Engineering the tendon-to-bone tissue interface mimicking its microenvironment: from stem cells to gradient scaffolds

Helena Isabel Pinto Cardoso Teixeira Calejo

UMinho | 2021

Universidade do Minho
I3Bs - Instituto de Investigação em Biomateriais, Biodegradáveis e Biomiméticos

Helena Isabel Pinto Cardoso Teixeira Calejo

Engineering the tendon-to-bone tissue interface mimicking its microenvironment: from stem cells to gradient scaffolds

Março de 2021

Universidade do Minho

I3Bs - Instituto de Investigação em Biomateriais, Biodegradáveis e Biomiméticos

Helena Isabel Pinto Cardoso Teixeira Calejo

Engineering the tendon-to-bone tissue interface mimicking its microenvironment: from stem cells to gradient scaffolds

Tese de Doutoramento

Doutoramento em Engenharia de Tecidos, Medicina Regenerativa e Células Estaminais

Trabalho efetuado sob a orientação do

Professor Manuela Estima Gomes

Março 2021

ACKNOWLEDGMENTS

After four year, it's time to recognize the support and help of all people that accompanied me during this long journey.

First of all, I want to thank to my supervisor, Prof. Manuela Gomes, who believed in me from day zero and allowed me to join her team. I was fortunate to receive all the opportunities she gave me throughout these years and for the way she believed in me.

I would also like to thank Professor Rui L. Reis for giving me the opportunity to develop my work at the 3B's Research Group.

To all my colleagues from 3B's, thanks for all the cooperation and challenges in such a big group and for the helpful insights. To my good friends from this institution and to no longer 3B's friends, thanks for being part of such an achievement.

To Raphael, to whom I will also dedicate this thesis. I can hardly put into words the way he encouraged me and supported me. He has guided me to be a better scientist. Independently of his mood, frustrations and workload, he was always there, and he always made me believe everything is possible, even when nothing was going well or even when we did not have nothing to hold on to. During these years, we have also started new chapters of our life together while embracing new adventures. Thanks for being my best friend, my partner!

To my family, I will thank them in portuguese: Obrigada por terem sempre acreditado em mim e em todos os meus devaneios e sonhos ao longo deste meu percurso. Muito Obrigada! Dedico-vos esta tese, sem vocês não teria sido possível.

I also would like to acknowledge the financial support of "Fundação para a Ciência e Tecnologia – FCT" for my PhD scholarship (PD/BD/128088/2016).

To finish:

"Only those who attempt the absurd can achieve the impossible."

Albert Einstein

STATEMENT OF INTEGRITY

I hereby declare having conducted this academic work with integrity. I confirm that I have not used plagiarism or any form of undue use of information or falsification of results along the process leading to its elaboration.

I further declare that I have fully acknowledged the Code of Ethical Conduct of the University of Minho.

University of Minho,

ENGINEERING THE TENDON-TO-BONE TISSUE INTERFACE MIMICKING ITS MICROENVIRONMENT: FROM STEM CELLS TO GRADIENT SCAFFOLDS

ABSTRACT

Within the human body, musculoskeletal tissues interfaces, such as the tendon-to-bone, are characterized by a unique compositional and structural gradient between dissimilar tissues. Interface injuries are very challenging to treat, and clinical outcomes using currently available therapies are unsatisfactory, mostly leading to the formation of a fibrotic tissue. To overcome this, interface tissue engineering has evolved over the past years taking advantage from major advances in biomaterial design to precisely control biophysical cues coupled with bioactive molecules for efficient regulation of cells towards the formation of a functional tissue. In this thesis, different strategies were explored for a better understanding of the basic molecular events occurring in tendon-to-bone interface while developing biomimetic templates to govern cellular responses, aiming at developing mimetic *in vitro* models and efficient regenerative strategies to treat tendon-to-bone interface injuries.

In the first study of this thesis (Chapter 5), direct co-cultures of human tendon-derived stem cells and pre-differentiated human adipose-derived stem cells towards the osteogenic lineage were established to determine optimal culture conditions to maintain both phenotypes and understand the effect of direct contact in the expression of interface markers. In the subsequent work (Chapter 6), the microenvironment oxygen tension (hypoxia vs normoxia) was modulated to study and control cells phenotype. The concept of gradient scaffolds was then explored (Chapter 7) to create a continuous fibrous structure composed of mechanically robust microfibers with topographical cues to stimulate the differentiation of hASCs towards enthesis specific lineages. In Chapter 8, topographically different fibers were biofunctionalized with platelet lysates and assembled into continuous 3D functionally graded scaffolds to replicate the tendon-to-bone microstructure while providing the cues for hASCs multi-differentiation in a single construct. Finally (Chapter 9), *in vitro* physiological and pathological bioengineered models of tendon were investigated through the use of hierarchically assembled yarns coated with a hydrogel coating of platelet lysates. Overall, the work developed under this thesis allowed the understanding of the effect of medium conditions and oxygen tension on the modulation of cell's phenotype along with the importance of cell-cell contact on the regulation of tendon-to-bone biomarkers. Additionally, fabricated scaffolds supported the native behavior of tendon-to-bone cells in artificial 3D constructs. These systems are expected to boost tissue *in vitro* modulation, surgical host integration and further tissue regeneration.

Keywords: Biomaterials, Gradients; Tendon-bone interface; Tissue Engineering; Oxygen tension

PRODUÇÃO DA INTERFACE TENDÃO-OSSO REPLICANDO O SEU MICROAMBIENTE: DESDE CÉLULAS ESTAMINAIS ATÉ ESTRUTURAS COM GRADIENTES

RESUMO

No corpo humano, as interfaces dos tecidos músculo-esqueléticos, como o tendão-osso, são caracterizadas por um gradiente de composição e estrutura entre diferentes tecidos. Lesões na interface são difíceis de tratar e os resultados clínicos, usando as terapias atualmente disponíveis, são insatisfatórios, principalmente devido à formação de tecido fibrótico. Para ultrapassar isso, a engenharia de tecidos de interface evoluiu nos últimos anos, aproveitando os principais avanços no design de biomateriais para controlar com precisão os fatores biofísicos conjuntamente com moléculas bioativas para a regulação das células e formação de um tecido funcional. Nesta tese, diferentes estratégias foram exploradas de forma a compreender vias moleculares que ocorrem na interface tendão-osso, através do desenvolvimento de modelos biomiméticos *in vitro* e estratégias regenerativas para tratar lesões na interface tendão-osso.

No primeiro estudo desta tese (Capítulo 5), co-culturas diretas de células estaminais derivadas do tendão e células estaminais derivadas do tecido adiposo, pré-diferenciadas na linhagem osteogênica, foram estabelecidas para determinar as condições ideais de cultura de forma a manter ambos os fenótipos e compreender o efeito do contato direto na expressão dos marcadores de interface. Subsequentemente (Capítulo 6), a tensão de oxigênio no microambiente (hipóxia vs normóxia) foi modulada para estudar e controlar o fenótipo das células. O conceito de estruturas com gradientes foi então explorado (Capítulo 7). Estruturas fibrosas compostas de microfibras mecanicamente robustas diferentes topografias foram criadas para estimular a diferenciação de células estaminais nas linhagens específicas de interface. No Capítulo 8, fibras topograficamente diferentes foram funcionalizadas com lisado de plaquetas e criadas estruturas funcionais 3D contínuas para replicar a microestrutura do tendão-osso, fornecendo fatores necessários para a diferenciação de hASCs. Finalmente (Capítulo 9), modelos de saúde e doença de tendão *in vitro* foram investigados através do uso de fibras hierarquicamente montados e revestidas com um hidrogel de lisado de plaquetas. De maneira geral, o trabalho desenvolvido nesta tese permitiu a compreensão do efeito das condições do meio e da tensão de oxigênio na modulação do fenótipo celular, juntamente com a importância do contato célula-célula na regulação de biomarcadores do tendão-osso. Além disso, as estruturas 3D fabricadas induziram a expressão de marcadores tendão-osso. Espera-se que esses sistemas aumentem a modulação *in vitro* do tecido, a integração cirúrgica e a regeneração do tecido.

Palavras-chave: Biomateriais; Engenharia Tecidos; Gradientes; Interface tendão-osso; Tensão Oxigénio

TABLE OF CONTENTS

LIST OF ABBREVIATIONS AND ACRONYMS

2D – Two-dimensional

3D – Three-dimensional

βGP – beta-glycerophosphate

β-TCP – Tricalcium Phosphate

α-MEM – Alpha Minimum Essential Medium

A

AA – Ascorbic Acid

ACL – Anterior Cruciate Ligament

ACAN – Aggrecan

ALP – Alkaline Phosphatase

ALPL – Alkaline Phosphatase gene

ASCs – Adipose derived Stem Cells

B

bFGF – Basic Fibroblast Growth Factor

BG – Bioactive Glass

Bglap – Osteocalcin

BMSCs – Bone Marrow Derived Mesenchymal Stem Cells

BMU – Basic Multicellular Unit

BMP – Bone Morphogenetic Protein

BSP – Bone Sialoprotein

C

CHF – Chloroform

CHON – Chondrogenic

CLF – Composite living fibers

COL1A1 – Collagen Type 1, Alpha Chain 1

COL1A2 – Collagen Type 1, Alpha Chain 2

COMP – Cartilage Oligomeric Matrix Protein

CS-TSA – Cell Sheets Treated with Trichostatin

CTGF – Connective Tissue Growth Factor

D

DMF – Dimethylformamide

E

ECs – Endothelial Cells

ECM – Extracellular Matrix

EGF – Endothelial Growth Factor

EMF – External Magnetic Field

F

FBS – Fetal Bovine Serum

FGF – Fibroblast Growth Factor

G

G-CSF – Granulocyte-Colony Stimulating Factor

GDF – Growth/Differentiation Factor

GHS – Gelatin Hydrogel Sheet

GLI1 – Gli Family Zinc Finger 1

H

Hap - Hydroxyapatite

hASCs – Human Adipose Tissue Derived Stem Cells

HDAC – Histone Deacetylase

HGF – Hepatic Growth Factor

Hh – Hedgehog

HIF-1α – Hypoxia-Inducible Factor-1 Alpha

HIF-2α – Hypoxia-Inducible Factor-2 Alpha

hTDCs – Human tendon-derived cells

Hz – Hertz

I

IBSP – Integrin Binding Sialoprotein

IGF-1 – Insulin-Like Growth Factor 1

Ihh – Indian Hedgehog

ITE – Interfacial Tissue Engineering

L

-

M

MA/MMA – Methyl Acrylate/Methyl Methacrylate

MA-CS – Methacrylated Chondroitin Sulfate

magCS – magnetic Cell Sheets

Min – Minute

MMP – Matrix metalloproteinase

MMP13 – Matrix Metallopeptidase 13

MSCs – Mesenchymal Stem Cells

MKX – Mohawk

N

nACP – Amorphous Calcium Phosphate nanoparticles

nHAp – Nano-hydroxyapatite

NMR – Nuclear Magnetic Resonance

O

O_2 – Oxygen Tension

OB – Osteoblastic

OCN – Osteocalcin

OPN – Osteopontin

ORAC – Oxygen Radical Absorbance Capacity

P

PCL - Polycaprolactone

PDGF – Platelet-derived Growth Factor

PDSCs – Periosteum-derived Stem Cells

PEG – Polyethylene Glycol

PEGDA - Polyethylene Glycol Diacrylate

Pre-OBs – Pre-Osteoblasts

PL – Platelet Lysate

PLGA – Poly(D-L-Lactide-coglycolide)

PLLA – Poly(Lactic Acid)

pNPP – p-nitrophenyl phosphate

PPP – Platelet Poor Plasma

PRP – Platelet-Rich Plasma

PTHrP – Parathyroid Hormone-Related Protein

R

RGD – Arginylglycylaspartic Acid

rhBMP-2 – Recombinant Human Bone Morphogenetic Protein-2

RNA – Ribonucleic Acid

ROS – Reactive Oxygen Species

RUNX – Runt-related transcription factor

S

SBF – Simulated Body Fluid

SCX – Scleraxis

SIS – Small Intestinal Submucosa

SMO – Smoothened Protein

sMSCs – Synovial Mesenchymal Stem Cells

SOX – SRY-Box Transcription Factor

SPP1 – Osteopontin gene

T

TCP – Tissue Culture Plastic

TCs – Tenocytes

TDSCs – Tendon-derived Stem Cells

TERM – Tissue Engineering and Regenerative Medicine

TGFβ – Transforming Growth Factor Beta

TgfBrII – Transforming Growth Factor Beta Receptor II

TNMD - Tenomodulin

TSPC – Tendon Stem/Progenitor Cells

TTE – Tendon Tissue Engineering

U

-

V

VEGF – Vascular Endothelial Growth Factor

LIST OF FIGURES

LIST OF SUPPLEMENTARY FIGURES

LIST OF TABLES

LIST OF SUPPLEMENTARY TABLES

SHORT *CURRICULUM VITAE*

Helena Isabel Calejo was born on the 31st of May 1991 in Porto, Portugal. She concluded her Degree in Biomedical Bioengineering in 2012 in the Superior School of Biotechnology of Catholic University of Porto and, in 2015, her master's in Forensic Toxicology in Faculty of Medicine of University of Porto. During that period (1 year), she worked at the Department of Biological Sciences of Faculty of Medicine, University of Porto, where she developed an analytical technique of GC-MS for the identification of characteristic volatile compounds in urine enabling the discrimination of patients with and without prostate cancer, resulting in her first publication. From 2012 to 2016, Isabel simultaneously worked as a researcher in the Centre for Drug Discovery and Innovative Medicines of Institute of Biomedical Sciences Abel Salazar, specifically in the Laboratory of Pharmacology and Neurobiology. During that period, she was involved in a project focused on the study of the purinergic signaling in human bone remodeling, where she started developing her skills in cell culture and biological assays. Simultaneously, Isabel learned how to perform the quantification of purine and pyrimidine nucleotides by HPLC-UV/VIS. Consequently, she also participated in other ongoing projects during this period, such as the study of the role of ATP on Neuromuscular Transmission in experimental autoimmune myasthenia gravis, among others. As academic contributions, Isabel Calejo has also actively participated in the preparation and technical assistance of practical lessons designed for the 3rd year students of the master's in human medicine, Veterinary Medicine and Biochemistry (2015/2016), within the Pharmacology and Therapeutics course.

Since 2016, she is enrolled in the Doctoral Program of Tissue Engineering, Regenerative Medicine and Stem Cells (TERM&SC) from the University of Minho. Her work is being develop in 3B's Research Group from University of Minho and focuses the fundamental understanding and regeneration of a soft-to-hard musculoskeletal interface, the enthesis. Her first study approached the understanding of cellular and biochemical interactions occurring at the tendon-to-bone interface. Then, Isabel studied the effect of environmental cues (e.g., oxygen tension) on cells behavior, phenotype and genotype, while developing novel bioinstructive materials to guide cells differentiation towards osteogenic, chondrogenic and tenogenic lineages. She has also worked with platelet lysates to develop composite living fibers for tendon regeneration, and more recently she developed a controllable and biofunctionalized nanoelectrospun fiber threads incorporating PLs for tendon-to-bone interface applications.

Her work has resulted in several oral presentations and posters in international and national conferences. Moreover, as a result of the research carried out, she is the author and co-author of several publications in international scientific meetings, and original articles in international journals (8 published and 2 submitted), as well as published literature reviews (2) and a chapter (1).

LIST OF PUBLICATIONS

The work performed during the PhD period resulted in the publications listed below.

PAPERS IN INTERNATIONAL REFEREED JOURNALS:

I. Calejo, C. J. Labrador-Rached, M. Gomez-Florit, D. Docheva, R. L. Reis, R.M.A. Domingues, M. E. Gomes (2021) Microengineered composite living fibers as 3D in vitro models of tendon physiology and pathology *(Submitted)*

I. Calejo, R. M. A. Domingues, R. L. Reis, M. E. Gomes (2021) Functionally graded fibrous scaffolds as tendon-to-bone tissue interface replicates *(Submitted)*

I. Calejo, R. Costa-Almeida, R. L. Reis, M. E. Gomes (2020) *In vitro* temporal HIF-mediated deposition of osteochondrogenic matrix governed by hypoxia and osteogenic factors synergy. *Journal of Cellular Physiology.* DOI: 10.1002/jcp.30138.

I. Calejo, R. Costa-Almeida, R. L. Reis, M. E. Gomes (2019) A Textile Platform Using Continuous Aligned and Textured Composite Microfibers to Engineer Tendon-to-Bone Interface Gradient Scaffolds. *Advanced Healthcare Materials*, 8(15) 1900200. DOI: 10.1002/adhm.201900200

R. Costa-Almeida, **I. Calejo**, M. E. Gomes (2019) Mesenchymal Stem Cells Empowering Tendon Regenerative Therapies. *International Journal of Molecular Sciences,* 20(12):3002. DOI: 10.3390/ijms20123002. *(Author of journal cover)*

R. Costa-Almeida*, **I. Calejo***, R. Altieri, R. M. A. Domingues, E. Giordano, R. L. Reis, M. E. Gomes (2018) Exploring platelet lysate hydrogel-coated suture threads as biofunctional composite living fibers for cell delivery in tissue repair. *Biomedical Materials*, 14(3):034104. DOI:10.1088/1748-605X/ab0de6. (*Co-first authors)

I. Calejo, R. Costa-Almeida, A. I. Gonçalves, D. Berdecka, R. L. Reis, M. E. Gomes (2018) Bi-directional modulation of cellular interactions in an in vitro co-culture model of tendon-to-bone interface. *Cell Proliferation*, 51:e12493. DOI:10.1111/cpr.12493.

R. Costa-Almeida, **I. Calejo**, R. L. Reis, M. E. Gomes. (2018) Crosstalk between adipose stem cells and tendon cells reveals a temporal regulation of tenogenesis by matrix deposition and remodelling. *Journal of Cell Physiology* 2018;233: 5383–5395. DOI: 10.1002/jcp.26363.

REVIEW PAPERS:

I. Calejo, R. Costa-Almeida, R. L. Reis, M. E. Gomes (2020) A Physiology-Inspired Multifactorial Toolbox in Soft-to-Hard Musculoskeletal Interface Tissue Engineering. *Trends in Biotechnology*, 38:1. DOI: 10.1016/j.tibtech.2019.06.00.

I. Calejo, R. Costa-Almeida, M. E. Gomes (2019) Enthesis tissue engineering: biological requirements meet at the interface. *Tissue Engineering Part B Reviews.* DOI: 10.1089/ten.TEB.2018.0383.

BOOK CHAPTERS:

I. Calejo, R. Costa-Almeida, R. L. Reis, M. E. Gomes (2019) Cellular Complexity at the Interface: Challenges in Enthesis Tissue Engineering. In: *Advances in Experimental Medicine and Biology*, 1144:71-90. Springer, New York, NY. DOI:10.1007/5584_2018_307.

COMMUNICATIONS IN INTERNATIONAL CONFERENCES

Oral Presentations:

I. Calejo, R. Costa-Almeida, R. L. Reis, M. E. Gomes. "Topological and compositional gradients to generate 3D textured living microfibers resembling tendon-to-bone interface". European Orthopaedic Research Society (EORS), 02nd-04th October 2019, Maastricht, Netherlands.

I. Calejo, R. Costa-Almeida, R. L. Reis, M. E. Gomes. "Hypoxia mediated response in an in vitro co-culture model of tendon-to-bone interface". 1st Achilles Conference – Molecular and biological mechanisms of tendon homeostasis and repair 2019, 08th-10th July, Porto, Portugal.

I. Calejo, R. Costa-Almeida, R. L. Reis, M. E. Gomes. "Oxygen conditioning effect on an in vitro co-culture model of tendon-to-bone interface". TERMIS European Chapter Meeting 2019, 27th-31st May, Rhodes, Greece. – Published in European Cells & Materials Conferences.

R. Costa-Almeida, **I. Calejo**, R. L. Reis, M. E. Gomes. "Platelet lysate cell-laden hydrogel-coated suture threads for tendon repair". European Orthopaedic Research Society (EORS) 26th Annual Meeting, 25th-28th September 2018, Galway, Ireland. – Published in Orthopaedic Proceedings, 100.

I. Calejo, R. Costa-Almeida, R. L. Reis, M. E. Gomes. "Optimization and establishment of a co-culture model to study cellular interactions in tendon-to-bone interface" European Orthopaedic Research Society (EORS) 25th Annual Meeting, 13th-15th September 2017, Munich, Germany – Published in Orthopaedic Proceedings, 100:3

Poster Presentations:

I. Calejo, R. Costa-Almeida, R. L. Reis, M. E. Gomes. "Textured microfibers with topological and compositional gradients resembling tendon-to-bone interface" 1st Discoveries Forum on Regenerative and Precision Medicine, 25th-27th September 2019, Porto, Portugal.

I. Calejo, R. Costa-Almeida, R. L. Reis, M. E. Gomes. "Hypoxia conditioning effect on an in vitro tendon-to-bone interface co-culture model". Gene2Skin/CHEM2NATURE Final Conference, 23rd-26th October 2018, Guimaraes, Portugal.

I. Calejo, R. Costa-Almeida, A. I. Gonçalves, D. Berdecka, R. L. Reis, M. E. Gomes. "Unraveling the crosstalk between pre-osteoblasts and tendon cells in tendon-to-bone regeneration" 5th TERMIS World Congress, 04th-07th September 2018, Kyoto, Japan.

I. Calejo, R. Costa-Almeida, R. L. Reis, M. E. Gomes. "Wet-spinning technique for the production of PCL/Gel and PCL/Gel/nHA continuous fibers for tendon-to-bone insertion regeneration". Chem2Nature/Gene2skin – Summer School 2018, 03rd-08th June 2018, Porto, Portugal.

I. Calejo, R. Costa-Almeida, R. L. Reis, M. E. Gomes. "Bi-directional crosstalk between tendon cells and pre-osteoblasts: a co-culture approach for tendon-to-bone interfacial tissue engineering". TERMSTEM/FORECAST 2017 - 1° Workshop of FoReCaST -The Tumour Microenvironment, 15th-17th November 2017, Porto, Portugal.

I. Calejo, R. Costa-Almeida, R. L. Reis, M. E. Gomes. "Co-culture model to study the role of cellular interactions in enthesis" CHEM2NATURE Second school, 05th-09th June 2017. Porto, Portugal

Conference abstracts published in international scientific journals:

I. Calejo, R. Costa-Almeida, R. L. Reis, M. E. Gomes. "Topological and compositional gradients to generate 3d textured living microfibers resembling tendon-to-bone interface." European Orthopaedic Research Society (EORS) 27th Annual Meeting, 2nd-4th October 2019, Maastricht, The Netherlands – Published in Orthopaedic Proceedings Supplements.

I. Calejo, R. Costa-Almeida, R. L. Reis, M. E. Gomes. "Oxygen conditioning effect on an in vitro co-culture model of tendon-to-bone interface". TERMIS European Chapter Meeting 2019, 27th-31st May, Rhodes, Greece. – Published in European Cells & Materials Conferences.

R. Costa-Almeida, **I. Calejo**, R. L. Reis, M. E. Gomes. "Platelet lysate cell-laden hydrogel-coated suture threads for tendon repair". European Orthopaedic Research Society (EORS) 26th Annual Meeting, 25th-28th September 2018, Galway, Ireland. – Published in Orthopaedic Proceedings, 100.

I. Calejo, R. Costa-Almeida, R. L. Reis, M. E. Gomes. "Optimization and establishment of a co-culture model to study cellular interactions in tendon-to-bone interface" European Orthopaedic Research Society (EORS) 25th Annual Meeting, 13th-15th September 2017, Munich, Germany – Published in Orthopaedic Proceedings, 100:3

AWARDED GRANTS

Fundação para a Ciência e Tecnologia (FCT) PhD Scholarship - PD/BD/128088/2016

ON Travel grant – EORS

To my Family

Thank you, for never stop believing

SECTION I: General Introduction

CHAPTER 1. Musculoskeletal interfaces: A brief overview of soft-to-hard tissue interface engineering strategies

This chapter was adapted from the following publication:

I. Calejo, R. Costa-Almeida, R. L. Reis, M. E. Gomes (2020) A Physiology-Inspired Multifactorial Toolbox in Soft-to-Hard Musculoskeletal Interface Tissue Engineering. *Trends in Biotechnology*, 38:1. DOI: 10.1016/j.tibtech.2019.06.003

ABSTRACT

Musculoskeletal diseases are increasing the prevalence of physical disability worldwide. Within the body, musculoskeletal soft and hard tissues integrate through specific multi-tissue transitions, allowing for body movements. Owing to their unique compositional and structural gradients, injuries challenge the native interfaces, and tissue regeneration is unlikely to occur.

Tissue engineering strategies are emerging to emulate the physiological environment of soft-to-hard tissue interfaces. Advances in biomaterial design enable control over biophysical parameters, but biomaterials alone are not sufficient to provide adequate support and guide transplanted cells. Therefore, in this chapter, biological, biophysical, and biochemical tools are integrated into a multifactorial toolbox, steering prospective advances toward engineering clinically relevant soft-to-hard tissue interfaces.

Keywords: Biomaterial design; Biomimetics; Gradients; Multi-tissue transitions; Osteochondral; Regenerative Medicine; Stem cell differentiation; Soft-hard tissue interfaces; Tendon-to-bone

1.1. MUSCULOSKELETAL INTERFACES AND REGENERATION REQUIREMENTS: A GLOBAL BURDEN

Body tissues and organs are inherently composed of multiple tissues interfacing with each other and allowing extremely complex biological functions to take place. In the musculoskeletal system, these tissue interfaces integrate extremely dissimilar tissues with distinctive characteristics ranging from a hard and highly vascularized tissue with lightweight stiffness and strength, as the bone, to extremely viscoelastic and avascular tissues, such as articular cartilage, or tough, resilient and elastic as the tendons. Interestingly, the defining characteristic of musculoskeletal interfaces is their primary load-bearing function while mediating the multiple transitions in tissues stiffness [1, 2], which structurally requires the presence of hierarchically assembled proteins in highly specialized extracellular matrices (Supplementary Figure 1.1). Examples of soft-to-hard tissue interfaces are the tendon/ligament-to-bone interface, commonly found in the rotator cuff and anterior cruciate ligament, respectively, and osteochondral unit (cartilage-to-bone interface) located in the knee joints. However, these tissue interfaces are commonly affected by diseases and disorders at all stages of life. Strikingly, musculoskeletal diseases have been estimated to correspond to the major cause of disability worldwide with significant healthcare and social support costs [3]. Rotator cuff and anterior cruciate ligament tears or detachment affect the daily life of both adult and elderly resulting in pain and movement impairment [4]. Similarly, in adulthood, osteoarthritis, a degenerative process resulting in progressive articular cartilage and joint destruction, especially at the osteochondral interface, is one of the major contributors to immobility, pain, and productivity lose [3].

Current strategies used in the clinics to manage ligament/tendon injuries include the application of grafts (auto-, allo-, and synthetic grafts) and, alternatively, microfracture surgery where the subchondral bone is perforated to enable a localized transport of bone marrow and blood into contact with the degenerate tissue in the osteochondral unit. However, unsatisfactory functional outcomes of repaired tissues due to previous degeneration, together with increased risk of re-injury, lay the foundation for the development of soft-to-hard interface tissue engineering and regenerative therapies. Alternative strategies reaching the stage of commercialization or clinical trials for managing osteochondral defects and tendon-to-bone injuries encompass mainly the application of biomaterials, including biologic and synthetic scaffolds, injectable hydrogels, or decellularized matrices [5, 6]. However, these are often used as tissue substitutes, not accurately resembling the native architecture, structure, composition, and therefore mechanical needs of the native tissue, as well as lacking the ability to generate the proper interface.

Hence, the regeneration of soft-to-hard tissue interfaces after an injury is still far from being achieved and constitutes a global clinical and economic burden.

The field of tissue engineering and regenerative medicine (TERM) envisions the generation of novel approaches toward restoring functionality upon tissue repair. The ideal strategy for soft-to-hard tissue regeneration would recreate interfacial physiological complexity, assure mechanical performance of the tissue during the reparative process, and deliver therapeutic elements essential to promote tissue regeneration and to modulate the inflammatory milieu. Besides these challenges, healing must occur within an optimal temporal window toward limiting scar tissue formation. Several studies addressed the role of biological actors, including competent regenerative cells and inflammatory cells, as well as biochemical factors, namely cytokines and growth factors. Alternatively, recent progresses on biomaterial-guided cell behaviors [7] have been providing novel tools to direct cell fate.

In this chapter, we give an overview of two well-known soft-to-hard tissue interfaces, osteochondral and tendon-bone, while generally discussing the use of biophysical, biochemical, and biomechanical cues together as a toolbox steering prospective advances toward engineering physiological niches aiming at musculoskeletal soft-to-hard tissue interface regeneration (Figure 1.1).

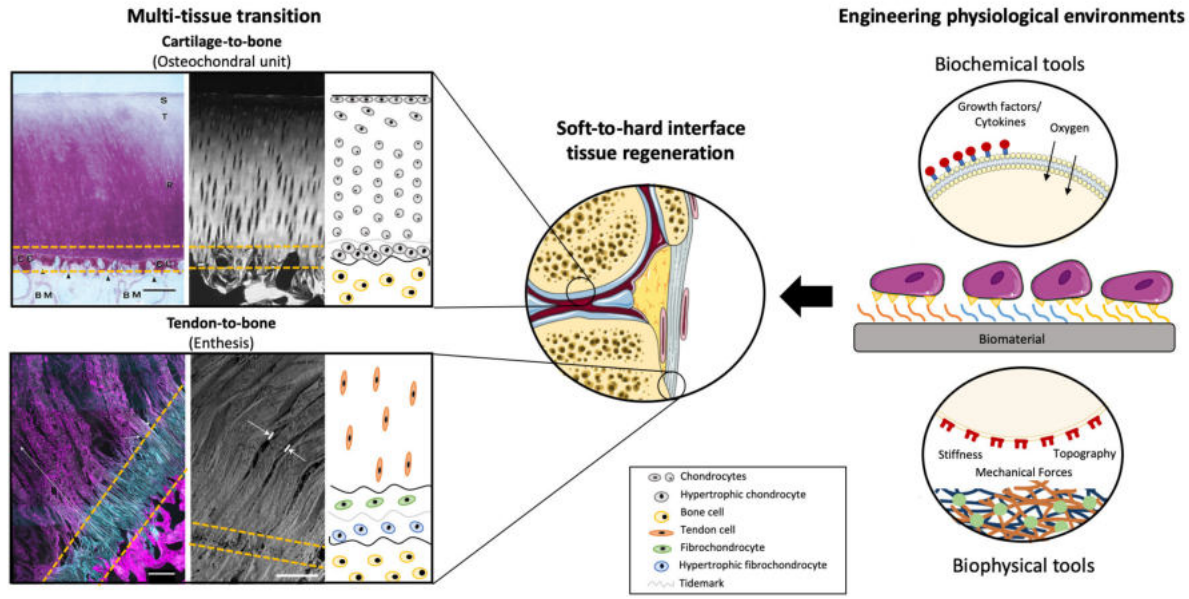

Figure 1.1 | Schematic representation of multifactorial strategies targeting soft-to-hard interface tissue regeneration. Taking a close look at the osteochondral unit (left, top pannel), a transitional region is distinguished, as well as a distinct shift in tissue matrix organization, composition, and cell phenotype (between dashed lines). Scale bar, 500 μm. Reproduced, with permission, from [8] and [9]. Similarly, tendon and bone are interfaced within a region of ~500 μm (left, bottom panel, blue coloured, between dashed lines), exhibiting a smooth gradient in fiber organization, architecture, and

therefore mechanical properties. A heterotypic cellular environment is observed with a gradual change from tendon cells, to fibrochondrocytes, hypertrophic chondrocytes, and bone cells. Scale bars, 300 μm (left) and 250 μm (right). Reproduced, with permission, from [2]. Interfacial tissue engineering (ITE) strategies targeting soft-to-hard interface tissue regeneration encompass the combination of biochemical and biophysical tools to recreate the native morphological and regional features of soft-to-hard tissue interfaces, while carefully controlling stem cells fate to mimic the naturally present cellular microenvironments.

1.2. A MULTIFACTORIAL TOOLBOX FOR DESIGNING TISSUE ENGINEERING STRATEGIES

Based on the hierarchical organization of soft-to-hard tissue interfaces, various biomaterials-based approaches have been proposed over the past decade. For tendon/ligament-bone interface, scaffold design has long relied on the creation of stratified layers with or without minerals and reconstructed graft materials for interface repair [10], however not truly recreating the physiological structure. Therefore, multmultiphasic gradient fiber-based scaffold designs, along with strategic patterning of key biochemical cues, such as growth factors, have emerged to emulate multi-tissue architecture[11, 12] while controlling stem cell distribution and differentiation both *in vitro* and *in vivo* [13, 14]. Comparably, biomaterials-based strategies for osteochondral defects have been relying on the use of multilayered polymeric scaffolds, which are designed to generate structural templates to mimic the cartilaginous layer, the calcified cartilage and subchondral bone, and metallic scaffolds with architectural and biochemical gradients [15, 16]. However, these structures do not functionally generate different cellular phenotypes in a spatially and temporally defined way, which allow to mimic the native osteochondral tissue cellular environment. Furthermore, in the case of laminate composites, the weak strength bonding between layers normally results in phase separation, not leading to tissue regeneration. Therefore, some reports focused on the use of single scaffolds for osteochondral regeneration [17, 18]. These scaffolds ensure continuity between phases to avoid a barrier in the interface, together with biomaterials integrity, while mimicking the natural hierarchical structure of the osteochondral tissue. Developed functional materials focused on mimicking specific anisotropic orientation of the subchondral bone and calcified cartilage region in single 3D constructs have demonstrated a favorable control of stem cell fate toward osteogenic and chondrogenic-lineages [19, 20]. Cartilage-to-bone engineered strategies mainly rely on scaffold-based approaches due to the tunability and versatility of materials to achieve the mechanical and physical requirements of the tissue for proper regeneration. However, developed technologies still fail in providing the necessary

signals in a controllable and precise manner for an enhanced and effective biological response, therefore, failing in the conjugation with cellular-based strategies.

From a biomimetic perspective, the recapitulation of multi-tissue spatial properties goes beyond the application of a single strategy.

Engineering a functional soft-to-hard tissue interface requires a multi-scale, multi-component approach to integrate region-specific cell populations, matrix composition and organization and, consequently, mechanical requirements in a single unit.

1.2.1. BIOLOGICAL TOOLS

Upon injury, hypovascular dense regular connective tissues (e.g., meniscus, tendons, and ligaments) have a limited self-repair ability and depend on resident or neighboring cells to orchestrate tissue repair, as opposed to the majority of tissues that are supplied by a vascular network, benefiting from circulating progenitor cells. Up to date, the identification of regeneration competent cells within soft-to-hard tissue interfaces remains a mystery, particularly for tendon-/ligament-to-bone interfaces since resident cells and their heterogeneity is not fully understood.

Different cell populations, particularly bone marrow derived mesenchymal stem cells (BMSCs), and other cell sources ranging from resident/tissue-specific cells to induced pluripotent stem cells, are explored for musculoskeletal tissue regeneration using various delivery strategies (e.g., injection, arthroscopy, implantation), as reviewed elsewhere [21]. Autologous chondrocyte implantation aiming at osteochondral repair was one of the first cell-based tissue engineering interventions reaching the clinical application. Similarly, autologous tenocyte implantation is also explored (Phase 2-3 clinical study NCT01343836). Nonetheless, the need for cell support has been recognized and the combination with matrix-based cell implantation is pursued nowadays.

1.2.1.1. *Scaffold-free cell delivery technologies*

Cell sheet engineering (Figure 1.2) has been proposed to overcome shortcomings of single-cell suspension injection in tissue reconstruction through the preservation of cell-cell contacts and deposited extracellular matrix (ECM) [22]. Autologous cell sheet transplantation has been explored for regenerating thin-layered tissues (e.g., cornea, esophagus, periodontal tissues), but advances in three-dimensional (3D) cell sheet manipulation enable the reconstruction of thicker and more complex tissue architectures (Figure 1.2A-E). Layered chondrocyte sheets alone and in combination with synovial cells or even further combined with scaffolds have been reported to facilitate osteochondral regeneration through barrier

functionality and supporting chondrocyte phenotype and chondrogenic differentiation [23, 24] [25]. In the case of tendon and tendon-to-bone repair, the use of native tissue cells and derived cell sheets has been defied by the phenotypic drift and senescence of tendon cells upon *in vitro* expansion, leading to limited healing capacity. Recently, this has been associated with increased activity of histone deacetylase (HDAC) [26]. Hence, epigenomic modifications targeting the inhibition of different HDAC subtypes allowed the recovery of tendon-marker *scleraxis* expression, supporting the use of tendon stem/progenitor cells (TSPC) sheets (Figure 1.2F) in accelerating tendon repair [26]. Further combining stem cell sheets with native tendon-fibrocartilage-bone composite as a biological patch to augment rotator cuff healing resulted in enhanced fibrocartilage formation and collagen fiber organization while providing biomechanical support during tissue repair [27]. The value of cell sheets in tissue repair is well-recognized as they overcome cell loss and reduced engraftment upon transplantation. Nevertheless, engineering functional soft-to-hard tissue interfaces is postulated to require an integration of physiologically relevant ECM signals and mechanical stimuli toward guiding stem cell fate.

Next-generation cell sheet engineering is taking this technology to a higher level of organization in recreating complex tissues. The development of anisotropic cell sheets using stripe-like micropatterned thermoresponsive surfaces [28] (Figure 1.2A) and, recently, light-induced cell alignment and cell sheet harvest [29] (Figure 1.2B-D) hold promising results to be explored for interfacial tissue engineering. More recent trends have been exploring magnetic force-based tissue engineering. The generation of magnetic cell sheets by cellular internalization of magnetic nanoparticles enabled the fabrication of tenogenic living ECM-rich patches (Figure 1.2E) with potential for remote control upon application of an external magnetic field as mechano-magnetic stimulus [30].

Biotechnological advances are pushing forward the complexity of cell-based therapies, paving the way to engineer living constructs with physiological and clinical relevance. Despite the promising reported outcomes, unsolved issues remain that challenge the field, including the development of off-the-shelf cellular therapies. Further, the refinement of cellular approaches in combination with biophysical and biochemical tools to manipulate cell fate is a current need toward generating physiologically relevant cellular gradients to emulate the cellular niche from the different musculoskeletal interfaces.

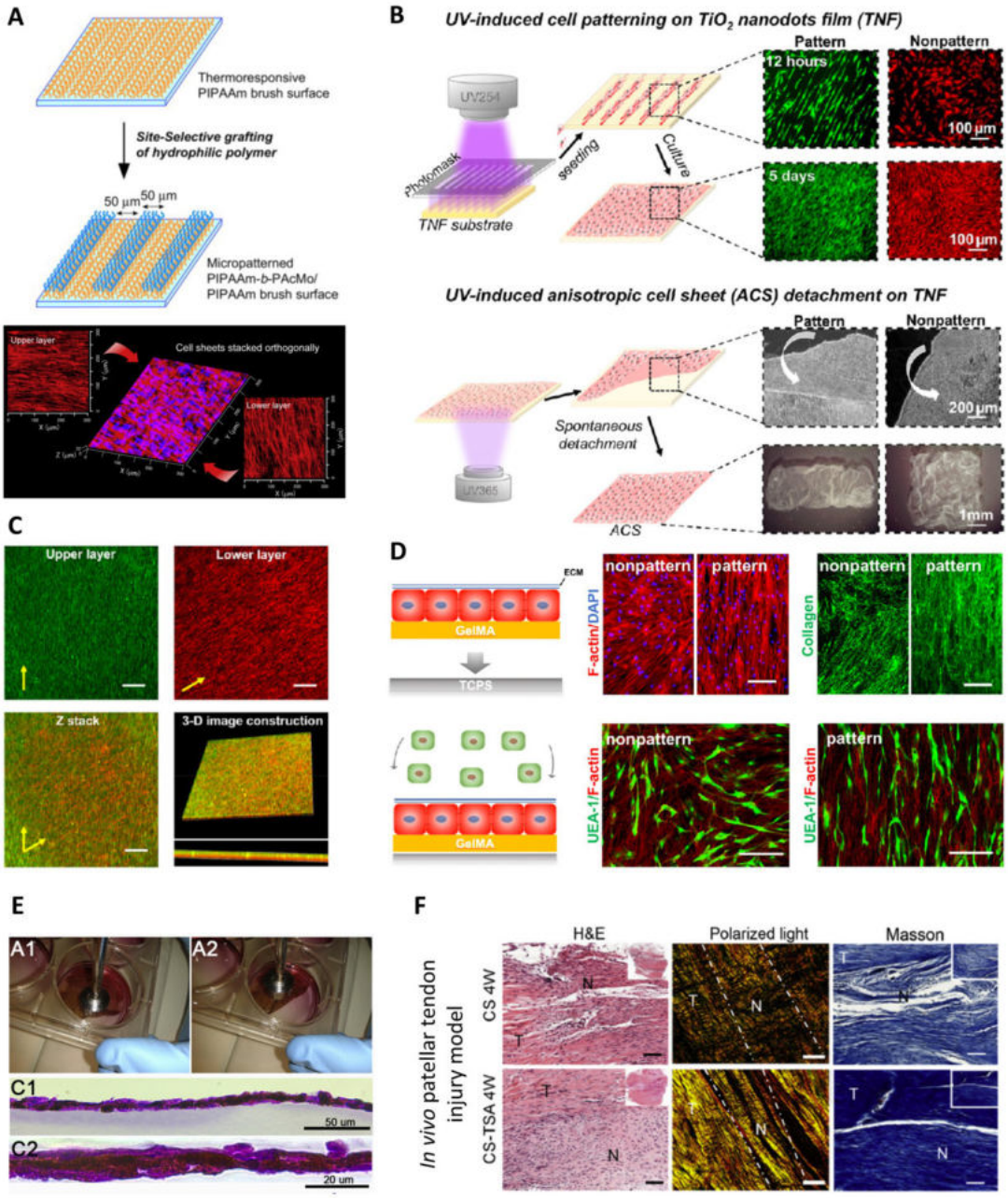

Figure 1.2| Advances in cellular-based technologies. Cell sheet engineering enables the delivery of cells along with their extracellular matrix. Site-selective polymer grafting onto thermoresponsive surfaces enabled the generation of anisotropic cell sheets upon one-pot cell seeding of human dermal fibroblasts (A). Reproduced with permission from [28]. Recently, light-induced cell alignment and harvest was achieved through the combination of light-responsive nanodots and photocrosslinkable gelatin (B). These anisotropic cell sheets retain an aligned ECM and can be stacked together in several layers to generate more complex 3D constructs (A, top; C). Besides the control over cell and matrix orientation, anisotropic cell sheets induce endothelial cells seeded on top to orient themselves, favoring vascularization (D). Although not yet applied to soft-to-hard interface tissue engineering, these strategies

hold promising features to be manipulated envisioning the creation of a gradient of cells, cellular alignment and cellular environments. (B-D) Reproduced with permission from [29]. Progresses in magnetic force-based tissue engineering are supporting also the development of magnetic cell sheets (magCS). MagCS have been fabricated using a subpopulation of tenomodulin-expressing human adipose derived stem cells (hASCs) to support the development of tendon-like living patches, which can be harvested through the use of a permanent magnet (E). Reproduced with permission from [30]. Further manipulation of tendon stem/progenitor cells through epigenetics tools (cell sheets treated with trichostatin A, CS-TSA, to inhibit histone deacetylase) allowed long-term cell expansion until reaching a sufficient cell number for cellular therapies with *in vivo* evidences of therapeutic efficiency in a rat patellar tendon injury model. Reproduced with permission from [26]].

1.2.2. BIOPHYSICAL PARAMETERS

Soft-to-hard musculoskeletal interfaces are highly structured nanocomposites arranged into microarchitectures with unique directionalities, gradients and cellular environments. Attachment of cells to the ECM regulates diverse cellular functions. It is well recognized that a precise control over nano-to-macro structural features of biomaterials is of major importance to recreate key properties of the native ECM. However, the development of multi-tissue transitions is still a challenge.

Advances in biomaterials design allow for refining microenvironmental features, paving the way to generate physiologically relevant niches and engineering soft-to-hard tissue interfaces. Over the years, different fabrication methods have been enabling the control over a panoply of interdependent biophysical parameters (Table 1.1).

Table 1.1 | Interplay of biophysical and biochemical properties in gradient biomaterials.

Feature	Strategy	Technique	Effects on biological functions	Interplay with other features	References
Biophysical					
Architecture/ geometry	Multiphasic scaffolds	Directional freezing and freeze-drying	• Macro/micro/nano interconnected porosity favors osteogenesis • Constrained areas promote chondrogenesis • Pore shape controls stem cell differentiation toward chondrogenic (cubic) or osteogenic (cylindrical) phenotypes • Aligned 3D geometry induces cell alignment	Dimension and pore shape gradients induce gradients of oxygen concentrations	[31-33]
	Gradient scaffolds and hydrogels	Electrospinning; 3D printing			
Surface topography	Fiber-based biomaterials	Electrospinning; Wetspinning	• Disordered/random topography supports osteogenesis • Greater topographical depth (100 nm) promotes osteogenesis • Anisotropic alignment promotes tenogenesis	Organization of topography alters mechanical properties	[34, 35]
	Patterning techniques	Soft lithography			
Mechanical properties	Hydrogel gradients				[36-38] [39-41]

	Fiber-based biomaterials	Electrospinning; Wetspinning; Textile assembling	• Higher substrate stiffness (>60KPa) and elastic moduli induce osteogenesis • Intermediate substrate stiffness results in the chondrogenic commitment of stem cells (30-50 KPa) • Textile assembling of aligned nanofibers improves biomechanical performance and enhances tenogenic differentiation		
Biochemical					
Oxygen	Hypoxia conditioning	Hypoxic culture	• Enhanced differentiation potential toward tenogenic and chondrogenic lineages • Reduced osteogenic differentiation commitment of stem cells • Improve interface integration		[42, 43]
		Chemical induction	• Gradient of oxygen delivery to control stem cells differentiation		
Composition	Growth factors and other biomolecules	Click reactions; Tethering/immobilization; Encapsulation; Electrostatic reaction	• Osteoinductive growth factors like bone morphogenetic protein (BMP) -2 and inorganic elements benefit osteogenesis • Growth factors like transforming growth factor-beta 3 (TGFβ-3) and BMP-2 induce endochondral ossification		[14, 44]

			• TGFβ1 and 3 induce chondrogenic and hypertrophic chondrogenic commitment of stem cells, respectively • Compositional gradients enable a spatial control over stem cell differentiation		
	Biomineralization	Crosslinking densities of polydopamine coatings	• Spatial control over mineral deposition and control over stem cells differentiation	Biomineralization alters mechanical properties (increased stiffness)	[45, 46]
Gene delivery	Growth factors and transcription factors	Cells Scaffolds	• Plasmid, adenovirus and retrovirus, baculovirus as vectors for delivery • Trio-co-transduction of SRY-Box Transcription Factor (SOX) -5, -6 and -9 combined with runt-related transcription factor 2 (RUNX2) enable osteochondral defect regeneration • Transfection with fibroblast growth factor (FGF) -2, growth/differentiation factor (GDF) -5 and BMPs benefits chondrogenesis and endochondral ossification		[47-50]

1.2.2.1. *Tailoring biomaterial architecture, surface topography and mechanical properties.*

As biophysical properties of native ECM are difficult to emulate, synthetic fibrous scaffolds have been essential to study and regulate specific matrix properties, necessary for cellular proliferation and function. From electrospinning to hydrogel systems, tendon-to-bone regeneration has been relying on the fabrication of variable scaffolds for the replication of architectural and mechanical properties of the graded tissue. Nanofibrous scaffolds have been widely used for tendon-to-bone regeneration as these biomaterials act as a physical platform mimicking 3D fibrous collagenous hierarchical structure [51, 52]. In contrast, 3D printing and hydrogels have been used for mimicking the physical properties of the osteochondral unit as this combination demonstrates good physical and mechanical performance [14, 53].

The development of injectable hydrogel systems with control over the architecture of the fibrillar network has also been demonstrated to have biological relevance [54]. These hydrogels have a controllable and precise internal fibrous structure, which determines their pore size and mechanical properties while replicating the filamentous architecture of the ECM. Moreover, hydrogels can also be tuned to present an anisotropic architecture, for instance taking advantage of magnetic stimulation to nanoparticle alignment [55]. Strikingly, these hydrogels provide biochemical and physical cues enabling to tune the behavior of encapsulated stem cells, with prospective applications in minimally invasive defect filling surgeries.

Within every tissue and organ, cells sense the properties of their supporting environment at multiple length scales. Hence, new biomaterial designs must consider the role of mechanosensing. By generating methacrylated dextran fibrillar matrices resembling collagen type I networks, Baker and colleagues have demonstrated the role of fibrillar topography in directing cellular morphology, impacting cellular alignment and matrix remodeling by cellular traction forces [56]. Remarkably, cellular forces at the microscale, together with tissue-generated forces at the macroscale, are two essential parameters guiding numerous tissue differentiation and maturation during soft-to-hard tissue development [35]. In turn, cellular processes, including stem cell lineage specification, can be guided by contact with the surrounding physical microenvironment. Matrix stiffness as a stand-alone stimulus directing multilineage differentiation of bone marrow mesenchymal stem cells was first demonstrated in 2006; for instance, rigid matrices resembling collagenous bone triggered osteogenic differentiation [57]. Surface stiffness was shown to modulate stem cell adhesion, proliferation, and differentiation (Figure 1.3A). Indeed, MSCs tend to become more spread on

substrates with higher stiffness (ranging from 50 to 90 kPa) and differentiate toward chondrogenic- [37, 38] and osteogenic- lineages [38, 39] (Figure 1.3A, a-c), whereas softer surfaces (~30-50 kPa) result in a tenogenic-like phenotype [39, 40] (Figure 1.3A, C). These results support the creation of material stiffness gradients to guide stem cell differentiation along tendon-to-bone and bone-cartilage bioengineered constructs. Such gradients can be reproduced as a consequence of mineral content in nanofibrous systems, taking advantage of simple mineral coatings to increase nanofibrous stiffness to direct stem cells differentiation toward the osteogenic lineage [58].Comparably, hydrogel stiffness has been shown to have a role in modulating cell-based osteochondral formation in 3D, as soft hydrogels have been shown to support the deposition of neocartilage by cells due to their permissiveness [59] and stiffer hydrogels to support the deposition of osteogenic-like matrix [41]. Complementarily, micro/nanostructured surface architectures have been developed as an easy and smart strategy to induce bi-lineage differentiation in single scaffolds (Figure 1.3B). Interestingly, tailoring the surface topography of scaffolds by increasing either the roughness or the use of nano-scaled matrices has shown to allow a better cell adhesion to the matrix, followed by subsequent tenogenic, osteogenic and chondrogenic commitment of stem cells when in contact with oriented groove materials or just by creating dense or fibrous topologies in scaffolds, respectively [20, 45, 60-63].

In this sense, it is worth mentioning that phenotypic alterations induced by biophysical sensing have been shown to have a dose-dependent response and to be cell-type-specific and context dependent [64]. It has been recognized for long that material properties (e.g., matrix stiffness, topography) can sensitize cells to other microenvironmental features, impacting cell response [65-68]. Notwithstanding, recent studies using ribonucleic acid (RNA) sequencing and differential expression analyses have demonstrated that one specific parameter has the power to contextualize the response to other features, through a dose-dependent effect [64, 68]. Besides this context-dependence of coupling biophysical cues, the type of cell also determines the downstream response and the way the biophysical sensing happens. Indeed, the ability of cells to cluster adhesion ligands in response to a specific material parameter has been demonstrated to occur in a cell-type-specific manner and to be dependent on cellular intrinsic characteristics (lineage, species) [64].

These findings raise several questions particularly concerning the interplay of downstream cell regulatory networks in response to specific combinations of biophysical features. Hence, challenges emerge regarding the establishment of adequate gradient biomaterials for interfacial

tissue engineering. Other challenges include the impact on selection of cell sources and cell history for developing adequate tissue mimetics. Biophysical gradients are expected to guide the behavior of different cells types, which will, in turn, establish a cross-communication and influence each other, resulting in a highly complex system.

1.2.2.2. *The role of mechanotransduction*

Since the function of musculoskeletal interfaces is to bear and transmit loads between mechanically different tissues, it is not a surprise that mechanical loading contributes to the development and function (and even pathology onset) of such multi-tissue interfaces, contributing to a gradation in tissue cellularity and structure. During the last years, growing evidences have demonstrated that cells sense the mechanical forces in different ways, transducing these mechanosignals into gene regulation that will impact not only cell migration or ECM adhesion but also proliferation and differentiation [69]. Therefore, understanding cellular responses upon stimulation by mechanical inputs from the surrounding environment may provide key information for manipulating cellular behaviors toward pro-regenerative phenotypes.

Active loading has been used *in vivo* to guide tissue formation upon construct implantation, but issues remain regarding the lack of control over mechanical loading regimes. Alternatively, effects of mechanical stresses have been increasingly explored *in vitro* using dynamic systems as bioreactors. The potential regeneration of tendon/ligament-bone has been evaluated mainly through the use of cyclic tension, whereas bone-cartilage regeneration has been relying on the use of compressive stress. For instance, a dynamic compression bioreactor was used in a semi-confined compression model to direct MSC differentiation throughout the depth of a hydrogel to resemble the spatial endochondral progression [70]. The application of dynamic compression increased strains across the top of the construct while the confinement reduced oxygen levels (see section 'Biochemical tools') at the bottom of the construct, resulting in increased glycosaminoglycan accumulation in the bottom, increased collagen accumulation in the top along with a suppression of hypertrophy and calcification throughout the construct [70]. In contrast, mechanical and biological properties of an engineered tendon-to-bone composite have been investigated after culturing bone marrow-derived MSCs sheets under cyclic tension for 7 days [71]. Mechanical tension led to increased cell migration and aligned distribution of cells within the scaffold, resulting in the upregulation of tenogenic genes as scleraxis [71].

While there are some challenges to overcome in engineering a native-like soft-to-hard tissue interface, and whether bioreactors systems will be ultimately used for tissue maturation for the clinics remains an open question. However, these systems present an advantage over current *in vitro* systems as they allow fine control over mechanical cues, improving both local cell modulation and ultimately, tissue regeneration after implantation.

1.2.3. BIOCHEMICAL TOOLS

Supplementation of cell cultures using biomolecules has been explored to maintain the phenotype of permanently differentiated cells or to modulate stem cell fate and induce differentiation. Among different biochemical factors, oxygen is a crucial molecule and we will discuss the influence of oxygen tension on cellular behavior. Additionally, small molecules, like ascorbic acid, can be employed to accelerate ECM deposition, particularly for cell sheet engineering [72-75], or to promote cellular proliferation in cell expansion protocols (e.g, glucose and essential aminoacids). Other signals include hormones, growth factors and cytokines. Although high-throughput analysis of combinatorial approaches has been troublesome, the use of such biochemical cues has been at the forefront of cell- and material-based therapies development and is herein addressed.

1.2.3.1. *Oxygen tension and hypoxic niches*

In the human body, normal physiological conditions of oxygen tension fall between 2-9% in most organs and between 10-13% in arteries, lungs and liver [76]. The musculoskeletal system is a good example of where hypoxia plays an important role during tissue development and homeostasis. Soft-to-hard tissue interfaces present a gradual transition in vascularity and, consequently, in oxygen concentrations. Given the physiology of the native tissues, tendon cells are known to maintain their phenotype *in vitro* under hypoxic conditions, as the ones observed in the native hypovascular tendon niche (<5% oxygen tension (O_2)) [76, 77]. Contrarily, hypoxia has been shown to profoundly inhibit osteoclastogenesis in bone remodeling [78] given that bone physiological oxygen tension remains above 5% [79].

Nonetheless, the beneficial effect of hypoxia has been demonstrated using differently sized engineered endochondral cartilage intermediates prior to implantation, where hypoxia activation resulted in improved bone formation and enhanced chondrogenesis without the formation of fibrotic tissue [42]. Moreover, several studies have demonstrated the role of oxygen in directing both cartilage and bone integration whereby hypoxic conditions (2.5% O_2) have been shown to

suppress hypertrophy and endochondral ossification within chondrogenically primed MSCs [80]. Tissue engineering strategies have been addressing the effects of cell conditioning under hypoxic culture. Indeed, pre-conditioning (5% O_2) a 3D bioprinted stratified construct carrying ASCs reduced uncontrolled differentiation by inhibiting spontaneous calcification and promoted interface integration *in vivo* [81]. Nonetheless, recreating hypoxic niches through culture conditions limits the maintenance of this biomimetic feature to *in vitro* settings. Strikingly, a minute control over physical features of produced scaffolds has been shown to have an impact on oxygen supply. For example, through variations in pore size (higher to smaller), oxygen diffusion will decrease, resulting in the recreation of a gradient of hypoxic environments within a single structure. This enables a control over stem cell differentiation toward osteogenic- and chondrogenic lineages [31].

The role of oxygen tension is frequently disregarded in tissue engineering strategies, but it has been increasingly recognized as a critical biochemical parameter to address in soft-to-hard tissue interface regeneration. Novel approaches deploying a control over oxygen gradients are likely to provide strategic management of multi-differentiation of a single stem cell source.

1.2.3.2. *Growth factors and biofunctionalization strategies*

Musculoskeletal interface tissue repair relies on the use of growth factors to elicit a desired phenotypic response from a host tissue or when co-delivered with cells, through localized and controlled multifunctional delivery systems. Interestingly, growth factors involved in growth plate development have been elucidated as possible targets for both tendon-to-bone and osteochondral tissue regeneration, particularly bone morphogenetic proteins and transforming growth factor beta superfamily [82-84].

Biofunctionalization of biomaterial surfaces have demonstrated good results toward the induction of different phenotypes in single structures. Multifunctional gradients using controllable and reversed click reactions [85] or polymerization of dopamine [45, 46] have been explored for tendon-bone interface regeneration. Resulting available groups provide accessibility for biomolecule immobilization and biomineralization [46], allowing a gradual differentiation of stem cells (Figure 1.3C). Comparably, strategies aiming at the delivery of growth factors for osteochondral unit regeneration have focused on bulk phase delivery where the release of bioactive factors is dependent on the interaction between the growth factor and the matrix, either by tethering/immobilization [44] or encapsulation [14] resulting in the chondrogenic and osteogenic differentiation of stem cells in single units. In this regard, gradients of growth factors and the rate

of release have been demonstrated to affect tissue formation. Even though the immobilization of growth factors has shown satisfactory results in *in vitro* applications, this strategy faces some challenges *in vivo*, such as ion exchange with physiological fluids. Therefore, the undefined and negative cross-effects in *in vivo* defect studies suggest that these methodologies still require a fine-tuning. Effectively, it is well acknowledged the need for an "ideal" spatial and temporal delivery of growth factors in order to potentiate their highest therapeutic efficacy in future tissue engineered approaches.

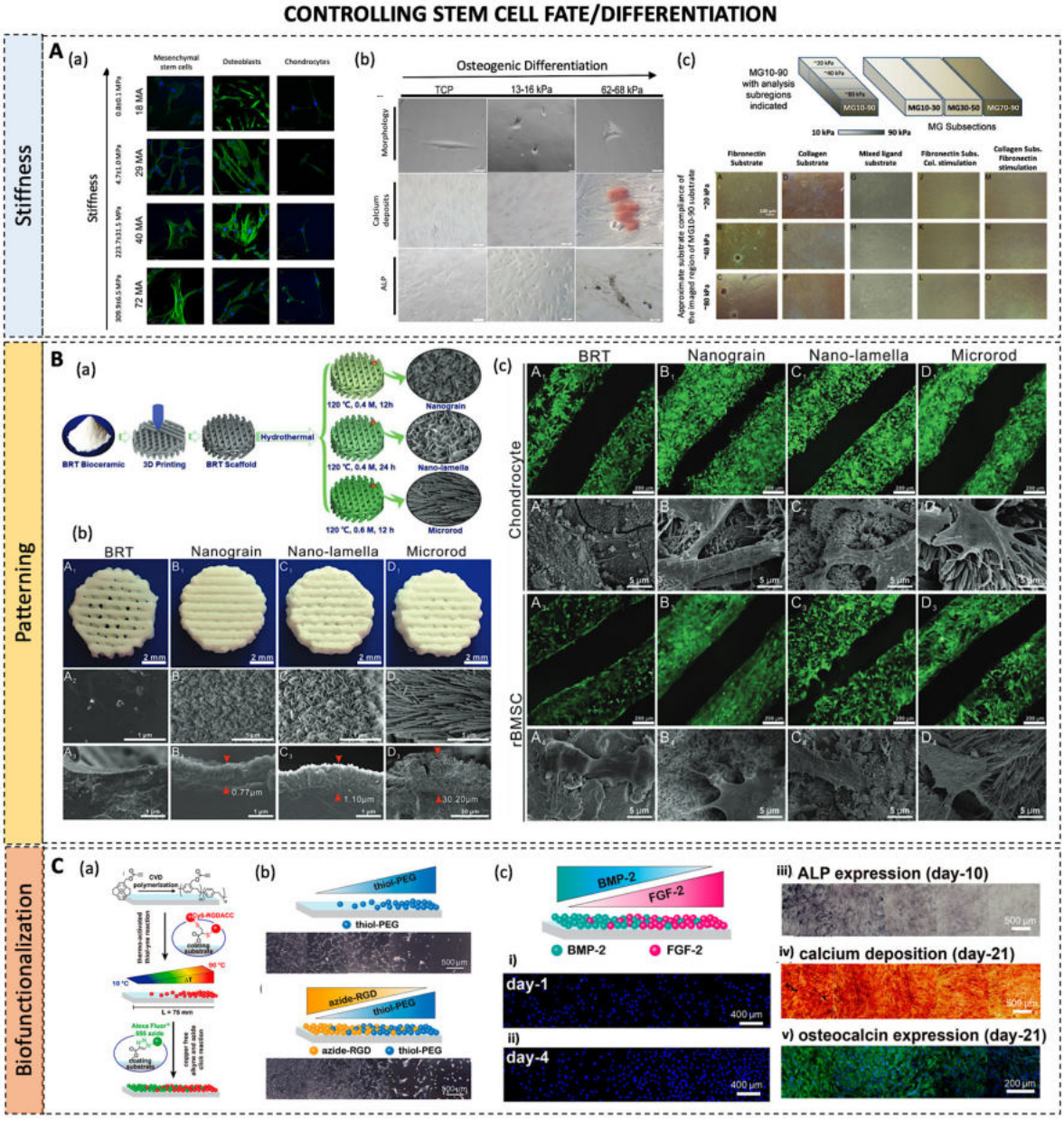

Figure 1.3 | Examples of biophysical cues to control stem cell fate for tendon-to-bone and osteochondral tissue engineering and regeneration. As elastic modulus and

toughness vary between distinct tissues such as cartilage, tendon/ligament and bone, a variation between stiffer and softer surfaces has been proven to control stem cell differentiation (A). The stiffness of different methyl acrylate/methyl methacrylate (MA/MMA) polymer surfaces without major changes in surface chemistry were used to evaluate human MSC commitment toward osteoblastic (OB) and chondrogenic (CHON) lineages. Simply by increasing surface stiffness, the tunability of the cytoskeletal structural organization was demonstrated (a). Round OBs were found in stiffer substrates (>10MPa), CHON presented a similar morphology with long extensions and few points of contact and MSCs presented longer cytoskeletal arrangements in less stiff surfaces (<10 MPa). Reproduced with permission from [39]. The same effect was demonstrated by assessing MSCs response to tunable polyacrylamide hydrogels coated with fibronectin with increasing stiffness. After 1-week, cells seeded in stiffer substrates (62-68 kPa) were found to produce calcium nodules (Alizarin Red-positive) and express more alkaline phosphatase (ALP-stained crystals), even compared to substrates such as tissue culture plastic (TCP) (b). Reproduced with permission from [39]. Materials stiffness can also influence tendon differentiation. Polyacrylamide hydrogels with a mechanical gradient comprising a moderately rigid collagen type I substrate (~30–50 kPa) were found to induce MSC differentiation into the tenogenic lineage, while MSCs differentiate into osteogenic cells on more rigid substrates (70–90 kPa) (c). Reproduced with permission from [40]. (B) Surface patterning of 3D scaffolds with different morphological micro/nanostructured surfaces has demonstrated potential use for cartilage and subchondral bone application (a). Pure bredigite, a bioactive composite made of silica, magnesium and calcium, with good bioactivity, biodegradability and mechanical properties, was used to produce the 3D scaffolds. Structured surfaces distinctly facilitated the spread and differentiation of chondrocytes, regulated cell morphology, and promoted osteogenic differentiation of rat BMSCs (b-c). Reproduced with permission from [62]. (C) Surface modification by dual reverse click reactions producing a continuous and gradient biofunctionalization to control stem cell differentiation for tendon-to-bone regeneration. (a) Seeding with 3T3 fibroblasts on surfaces containing (a) only polyethylene glycol (PEG) immobilized to the first gradient and (b) two gradients of PEG and arginyl glycyl aspartic acid (RGD) contrary gradients, demonstrated a cell-dependent behavior for PEG. After 21 days with adipose ASCs in functionalized surfaces with BMP2 and FGF-2, it was observed a gradient of (iii) ALP expression (iv) calcium deposition and (v) osteocalcin expression, showing the osteogenic commitment of hASCs in a continuous and gradient manner. Reproduced with permission from [85].

1.3. CONCLUDING REMARKS AND FUTURE PERSPECTIVES

Soft-to-hard tissue interfaces have primary mechanical roles. Thus, tissue engineering dedicates a considerable effort toward recapitulating these structures through biomaterial design. Nonetheless, the characteristic complexity of interfacial tissues requires integrative tissue engineering approaches that combine a set of tools – biological, biophysical and biochemical – toward guiding native or transplanted cells.

Over the years, advances in biotechnological tools have refined TERM strategies. The development of adequate constructs for soft-to-hard tissue interface regeneration is challenged by limited knowledge of the biology of these multi-tissue transitions.

Taking advantage of the body's self-healing ability, advanced cell therapies have been increasingly explored. Cell injections rely on taking cells out of their 'comfort zone' and leaving them to face a very harsh environment that is the injury site, leading to cell loss and poor cell engraftment. Although with disadvantages associated with *in vitro* cellular expansion and extensive manipulation, advanced cell therapies, either based on scaffold-free cell delivery technologies or on cellular actuation through mechanical/magnetic forces, hold potential to change the clinical landscape. Indeed, biotechnological advances enable the generation of regeneration competent cellular phenotypes and tissue-specific living patches aiming at shifting the pro-fibrotic healing toward a pro-regenerative environment, which is of particular importance in the case of non-healing and chronic injuries.

Furthermore, the combination of cell therapies with a support matrix is undoubtedly important, but the reduced size of soft-to-hard tissue insertions also defies the design of gradient biomaterials. Alternative biomaterial designs may focus on aligned-random fibrous scaffolds assembled through textile techniques to guide different cellular phenotypes within the two distinct regions and rely on the cellular crosstalk to recreate an interfacial phenotype when the two cell types merge. Although particularly unpredictable, evidences have been supporting the role of cellular communication in recreating tissue-specific zones. However, future research could focus on improving the resolution of material processing techniques to achieve better spatial control over physical and biochemical properties and, consequently, cell fate determination.

High-throughput screening technologies have elucidated cellular responses to changes in biophysical and biochemical properties, both at the single cell level and on long-range cell behaviors. Combining these transcriptomics and proteomics insights with high-resolution

fabrication techniques may help to develop more physiologically representative tissue engineered products.

An important aspect of future advanced tissue engineering therapies for soft-to-hard interface regeneration is the establishment of adequate regimes of mechanical stimulation to promote pro-regenerative cellular responses. For instance, walking steps stimulate soft-to-hard musculoskeletal systems at 1.5 hertz (Hz) frequency, under 30.6 $Kg/m^{2.}$ according to the averaged walking speed and body mass index. To replicate this scenario, dynamic cell culture systems, as bioreactors, have been refined. However, a spatial control over vascularization and innervation in distinct but integrated microtissues is still a main challenge in the field, due to a lack of simultaneous control over biochemical (e.g., growth factors and oxygen tension) and mechanical cues. This way already reported mechanical and biochemical stimulating bioreactors should be combined in a single concept as a way to stimulate distinct microenvironments allowing a biomimetic regenerative response in soft-hard interfaced tissues.

1.4. REFERENCES

[1] S.R. Goldring, M.B. Goldring, Changes in the osteochondral unit during osteoarthritis: structure, function and cartilage–bone crosstalk, Nature Reviews Rheumatology 12 (2016) 632, 10.1038/nrrheum.2016.148.

[2] L. Rossetti, L.A. Kuntz, E. Kunold, J. Schock, K.W. Müller, H. Grabmayr, J. Stolberg-Stolberg, F. Pfeiffer, S.A. Sieber, R. Burgkart, A.R. Bausch, The microstructure and micromechanics of the tendon–bone insertion, Nature Materials 16 (2017) 664, 10.1038/nmat4863

[3] A.M. Briggs, M.J. Cross, D.G. Hoy, L. Sànchez-Riera, F.M. Blyth, A.D. Woolf, L. March, Musculoskeletal Health Conditions Represent a Global Threat to Healthy Aging: A Report for the 2015 World Health Organization World Report on Ageing and Health, The Gerontologist 56(Suppl_2) (2016) S243-S255, 10.1093/geront/gnw002.

[4] S.N. Sambandam, V. Khanna, A. Gul, V. Mounasamy, Rotator cuff tears: An evidence based approach, World J Orthop 6(11) (2015) 902-918, 10.5312/wjo.v6.i11.902.

[5] J. Chen, J. Xu, A. Wang, M. Zheng, Scaffolds for tendon and ligament repair:
review of the efficacy of
commercial products, Expert Rev Med Devices 6 (2009) 61-73, 10.1586/17434440.6.1.61.

[6] D. Bicho, S. Pina, R.L. Reis, J.M. Oliveira, Commercial Products for Osteochondral Tissue Repair and Regeneration, Adv Exp Med Biol 1058 (2018) 415-428, 10.1007/978-3-319-76711-6_19.

[7] Y. Li, Y. Xiao, C. Liu, The Horizon of Materiobiology: A Perspective on Material-Guided Cell Behaviors and Tissue Engineering, Chemical reviews 117 5 (2017) 4376-4421,

[8] E.B. Hunziker, T.M. Quinn, H.J. Häuselmann, Quantitative structural organization of normal adult human articular cartilage, Osteoarthritis and Cartilage 10(7) (2002) 564-572, 10.1053/joca.2002.0814.

[9] J. Rieppo, M.M. Hyttinen, E. Halmesmaki, H. Ruotsalainen, A. Vasara, I. Kiviranta, J.S. Jurvelin, H.J. Helminen, Changes in spatial collagen content and collagen network architecture in porcine articular cartilage during growth and maturation, Osteoarthritis and Cartilage 17(4) (2009) 448-455, 10.1016/j.joca.2008.09.004.

[10] B. Soo Kim, E. Ji Kim, J. Suk Choi, J. Hoon Jeong, C. Hyunchul Jo, Y. Woo Cho, Human collagen-based multilayer scaffolds for tendon-to-bone interface tissue engineering, Journal of Biomedical Materials Research Part A 102(11) (2014) 4044-4054, 10.1002/jbm.a.35057.

[11] G.X. Huang, P.R. Arany, D.J. Mooney, Modeling and Validation of Multilayer Poly(Lactide-Co-Glycolide) Scaffolds for In Vitro Directed Differentiation of Juxtaposed Cartilage and Bone, Tissue Engineering Part A 21(15-16) (2015) 2228-2240, 10.1089/ten.tea.2015.0089.

[12] S.K.M. Perikamana, J. Lee, T. Ahmad, E.M. Kim, H. Byun, S. Lee, H. Shin, Harnessing biochemical and structural cues for tenogenic differentiation of adipose derived stem cells (ADSCs) and development of an in vitro tissue interface mimicking tendon-bone insertion graft, Biomaterials 165 (2018) 79-93, 10.1016/j.biomaterials.2018.02.046.

[13] S.F. Tellado, S. Chiera, W. Bonani, P.S.P. Poh, C. Migliaresi, A. Motta, E.R. Balmayor, M. van Griensven, Heparin functionalization increases retention of TGF-β2 and GDF5 on biphasic silk fibroin scaffolds for tendon/ligament-to-bone tissue engineering, Acta Biomaterialia 72 (2018) 150-166, 10.1016/j.actbio.2018.03.017.

[14] F. Gao, Z. Xu, Q. Liang, B. Liu, H. Li, Y. Wu, Y. Zhang, Z. Lin, M. Wu, C. Ruan, W. Liu, Direct 3D Printing of High Strength Biohybrid Gradient Hydrogel Scaffolds for Efficient Repair of Osteochondral Defect, Advanced Functional Materials 28(13) (2018) 1706644, 10.1002/adfm.201706644.

[15] T.J. Levingstone, E. Thompson, A. Matsiko, A. Schepens, J.P. Gleeson, F.J. O'Brien, Multi-layered collagen-based scaffolds for osteochondral defect repair in rabbits, Acta Biomater 32 (2016) 149-160, 10.1016/j.actbio.2015.12.034.

[16] J. Chen, H. Chen, P. Li, H. Diao, S. Zhu, L. Dong, R. Wang, T. Guo, J. Zhao, J. Zhang, Simultaneous regeneration of articular cartilage and subchondral bone in vivo using MSCs induced

by a spatially controlled gene delivery system in bilayered integrated scaffolds, Biomaterials 32(21) (2011) 4793-4805, 10.1016/j.biomaterials.2011.03.041.

[17] V. Bunpetch, X. Zhang, T. Li, J. Lin, E.P. Maswikiti, Y. Wu, D. Cai, J. Li, S. Zhang, C. Wu, H. Ouyang, Silicate-based bioceramic scaffolds for dual-lineage regeneration of osteochondral defect, Biomaterials 192 (2019) 323-333, 10.1016/j.biomaterials.2018.11.025.

[18] Y. Zhu, L. Kong, F. Farhadi, W. Xia, J. Chang, Y. He, H. Li, An injectable continuous stratified structurally and functionally biomimetic construct for enhancing osteochondral regeneration, Biomaterials 192 (2019) 149-158, 10.1016/j.biomaterials.2018.11.017.

[19] R.F. Canadas, T. Ren, A.P. Marques, J.M. Oliveira, R.L. Reis, U. Demirci, Biochemical Gradients to Generate 3D Heterotypic-Like Tissues with Isotropic and Anisotropic Architectures, Advanced Functional Materials 28(48) (2018) 10.1002/adfm.201804148.

[20] J. Radhakrishnan, A. Manigandan, P. Chinnaswamy, A. Subramanian, S. Sethuraman, Gradient nano-engineered in situ forming composite hydrogel for osteochondral regeneration, Biomaterials 162 (2018) 82-98, 10.1016/j.biomaterials.2018.01.056.

[21] C. Loebel, J.A. Burdick, Engineering Stem and Stromal Cell Therapies for Musculoskeletal Tissue Repair, Cell Stem Cell 22(3) (2018) 325-339, 10.1016/j.stem.2018.01.014.

[22] M. Yamato, T. Okano, Cell sheet engineering, Materials Today 7(5) (2004) 42-47, 10.1016/S1369-7021(04)00234-2.

[23] G. Ebihara, M. Sato, M. Yamato, G. Mitani, T. Kutsuna, T. Nagai, S. Ito, T. Ukai, M. Kobayashi, M. Kokubo, T. Okano, J. Mochida, Cartilage repair in transplanted scaffold-free chondrocyte sheets using a minipig model, Biomaterials 33(15) (2012) 3846-51, 10.1016/j.biomaterials.2012.01.056.

[24] S. Ito, M. Sato, M. Yamato, G. Mitani, T. Kutsuna, T. Nagai, T. Ukai, M. Kobayashi, M. Kokubo, T. Okano, J. Mochida, Repair of articular cartilage defect with layered chondrocyte sheets and cultured synovial cells, Biomaterials 33(21) (2012) 5278-86, 10.1016/j.biomaterials.2012.03.073.

[25] F. Wang, Y. Hu, D. He, G. Zhou, E. Ellis, 3rd, Scaffold-free cartilage cell sheet combined with bone-phase BMSCs-scaffold regenerate osteochondral construct in mini-pig model, Am J Transl Res 10(10) (2018) 2997-3010,

[26] C. Zhang, E. Zhang, L. Yang, W. Tu, J. Lin, C. Yuan, V. Bunpetch, X. Chen, H. Ouyang, Histone deacetylase inhibitor treated cell sheet from mouse tendon stem/progenitor cells promotes tendon repair, Biomaterials 172 (2018) 66-82, 10.1016/j.biomaterials.2018.03.043.

[27] Q. Liu, Y. Yu, R.L. Reisdorf, J. Qi, C.-K. Lu, L.J. Berglund, P.C. Amadio, S.L. Moran, S.P. Steinmann, K.-N. An, A. Gingery, C. Zhao, Engineered tendon-fibrocartilage-bone composite and bone marrow-derived mesenchymal stem cell sheet augmentation promotes rotator cuff healing in a non-weight-bearing canine model, Biomaterials 192 (2019) 189-198, 10.1016/j.biomaterials.2018.10.037.

[28] H. Takahashi, M. Nakayama, T. Shimizu, M. Yamato, T. Okano, Anisotropic cell sheets for constructing three-dimensional tissue with well-organized cell orientation, Biomaterials 32(34) (2011) 8830-8838, 10.1016/j.biomaterials.2011.08.006.

[29] C. Liu, Y. Zhou, M. Sun, Q. Li, L. Dong, L. Ma, K. Cheng, W. Weng, M. Yu, H. Wang, Light-Induced Cell Alignment and Harvest for Anisotropic Cell Sheet Technology, ACS Applied Materials & Interfaces 9(42) (2017) 36513-36524, 10.1021/acsami.7b07202.

[30] A.I. Gonçalves, M.T. Rodrigues, M.E. Gomes, Tissue-engineered magnetic cell sheet patches for advanced strategies in tendon regeneration, Acta Biomaterialia 63 (2017) 110-122, 10.1016/j.actbio.2017.09.014.

[31] A. Di Luca, I. Lorenzo-Moldero, C. Mota, A. Lepedda, D. Auhl, C. Van Blitterswijk, L. Moroni, Tuning Cell Differentiation into a 3D Scaffold Presenting a Pore Shape Gradient for Osteochondral Regeneration, Adv Healthc Mater 5(14) (2016) 1753-63, 10.1002/adhm.201600083.

[32] K.M. Park, S. Gerecht, Hypoxia-inducible hydrogels, Nature Communications 5 (2014) 4075, 10.1038/ncomms5075.

[33] K.M. Ferlin, M.E. Prendergast, M.L. Miller, D.S. Kaplan, J.P. Fisher, Influence of 3D printed porous architecture on mesenchymal stem cell enrichment and differentiation, Acta Biomaterialia 32 (2016) 161-169, 10.1016/j.actbio.2016.01.007.

[34] O.F. Zouani, C. Chanseau, B. Brouillaud, R. Bareille, F. Deliane, M.-P. Foulc, A. Mehdi, M.-C. Durrieu, Altered nanofeature size dictates stem cell differentiation, Journal of Cell Science 125(5) (2012) 1217, 10.1242/jcs.093229.

[35] N. Felsenthal, E. Zelzer, Mechanical regulation of musculoskeletal system development, Development 144(23) (2017) 4271-4283, 10.1242/dev.151266.

[36] M. Sun, G. Chi, J. Xu, Y. Tan, J. Xu, S. Lv, Z. Xu, Y. Xia, L. Li, Y. Li, Extracellular matrix stiffness controls osteogenic differentiation of mesenchymal stem cells mediated by integrin alpha5, Stem Cell Res Ther 9(1) (2018) 52, 10.1186/s13287-018-0798-0.

[37] Y. Wu, Z. Yang, J.B. Law, A.Y. He, A.A. Abbas, V. Denslin, T. Kamarul, J.H. Hui, E.H. Lee, The Combined Effect of Substrate Stiffness and Surface Topography on Chondrogenic Differentiation

of Mesenchymal Stem Cells, Tissue Eng Part A 23(1-2) (2017) 43-54, 10.1089/ten.TEA.2016.0123.

[38] R. Olivares-Navarrete, E.M. Lee, K. Smith, S.L. Hyzy, M. Doroudi, J.K. Williams, K. Gall, B.D. Boyan, Z. Schwartz, Substrate Stiffness Controls Osteoblastic and Chondrocytic Differentiation of Mesenchymal Stem Cells without Exogenous Stimuli, PLoS One 12(1) (2017) e0170312, 10.1371/journal.pone.0170312.

[39] R.I. Sharma, J.G. Snedeker, Biochemical and biomechanical gradients for directed bone marrow stromal cell differentiation toward tendon and bone, Biomaterials 31(30) (2010) 7695-704, 10.1016/j.biomaterials.2010.06.046.

[40] R.I. Sharma, J.G. Snedeker, Paracrine interactions between mesenchymal stem cells affect substrate driven differentiation toward tendon and bone phenotypes, PloS one 7(2) (2012) e31504-e31504, 10.1371/journal.pone.0031504.

[41] T. Wang, J.H. Lai, F. Yang, Effects of Hydrogel Stiffness and Extracellular Compositions on Modulating Cartilage Regeneration by Mixed Populations of Stem Cells and Chondrocytes In Vivo, Tissue engineering. Part A 22(23-24) (2016) 1348-1356, 10.1089/ten.TEA.2016.0306.

[42] P.J. Stiers, S. Stegen, N. van Gastel, R. Van Looveren, S. Torrekens, G. Carmeliet, Inhibition of the Oxygen Sensor PHD2 Enhances Tissue-Engineered Endochondral Bone Formation, J Bone Miner Res 10.1002/jbmr.3599 (2018) 10.1002/jbmr.3599.

[43] A.L. Farris, A.N. Rindone, W.L. Grayson, Oxygen Delivering Biomaterials for Tissue Engineering, Journal of materials chemistry. B 4(20) (2016) 3422-3432, 10.1039/C5TB02635K.

[44] C. Stüdle, Q. Vallmajó-Martín, A. Haumer, J. Guerrero, M. Centola, A. Mehrkens, D.J. Schaefer, M. Ehrbar, A. Barbero, I. Martin, Spatially confined induction of endochondral ossification by functionalized hydrogels for ectopic engineering of osteochondral tissues, Biomaterials 171 (2018) 219-229, 10.1016/j.biomaterials.2018.04.025.

[45] S.K.M. Perikamana, Y.M. Shin, J.K. Lee, Y.B. Lee, Y. Heo, T. Ahmad, S.Y. Park, J. Shin, K.M. Park, H.S. Jung, S.W. Cho, H. Shin, Graded functionalization of biomaterial surfaces using mussel-inspired adhesive coating of polydopamine, Colloids Surf B Biointerfaces 159 (2017) 546-556, 10.1016/j.colsurfb.2017.08.022.

[46] S.K.M. Perikamana, J.K. Lee, Y.M. Shin, T. Ahmad, S.-j. Kim, K.M. Park, H. Shin, Oxygen-dependent generation of a graded polydopamine coating on nanofibrous materials for controlling stem cell functions, Journal of Materials Chemistry B 5(44) (2017) 8865-8878, 10.1039/c7tb00995j.

[47] J.-M. Lee, G.-I. Im, SOX trio-co-transduced adipose stem cells in fibrin gel to enhance cartilage repair and delay the progression of osteoarthritis in the rat, Biomaterials 33(7) (2012) 2016-2024, 10.1016/j.biomaterials.2011.11.050.

[48] C.J. Needham, S.R. Shah, R.L. Dahlin, L.A. Kinard, J. Lam, B.M. Watson, S. Lu, F.K. Kasper, A.G. Mikos, Osteochondral tissue regeneration through polymeric delivery of DNA encoding for the SOX trio and RUNX2, Acta Biomaterialia 10(10) (2014) 4103-4112, 10.1016/j.actbio.2014.05.011.

[49] C. An, Y. Cheng, Q. Yuan, J. Li, IGF-1 and BMP-2 induces differentiation of adipose-derived mesenchymal stem cells into chondrocytes-like cells, Ann Biomed Eng 38(4) (2010) 1647-54, 10.1007/s10439-009-9892-x.

[50] M. Cucchiarini, M. Ekici, S. Schetting, D. Kohn, H. Madry, Metabolic Activities and Chondrogenic Differentiation of Human Mesenchymal Stem Cells Following Recombinant Adeno-Associated Virus–Mediated Gene Transfer and Overexpression of Fibroblast Growth Factor 2, Tissue Engineering Part A 17(15-16) (2011) 1921-1933, 10.1089/ten.tea.2011.0018.

[51] S. Sant, D.F. Coutinho, A.K. Gaharwar, N.M. Neves, R.L. Reis, M.E. Gomes, A. Khademhosseini, Self-Assembled Hydrogel Fiber Bundles from Oppositely Charged Polyelectrolytes Mimic Micro-/Nanoscale Hierarchy of Collagen, Advanced Functional Materials 27(36) (2017) 1606273, 10.1002/adfm.201606273.

[52] I. Calejo, R. Costa-Almeida, R.L. Reis, M.E. Gomes, A textile platform using continuous aligned and textured composite microfibers to engineer tendon, Advanced Healthcare Materials 10.1002/adhm.201900200 (2019) 10.1002/adhm.201900200.

[53] L. Li, J. Li, J. Guo, H. Zhang, X. Zhang, C. Yin, L. Wang, Y. Zhu, Q. Yao, 3D Molecularly Functionalized Cell-Free Biomimetic Scaffolds for Osteochondral Regeneration, Advanced Functional Materials 29(6) (2019) 1807356, 10.1002/adfm.201807356.

[54] B.B. Mendes, M. Gómez-Florit, R.A. Pires, R.M.A. Domingues, R.L. Reis, M.E. Gomes, Human-based fibrillar nanocomposite hydrogels as bioinstructive matrices to tune stem cell behavior, Nanoscale 10(36) (2018) 17388-17401, 10.1039/C8NR04273J.

[55] S. Araújo-Custódio, M. Gomez-Florit, A.R. Tomás, B.B. Mendes, P.S. Babo, S.M. Mithieux, A. Weiss, R.M.A. Domingues, R.L. Reis, M.E. Gomes, Injectable and Magnetic Responsive Hydrogels with Bioinspired Ordered Structures, ACS Biomaterials Science & Engineering 5(3) (2019) 1392-1404, 10.1021/acsbiomaterials.8b01179.

[56] B.M. Baker, B. Trappmann, W.Y. Wang, M.S. Sakar, I.L. Kim, V.B. Shenoy, J.A. Burdick, C.S. Chen, Cell-mediated fibre recruitment drives extracellular matrix mechanosensing in engineered fibrillar microenvironments, Nature Materials 14(12) (2015) 1262-1268, 10.1038/nmat4444.

[57] A.J. Engler, S. Sen, H.L. Sweeney, D.E. Discher, Matrix elasticity directs stem cell lineage specification, Cell 126(4) (2006) 677-89, 10.1016/j.cell.2006.06.044.

[58] W. Liu, J. Lipner, J. Xie, C.N. Manning, S. Thomopoulos, Y. Xia, Nanofiber Scaffolds with Gradients in Mineral Content for Spatial Control of Osteogenesis, ACS Applied Materials & Interfaces 6(4) (2014) 2842-2849, 10.1021/am405418g.

[59] S.Q. Liu, Q. Tian, J.L. Hedrick, J.H. Po Hui, P.L. Rachel Ee, Y.Y. Yang, Biomimetic hydrogels for chondrogenic differentiation of human mesenchymal stem cells to neocartilage, Biomaterials 31(28) (2010) 7298-7307, 10.1016/j.biomaterials.2010.06.001.

[60] Y. Shi, K. Zhou, W. Zhang, Z. Zhang, G. Zhou, Y. Cao, W. Liu, Microgrooved topographical surface directs tenogenic lineage specific differentiation of mouse tendon derived stem cells, Biomedical Materials 12(1) (2017) 10.1088/1748-605x/12/1/015013.

[61] C. Mahapatra, J.-J. Kim, J.-H. Lee, G.-Z. Jin, J.C. Knowles, H.-W. Kim, Differential chondro- and osteo-stimulation in three-dimensional porous scaffolds with different topological surfaces provides a design strategy for biphasic osteochondral engineering, Journal of Tissue Engineering 10 (2019) 2041731419826433, 10.1177/2041731419826433.

[62] C. Deng, R. Lin, M. Zhang, C. Qin, Q. Yao, L. Wang, J. Chang, C. Wu, Micro/Nanometer-Structured Scaffolds for Regeneration of Both Cartilage and Subchondral Bone, Advanced Functional Materials 29 (2019) 10.1002/adfm.201806068.

[63] J. Nowlin, M.A. Bismi, B. Delpech, P. Dumas, Y. Zhou, G.Z. Tan, Engineering the hard-soft tissue interface with random-to-aligned nanofiber scaffolds, Nanobiomedicine (Rij) 5 (2018) 1849543518803538, 10.1177/1849543518803538.

[64] M. Darnell, A. O'Neil, A. Mao, L. Gu, L.L. Rubin, D.J. Mooney, Material microenvironmental properties couple to induce distinct transcriptional programs in mammalian stem cells, Proceedings of the National Academy of Sciences 115(36) (2018) E8368, 10.1073/pnas.1802568115.

[65] M.J. Dalby, N. Gadegaard, R.O.C. Oreffo, Harnessing nanotopography and integrin–matrix interactions to influence stem cell fate, Nature Materials 13 (2014) 558, 10.1038/nmat3980.

[66] O. Chaudhuri, S.T. Koshy, C. Branco da Cunha, J.-W. Shin, C.S. Verbeke, K.H. Allison, D.J. Mooney, Extracellular matrix stiffness and composition jointly regulate the induction of malignant phenotypes in mammary epithelium, Nature Materials 13 (2014) 970, 10.1038/nmat4009.

[67] J.H. Wen, L.G. Vincent, A. Fuhrmann, Y.S. Choi, K.C. Hribar, H. Taylor-Weiner, S. Chen, A.J. Engler, Interplay of matrix stiffness and protein tethering in stem cell differentiation, Nature Materials 13 (2014) 979, 10.1038/nmat4051.

[68] M. Darnell, L. Gu, D. Mooney, RNA-seq reveals diverse effects of substrate stiffness on mesenchymal stem cells, Biomaterials 181 (2018) 182-188, 10.1016/j.biomaterials.2018.07.039.

[69] C. Yang, M.W. Tibbitt, L. Basta, K.S. Anseth, Mechanical memory and dosing influence stem cell fate, Nat Mater 13(6) (2014) 645-52, 10.1038/nmat3889.

[70] S.D. Thorpe, T. Nagel, S.F. Carroll, D.J. Kelly, Modulating gradients in regulatory signals within mesenchymal stem cell seeded hydrogels: a novel strategy to engineer zonal articular cartilage, PLoS One 8(4) (2013) e60764, 10.1371/journal.pone.0060764.

[71] Q. Liu, T. Hatta, J. Qi, H. Liu, A.R. Thoreson, P.C. Amadio, S.L. Moran, S.P. Steinmann, A. Gingery, C. Zhao, Novel engineered tendon-fibrocartilage-bone composite with cyclic tension for rotator cuff repair, J Tissue Eng Regen Med 12(7) (2018) 1690-1701, 10.1002/term.2696.

[72] M. Ni, Y.F. Rui, Q. Tan, Y. Liu, L.L. Xu, K.M. Chan, Y. Wang, G. Li, Engineered scaffold-free tendon tissue produced by tendon-derived stem cells, Biomaterials 34(8) (2013) 2024-37, 10.1016/j.biomaterials.2012.11.046.

[73] P.P. Lui, O.T. Wong, Y.W. Lee, Transplantation of tendon-derived stem cells pre-treated with connective tissue growth factor and ascorbic acid in vitro promoted better tendon repair in a patellar tendon window injury rat model, Cytotherapy 18(1) (2016) 99-112, 10.1016/j.jcyt.2015.10.005.

[74] C.F. Hsieh, Z. Yan, R.G. Schumann, S. Milz, C.G. Pfeifer, M. Schieker, D. Docheva, In Vitro Comparison of 2D-Cell Culture and 3D-Cell Sheets of Scleraxis-Programmed Bone Marrow Derived Mesenchymal Stem Cells to Primary Tendon Stem/Progenitor Cells for Tendon Repair, Int J Mol Sci 19(8) (2018) 10.3390/ijms19082272.

[75] R. Shimizu, N. Kamei, N. Adachi, M. Hamanishi, G. Kamei, E.E. Mahmoud, T. Nakano, T. Iwata, M. Yamato, T. Okano, M. Ochi, Repair mechanism of osteochondral defect promoted by bioengineered chondrocyte sheet, Tissue Eng Part A 21(5-6) (2015) 1131-41, 10.1089/ten.TEA.2014.0310.

[76] M.Y. Koh, G. Powis, Passing the baton: the HIF switch, Trends Biochem Sci 37(9) (2012) 364-72, 10.1016/j.tibs.2012.06.004.

[77] Y. Yu, L. Lin, Y. Zhou, X. Lu, X. Shao, C. Lin, K. Yu, X. Zhang, J. Hong, Y. Chen, Effect of Hypoxia on Self-Renewal Capacity and Differentiation in Human Tendon-Derived Stem Cells, Medical Science Monitor 23 (2017) 1334-1339, 10.12659/msm.903892.

[78] H. Kang, K. Yang, L. Xiao, L. Guo, C. Guo, Y. Yan, J. Qi, F. Wang, B. Ryffel, C. Li, L. Deng, Osteoblast Hypoxia-Inducible Factor-1alpha Pathway Activation Restrains Osteoclastogenesis via the Interleukin-33-MicroRNA-34a-Notch1 Pathway, Front Immunol 8 (2017) 1312, 10.3389/fimmu.2017.01312.

[79] M. Marenzana, T.R. Arnett, The Key Role of the Blood Supply to Bone, Bone research 1(3) (2013) 203-215, 10.4248/BR201303001.

[80] X. Huang, Y. Hou, L. Zhong, D. Huang, H. Qian, M. Karperien, W. Chen, Promoted Chondrogenesis of Cocultured Chondrocytes and Mesenchymal Stem Cells under Hypoxia Using In-situ Forming Degradable Hydrogel Scaffolds, Biomacromolecules 19(1) (2018) 94-102, 10.1021/acs.biomac.7b01271.

[81] Y. Wang, S. Wu, M.A. Kuss, P.N. Streubel, B. Duan, Effects of Hydroxyapatite and Hypoxia on Chondrogenesis and Hypertrophy in 3D Bioprinted ADMSC Laden Constructs, ACS Biomaterials Science & Engineering 3(5) (2017) 826-835, 10.1021/acsbiomaterials.7b00101.

[82] J. Liao, N. Hu, N. Zhou, L. Lin, C. Zhao, S. Yi, T. Fan, W. Bao, X. Liang, H. Chen, W. Xu, C. Chen, Q. Cheng, Y. Zeng, W. Si, Z. Yang, W. Huang, Sox9 Potentiates BMP2-Induced Chondrogenic Differentiation and Inhibits BMP2-Induced Osteogenic Differentiation, PLOS ONE 9(2) (2014) e89025, 10.1371/journal.pone.0089025.

[83] N. Zhou, Q. Li, X. Lin, N. Hu, J.-Y. Liao, L.-B. Lin, C. Zhao, Z.-M. Hu, X. Liang, W. Xu, H. Chen, W. Huang, BMP2 induces chondrogenic differentiation, osteogenic differentiation and endochondral ossification in stem cells, Cell and Tissue Research 366(1) (2016) 101-111, 10.1007/s00441-016-2403-0.

[84] L.F. Mendes, H. Katagiri, W.L. Tam, Y.C. Chai, L. Geris, S.J. Roberts, F.P. Luyten, Advancing osteochondral tissue engineering: bone morphogenetic protein, transforming growth factor, and fibroblast growth factor signaling drive ordered differentiation of periosteal cells resulting in stable cartilage and bone formation in vivo, Stem Cell Research & Therapy 9(1) (2018) 42, 10.1186/s13287-018-0787-3.

[85] Z.-Y. Guan, C.-Y. Wu, J.-T. Wu, C.-H. Tai, J. Yu, H.-Y. Chen, Multifunctional and Continuous Gradients of Biointerfaces Based on Dual Reverse Click Reactions, ACS Applied Materials & Interfaces 8(22) (2016) 13812-13818, 10.1021/acsami.6b03908.

[86] E.A. McNally, H.P. SChwarcz, G.A. Botton, A.L. Arsenault, A Model for the Ultrastructure of Bone Based on Electron Microscopy of Ion-Milled Sections, Plos One 7(1) (2012) 10.1371/journal.pone.0029258.

[87] H. Fujie, K. Imade, Effects of low tangential permeability in the superficial layer on the frictional property of articular cartilage, Biosurface and Biotribology 1(2) (2015) 124-129, 10.1016/j.bsbt.2015.06.001.

SUPPLEMENTARY INFORMATION

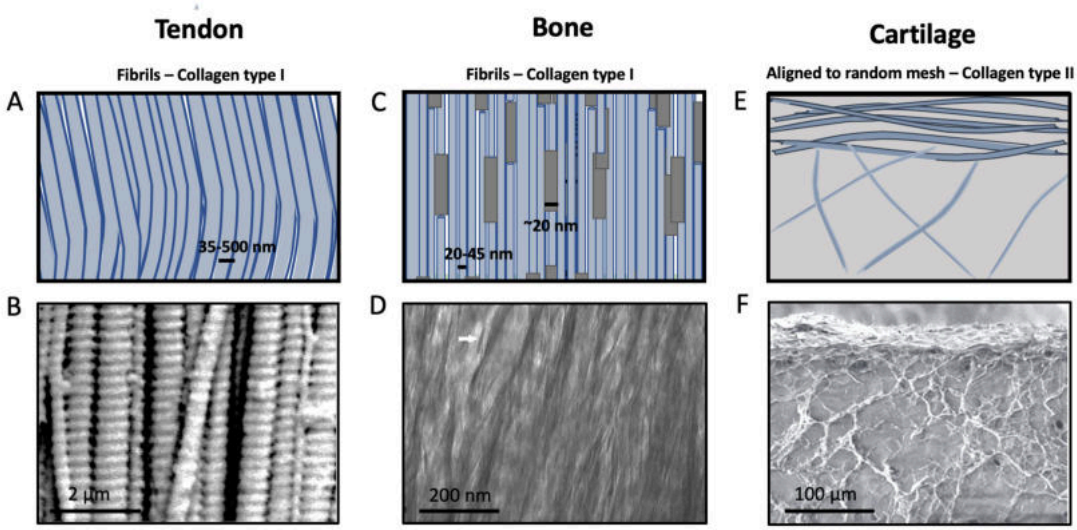

Supplementary Figure S1.1 | Matrix organization of soft-to-hard tissue interfaces. A collagen rich composition is observed in musculoskeletal tissues, although with different architectural assembly. (A-B) Tendon presents unidirectional collagen type I fibrils (average size, 35-500 nm, blue) arranged in bundles, coupled together in fascicles and these make up the tendon unit. (B) Scale bar, 2 µm. Reproduced with permission from [Provenzano, 2006 #20}. (C-D) In contrast, bone is constituted by a type I collagenous matrix comprised of stacked fibrils with diameters between 20-45 nm (blue), which are intercepted by mineral spindles of hydroxiapatite (average size ~20 nm, grey). (D), Scale bar, 200 nm. Reproduced with permission from [86]. (E-F) Mature cartilage owns depth-dependent architecture where collagen type II fibers are

unidirectionally oriented at the superficial layer while with depth it is observed the formation of randomly organized meshes (F) Scale bar, 100 μm. Reproduced with permission from [87].

CHAPTER 2. The Tendon-to-Bone interface: Multi-tissue Physiology and Cellular Microenvironment

This chapter was based on the following publication:

I. Calejo, R. Costa-Almeida, R. L. Reis, M. E. Gomes (2019) Cellular Complexity at the Interface: Challenges in Enthesis Tissue Engineering. In: *Advances in Experimental Medicine and Biology*, 1144:71-90. Springer, New York, NY. DOI:10.1007/5584_2018_307.

ABSTRACT

The complex heterogeneous cellular environment found in the tendon-to-bone interface makes this structure a challenge for interface tissue engineering. Orthopedic surgeons still face some problems associated with the formation of fibrotic tissue or retear occurring after surgical re-attachment of tendons to the bony insertion or the application of grafts. Unfortunately, an understanding of the cellular component of the tendon-to-bone interface (enthesis) lags far behind of other well-known musculoskeletal interfaces, which blocks the development of new treatment options for the healing and regeneration of this multifaceted junction.

Thus, in this chapter, the main characteristics of tendon and bone cell populations are introduced, followed by a brief description of the interfacial cellular niche, highlighting molecular mechanisms governing tendon-to-bone attachment and mineralization. Simultaneously, we describe and critically assess some challenges faced concerning the use of cell-based strategies in tendon-to-bone healing and regeneration.

Keywords: Biomarkers; Bone; Cell-based therapies; Cellular complexity; Cell Biology; Enthesis healing/repair; Regeneration; Microenvironment

2.1. THE TENDON-TO-BONE INTERFACE: AN INTRODUCTION

Tendon-to-bone interface, also known as enthesis, is a musculoskeletal structure that allows a smooth transition between two widely different tissues. This soft-to-hard tissue is prone to acute and overuse injuries, being the rotator cuff the most common and debilitating injury sites.

In trauma and orthopedic surgery, these injuries are very common and affect both young people, from professional athletes to active workers, and elderly patients [1]. Commonly, orthopedic surgeons are faced with partial and/or complete rupture of Achilles and rotator cuff tendons, which are very difficult to heal due to the complexity of interface tissue structure and the formation of scar tissue [2]. Even though some patients are asymptomatic, the damage caused in these sites significantly affects daily life due to associated morbidity. Besides conservative therapies, which frequently fail or are not appropriate, current surgical treatments rely on the use of grafts, but it has already been reported that these procedures present structural and mechanical failure rates of 20% to 94% at the surgical site [3, 4]. Therefore, it is crucial to explore easy and suitable strategies to improve tendon-to-bone junction healing and regeneration.

Enthesis tissue engineering approaches have been receiving increased attention as strategies to overcome some of the challenges encountered in the regeneration of the tendon-to-bone interface. Enthesis is a multiphasic tissue that displays a complex gradient in composition, tissue organization and, therefore, mechanical properties, while it is maintained by a heterogeneous cell population. Therefore, different approaches, such as cell-based strategies, growth factors and gene therapy, scaffold-based strategies and mechanical stimulation, have been explored [5-7]. However, up to now, the existing challenges faced in the clinics, when trying to restore musculoskeletal interfaces functionality, have led to a preference toward stem cell-mediated treatments, due to their regenerative and differentiation potential as nature tissue engineers. Hence, it is crucial to understand the cellular complexity observed at this junction toward generating adequate and straightforward cell-based approaches.

This chapter reviews the main characteristics of tendon-to-bone biology, including the cellular phenotypes and native niche microenvironment, highlighting some of the major challenges encountered in enthesis tissue engineering.

2.2. OVERVIEW ON TENDON-TO-BONE BIOLOGY

To clearly understand the complexity associated with enthesis, a small overview will be made on its soft – tendon - and hard – bone - tissue constitutes. Additionally, the interface between these

two tissues will be explored in detail. Therefore, some characteristics of these tissues will be described in the following sections.

2.2.1. TENDON TISSUE

Tendons are well-organized and dense fibrous connective tissues that link muscle to bone. Due to their mechanosensitive nature, tendons have the ability to respond and adapt to the transmission of contraction-forces by muscles to the skeleton, allowing motion and maintenance of posture. Normally, tendons vary in structure, composition and mechanical properties, depending on their anatomic location, which is coupled with their function while interacting within myotendinous (tendon-to-muscle) or tendon-to-bone junctions [8-10].

Naturally, tendons have very limited and inefficient healing capacity. Intrinsic and extrinsic mechanisms are known to occur simultaneously during tendon healing, where resident cells and surrounding cells, respectively, are recruited [11]. However, cell infiltration into the injury site and the creation of adhesions leads to the formation of fibrotic tissue [12]. Additionally, cells regulating fibrotic tendon healing have not yet been defined [13].

The limited knowledge on tendon biology relies on the fact that mature tendon tissue is relatively hypocellular, hypovascularized and mainly composed of ECM. Indeed, collagens account for up to 85% of its dry weight [12]. This tissue is a good example of a highly organized and multi-hierarchical structure composed of collagen fibrils densely packed into fiber bundles and these ones into fascicles (Figure 2.1), interspersed at each level with different amounts of non-collagenous matrix [14]. Although collagen type I is the most abundant element, other fibrillar collagens can also be found, including collagen type III, V and IX. Additionally, although in smaller amounts, non-collagenous ECM elements, such as decorin, biglycan, fibromodulin, tenascin C, fibronectin, thrombospondin, and elastin, also compose tendon ECM.

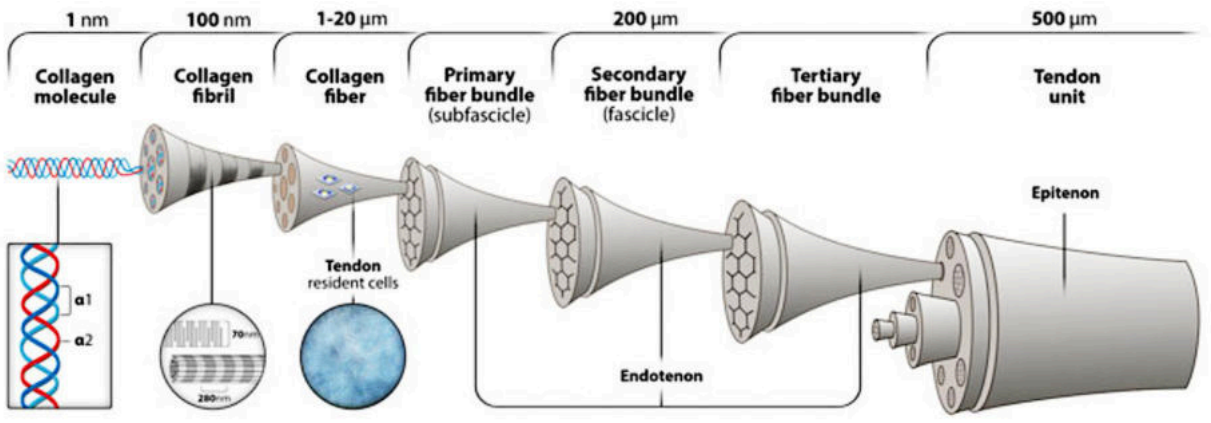

Figure 2.1 | Hierarchical structure of tendon. Tendons are organized in a hierarchical manner, with type I collagen parallelly-oriented to the mechanical axis. Fibrils are composed of dense microfibrils organized by lateral and longitudinal stacking, forming a moderately twisted configuration. Packed fibrils form large fibers, which are further combined to form fascicles. Within these collagen fibers, tendon resident cells, the tenocytes, can be found. The bundling of fascicles by connective tissue sheaths is known as endotenon and epitenon, and encounters a multipotent stem cell population, termed tendon stem/progenitor cells, that can also be found in the perivascular niche. Reproduced from Costa-Almeida et al. [15]. Copyright © Springer International Publishing Switzerland 2015.

2.2.1.1. TENDON CELL POPULATIONS

Together with the collagenous and non-collagenous matrix, tendon resident cells coordinate the necessary cues to promote tissue repair and eventual regeneration [16]. Strikingly, tendons were considered to be only composed of terminally differentiated cells. But, despite its hypocellular nature, a mixed population of mature cells (tenocytes) and stem/progenitor cells [17] was found to compose the cellular environment, as addressed in detail below.

2.2.1.1.1. *Tenocytes*

Tenocytes (TCs) or tendon cells are elongated fibroblast-like cells that lie arranged in long and parallel chains between collagen fibers and comprise about 90% of the cellular components of the tendon. Therefore, they exhibit a stretched cytoplasm as a result of the stretching mechanical forces acting on tendons. Moreover, these cells present a prominent nucleus, a well-developed rough endoplasmic reticulum and are responsible for the synthesis, degradation and maintenance of the ECM [18]. Tenocytes either reside between the collagen fibers within the fascicles or together in the interfascicular matrix between the fascicles, being denominated as intrafascicular or interfascicular TCs, respectively [19]. Tenocytes communicate with each other by extending cytoplasmic processes into the 3D tendon ECM network and establishing cell-cell contacts through adherens and gap junctions [18]. Interestingly, differences have been highlighted regarding the influence of aging on the morphology, biochemistry and composition of tendon cells [20, 21]. Tendons from young donors have been referred as having spindle-shaped cells, namely tenoblasts, while aged tendons tend to contain fewer and elongated cells, the tenocytes [21]. Such morphological changes have also been shown to be accompanied by an evident decrease both in

cell number and cell activity [20]. Moreover, the conversion of tenoblasts to tenocytes has been reported to occur under the influence of different stimuli, such as exercise or trauma [22]. Therefore, from the developmental stage to adulthood, evidences confirm a gradual decrease in cell-to-matrix ratio; thus, the native cell-mediated reparative response seems to become very limited.

2.2.1.1.2. *Tendon-derived stem cells*

A minor population of cells has been firstly identified in human and mouse tendons (Bi et al. 2007) and later in tendon samples of rabbit [23], rat [24-26], fetal bovine [27], horse [28] and fetal human [29]. These cells have been reported to fulfill universal criteria of stem cells, namely clonogenicity, self-renewal and multilineage differentiation capacities after *in vitro* expansion and *in vivo* transplantation [17]. However, some heterogeneous properties have been reported, suggesting the existence of progenitor cells. Therefore, this cell population is usually termed as tendon-derived stem cells (TDSCs) or TSPCs [17].

Concerning the physiological niche, as cells residing within tendons, TDSCs share the same microenvironment with tenocytes and are expected to play an important role in tissue maintenance and repair. Mechanical loading, biological factors, matrix structure, resident cells, physiological factors (oxygen tension and metabolic products), topographical cues, among other possible signals, seem to influence the fate of TDSCs [29, 30]. *In vitro* induction studies have shown the ability of these cells into tenocytes or towards the chondrogenic, osteogenic and adipogenic lineages and animal model studies have reported the formation of tendon-, cartilage-, bone- and tendon-bone junction-like tissues [17, 23, 24, 27-29].

Therefore, the application of this cell population in tendon and interfacial tissue engineering would be of great interest. However, its application still faces several limitations, including the lack of well-established enrichment and selection protocols for straightforward isolation. A large uncertainty also remains around the markers that enable the differentiation between TDSCs, mesenchymal stem cells (MSCs) and TCs. Thus, the establishment of a set of criteria to differentiate the different cell types would be of great interest, enabling a better assessment of the tendon niche, the influence of pathologies and, even, for interface tissue applications.

2.2.2. BONE TISSUE

Bone is a highly mineralized connective tissue essential in important functions in the human body, such as locomotion, support of other organs, protection of soft tissues, harbor of bone marrow and blood production, as well as, storage and homeostasis of minerals (phosphate and calcium). Its structure and composition determines some unique mechanical properties that allow it to have, not only, structural strength and lightweight design, but also stiffness, elasticity, resistance to deformation and capacity to absorb energy [31]. Macroscopically, two structural features can be distinguished: the cortical and trabecular bone (Figure 2.2). Cortical bone is present around the bone, forming a dense and parallel shell of lamellar units – the osteons [31]. On the contrary, trabecular bone presents a less dense, spongy-like and homogeneous network of trabeculae, being always surrounded by the cortical bone [31].

Bone, as a dynamic organ, undergoes a complex but continuous remodeling process in a cycle comprising three different phases: (1) bone resorption, (2) transition from resorption to new bone and (3) bone formation [32]. This process is only possible due to the balanced coordination of bone cells – osteoblasts, osteoclasts, osteocytes and bone lining cells – that altogether form a temporary anatomical structure, the so-called basic multicellular unit (BMU) [32].

Herein, the characteristics of the distinct cellular phenotypes will be highlighted, addressing their role in bone physiology.

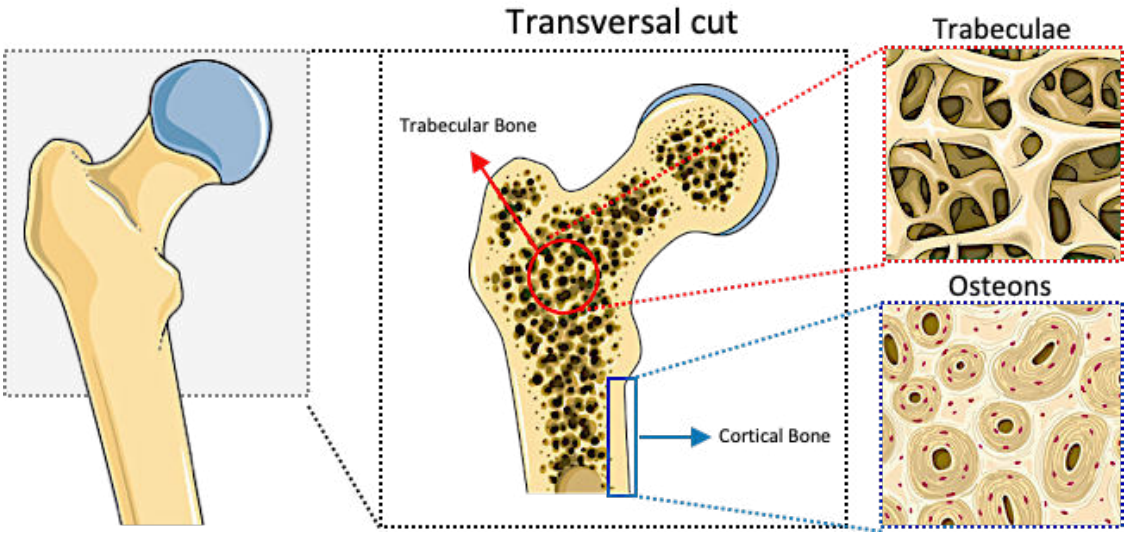

Figure 2.2 | Structural features of bone: cortical and trabecular bone. The bone is composed of a dense porous structure, the cortical bone, also called compact bone, composed by osteons. In contrast, the trabecular bone is much more porous structure, which the basic first-level structure is the trabeculae.

2.2.2.1. BONE CELL POPULATIONS

2.2.2.1.1. *Osteoblasts – Bone forming cells*

Osteoblasts, the bone-forming cells, comprise up to 6% of the total bone resident cell population and are located along the bone surface. These cells derive from MSCs whose differentiation is controlled by the master transcription factor, RUNX2 [33]. Once this transcription factor is activated, osteoprogenitor cells undergo a proliferation process characterized by the expression of specific markers being afterward denominated as pre-osteoblasts [34] (Figure 2.3). These cells undergo morphological changes, becoming larger and with a cuboidal shape. The activity of ALP increases and the cells start to secrete more bone matrix-related proteins [35]. Mature osteoblasts express higher levels of bone matrix proteins such as osteocalcin (OCN), bone sialoprotein (BSP) I/II and collagen type I, among others (Figure 2.3). Eventually, these cells will be trapped within the bone matrix and start the deposition of the organic matrix and its subsequent mineralization [32]. After osteoblast maturation, these cells can undergo one of three different fates: (1) become osteocytes as they are embedded in the bone, (2) transform into inactivated surface osteoblasts called bone-lining cells or (3) undergo programmed apoptosis [36].

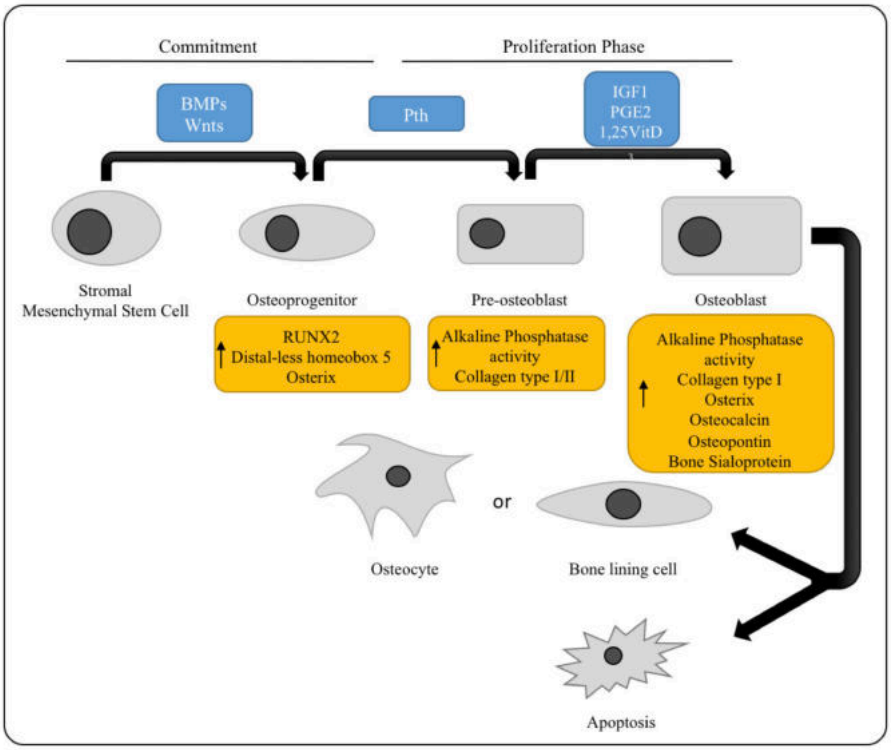

Figure 2.3 | Osteoblast differentiation process: from commitment to matrix synthesis. Schematic representation of the process of osteoblast differentiation and the possible

fate of mature osteoblast (BMPs: bone morphogenic proteins (Pth: Parathyroid hormone; Wnts: Wingless; IGF: insulin-like growth factor; PGE: prostaglandin; VitD3: vitamin D3).

2.2.2.1.2. *Osteocytes – Bone remodeling cells*

Osteocytes comprise up to 95% of bone cellular niche, being the most abundant and long-living cells with a lifespan of decades [35]. These cells are known for their central role in bone formation and resorption. Contrary to osteoblasts, osteocytes are easily identified in a bone section because of their dendritic shape and localization within small lacuna spaces in the hard-mineralized bone matrix [37]. Nevertheless, cell morphology varies between rounded and elongated shape depending on the bone type [37].

As already mentioned, osteocytes are originated from old osteoblasts buried in the bone matrix. Cells at early stages of osteoblast to osteocyte differentiation have been extensively named as "preosteocytes", "young osteocytes" or "large osteocytes [36]. When mature, osteocytes are completely trapped in the mineralized matrix and previously expressed osteoblast markers are downregulated or switched off, while osteocyte markers start to be expressed (e.g., sclerostin) [38, 39]. The majority of these markers are regulated, among other signals, by mechanical loading [39]. Once inside the lacunae, osteocyte cytoplasmic processes originate tinny tunnels, forming the so-called canaliculi, which will form the lacunocanalicular system, allowing not only the connection with neighboring osteocytes but also osteoblasts and bone-lining cells at the bone surface [39, 40]. These communications are performed through the transport of small signaling molecules (such as prostaglandins and nitric oxide) and by interstitial fluid [41]. Furthermore, the mechanosensitive function of osteocytes is possible due to the canalicular network and the spatial arrangement and shape of osteocytes [39]. However, the molecular mechanisms that trigger the conversion of mechanical stimuli to biochemical signals in osteocytes are not yet fully understood, even though some mechanisms have already been proposed [42, 43].

2.2.2.1.3. *Bone lining cells*

Bone lining cells are quiescent flat-shaped cells, originated from inactivated osteoblasts and are found at the bone surface, where neither bone resorption nor formation occurs [36, 44]. Some of these cells exhibit cytoplasmic processes and gap junctions to communicate with adjacent bone lining cells and osteocytes. Together with other bone cells, they are a component of the BMU, having a role in the bone remodeling cycle [45]. The function of bone lining cells is not fully

understood, but it is known that they have a secretory activity depending on the bone's physiological status [46]. Moreover, until now, there are no defined markers for the identification of bone lining cells or well-established and effective isolation protocols [46].

2.2.2.1.4. *Osteoclasts - Bone resorption cells*

Osteoclasts are large and terminally differentiated multinucleated cells originated from mononuclear precursors of the hematopoietic stem cell lineage. During osteoclastogenesis, or bone resorption, osteoclasts suffer a rearrangement of the cytoskeleton and become polarized; thus, different unique membrane domains can be distinguished: (1) the sealing zone and (2) ruffled border – that are in contact with the bone matrix – (3) basolateral and (4) functional secretory domains – which are not in contact with the bone matrix but with the extracellular fluid of other cells [47]. The ruffled border is responsible for the resorptive activity of osteoclasts, including the dissolution of hydroxyapatite due to the acidification in the resorption lacuna [47]. After mineral dissolution, the organic part is exposed to the action of proteolytic enzymes, leading to the degradation of both inorganic and organic matrix components [47], resulting in bone matrix resorption.

2.2.3. INTERFACING TENDON AND BONE

Although enthesis bridges tendon and bone, cells within this interface reside within a unique microenvironment that is different from that found in tendon and bone niches, exhibiting geometrical and compositional dissimilarities [48]. Two types of tendon-to-bone interface have been distinguished according to their location and structure: “fibrous” and “fibrocartilaginous” entheses [49]. In fibrous attachments, tendon or ligaments attach directly or indirectly to long bones via the periosteum. In fibrocartilaginous attachments, typical of epiphyses and apophyses, there are locations where chondrogenesis has occurred. These insertions are the most common and with major clinical relevance and include the bony attachments of rotator cuff and Achilles tendons.

The most commonly found enthesis, denominated as fibrocartilaginous, is described as a four-divided zone structure: zone 1, tendon/ligament; zone 2, unmineralized fibrocartilage; zone 3, mineralized fibrocartilage; and zone 4, bone [50, 51] (Figure 2.4). Tendon constitutes the first part of enthesis, where mechanical properties, as well as composition are similar to those found in the mid-substance tendon. This zone is characterized by its predominantly aligned collagen type I

fibers, proteoglycans, biglycan and small amounts of decorin with interspaced spindle-shaped tendon resident cells aligned in the direction of tendon tension [51-53] (Figure 2.5A, C). Strikingly, advanced imaging techniques have demonstrated a ~500 μm zone where tendon crimped fibers unravel into smoother and thinner interface fibers before attaching to bone (Figure 2.5A-B). This small area is constituted by two distinct zones, the unmineralized or noncalcified (zone 2) and mineralized fibrocartilage (zone 3). The unmineralized zone is populated by fibrochondrocytes that are responsible for ECM production of small amounts of collagen type I, IX and X and proteoglycans (decorin and aggrecan), together with higher amounts of collagen type III (Figure 2.4) [52-54]. This zone is also characterized by its low vascularization. Interestingly, mineral deposition and calcification starts at the mineralized fibrocartilage with a clearly visible straight line, called as tidemark, that delimitates the true transition between mineralized and unmineralized tissue [18]. The mineralized or calcified fibrocartilage (zone 3) is populated by hypertrophic fibrochondrocytes and is mainly constituted by collagens type I, II and X and aggrecan produced by the cells [52, 55]. This zone is described as the true transition between tendon and bone [56]. Finally, bone constitutes the last zone, thus containing osteoblasts, osteocytes and osteoclasts residing within a non-aligned collagen type I matrix together with high amounts of carbonated apatite minerals [51, 56]

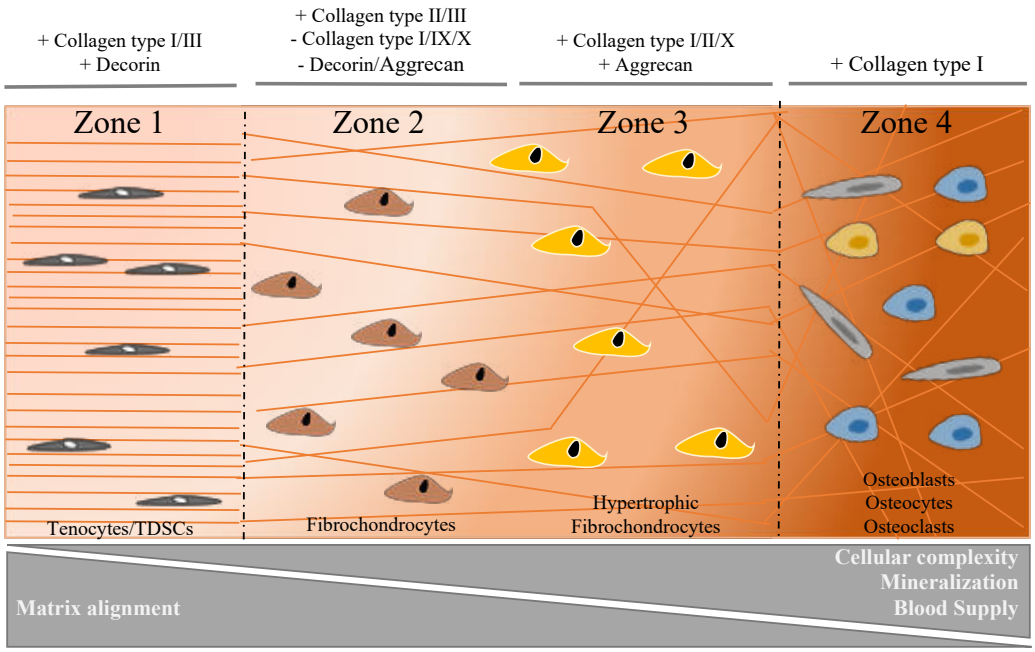

Figure 2.4 | Schematical image of tendon-to-bone structure and composition. Fibrocartilaginous insertion composed of four characteristic zones with the main ECM components and cellular microenvironment. Adapted from Tellado et al. [57].

Several studies have been performed to understand the composition and structure of enthesis. It is widely recognized that soft-to-hard tissue interfaces exhibit variations in viscoelastic and mechanical properties, architecture/structure, cellular and matrix composition along their length. Distinct regions along the supraspinatus tendon-to-bone insertion in rats and mice have been studied and gene expression, collagen organization, mineral content and biochemical properties evaluated [57-59]. At the gene level, the expression of decorin and biglycan was observed at the tendon end, while going to the bone end, only the expression of cartilage specific matrix genes was observed (such as aggrecan and collagen type II) [52]. Polarized light and angular deviation have demonstrated a lower orientation of the collagen fibers at the bone insertion site compared to tendon [60]. Moreover, analysis using Raman microprobe demonstrated a linear increase in mineral content towards the interface [58, 59]. Interestingly, collagen type I is universally found along all the regions comprising tendon-to-bone interface; but the main striking difference relies on its organization. Genin et al. observed that a gradual increase in mineral composition was accompanied by a decrease in collagen fiber organization while moving from tendon to bone [61]. Based on these results, evidence support a continuous change in collagen fiber organization, but also in mineral content, ECM composition, geometry and, consequently, mechanical properties along the tendon-to-bone interface (Figure 2.4, Figure 2.5). Altogether, these intrinsic properties are likely to effectively distribute the forces from a soft and flexible tissue like tendon, to a more rigid material as bone.

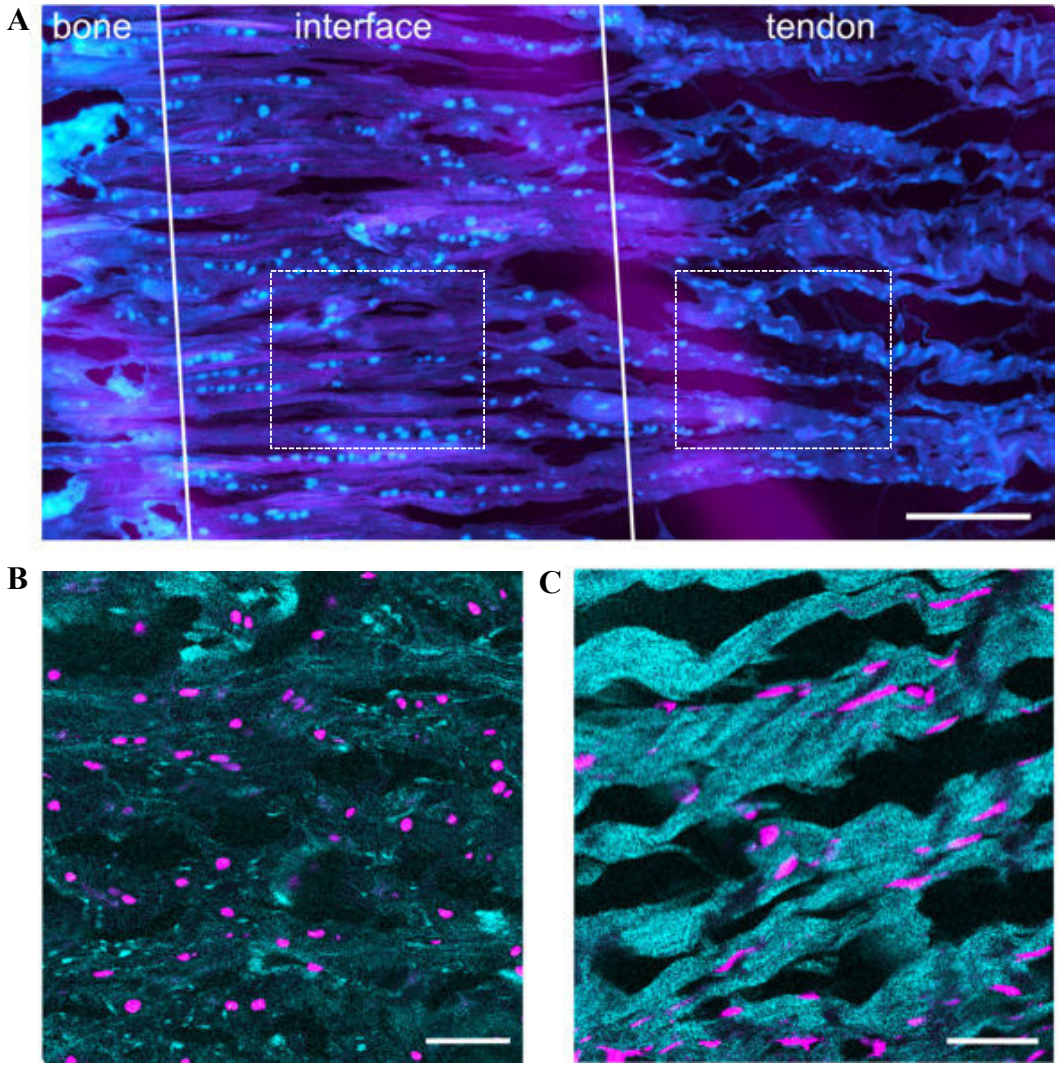

Figure 2.5 | Structure and cells morphology and localization in the tendon-to-bone insertion site. (A) Localization of cells in tendon-to-bone interface. Confocal images staining cells with SYTO® 13. Scale bar 150 μm (B) Cells residing within interface showing a round-like shape. Scale bar 50 μm. (C) Tendon cells in arranged between tendon fibers. Scale bar 50 μm. (A-C) Copyright © 2018 Kuntz et al. [62].

The structural and compositional complexity inherent to the tendon-to-bone interface has led to the development of several tissue engineered strategies. However, a lack of understanding regarding molecular mechanisms and cellular interactions, makes enthesis regeneration a challenge. Thomopoulos et al. pointed out the importance of clearly understanding the development and morphogenesis of enthesis before trying to address the healing process [60]. The unique and transitional gradient present in the tendon-to-bone interface is not recreated during the naturally occurring healing process. As already reported by Newsham-West et al., in a patella sheet model

following surgical re-attachment, the repaired enthesis resembled more fibrous tissue than the original fibrocartilaginous interface, characterized by a gradient of morphological changes on the collagen fibrils between the two tissues and a hypercellular environment [63]. Moreover, studies in animal models of the rotator cuff and anterior cruciate ligament (ACL) have clearly demonstrated a failed regeneration of tendon and bone with the formation of scar tissue and high probability of retear [60, 64, 65]. Therefore, there is a fundamental need to better understand the relationship between structure, function and the healing process of the native tissue to be able to develop and regenerate tendon-to-bone interface.

2.2.4. MOLECULAR MECHANISMS GOVERNING ENTHESIS ATTACHMENTS

Currently, very little is known about the main mechanisms behind the embryonic development of this complex structure. It is believed that a synergistic effect between biological and biophysical cues triggers the generation of the highly multifaceted composition found at tendon-to-bone insertion sites. During fetal development, tendon and bone are formed almost at the same time, but the formation of the transition between them only occurs postnatally [66-68]. At this point, biological factors are likely to have a fundamental role in interfacial growth plate development. Tendon-to-bone developmental studies have demonstrated that the development of this tendon attachment occurs separately from bone development. This modular process provides a checkpoint to control musculoskeletal system assembly, without interfering with bone tissue morphogenesis [69].

Transcription factors associated with tenogenesis, scleraxis (SCX), and chondrogenesis, SOX9, have been highlighted as important elements for enthesis development [70-73]. Interestingly, the deletion of *Scx* has been shown to prevent the formation of bony tuberosities where tendons attach, defective maturation of tendons and a decrease in the expression of *Sox9* in developing entheseal cartilage in mice [72, 73].

A common *Scx+/Sox9+* progenitor pool to tenocytes and chondrocytes has been proposed [71, 74] but the regulation of the divergence process during lineage specification is still poorly understood. Recently, the interplay of these two factors on the development of bone eminence suggested different regulatory mechanisms to control the different pool of progenitor cells [70, 71]. In a first study, the formation of the deltoid tuberosity was demonstrated to be initially regulated by tendon and, subsequently, muscle dependent [70]. Tendon *Scx*-expressing cells have been shown to drive the expression of *Bmp4* and the deletion of either *Scx* or *Bmp4* in the limb arrested the

development of cartilaginous bone eminences [70, 71]. Therefore, the expression of *Bmp4* seems to be crucial for enthesis and associated bone ridges formation. In another study, a new regulatory mechanism for attachment formation was described. A distinct pool of *Scx*/*Sox9*-expressing progenitor cells has been shown to form bone eminences in a modular fashion, independent of primary cartilage chondrocytes descendance [71] (Figure 2.6). Moreover, a lack of eminences in limb mesenchyme of mouse embryos, where a loss of TGFß signaling was induced by genetic ablation of transforming growth factor beta receptor II (TgfBrII), clearly demonstrated an earlier role of TGFß signaling pathway in skeletal/tendon progenitors [75]. Interestingly, the loss of *Scx* has been shown to affect also *Sox9* expression in the developing deltoid tuberosity while decreasing the phosphorylation of Smad1/5 and Smad 3, intracellular downstream mediators of TGFß and BMP signaling pathways [73]. Thus, it is tempting to assume that TGFß signaling plays an important role in tendon-to-bone formation, trough the regulation of both tendon and bone eminence progenitors.

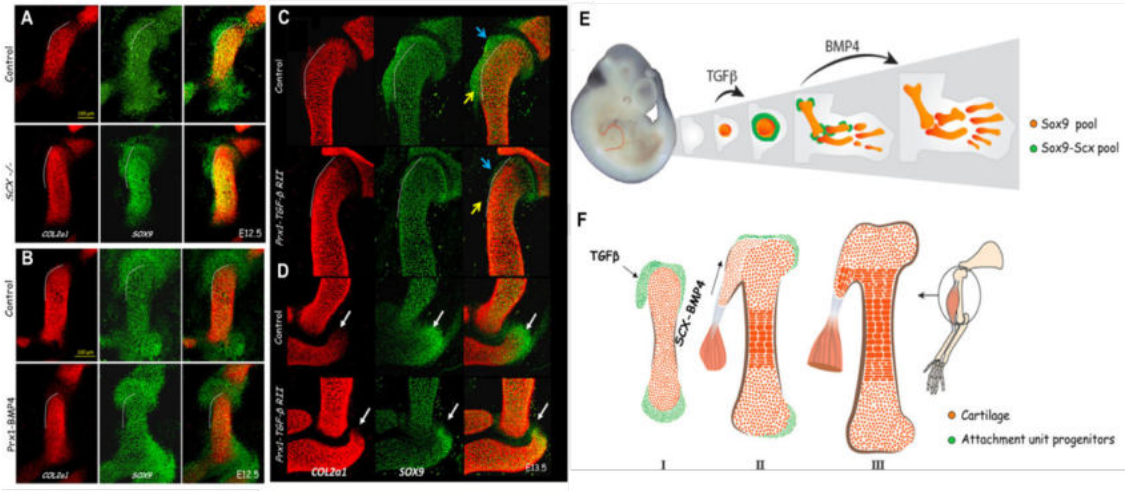

Figure 2.6 | SCX/BMP4 and TGFß signaling regulation of bone imminences. (A-B) Sections of *Scx–/–* and *Prx1-Bmp4* mutants showed the presence of S*ox9*-positive eminence progenitors. (C-D) Sections of *Prx1-Tgf-ßRII* mutants demonstrating a lack of S*ox9*-positive progenitors. (E-F) Modular model of bone eminence development. Figure adapted from Blitz et al. [71]. Copyright © 2013. Published by The Company of Biologists Ltd.

Other promising candidates have been pointed because of their involvement in the regulation of different stages of attachment development [76, 77]. Evidences have shown that the depletion of *Bmp4* in limbs did not lead to a complete loss of bone eminences. Moreover, the blockage of bone

morphogenetic protein receptor 1a (*Bmpr1a*) in limb mesenchyme and a dominant-negative *Bmp5* mutation has led to alterations in bone eminences formation.

A more profound gene profiling of these candidates and other molecules playing a critical role in tendon-to-bone attachment and bone eminence formation would be of great interest. Nevertheless, exploring the role of growth factors implicated in skeletal morphogenesis and tendon or bone formation could light up some mechanisms important in the development and attachment of the tendon-to-bone junction.

2.2.5. MINERALIZATION PROCESS

The cellular and molecular mechanisms associated with matrix mineralization of tendon-to-bone interface follow a similar pathway to the mechanism observed in chondrocyte hypertrophy in the growth plate [2, 69].

A small population of cells pointed as responsible for entheseal mineralization has been identified in the fibrocartilage region between tendon and bone and denominated Gli1-positive cells [78-80]. These cells have been identified in neonatal enthesis but known to persist in the mature enthesis at the edge of mineralization and pointed as hedgehog (Hh)-responsive cell [79, 81]. The Indian hedgehog (Ihh) and parathyroid hormone-related protein (PTHrP) signaling pathways have been highlighted in a large number of mouse models due to their role in the regulation of chondrocyte differentiation towards hypertrophic chondrocytes and, therefore, preventing the mineralization at inappropriate zones of the growth plate [79, 81, 82]. For example, the deletion of *PTHrP* led to an arrestment of fibrous enthesis, meaning that a hypermineralized tuberosity was observed instead of a normal tibial crest [83, 84]. Similarly, when studying the role of Ihh in tendon-to-bone development, the deletion of smoothened (SMO), a transmembrane protein responsible for the Ihh signals transduction, in *Scx*-expressing cells led to an impairment in the formation of a fibrocartilaginous interface, evidenced by a downregulation of chondrogenic- and interface-related genes expression, along with a decrease in matrix mineralization [81].

Even though the molecular mechanisms are not yet fully understood, biomechanical cues, such as loading, have also been associated with the expression of PTHrP [82, 85], and shown to modulate Ihh signaling and the size of Hh-responsive cells population [79]. Unloading of the medial collateral ligament, semimembranosus and semitendinosus mouse enthesis led to a marked decrease in PTHrP expression. Nevertheless, cyclic mechanical stress has also been reported to influence Ihh expression in chondrocytes culture [86] and, more recently, Ihh expression has been correlated

with the mechanical levels while studying mechanosensitive genes expression during embryonic bone formation [87].

Therefore, the expression of PTHrP and Ihh, along with the presence of Gli1-positive cells, can be associated with the onset of mineralization in developing insertion sites of the tendon-to-bone interface.

2.3. MAIN CHALLENGES IN CELLULAR THERAPIES FOR ENTHESIS TISSUE ENGINEERING

Cells are nature engineers that would ideally replicate tissue development when regeneration of a damaged enthesis is needed. Currently, various cell-based or culture-based strategies are used [57]. However, up to now, several issues remain unsolved regarding the application of cell-based therapies for enthesis tissue engineering and regeneration.

2.3.1. CELL SOURCE SELECTION AND CELL DIFFERENTIATION PROTOCOLS

Given the cellular complexity described above, the identification of an ideal cell source poses a great challenge to the establishment of adequate cellular therapies. Co-culture systems have been demonstrated to be a useful tool while trying to mimic the heterotypic cellular environment found in tendon-to-bone junction. However, the attempt to replicate the native cell-cell communication and understand the molecular mechanisms behind tendon-to-bone healing and regeneration is far from resolution. Till now, culture-based strategies have focused on the use of multiple terminally differentiated cells [88, 89] or stem cells with terminally differentiated cells [90-92]. For instance, osteoblast-fibroblast interactions have been explored [88] under the rationale that the synergistic communication between distinct phenotypes could induce the formation of enthesis-like tissue. Although the oversimplicity of the system limited the formation of a true tendon-to-bone interface *in vitro*, it could support the deposition of fibrocartilage ECM components (e.g., collagen type II and aggrecan). Nevertheless, this type of strategy requires the isolation of cells from different tissues, often through invasive procedures, which limits clinical translation.

On the other hand, exploring the use of stem cells relies on the establishment of adequate differentiation protocols. So far, diverse sources have been explored from, for example, not so well-known ACL-derived stem cells [93] to more established and readily available adipose-derived stem cells (ASCs) [94-98]. Although there are well-established inductive protocols for the osteogenic and chondrogenic commitment of MSCs [99-101], diverse attempts have been made to commit stem

cells towards the tenogenic lineage. Normally, treatments with GDF or genetic manipulation are applied. For example, ASCs cultured in the presence of different growth factors associated with tendon development and healing (endothelial growth factor, platelet-derived growth factor) showed an upregulation of tendon-related genes [102], demonstrating the potential use of biochemical molecules to induce the cell commitment toward the tenogenic lineage. However, an ideal medium formulation is not yet available.

Furthermore, bone repair involves a progression from undifferentiated progenitors to actively mature cells with distinct phenotypes. Thus, the identification of an ideal skeletal progenitor is defying the fields of bone and tendon-to-bone tissue engineering.

2.3.2. CELL ISOLATION PROTOCOLS AND PURITY

Concerning the isolation methods of bone cells, osteoblast-like cells are often modeled through the use of immortalized cell lines derived from sarcomas. Alternatively, with interest in tissue engineering and clinical applications, primary cultures can be obtained by explant digestion or stem cell differentiation. These cell cultures are able to represent bone cells and to deposit mineralized ECM in response to osteoinductive stimuli [103], but their fundamental biology may not be comparable, limiting the comprehension of their effectiveness and requiring extensive studies to understand their potential in tendon-to-bone therapies.

Furthermore, up to now, several problems remain unsolved regarding the use of tendon cell populations, and in particular of TDSCs for tendon-to-bone regeneration. The isolation of TDSCs still remains largely dependent on a well-established enrichment and selection approach. Several methods of tissue digestion have already been used [104-107]. Some authors reported the use of only collagenase type, collagenase type I with dispase [17, 23], collagenase type II [108] and collagenase type V [109] for tendon tissue digestion. Besides the lack of consensus between the described isolation methods, it is most likely that a mixed population of cells with heterogeneous characteristics in terms of clonogenicity, multidifferentiation potential, and self-renewal capability will be obtained, including also terminally differentiated cells, such as tenocytes [104, 110]. Isolation and characterization of these cells are of major importance because it will generate new insights on basic tendon biology and allow a correct use of the obtained cell population. The same problem is applied to the isolation of ACL-derived stem cells, which still lack standardized isolation methods [111-113].

2.3.3. MOLECULAR SIGNATURES

The lack of molecular markers to discriminate the tendon cell population at every discrete step of cell lineage differentiation, makes the expansion and purification of TDSCs and fully differentiated cells very difficult. Several additional factors have been reported to influence markers expression in TDSCs, such as cell source (age, donor variability, tendon type) and cell culture procedures (culture conditions and cell passaging). Indeed, some studies have reported depletion in the number of TDSCs when comparing cell populations isolated from young and aged individuals, as well as a variation in the number of obtained TDSCs according to the location of tissue collection, as mentioned above. Currently, there is no specific marker that is able to accurately distinguish between tendon cell populations and other cells from mesenchymal original, like MSCs and fibroblasts. Although TDSCs share common surface markers, express identical genes and respond to different growth factors in a similar manner to that of other MSCs (such as bone-marrow MSCs), it was observed that expression patterns were closely related but not identical [17, 25]. Hence, some controversy may arise regarding the identity of these cell populations.

Furthermore, the limited knowledge regarding enthesis cells molecular biomarkers is challenging the interpretation of stem cell differentiation strategies for enthesis tissue engineering. Indeed, cell-based approaches relying on the transplantation of MSCs or on the seeding of MSCs (and other stem cells) onto bioengineered scaffolds require that the differentiated phenotype resembles the physiological phenotype of interface cells. Recently, several biomarkers have been proposed for tendon-to-bone interface. Despite morphological disparities, a transcriptomic analysis along with proteome data were used and the cellular patterns of enthesis cells were assessed and compared with tendon and cartilage cells. Kuntz and colleagues explored the transcriptome of Achilles tendon-to-bone interface from porcine legs and have found 3980 differentially regulated transcripts for enthesis and tendon and 395 for enthesis and cartilage, suggesting that cells at the interface are more chondrocyte-like than tenocyte-like given the strong overlap between cartilage and enthesis cells transcriptomes [62]. Interestingly, symmetric differences were shown in the transcriptome of the tendon in comparison with enthesis, where two genes showed enrichment in the tendon proteome but conversely in enthesis transcriptome (collagen type XIV alpha-1 chain and extracellular matrix protein 1), raising the hypothesis that differences resulted from the influence of mechanical stimuli that cells undergo [62]. Moreover, several markers of terminally differentiated hypertrophic chondrocytes were detected in cells within the interface (namely RUNX2, integrin-binding sialoprotein (IBSP) and matrix metallopeptidase 13 (MMP13)), among other cartilage-

related biomarkers (aggrecan, chondroadherin, collagen type II and versican) [62]. Altogether, the integration of transcriptomics [62] and proteomics data [48] demonstrates that enthesis cells resemble chondrocyte-like cells, but in a different stage of chondrogenic differentiation, being less committed than cartilage cells.

The identification of several biomarkers is of major importance while trying to characterize the single cell unit or cells on tendon-to-bone interface. However, there is still a lack of knowledge about the cells at the interface, along with a lack of molecular biomarkers for its identification. Even though advanced genetic tools have been developed, there is not a well-established molecular signature for each cell type, being difficult to identify or clarify within the proper tissue or to clearly understand the differentiation process occurring in the tendon-to-bone interface.

2.4. CONCLUSIONS

Tendon-to-bone interface physiology and healing are still far from being completely understood. Insights from tendon and bone biology have been helping in the development of tissue engineering strategies for enthesis regeneration, but the fundamental differences within this interface need to uncover. It is of major importance to understand the heterotypic cellular interactions occurring in the native tissues, such as the role of ECM-cell contact, cell-cell contact and production of paracrine factors for the development of a fully functional tissue. Input signals from very dissimilar tissues, tendon (soft tissue) and bone (hard tissue) render the interface with a unique niche exhibiting specific structural and compositional properties. The identification of transcription factors and signaling pathways involved in enthesis development has been shedding light on putative mechanisms underlying interface repair and ultimately regeneration. The integration of transcriptomics and proteomics data has brought hope to a more precise identification of enthesis cells, which resemble a more chondrocyte-like than tenocyte-like phenotype. Nonetheless, the molecular signature (of both tendon cells and enthesis cells) is still to be unveiled, posing a strong challenge to the development of future cell-based therapies. Hence, further investigations are required to improve the knowledge on the molecular mechanisms regulating the physiology, as well as pathology and repair/regeneration of these musculoskeletal tissues.

2.5. REFERENCES

[1] I. Gans, J.S. Retzky, L.C. Jones, M.J. Tanaka, Epidemiology of Recurrent Anterior Cruciate Ligament Injuries in National Collegiate Athletic Association Sports: The Injury Surveillance

Program, 2004-2014, Orthop J Sports Med 6(6) (2018) 2325967118777823, 10.1177/2325967118777823.

[2] H.H. Lu, S. Thomopoulos, Functional attachment of soft tissues to bone: development, healing, and tissue engineering, Annual review of biomedical engineering 15 (2013) 201-26, 10.1146/annurev-bioeng-071910-124656.

[3] N.S. Cho, Y.G. Rhee, The factors affecting the clinical outcome and integrity of arthroscopically repaired rotator cuff tears of the shoulder, Clin Orthop Surg 1(2) (2009) 96-104, 10.4055/cios.2009.1.2.96.

[4] B.E. Øiestad, L. Engebretsen, K. Storheim, M.A. Risberg, Knee osteoarthritis after anterior cruciate ligament injury: a systematic review, Am J Sports Med 37(7) (2009) 1434-43, 10.1177/0363546509338827.

[5] J.E. Phillips, K.L. Burns, J.M. Le Doux, R.E. Guldberg, A.J. García, Engineering graded tissue interfaces, Proceedings of the National Academy of Sciences 105(34) (2008) 12170, 10.1073/pnas.0801988105.

[6] E. Bayrak, P. Yilgor Huri, Engineering Musculoskeletal Tissue Interfaces, Frontiers in Materials 5 (2018) 24,

[7] E.D. Bonnevie, R.L. Mauck, Physiology and Engineering of the Graded Interfaces of Musculoskeletal Junctions, Annual review of biomedical engineering 20(1) (2018) 403-429, 10.1146/annurev-bioeng-062117-121113.

[8] S.P. Magnusson, P. Hansen, M. Kjaer, Tendon properties in relation to muscular activity and physical training, Scandinavian journal of medicine & science in sports 13(4) (2003) 211-23,

[9] M. Kjaer, Role of extracellular matrix in adaptation of tendon and skeletal muscle to mechanical loading, Physiol Rev 84 (2004) 649–698, 10.1152/physrev.00031.2003.

[10] M. Franchi, A. Trire, M. Quaranta, E. Orsini, V. Ottani, Collagen structure of tendon relates to function, ScientificWorldJournal 7 (2007) 404-20, 10.1100/tsw.2007.92.

[11] S.A. Fenwick, B.L. Hazleman, G.P. Riley, The vasculature and its role in the damaged and healing tendon, Arthritis Res 4(4) (2002) 252-60, 10.1186/ar416.

[12] D. Docheva, S.A. Muller, M. Majewski, C.H. Evans, Biologics for tendon repair, Adv Drug Deliv Rev 84 (2015) 222-39, 10.1016/j.addr.2014.11.015.

[13] K. Howell, C. Chien, R. Bell, D. Laudier, S.F. Tufa, D.R. Keene, N. Andarawis-Puri, A.H. Huang, Novel Model of Tendon Regeneration Reveals Distinct Cell Mechanisms Underlying Regenerative and Fibrotic Tendon Healing, Scientific reports 7 (2017) 45238-45238, 10.1038/srep45238.

[14] C.T. Thorpe, H.L. Birch, P.D. Clegg, H.R. Screen, The role of the non-collagenous matrix in tendon function, Int J Exp Pathol 94(4) (2013) 248-59, 10.1111/iep.12027.

[15] G.A.I. Costa-Almeida R., Gershovich P., Rodrigues M.T., Reis R.L., Gomes M.E., Tendon Stem Cell Niche, In: Turksen K. (eds) e. Springer, Cham. Tissue-Specific Stem Cell Niche. Stem Cell Biology and Regenerative Medicin (2015)

[16] F. Gattazzo, A. Urciuolo, P. Bonaldo, Extracellular matrix: A dynamic microenvironment for stem cell niche, Biochimica et Biophysica Acta (BBA) - General Subjects 1840(8) (2014) 2506-2519, 10.1016/j.bbagen.2014.01.010.

[17] Y. Bi, D. Ehirchiou, T.M. Kilts, C.A. Inkson, M.C. Embree, W. Sonoyama, L. Li, A.I. Leet, B.-M. Seo, L. Zhang, S. Shi, M.F. Young, Identification of tendon stem/progenitor cells and the role of the extracellular matrix in their niche, Nature Medicine 13(10) (2007) 1219-1227, 10.1038/nm1630.

[18] J.C. Patterson-Kane, T. Rich, Achilles Tendon Injuries in Elite Athletes: Lessons in Pathophysiology from Their Equine Counterparts, ILAR Journal 55(1) (2014) 86-99, 10.1093/ilar/ilu004.

[19] C.T. Thorpe, H.L. Birch, P.D. Clegg, H.R.C. Screen, Chapter 1 - Tendon Physiology and Mechanical Behavior: Structure–Function Relationships, Tendon Regeneration, Academic Press, Boston, 2015, pp. 3-39.

[20] E. Ippolito, P.G. Natali, F. Postacchini, L. Accinni, C. De Martino, Morphological, immunochemical, and biochemical study of rabbit achilles tendon at various ages, The Journal of bone and joint surgery. American volume 62(4) (1980) 583-98,

[21] P. Kannus, Structure of the tendon connective tissue, Scandinavian journal of medicine & science in sports 10(6) (2000) 312-20,

[22] F.S. Chuen, C.Y. Chuk, W.Y. Ping, W.W. Nar, H.L. Kim, C.K. Ming, Immunohistochemical characterization of cells in adult human patellar tendons, J Histochem Cytochem 52(9) (2004) 1151-7, 10.1369/jhc.3A6232.2004.

[23] J. Zhang, J.H. Wang, Characterization of differential properties of rabbit tendon stem cells and tenocytes, BMC Musculoskelet Disord 11 (2010) 10, 10.1186/1471-2474-11-10.

[24] R. Yung-Feng, P.Y.L. Pauline, L. Gang, e. al., Isolation and Characterization of Multipotent Rat Tendon-Derived Stem Cells, Tissue Engineering: Part A 16(5) (2010) 10.1089=ten.tea.2009.0529.

[25] Q. Tan, P.P. Lui, Y.F. Rui, Y.M. Wong, Comparison of potentials of stem cells isolated from tendon and bone marrow for musculoskeletal tissue engineering, Tissue Eng Part A 18(7-8) (2012) 840-51, 10.1089/ten.TEA.2011.0362.

[26] Y.F. Rui, P.P.Y. Lui, Y.M. Wong, Q. Tan, K.M. Chan, Altered fate of tendon-derived stem cells isolated from a failed tendon-healing animal model of tendinopathy, Stem cells and development 22(7) (2013) 1076-1085, 10.1089/scd.2012.0555.

[27] J. Yang, Q. Zhao, K. Wang, H. Liu, C. Ma, H. Huang, Y. Liu, Isolation and biological characterization of tendon-derived stem cells from fetal bovine, In Vitro Cellular & Developmental Biology - Animal 52(8) (2016) 846-856, 10.1007/s11626-016-0043-z.

[28] A.B. Lovati, B. Corradetti, A. Lange Consiglio, C. Recordati, E. Bonacina, D. Bizzaro, F. Cremonesi, Characterization and differentiation of equine tendon-derived progenitor cells, Journal of biological regulators and homeostatic agents 25(2 Suppl) (2011) S75-84,

[29] Z. Yin, X. Chen, J.L. Chen, W.L. Shen, T.M. Hieu Nguyen, L. Gao, H.W. Ouyang, The regulation of tendon stem cell differentiation by the alignment of nanofibers, Biomaterials 31(8) (2010) 2163-75, 10.1016/j.biomaterials.2009.11.083.

[30] Y. Yu, L. Lin, Y. Zhou, X. Lu, X. Shao, C. Lin, K. Yu, X. Zhang, J. Hong, Y. Chen, Effect of Hypoxia on Self-Renewal Capacity and Differentiation in Human Tendon-Derived Stem Cells, Medical Science Monitor 23 (2017) 1334-1339, 10.12659/msm.903892.

[31] E. Seeman , P.D. Delmas Bone Quality — The Material and Structural Basis of Bone Strength and Fragility, New England Journal of Medicine 354(21) (2006) 2250-2261, 10.1056/NEJMra053077.

[32] J.C. Crockett, M.J. Rogers, F.P. Coxon, L.J. Hocking, M.H. Helfrich, Bone remodelling at a glance, Journal of Cell Science 124(7) (2011) 991-998, 10.1242/jcs.063032.

[33] E.D. Jensen, R. Gopalakrishnan, J.J. Westendorf, Regulation of gene expression in osteoblasts, Biofactors 36(1) (2010) 25-32, 10.1002/biof.72.

[34] F. Long, Building strong bones: molecular regulation of the osteoblast lineage, Nat Rev Mol Cell Biol 13(1) (2011) 27-38, 10.1038/nrm3254.

[35] M. Capulli, R. Paone, N. Rucci, Osteoblast and osteocyte: games without frontiers, Arch Biochem Biophys 561 (2014) 3-12, 10.1016/j.abb.2014.05.003.

[36] G.Y. Rochefort, S. Pallu, C.L. Benhamou, Osteocyte: the unrecognized side of bone tissue, Osteoporos Int 21(9) (2010) 1457-69, 10.1007/s00198-010-1194-5.

[37] B.S. Noble, The osteocyte lineage, Arch Biochem Biophys 473(2) (2008) 106-11, 10.1016/j.abb.2008.04.009.

[38] C. Palumbo, S. Palazzini, D. Zaffe, G. Marotti, Osteocyte differentiation in the tibia of newborn rabbit: an ultrastructural study of the formation of cytoplasmic processes, Acta anatomica 137(4) (1990) 350-8,

[39] L.F. Bonewald, The amazing osteocyte, J Bone Miner Res 26(2) (2011) 229-38, 10.1002/jbmr.320.

[40] R. Civitelli, Cell-Cell Communication in the Osteoblast/Osteocyte Lineage, Archives of biochemistry and biophysics 473(2) (2008) 188-192, 10.1016/j.abb.2008.04.005.

[41] M.B. Schaffler, O.D. Kennedy, Osteocyte signaling in bone, Curr Osteoporos Rep 10(2) (2012) 118-25, 10.1007/s11914-012-0105-4.

[42] Z. Xiao, S. Zhang, J. Mahlios, G. Zhou, B.S. Magenheimer, D. Guo, S.L. Dallas, R. Maser, J.P. Calvet, L. Bonewald, L.D. Quarles, Cilia-like structures and polycystin-1 in osteoblasts/osteocytes and associated abnormalities in skeletogenesis and Runx2 expression, J Biol Chem 281(41) (2006) 30884-95, 10.1074/jbc.M604772200.

[43] A. Santos, A.D. Bakker, B. Zandieh-Doulabi, J.M. de Blieck-Hogervorst, J. Klein-Nulend, Early activation of the beta-catenin pathway in osteocytes is mediated by nitric oxide, phosphatidyl inositol-3 kinase/Akt, and focal adhesion kinase, Biochem Biophys Res Commun 391(1) (2010) 364-9, 10.1016/j.bbrc.2009.11.064.

[44] S.C. Miller, L. de Saint-Georges, B.M. Bowman, W.S. Jee, Bone lining cells: structure and function, Scanning microscopy 3(3) (1989) 953-60; discussion 960-1,

[45] E.F. Eriksen, Normal and Pathological Remodeling of Human Trabecular Bone: Three Dimensional Reconstruction of the Remodeling Sequence in Normals and in Metabolic Bone Disease*, Endocrine Reviews 7(4) (1986) 379-408, 10.1210/edrv-7-4-379.

[46] I. Matic, B.G. Matthews, X. Wang, N.A. Dyment, D.L. Worthley, D.W. Rowe, D. Grcevic, I. Kalajzic, Quiescent Bone Lining Cells Are a Major Source of Osteoblasts During Adulthood, Stem Cells 34(12) (2016) 2930-2942, 10.1002/stem.2474.

[47] V.E. Arana-Chavez, V. Bradaschia-Correa, Clastic cells: Mineralized tissue resorption in health and disease, The International Journal of Biochemistry & Cell Biology 41(3) (2009) 446-450, 10.1016/j.biocel.2008.09.007.

[48] L. Rossetti, L.A. Kuntz, E. Kunold, J. Schock, K.W. Müller, H. Grabmayr, J. Stolberg-Stolberg, F. Pfeiffer, S.A. Sieber, R. Burgkart, A.R. Bausch, The microstructure and micromechanics of the tendon–bone insertion, Nature Materials 16(6) (2017) 664-670, 10.1038/nmat4863.

[49] M. Benjamin, H. Toumi, J.R. Ralphs, G. Bydder, T.M. Best, S. Milz, Where tendons and ligaments meet bone: attachment sites ('entheses') in relation to exercise and/or mechanical load, Journal of anatomy 208(4) (2006) 471-90, 10.1111/j.1469-7580.2006.00540.x.

[50] M. Benjamin, T. Kumai, S. Milz, B.M. Boszczyk, A.A. Boszczyk, J.R. Ralphs, The skeletal attachment of tendons—tendon 'entheses' Comp Biochem Physiol A Mol Integr Physiol 133(4) (2002) 931-945, 10.1016/S1095-6433(02)00138-1.

[51] S. Thomopoulos, G. Hattersley, V. Rosen, M. Mertens, L. Galatz, G.R. Williams, L.J. Soslowsky, The localized expression of extracellular matrix components in healing tendon insertion sites: an in situ hybridization study, Journal of orthopaedic research : official publication of the Orthopaedic Research Society 20(3) (2002) 454-63, 10.1016/s0736-0266(01)00144-9.

[52] S. Thomopoulos, G.R. Williams, J.A. Gimbel, M. Favata, L.J. Soslowsky, Variation of biomechanical, structural, and compositional properties along the tendon to bone insertion site, Journal of Orthopaedic Research 21 (2003) 413-419, 10.1016/SO736-0266(03)000S7-3.

[53] A.D. Waggett, J.R. Ralphs, A.P. Kwan, D. Woodnutt, M. Benjamin, Characterization of collagens and proteoglycans at the insertion of the human Achilles tendon, Matrix Biol 16(8) (1998) 457-70,

[54] S. Fukuta, M. Oyama, K. Kavalkovich, F.H. Fu, C. Niyibizi, Identification of types II, IX and X collagens at the insertion site of the bovine achilles tendon, Matrix Biol 17(1) (1998) 65-73,

[55] S. Thomopoulos, The role of mechanobiology in the attachment of tendon to bone, IBMS BoneKEy 8(6) (2011) 271-285, 10.1138/20110515.

[56] S. Thomopoulos, G.M. Genin, L.M. Galatz, The development and morphogenesis of the tendon-to-bone insertion What development can teach us about healing, Journal of musculoskeletal & neuronal interactions 10(1) (2010) 35-45,

[57] S. Font Tellado, E.R. Balmayor, M. Van Griensven, Strategies to engineer tendon/ligament-to-bone interface: Biomaterials, cells and growth factors, Adv Drug Deliv Rev 94 (2015) 126-40, 10.1016/j.addr.2015.03.004.

[58] B. Wopenka, A. Kent, J.D. Pasteris, Y. Yoon, S. Thomopoulos, The tendon-to-bone transition of the rotator cuff: a preliminary Raman spectroscopic study documenting the gradual

mineralization across the insertion in rat tissue samples, Appl Spectrosc 62(12) (2008) 1285-94, 10.1366/000370208786822179.

[59] A.G. Schwartz, J.D. Pasteris, G.M. Genin, T.L. Daulton, S. Thomopoulos, Mineral distributions at the developing tendon enthesis, PLoS One 7(11) (2012) e48630, 10.1371/journal.pone.0048630.

[60] S. Thomopoulos, Tendon to Bone Healing: Differences in Biomechanical, Structural, and Compositional Properties Due to a Range of Activity Levels, Journal of Biomechanical Engineering 125(1) (2003) 10.1115/1.1536660.

[61] G.M. Genin, A. Kent, V. Birman, B. Wopenka, J.D. Pasteris, P.J. Marquez, S. Thomopoulos, Functional grading of mineral and collagen in the attachment of tendon to bone, Biophys J 97(4) (2009) 976-85, 10.1016/j.bpj.2009.05.043.

[62] L.A. Kuntz, L. Rossetti, E. Kunold, A. Schmitt, R. von Eisenhart-Rothe, A.R. Bausch, R.H. Burgkart, Biomarkers for tissue engineering of the tendon-bone interface, PLOS ONE 13(1) (2018) e0189668, 10.1371/journal.pone.0189668.

[63] R. Newsham-West, H. Nicholson, M. Walton, P. Milburn, Long-term morphology of a healing bone?tendon interface: a histological observation in the sheep model, Journal of anatomy 210(3) (2007) 318-327, 10.1111/j.1469-7580.2007.00699.x.

[64] J.E. Carpenter, S. Thomopoulos, C.L. Flanagan, C.M. DeBano, L.J. Soslowsky, Rotator cuff defect healing: A biomechanical and histologic analysis in an animal model, Journal of Shoulder and Elbow Surgery 7(6) (1998) 599-605, 10.1016/S1058-2746(98)90007-6.

[65] L. Galatz, S. Rothermich, K. VanderPloeg, B. Petersen, L. Sandell, S. Thomopoulos, The development and morphogenesis of the tendon-to-bone insertion What development can teach us about healing, J Musculoskelet Neuronal Interact 10(1) (2010) 35-45,

[66] Y.S. Bland, D.E. Ashhurst, The hip joint: the fibrillar collagens associated with development and ageing in the rabbit, Journal of anatomy 198(Pt 1) (2001) 17-27, 10.1046/j.1469-7580.2001.19810017.x.

[67] Y.S. Bland, D.E. Ashhurst, Fetal and postnatal development of the patella, patellar tendon and suprapatella in the rabbit; changes in the distribution of the fibrillar collagens, Journal of anatomy 190 (Pt 3)(Pt 3) (1997) 327-342, 10.1046/j.1469-7580.1997.19030327.x.

[68] L. Galatz, S. Rothermich, K. VanderPloeg, B. Petersen, L. Sandell, S. Thomopoulos, Development of the supraspinatus tendon-to-bone insertion: localized expression of extracellular

matrix and growth factor genes, Journal of orthopaedic research : official publication of the Orthopaedic Research Society 25(12) (2007) 1621-8, 10.1002/jor.20441.

[69] E. Zelzer, E. Blitz, M.L. Killian, S. Thomopoulos, Tendon-to-bone attachment: from development to maturity, Birth Defects Res C Embryo Today 102(1) (2014) 101-12, 10.1002/bdrc.21056.

[70] E. Blitz, S. Viukov, A. Sharir, Y. Shwartz, J.L. Galloway, B.A. Pryce, R.L. Johnson, C.J. Tabin, R. Schweitzer, E. Zelzer, Bone Ridge Patterning during Musculoskeletal Assembly Is Mediated through SCX Regulation of Bmp4 at the Tendon-Skeleton Junction, Developmental Cell 17(6) (2009) 861-873, 10.1016/j.devcel.2009.10.010.

[71] E. Blitz, A. Sharir, H. Akiyama, E. Zelzer, Tendon-bone attachment unit is formed modularly by a distinct pool of Scx- and Sox9-positive progenitors, Development 140(13) (2013) 2680-90, 10.1242/dev.093906.

[72] M.L. Killian, S. Thomopoulos, Scleraxis is required for the development of a functional tendon enthesis, FASEB J 30(1) (2016) 301-11, 10.1096/fj.14-258236.

[73] Y. Yoshimoto, A. Takimoto, H. Watanabe, Y. Hiraki, G. Kondoh, C. Shukunami, Scleraxis is required for maturation of tissue domains for proper integration of the musculoskeletal system, Sci Rep 7 (2017) 45010, 10.1038/srep45010.

[74] Y. Sugimoto, A. Takimoto, H. Akiyama, R. Kist, G. Scherer, T. Nakamura, Y. Hiraki, C. Shukunami, Scx+/Sox9+ progenitors contribute to the establishment of the junction between cartilage and tendon/ligament, Development 140(11) (2013) 2280-8, 10.1242/dev.096354.

[75] B.A. Pryce, S.S. Watson, N.D. Murchison, J.A. Staverosky, N. Dünker, R. Schweitzer, Recruitment and maintenance of tendon progenitors by TGFβ signaling are essential for tendon formation, Development 136(8) (2009) 1351, 10.1242/dev.027342.

[76] D.A. Ovchinnikov, J. Selever, Y. Wang, Y.T. Chen, Y. Mishina, J.F. Martin, R.R. Behringer, BMP receptor type IA in limb bud mesenchyme regulates distal outgrowth and patterning, Dev Biol 295(1) (2006) 103-15, 10.1016/j.ydbio.2006.03.013.

[77] A.M. Ho, P.C. Marker, H. Peng, A.J. Quintero, D.M. Kingsley, J. Huard, Dominant negative Bmp5 mutation reveals key role of BMPs in skeletal response to mechanical stimulation, BMC Dev Biol 8 (2008) 35-35, 10.1186/1471-213X-8-35.

[78] A.P. Breidenbach, L. Aschbacher-Smith, Y. Lu, N.A. Dyment, C.-F. Liu, H. Liu, C. Wylie, M. Rao, J.T. Shearn, D.W. Rowe, K.E. Kadler, R. Jiang, D.L. Butler, Ablating hedgehog signaling in tenocytes during development impairs biomechanics and matrix organization of the adult murine

patellar tendon enthesis, Journal of orthopaedic research : official publication of the Orthopaedic Research Society 33(8) (2015) 1142-1151, 10.1002/jor.22899.

[79] A.G. Schwartz, F. Long, S. Thomopoulos, Enthesis fibrocartilage cells originate from a population of Hedgehog-responsive cells modulated by the loading environment, Development (Cambridge, England) 142(1) (2015) 196-206, 10.1242/dev.112714.

[80] A.G. Schwartz, L.M. Galatz, S. Thomopoulos, Enthesis regeneration: a role for Gli1+ progenitor cells, Development 144(7) (2017) 1159, 10.1242/dev.139303.

[81] C.-F. Liu, A. Breidenbach, L. Aschbacher-Smith, D. Butler, C. Wylie, A Role for Hedgehog Signaling in the Differentiation of the Insertion Site of the Patellar Tendon in the Mouse, PLOS ONE 8(6) (2013) e65411, 10.1371/journal.pone.0065411.

[82] X. Chen, C.M. Macica, B.E. Dreyer, V.E. Hammond, J.R. Hens, W.M. Philbrick, A.E. Broadus, Initial characterization of PTH-related protein gene-driven lacZ expression in the mouse, J Bone Miner Res 21(1) (2006) 113-23, 10.1359/jbmr.051005.

[83] M. Wang, J.N. VanHouten, A.R. Nasiri, R.L. Johnson, A.E. Broadus, PTHrP regulates the modeling of cortical bone surfaces at fibrous insertion sites during growth, Journal of Bone and Mineral Research 28(3) (2013) 598-607, 10.1002/jbmr.1801.

[84] M. Wang, J.N. VanHouten, A.R. Nasiri, S.M. Tommasini, A.E. Broadus, Periosteal PTHrP regulates cortical bone modeling during linear growth in mice, Journal of anatomy 225(1) (2014) 71-82, 10.1111/joa.12184.

[85] X. Chen, C. Macica, A. Nasiri, S. Judex, A.E. Broadus, Mechanical Regulation of PTHrP Expression in Entheses, Bone 41(5) (2007) 752-759, 10.1016/j.bone.2007.07.020.

[86] Q. Wu, Y. Zhang, Q. Chen, Indian hedgehog is an essential component of mechanotransduction complex to stimulate chondrocyte proliferation, J Biol Chem 276(38) (2001) 35290-6, 10.1074/jbc.M101055200.

[87] N.C. Nowlan, P.J. Prendergast, P. Murphy, Identification of mechanosensitive genes during embryonic bone formation, PLoS Comput Biol 4(12) (2008) e1000250, 10.1371/journal.pcbi.1000250.

[88] I.E. Wang, J. Shan, R. Choi, S. Oh, C.K. Kepler, F.H. Chen, H.H. Lu, Role of osteoblast-fibroblast interactions in the formation of the ligament-to-bone interface, Journal of orthopaedic research : official publication of the Orthopaedic Research Society 25(12) (2007) 1609-20, 10.1002/jor.20475.

[89] J.O. Cooper, J.D. Bumgardner, J.A. Cole, R.A. Smith, W.O. Haggard, Co-cultured tissue-specific scaffolds for tendon/bone interface engineering, Journal of tissue engineering 5 (2014) 2041731414542294, 10.1177/2041731414542294.

[90] P. He, K.S. Ng, S.L. Toh, J.C. Goh, In vitro ligament-bone interface regeneration using a trilineage coculture system on a hybrid silk scaffold, Biomacromolecules 13(9) (2012) 2692-703, 10.1021/bm300651q.

[91] I. Calejo, R. Costa-Almeida, A.I. Gonçalves, D. Berdecka, R.L. Reis, M.E. Gomes, Bi-directional modulation of cellular interactions in an in vitro co-culture model of tendon-to-bone interface, Cell proliferation 51(6) (2018) e12493-e12493, 10.1111/cpr.12493.

[92] S.S. He P.F., Goh J.C., Toh S.L. , Establishing a Coculture System for Ligament-Bone Interface Tissue Engineering. In: Lim C.T., Goh J.C.H. (eds) 13th International Conference on Biomedical Engineering. IFMBE Proceedings, vol 23. Springer, Berlin, Heidelberg, (2009)

[93] Y. Mifune, T. Matsumoto, S. Ota, M. Nishimori, A. Usas, S. Kopf, R. Kuroda, M. Kurosaka, F.H. Fu, J. Huard, Therapeutic potential of anterior cruciate ligament-derived stem cells for anterior cruciate ligament reconstruction, Cell transplantation 21(8) (2012) 1651-65, 10.3727/096368912x647234.

[94] H.K. Min, S.H. Oh, J.M. Lee, G.I. Im, J.H. Lee, Porous membrane with reverse gradients of PDGF-BB and BMP-2 for tendon-to-bone repair: in vitro evaluation on adipose-derived stem cell differentiation, Acta Biomater 10(3) (2014) 1272-9, 10.1016/j.actbio.2013.12.031.

[95] M. Kosaka, J. Nakase, K. Hayashi, H. Tsuchiya, Adipose-Derived Regenerative Cells Promote Tendon-Bone Healing in a Rabbit Model, Arthroscopy : the journal of arthroscopic & related surgery : official publication of the Arthroscopy Association of North America and the International Arthroscopy Association 32(5) (2016) 851-9, 10.1016/j.arthro.2015.10.012.

[96] R. McGoldrick, A. Chattopadhyay, C. Crowe, G. Chiou, K. Hui, S. Farnebo, C. Davis, A. Le Grand, M. Jacobs, H. Pham, J. Chang, The Tissue-Engineered Tendon-Bone Interface: In Vitro and In Vivo Synergistic Effects of Adipose-Derived Stem Cells, Platelet-Rich Plasma, and Extracellular Matrix Hydrogel, Plastic and reconstructive surgery 140(6) (2017) 1169-1184, 10.1097/prs.0000000000003840.

[97] E.D. Silva, P.S. Babo, R. Costa-Almeida, R.M.A. Domingues, B.B. Mendes, E. Paz, P. Freitas, M.T. Rodrigues, P.L. Granja, M.E. Gomes, Multifunctional magnetic-responsive hydrogels to engineer tendon-to-bone interface, Nanomedicine : nanotechnology, biology, and medicine 10.1016/j.nano.2017.06.002 (2017) 10.1016/j.nano.2017.06.002.

[98] S.K. Madhurakkat Perikamana, J. Lee, T. Ahmad, E.M. Kim, H. Byun, S. Lee, H. Shin, Harnessing biochemical and structural cues for tenogenic differentiation of adipose derived stem cells (ADSCs) and development of an in vitro tissue interface mimicking tendon-bone insertion graft, Biomaterials 165 (2018) 79-93, 10.1016/j.biomaterials.2018.02.046.

[99] L.A. Solchaga, K.J. Penick, J.F. Welter, Chondrogenic differentiation of bone marrow-derived mesenchymal stem cells: tips and tricks, Methods in molecular biology (Clifton, N.J.) 698 (2011) 253-278, 10.1007/978-1-60761-999-4_20.

[100] A. Kwon, Y. Kim, M. Kim, J. Kim, H. Choi, D.W. Jekarl, S. Lee, J.M. Kim, J.-C. Shin, I.Y. Park, Tissue-specific Differentiation Potency of Mesenchymal Stromal Cells from Perinatal Tissues, Scientific Reports 6(1) (2016) 23544, 10.1038/srep23544.

[101] B.A. Bunnell, M. Flaat, C. Gagliardi, B. Patel, C. Ripoll, Adipose-derived stem cells: isolation, expansion and differentiation, Methods 45(2) (2008) 115-20, 10.1016/j.ymeth.2008.03.006.

[102] A.I. Gonçalves, M.T. Rodrigues, S.J. Lee, A. Atala, J.J. Yoo, R.L. Reis, M.E. Gomes, Understanding the role of growth factors in modulating stem cell tenogenesis, PLoS One 8(12) (2013) e83734, 10.1371/journal.pone.0083734.

[103] K.B. Jonsson, A. Frost, O. Nilsson, S. Ljunghall, Ö. Ljunggren, Three isolation techniques for primary culture of human osteoblast-like cells: A comparison, Acta Orthopaedica Scandinavica 70(4) (1999) 365-373, 10.3109/17453679908997826.

[104] M. Vigano, C. Perucca Orfei, A. Colombini, D. Stanco, P. Randelli, V. Sansone, L. de Girolamo, Different culture conditions affect the growth of human tendon stem/progenitor cells (TSPCs) within a mixed tendon cells (TCs) population, J Exp Orthop 4(1) (2017) 8, 10.1186/s40634-017-0082-8.

[105] I. Nagura, T. Kokubu, Y. Mifune, A. Inui, F. Takase, Y. Ueda, T. Kataoka, M. Kurosaka, Characterization of progenitor cells derived from torn human rotator cuff tendons by gene expression patterns of chondrogenesis, osteogenesis, and adipogenesis, Journal of Orthopaedic Surgery and Research 11(1) (2016) 40, 10.1186/s13018-016-0373-2.

[106] L. Ruzzini, F. Abbruzzese, A. Rainer, U.G. Longo, M. Trombetta, N. Maffulli, V. Denaro, Characterization of age-related changes of tendon stem cells from adult human tendons, Knee Surg Sports Traumatol Arthrosc 22(11) (2014) 2856-66, 10.1007/s00167-013-2457-4.

[107] L. Yao, C.S. Bestwick, L.A. Bestwick, N. Maffulli, R.M. Aspden, Phenotypic drift in human tenocyte culture, Tissue engineering 12(7) (2006) 1843-9, 10.1089/ten.2006.12.1843.

[108] J. Kohler, C. Popov, B. Klotz, P. Alberton, W.C. Prall, F. Haasters, S. Muller-Deubert, R. Ebert, L. Klein-Hitpass, F. Jakob, M. Schieker, D. Docheva, Uncovering the cellular and molecular changes in tendon stem/progenitor cells attributed to tendon aging and degeneration, Aging Cell 12(6) (2013) 988-99, 10.1111/acel.12124.

[109] H. Utsunomiya, S. Uchida, I. Sekiya, A. Sakai, K. Moridera, T. Nakamura, Isolation and characterization of human mesenchymal stem cells derived from shoulder tissues involved in rotator cuff tears, Am J Sports Med 41(3) (2013) 657-68, 10.1177/0363546512473269.

[110] P.P. Lui, Markers for the identification of tendon-derived stem cells in vitro and tendon stem cells in situ - update and future development, Stem Cell Res Ther 6 (2015) 106, 10.1186/s13287-015-0097-y.

[111] Y. Mifune, T. Matsumoto, K. Takayama, S. Terada, N. Sekiya, R. Kuroda, M. Kurosaka, F.H. Fu, J. Huard, Tendon graft revitalization using adult anterior cruciate ligament (ACL)-derived CD34+ cell sheets for ACL reconstruction, Biomaterials 34(22) (2013) 5476-87, 10.1016/j.biomaterials.2013.04.013.

[112] T.F. Huang, Y.T. Chen, T.H. Yang, L.L. Chen, S.H. Chiou, T.H. Tsai, C.C. Tsai, M.H. Chen, H.L. Ma, S.C. Hung, Isolation and characterization of mesenchymal stromal cells from human anterior cruciate ligament, Cytotherapy 10(8) (2008) 806-14, 10.1080/14653240802474323.

[113] A.F. Steinert, M. Kunz, P. Prager, T. Barthel, F. Jakob, U. Nöth, M.M. Murray, C.H. Evans, R.M. Porter, Mesenchymal stem cell characteristics of human anterior cruciate ligament outgrowth cells, Tissue Eng Part A 17(9-10) (2011) 1375-88, 10.1089/ten.TEA.2010.0413.

CHAPTER 3. Enthesis Tissue Engineering:

Biological, Biochemical and Biophysical (3B's) strategies

This chapter was based on the following publication:

I. Calejo, R. Costa-Almeida, M. E. Gomes (2019) Enthesis tissue engineering: biological requirements meet at the interface. *Tissue Engineering Part B Reviews.* DOI: 10.1089/ten.TEB.2018.0383.

ABSTRACT

The tendon-bone interface (enthesis) exhibits a complex multi-scale architectural and compositional organization maintained by a heterogeneous cellular environment. Orthopedic surgeons have been facing several challenges when treating tendon pullout or tear from the bony insertion due to unsatisfactory surgical outcomes and high re-tear rates. The limited understanding of enthesis hinders the development of new treatment options toward enhancing regeneration. Mimicking the natural tissue structure and composition is still a major challenge to be overcome. Therefore, it is of major importance to deeply investigate the tendon-to-bone biology toward establishing foundational expertise and integrate cues from the native niche into novel biomaterial engineering, aiming at moving today's research advances into tomorrow's regenerative therapies.

In this chapter, we critically assess current tendon-to-bone interface tissue engineering strategies through the use of biological, biochemical or biophysical cues, which must be ultimately combined into sophisticated gradient systems. Cellular strategies are described, focusing on cell sources and co-cultures to emulate a physiological heterotypic niche, as well as hypoxic environments, alongside with growth factor delivery and the use of platelet-rich hemoderivatives. Biomaterials design considerations are revisited, highlighting recent progresses in tendon-to-bone scaffolds. Mechanical loading is addressed to uncover prospective engineering advances. Finally, research challenges and translational aspects are considered.

Keywords: 2D vs 3D culture, Cell-based strategies; Gradient Biomaterials; Growth factors; Tendon-to-bone interface; Tissue Engineering.

3.1. INTRODUCTION TO ENTHESIS TISSUE ENGINEERING

Soft-to-hard tissue interfaces, such as tendon-to-bone insertions, are compelled to deal with large mismatch mechanical needs of two widely different tissues and, therefore, known to be under increased failure chances. Orthopedic surgeons frequently face the challenge of torn enthesis, partial or complete rupture of tendons and ligaments and bone avulsions. Statistically, 20%-80% of the general population above 50 to 80 years has been diagnosed with a rotator cuff tear [1]. Similarly, younger patients are affected by acute or overuse sports injuries, such as tennis and golfer's elbow, jumper's knee and Achilles insertional tendinopathies [2, 3]. Nevertheless, the enthesis can also be affected by extrinsic and intrinsic factors (such as trauma, systemic illness, age-related degeneration or pharmacotherapy) resulting in general insertional disorders, known as enthesopathies, and/or enthesitis, if an inflammatory process is involved [4]. Current methods to manage enthesis pathologies include, in a first approach, conservative treatments (e.g., rest, mechanical conditioning, corticosteroids injection, orthotics, among others) normally with limited success, or surgical interventions through the routine application of grafts (auto-, allo- and synthetic grafts). However, surgical repair still presents several major problems, including tissue harvesting, host tissue reaction, risk of disease transmission, slow or lack of tissue integration and donor tissue availability [5, 6]. Additionally, following repair, grafts are associated with high recurrence rates due to formation of neo-fibrovascular tissue, compromising the stability and consequently mechanical performance of the newly formed tissue [6, 7]. As a result, high probability of re-injury, deformation, pull-out and long rehabilitation periods are associated with these common surgical procedures [6, 8]. Thus, given the importance of this interface within the skeleton and all the clinical challenges concerning its repair, there is a crucial need to regenerate this critical soft-to-hard tissue transition.

In the past decades, enthesis tissue engineering arised aiming at the recreation of complex and hierarchical interfacial tissue in order to repair or to regenerate diseased or damaged junctions [9]. Many attempts have been made to improve the repair and ultimately regenerate the tissue but challenges still exist toward mimicking the micro- and nanostructure of the native interface, as well as replicating the spatial distribution of signaling factors and cellular interactions, which are essential for a normal interfacial function and homeostasis [10, 11]. A variety of interdependent tissue engineered strategies have been proposed over the years [12-14] and can be roughly grouped into four connected categories: (1) scaffold-based strategies, (2) cell-based strategies, (3) growth factors and gene therapy and, finally, (4) mechanical stimulation. However, up to now, the existing challenges faced in the clinics, when trying to restore musculoskeletal interfaces functionality, including graft laxity and inferior mechanical properties associated with a lack in the identification of appropriate healing factors and time of administration at the

repair site, have led to a preference toward stem cell-mediated treatments, due to their regenerative and differentiation potential as Nature tissue engineers.

As cells are the major players in orchestrating tissue regeneration, in this chapter, we will discuss current cell- and material-based strategies with and without biomaterial constructs for tendon-to-bone repair. In light of this, cellular/biological, biochemical and biophysical components (Figure 3.1) will be discussed. Instead of extensively analyzing currently explored strategies, this review intends to collect insights illustrating the usefulness of different approaches and highlight main challenges and prospective successes.

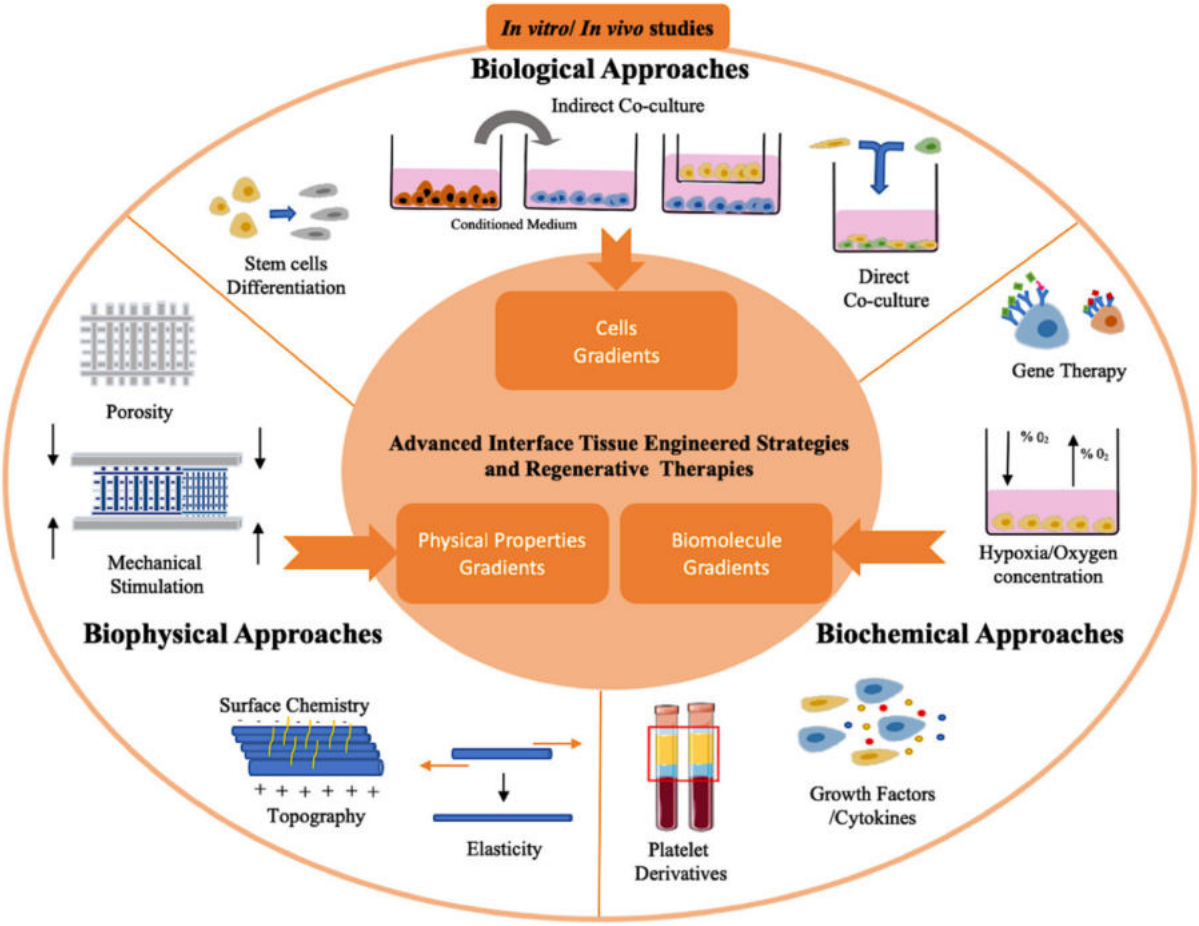

Figure 3.1 | Schematic representation of biological, biophysical and biochemical components for enthesis tissue engineering and regenerative strategies.

3.2. MULTI-SCALE STRUCTURAL AND COMPOSITIONAL ORGANIZATION

The enthesis is a musculoskeletal structure that allows a smooth transition between two widely different tissues, displaying a gradient in composition, tissue organization and, therefore, mechanical properties. Hence, this interface displays a unique microenvironment, which maintains specific cellular phenotypes

throughout different localizations within the tissue, playing an important role in its composition, maintenance and regeneration. A close look reveals a well-organized structure with spatiotemporal distribution of extracellular proteins and biochemical signals produced by distinct cell populations that work in synchrony to enable the biological function of the whole tissue (Figure 3.2). For instance, besides matrix mineralization increase along the interface, a gradient in collagen fibers orientation is observed from the tendon (fiber alignment) to bone. This allows the mitigation at the interface of stress concentrations [15]. Moreover, the collagen fibrils mineral arrangement, either extrafibrillar or intrafibrillar, leads to a controlled and graded increase of stiffness, resulting in a smooth load transfer [16] (Figure 3.3).

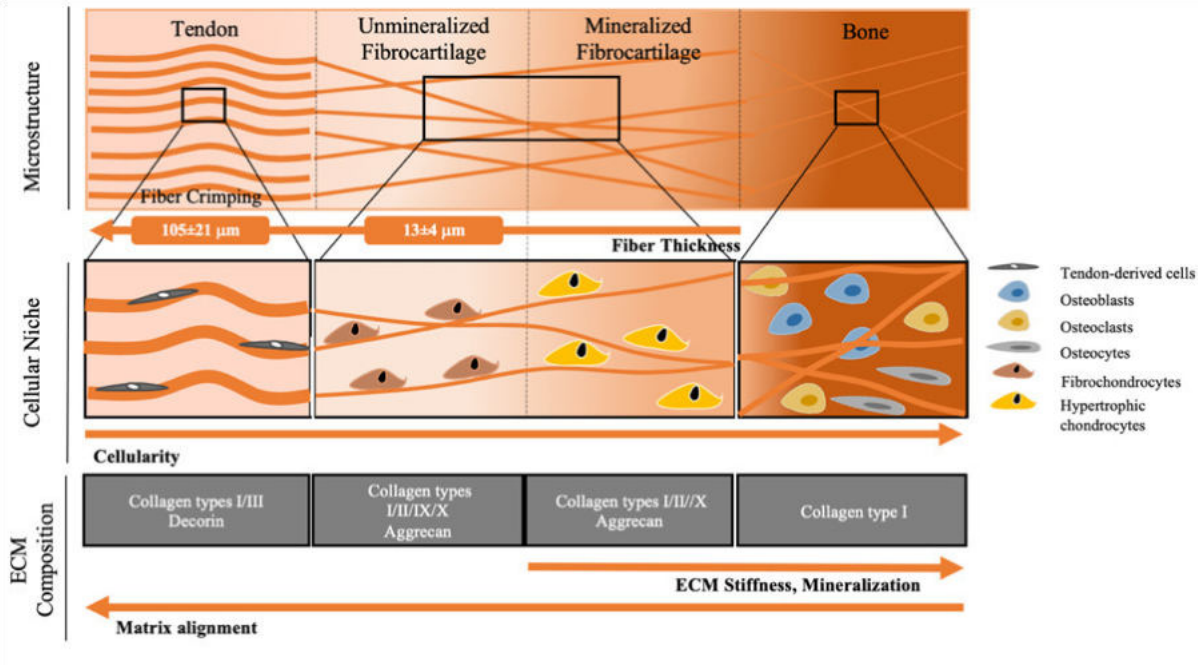

Figure 3.2 | Structure and composition of tendon-to-bone interface. Values of mean fiber diameter were obtained from Rossetti et al. [17].

Interestingly, the fibrocartilaginous insertion is regarded as avascular and aneural recalling the nature of articular cartilage [18], which can be explained by the levels of compression it is subjected to or by the presence of aggrecan, known by its axonal growth inhibitory effect in the nervous system [19]. However, tissue microdamage is very common to occur and appears to be responsible for vessel ingrowth, thus leading to immune cells infiltration and the onset of inflammatory events [20]. Moreover, the presence of vessels and nerve ingrowth have been also reported in enthesis of elderly human Achilles tendons as a consequence of degenerative changes [21]. Therefore, altered vascularity may provide an anatomic

explanation for enthesis-related diseases and damage. Additionally, many fibrocartilage sites present fat pad near the insertion site which, in combination with the bursa, serve to promote frictionless movements, being these movements compromised in patients with entheseal degenerative diseases [22, 23]. Nevertheless, fat pad present other functions in the enthesis such as proprioceptive function in monitoring changes in the insertional angle, immune function due to its rich macrophage population and source of pain in enthesopathies [18].

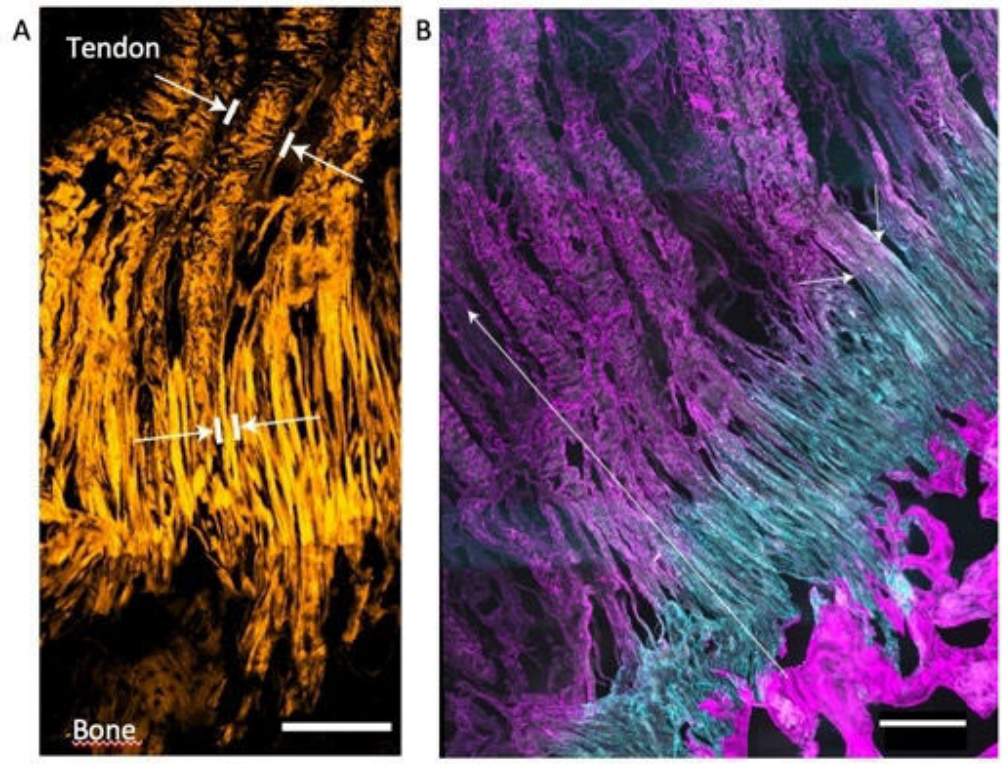

Figure 3.3 | The structure and collagen composition of tendon-to-bone attachment. (A) Confocal reflection microscopy image of enthesis cryosection demonstrating that tendon fibers unravel into thinner fibers at the interface preceding bone attachment. Scale bar, 250 μm. (B) Confocal image immunostained for collagen type I (magenta) and collagen type II (cyan) showing a fiber composition change at ~500 μm before reaching the bone. Scale bar, 300 μm. From Rossetti et al. [17]. All rights reserved Copyright © 2017, Springer Nature.

When trying to mimic the native tissue, one of the major challenges is the replication of all the structural features of the enthesis, as well as meeting the specific requirements for each cell type. Although tendon and bone exhibit their own cellular niche and cell populations, cells residing at the enthesis present distinctive features. Therefore, it is important to develop tissue engineered constructs that not only

support the deposition and formation of compositionally different tissues in an organized, continuous and graded manner but also sustain a spatially varying cellular content, which play a critical role in orchestrating the formation and repair of interfacial tissues.

3.3. CELL-BASED STRATEGIES

3.3.1. GENERAL CONSIDERATIONS

Cell-based strategies for tendon-to-bone interface face some challenges due to the complexity of the cellular environment, tissue vascularization and oxygen tension, and different mechanical requirements associated with the distinct tissues.

The search for a single cell source or the use of mixed cultures along with the determination of adequate cell ratios are being explored. In particular, the use of co-cultured cells has shown promising outcomes while trying to overcome the limitations associated with the mimicry of the heterotypic communications occurring within the native junction. However, many challenges still have to be addressed before stem cells, or even terminally differentiated cells, can break the barrier between the laboratory and the clinics. There is still a real need to evaluate the efficacy of cells and cell-based products in long-term safety and well controlled tendon-to-bone healing animal models. Therewithal, it is important to have in mind that, even though evidences show a substantial development in cell-based therapies and these are recognized as new biotechnological innovations, the translation to the clinical environment still faces very strict and complex global regulatory issues [24].

In the following sections, recent advances regarding cell- and culture-based strategies for tendon-to-bone regeneration will be further illustrated and discussed in detail.

3.3.2. CELL SOURCES FROM STEM CELLS TO TERMINALLY DIFFERENTIATED CELLS

Stem cells, normally from mesenchymal origin, are widely used in interfacial tissue engineering. These cells can be isolated from a wide number of human tissues (including bone, tendon, cartilage, ligament, adipose, synovial), have self-replication capability and are able to differentiate toward mature cells of different lineages such as tendon, bone and cartilage [25]. Several studies have demonstrated an improvement in tendon-to-bone healing and mechanical properties after transplantation of bone marrow mesenchymal stem cells [26-28]. Still, other stem cell sources have been exploited for tendon-to-bone healing, mainly in animal models.

An interesting example is the emerging use of ACL-derived stem cells. These cells have been isolated from ACL and exhibit stem cell properties, such as clonogenicity, self-renewal and multidifferentiation capability [29]. Recently, ACL-derived $CD34^+$ stem cells were identified in injured ACL tissues, displaying higher expansion and multidifferentiation potential [30]. The efficacy of these cells has been tested on tendon-to-bone healing. Injections of adult human ACL-derived $CD34^+$ stem cells into nude mice after ACL reconstruction resulted in an increased number of fibrocartilage cells, enhanced angiogenesis and osteogenesis in the presence of CD34+ cells and non-sorted cells in comparison with control groups (PBS and $CD34^-$ groups) and similar failure load as uninjured ACL [31]. However, migration of cells to other tissues was reported. Alternatively, the use of cell sheet technology by incorporating ACL-derived $CD34^+$ in a cell sheet wrapped tendon graft demonstrated the potential application of these cells in ACL reconstruction and recovery [32]. This strategy resulted in *ex vivo* gradual cell migration within grafted tendon and bone tunnel site, as well as *in vivo* promotion of angiogenesis and osteogenesis, together with accelerated early remodeling observed by the faster recovery time, graft maturation and biochemical strength [32].

Tendon-derived stem cells have also demonstrated great potential to form enthesis-like tissues, alone or in the presence of a carrier. *In vivo* studies, including treatment with BMP-2 and subcutaneous transplantation in immunocompromised mice [33] or even incorporation in knitted silk-collagen sponge scaffold for rotator cuff regeneration in a rabbit model [34], led to improved mechanical and structural properties in comparison with controls and possible formation of a osteotendinous-like tissue [33, 34]. Even though TDSCs and ACL-derived stem cells seem to constitute promising cell types for tendon-to-bone junction regeneration, donor site morbidity, cell number and the need for long expansion periods together with consequent phenotypic drift are still a limiting factor for future clinical applications [35]. Furthermore, the impracticality of isolating these stem cell populations for further exogenous applications still poses a limiting step owing to the need for invasive collection procedures.

Alternatively, synovial mesenchymal stem cells (sMSCs) and periosteum-derived stem cells (PDSCs) have been reported in the literature as reliable cell populations for tendon-to-bone healing [36] [37, 38]. Although there is still a limited number of studies, some encouraging outcomes have been reported. For example, *in vivo* injection of sMSCs in a bone tunnel enhanced the production of collagen fibers and Sharpey's fibers between tendon and bone [38]. However, after 4 weeks, bone and tendon were attached together, without the presence of sMSCs or the formation of a fibrocartilage transition region [38]. In this case, even though these cells have shown an effective potential to improve tissue healing, they failed in the regeneration of the proper tissue. On the other hand, PDSCs are progenitor cells found in the inner

layer of the periosteum with the capability to differentiate, under appropriate stimulus, toward de chondrogenic and osteogenic lineages [39, 40]. The combination of these cells along with the appropriate stimulus, e.g. growth factors, has been applied to enhance tendon-to-bone healing. Injectable hydrogels containing PDSCs and BMP-2 were reported to have a strong inductive ability along with an enhanced tendon-to-bone healing at 8 weeks postoperatively through the formation of fibrocartilage in a rabbit rotator cuff healing model [36]. More recently, PDSCs cell sheets were evaluated in a rabbit extra-articular bone tunnel model. Results demonstrated enhanced deposition of collagen and glycosaminoglycans with fibrocartilage formation at 4 weeks postoperatively, showing the promising application of periosteum-derived cells monolayer in tendon-to-bone healing [37]. But the question still remains in the isolation method and either or not a mixture of cells is obtained from the different layers of the periosteum, and in the limited differentiation capability demonstrated by clonal cultures of periosteum-derived cells [41].

A well-known alternative is the use of ASCs. This stem cell population is more readily accessible from adipose tissue through a minimally invasive method, providing higher yield and lower morbidity and pain, as well as higher proliferation rate and lower senescence upon *in vitro* expansion [42]. Recent studies have also demonstrated the feasibility of using ASCs and ASCs subpopulations for the generation of tendon- [43-45], bone- [46, 47, 48 and cartilage-like tissues {Popa, 2016 #351, 49, 50] and the potential use of ASCs for tendon-to-bone regeneration has been under study [27, 51-54]. A recent report by Kosaka et al. [27], where ASCs were locally injected in a rabbit ACL reconstruction model, demonstrated a temporal improvement of tendon-to-bone integration with the appearance of a more organized and cartilaginous-like tissue in the ASCs-treated group, accompanied by a significantly better failure load 2 and 4 weeks after surgery, in comparison to controls [27]. Additionally, ASCs multilineage differentiation potential has been also demonstrated after seeding onto a micropore surface of a porous membrane with a dual reverse gradient of growth factors concentrations (PDGF-BB gradient from the left to right side of the membrane and BMP-2 gradient from the right to left side) to generate a tendon-to-bone like construct [52]. This strategy allowed a spatially modulated differentiation of ASCs toward tenogenic and osteogenic lineages according to the gradient of growth factor concentration along the construct.

Rather than applying a multipotent cell source, the interposition of chondrocytes between two tissues (tendon and bone) to mimic the cellular environment found in the native niche, has shown great promise in tissue engineering. In a rabbit partial patellectomy model, Wong et al. investigated the use of an allogeneic chondrocyte pellet in restoring the transitional fibrocartilage and tendon-to-bone healing, demonstrating an early integration and formation of a fibrocartilage-like zone, without immune rejection, suggesting a possible stimulatory effect of these cells [55]. Comparably, Nourissat et al. [56] studied the

ability of chondrocytes to restore the normal function of tendon-to-bone while comparing it with the ability of BMSCs. An Achilles tendon repair model was induced in rats by destroying the enthesis; afterwards chondrocytes and BMSCs were injected and the healing rate, tissue remodeling and biomechanical load were assessed [56]. The injection of both cell types resulted in the production of enthesis-like tissue as soon as 15 days, which was not observed in control groups (not injected rats) [56]. However, only MSCs-injected were able to recapitulate the enthesis organization with columnar chondrocytes as observed in uninjured tissues [56]. Nonetheless, the ability of chondrocytes to improve tendon-to-bone healing is still relatively unexplored.

As said before, several cell sources are being explored to restore the normal function of tendon-to-bone interface through the improvement of fibrocartilage formation and enhancement of mechanical properties. The use of stem cells for tendon-to-bone interface tissue engineering presents several advantages compared to terminally differentiated cells. Multipotent stem cells can be expanded until a sufficient number for transplantation is achieved, whereas terminally differentiated cells present limited expansion, and can be induced to differentiate into the distinct phenotypes found at the enthesis. Moreover, a lack of immunological reaction, together with their capability to "empower" other cell types residing at the injured tissue makes them an optimal option while trying to be incorporated *in vivo*.

3.3.3. CO-CULTURE SYSTEMS

The use of novel multi-cell type co-culture systems can substantially facilitate the formation of transition regions of the tendon-to-bone interface, while giving better insights about the developmental process of enthesis insertion site.

Generally, culture systems can be divided in 2D or 3D [57]. Particularly, co-culture systems can be further divided into direct and indirect contact co-cultures (Figure 3.1). Direct contact co-cultures are based on cell-cell interactions, paracellular diffusion of paracrine factors and also cell-ECM communication [57]. On the other hand, in indirect contact or noncontact co-cultures, cells are separated by a porous membrane (normally a transwell), thus only the culture medium is shared, allowing the study of paracrine interactions between different cell populations [57]. Other approaches are based on conditioned media from one type of cells that can be used to culture other type of cells, and even the use of decellularized matrices [58]. These strategies can be applied to assess the effect of paracrine factors without the need of pre-labelling the different cell populations [58]. In interface tissue engineering, usually two types of strategies are applied: co-culture of terminally differentiated cells and co-culture of terminally

differentiated cells with stem cells [57]. Table 3.1 highlights main outcomes regarding 2D and 3D co-culture systems for tendon-to-bone tissue engineering and regenerative medicine applications.

Table 3.1 | Examples of co-culture systems for tendon-to-bone TERM applications.

	In vitro/ In vivo	**Cell types**	**Culture system**	**Main outcomes**	**References**
Differentiated cells only	*In vitro*	• Fibroblasts (ligament/tendon) • Osteoblasts	2D using a spacer until confluent	• After 14 days, 3 regions were distinguished: fibroblasts, fibroblasts plus osteoblasts (interface) and osteoblasts; • Presence of osteoblasts induced ALP activity and mineralization by fibroblasts; • Higher transcription levels of collagen type II, aggrecan (*ACAN*) and cartilage oligomeric matrix protein (*COMP*) at the interface	[59]
			3D triphasic scaffold with cells seeded at different extremities	• Fibroblasts-osteoblasts interaction in phase B of the scaffold (interface); • Higher ALP activity and mineralization by osteoblasts in phase C (hard tissue); • Higher collagen type I expression by fibroblasts (phase A)	[60]
		• Fibroblasts (NIH 3T3 line) • Osteoblasts (MC 3T3)	3D scaffolds with cells seeded at different extremities	• The use of 3 mM beta-glycerophosphate (βGP), and 25 μg/mL ascorbic acid (AA) reduced fibroblasts mineralization while enhancing osteoblasts response; • Deposition of collagen and glycosaminoglycan at the interface	[61]

	In vivo	• Fibroblasts (ligament/tendon) • Chondrocytes • Osteoblasts	3D triphasic scaffolds	• Deposition of collagenous-rich matrix in all phases; • Higher deposition of collagen type III by fibroblasts (phase A); • Deposition of collagen types I, II and X phase B by chondrocytes; • Mineralization confinement in phase C (osteoblasts);	[62]
Differentiated cells with stem cells	*In vitro*	• Fibroblasts • BMSCs • Osteoblasts	2D tri-culture using an agarose gel to embed cells (middle)	• Gene expression of proteoglycans, collagen type I and II by BMSCs; • Conditioned medium of fibroblasts and osteoblasts decreased proliferation, glycosaminoglycan deposition and ALP activity by BMSCs • Conditioned media from fibroblasts-osteoblasts contact cultures promoted proteoglycan and TGF-ß1 synthesis and expression of SOX9 in BMSCs; • The presence of TGF-ß3 supplementation in co-cultured BMSCs resulted in delayed mineralization	[63]
			3D knitted scaffolds	• Direct interaction between BMSCs with fibroblasts and osteoblasts resulted in gradual mineral deposition; • Up-regulation of collagen type II, SOX9 and aggrecan genes in co-cultures in comparison with BMSCs monoculture	[64]
		• Tendon-derived stem cells (TDCs)	2D direct co-culture system	• Phenotype of single cultures maintained using an intermediate medium condition containing osteogenic and basal medium (1:1 ratio);	[65]

		• Osteogenically induced ASCs (pre-osteoblasts)	• Higher expression of *OPN* and *RUNX2* in co-culture in comparison with single cultures of pre-osteoblasts; • Increased expression of ACAN and COMP in co-culture

***Abbreviations**: ACAN – Aggrecan; ALP - Alkaline phosphatase; ASCs – Adipose-derived stem cells; BMSCs – Bone marrow stem cells; COMP – Cartilage-oligomeric matrix protein; TDCs – Tendon-derived stem cells; TGF-β1/3 – Transforming growth factor – beta 1/3; SOX9 – SRY-box9*

The role of stem cells in these systems goes beyond their multidifferentiation capacity. Normally, in co-cultures, stem cells are the target cells to differentiate and eventually synthetize ECM or metabolites favorable to a tissue. The employment of co-cultures using terminally differentiated cells with stem cells underwent significant advances in the last years. However, even though exogenous factors are applied to induce a more controlled cellular response, the crosstalk between the different cell types turns this phenomenon more complex than it was initially believed. Therefore, novel co-culture strategies based on the manipulation of the *in vitro* supplementation to modulate the communication occurring between these cell types is of major importance.

3.3.3.1. *Co-cultures using terminally differentiated cells*

In the field of tendon-to-bone tissue engineering, there are few studies reporting the use of co-culture systems for tendon-to-bone regeneration. Wang et al. [59] studied the interactions occurring between osteoblasts and ligament fibroblasts using a direct contact co-culture model. Primary osteoblasts and fibroblasts, obtained from trabecular bone fragments and ACL, respectively, were first seeded using 1:1 ratio in a tissue culture plate separated by a hydrogel divider to mimic the interface region, which upon confluency, was removed, allowing cells to migrate and interact directly (Figure 3.4 A-B). Cells were pre-labelled to control cell migration and subsequent interactions. After 14 days, three regions could be distinguished: fibroblasts, fibroblasts plus osteoblasts (interface) and osteoblasts [64], demonstrating the effectiveness of direct cell-cell physical contact in the establishment of different regions. ALP activity and mineralization by fibroblasts seemed to be influenced by the presence of osteoblasts, suggesting that osteoblast–fibroblast interactions may lead to fibroblasts trans-differentiation {Wang, 2007 #178} (Figure 3.4 C-E). Furthermore, at the gene level, an up-regulation of collagen type II, aggrecan (*ACAN*) and cartilage-oligomeric protein (*COMP*), interface-relevant markers, was observed in the interface region, in comparison with the regions containing only osteoblasts or fibroblasts [59]. Despite these interesting results regarding the expression of interface-related markers, using only terminally differentiated cells was not proven to be sufficient to trigger the formation of an interface-like region *in vitro* [59]. Interestingly, another approach by Cooper et al. [61] demonstrated the importance of medium supplementation for an appropriate matrix deposition in a multiphased co-culture setup. In this case, cell lines of NIH 3T3 fibroblasts and MC 3T3 osteoblasts were used and the medium supplemented with 3 mM βGP and 25 μg/mL AA to reduce fibroblasts mineralization while enhancing the osteoblasts response.

Overall, co-culture studies using terminally differentiated cells can represent simplified *in vitro* models of native tissue physiology. Altogether, these results have shown that the crosstalk between fibroblasts and

osteoblasts, representing tendon and bone cellular environments, respectively, can induce phenotypic alterations, particularly through fibroblast mineralization. Nonetheless, this constitutes a less controlled response given that these systems frequently require the use of cell-specific conditions or additional supplementation, challenging tissue engineering protocols.

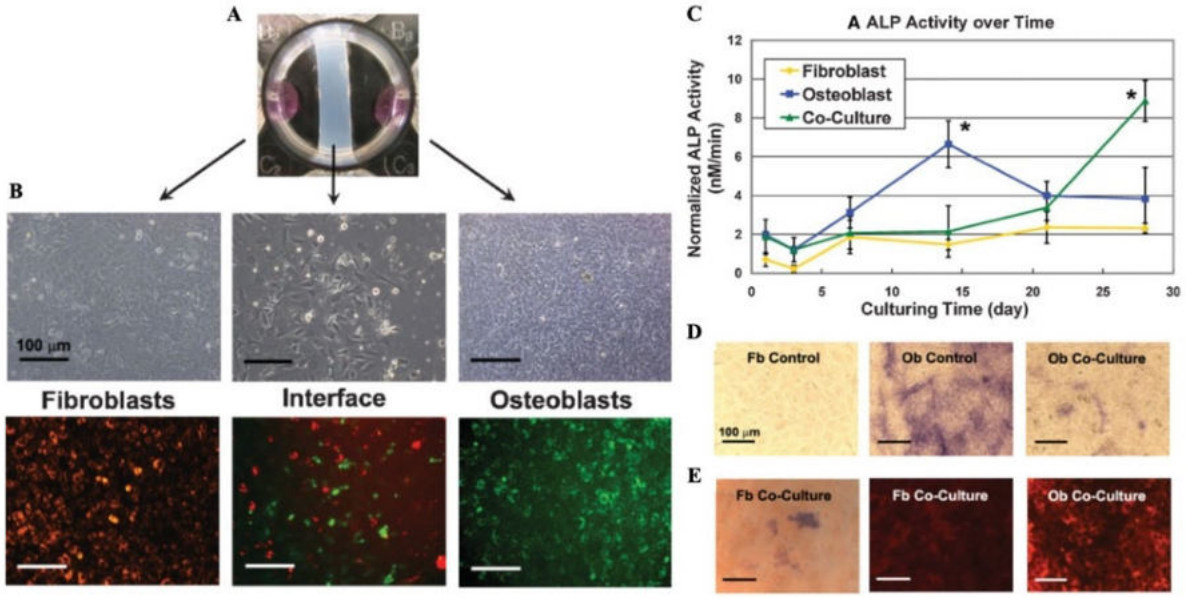

Figure 3.4 | Co-culture setup of fibroblasts and osteoblasts and effect on alkaline phosphatase activity. (A) Co-culture system using a hydrogel divider; (B) Light microscopy and fluorescence images of the three different regions. Fibroblasts are shown in red and osteoblasts in green after 14 days of culture. (C) Normalized ALP activity over time in culture revealed an increase in ALP levels in co-culture. * denotes significance at $p<0.05$. (D) Fast-Blue staining for ALP of the co-cultured osteoblasts and the correspondent control groups (fibroblasts and osteoblasts) and (E) fluorescence tracking of osteoblasts (CM-DiI) demonstrated an ALP positive staining of fibroblasts in the co-cultured well. Adapted from Wang et al. [59].

3.3.3.2. *Co-culture of terminally differentiated cells with stem cells*

Alternatively, to the sole use of differentiated cells, the crosstalk between these and stem cells has been increasingly exploited under the rationale that the intricate communication occurring within these systems will ultimately lead to stem cell differentiation into relevant phenotypes. In turn, stem cells are expected to contribute with key signaling molecules, "empowering" native cell populations. In this context, a tri-culture model has been developed using primary fibroblasts and osteoblasts in combination with BMSCs; cells were seeded in opposing sides of the tissue culture well and fibroblasts or BMSCs embedded in an

agarose-gel and placed in the middle region of the plate, allowing for individual analysis [61]. Additionally, the effect of fibroblasts-osteoblasts physical contact on BMSCs differentiation was studied using a mixture of fibroblasts-osteoblasts (1:1 ratio) in both sides of the agarose gel, resulting in three different regions: fibroblasts-osteoblasts, BMSCs and fibroblasts-osteoblasts [61]. Interestingly, in contrast to fibroblasts, BMSCs in tri-culture were found to express interface-relevant markers (such as proteoglycans, as well as collagen types I and II at the gene level) throughout time in culture [61]. Matrix mineralization potential was reduced, but BMSCs exhibited higher ALP activity in comparison with fibrochondrocytes and fibroblasts; and, in contrast to ALP activity in tri-culture, the highest ALP activity was delayed in time suggesting an enzyme suppression, resulting from osteoblasts-fibroblasts interaction [61]. Moreover, gene expression of *SOX9*, collagen type II and production of proteoglycans was significantly up-regulated in the mixed tri-culture demonstrating an important role of cell-cell communication in BMSCs differentiation toward fibrochondrogenic phenotype [61]. Together, these results support the hypothesis that the direct crosstalk between differentiated and stem cells within the system can potentiate fibrochondrogenic commitment characteristic of the chondrocyte-like phenotype observed for native enthesis cells [66]. Furthermore, conditioned media from parallel cultures of fibroblasts-only, osteoblasts-only, and fibroblast-osteoblast co-culture were collected and added to monocultures of BMSCs to evaluate the effect of paracrine communication [61]. Strikingly, glycosaminoglycan deposition was reduced when BMSCs were exposed to conditioned media from co-culture of fibroblasts and osteoblasts. The same decrease was observed in BMSCs proliferation and ALP activity in the presence of both osteoblast- and fibroblast-conditioned media [61]. Overall, fibroblasts-osteoblasts direct interactions seem to play an important role in regulating stem cell commitment.

Additionally, the use of mixed culture media in co-cultures of hTDCs and pre-osteoblasts (pre-OBs, osteogenically induced ASCs) has been studied to assess medium composition influence on the expression of tendon-, bone- and interface-related markers [65]. An intermediate condition of 1:1 ratio of basal medium and osteogenic medium was reported as optimal for the maintenance of tenogenic and osteogenic phenotypes in single cultures of hTDCs and pre-OBs, respectively [65]. A direct co-culture model with hTDCs and pre-OBs (1:1 cell ratio) was then established. Interestingly, the presence of osteogenic medium seemed to increase the expression of bone-related markers (osteopontin, *SPP1,* and Runt-related transcription factor 2, *RUNX2*) in comparison with pre-OBs expression levels, suggesting the existence of a bi-directional cellular communication. Moreover, the expression of interface-relevant markers (*ACAN* and *COMP*) was also increased in comparison with single cultures, suggesting a possible targeting toward chondrogenesis [65].

Altogether, the effect of medium supplementation and cell-cell interactions played an important role on the modulation of cells phenotype with future application in more complex systems to promote the formation of an enthesis-like tissue. These results constitute promising outcomes in light of recent descriptions of enthesis cells phenotype, which resemble chondrocyte-like cells [17, 66] and the use of an optimal culture condition that can maintain different phenotypes at the same time is a major advantage supporting the combination of stem cells with differentiated cells.

3.3.3.3. *Co-cultures using biomaterials*

The development of scaffold-based strategies along with the use of co-cultures has been also explored to overcome the structural complexity of tendon-to-bone junction. A biomimetic continuous triphasic scaffold was designed aiming at the regeneration of ACL-to-bone interface, consisting of three phases: phase A (soft tissue) formed from polyglactin 10:90 knitted mesh sheets; phase B (interface) made from poly(D-L-lactide-coglycolide) (PLGA) 85:15 copolymer microspheres; and phase C (hard tissue) comprised of composite microspheres consisting of a 4:1 ratio of PLGA and 45S5 bioactive glass [67]. Human hamstring tendon fibroblasts and primary human osteoblasts were seeded on the extremities of the scaffold and allowed to migrate during culture time. Cell tracking results showed that fibroblasts adhered to phase A and osteoblasts to phase C, and cells continuously proliferated, resulting in fibroblast-osteoblast interaction within phase B [67]. Higher ALP activity and mineralization were mainly restricted to phase C, confirming the osteoconductivity effect of this phase provided by the bioactive glass, while higher amounts of collagen type I were observed in the presence of fibroblasts in phase A, together with a controlled phase-specific distribution of ECM over time [67]. Unfortunately, the expression of fibrocartilage-related markers was not assessed in the interface region, limiting the interpretation of *in vitro* cellular crosstalk effects alone. Notwithstanding, *in vivo* implantation studies of this multi-phasic scaffold tri-cultured with fibroblasts, chondrocytes and osteoblasts were performed to evaluate the formation of a fibrocartilage-like structure [62]. Three experimental groups were considered: tri-cultured, co-cultured (fibroblasts and osteoblasts only) and acellular scaffolds. Seeded scaffolds were cultured for 4 days prior to implantation and implanted subcutaneously in rats for 8 weeks. Immunohistological staining's demonstrated the deposition of collagenous-rich matrix in all phases of the scaffold in co- and tri-cultures, in opposition to acellular scaffolds, with collagen type III majorly found in phase A [62]. Moreover, tissues mineral distribution by micro-CT confirmed the mineralization confinement in phase C in all experimental groups [62]. Interestingly, the presence of a tri-culture led to an enhanced degradation

of phase A, resulting in the formation of a fibrocartilage-like region revealed by the presence of collagen types I, II and X [62].

Another relevant approach is the combination of stem cells, terminally differentiated cells and scaffolds. For ligament-bone regeneration, He et al. [64] used knitted silk scaffolds tri-cultured with rabbit BMSCs, fibroblasts and osteoblasts. Separate scaffolds were firstly seeded individually and cultured for 7 days; the three parts were then knitted together, and a scaffold composed of 5 distinct regions (osteoblasts only, BMSCs plus osteoblasts, BMSCs only, BMSCs plus fibroblasts and fibroblasts only) was obtained. A gradual transition was formed from the region where BMSCs directly interacted with fibroblasts to the opposite region where BMSCs interacted with osteoblasts and BMSCs were found to differentiate toward the fibrocartilage lineage, exhibiting at gene level an up-regulation of collagen type II, SOX9 and aggrecan in comparison with monocultures of BMSCs [64].

Altogether, these results anticipate the potential of controlling cellular interactions while changing scaffolds porosity, architecture and composition which allowed selective cell ingrowth, stimulating the production of a heterogeneous cell matrix along the scaffold and, therefore, the generation of a gradual transition between a soft and hard tissue. Overall, the combination of co-cultures with scaffold design constitutes a multidisciplinary approach for studying possible cell-cell and cell-matrix interactions occurring in the native tissue.

Even tough co-cultures are presented as important *in vitro* cell culture methodologies, there is still a lack of understanding regarding the mechanisms governing tendon-to-bone interface development and regeneration. Therefore, further studies should first focus on the characterization of important cellular interactions while using co- or tri-cultures, as a relevant *in vitro* platform to mimic as close as possible the cellular environment found at tendon-to-bone interface.

3.3.4. HYPOXIC ENVIRONMENT

Oxygen concentration is an important signal for the development and maintenance of several tissues. Tendon-to-bone interface presents a "critical zone" near the proximal tendon/bone attachment, poorly vascularized, where the oxygen supply is very low. Similarly, tendons are also poorly vascularized tissues [68, 69] while, in contrast, bone is highly vascularized [70]. Oxygen concentrations (O_2) ranging from 5.5% to 15% have been estimated in bone tissue [71-73]. In contrast, as muscles oxygen tension varies between 3.6-4.0%, tendon oxygen saturation falls below this value [74, 75]. This is corroborated by the quantification of oxygen consumption in tendons (5.3%/min) and muscles (10.5%/min) during rest [76, 77]. Over the past years, studies have been focusing on the effect of hypoxia on tenogenic [78-80],

chondrogenic [81-84] and osteogenic [84-88] differentiation of stem cells. Interestingly, *in vitro* studies comparing different oxygen tensions, revealed distinct cell responses. For instance, human tendon-derived stem cells cultured in 2D monolayers under low oxygen tension (2%-5%) exhibited higher proliferation and increased number of colonies in comparison with cells maintained under normoxia (20-21% O_2) [78-80]. The multilineage differentiation capability of this cell population seemed to be influenced by a myriad of oxygen concentrations (20%, 10%, 5%, 2%, 0.5%) both *in vitro* and *in vivo* [78-80]. Indeed, when expanded *in vitro* at 5% O_2 and afterwards implanted *in vivo* using an engineered tendon matrix, cells expressed osteogenic-, adipogenic- and chondrogenic- markers, such as osteocalcin, adiponectin, collagen type II, respectively, even though in lower levels compared to cells maintained at 20% O_2 prior *in vivo* implantation (control) [78]. Interestingly, these cells were found to be more prone to express tenogenic-markers, such as collagen type I, than the correspondent controls [82]. In contrast, this phenotypic commitment seemed to be inhibited in *in vitro* cultures maintained under lower oxygen concentrations (0.5-2% O_2) [79, 80].

Moreover, the influence of hypoxia in an indirect co-culture using tenocytes and ASCs was also studied to get deeper in the potential effect of oxygen concentration and paracrine factors on tenogenic differentiation of ASCs [89]. The expression of hypoxia-inducible factor-1 alpha (HIF-1α) was analyzed and, under hypoxic conditions, it seemed to play an important role in the differentiation of ASCs toward the tenogenic phenotype. Indeed, after HIF-1α inhibition, gene expression of collagen type I and III, tenomodulin, thrombospondin-4 and scleraxis, relevant tenogenic markers, was significantly inhibited in comparison with the control group, suggesting a potential role of HIF-1α on ASCs tenogenic differentiation under hypoxia [89]. Similarly, low oxygen tensions (1, 3, 5, and 10% O_2) seemed to have a negative effect on the osteogenic differentiation of human stem cells, given that a reduction in the expression of osteogenic-related markers, such as *RUNX2*, matrix mineralization and ALP activity has been described [85, 90-92]. Likewise, at 2% O_2, murine ASCs exhibited decreased chondrogenic and osteogenic potential, in comparison with cells cultured under normoxia [93]. Intriguingly, some reports in the literature have shown an enhancement of osteogenic differentiation of human and rat BMSCs under hypoxic conditions (1% and 5%). In both cases, low oxygen concentrations influenced BMSCs migration, enhancing cell attachment and survival, accompanied by increased cell proliferation, matrix mineralization, enhanced calcium content and ALP activity [94, 95]. Additionally, at gene level, human BMSCs expressed higher levels of osteocalcin and osteopontin, while, in contrast chondrogenic- (*COMP* and *ACAN*) and adipogenic-related (adipsin, fatty acid synthase) markers levels were significantly reduced [95]. Collectively, the lack of standardized cell isolation methods, experimental parameters, stem cells source and different oxygen

concentrations contribute to the challenge inherent to the determination of the role of oxygen in stem cells differentiation.

Notwithstanding, an interesting phenomenon was the influence of 2D and 3D cultures under hypoxic condition observed in human ASCs. In the presence of 1%-5% O_2 tension, ASCs presented a downregulation in the expression of osteogenic markers (ALP activity, mineralization and gene expression of *RUNX2*, collagen type 1, alpha chain 1 (*COL1A1*) and bone gamma-carboxyglutamate (gla) protein or osteocalcin (*Bglap*) in both 2D and 3D cultures, even though osteogenic differentiation in 2D was clearly more enhanced in comparison with 3D cultures [88] . However, differences in the osteogenic markers revealed a temporal change under different oxygen conditions. The expression of collagen type I was higher under 21% oxygen environment in 3D cultures than in 2D, increasing up to week 2, but even though 5% and 1% displayed lower expression levels, at each time point the expression was similar to that observed in 2D [88]. Moreover, in contrast with TDSCs, ASCs showed an independent HIF-1α inhibition of osteogenic differentiation, observed by a downregulation of osteogenic markers in both 1% and 2% oxygen in 2D and 3D cultures [96].

Therefore, oxygen variations in the culture environment seem to play an important role in stem cell fate. Hence, it is of major importance to have in mind the gradual heterotypic cellular environment that is found in tendon-to-bone interface. Future approaches should not only focus on the individual oxygen concentration found in tendon and bone but come up with a balanced concentration to support the tenogenic, chondrogenic and osteogenic phenotypes when trying to generate or regenerate this graded tissue.

3.3.5. GROWTH FACTORS

Growth factors also play an important role in the repair and development of a functional tissue as regulators of cell differentiation, proliferation and matrix deposition [97]. Interestingly, during tendon-to-bone healing process, a temporal expression of several growth factors seems to occur, as reported by different enthesis repair *in vivo* studies (Table 3.2). Therefore, the best time for growth factors delivery must be studied since it can potentiate the effectiveness of future treatments. Moreover, the correct combination of growth factors or the most effective growth factor must also be determined.

In a first approach, several *in vitro* studies have been focusing on the optimization of cell culture medium supplementation. BMP-2 [98], BMP-7 [99, 100] and TGF-β3 [101] are some examples of relevant growth factors used for medium supplementation that affect cell behavior *in vitro*. Supplementation with BMP-7 was tested in a co-culture model of murine osteoblasts and fibroblasts cell lines; agarose dividers were

used for two days and BMP-7 added at three different concentrations (100, 250 or 500 ng/mL) [99]. BMP-7 supplementation resulted in a suppression of *SPP1* (osteopontin) expression at the osteoblast region, while up-regulating alkaline phosphatase (*ALPL*) and *COL1A1*, as well as, *BGLAP* and *RUNX2* at the interface region; on the fibroblast region, *ALPL, BGLAP* and *RUNX2* were highly expressed [99]. Interestingly, the presence of BMP-7 seemed to influence *COL1A1* expression in all the regions, suggesting a possible increase in ECM formation and maturation [99]. In a similar study, Thomopoulos et al. [101] reported the importance of growth factor supplementation using tensile cyclic and compressive stresses for rat MSC differentiation in the presence and absence of TGF-β3. Actually, it was clearly observed that *SOX9* and *ACAN* were only expressed by cells maintained with medium supplemented with TGF-β3, in contrast with cells only maintained under influence of tensile and compressive stress [101]. Indeed, medium supplementation seems to play an important role in cell behavior. Thus, it is imperative to study the possible synergistic effects that may occur between mechanical cues and biochemical factors in tendon-to-bone healing.

Table 3.2 | *In vivo* studies of the temporal expression of growth factors and tissue formation along the healing process.

Growth factor	Model	Time period	Expression timeline	Ref.
TGF-β1 and TGF-β3	Rat bilateral supraspinatus tendon transection	8 weeks	Cell proliferation accompanied TGF-β1 temporal expression; Collagen remodeling, collagen types I and III production; TGF-β1 localized in the scar tissue and peaked at 10 days; TGF-β 3 was not detected in the healing insertion site.	[102]
bFGF, IGF-1, PDGF and TGF-β	Rabbit Rotator cuff tendon tear	4 weeks	Cell-specific expression: bFGF by fibroblast-like cells and ECs, IGF-1 by blood cells and ECs, PDGF by ECs, and TGF-β by blood cells; IGF-1 and TGF-β expressed during the inflammation period; Sequential peak expression of growth factors: TGF-β, IGF-1, bFGF, and PDGF.	[103]
BMP-2 and BMP-7	Ovine Extra-articular patellar	6 weeks	BMP-2 staining was more prominent at the tendon site at 6 weeks while BMP-7 was mainly observed at the interface close to the bone.	[104]

	tendon-to-bone			
BMP-12, -13, -14, bFGF, CTGF, PDGF, TGF-β1 and COMP	Rat Supraspinatus tendon insertion defect	16 weeks	At week 1: up regulation of all growth factors during inflammation period; COMP peaked at 1 week; PDGF-B expression at weeks 1 and 8; TGF-β1 expression at weeks 1, 2 and 8 in the midsubstance; BMP-12 moderately expressed at all time points; At 16 weeks, no expression of studied growth factors.	[105]
bFGF, VEGF, BMP-2 and BMP-7	Rabbit Anterior cruciate ligament repair	12 weeks	At week 1, FGF-2, BMP-2 and VEGF expression by fibroblasts and ECs at the interface; at week 3, VEGF expression by fibroblasts, FGF-2, and VEGF expression by osteoblasts; BMPs stained in fibroblasts and osteoblasts at the interface; At week 6, bFGF and VEGF in fibroblasts and osteoblasts at the interface; At week 12, bFGF and BMP-7 residually expressed by fibroblasts and osteoblasts at the interface; BMP-2 and BMP-7 in osteoblasts – expression more confined to later phases characterizing bone remodeling.	[106]

Abbreviations: *bFGF – basic fibroblast growth factor; ECs- endothelial cells; IGF-1 - insulin-like growth factor 1; PDGF – Platelet-derived growth factor; TGF-β – Transforming growth factor beta; BMP – Bone morphogenetic protein; CTGF – Connective tissue growth factor; COMP – Cartilage oligomeric matrix*

Another important challenge that must be overcome is the study and development of sustained-release vehicles for growth factor delivery. An interesting approach for a continuous and stable release of growth factors was introduced by gene therapy based on stem cells. This genetic intervention has shown promising results in comparison with the direct administration of growth factors to promote tendon-to-bone healing. Autologous MSCs transfected with platelet-derived growth factor-B (PDGF-B) [107], BMP-2 [108-110], TGF-β [111] and the combination of two different growth factors [112] genes have been reported in the literature for tendon-to-bone healing. Even though, transfected stem cells secrete several

growth factors in a steadily and continuous way, a decrease of the growth factor with time may lead to a loss of the primary objective after several weeks. Moreover, *in vivo* application involves delivering the vector directly into the cells of the tissue, which can lead to uncontrollable side effects, such as mutagenesis or development of malignancy [113, 114]. Instead, the use of biomaterials has been alternatively exploited for the controlled delivery of growth factors envisioning tendon-to-bone healing. Most of the reported literature is focused on *in vivo* studies to assess the influence of growth factors during different stages of tendon-to-bone healing. These studies use different gels, cements and glues for the local delivery of growth factors. Such systems overcome several limitations associated to bolus injections of growth factors, including rapid leakage, short half-life of soluble factors, denaturation, injection risks and the use of supraphysiological dosages. However, for example, rotator cuff surgeries are performed by arthroscopic surgery, therefore involving the placement trough cannulas, making the previous vehicles less appropriate and desired in comparison with scaffolds and patches. Diverse animal injury and repair models have been developed and overall, the presence of growth factors appear to increase the cellularity and tissue quality at the injury site. Table 3.3 summarizes the major outcomes obtained in these studies.

Table 3.3| *In vivo* studies using growth factors for tendon-to-bone healing.

Growth factors	Model	Vehicle	Time period	Animal	Major outcomes	Ref.
Bone Morphogenetic Proteins (BMPs)						
rhBMP-2	Bilateral anterior cruciate ligament reconstruction	Injectable calcium phosphate matrix	Phase I: 2 weeks Phase II: 1, 2 and 8 weeks	Rabbit	Phase I: BMP-2 increased bone width in a dose dependent way; Phase II: Smaller bone tunnels in comparison to controls; Significantly higher stiffness after 8 weeks in recombinant human bone morphogenetic protein-2 (rhBMP-2) treated groups, no differences in ultimate tensile load in comparison with control groups (carrier alone).	[115]
rhBMP-2	Achilles tendon repair	Local injection	Experiment I: 1, 2, 3 and 4 weeks Experiment II: 4 weeks	Rabbit	Experiment I: Spotty calcification in tendon 2 weeks after injection, being significantly higher at 3-4 weeks; Cartilaginous matrix formation 1 week after injection, expanding across the tendon after 2 weeks; At 3 weeks, hypertrophic chondrocytes embedded in the cartilaginous matrix, osteocalcin and collagen type II expression; Experiment II: Cartilaginous matrix formation between tendon and bone; Higher ultimate failure load in comparison with controls (buffer solution).	[116]
rhBMP-2	Rotator cuff repair	Phase I: Hyaluronan paste/sponge	8 weeks	Sheep	Phase I: Collagen sponges with rhBMP-2 led to greater maximum tensile load and stiffness at 8 weeks in comparison with hyaluronan paste with rhBMP-2;	[117]

		s and collagen sponges Phase II: Collagen sponges			Phase II: Decrease in cell density and increase in collagen fibers alignment in the tissue insertional zone in treated groups; No differences in the maximum load and stiffness between treated and untreated groups; Larger bone nodules in treated groups.	
BMP-2	Patellar repair	Fibrin glue and collagen gel	4 and 8 weeks	Rabbit	New bone formation, maturation and organized fibrocartilage formation at both 4 and 8 weeks in treated groups; Significantly higher failure to load in fibrin glue with BMP-2 treated group, comparing with control groups; Collagen type I, alpha chain 2 (*COL1A2*) and *ALPL*) gene expression decreased in BMP-2 treated groups.	[118]
BMP-2	Intrasynovial flexor tendon	Phase I: Calcium phosphate matrix Phase II: Collagen sponge	3 weeks	Dog	Increased osteoid formation, without increased mineral content; No maturation or bone ingrowth onto the tendon counterpart; No differences in biomechanical properties between treated and control groups; Fibrovascular scar tissue zone observed in all samples between tendon and tunnel wall.	[119]

rhBMP-2	Chronic rotator cuff tear	Dermal patch	4 or 8 weeks	Rabbit	Significantly higher formation of new bone in comparison with control groups (suture and dermal patch only) at both time points; Significantly higher ultimate tensile strength; After 8 weeks, higher cell penetration near the host bone as well as at interface, and presence of new fibrochondrocytes.	[120]
rhBMP-2	Rotator cuff repair	Tricalcium phosphate (β-TCP) material	2, 4 and 8 weeks	Rabbit	Mechanical strength increased at 4 weeks; Collagen fibers alignment and presence of fibrocartilage at week 4; No significant histological and biomechanical differences at week 8.	[121]
BMP-7	Rotator cuff repair	Gelatin hydrogel sheet (GHS)	2, 4 and 8 weeks	Rat	Improved collagen fiber orientation at week 8; Increased number of chondrocytes at the tendon-to-bone insertion; Histological staining demonstrated higher deposition of cartilage matrix at week 8 in GHS-BMP-7 group in comparison with BMP-7 group; No evident heterotopic ossification in the GHS-BMP-7 group; Higher tendon-to-bone maturing score and ultimate force-to-failure values	[122]
GDF-5 (BMP-14)	Achilles tendon repair	Suture	1, 2, 4 and 8 weeks	Rat	Increased tendon thickness with higher cell density until 8 weeks; Maximum failure load and tensile strength increased at week 2; At 4 weeks, cartilage-like cells appeared after tendon repair in the presence of collagen type II.	[123]

Cartilage-derived Morphogenetic Proteins (CDMPs)						
CDMP-2	Supraspinatus Tendon Repair	Sutures	2, 3, 4 and 6 weeks	Rat	Enhanced tendon healing: Regions of disorganized, hypercellular healed tendon tissue at the repair site at week 2; Improved tendon structure with greater cellular organization and collagen content at weeks 4 and 6; Significantly higher load to failure at week 4.	[124]
Transforming Growth Factors (TGF)						
TGF-β1	Anterior cruciate ligament replacement	Collagen Sponge	3 weeks	Dog	Rich collagen fibers between tendon and bone; TGF-β1 significantly increased the bonding strength of the graft to the tunnel wall at 3 weeks, although long-term effects are unknown.	[125]
TGF-β1	Supraspinatus tendon-to-bone repair	Gelatin hydrogel	2, 4, 6, 8 and 12 weeks	Rat	Significantly higher ultimate load to failure, higher tissue volume at 6 and 12 weeks and higher collagen content at 12 weeks; No normal fibrocartilaginous layer regeneration in all tested groups; No effects on MSCs-related markers and cell proliferation in the presence of TGF-β1.	[126]
TGF-β1	Bilateral supraspinatus tendon repair	Alginate scaffold	12 weeks	Rabbit	Significantly higher ultimate failure load in comparison with groups treated with single injections and non-treated ones; No differences in ultimate stress;	[127]

					More evident formation of new fibrocartilage, with better collagen orientation, organization and continuity.	
TGF-β1	Rotator cuff repair	Hydroxyapatite (HAp) microspheres	2, 4 and 8 weeks	Rat	Novel bone formation; Improved fibrocartilage formation and higher collagen organization at the insertion site at 2 and 4 weeks; Higher load to failure was obtained for HAp-TGF-β1 and HAp groups	[128]
TGF-β3	Supraspinatus Tendon repair	Heparin/fibrin-based delivery system	2 to 8 weeks	Rat	Increased inflammation, proliferation, cellularity and vascularity in early timepoints in the presence of TGF-β3; Increased ECM remodeling at late time points; Improved ultimate force, toughness, modulus, failure to stress and stiffness in the presence of TGF-β3.	[129]
TGF-β1 or TGF-β3	Supraspinatus tendon repair	Osmotic pump	1 and 4 weeks	Rat	Increased production of collagen type III, but shoulders with reduced mechanical properties in TGF-β1 group; No differences in TGF-β3 group.	[130]
Fibroblast Growth Factor (FGF)						
bFGF	Chronic Rotator cuff tear	PLGA fibrous membranes	2, 4 and 8 weeks	Rat	Membrane absorption as soon as 2 weeks; Improved collagen organization, formation of a more mature tissue compared to controls (membrane and repair only); Reduced ultimate stress due to increases in cross-sectional area; Improved ultimate load to failure and stiffness at week 4.	[131]

FGF-2	Supraspinatus tendon repair	Fibrin sealant	2, 4 and 6 weeks	Rat	Accelerated bone ingrowth at interface; At 2 weeks, according to a modified tendon maturing scoring system, tendon-to-bone presented higher maturity, with increased cellularity, parallel oriented fibers, vascularity, continuity, bone ingrowth, fibrocartilage cells, strength and tidemark in comparison with the untreated group; At 4 and 6 weeks, FGF-treated group and controls exhibited similar strength in relation to the degree of the tendon-to-bone insertion maturity.	[132]
FGF-2	Supraspinatus tendon repair	Gelatin hydrogel	2, 4, 6, 8 and 12 weeks	Rat	Higher number of cells expressing MSC markers at insertion site; At gene level, from 4 to 8 weeks: increased SCX expression levels, while tenomodulin (TNMD) expression levels significantly increased from 4 to 12 weeks; SOX9 significantly upregulated at 4 weeks; Overlapping localization for tenomodulin and aligned collagen fibers; Significant improvement in mechanical strength at 6 and 12 weeks.	[133]
FGF-2	Supraspinatus tendon repair	Suture coated with GHS/ Suture with FGF-2–	Experiment I: 12 weeks Experiment II: 2 and 6 weeks	Rabbit	Positive effects observed at ≥ 6 weeks postoperatively; At 12 weeks, loose fibrovascular tissues observed in the repair site in the suture and carrier groups; Significantly higher ultimate load-to-failure and stress-to-failure was found in the suture in comparison with carrier	[134]

		impregnated GHS			groups; bFGF promoted the formation of a new tendon-like tissue with highly oriented collagen fibers; Significantly higher load-to-failure and stress-to-failure registered in groups treated with bFGF in comparison with controls (buffered saline).	
Hepatocyte Growth Factor (HGF)						
HGF	Long Digital Extensor tendon insertion in proximal tibia	Cancellous bone	2, 4, 6 8 and 12 weeks	Rabbit	Lamellar bone and Sharpey-like fibers appeared at week 4; Significantly higher biomechanical properties at weeks 2 and 4; junctional adhesion between tendon and bone observed after 12 weeks, presenting higher failure load tunnel length ratio.	[135]
Granulocyte-colony stimulating factor (G-CSF)						
G-CSF	Supraspinatus tendon repair	Injectable vesicular phospholipid gels	3 and 9 weeks	Rat	Higher amounts of G-CSF (10 μg) resulted in a significant increase in collagen type III content in tendon in comparison with lower amounts (1 μg) and placebo; No differences between the tested groups in the mean load to failure and stiffness; Tissues treated with lower amounts of G-CSF presented higher load to failure ratio compared to control.	[136]

G-CSF	Supraspinatus tendon repair	Subcutaneous Injection	12-19 days	Rat	Significantly higher cellularity in treated animals in comparison with normal animals and controls; No differences in ultimate stress, strain, modulus between normal animals and treated ones at both 12 and 19 days; Lower bone volume.	[137]

More recently, blood derivatives have been receiving increased attention as cost-effective sources of human therapeutic factors that can be used in both autologous and allogeneic applications in regenerative medicine [138]. There is a wide range of platelet containing products with different biological characteristics, including platelet-rich plasma (PRP), platelet poor plasma (PPP), platelet lysate (PL) [139, 140]. The use of such blood derivatives for enthesis repair and regeneration is frequently investigated, either in the form of soluble preparations or gels. Table 3.4 summarizes the major outcomes of *in vivo* studies applying PRP preparations to enthesis healing models. In general, studies on PRP administration demonstrate conflicting results with some studies presenting improved tissue healing through enhanced cellular response and mechanical performance, while others report no differences in tissue healing response. Furthermore, clinical reports have demonstrated conflicting outcomes, including mid-term positive outcomes upon rotator cuff tendinopathy treatment using multiple PRP injections, but no differences in tissue integrity [141] or on re-tear rate [142]. Although contradictory results have been frequently found, the use of blood derivatives other than PRP in *in vitro* settings has been gaining attention to modulate cell behavior, particularly for tendon tissue engineering (TTE). Indeed, PL can be a more stable alternative since it shows a comparatively lower batch-to-batch variability in batches prepared from platelet concentrates of different donors [143], potentially resulting in more predictable clinical outcomes. Although no studies exist concerning the application of PL preparations for enthesis repair, PL membranes have been reported to result in an up-regulation of tenogenic genes and deposition of tendon-related ECM proteins by hTDCs [144]. Furthermore, nanocomposite hydrogels based on PL have been reported to modulate the behavior of ASCs according to nanofillers content [145], suggesting prospective applications for the development of gradient tissue engineered constructs *in vitro*.

Overall, studies have shown that several growth factors have the ability to increase the "quality" of repaired tissues in animal models. Given the complexity of tendon-to-bone interface, tissue repair is most probably orchestrated by a multitude of growth factors released in a temporally and spatially controlled manner. Hence, it has become clear that the application of multiple growth factors may be needed to regenerate the insertion site between tendon and bone. However, parameters such as optimal delivery time and vehicle are not effective. Although the use of growth factor gradients is being explored for providing adequate biochemical cues [12], this strategy can only be explored in combination with adequate cells and biomaterials, limiting their application *in vivo*.

Even though, growth factor therapy remains an important therapeutic for tendon-to-bone healing and regeneration and needs to be further exploited in light of the discussed current limitations.

Table 3.4 | *In vivo* studies using growth factors for tendon-to-bone healing.

Injury anatomical insertion location	Animal model	Blood derivative preparation	Administration mode	Main outcomes	References
Achilles tendon	New Zealand rabbits	PRP	Injection into the bone tunnel	• Improved tissue integration and reduced cellularity after 56 days	[146]
	Female Sprague Dawley rats	PRP gel, autologous	Local injection of PRP gel	• Formation of a transition zone with moderate collagen fiber organization after 3 months, no chondrocytes were observed; • Complete healing (not observed in controls); • Proteoglycan expression; • Improved mechanical strength	[147]
Supraspinatus tendon	Inbred Fischer 344 Adult male rats	PRP	Injection (pipped) onto tendon-bone approximation	• Increased acute cellular inflammation at day 7; • Enhanced biomechanical properties at day 21;	[148]

			• Better collagen fiber organization and alignment at day 21	
	Adult male Wistar rats	PRP	Local injection	• Reparative fibrous and granulation tissue between tendon and bone tissue, in comparison to acute inflammatory infiltrates and initiation of scar formation in controls; • Higher maximum load and stiffness after 21 days	[149]
	Adult male Wistar-Albino rats	PRP	Local injection PRP infused into an absorbable hemostatic gelatin sponge	• Improved biomechanical properties in comparison to no repair/primary repair controls, but no differences between administration modes	[150]
	New Zealand white rabbits	PRP	Suture sprayed with PRP Suture sprayed with PRP + bioactive glass (BG) powder	• Higher mean failure load after 6 and 12 weeks – highest for PRP + BG group; • Higher BMP-2 gene expression after 6 weeks	[151]

ACL	New Zealand white rabbits	PRP, autologous	PRP in combination with ACL grafts prepared by braid-twist canine small intestinal submucosa (SIS)	• Fibrous and vascularized tissue formed around SIS graft in SIS+PRP group; • More adhesions in SIS control; • Lower mechanical properties in SIS+PRP group, compared to SIS alone; • Improved cellular response, chondrocyte cell infiltration, and collagen fibers loosely attached to the bone	[152]
	New Zealand white rabbits	PRP immobilized in fibrin glue	Hamstring tendon graft wrapped with PRP immobilized in fibrin glue	• Aligned connective tissue, newly formed bone and cartilage at the tendon-to-bone interface after 8 weeks; • Formation of mineralized tissue at the tendon-to-bone interface after 8 weeks; • No differences in biomechanical properties	[153]

3.4. TWO- OR THREE-DIMENSIONAL (2D/3D): A BIOMATERIALS APPROACH

In vitro 2D culture systems are an oversimplified version of the human physiological conditions [154]. Indeed, shifting from 2D to 3D has a significant impact on cell proliferation, differentiation, survival and mechanical response. Novel 3D cell culture approaches were developed to mimic as close as possible the *in vivo* complex interactions of tissues and organs, opening new possibilities to study both biochemical and biomechanical signals [155]. Particularly, interfacial tissue engineering has put efforts to develop structures that mimic the anisotropic structural properties observed in interface tissues, such as the one found in tendon-to-bone interface. Therefore, biomimetic scaffolds with graded morphology/architecture, topography and composition are useful, especially when physical and chemical factors affect the fate of cultured cells in 3D scaffolds in a spatially orchestrated manner. interfacial tissue engineering is going beyond the production of multi-phasic scaffolds with the fabrication of graded biomaterials, capable of mimicking the gradual transition of interface tissues while supporting both heterotypic and homeotypic cell-cell interactions and cell-matrix integration. Common approaches include the fabrication of aligned nanofibers scaffolds with the incorporation of mineral gradients [16, 156-158], scaffolds with gradations in fiber organization [158-160], bi- and tri-phasic scaffolds Tellado [60, 67, 161, 162] and graded hydrogels [53, 163, 164].

3.4.1. 2D NANOFIBER-BASED MATERIALS

Conventional electrospinning process has evolved during the last years. Even though there is a pressing need for the development of 3D structures, approaches using 2D environment have demonstrated to be useful in mimicking the nanostructure and composition of tendon-to-bone junction. One interesting approach for 2D nanofibers was developed applying a 2-spinnerette device to create a nonwoven mat of polycaprolactone (PCL) nanofibers containing a gradient of amorphous calcium phosphate nanoparticles (nACP). Here, increasing nACP concentration resulted in increased proliferation of MC3T3-E1 murine pre-osteoblasts along the gradient, which suggested that the presence of nACP potentiated the adhesion and proliferation of osteoblasts [156]. Similarly, a nonwoven mat of electrospun PCL nanofibers was developed and submersed in 10 times concentrated simulated body fluid (SBF) solution to create a calcium phosphate gradient, resulting in an increase of Young's modulus [157], mimicking the spatially graded mineral composition and mechanics of enthesis. Likewise, Liu et al. [16] developed aligned PLGA electrospun mats with a similar SBF mineral gradient and also demonstrated the ability to spatially

control the differentiation of a single stem cell source. Indeed, ASCs exhibited increased ALP activity, as well as RUNX2 and OCN expression, indicating that osteogenic differentiation of ASCs was attained along the increasing mineral concentration on the scaffold [16].

Supplementation with growth factors has also been used as a potential approach for tendon-to-bone regeneration. Interestingly, Perikamana et al. [54] focused on the spatially combinatory effect of a matrix-bound growth factor (platelet-derived growth factor, PDGF), matrix alignment and calcium deposition to mimic tendon-to-bone regeneration in an *in vitro* system. Briefly, random-aligned-random poly(lactic acid) (PLLA) nanofibers meshes were produced and PDGF immobilized using an asymmetrical polydopamine gradient. Using a precision syringe pump infusion method, the extremities of the nanofiber meshes were immersed in SBF solution creating a gradient of mineral deposition in both margins. After seeding of ASCs, higher adhesion, ALP activity and osteogenic gene levels were observed in the both ends of the nanofibers meshes in comparison with the middle region (unmineralized zone) which lacked mineral deposition [54]. However, no results were shown concerning the tenogenic commitment of ASCs when in contact with the middle part of the nanofiber mesh where the immobilization took place.

Understanding the development of the nano-scale structure of tendon-to-bone interface may provide novel insights for the improvement of repair strategies. However, even though, biological evidences have shown the possible use of nanofibers to induce a spatially controlled cell differentiation on electrospun scaffolds, structures with 3D orientations mimicking the proper tissue are an upcoming topic in the fabrication of enthesis tissue engineered scaffolds.

3.4.2. 3D BIO-INSTRUCTIVE SCAFFOLDS

Remarkably, a 3D scaffold for bone-ligament applications was developed by coating the random part of PCL nanofibers with 5x SBF on a "random-aligned-random" scaffold structure [165]. Using two spin cones electrospinning design, non-aligned nanofibers were obtained, while the gap in between consisted mainly in aligned fibers, resulting in the generation of a transitional zone [165]. Higher ultimate tensile strength, tensile modulus and strain at break were observed in the aligned region in comparison with the random regions [165]. Scaffolds were then seeded with human BMSCs, which aligned following the direction of fibers alignment, with more spindle shaped cells at the aligned part and polygonal or round shaped cells in the random regions of the scaffold [165]. Moreover, through gene expression analysis, tendon-related markers (TNMD and MKX (mohawk)) were found to be up-regulated in the aligned region in comparison with the random and mineralized

regions, where bone-related markers (RUNX2, osteocalcin and osteopontin) were highly expressed [165]. Therefore, both chemical and structural characteristics of the scaffold seemed to influence the phenotype of hBMSCs toward tenogenic and osteogenic lineages. Another approach to obtain a 3D cylindrical composite scaffold was developed using an electrospinning set-up with a dual-drum collector [166]. Two spinnerets were used in a first approach to form a single transition zone, and a 3-spinnerets design was afterwards used to create two transition regions, while shields were placed in the dual drum to control the size of the transition regions [166]. The obtained 2D meshes of PCL and PLGA were cut into small pieces, rolled around a guide (20G needle) and withdrawn and bathed in 20% polyethylene glycol diacrylate (PEGDA) solution and PEGDA/Irgacure 2959 solution, respectively; the needle was removed afterwards originating a 3D cylindrical composite scaffold [166]. Mechanical testing was performed for both 2D meshes and 3D scaffolds, showing that 3D cylindrical composites were more mechanically robust but failed due to the stress concentration on the aligned region of the scaffold while 2D meshes presented the opposite mechanical behavior [166]; however, the biological behavior of cells in contact with the 3D composites was not assessed in this study.

Multi-phasic scaffolds have been also improving on the gradual transition between different tissues to try to mimic, as close as possible, the three zones observed in enthesis. For example, Tellado et al. [161] fabricated biphasic silk fibroin scaffolds with anisotropic and isotropic porous alignment, by directional freezing and salt leaching, to mimic the gradient in collagen molecule alignment found in tendon-to-bone interface. Aligned porosity represented the tendon/ligament side, while random porosity was designed for the bone side [161]. Young's modulus varied along the construct and culture with hASCs clearly demonstrated the cytoskeleton organization according to pore alignment [161]. Moreover, changes in gene expression of tendon, enthesis and cartilage markers in the different regions of the scaffold were observed. In this regard, SOX9 was more expressed in the isotropic region of the scaffold and SCX in the anisotropic part, suggesting the potential gradual cell differentiation to the chondrogenic and tenogenic lineages along the scaffold [161].

Up to now, efforts have been concentrated on the development of 3D scaffolds which replicate either the multi-structural alignment of the interface, the spatially mineral distribution or mechanical stimulation to drive cells differentiation to the different lineages. However, the conjugation of all factors to create bio-instructive scaffolds would be of great matter as demonstrated by Caliari et al. [167] through the development of an osteotendinous biomaterial

based on a collagen-GAG scaffold platform. Using freeze-drying method a collagen-GAG scaffold was created mimicking the gradients of mineralization with calcium phosphate and geometric anisotropy which allowed, within a unique 3D biomaterial, to control the spatially selective tenogenic and osteogenic stem cells differentiation [167] (Figure 3.5). Moreover, uniaxial tensile strain was also found to specifically guide along the scaffold the MSCs differentiation throughout the osteotendinous lineages [167].

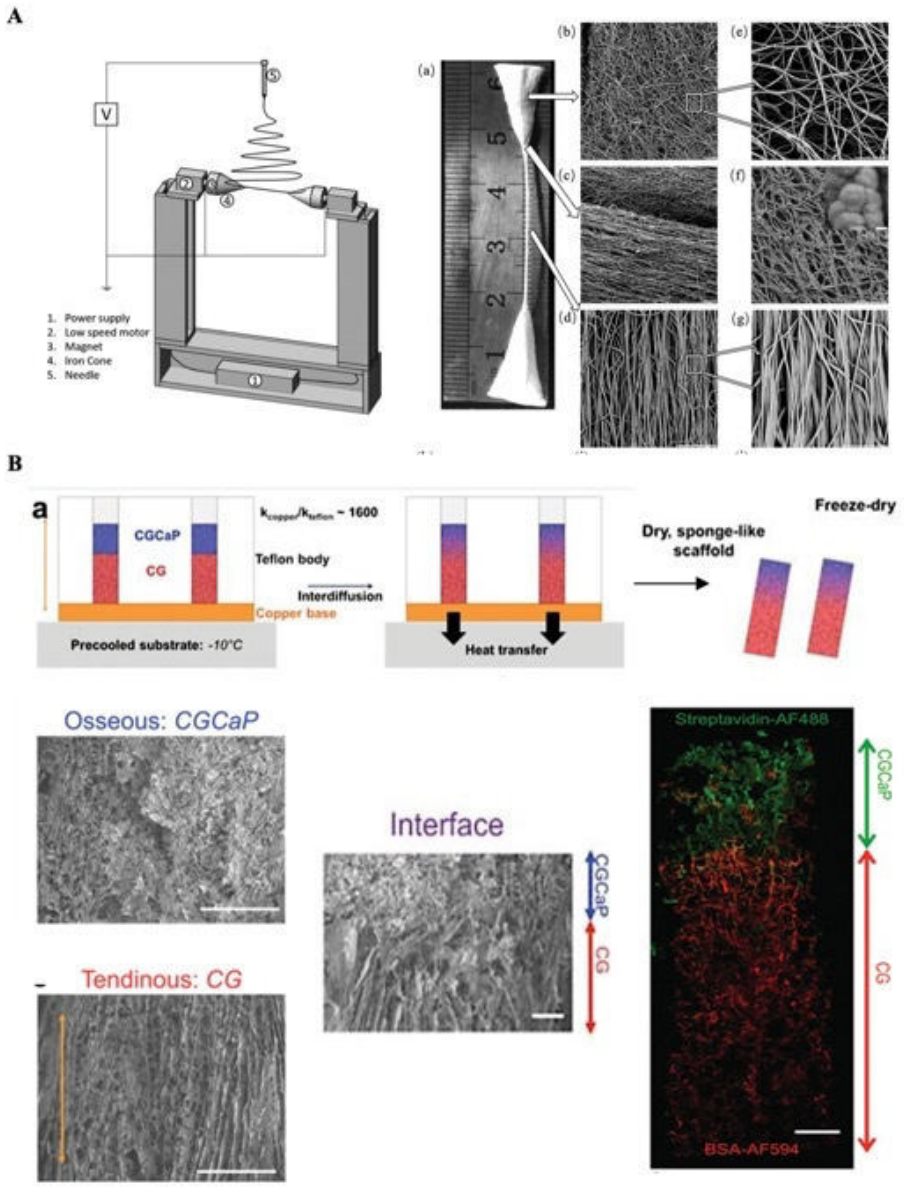

Figure 3.5 | Production setups of 3D cylindrical scaffold and osteotendinous scaffold. (A) Schematics of an electrospinning dual-motor collector for the production of random-aligned-random PCL fibrous scaffolds for ligament to bone application. Scale bars: 10 um and 100 nm.

Reproduced from Lin *et al.* [165] with permission from The Royal Society of Chemistry. (B) Schematic setup of the multi-comparted osteotendinous scaffolds production with distinct regions of pore anisotropy and mineral content. Scanning electron micrographs showing an isotropic porosity in the mineralized area (CGCaP) and aligned porosity in the tendinous region (CG). Scale bars, 200 μm. Confocal micrograph of the scaffold stained with AlexaFluor 488-streptavidin conjugate in the osseous (CGCaP) part and AlexaFluor 594-BSA conjugate in the tendinous (CG) compartment. Scale bar, 1 mm. Adapted from Caliari et al. [167].

New material designs for tendon-to-bone regeneration are also focused on the use of hydrogel gradient systems. Hydrogels present tunable chemical and physical properties suitable for tailoring the 3D cellular microenvironment. Therefore, the generation of biochemical and physical gradients within a hydrogel has become an attractive tool to generate a graded tissue. The development of hydrogels with spatially controlled patterning of cells has been explored for co-culturing different cell types [53, 168] [56,173]. Hammoudi et al. [168] designed tissue-scalable oligo(polyethylene glycol)-fumarate:poly(ethylene glycol)-diacrylate hydrogel-based scaffold for long-term 3D co-culture of primary tendon fibroblasts and BMSCs, showing their viability up to 2 weeks [168]. Additionally, hydrogels as magnetic-responsive materials have been also developed as a way to provide structures with the ability to modulate the biochemical, physical and mechanical properties of the surrounding tissues. For example, a magnetic-responsive hydrogel composed of methacrylated chondroitin sulfate (MA-CS) enriched with PL was developed to encapsulate osteogenically differentiated human adipose-derived stem cells or hTDCs within distinct hydrogel compartments [53]. Swelling, degradation and release of growth factors were modulated by the application of an external magnetic field (EMF), showing impact on both cell morphology and the expression of tendon- (decorin) and bone-related (osteopontin) genes in the different sections of the hydrogel after EMF application [53].

Textile techniques have been also used to produce more complex 3D structures. Knitting and braiding are some examples of textile assembly that have been applied to produce scaffolds and showed great similarity with, for example, tendons considering its architectural features, mechanical properties, and biological functionality [169, 170]. Interestingly, these techniques have been used to produce knitted silk scaffolds for ACL regeneration [171-173]. However, these

scaffolds were still unable to be competent and did not completely reproduce the structural integrity and functionality of the proper tissue.

Current advances in the development of 3D biomaterials with a combination of compositional, architectural and topographical properties allow the control over cell behavior without the need for external supplementation in all dimensions. Collectively, it is evident that scaffold topographies and composition influence both the morphology and differentiation capability of cells. However, several features still need to be optimized and further research of *in vitro* and *in vivo* effects on cell behavior could generate new insights to achieve a perfectly functional regenerated tissue. Nonetheless, the complexity of tendon-to-bone insertion, as well as of other musculoskeletal interfaces, requires the coordination between such systems and more complex and controllable factors, including oxygen concentration and biochemical factors, as discussed above.

3.5. STATIC OR DYNAMIC? THE ROLE OF MECHANICAL STIMULATION

There is still limited knowledge on the material properties of tendon-to-bone interface and the specific demands to achieve its full repair and regeneration. During developmental stage, biophysical cues influence the development of tendon, bone and cartilage [174-178]. First evidences were described in cortical bone with numerous studies demonstrating the importance of stress environment on the architecture of trabecular bone and thickness of cortical bone [179, 180]. Similarly, a comparable responsiveness was demonstrated on tendon, where the total removal of load led to structural and compositional changes and a fast deterioration of tendon strength [181]. Indeed, all cells found along tendon-to-bone interface are known to be mechanoresponsive, thus mechanobiology is expected to play an important role in the development and healing of this tissue interface. Several studies have shown the importance of mechanical loading in the development of enthesis in murine models. In a study by Galatz et al. [182], the effect of the mechanical environment was evaluated by paralyzing the supraspinatus muscle in a rat model of rotator cuff injury and repair. The complete removal of load and immobilization clearly had a detrimental effect on rotator cuff healing, in comparison with rats with free range of motion, in which structural properties increased and modest improvements in biomechanical properties were observed [182]. The role of muscular loading in the development of tendon-to-bone interface has been described using a murine shoulder model [183, 184]. Intramuscular injections of botulinum toxin A or laceration were used to paralyze rotator cuff muscles in postnatal mice and saline injections were used as controls [183, 184]. Diminished muscle loading led to a reduction

in mineral deposition and deficient fibrocartilage formation, with disorganized fiber distribution and inferior tendon mechanical properties at the enthesis [183, 184]. In the absence of mechanical loading, a decrease in bone volume and a change in bone architecture were also noticed [183, 184]. Interestingly, the effect of muscle loading did not seem to be necessary for initiating enthesis development; however, the signal from tendons has an important effect, whereas mechanical loading has an impact on growth and maturation of enthesis[183-187]. Hence, it is evident that mechanical loading contributes to a gradation in structure and cellular environment, which for itself will turn to a gradation in mechanical properties along the enthesis, enabling an efficient load transfer and reduced stress concentration [10, 188].

Normally, interfacial tissue engineered strategies are based on dynamic cultures to better mimic the human physiology in an organ-specific context. For this purpose, bioreactors have been designed to spatially control biomechanical and physical signals to guide cell proliferation, differentiation and, ultimately, tissue formation [189-193], with the application of uniaxial tensile loads and dynamic compressive loading to emulate tendon and bone mechanophysiology, respectively. Using this concept, MSCs have been differentiated in several scaffolds under the influence of different biomechanical stimuli provided in bioreactors [194-197]. Several strategies have focused on the use of diffusing-based bioreactors to co-differentiate cells along a unique platform creating an interface [191, 198, 199], but, no studies are still available with the use of these dynamic platforms for tendon-to-bone interface. Instead, static cell cultures are commonly used to study the developmental stage and mechanical loading influence on tendon-to-bone development and healing is often disregarded. Therefore, the development of bioreactors for enthesis engineering is a major need, due to the advantageous application of such dynamic systems to create a graded interface along a single unit while controlling the environment, presenting some advantageous characteristics over the currently used *in vitro* cultures. Finer spatial control should also be focused to enhance knowledge on the effect of several chemical stimulus and, therefore, improving local cellular modulation and control.

3.6. CLINICAL TRANSLATION

Clinical translation of *in vivo* results is still a very slow process even though there is growing evidence of the benefits of cell-based therapies in tendon-to-bone healing. Few victories have been also observed in the clinics using scaffolds for human enthesis repair. Many preclinical devices, such as interpositional grafting [200] and rotator cuff augmentation [201, 202], have failed to

restore the normal function of the tissue due to inadequate mechanical forces and structural properties of the grafts. Moreover, variations between small and larger tears in some follow up studies makes comparisons impossible [203, 204]. Nevertheless, commercial scaffolds have focused on tendon/ligament repair for rotator cuff and ACL augmentation, not properly restoring the interface. For example, porcine small-intestinal submucosa (SIS) patches such as Restore™ SIS (DePuy Orthopedics, West Chester, PA, USA) were implanted in 62 patients with rotator cuff tear characteristics [205]. An evaluation after 1 year did not reveal significant differences in strength and motion between patients treated with SIS and non-treated groups [205]. Similarly, Iannotti et al. [206] tested Restore™ SIS in human rotator cuff repair and found inferior tendon healing accompanied of increasing pain, thus not recommending the use of these patches for augmentating massive chronic rotator cuff tears [206]. Contrarily, GraftJacket (Wright Medical Arlington, TN, USA), made from a human cadaveric dermis ECM scaffold, demonstrated significant improvements in pain scores, forward flexion, external rotation strength with full incorporation of the graft as observed by Bond et al. [207] and Burkhead et al. [208]. But overall these technologies fail when mechanical properties are tested, suggesting limited mechanical performance of existing biological scaffolds for rotator cuff augmentation.

Interestingly, few clinical studies investigated the use of stem cells in enthesis healing or regeneration. However, once more studies focused solely on tendon/ligament repair when targeting interface regeneration and functional recovery. For example, Hernigou et al. [209] evaluated the efficiency of biological augmentation of rotator cuff repair with iliac MSCs in forty-five patients for a period of 10 years and a significant improvement of tendon integrity with lower levels of re-tear was observed while using concentrates containing MSCs. More recently, in a cohort study, among 182 patients treated through arthroscopic surgery for a rotator cuff tear, 35 received an injection of ASCs loaded in fibrin glue [210]. In contrast to the previous study, no differences were found between the conventional repaired group and the injection group with respect to the internal rotation at the back and the functional measures of the constant score and final follow-up [210]. Nonetheless, a higher re-tear rate was observed in the conventional group in comparison with the injection group, even though no clinical differences were found in the follow-up [210].

Despite the promising results of these clinical therapies, achieving regeneration of tendon-to-bone interface still remains in its infancy. Several basic challenges have to be overcome, including understanding the differences in cellular responses between acute and chronic injuries along with the identification of the best strategies. Overall, current clinical outcomes support the need for

more refined tissue engineering strategies that should integrate the complexity of this interface. Furthermore, the knowledge gap regarding the molecular characterization of resident cell populations, as mentioned above, has been limiting the understanding of cellular differentiation strategies and the evaluation of bioengineered strategies effectiveness. Hence, it is of utmost importance to investigate deeper the biology of these tissues toward establishing foundational expertise, aiming at moving today's research advances into tomorrow's regenerative therapies.

3.7. CONCLUSIONS/ FUTURE TRENDS

Despite biotechnological advances of tissue engineering, it is well-recognized that there is still a critical need to understand the development and healing of tendon-to-bone interface. Over the years, tissue engineers have been trying to replicate the complexity of different tissues by attempting to understand the signals involved in the initiation of regenerative processes. However, the field of tendon-to-bone biology is lagging far behind owing to the peculiarities of this multi-tissue transition. We highlighted that it is of major importance to understand the heterotypic cellular interactions occurring in the native tissues, particularly the role of cell-cell and cell-ECM contacts and production of paracrine factors, for the development of a functional tissue. Co-culture systems have been increasingly exploited as platforms to study bidirectional communication. Although disparities on selection of cell sources and culture conditions have been hampering the establishment of an optimal *in vitro* system, stem cells of mesenchymal origin have been gaining increasing attention for the generation of bioengineered strategies, overcoming main limitations of tissue-specific cell populations. *In vitro* studies using differentiated cells and stem cells have been opening new avenues toward understanding the crosstalk between distinct cell types in directing pro-regenerative responses, either by stem cell differentiation or through synergistic effects in promoting fibrocartilage-like phenotype. Furthermore, given the mechanical nature of tendon-to-bone interface, (bio)physical elements are postulated to be needed in combination with cellular therapies. Different signals can be considered, from mechanical loading to biomaterial properties. Biomaterial properties can be tuned through different fabrication strategies to emulate structural, architectural and topographical signals of native interfacial tissue. Nonetheless, the application of adequate mechanical signals requires refinement and efforts should be focused on understanding the mechanical interplay and its implications on biological functions toward the development of sophisticated platforms to support the development of functional and physiologically relevant tendon-to-bone tissue engineered constructs.

The establishment of relevant animal models for translation of novel treatments is also a need, as researchers, providers and regulatory agencies should come up with a standardized animal model. In this regard, the definition of optimal rehabilitation periods and/or sex determining role on healing as variables of tendon-to-bone healing is of major importance. Preclinical data is still a crucial step toward clinical translation. However, suitable strategies for tendon-to-bone healing and/or regeneration require not only the use of graded biomaterials but also the ideal combination of cells, growth factors and culture conditions. Nevertheless, simple and ease handling constructs need to be developed and integrate appropriate biophysical, biological and biochemical signals to promote tissue integration and regeneration. Still, regulatory constraints and cost considerations will always be a concern while developing the best tissue engineering strategies. Strikingly, issues concerning the developed technologies, such as feasible sterilization, tracking and storage need to be addressed and optimized for efficient translation.

3.8. REFERENCES

[1] A. Yamamoto, K. Takagishi, T. Osawa, T. Yanagawa, D. Nakajima, H. Shitara, T. Kobayashi, Prevalence and risk factors of a rotator cuff tear in the general population, J Shoulder Elbow Surg 19(1) (2010) 116-20, 10.1016/j.jse.2009.04.006.

[2] M. Benjamin, T. Kumai, S. Milz, B.M. Boszczyk, A.A. Boszczyk, J.R. Ralphs, The skeletal attachment of tendons—tendon 'entheses' Comp Biochem Physiol A Mol Integr Physiol 133(4) (2002) 931-945, 10.1016/S1095-6433(02)00138-1.

[3] M. Benjamin, H. Toumi, J.R. Ralphs, G. Bydder, T.M. Best, S. Milz, Where tendons and ligaments meet bone: attachment sites ('entheses') in relation to exercise and/or mechanical load, Journal of anatomy 208(4) (2006) 471-90, 10.1111/j.1469-7580.2006.00540.x.

[4] M. Benjamin, D. McGonagle, The anatomical basis for disease localisation in seronegative spondyloarthropathy at entheses and related sites, J Anat. 199(5) (2001) 503-526,

[5] A. Robertson, R.W. Nutton, J.F. Keating, Current trends in the use of tendon allografts in orthopaedic surgery, J Bone Joint Surg Br 88(8) (2006) 988-992, 10.1302/0301-620X.88B8.

[6] C.C. Kaeding, B. Aros, A. Pedroza, E. Pifel, A. Amendola, J.T. Andrish, W.R. Dunn, R.G. Marx, E.C. McCarty, R.D. Parker, R.W. Wright, K.P. Spindler, Allograft Versus Autograft Anterior Cruciate Ligament Reconstruction: Predictors of Failure From a MOON Prospective Longitudinal Cohort, Sports Health 3(1) (2011) 73-81, 10.1177/1941738110386185.

[7] P.P. Lui, P. Zhang, K. Chan, L. Qin, Biology and augmentation of tendon-bone insertion repair, Journal of Orthopaedic Surgery and Research 5(59) (2010) 10.1186/1749-799X-5-59.

[8] S. Thomopoulos, Tendon to Bone Healing: Differences in Biomechanical, Structural, and Compositional Properties Due to a Range of Activity Levels, Journal of Biomechanical Engineering 125(1) (2003) 10.1115/1.1536660.

[9] E.D. Bonnevie, R.L. Mauck, Physiology and Engineering of the Graded Interfaces of Musculoskeletal Junctions, Annual review of biomedical engineering 20(1) (2018) 403-429, 10.1146/annurev-bioeng-062117-121113.

[10] H.H. Lu, S. Thomopoulos, Functional attachment of soft tissues to bone: development, healing, and tissue engineering, Annual review of biomedical engineering 15 (2013) 201-26, 10.1146/annurev-bioeng-071910-124656.

[11] E. Zelzer, E. Blitz, M.L. Killian, S. Thomopoulos, Tendon-to-bone attachment: from development to maturity, Birth Defects Res C Embryo Today 102(1) (2014) 101-12, 10.1002/bdrc.21056.

[12] S. Font Tellado, E.R. Balmayor, M. Van Griensven, Strategies to engineer tendon/ligament-to-bone interface: Biomaterials, cells and growth factors, Adv Drug Deliv Rev 94 (2015) 126-40, 10.1016/j.addr.2015.03.004.

[13] L. Smith, Y. Xia, L.M. Galatz, G.M. Genin, S. Thomopoulos, Tissue-engineering strategies for the tendon/ligament-to-bone insertion, Connect Tissue Res 53(2) (2012) 95-105, 10.3109/03008207.2011.650804.

[14] N. Lee, J. Robinson, H. Lu, Biomimetic strategies for engineering composite tissues, Current Opinion in Biotechnology 40 (2016) 64-74, 10.1016/j.copbio.2016.03.006.

[15] G.M. Genin, A. Kent, V. Birman, B. Wopenka, J.D. Pasteris, P.J. Marquez, S. Thomopoulos, Functional grading of mineral and collagen in the attachment of tendon to bone, Biophys J 97(4) (2009) 976-85, 10.1016/j.bpj.2009.05.043.

[16] W. Liu, J. Lipner, J. Xie, C.N. Manning, S. Thomopoulos, Y. Xia, Nanofiber scaffolds with gradients in mineral content for spatial control of osteogenesis, ACS applied materials & interfaces 6(4) (2014) 2842-9, 10.1021/am405418g.

[17] L. Rossetti, L.A. Kuntz, E. Kunold, J. Schock, K.W. Müller, H. Grabmayr, J. Stolberg-Stolberg, F. Pfeiffer, S.A. Sieber, R. Burgkart, A.R. Bausch, The microstructure and micromechanics of the tendon–bone insertion, Nature Materials 16(6) (2017) 664-670, 10.1038/nmat4863.

[18] H.M. Shaw, R.M. Santer, A.H.D. Watson, M. Benjamin, Adipose tissue at entheses: the innervation and cell composition of the retromalleolar fat pad associated with the rat Achilles tendon, Journal of anatomy 211(4) (2007) 436-443, 10.1111/j.1469-7580.2007.00791.x.

[19] W.E. Johnson, B. Caterson, S.M. Eisenstein, S. Roberts, Human intervertebral disc aggrecan inhibits endothelial cell adhesion and cell migration in vitro, Spine (Phila Pa 1976) 30(10) (2005) 1139-47, 10.1097/01.brs.0000162624.95262.73.

[20] M. Benjamin, H. Toumi, D. Suzuki, S. Redman, P. Emery, D. McGonagle, Microdamage and altered vascularity at the enthesis-bone interface provides an anatomic explanation for bone involvement in the HLA-B27-associated spondylarthritides and allied disorders, Arthritis Rheum 56(1) (2007) 224-33, 10.1002/art.22290.

[21] A. Rufai, J.R. Ralphs, M. Benjamin, Ultrastructure of fibrocartilages at the insertion of the rat Achilles tendon, Journal of anatomy 189 (Pt 1)(Pt 1) (1996) 185-191,

[22] P. Theobald, G. Bydder, C. Dent, L. Nokes, N. Pugh, M. Benjamin, The functional anatomy of Kager's fat pad in relation to retrocalcaneal problems and other hindfoot disorders, Journal of anatomy 208(1) (2006) 91-97, 10.1111/j.1469-7580.2006.00510.x.

[23] J.J. Canoso, N. Liu, M.R. Traill, V.M. Runge, Physiology of the retrocalcaneal bursa, Ann Rheum Dis 47(11) (1988) 910-2, 10.1136/ard.47.11.910.

[24] D.G.M. Coppens, M.L. De Bruin, H.G.M. Leufkens, J. Hoekman, Global Regulatory Differences for Gene- and Cell-Based Therapies: Consequences and Implications for Patient Access and Therapeutic Innovation, Clin Pharmacol Ther 103(1) (2018) 120-127, 10.1002/cpt.894.

[25] N.W. Marion, J.J. Mao, Mesenchymal Stem Cells and Tissue Engineering, Methods in Enzymology, Academic Press2006, pp. 339-361.

[26] Y.G. Li, J.N. Wei, J. Lu, X.T. Wu, G.J. Teng, Labeling and tracing of bone marrow mesenchymal stem cells for tendon-to-bone tunnel healing, Knee Surg Sports Traumatol Arthrosc 19(12) (2011) 2153-8, 10.1007/s00167-011-1506-0.

[27] M. Kosaka, J. Nakase, K. Hayashi, H. Tsuchiya, Adipose-Derived Regenerative Cells Promote Tendon-Bone Healing in a Rabbit Model, Arthroscopy : the journal of arthroscopic & related surgery : official publication of the Arthroscopy Association of North America and the International Arthroscopy Association 32(5) (2016) 851-9, 10.1016/j.arthro.2015.10.012.

[28] H.W. Ouyang, J.C. Goh, E.H. Lee, Use of bone marrow stromal cells for tendon graft-to-bone healing: histological and immunohistochemical studies in a rabbit model, Am J Sports Med 32(2) (2004) 321-7, 10.1177/0095399703258682.

[29] J. Zhang, T. Pan, H.J. Im, F.H. Fu, J.H. Wang, Differential properties of human ACL and MCL stem cells may be responsible for their differential healing capacity, BMC Med 9 (2011) 68, 10.1186/1741-7015-9-68.

[30] T. Matsumoto, S.M. Ingham, Y. Mifune, A. Osawa, A. Logar, A. Usas, R. Kuroda, M. Kurosaka, F.H. Fu, J. Huard, Isolation and characterization of human anterior cruciate ligament-derived vascular stem cells, Stem Cells Dev 21(6) (2012) 859-72, 10.1089/scd.2010.0528.

[31] Y. Mifune, T. Matsumoto, S. Ota, M. Nishimori, A. Usas, S. Kopf, R. Kuroda, M. Kurosaka, F.H. Fu, J. Huard, Therapeutic potential of anterior cruciate ligament-derived stem cells for anterior cruciate ligament reconstruction, Cell transplantation 21(8) (2012) 1651-65, 10.3727/096368912x647234.

[32] Y. Mifune, T. Matsumoto, K. Takayama, S. Terada, N. Sekiya, R. Kuroda, M. Kurosaka, F.H. Fu, J. Huard, Tendon graft revitalization using adult anterior cruciate ligament (ACL)-derived CD34+ cell sheets for ACL reconstruction, Biomaterials 34(22) (2013) 5476-87, 10.1016/j.biomaterials.2013.04.013.

[33] Y. Bi, D. Ehirchiou, T.M. Kilts, C.A. Inkson, M.C. Embree, W. Sonoyama, L. Li, A.I. Leet, B.-M. Seo, L. Zhang, S. Shi, M.F. Young, Identification of tendon stem/progenitor cells and the role of the extracellular matrix in their niche, Nature Medicine 13(10) (2007) 1219-1227, 10.1038/nm1630.

[34] W. Shen, J. Chen, Z. Yin, X. Chen, H. Liu, B.C. Heng, W. Chen, H.W. Ouyang, Allogenous tendon stem/progenitor cells in silk scaffold for functional shoulder repair, Cell transplantation 21(5) (2012) 943-58, 10.3727/096368911x627453.

[35] P.P.Y. Lui, O.T. Wong, Tendon stem cells: experimental and clinical perspectives in tendon and tendon-bone junction repair, Muscles, ligaments and tendons journal 2(3) (2012) 163-168,

[36] C.H. Chen, C.H. Chang, K.C. Wang, C.I. Su, H.T. Liu, C.M. Yu, C.B. Wong, I.C. Wang, S.W. Whu, H.W. Liu, Enhancement of rotator cuff tendon-bone healing with injectable periosteum progenitor cells-BMP-2 hydrogel in vivo, Knee Surg Sports Traumatol Arthrosc 19(9) (2011) 1597-607, 10.1007/s00167-010-1373-0.

[37] C.H. Chang, C.H. Chen, H.W. Liu, S.W. Whu, S.H. Chen, C.L. Tsai, G.H. Hsiue, Bioengineered periosteal progenitor cell sheets to enhance tendon-bone healing in a bone tunnel, Biomed J 35(6) (2012) 473-80, 10.4103/2319-4170.104412.

[38] Y.J. Ju, T. Muneta, H. Yoshimura, H. Koga, I. Sekiya, Synovial mesenchymal stem cells accelerate early remodeling of tendon-bone healing, Cell Tissue Res 332(3) (2008) 469-78, 10.1007/s00441-008-0610-z.

[39] C. Ferretti, V. Borsari, M. Falconi, A. Gigante, R. Lazzarini, M. Fini, R. Di Primio, M. Mattioli-Belmonte, Human periosteum-derived stem cells for tissue engineering applications: the role of VEGF, Stem Cell Rev Rep 8(3) (2012) 882-90, 10.1007/s12015-012-9374-7.

[40] Y.S. Choi, S.M. Lim, H.C. Shin, C.W. Lee, S.L. Kim, D.I. Kim, Chondrogenesis of human periosteum-derived progenitor cells in atelocollagen, Biotechnol Lett 29(2) (2007) 323-9, 10.1007/s10529-006-9240-2.

[41] S. Stich, A. Loch, S.-J. Park, T. Häupl, J. Ringe, M. Sittinger, Characterization of single cell derived cultures of periosteal progenitor cells to ensure the cell quality for clinical application, PLOS ONE 12(5) (2017) e0178560, 10.1371/journal.pone.0178560.

[42] Y. Zhu, T. Liu, K. Song, X. Fan, X. Ma, Z. Cui, Adipose-derived stem cell: a better stem cell than BMSC, Cell Biochem Funct 26(6) (2008) 664-75, 10.1002/cbf.1488.

[43] G. Yang, B.B. Rothrauff, H. Lin, R. Gottardi, P.G. Alexander, R.S. Tuan, Enhancement of tenogenic differentiation of human adipose stem cells by tendon-derived extracellular matrix, Biomaterials 34(37) (2013) 9295-306, 10.1016/j.biomaterials.2013.08.054.

[44] A.I. Gonçalves, P.M. Gershovich, M.T. Rodrigues, R.L. Reis, M.E. Gomes, Human adipose tissue-derived tenomodulin positive subpopulation of stem cells: A promising source of tendon progenitor cells, Journal of Tissue Engineering and Regenerative Medicine 12(3) (2018) 762-774, 10.1002/term.2495.

[45] R. James, S.G. Kumbar, C.T. Laurencin, G. Balian, A.B. Chhabra, Tendon tissue engineering: adipose-derived stem cell and GDF-5 mediated regeneration using electrospun matrix systems, Biomedical materials (Bristol, England) 6(2) (2011) 025011, 10.1088/1748-6041/6/2/025011.

[46] O. Jeon, J.W. Rhie, I.K. Kwon, J.H. Kim, B.S. Kim, S.H. Lee, In vivo bone formation following transplantation of human adipose-derived stromal cells that are not differentiated osteogenically, Tissue Eng Part A 14(8) (2008) 1285-94, 10.1089/ten.tea.2007.0253.

[47] C.M. Cowan, Y.-Y. Shi, O.O. Aalami, Y.-F. Chou, C. Mari, R. Thomas, N. Quarto, C.H. Contag, B. Wu, M.T. Longaker, Adipose-derived adult stromal cells heal critical-size mouse calvarial defects, Nature Biotechnology 22 (2004) 560, 10.1038/nbt958.

[48] Y.D. Halvorsen, D. Franklin, A.L. Bond, D.C. Hitt, C. Auchter, A.L. Boskey, E.P. Paschalis, W.O. Wilkison, J.M. Gimble, Extracellular matrix mineralization and osteoblast gene expression by

human adipose tissue-derived stromal cells, Tissue engineering 7(6) (2001) 729-41, 10.1089/107632701753337681.

[49] H.A. Awad, M.Q. Wickham, H.A. Leddy, J.M. Gimble, F. Guilak, Chondrogenic differentiation of adipose-derived adult stem cells in agarose, alginate, and gelatin scaffolds, Biomaterials 25(16) (2004) 3211-22, 10.1016/j.biomaterials.2003.10.045.

[50] T. Rada, P.P. Carvalho, T.C. Santos, A.G. Castro, R.L. Reis, M.E. Gomes, Chondrogenic potential of two hASCs subpopulations loaded onto gellan gum hydrogel evaluated in a nude mice model, Current stem cell research & therapy 8(5) (2013) 357-64, 10.2174/1574888x113089990049.

[51] R. McGoldrick, A. Chattopadhyay, C. Crowe, G. Chiou, K. Hui, S. Farnebo, C. Davis, A. Le Grand, M. Jacobs, H. Pham, J. Chang, The Tissue-Engineered Tendon-Bone Interface: In Vitro and In Vivo Synergistic Effects of Adipose-Derived Stem Cells, Platelet-Rich Plasma, and Extracellular Matrix Hydrogel, Plastic and reconstructive surgery 140(6) (2017) 1169-1184, 10.1097/prs.0000000000003840.

[52] H.K. Min, S.H. Oh, J.M. Lee, G.I. Im, J.H. Lee, Porous membrane with reverse gradients of PDGF-BB and BMP-2 for tendon-to-bone repair: in vitro evaluation on adipose-derived stem cell differentiation, Acta Biomater 10(3) (2014) 1272-9, 10.1016/j.actbio.2013.12.031.

[53] E.D. Silva, P.S. Babo, R. Costa-Almeida, R.M.A. Domingues, B.B. Mendes, E. Paz, P. Freitas, M.T. Rodrigues, P.L. Granja, M.E. Gomes, Multifunctional magnetic-responsive hydrogels to engineer tendon-to-bone interface, Nanomedicine : nanotechnology, biology, and medicine 10.1016/j.nano.2017.06.002 (2017) 10.1016/j.nano.2017.06.002.

[54] S.K. Madhurakkat Perikamana, J. Lee, T. Ahmad, E.M. Kim, H. Byun, S. Lee, H. Shin, Harnessing biochemical and structural cues for tenogenic differentiation of adipose derived stem cells (ADSCs) and development of an in vitro tissue interface mimicking tendon-bone insertion graft, Biomaterials 165 (2018) 79-93, 10.1016/j.biomaterials.2018.02.046.

[55] M.W. Wong, L. Qin, J.K. Tai, S.K. Lee, K.S. Leung, K.M. Chan, Engineered allogeneic chondrocyte pellet for reconstruction of fibrocartilage zone at bone-tendon junction–a preliminary histological observation, J Biomed Mater Res B Appl Biomater 70(2) (2004) 362-7, 10.1002/jbm.b.30049.

[56] G. Nourissat, A. Diop, N. Maurel, C. Salvat, S. Dumont, A. Pigenet, M. Gosset, X. Houard, F. Berenbaum, Mesenchymal Stem Cell Therapy Regenerates the Native Bone-Tendon Junction after

Surgical Repair in a Degenerative Rat Model, PLOS ONE 5(8) (2010) e12248, 10.1371/journal.pone.0012248.

[57] N.K. Paschos, W.E. Brown, R. Eswaramoorthy, J.C. Hu, K.A. Athanasiou, Advances in tissue engineering through stem cell-based co-culture, J Tissue Eng Regen Med 9(5) (2015) 488-503, 10.1002/term.1870.

[58] R. Costa-Almeida, R. Soares, P.L. Granja, Fibroblasts as maestros orchestrating tissue regeneration, J Tissue Eng Regen Med 12(1) (2018) 240-251, 10.1002/term.2405.

[59] I.E. Wang, J. Shan, R. Choi, S. Oh, C.K. Kepler, F.H. Chen, H.H. Lu, Role of osteoblast-fibroblast interactions in the formation of the ligament-to-bone interface, Journal of orthopaedic research : official publication of the Orthopaedic Research Society 25(12) (2007) 1609-20, 10.1002/jor.20475.

[60] G. Criscenti, A. Longoni, A. Di Luca, C. De Maria, C.A. van Blitterswijk, G. Vozzi, L. Moroni, Triphasic scaffolds for the regeneration of the bone-ligament interface, Biofabrication 8(1) (2016) 015009, 10.1088/1758-5090/8/1/015009.

[61] J.O. Cooper, J.D. Bumgardner, J.A. Cole, R.A. Smith, W.O. Haggard, Co-cultured tissue-specific scaffolds for tendon/bone interface engineering, Journal of tissue engineering 5 (2014) 2041731414542294, 10.1177/2041731414542294.

[62] J.P. Spalazzi, E. Dagher, S.B. Doty, X.E. Guo, S.A. Rodeo, H.H. Lu, In vivo evaluation of a multiphased scaffold designed for orthopaedic interface tissue engineering and soft tissue-to-bone integration, Journal of Biomedical Materials Research Part A 86A(1) (2008) 1-12, 10.1002/jbm.a.32073.

[63] I.E. Wang, D.R. Bogdanowicz, S. Mitroo, J. Shan, S. Kala, H.H. Lu, Cellular interactions regulate stem cell differentiation in tri-culture, Connect Tissue Res 57(6) (2016) 476-487, 10.1080/03008207.2016.1230106.

[64] P. He, K.S. Ng, S.L. Toh, J.C. Goh, In vitro ligament-bone interface regeneration using a trilineage coculture system on a hybrid silk scaffold, Biomacromolecules 13(9) (2012) 2692-703, 10.1021/bm300651q.

[65] I. Calejo, R. Costa-Almeida, A.I. Gonçalves, D. Berdecka, R.L. Reis, M.E. Gomes, Bi-directional modulation of cellular interactions in an in vitro co-culture model of tendon-to-bone interface, Cell proliferation 51(6) (2018) e12493-e12493, 10.1111/cpr.12493.

[66] L.A. Kuntz, L. Rossetti, E. Kunold, A. Schmitt, R. von Eisenhart-Rothe, A.R. Bausch, R.H. Burgkart, Biomarkers for tissue engineering of the tendon-bone interface, PLOS ONE 13(1) (2018) e0189668, 10.1371/journal.pone.0189668.

[67] J.P. Spalazzi, S.B. Doty, K.L. Moffat, W.N. Levine, H.H. Lu, Development of controlled matrix heterogeneity on a triphasic scaffold for orthopedic interface tissue engineering, Tissue engineering 12(12) (2006) 3497-508, 10.1089/ten.2006.12.3497.

[68] I.M. Ahmed, M. Lagopoulos, P. McConnell, R.W. Soames, G.K. Sefton, Blood supply of the Achilles tendon, Journal of orthopaedic research : official publication of the Orthopaedic Research Society 16(5) (1998) 591-6, 10.1002/jor.1100160511.

[69] W. Petersen, V. Stein, B. Tillmann, Blood supply of the tibialis anterior tendon, Archives of Orthopaedic and Trauma Surgery 119(7) (1999) 371-375, 10.1007/s004020050431.

[70] M.-H. Lafage-Proust, B. Roche, M. Langer, D. Cleret, A. Vanden Bossche, T. Olivier, L. Vico, Assessment of bone vascularization and its role in bone remodeling, BoneKEy Rep 4 (2015) 10.1038/bonekey.2015.29.

[71] P.M. Gross, D.D. Heistad, M.L. Marcus, Neurohumoral regulation of blood flow to bones and marrow, American Journal of Physiology-Heart and Circulatory Physiology 237(4) (1979) H440-H448, 10.1152/ajpheart.1979.237.4.H440.

[72] R.D. Ray, M. Kawabata, J. Galante, Experimental Study of Peripheral Circulation and Bone Growth: An Experimental Method for the Quantitative Determination of Bone Blood Flow PART III, Clinical Orthopaedics and Related Research® 54 (1967)

[73] M. Marenzana, T.R. Arnett, The Key Role of the Blood Supply to Bone, Bone Res 1(3) (2013) 203-215, 10.4248/BR201303001.

[74] R.S. Richardson, S. Duteil, C. Wary, D.W. Wray, J. Hoff, P.G. Carlier, Human skeletal muscle intracellular oxygenation: the impact of ambient oxygen availability, The Journal of physiology 571(Pt 2) (2006) 415-24, 10.1113/jphysiol.2005.102327.

[75] T. Kiaer, K.D. Kristensen, Intracompartmental pressure, PO2, PCO2 and blood flow in the human skeletal muscle, Archives of orthopaedic and traumatic surgery. Archiv fur orthopadische und Unfall-Chirurgie 107(2) (1988) 114-6,

[76] K. Kubo, T. Ikebukuro, N. Tsunoda, H. Kanehisa, Changes in oxygen consumption of human muscle and tendon following repeat muscle contractions, European Journal of Applied Physiology 104(5) (2008) 859, 10.1007/s00421-008-0841-4.

[77] R. Boushel, H. Langberg, J. Olesen, J. Gonzales-Alonzo, J. Bülow, M. Kjær, Monitoring tissue oxygen availability with near infrared spectroscopy (NIRS) in health and disease, Scandinavian journal of medicine & science in sports 11(4) (2001) 213-222, 10.1034/j.1600-0838.2001.110404.x.

[78] J. Zhang, J.H.C. Wang, Human Tendon Stem Cells Better Maintain Their Stemness in Hypoxic Culture Conditions, PLOS ONE 8(4) (2013) e61424, 10.1371/journal.pone.0061424.

[79] Y. Yu, L. Lin, Y. Zhou, X. Lu, X. Shao, C. Lin, K. Yu, X. Zhang, J. Hong, Y. Chen, Effect of Hypoxia on Self-Renewal Capacity and Differentiation in Human Tendon-Derived Stem Cells, Medical Science Monitor 23 (2017) 1334-1339, 10.12659/msm.903892.

[80] W.Y. Lee, P.P. Lui, Y.F. Rui, Hypoxia-mediated efficient expansion of human tendon-derived stem cells in vitro, Tissue Eng Part A 18(5-6) (2012) 484-98, 10.1089/ten.TEA.2011.0130.

[81] T. Gómez-Leduc, M. Desancé, M. Hervieu, F. Legendre, D. Ollitrault, C. de Vienne, M. Herlicoviez, P. Galéra, M. Demoor, Hypoxia Is a Critical Parameter for Chondrogenic Differentiation of Human Umbilical Cord Blood Mesenchymal Stem Cells in Type I/III Collagen Sponges, Int J Mol Sci 18(9) (2017) 10.3390/ijms18091933.

[82] F. Legendre, D. Ollitrault, T. Gomez-Leduc, M. Bouyoucef, M. Hervieu, N. Gruchy, F. Mallein-Gerin, S. Leclercq, M. Demoor, P. Galéra, Enhanced chondrogenesis of bone marrow-derived stem cells by using a combinatory cell therapy strategy with BMP-2/TGF-β1, hypoxia, and COL1A1/HtrA1 siRNAs, Sci Rep 7(1) (2017) 3406, 10.1038/s41598-017-03579-y.

[83] J. Shang, H. Liu, J. Li, Y. Zhou, Roles of hypoxia during the chondrogenic differentiation of mesenchymal stem cells, Current stem cell research & therapy 9(2) (2014) 141-7, 10.2174/1574888x09666131230142459.

[84] E.J. Sheehy, C.T. Buckley, D.J. Kelly, Oxygen tension regulates the osteogenic, chondrogenic and endochondral phenotype of bone marrow derived mesenchymal stem cells, Biochem Biophys Res Commun 417(1) (2012) 305-10, 10.1016/j.bbrc.2011.11.105.

[85] S.H. Hsu, C.T. Chen, Y.H. Wei, Inhibitory effects of hypoxia on metabolic switch and osteogenic differentiation of human mesenchymal stem cells, Stem Cells 31(12) (2013) 2779-88, 10.1002/stem.1441.

[86] E. Potier, E. Ferreira, R. Andriamanalijaona, J.P. Pujol, K. Oudina, D. Logeart-Avramoglou, H. Petite, Hypoxia affects mesenchymal stromal cell osteogenic differentiation and angiogenic factor expression, Bone 40(4) (2007) 1078-87, 10.1016/j.bone.2006.11.024.

[87] S.S. Lin, S.W. Ueng, C.C. Niu, L.J. Yuan, C.Y. Yang, W.J. Chen, M.S. Lee, J.K. Chen, Effects of hyperbaric oxygen on the osteogenic differentiation of mesenchymal stem cells, BMC Musculoskelet Disord 15 (2014) 56, 10.1186/1471-2474-15-56.

[88] J. He, D.C. Genetos, C.E. Yellowley, J.K. Leach, Oxygen tension differentially influences osteogenic differentiation of human adipose stem cells in 2D and 3D cultures, Journal of cellular biochemistry 110(1) (2010) 87-96, 10.1002/jcb.22514.

[89] Y. Yu, Y. Zhou, T. Cheng, X. Lu, K. Yu, Y. Zhou, J. Hong, Y. Chen, Hypoxia enhances tenocyte differentiation of adipose-derived mesenchymal stem cells by inducing hypoxia-inducible factor-1alpha in a co-culture system, Cell Prolif 49(2) (2016) 173-84, 10.1111/cpr.12250.

[90] G. D'Ippolito, S. Diabira, G.A. Howard, B.A. Roos, P.C. Schiller, Low oxygen tension inhibits osteogenic differentiation and enhances stemness of human MIAMI cells, Bone 39(3) (2006) 513-22, 10.1016/j.bone.2006.02.061.

[91] C. Merceron, C. Vinatier, S. Portron, M. Masson, J. Amiaud, L. Guigand, Y. Chérel, P. Weiss, J. Guicheux, Differential effects of hypoxia on osteochondrogenic potential of human adipose-derived stem cells, Am J Physiol Cell Physiol 298(2) (2010) C355-64, 10.1152/ajpcell.00398.2009.

[92] A. Youssef, V.K.M. Han, Regulation of Osteogenic Differentiation of Placental-Derived Mesenchymal Stem Cells by Insulin-Like Growth Factors and Low Oxygen Tension, Stem cells international 2017 (2017) 4576327-4576327, 10.1155/2017/4576327.

[93] P. Malladi, Y. Xu, M. Chiou, A.J. Giaccia, M.T. Longaker, Effect of reduced oxygen tension on chondrogenesis and osteogenesis in adipose-derived mesenchymal cells, Am J Physiol Cell Physiol 290(4) (2006) C1139-46, 10.1152/ajpcell.00415.2005.

[94] S.P. Hung, J.H. Ho, Y.R. Shih, T. Lo, O.K. Lee, Hypoxia promotes proliferation and osteogenic differentiation potentials of human mesenchymal stem cells, Journal of orthopaedic research : official publication of the Orthopaedic Research Society 30(2) (2012) 260-6, 10.1002/jor.21517.

[95] D.P. Lennon, J.M. Edmison, A.I. Caplan, Cultivation of rat marrow-derived mesenchymal stem cells in reduced oxygen tension: effects on in vitro and in vivo osteochondrogenesis, J Cell Physiol 187(3) (2001) 345-55, 10.1002/jcp.1081.

[96] S. Sahai, A. Williams, M.L. Skiles, J.O. Blanchette, Osteogenic differentiation of adipose-derived stem cells is hypoxia-inducible factor-1 independent, Tissue Eng Part A 19(13-14) (2013) 1583-91, 10.1089/ten.TEA.2012.0378.

[97] I.H. Ali, D.P. Brazil, Bone morphogenetic proteins and their antagonists: current and emerging clinical uses, British journal of pharmacology 171(15) (2014) 3620-32, 10.1111/bph.12724.

[98] T. Schwarting, D. Schenk, M. Frink, M. Benölken, F. Steindor, M. Oswald, S. Ruchholtz, P. Lechler, Stimulation with bone morphogenetic protein-2 (BMP-2) enhances bone-tendon integration in vitro, Connect Tissue Res 57(2) (2016) 99-112, 10.3109/03008207.2015.1087516.

[99] T. Schwarting, M. Benolken, S. Ruchholtz, M. Frink, P. Lechler, Bone morphogenetic protein-7 enhances bone-tendon integration in a murine in vitro co-culture model, Int Orthop 39(4) (2015) 799-805, 10.1007/s00264-015-2688-8.

[100] T. Schwarting, P. Lechler, J. Struewer, M. Ambrock, T.M. Frangen, S. Ruchholtz, E. Ziring, M. Frink, Bone morphogenetic protein 7 (BMP-7) influences tendon-bone integration in vitro, PLoS One 10(2) (2015) e0116833, 10.1371/journal.pone.0116833.

[101] S. Thomopoulos, R. Das, V. Birman, L. Smith, K. Ku, E.L. Elson, K.M. Pryse, J.P. Marquez, G.M. Genin, Fibrocartilage tissue engineering: the role of the stress environment on cell morphology and matrix expression, Tissue Eng Part A 17(7-8) (2011) 1039-53, 10.1089/ten.TEA.2009.0499.

[102] L.M. Galatz, L.J. Sandell, S.Y. Rothermich, R. Das, A. Mastny, N. Havlioglu, M.J. Silva, S. Thomopoulos, Characteristics of the rat supraspinatus tendon during tendon-to-bone healing after acute injury, Journal of orthopaedic research : official publication of the Orthopaedic Research Society 24(3) (2006) 541-50, 10.1002/jor.20067.

[103] M. Kobayashi, E. Itoi, H. Minagawa, N. Miyakoshi, S. Takahashi, Y. Tuoheti, K. Okada, Y. Shimada, Expression of growth factors in the early phase of supraspinatus tendon healing in rabbits, J Shoulder Elbow Surg 15(3) (2006) 371-7, 10.1016/j.jse.2005.09.003.

[104] Y. Yu, J.P. Bliss, W.J. Bruce, W.R. Walsh, Bone morphogenetic proteins and Smad expression in ovine tendon-bone healing, Arthroscopy : the journal of arthroscopic & related surgery : official publication of the Arthroscopy Association of North America and the International Arthroscopy Association 23(2) (2007) 205-10, 10.1016/j.arthro.2006.08.023.

[105] C.C. Würgler-Hauri, L.M. Dourte, T.C. Baradet, G.R. Williams, L.J. Soslowsky, Temporal expression of 8 growth factors in tendon-to-bone healing in a rat supraspinatus model, J Shoulder Elbow Surg 16(5 Suppl) (2007) S198-203, 10.1016/j.jse.2007.04.003.

[106] T. Kohno, Y. Ishibashi, E. Tsuda, T. Kusumi, M. Tanaka, S. Toh, Immunohistochemical demonstration of growth factors at the tendon–bone interface in anterior cruciate ligament reconstruction using a rabbit model, Journal of Orthopaedic Science 12(1) (2007) 67-73, 10.1007/s00776-006-1088-8.

[107] F. Li, H. Jia, C. Yu, ACL reconstruction in a rabbit model using irradiated Achilles allograft seeded with mesenchymal stem cells or PDGF-B gene-transfected mesenchymal stem cells, Knee Surg Sports Traumatol Arthrosc 15(10) (2007) 1219-27, 10.1007/s00167-007-0385-x.

[108] Y. Dong, Q. Zhang, Y. Li, J. Jiang, S. Chen, Enhancement of tendon-bone healing for anterior cruciate ligament (ACL) reconstruction using bone marrow-derived mesenchymal stem cells infected with BMP-2, Int J Mol Sci 13(10) (2012) 13605-20, 10.3390/ijms131013605.

[109] V. Martinek, C. Latterman, A. Usas, S. Abramowitch, S.L. Woo, F.H. Fu, J. Huard, Enhancement of tendon-bone integration of anterior cruciate ligament grafts with bone morphogenetic protein-2 gene transfer: a histological and biomechanical study, The Journal of bone and joint surgery. American volume 84(7) (2002) 1123-31, 10.2106/00004623-200207000-00005.

[110] S. Shahab-Osterloh, F. Witte, A. Hoffmann, A. Winkel, S. Laggies, B. Neumann, V. Seiffart, W. Lindenmaier, A.D. Gruber, J. Ringe, T. Häupl, F. Thorey, E. Willbold, P. Corbeau, G. Gross, Mesenchymal stem cell-dependent formation of heterotopic tendon-bone insertions (osteotendinous junctions), Stem Cells 28(9) (2010) 1590-601, 10.1002/stem.487.

[111] R. Wang, B. Xu, H.G. Xu, Up-Regulation of TGF-β Promotes Tendon-to-Bone Healing after Anterior Cruciate Ligament Reconstruction using Bone Marrow-Derived Mesenchymal Stem Cells through the TGF-β/MAPK Signaling Pathway in a New Zealand White Rabbit Model, Cell Physiol Biochem 41(1) (2017) 213-226, 10.1159/000456046.

[112] B. Chen, B. Li, Y.-J. Qi, Q.-B. Ni, Z.-Q. Pan, H. Wang, L.-B. Chen, Enhancement of tendon-to-bone healing after anterior cruciate ligament reconstruction using bone marrow-derived mesenchymal stem cells genetically modified with bFGF/BMP2, Scientific Reports 6(1) (2016) 25940, 10.1038/srep25940.

[113] J. Kimmelman, The ethics of human gene transfer, Nature Reviews Genetics 9(3) (2008) 239-244, 10.1038/nrg2317.

[114] R.G. Crystal, Transfer of genes to humans: early lessons and obstacles to success, Science (New York, N.Y.) 270(5235) (1995) 404-10, 10.1126/science.270.5235.404.

[115] C.B. Ma, S. Kawamura, X.H. Deng, L. Ying, J. Schneidkraut, P. Hays, S.A. Rodeo, Bone morphogenetic proteins-signaling plays a role in tendon-to-bone healing: a study of rhBMP-2 and noggin, Am J Sports Med 35(4) (2007) 597-604, 10.1177/0363546506296312.

[116] Y. Hashimoto, G. Yoshida, H. Toyoda, K. Takaoka, Generation of tendon-to-bone interface "enthesis" with use of recombinant BMP-2 in a rabbit model, Journal of orthopaedic research :

official publication of the Orthopaedic Research Society 25(11) (2007) 1415-24, 10.1002/jor.20447.

[117] H.J. Seeherman, J.M. Archambault, S.A. Rodeo, A.S. Turner, L. Zekas, D. D'Augusta, X.J. Li, E. Smith, J.M. Wozney, rhBMP-12 Accelerates Healing of Rotator Cuff Repairs in a Sheep Model, JBJS 90(10) (2008)

[118] J.G. Kim, H.J. Kim, S.E. Kim, J.H. Bae, Y.J. Ko, J.H. Park, Enhancement of tendon-bone healing with the use of bone morphogenetic protein-2 inserted into the suture anchor hole in a rabbit patellar tendon model, Cytotherapy 16(6) (2014) 857-67, 10.1016/j.jcyt.2013.12.012.

[119] S. Thomopoulos, H.M. Kim, M.J. Silva, E. Ntouvali, C.N. Manning, R. Potter, H. Seeherman, R.H. Gelberman, Effect of bone morphogenetic protein 2 on tendon-to-bone healing in a canine flexor tendon model, Journal of orthopaedic research : official publication of the Orthopaedic Research Society 30(11) (2012) 1702-9, 10.1002/jor.22151.

[120] K.W. Lee, J.S. Lee, Y.S. Kim, Y.B. Shim, J.W. Jang, K.I. Lee, Effective healing of chronic rotator cuff injury using recombinant bone morphogenetic protein-2 coated dermal patch in vivo, J Biomed Mater Res B Appl Biomater 105(7) (2017) 1840-1846, 10.1002/jbm.b.33716.

[121] Y. Hirakawa, T. Manaka, K. Orita, Y. Ito, K. Ichikawa, H. Nakamura, The accelerated effect of recombinant human bone morphogenetic protein 2 delivered by β-tricalcium phosphate on tendon-to-bone repair process in rabbit models, J Shoulder Elbow Surg 27(5) (2018) 894-902, 10.1016/j.jse.2017.11.025.

[122] Y. Kabuto, T. Morihara, T. Sukenari, Y. Kida, R. Oda, Y. Arai, K. Sawada, K.-I. Matsuda, M. Kawata, Y. Tabata, H. Fujiwara, T. Kubo, Stimulation of Rotator Cuff Repair by Sustained Release of Bone Morphogenetic Protein-7 Using a Gelatin Hydrogel Sheet, Tissue engineering. Part A 21(13-14) (2015) 2025-2033, 10.1089/ten.TEA.2014.0541.

[123] M. Rickert, M. Jung, M. Adiyaman, W. Richter, H.G. Simank, A growth and differentiation factor-5 (GDF-5)-coated suture stimulates tendon healing in an Achilles tendon model in rats, Growth Factors 19(2) (2001) 115-26, 10.3109/08977190109001080.

[124] D.H. Murray, E.N. Kubiak, L.M. Jazrawi, A. Araghi, F. Kummer, M.I. Loebenberg, J.D. Zuckerman, The effect of cartilage-derived morphogenetic protein 2 on initial healing of a rotator cuff defect in a rat model, J Shoulder Elbow Surg 16(2) (2007) 251-4, 10.1016/j.jse.2006.07.002.

[125] S. Yamazaki, K. Yasuda, F. Tomita, H. Tohyama, A. Minami, The Effect of Transforming Growth Factor-β1 on Intraosseous Healing of Flexor Tendon Autograft Replacement of Anterior

Cruciate Ligament in Dogs, Arthroscopy: The Journal of Arthroscopic & Related Surgery 21(9) (2005) 1034-1041, 10.1016/j.arthro.2005.05.011.

[126] H. Arimura, C. Shukunami, T. Tokunaga, T. Karasugi, N. Okamoto, T. Taniwaki, H. Sakamoto, H. Mizuta, Y. Hiraki, TGF-β1 Improves Biomechanical Strength by Extracellular Matrix Accumulation Without Increasing the Number of Tenogenic Lineage Cells in a Rat Rotator Cuff Repair Model, Am J Sports Med 45(10) (2017) 2394-2404, 10.1177/0363546517707940.

[127] J.P. Yoon, C.H. Lee, J.W. Jung, H.J. Lee, Y.S. Lee, J.Y. Kim, G.Y. Park, J.H. Choi, S.W. Chung, Sustained Delivery of Transforming Growth Factor β1 by Use of Absorbable Alginate Scaffold Enhances Rotator Cuff Healing in a Rabbit Model, Am J Sports Med 46(6) (2018) 1441-1450, 10.1177/0363546518757759.

[128] X. You, Y. Shen, W. Yu, Y. He, Enhancement of tendon-bone healing following rotator cuff repair using hydroxyapatite with TGFβ1, Mol Med Rep 17(4) (2018) 4981-4988, 10.3892/mmr.2018.8499.

[129] C.N. Manning, H.M. Kim, S. Sakiyama-Elbert, L.M. Galatz, N. Havlioglu, S. Thomopoulos, Sustained delivery of transforming growth factor beta three enhances tendon-to-bone healing in a rat model, Journal of orthopaedic research : official publication of the Orthopaedic Research Society 29(7) (2011) 1099-105, 10.1002/jor.21301.

[130] H.M. Kim, L.M. Galatz, R. Das, N. Havlioglu, S.Y. Rothermich, S. Thomopoulos, The role of transforming growth factor beta isoforms in tendon-to-bone healing, Connect Tissue Res 52(2) (2011) 87-98, 10.3109/03008207.2010.483026.

[131] S. Zhao, J. Zhao, S. Dong, X. Huangfu, B. Li, H. Yang, J. Zhao, W. Cui, Biological augmentation of rotator cuff repair using bFGF-loaded electrospun poly(lactide-co-glycolide) fibrous membranes, Int J Nanomedicine 9 (2014) 2373-85, 10.2147/ijn.S59536.

[132] J. Ide, K. Kikukawa, J. Hirose, K. Iyama, H. Sakamoto, T. Fujimoto, H. Mizuta, The effect of a local application of fibroblast growth factor-2 on tendon-to-bone remodeling in rats with acute injury and repair of the supraspinatus tendon, J Shoulder Elbow Surg 18(3) (2009) 391-8, 10.1016/j.jse.2009.01.013.

[133] T. Tokunaga, C. Shukunami, N. Okamoto, T. Taniwaki, K. Oka, H. Sakamoto, J. Ide, H. Mizuta, Y. Hiraki, FGF-2 Stimulates the Growth of Tenogenic Progenitor Cells to Facilitate the Generation of Tenomodulin-Positive Tenocytes in a Rat Rotator Cuff Healing Model, Am J Sports Med 43(10) (2015) 2411-22, 10.1177/0363546515597488.

[134] T. Tokunaga, T. Karasugi, H. Arimura, R. Yonemitsu, H. Sakamoto, J. Ide, H. Mizuta, Enhancement of rotator cuff tendon-bone healing with fibroblast growth factor 2 impregnated in gelatin hydrogel sheets in a rabbit model, J Shoulder Elbow Surg 26(10) (2017) 1708-1717, 10.1016/j.jse.2017.03.020.

[135] J. Nakase, K. Kitaoka, K. Matsumoto, K. Tomita, Facilitated tendon-bone healing by local delivery of recombinant hepatocyte growth factor in rabbits, Arthroscopy : the journal of arthroscopic & related surgery : official publication of the Arthroscopy Association of North America and the International Arthroscopy Association 26(1) (2010) 84-90, 10.1016/j.arthro.2009.06.029.

[136] S. Buchmann, G.H. Sandmann, L. Walz, T. Reichel, K. Beitzel, G. Wexel, W. Tian, A. Battmann, S. Vogt, G. Winter, A.B. Imhoff, Growth factor release by vesicular phospholipid gels: in-vitro results and application for rotator cuff repair in a rat model, BMC Musculoskelet Disord 16 (2015) 82, 10.1186/s12891-015-0542-1.

[137] D. Ross, T. Maerz, M. Kurdziel, J. Hein, S. Doshi, A. Bedi, K. Anderson, K. Baker, The effect of granulocyte-colony stimulating factor on rotator cuff healing after injury and repair, Clin Orthop Relat Res 473(5) (2015) 1655-64, 10.1007/s11999-015-4218-9.

[138] E. Anitua, R. Prado, G. Orive, Allogeneic Platelet-Rich Plasma: At the Dawn of an Off-the-Shelf Therapy?, Trends Biotechnol 35(2) (2017) 91-93, 10.1016/j.tibtech.2016.11.001.

[139] D.M. Dohan Ehrenfest, L. Rasmusson, T. Albrektsson, Classification of platelet concentrates: from pure platelet-rich plasma (P-PRP) to leucocyte- and platelet-rich fibrin (L-PRF), Trends Biotechnol 27(3) (2009) 158-67, 10.1016/j.tibtech.2008.11.009.

[140] B.B. Mendes, M. Gómez-Florit, P.S. Babo, R.M. Domingues, R.L. Reis, M.E. Gomes, Blood derivatives awaken in regenerative medicine strategies to modulate wound healing, Adv Drug Deliv Rev 129 (2018) 376-393, 10.1016/j.addr.2017.12.018.

[141] J.R. Ebert, A. Wang, A. Smith, R. Nairn, W. Breidahl, M.H. Zheng, T. Ackland, A Midterm Evaluation of Postoperative Platelet-Rich Plasma Injections on Arthroscopic Supraspinatus Repair: A Randomized Controlled Trial, Am J Sports Med 45(13) (2017) 2965-2974, 10.1177/0363546517719048.

[142] J. Yang, Y. Sun, P. Xu, B. Cheng, Can patients get better clinical outcomes by using PRP in rotator cuff repair: a meta-analysis of randomized controlled trials, J Sports Med Phys Fitness 56(11) (2016) 1359-1367,

[143] R. Crespo-Diaz, A. Behfar, G.W. Butler, D.J. Padley, M.G. Sarr, J. Bartunek, A.B. Dietz, A. Terzic, Platelet lysate consisting of a natural repair proteome supports human mesenchymal stem cell proliferation and chromosomal stability, Cell transplantation 20(6) (2011) 797-811, 10.3727/096368910x543376.

[144] R. Costa-Almeida, A.R. Franco, T. Pesqueira, M.B. Oliveira, P.S. Babo, I.B. Leonor, J.F. Mano, R.L. Reis, M.E. Gomes, The effects of platelet lysate patches on the activity of tendon-derived cells, Acta Biomaterialia 68 (2018) 29-40, 10.1016/j.actbio.2018.01.006.

[145] B.B. Mendes, M. Gómez-Florit, R.A. Pires, R.M.A. Domingues, R.L. Reis, M.E. Gomes, Human-based fibrillar nanocomposite hydrogels as bioinstructive matrices to tune stem cell behavior, Nanoscale 10(36) (2018) 17388-17401, 10.1039/C8NR04273J.

[146] İ. Ağır, M.N. Aytekin, F. Küçükdurmaz, B. Kocaoğlu, S. Çetinel, M. Karahan, The effect of platelet-rich plasma in bone-tendon integration, Adv Clin Exp Med 26(2) (2017) 193-199, 10.17219/acem/61384.

[147] J. Zhang, T. Yuan, N. Zheng, Y. Zhou, M.V. Hogan, J.H.C. Wang, The combined use of kartogenin and platelet-rich plasma promotes fibrocartilage formation in the wounded rat Achilles tendon entheses, Bone & Joint Research 6(4) (2017) 231-244, 10.1302/2046-3758.64.BJR-2017-0268.R1.

[148] J. Beck, D. Evans, P.M. Tonino, S. Yong, J.J. Callaci, The biomechanical and histologic effects of platelet-rich plasma on rat rotator cuff repairs, Am J Sports Med 40(9) (2012) 2037-44, 10.1177/0363546512453300.

[149] O. Dolkart, O. Chechik, Y. Zarfati, T. Brosh, F. Alhajajra, E. Maman, A single dose of platelet-rich plasma improves the organization and strength of a surgically repaired rotator cuff tendon in rats, Archives of orthopaedic and traumatic surgery. Archiv fur orthopadische und Unfall-Chirurgie 134(9) (2014) 1271-7, 10.1007/s00402-014-2026-4.

[150] A. Ersen, M. Demirhan, A.C. Atalar, M. Kapicioğlu, G. Baysal, Platelet-rich plasma for enhancing surgical rotator cuff repair: evaluation and comparison of two application methods in a rat model, Archives of orthopaedic and traumatic surgery. Archiv fur orthopadische und Unfall-Chirurgie 134(3) (2014) 405-11, 10.1007/s00402-013-1914-3.

[151] Y. Wu, Y. Dong, S. Chen, Y. Li, Effect of platelet-rich plasma and bioactive glass powder for the improvement of rotator cuff tendon-to-bone healing in a rabbit model, International journal of molecular sciences 15(12) (2014) 21980-21991, 10.3390/ijms151221980.

[152] A.J. Lee, W.-H. Chung, D.-H. Kim, K.-P. Lee, D.-J. Chung, S.H. Do, H.-Y. Kim, Anterior cruciate ligament reconstruction in a rabbit model using canine small intestinal submucosa and autologous platelet-rich plasma, Journal of Surgical Research 178(1) (2012) 206-215, 10.1016/j.jss.2012.01.052.

[153] C. Teng, C. Zhou, D. Xu, F. Bi, Combination of platelet-rich plasma and bone marrow mesenchymal stem cells enhances tendon-bone healing in a rabbit model of anterior cruciate ligament reconstruction, J Orthop Surg Res 11(1) (2016) 96, 10.1186/s13018-016-0433-7.

[154] G.D. Prestwich, Simplifying the extracellular matrix for 3-D cell culture and tissue engineering: a pragmatic approach, Journal of cellular biochemistry 101(6) (2007) 1370-83, 10.1002/jcb.21386.

[155] K. Duval, H. Grover, L.H. Han, Y. Mou, A.F. Pegoraro, J. Fredberg, Z. Chen, Modeling Physiological Events in 2D vs. 3D Cell Culture, Physiology (Bethesda) 32(4) (2017) 266-277, 10.1152/physiol.00036.2016.

[156] M. Ramalingam, M.F. Young, V. Thomas, L. Sun, L.C. Chow, C.K. Tison, K. Chatterjee, W.C. Miles, C.G. Simon, Jr., Nanofiber scaffold gradients for interfacial tissue engineering, J Biomater Appl 27(6) (2013) 695-705, 10.1177/0885328211423783.

[157] X. Li, J. Xie, J. Lipner, X. Yuan, S. Thomopoulos, Y. Xia, Nanofiber Scaffolds with Gradations in Mineral Content for Mimicking the Tendon-to-Bone Insertion Site, Nano Letters 9(7) (2009) 2763-2768, 10.1021/nl901582f.

[158] J. Xie, B. Ma, P.L. Michael, F.D. Shuler, Fabrication of nanofiber scaffolds with gradations in fiber organization and their potential applications, Macromol Biosci 12(10) (2012) 1336-41, 10.1002/mabi.201200115.

[159] J. Xie, X. Li, J. Lipner, C.N. Manning, A.G. Schwartz, S. Thomopoulos, Y. Xia, "Aligned-to-random" nanofiber scaffolds for mimicking the structure of the tendon-to-bone insertion site, Nanoscale 2(6) (2010) 923-6, 10.1039/c0nr00192a.

[160] S. Samavedi, C. Olsen Horton, S.A. Guelcher, A.S. Goldstein, A.R. Whittington, Fabrication of a model continuously graded co-electrospun mesh for regeneration of the ligament–bone interface, Acta Biomaterialia 7(12) (2011) 4131-4138, 10.1016/j.actbio.2011.07.008.

[161] S. Font Tellado, W. Bonani, E.R. Balmayor, P. Foehr, A. Motta, C. Migliaresi, M. van Griensven, Fabrication and Characterization of Biphasic Silk Fibroin Scaffolds for Tendon/Ligament-to-Bone Tissue Engineering, Tissue Eng Part A 23(15-16) (2017) 859-872, 10.1089/ten.TEA.2016.0460.

[162] B.S. Kim, E.J. Kim, J.S. Choi, J.H. Jeong, C.H. Jo, Y.W. Cho, Human collagen-based multilayer scaffolds for tendon-to-bone interface tissue engineering, J Biomed Mater Res A 102(11) (2014) 4044-54, 10.1002/jbm.a.35057.

[163] R.I. Sharma, J.G. Snedeker, Biochemical and biomechanical gradients for directed bone marrow stromal cell differentiation toward tendon and bone, Biomaterials 31(30) (2010) 7695-704, 10.1016/j.biomaterials.2010.06.046.

[164] R. Newsham-West, H. Nicholson, M. Walton, P. Milburn, Long-term morphology of a healing bone?tendon interface: a histological observation in the sheep model, Journal of anatomy 210(3) (2007) 318-327, 10.1111/j.1469-7580.2007.00699.x.

[165] Z. Lin, X. Zhao, S. Chen, C. Du, Osteogenic and tenogenic induction of hBMSCs by an integrated nanofibrous scaffold with chemical and structural mimicry of the bone–ligament connection, Journal of Materials Chemistry B 5(5) (2017) 1015-1027, 10.1039/C6TB02156E.

[166] S. Samavedi, P. Vaidya, P. Gaddam, A.R. Whittington, A.S. Goldstein, Electrospun meshes possessing region-wise differences in fiber orientation, diameter, chemistry and mechanical properties for engineering bone-ligament-bone tissues, Biotechnol Bioeng 111(12) (2014) 2549-59, 10.1002/bit.25299.

[167] S.R. Caliari, D.W. Weisgerber, W.K. Grier, Z. Mahmassani, M.D. Boppart, B.A. Harley, Collagen Scaffolds Incorporating Coincident Gradations of Instructive Structural and Biochemical Cues for Osteotendinous Junction Engineering, Adv Healthc Mater 4(6) (2015) 831-7, 10.1002/adhm.201400809.

[168] T.M. Hammoudi, H. Lu, J.S. Temenoff, Long-term spatially defined coculture within three-dimensional photopatterned hydrogels, Tissue Eng Part C Methods 16(6) (2010) 1621-8, 10.1089/ten.TEC.2010.0146.

[169] M. Laranjeira, R.M.A. Domingues, R. Costa-Almeida, R.L. Reis, M.E. Gomes, 3D Mimicry of Native-Tissue-Fiber Architecture Guides Tendon-Derived Cells and Adipose Stem Cells into Artificial Tendon Constructs, Small 13(31) (2017) 10.1002/smll.201700689.

[170] M. Younesi, A. Islam, V. Kishore, J.M. Anderson, O. Akkus, Tenogenic Induction of Human MSCs by Anisotropically Aligned Collagen Biotextiles, Adv Funct Mater 24(36) (2014) 5762-5770, 10.1002/adfm.201400828.

[171] H. Liu, H. Fan, Y. Wang, S.L. Toh, J.C. Goh, The interaction between a combined knitted silk scaffold and microporous silk sponge with human mesenchymal stem cells for ligament tissue engineering, Biomaterials 29(6) (2008) 662-74, 10.1016/j.biomaterials.2007.10.035.

[172] W. Shen, X. Chen, Y. Hu, Z. Yin, T. Zhu, J. Hu, J. Chen, Z. Zheng, W. Zhang, J. Ran, B.C. Heng, J. Ji, W. Chen, H.W. Ouyang, Long-term effects of knitted silk-collagen sponge scaffold on anterior cruciate ligament reconstruction and osteoarthritis prevention, Biomaterials 35(28) (2014) 8154-63, 10.1016/j.biomaterials.2014.06.019.

[173] H. Li, J. Fan, L. Sun, X. Liu, P. Cheng, H. Fan, Functional regeneration of ligament-bone interface using a triphasic silk-based graft, Biomaterials 106 (2016) 180-92, 10.1016/j.biomaterials.2016.08.012.

[174] E. Tanck, G. Hannink, R. Ruimerman, P. Buma, E.H. Burger, R. Huiskes, Cortical bone development under the growth plate is regulated by mechanical load transfer, Journal of anatomy 208(1) (2006) 73-9, 10.1111/j.1469-7580.2006.00503.x.

[175] I.A. Stokes, Mechanical effects on skeletal growth, J Musculoskelet Neuronal Interact 2(3) (2002) 277-80,

[176] Q. Liu, X. Hu, X. Zhang, X. Duan, P. Yang, F. Zhao, Y. Ao, Effects of mechanical stress on chondrocyte phenotype and chondrocyte extracellular matrix expression, Sci Rep 6 (2016) 37268, 10.1038/srep37268.

[177] N.R. Schiele, J.E. Marturano, C.K. Kuo, Mechanical factors in embryonic tendon development: Potential cues for stem cell tenogenesis, Current opinion in biotechnology 24(5) (2013) 10.1016/j.copbio.2013.07.003, 10.1016/j.copbio.2013.07.003.

[178] M.T. Galloway, A.L. Lalley, J.T. Shearn, The Role of Mechanical Loading in Tendon Development, Maintenance, Injury, and Repair, The Journal of bone and joint surgery. American volume 95(17) (2013) 1620-1628, 10.2106/JBJS.L.01004.

[179] M. Brandt, M.I. Siegel, The effects of stress on cortical bone thickness in rodents, American Journal of Physical Anthropology 49(1) (1978) 31-34, 10.1002/ajpa.1330490106.

[180] L.M. McNamara, J.C. Van der Linden, H. Weinans, P.J. Prendergast, Stress-concentrating effect of resorption lacunae in trabecular bone, J Biomech 39(4) (2006) 734-41, 10.1016/j.jbiomech.2004.12.027.

[181] S.L. Woo, M.A. Gomez, Y.K. Woo, W.H. Akeson, Mechanical properties of tendons and ligaments. II. The relationships of immobilization and exercise on tissue remodeling, Biorheology 19(3) (1982) 397-408,

[182] L.M. Galatz, N. Charlton, R. Das, H.M. Kim, N. Havlioglu, S. Thomopoulos, Complete removal of load is detrimental to rotator cuff healing, Journal of Shoulder and Elbow Surgery 18(5) (2009) 669-675, 10.1016/j.jse.2009.02.016.

[183] S. Thomopoulos, H.-M. Kim, S.Y. Rothermich, C. Biederstadt, R. Das, L.M. Galatz, Decreased muscle loading delays maturation of the tendon enthesis during postnatal development, Journal of Orthopaedic Research 25(9) (2007) 1154-1163, 10.1002/jor.20418.

[184] H.M. Kim, L.M. Galatz, R. Das, N. Patel, S. Thomopoulos, Musculoskeletal deformities secondary to neurotomy of the superior trunk of the brachial plexus in neonatal mice, Journal of orthopaedic research : official publication of the Orthopaedic Research Society 28(10) (2010) 1391-1398, 10.1002/jor.21128.

[185] A.M. Tatara, J.H. Lipner, R. Das, H.M. Kim, N. Patel, E. Ntouvali, M.J. Silva, S. Thomopoulos, The role of muscle loading on bone (Re)modeling at the developing enthesis, PloS one 9(5) (2014) e97375-e97375, 10.1371/journal.pone.0097375.

[186] E. Blitz, S. Viukov, A. Sharir, Y. Shwartz, J.L. Galloway, B.A. Pryce, R.L. Johnson, C.J. Tabin, R. Schweitzer, E. Zelzer, Bone Ridge Patterning during Musculoskeletal Assembly Is Mediated through SCX Regulation of Bmp4 at the Tendon-Skeleton Junction, Developmental Cell 17(6) (2009) 861-873, 10.1016/j.devcel.2009.10.010.

[187] B. Mikic, T.L. Johnson, A.B. Chhabra, B.J. Schalet, M. Wong, E.B. Hunziker, Differential effects of embryonic immobilization on the development of fibrocartilaginous skeletal elements, Journal of rehabilitation research and development 37(2) (2000) 127-33,

[188] S. Thomopoulos, G.M. Genin, L.M. Galatz, The development and morphogenesis of the tendon-to-bone insertion What development can teach us about healing, Journal of musculoskeletal & neuronal interactions 10(1) (2010) 35-45,

[189] I. Martin, D. Wendt, M. Heberer, The role of bioreactors in tissue engineering, Trends in Biotechnology 22(2) (2004) 80-86, 10.1016/j.tibtech.2003.12.001.

[190] M.C. McCorry, M.M. Mansfield, X. Sha, D.J. Coppola, J.W. Lee, L.J. Bonassar, A model system for developing a tissue engineered meniscal enthesis, Acta Biomater 56 (2017) 110-117, 10.1016/j.actbio.2016.10.040.

[191] S.M. Goldman, G.A. Barabino, Spatial Engineering of Osteochondral Tissue Constructs Through Microfluidically Directed Differentiation of Mesenchymal Stem Cells, Biores Open Access 5(1) (2016) 109-17, 10.1089/biores.2016.0005.

[192] S.M. Goldman, G.A. Barabino, Cultivation of agarose-based microfluidic hydrogel promotes the development of large, full-thickness, tissue-engineered articular cartilage constructs, J Tissue Eng Regen Med 11(2) (2017) 572-581, 10.1002/term.1954.

[193] M. Peroglio, D. Gaspar, D.I. Zeugolis, M. Alini, Relevance of bioreactors and whole tissue cultures for the translation of new therapies to humans, Journal of orthopaedic research : official publication of the Orthopaedic Research Society 10.1002/jor.23655 (2017) 10.1002/jor.23655.

[194] L.A. McMahon, A.J. Reid, V.A. Campbell, P.J. Prendergast, Regulatory effects of mechanical strain on the chondrogenic differentiation of MSCs in a collagen-GAG scaffold: experimental and computational analysis, Ann Biomed Eng 36(2) (2008) 185-94, 10.1007/s10439-007-9416-5.

[195] A.C. Daly, B.N. Sathy, D.J. Kelly, Engineering large cartilage tissues using dynamic bioreactor culture at defined oxygen conditions, Journal of tissue engineering 9 (2018) 2041731417753718, 10.1177/2041731417753718.

[196] S.F. Carroll, C.T. Buckley, D.J. Kelly, Cyclic Tensile Strain Can Play a Role in Directing both Intramembranous and Endochondral Ossification of Mesenchymal Stem Cells, Front Bioeng Biotechnol 5 (2017) 73-73, 10.3389/fbioe.2017.00073.

[197] Y. Qiu, J. Lei, T.J. Koob, J.S. Temenoff, Cyclic tension promotes fibroblastic differentiation of human MSCs cultured on collagen-fibre scaffolds, J Tissue Eng Regen Med 10(12) (2016) 989-999, 10.1002/term.1880.

[198] A.J. Boys, M.C. McCorry, S. Rodeo, L.J. Bonassar, L.A. Estroff, Next generation tissue engineering of orthopedic soft tissue-to-bone interfaces, MRS Communications 7(3) (2017) 289-308, 10.1557/mrc.2017.91.

[199] W.L. Grayson, S. Bhumiratana, P.H. Grace Chao, C.T. Hung, G. Vunjak-Novakovic, Spatial regulation of human mesenchymal stem cell differentiation in engineered osteochondral constructs: effects of pre-differentiation, soluble factors and medium perfusion, Osteoarthritis and cartilage 18(5) (2010) 714-23, 10.1016/j.joca.2010.01.008.

[200] R. Omi, A. Gingery, S.P. Steinmann, P.C. Amadio, K.N. An, C. Zhao, Rotator cuff repair augmentation in a rat model that combines a multilayer xenograft tendon scaffold with bone marrow stromal cells, J Shoulder Elbow Surg 25(3) (2016) 469-77, 10.1016/j.jse.2015.08.008.

[201] D.R. Peterson, K.L. Ohashi, H.M. Aberman, P.A. Piza, H.C. Crockett, J.I. Fernandez, P.J. Lund, K.A. Funk, M.L. Hawes, B.G. Parks, R.-H. Mattern, Evaluation of a collagen-coated, resorbable fiber scaffold loaded with a peptide basic fibroblast growth factor mimetic in a sheep model of rotator cuff repair, Journal of Shoulder and Elbow Surgery 24(11) (2015) 1764-1773, 10.1016/j.jse.2015.06.009.

[202] S.A. Rodeo, H.G. Potter, S. Kawamura, A.S. Turner, H.J. Kim, B.L. Atkinson, Biologic augmentation of rotator cuff tendon-healing with use of a mixture of osteoinductive growth factors,

The Journal of bone and joint surgery. American volume 89(11) (2007) 2485-97, 10.2106/JBJS.C.01627.

[203] I. Encalada-Diaz, B.J. Cole, J.D. Macgillivray, M. Ruiz-Suarez, J.S. Kercher, N.A. Friel, F. Valero-Gonzalez, Rotator cuff repair augmentation using a novel polycarbonate polyurethane patch: preliminary results at 12 months' follow-up, J Shoulder Elbow Surg 20(5) (2011) 788-94, 10.1016/j.jse.2010.08.013.

[204] J.A. McCarron, R.A. Milks, X. Chen, J.P. Iannotti, K.A. Derwin, Improved time-zero biomechanical properties using poly-L-lactic acid graft augmentation in a cadaveric rotator cuff repair model, Journal of Shoulder and Elbow Surgery 19(5) (2010) 688-696, 10.1016/j.jse.2009.12.008.

[205] D. Bryant, R. Holtby, K. Willits, R. Litchfield, D. Drosdowech, A. Spouge, D. White, G. Guyatt, A randomized clinical trial to compare the effectiveness of rotator cuff repair with or without augmentation using porcine small intestine submucosa for patients with moderate to large rotator cuff tears: a pilot study, J Shoulder Elbow Surg 25(10) (2016) 1623-33, 10.1016/j.jse.2016.06.006.

[206] J.P. Iannotti, M.J. Codsi, Y.W. Kwon, K. Derwin, J. Ciccone, J.J. Brems, Porcine small intestine submucosa augmentation of surgical repair of chronic two-tendon rotator cuff tears. A randomized, controlled trial, The Journal of bone and joint surgery. American volume 88(6) (2006) 1238-44, 10.2106/jbjs.E.00524.

[207] J.L. Bond, R.M. Dopirak, J. Higgins, J. Burns, S.J. Snyder, Arthroscopic Replacement of Massive, Irreparable Rotator Cuff Tears Using a GraftJacket Allograft: Technique and Preliminary Results, Arthroscopy: The Journal of Arthroscopic & Related Surgery 24(4) (2008) 403.e1-403.e8, 10.1016/j.arthro.2007.07.033.

[208] W.Z. Burkhead, S.C. Schiffern, S.G. Krishnan, Use of Graft Jacket as an Augmentation for Massive Rotator Cuff Tears, Seminars in Arthroplasty 18(1) (2007) 11-18, 10.1053/j.sart.2006.11.017.

[209] P. Hernigou, C.H. Flouzat Lachaniette, J. Delambre, S. Zilber, P. Duffiet, N. Chevallier, H. Rouard, Biologic augmentation of rotator cuff repair with mesenchymal stem cells during arthroscopy improves healing and prevents further tears: a case-controlled study, Int Orthop 38(9) (2014) 1811-8, 10.1007/s00264-014-2391-1.

[210] Y.S. Kim, C.H. Sung, S.H. Chung, S.J. Kwak, Y.G. Koh, Does an Injection of Adipose-Derived Mesenchymal Stem Cells Loaded in Fibrin Glue Influence Rotator Cuff Repair Outcomes? A Clinical

and Magnetic Resonance Imaging Study, Am J Sports Med 45(9) (2017) 2010-2018, 10.1177/0363546517702863.

SECTION II: Experimental Design

CHAPTER 4. Materials and Methods

OVERVIEW

This chapter aims at providing a detailed description for the selection of the materials and strategies followed to achieve the main objectives proposed by this doctoral project. Moreover, herein the experimental procedures used throughout the developed work are detailed in the present chapter.

Although each chapter of the present thesis contains the respective "material and methods", this section intends to provide a broad view of the used protocols, while providing complete information on the rationale behind the selection of cells and materials, methodology and the chosen characterization assays used in this PhD thesis.

4.1. MATERIALS

Tissue engineering offers different materials with tunable characteristics to obtain an end product that will mimic as close as possible the native ECM of target tissues. In this regard, reliable biomimetic components have to be chosen in order to constitute a major tool for the progress of the therapeutic field. Having this is mind, we believe that the conjugation of natural and synthetic biopolymers, with or without the incorporation of nano/microparticles, for the development of biofunctional biosystems, provides a reliable solution to address the main goal of this thesis, the mimicry of the native microenvironment of the tendon-to-bone interface.

Therefore, in the present thesis, different materials were explored for the production of different systems for enthesis tissue regeneration, including nano/microfibers and scaffolds.

A summary of the materials used alongside the correspondent production/processing techniques is presented on Table 4.1.

Table 4.1 | Summary of materials used, type, and production and processing techniques applied.

Material	Chapter	Origin	Method(s)	Obtained system
Poly(ε-caprolactone) (PCL)		Synthetic	Wet-spinning; Electrospinning	Microfibers/Nanofibers Gradient Scaffold
Hydroxyapatite Particles (HAp)		Synthetic	Wet-spinning; Electropinning	Microfibers; Gradient Scaffold
Gelatin (GEL)		Natural *(Protein)*	Wet-spinning – Crosslinking	Microfibers/nanofibers; Gradient Scaffold
Platelet lysate (PL)		Natural *(Pool of biomolecules)*	Electrospinning; Hydrogel coating	Nanofibers; Gradient scaffolds

4.1.1. SYNTHETIC ORIGIN MATERIALS

4.1.1.1. Poly(ε-caprolactone)

Poly(ε-caprolactone) is a hydrophobic and semicrystalline biodegradable polyester (Table 4.1). It presents an excellent chain flexibility and can be synthesized by an ionic or metal catalyzed ring-opening

polymerization of epsilon-caprolactone, commonly derived from fossil carbon [1] (Figure 4.1). Having a rather low melting point and glass transition temperature compared to other biodegradable polymers (Table 4.2), its properties depend on molecular weight (Mw). For instance, Mw of 15,000 g/mol means a brittle material while higher Mw (~40,000 g/mol) indicate a softer and semicrystalline material [2].

Table 4.2 | Physicochemical properties of PCL [3].

Melting Point (T_m)	65 °C
Glass transition temperature (T_g)	-65°C to -61°C
Crystallinity (%)	67
Water permeability at 25ºC ($g/m^2/day$)	177
Surface tension (mN/m)	51
Solubility (at room temperature)	Highly soluble in: Benzene, Chloroform, Toluene and Dichloromethane; Slightly soluble: Acetonitrile, Acetone, 2-Butanone, Dimethylformamide; Insoluble: Water, Alcohols, Diethyl Ether

This polymer is degraded by hydrolytic scission of its aliphatic-ester linkage, presenting a slow degradation duration in the human body [4, 5]. PCL has low tensile strength (up to 23MPa) but a high elongation at breakage (>300 MPa) [3, 6].

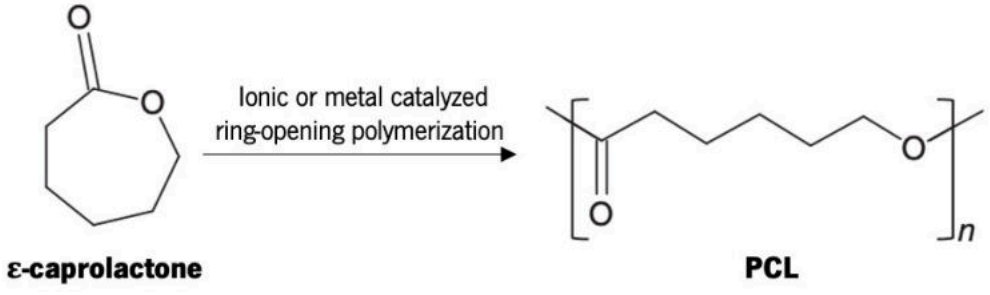

Figure 4.1 | Synthetic path to PCL by ionic or metal-catalyzed of ε-caprolactone.

This polymer was recognized and approved by Food and Drug Administration (FDA) as a biomaterial for some specific biomedical applications [6] and, in essence, due to its low cost, biocompatibility, degradation and mechanical strength properties, it has been extensively studied for orthopedic applications.

The limitations of PCL lie on its hydrophobicity and inadequate wettability which results in poor cell attachment, being this problem overcome with several surface modifications [3]. Additionally, its poor antimicrobial properties and use of strong and toxic solvents are pointed as problems associated with the use of PCL.

In this thesis, PCL with Mw of 80,000 (determined by GPC) was purchased by Sigma-Aldrich (St. Louis, MO; USA) and used for the production of textured microfibers by wet-spinning (**CHAPTER 7**) and nano/microfibers threads/yarns by electrospinning (**CHAPTER 8** and **9**) to mimic as close as possible the hierarchical and mechanical properties found at the tendon-to-bone interface and healthy and diseased tendon ECM.

4.1.1.2. Hydroxyapatite particles

Hydroxyapatite (HAp), commonly represented by the chemical formula $Ca_{10}(PO_4)_6(OH)_2$, is a naturally occurring mineral form of calcium apatite and has been an attractive material for human hard tissue engineering. The human natural bone contains approximately 70% of HAp by weight and 50% by volume [7]. Interestingly, the crystallography and chemical composition of hydroxyapatite closely resemble those of bone and tooth mineral [7]. Pure HAp has the theoretical density of 3.156 g/cm^3 [8], a theoretical composition (%wt) of 39.68 of calcium (Ca), 18.45 of phosphate (P); a calcium phosphate (CaP) ratio of 3.151 and CaP molar ratio of 1.667 [9].

Hydroxyapatite can be found in different phases, such as solutions, slurries, powders, dispersion media (gas, liquid, or solid), dispersion tools (nozzle, propeller, sieve, mould), being the powder the most commonly used. Different ceramic processing routes can be used to obtain HAp powder; however, the resulting microstructure and properties vary considerably. Hydroxyapatite can be synthesized by a variety of techniques that can be broadly grouped into six sets of methods (Table 4.3): 1) dry methods (solid state and mechanochemical reactions [10, 11]); 2) wet methods (low-temperature chemical precipitation, co-precipitation, sol-gel route and hydrolysis) [12]; 3) hydrothermal methods (aqueous solutions of high temperature and high voltage, emulsion and microemulsion, sonochemical) [13, 14]; 4) high temperature

processes (combustion, pyrolysis) [15]; 5) biogenic sources (extracted from fish bones, shells, eggshells, bovine bones) [16]; and 6) combination of the aforementioned methods [17].

Table 4.3 | Methods used for the production of hydroxyapatite. Adapted from [18].

Method	Type of reaction	Temp (°C)	Purity	CaP ratio	Obtained morphology	Particle size
Dry	Solid-state	±1000	Low	Variable	Miscellaneous	Micron
	Mechano-chemical			Non-stoichiometric		Nano
Wet	Precipitation	100-1300	Variable	Non-stoichiometric	Miscellaneous	Nanosized
	Hydrolysis	±900	High	Stoichiometric		Variable
	Sol-Gel	500-1300	Variable			Nano
Hydrothermal	Emulsion	±25	Variable	Non-stoichiometric	Spherical/ needle-like	Nano/ micro
	Hydrothermal	±120	High	Stoichiometric		Nano
	Sonochemical	600-1000		Variable	Miscellaneous	
High Temperature	Combustion	100-1300	High	Variable	Miscellaneous	Nanosized
	Pyrolysis	±600	Variable	Stoichiometric		Nano/ micro
Biogenic	-	-	Variable	Stoichiometric	Miscellaneous	Nanosized

The development of synthesis procedures by precipitation, sol-gel and hydrothermal reaction have been emphasized as with these techniques highly homogenous microstructure can be acquired [19]. Nonetheless, the preparation of HAp particles with well-defined stoichiometry, high aspect ratio and high crystallinity still presents several limitations. Even though, using conventional mechanical and wet chemical methods a better final product can be obtained, if the Ca/P stoichiometry is not adjusted to 1.67 during the precipitation step, β-TCP and CaO can be formed [20].

Interestingly, with the application of different synthesis/fabrication methods over the years, a diversity of particles with different shapes, sizes and diameters have been arising. Among them, nanoparticles,

nanodots, or nano-powder are the most predominant particles that have been an important part for the fabrication of pastes and cements used for minimally invasive approaches. HAp has demonstrated great potential for biomedical applications, being used in the orthopedic field as material for bone and dental implant and protheses [21, 22]. Among the most important biomedical applications, HAp can be used in the controlled release of drugs (drug delivery systems), coating of implants, and bone grafts and scaffolds for tissue engineering [22].

In **CHAPTER 7** of this thesis, microparticles of HAp were synthetized and incorporated into a polymeric solution of PCL/GEL to produce wet-spun textured microfibers aiming the replication of bone-ECM, while inducing the osteogenic differentiation of stem cells, and the creation of HAp gradient within a produced tri-dimensional (3D) scaffold for tendon-to-bone interface replication. For HAp synthesis, a precipitation reaction of calcium hydroxide (Riedel-de Haën, Germany) and orthophosphoric acid 85% (Panreac, Spain) solutions was performed in an aqueous system at room temperature. The mixing was performed in a basic environment (pH 11), adjusted with concentrated ammonium hydroxide (1 m, Riedel-de Haën, Germany) at a continuous flow rate ranging from 8 to 15 mL min−1. The formed ceramic powder was sieved to obtain particles smaller than 63 μm.

Lately, in chapter 9, HAp was incorporated in electrospun hollow and emulsion isotropic threads to induce an osteogenic commitment of stem cells without the need of medium supplementation while replication the mineral composition of bone tissue. For the incorporation, nanohydroxyapatite (nHAp, < 200 nm) was chosen and added to a PCL solution (17% w/v), representing 1% w/w of PCL. The presence of nHAp within produced threads was visualized after alizarin red staining under the optical microscope

4.1.2. NATURAL ORIGIN MATERIALS

4.1.2.1. Gelatin

Gelatin (GEL) is a fibrous protein derived from collagen. This protein is normally extracted from the skin, bones and connective tissues of animal collagen, normally through heat dissolution under acidic or alkaline pH, and partial hydrolysis. During extraction, the tertiary structure of interconnected collagen chains is broken, originating single chains that retain collagen's natural cell binding motifs, such as the tripeptide Arg-Gly-Asp (RGD) [23, 24], as well as matrix metalloproteinase (MMP) recognition sites [25]. This feature is described to increase biodegradability improving the *in vivo* remodeling [26]. Notably, compared to collagen, gelatin presents several other advantages, namely low cost, high biocompatibility, biodegradability and lower antigenicity. Additionally, gelation of gelatin has been shown to occur at low temperatures and several chemical reagents have been applied to covalently crosslink gelatin [27].

Among these reagents, glutaraldehyde (GTA) is one of the most used. Crosslinking with GTA involves reactions between the free amines groups of lysine or hydroxylysine amino acid residues in the collagenous polypeptide chains and the aldehyde groups of GTA to produce imine linkages (Figure 4.2) [28-30]. Nevertheless, GTA is known to be cytotoxic being necessary a careful preparation of produced materials prior to use.

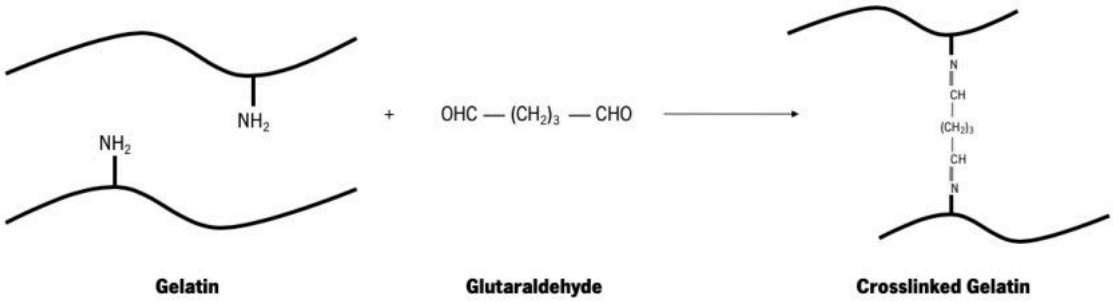

Figure 4.2 | Chemical reaction of gelatin crosslinking using glutaraldehyde.

Biomaterials using gelatin alone or in combination with synthetic polymers have been widely explored, especially in the case of both soft and hard tissues as it mimics the collagen-rich ECM [27, 31-33]. Therefore, in **CHAPTER 7** of this thesis, type B gelatin from porcine skin was purchased from Sigma-Aldrich and mixed with a polymeric solution of PCL to replicate as close as possible the ECM composition of tendon, interface of bone tissues. Moreover, in **CHAPTER 9**, gelatin from porcine skin (type A, gel strength~300 bloom, Sigma-Aldrich) was used to produce a hydrogel around PCL yarns and used as control to platelet lysates hydrogels.

4.1.2.2. Platelet lysate

Platelet lysate (PL) is a by-product of freeze/thaw processing of outdated platelet concentrate (PC), commonly known as platelet rich plasm (PRP). In comparison with other hemoderivatives, PL holds numerous advantages such as: 1) discards the necessity of an invasive blood collection from donors; 2) requires an easy and straightforward processing protocol without the need of any clot activator to release the platelet factors; 3) it can be freeze and stored to be redly used after thaw; and 4) the concentration of growth factors and cytokines is highly reproducible between batches, reducing the variability and contributing for more predicable outcomes [34]. Different activation mechanisms can be used for the release of endogenous growth factors stored in PC and ultimately producing PL, namely contact with thrombin [35, 36], calcium salts [35, 37, 38] or by simply causing the physical disruption of platelets through thermal and osmotic shock [39-41]. Moreover, PL is rich in transforming growth factor-β (TGF-

β), insulin growth factor-1 (IGF-1), endothelial growth factor (EGF), platelet derived growth factor (PDGF), vascular endothelial growth factor (VEGF) and fibroblast growth factor (FGF), among others, which are involved in relevant biological processes (e.g., cell adhesion, proliferation, differentiation and angiogenesis) [34, 42, 43]. In this sense, platelet rich hemoderivatives (PRHd) are being used in TE as an autologous/allogeneic cost-effective source of bioactive molecules (growth factors, cytokines, structural and adhesion proteins) aiming the replacement of complex delivery systems that require, as an example, the combination of expensive recombinant growth factors and biomaterial [44, 45].

For the works developed under the scope of this thesis, PC were obtained from Serviço de Imunohemoterapia do Centro Hospitalar São João (CHSJ, Porto, Portugal), under a previously established collaboration protocol approved by the Ethical Committee, and all collected samples were biologically qualified according to the Portuguese legislation. In Figure 4.3, the process to obtain PL was detailed. Briefly, PC were thaw in a 37°C water bath (1st cycle) and samples with a platelet count of 10^6 platelets/μL were pooled using 5-10 donors. The obtained mixture was afterwards aliquot and subjected to one more freezing/thaw cycle (2nd; frozen at −196°C and thaw in a 37°C water bath) lysing the platelets and releasing their content, and aliquoted for sterile polypropylene tubes. The last cycle (3rd) is started by the freezing of the aliquots in liquid nitrogen before storage at -80°C (if necessary) and concluded by thawing the PL before centrifugation at 1400g for 10 min to remove the deposited cellular debris. When necessary, the PL was filtered through 0.45μm filters. All the procedures were performed under aseptic conditions.

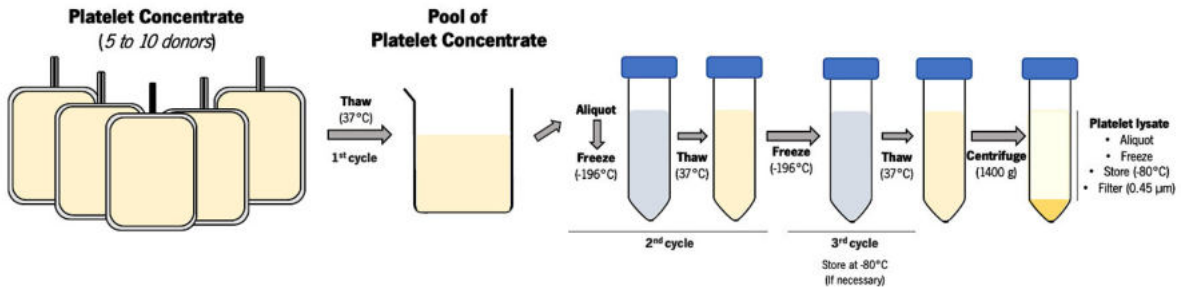

Figure 4.3 | Preparation of platelet lysate aliquots from platelet concentrate samples obtained from different donors.

In **CHAPTERs 8** and **9**, the potential of PL hydrogels and encapsulation within PCL nanofibers was explored relying on the fact that they can act as reservoirs of bioactive factors with benefits for tendon and interface tissue regeneration.

4.2. METHODS

4.2.1. MATERIAL PROCESSING

4.2.1.1. Wet spinning - Production of PCL/Gelatin and PCL/Gelatin/Hap microfibers

Wet spinning is a well-known industrial method emerged in the 1930s and nowadays widely employed in the textile sector for the production of synthetic polymeric fibers, such as nylon and acrylic fibers. This technique is based on a non-solvent-induced phase inversion process involving the extrusion of a polymeric solution directly into a coagulation bath, usually composed by a poor solvent (non-solvent) or a non-solvent/solvent mixture with respect to the processed polymer, to form a coagulating filament that finally solidifies as continuous polymeric fiber with a final diameter of tens to hundreds of micrometers [46]. A standard setup is composed by a syringe mounted on a pump and equipped with an extruding needle immersed in a coagulation medium and a collector (Figure 4.4).

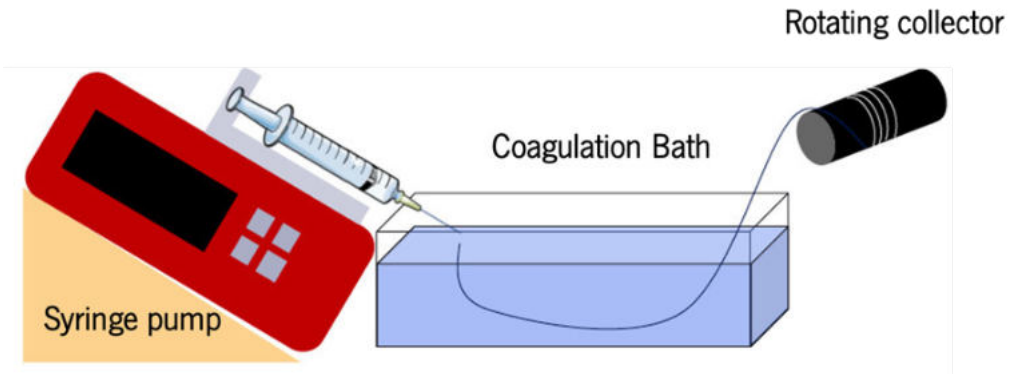

Figure 4.4 | Wet spinning common setup composed of a syringe pump, coagulation bath and collector.

Wet spinning has been widely used for the production of fibers based on polymers derived from natural sources, namely collagen [47], chitosan [48], silk fibroin [49], and from biodegradable polymers, such as poly-L-lactide acid (PLLA) [50], poly(lactic-co-glycolic acid) (PLGA) [51] and PCL [52]. The versatility of this method in terms of material selection and loading strategy (e.g. encapsulation in a core-shell structure) has allowed the functionalization of polymeric fibers with a huge range of bioactive compounds and the production of electrospun fibers widely used for blood vessel tissue engineering [53]

In **CHAPTER 7**, wet spinning was used for the continuous production of PCL/Gelatin and PCL/Gelatin/Hap microfibers for the replication of both tendon and bone microstructures, respectively. To do so, a PCL solution (22% w/v, initial concentration) was prepared by dissolving PCL in formic acid/acetic acid (3:1 v/v) and stirring at 150 rpm for 4 hours. Gelatin (9% w/v, initial concentration) was

dissolved in a solution of 80% acetic acid/water (v/v) and stirred at 150 rpm for 4 hours. The final solution of PCL/Gelatin was prepared by mixing PCL and gelatin solutions at a ratio of 70:30, respectively. In the case of PCL/Gelatin/HAp blend, HAp nano-to-microparticles were first completely dispersed in PCL solution and, afterwards, gelatin (9% w/v) solution was added to the mixture. HAp content represents 7.7% w/v of the final solution. Both solutions were prepared at room temperature and used within the day of preparation. A customized device was used to produce textured wet-spun microfibers (Figure 4.5). A coagulation bath containing 1.25% (v/v) glutaraldehyde/water solution was used as crosslinker. The prepared solutions were injected using a 10 mL syringe with a 21G needle and extruded to the coagulation bath at a constant flow rate. Three different flow rates were tested: 1 mL/h, 0.5 mL/h and 0.25 mL/h. The vertical distance from the needle to the collector was set at 6 cm. A collector was set after the coagulation bath at a horizontal distance of 8 cm from the needle and the fibers were collected at a constant speed (2 rotations per minute). All produced fibers were left inside the hood overnight to eliminate possible solvent and/or glutaraldehyde residues from the production process.

Figure 4.5 | Customized wet spinning setup for the continuous production of PCL/gelatin and PCL/gelatin/HAp microfibers.

4.2.1.2. Electrospinning - Fabrication of anisotropic and isotropic PCL electrospun nanofiber threads

Back to 1887, Charles V. Boys described that fibers could be drawn from a viscoelastic liquid in the presence of an external electric filed [54]. Widely known as electrospinning nowadays, this technique opened the door to the production of micro- to nanometer scale fibers. Electrospinning involves an electrohydrodynamic process, in which a liquid droplet is electrified generating a jet, followed by stretching and elongation to generate single fiber(s) (Figure 4.6). This basic setup must include four major components: a high-voltage power supply, a syringe pump, a spinneret (hypodermic needle with blunt

tip), and a conductive collector. During electrospinning, the liquid is extruded from the spinneret to produce a suspended droplet as result of surface tension. After electrification, the electrostatic repulsion between the surface charges, deforms the droplet into a Taylor cone, from which the jet is ejected. The jet initially extends in a straight line and then, due to bending instabilities, undergoes vigorous whipping motions. Finally, as the jet is stretched into finer diameters, allowing the evaporation of solvent or the cooling of melt, and afterwards the deposition of fibers on grounded collector [55-57].

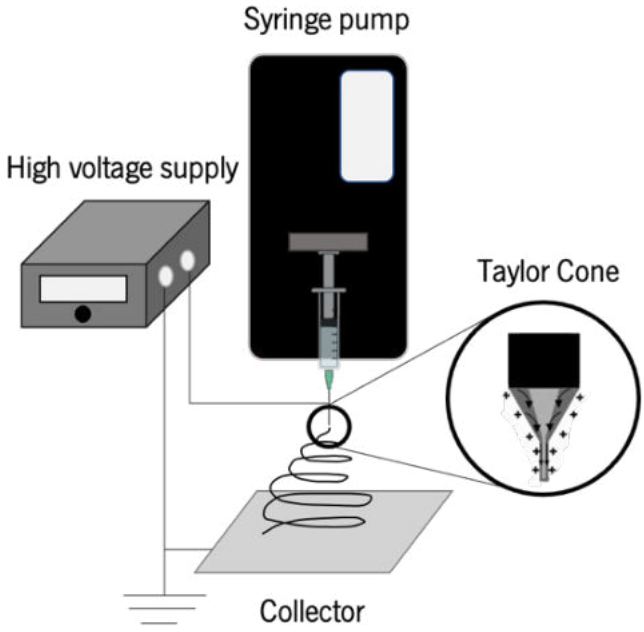

Figure 4.6 | Electrospinning common setup.

In general, the successful electrospinning of polymeric solutions (natural and synthetic materials), as well as electrospun fibers morphology and structure, relies on a set of parameters related to solvent, polymer solution, processing parameters and ambient conditions [55-57]. Processing parameters such as, the applied voltage, the flow rate of the liquid, and the distance between the tip of the spinneret and the collector, are determinant for the formation of electrospun fibers and control of their diameters. For instance, the distance between the tip of the spinneret (blunt needle tip) and the collector determines the stage of instability at which the jet is deposited on the collector. A moderately long distance is required to ensure full extension and solidification of the jet, and thus the formation of electrospun fibers [56]. Thinner fibers will be formed as the distance is increased. On the opposite, higher flow rates of solutions, typically result in thicker diameters [56]. Nonetheless, fibers morphology can similarly be altered by the changing the ground collector. For example, rotating mandrels can be used to achieve a desired degree of alignment mainly by regulation the linear velocity [58, 59].

In this work, a customized electrospinning setup [60] was used for the production of nanofiber threads with different topographies (Figure 4.7, **CHAPTER 8**) to replicate as close as possible tendon and bone topographies. Additionally, in **CHAPTER 9**, the same setting was used for the production of electrospun nanofiber threads with two topographies for healthy and diseased tendon ECM mimicry. Briefly, an electrospinning solution was prepared with 17% w/v of PCL dissolved in a chloroform (CHF)/dimethylformamide (DMF; v/v, 7:3) solution, which was stirred overnight at room temperature (RT). Afterwards, a 21G needle was filled with the PCL solution and jetted, under a constant flow rate of 1.0 mL/h and voltage of 8.0-9.0 kV, into an 20% (v/v) ethanol/water bath.

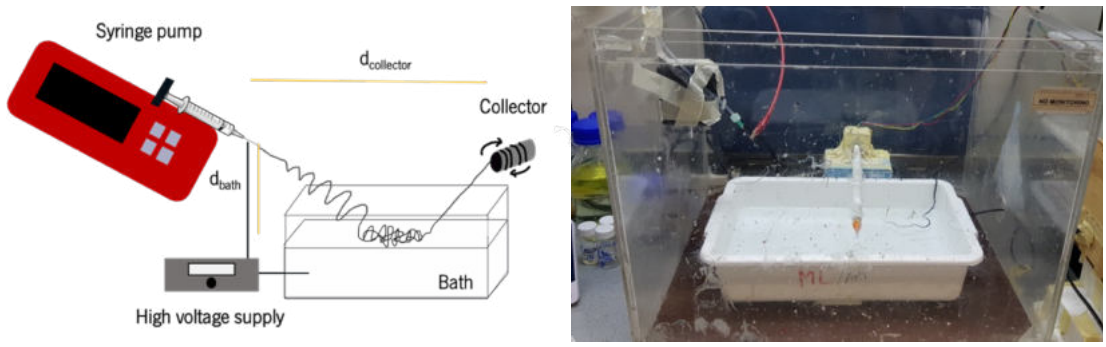

Figure 4.7 | Customized electrospinning setup with ethanol/water bath and rotating collector.

Nanofiber threads topographies were altered by changing the both the distance between the needle and bath (Figure 4.5, d_{bath}) and to the collector ($d_{collector}$), as well as collection speed. Continuous anisotropic fiber threads were collected with the jetting needle at 16 cm from the surface of the bath by a roller located 20 cm away from the needle at a constant winding speed of 1.09 cm/s. For isotropic fiber threads, the needle was placed 13 cm above the surface of the bath, the roller was located 13 cm away from the needle, and threads were collected at a constant winding speed of 0.14 cm/s. Samples were collected and left to complete dry at room temperature, enabling the evaporation of still remaining solvents.

4.2.1.3. Emulsion electrospinning - Incorporation of platelet lysates in electrospun PCL nanofiber threads

Over the past decade, intensive research has been conducted on electrospinning of fibrous scaffolds and their potential applications for tissue regeneration. For providing multifunction and enhancing the biological performance, drugs and bioactive molecules have been incorporated within fibers, normally using emulsion electrospinning. Emulsion electrospinning is a simple technique that takes advantage of

the normal electrospinning setting for the fabrication of nanofibers with core-shell structure and incorporation of bioactive molecules [61]. Either oil-in-water or water-in-oil, in emulsion electrospinning a phase separation can be induced in the jet by the de-emulsification caused by the evaporation of solvent, leading to the formation of core–sheath nanofibers [56, 62]. The use of different types of emulsions allows both the encapsulation of hydrophilic and/or hydrophobic compounds. Normally two immiscible liquids are mixed together forming a single-phase system containing emulsifiers, and then the droplet phase is dispersed in the immiscible phase (normally the solution containing the solvent) [63]. During the spinning process, the immiscible phase is converted into the shell of fibers, and the droplet phase is stretched to form the fiber core (Figure 4.8). The core section of the emulsion electrospun fibers is available enabling the encapsulation of bioactive compounds without compromising their bioactivity, while the presence of the core–shell fiber matrix may effectively circumvent the burst release of the encapsulated bioactive compounds [63].

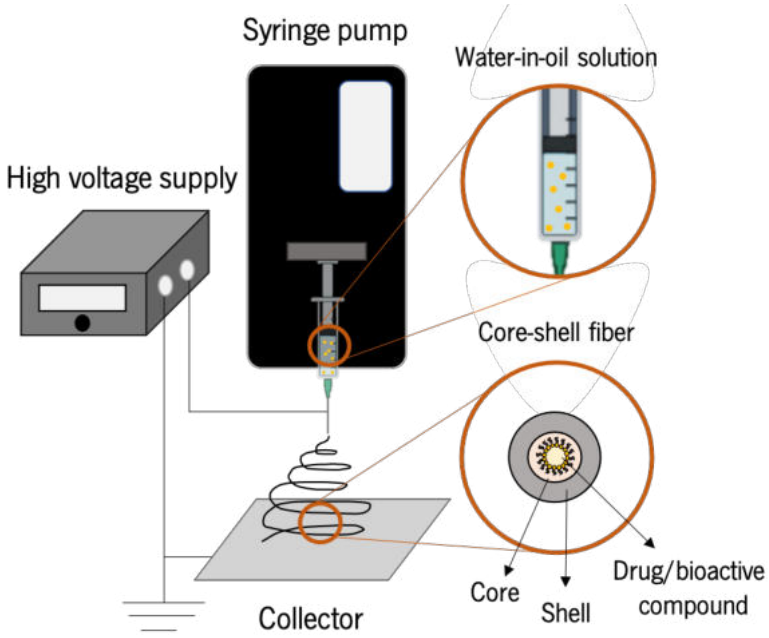

Figure 4.8 | Emulsion electrospinning setup for the production of bioactive core-shell fibers.

Yet this technique presents some drawbacks, namely the instability of an emulsified solution and the presence of an emulsifier may affect the applications of the nanofibers, and separate blobs can be observed instead of core-sheath structures [56, 62, 64, 65]. Nonetheless, compared to coaxial electrospinning, a single nozzle is employed being obtained continuous fibers in a relatively simpler way [66].

In **CHAPTER 8**, emulsion electrospinning was used for the incorporation of PLs and nHAp in electrospun nanofiber threads with two different topographies: anisotropic and isotropic. Briefly, in this work, a previously used PCL solution (17%, w/v in CHF/DMF, v/v, 7:3) was used as the continuous phase. For the incorporation of nHAP, particles with < 200 nm were added to the polymeric solution representing 1% w/w of PCL and the obtained mixture stirred at 150 rpm for 1-3 hour, at room temperature, until all the nHAP powder was blended. Water-in-oil emulsion of platelet lysates were prepared at the same day of electrospinning. For the aqueous phase preparation, filtered PLs and MilliQ were mixed together in a ratio of 1:1 (v/v), and a final volume of 200 μL dropped-wise to the polymeric solution, where the instantaneously formation of micelles was observed. Afterwards, using previously optimized conditions, the obtained solution was ultrasonicated on ice for 2 minutes at 50% amplitude. Immediately after, the acquired emulsion solutions were contained in a syringe with a 21G needle were electrospun at a constant flow rate of 1.00 mL/h and a voltage of 8-12 KV during all the process. For the production of anisotropic nanofiber threads, the vertical distance from the needle to the support liquid bath water/ethanol (8:2, v/v) was set at 16 cm, and the horizontal distance to the collector were set at 20 cm. For the production of isotropic nanofiber threads, the vertical and horizontal distances were set at 13 and 13 cm, respectively. Nanofiber threads were collected at RT (23±2 °C) and humidity ranging from 45% to 50%. Samples were collected, left to complete dry at room temperature, enabling the evaporation of still remaining solvents, and stored at 4°C inside an exicator until use.

4.2.1.4. Hydrogel coating - Production of platelet lysate (PL)-coated electrospun fiber threads

Hydrogels are 3D crosslinked polymeric systems with a high content in water and that can be produced with a variety of shapes. Particularly, for tendon tissue applications, biomaterials with a fibrous structure hold great promise to replicate the native tissue architecture. Different techniques exist for the production of hydrogel fibers, including wet spinning [50], microfluidics [51] and microfluidic spinning [52, 53]. Additionally, hydrogels can be produced using two roughly divided gelation mechanisms, namely physical and chemical. Physical mechanisms include temperature- and pH-induced crosslinking, peptide self-assembling, ionic gelation and polyelectrolyte complexation [67]. However, the stability of physically crosslinked hydrogels relies on relatively weak, non- covalent interactions, and the formation of these bonds leads to hydrogels with properties that are extremely dependent on the conditions of the surrounding environment [67]. Thus, more stable hydrogels are produced taking advantage of chemical

crosslinking mechanisms (e.g., photocrosslinking) as covalent bonds are established and the use of toxic crosslinkers is avoided [67].

Hydrogels based on PL have been increasingly investigated either employing self-crosslinking mechanisms [68] or incorporating PL in hydrogel matrices [69, 70]. Additionally, some studies have been demonstrating a sustained release of endogenous biomolecules from PL-based hydrogels, resulting in a bio-functionality and modulation of cell behavior, such as stem cell differentiation [71].

In the present thesis, the production of PL-hydrogel fibers through optimized gelation mechanism was explored in **Chapter 9** for the mimicry of physiological and pathophysiological tendon microenvironment. Herein, previously produced anisotropic and isotropic nanofiber yarns/threads were used and fixed inside the 3D-printed holder. Afterwards samples were immersed into thrombin solution prepared in 5 mM calcium chloride ($CaCl_2$) at a final concentration of 10 U/mL for 45 minutes at RT. The presence of these clotting factors induces a rapid self-assembly of PL into a 3D hydrogel [72]. Then, a clean multichannel piece was placed and filled with equal amounts of fresh PL and human tendon-derived cells (hTDCs). Sutures were incubated in PL at 37° C for 2 hours under humidified conditions to allow gelation. The morphology of PL hydrogel coated yarns was analyzed by optical microscopy (DM750, Leica, Schweiz), in order to observe hydrogel layer formation around nanofiber yarns/threads core.

4.2.1.5. Textile assembling of fibers - Fabrication of gradient scaffolds

Textile technologies have recently attracted great attention as potential biofabrication tools for engineering tissue constructs. Fibrous structures can be designed and engineered to reach the required properties that are demanded by different tissue engineering applications through the use of textile techniques [73]. Several key parameters, namely physiochemical characteristics of fibers, the pore size and mechanical properties, play an important role in the effective use of textile technologies in tissue engineering [73]. Different textile methods such as knitting, weaving, and braiding, constitute an appealing tool for engineering artificial tissues and organs [74].

First, knitting (Figure 4.9) was used as the main textile technique for the fabrication of a scaffold with a gradient of HAp content (**CHAPTER 7**). Briefly, four PCL/gelatin fibers were knot together and, with a hook needle, over hook and draw through to form a new loop without tightening the previous one, forming a chain stitch. In the middle region of the 3D scaffold, two PCL/gelatin fibers were removed, and two fibers of PCL/gelatin/HAp were interlocked with the remaining ones to produce the interface. Finally, PCL/gelatin fibers were completely removed to obtain a third part of the scaffold comprising only PCL/gelatin/HAp fibers.

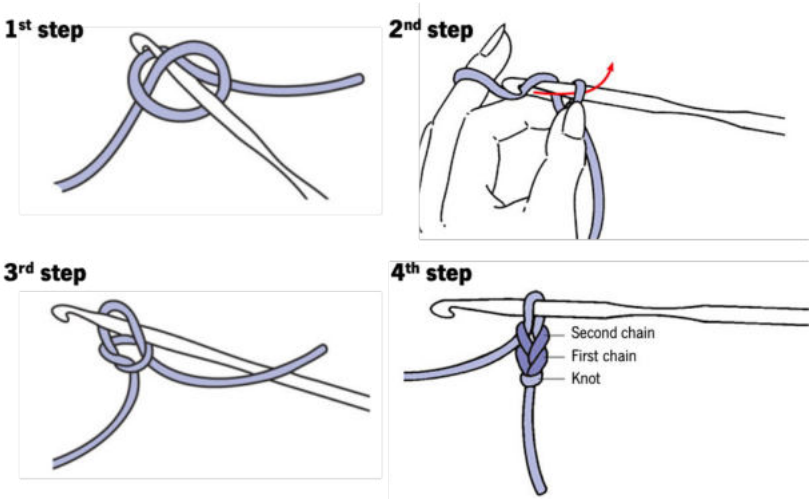

Figure 4.9 | Schematic illustration of knitting process for assembly of microfibers.

In **CHAPTER 9**, electrospun and emulsion yarns and threads were assembled in 3D constructs using weaving technique (Figure 4.10). Briefly, a 3D platform was produced where 8 weft cotton threads were placed side by side with a distance of 0.5 cm. Anisotropic yarns and isotropic threads were used as warp/weft threads. This sequence was modified during the fabrication of scaffolds. On the middle, threads were interlocked creating a continues gradient of threads topography and composition. As a final step, respective threads were passed in between warp/weft threads and in the middle, as a way to maintain the structural integrity of the scaffold. Scaffolds composed of electrospun and emulsion electrospun anisotropic yarns and isotropic threads with nHAp were produced, and only electrospun anisotropic and isotropic threads were used as controls.

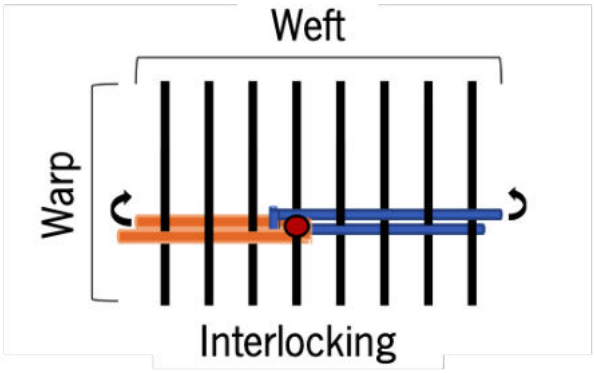

Figure 4.10 | Schematic illustration of weaving process for the fabrication of 3D gradient scaffolds.

4.2.2. PHYSICOCHEMICAL CHARACTERIZATION OF PRODUCED MATERIALS AND STRUCTURES

4.2.2.1. Morphological Characterization

Optical microscopy

The optical microscope also known as a light microscope, commonly uses visible light and a system of lenses to generate magnified images of small objects. Optical microscopes are the oldest design of microscope and were possibly invented in their present compound form in the 17th century. Basic optical microscopes can be very simple, although many complex designs aim to improve resolution and contrast. In this thesis, optical microscopy was used to evaluate the morphology of produced wet spun microfibers (**CHAPTER 7**), electrospun and emulsion anisotropic yarns and isotropic threads (**CHAPTER 8**) and PL-coated yarns and threads (**CHAPTER 9**). Moreover, optical images were used to assess fibers and droplets diameters using Fiji Software.

Scanning electron microscopy (SEM)

Scanning electron microscopy (SEM) is an extensively used technique to study the morphology of structures using a focused electron beam. Briefly, SEM micrographs are obtained from secondary electrons emitted from the surface of the specimen under analysis, generating information on the 3D morphology of the sample at a sub-micron level. In conventional SEM, specimens are observed in high vacuum, or in low vacuum or wet conditions when in variable pressure or low/high temperature SEM [75].

In **CHAPTER 7**, SEM was used to evaluate the morphology of produced microfibers of PCL/Gelatin and PCL/Gelatin/HAp. Additionally, the organization and morphology of stem cells seeded on microfibers was similarly evaluated by SEM. To do so, after 7 and 14 days, cell-seeded microfibers were washed three times with PBS, fixed with 2.5% (v/v) glutaraldehyde in PBS solution and stored at 4 °C until preparation. After this, all samples were dehydrated in a series of increasing concentrations of ethanol in water (10% to 100%, 30 min of incubation in each solution). After dehydration, all samples were left to air-dry and mounted on aluminum stubs. Prior to SEM analysis (SEM, MP1000001280128, JSM-6010 LV, JEOL), a coating with platinum was performed and the samples were observed at an accelerating voltage of 5 kV. Lastly, SEM was used to assess the morphology of emulsion anisotropic yarns and isotropic threads (**CHAPTER 8**) and of electrospun nanofiber threads (**CHAPTER 9**). To address the production of electrospun nanofibers, obtained threads were first embedded in a solution of PDMS (2:8) and allowed to solidify at 37° C, overnight. Afterward, samples were placed inside liquid nitrogen and, with the help

of tweezers, broken into several pieces. Samples were coated with 2 nm of platinum (Cressigton) before analysis. For anisotropic EE threads incorporated with nHAp, samples were coated with 2 nm of gold (Cressigton) and analyzed by High-Resolution Field Emission Scanning Electron Microscope with Focused Ion Beam (FIB – SEM).

Micro computed tomography (Micro-CT)

Micro-computed tomography (micro-CT) is a non-destructive imaging technique to scan objects. Briefly, micro-CT scanners capture a series of 2D planar X-ray images and reconstruct the data into 2D cross-sectional slices [76]. These ones can be further processed into 3D models and even printed as 3D physical objects for analysis. With 2D X-ray systems you can see through an object, but with the power of 3D micro-CT systems you can see inside the object and reveal its internal features. This technique provides volumetric information about the microstructure, nondestructively [76].

In this thesis (**CHAPTERs 7** and **8**), samples microstructure was evaluated by X-rays micro-computed tomography (micro-CT) using a high-resolution system Skyscan scanner (Skyscan 1272; Bruker, Billerica, MA, USA). The acquisition of X-ray images was performed with a pixel size of 4.25 to 10 μm, a rotation step of 0.2° over 360°, and a smoothing averaging of every two to three images, using the SkyScan acquisition software version 1.1.3. The X-ray source was fixed at 35-50 kV and 181-200 μA, of voltage and current, respectively. Following the acquisition, gray-scale images were reconstructed using the NRecon software (version 1.7.1.0). Then, when needed, the samples were vertically aligned for the cross-sectional analysis of the fibers using the DataViewer software (version 1.5.3.6). Qualitative visualization of the 3D morphology was performed using CT-Vox software (version 3.3.0). Quantitative analysis was performed after converting the regions of interest into binary images, by a dynamic threshold (30–255—polymeric phase; 80–255 ceramic phase, CT Analyzer v1.17.0.0). The binary images were used for morphometric examination of inner-porosity, pore size, pore volume and interconnectivity.

Directionality analysis

Directionality analysis using Fourier components method is a plugin available in Fiji software. This method is based on Fourier spectrum analysis. For a square image, structures with a preferred orientation generate a periodic pattern at +90° orientation in the Fourier transform of the image, compared to the direction of the objects in the input image. This plugin chops the image into square pieces and computes their Fourier power spectra. The later are analyzed in polar coordinates, and the power is measured for each angle using the spatial filters proposed in a directionality results window.

In **CHAPTERs 7**, **8** and **9**, the degree of surface alignment was determined through directionality analysis applying the Fourier components method using the FIJI software. For this purpose, scanning electron images were converted to 32-bit images and cropped into three different images. The radial intensities were calculated, and the orientation map was also obtained. Data from a directionality results window were collected and a graph elaborated. Briefly, if a sharp peak is observed in the orientation angle frequency it demonstrates a tendency of the sample to align in a specific orientation. When absent, a random orientation is observed.

4.2.2.2. Physical Characterization

Degradation assays

In vivo degradability of biomaterials is dependent on several factors that include the dissolution or erosion, hydrolysis, degradation with specific enzymes or phagocytosis [77, 78]. Given that tissue engineered scaffolds should maintain their function during the regeneration process, it is important to assess the stability of the materials in vitro.

Herein, two strategies were followed to investigate the stability of the materials herein developed: incubation in PBS (physiological environment, pH=7.4) or incubation in acidic environment (inflammatory environment, pH=6.4). Briefly, in **CHAPTER 8**, both anisotropic emulsion electrospun (EE) yarns and isotropic EE threads incorporating PLs were cut into pieces (20–30 mg) and placed in both physiological and inflammatory environments as previously described. At the end of each time point, samples of each formulation were collected and rinsed with distilled water (dH_2O) and the weight of the samples was measured. The percentage of weight loss kinetics was calculated according to the equation 4.1:

Equation 4.1: $\text{Weight loss} = (mi-mf) \times 100\%.$

Where, mi is the initial weight and mf the final weight.

4.2.2.3. Mechanical characterization - Tensile testing

Tensile testing was chosen over other methods for mechanical characterization of fabricated fibrous scaffolds, since this method best mimics the native mechanical stress underwent by the tissues in the native tendon-to-bone tissue interface. Tensile properties indicate how the material will react to forces applied, namely tension. A tensile test is a fundamental mechanical test where a specimen is loaded in a controlled manner while the applied load and elongation of the specimen are measured over some

distance. Tensile tests are used to determine the modulus of elasticity, elastic limit, elongation, proportional limit, reduction in area, tensile strength, yield point, yield strength and other tensile properties. Since both the engineering stress and the engineering strain are obtained by dividing the load and elongation by constant values, the load-elongation curve will have the same shape as the engineering stress-strain curve. The stress-strain curve relates the applied stress to the resulting strain and each material has its own unique stress-strain curve.

In the present thesis, to mimic the different tissues, several fibrous structures were developed, and their tensile properties were assessed (**CHAPTER 7** and **8**). To do so, mechanical properties of produced wet spun fibers (**CHAPTER 7**) and electropsun and emulsion electrospun anisotropic yarns and isotropic threads (**CHAPTER 8**) were assessed using the universal mechanical testing machine (5543K2942, 5543, Instron) equipped with a 1 kN and 50 N load cell, respectively. Images from optical microscope (DM750, Leica, Schweiz, Germany) were acquired and used for cross-sectional area calculations. Each specimen was measured along the length at three different locations using the ImageJ software (version 1.52d). Samples were cut into testing specimens with 1.5 cm and fixed in paper frames with a window of 1.2 × 1.2 cm in the case of wet spun fibers. For yarns and threads, samples were cut into testing specimens with 2 cm and fixed in paper frames with a window of 1 × 1 cm. After mounting the frames onto the tester grips, the lateral sides were cut, and the crosshead speed was set at a constant rate of 1 and 10 mm min^{-1}, respectively. At least six samples per condition were tested. The elastic modulus was calculated from the tangent slope of the linear section of the stress–strain curve.

4.2.2.4. Biochemical characterization

Fourier transform infrared spectroscopy

Fourier transform infrared spectroscopy (FTIR) is spectroscopic technique widely used to obtain information about the chemical structure of materials (in solid, liquid or gas state). The basic principle of FTIR relies on an interferometer that analysis the specific absorption and transmission of chemical compounds, exciting specific molecular vibrations when passed by infrared (IR) radiation[79]. The absorption/transmission peaks of a range of incident IR light are converted by a Fourier transformed mathematical processing, producing a characteristic spectrum which represent the “fingerprint” of each compound [79].

FTIR spectroscopy was used in **Chapter 7** and **8** of this thesis, to assess the chemistry of the raw PCL, the conjugation with gelatin and the successful incorporation of HAP and PLs. For this purpose, in **CHAPTER 7** all samples were first mixed with potassium bromide (KBr) and pressed into transparent

pellets, while in **CHAPTER 8**, prior to FTIR analysis by attenuated total reflectance (ATR), all samples were dissolved with a small amount of chloroform and allowed to dry at RT to form a small pellet. Then, IR spectra were recorded on an IRPrestige-21 Spectrophotometer (Shimadzu Scientific Instruments, USA) by averaging 32 individual scans at a resolution of 4 cm^{-1} over the wavenumber range between 4000 and 400 cm^{-1}.

Total protein release

Micro BCA™ Protein Assay is a detergent-compatible bicinchoninic acid formulation for the colorimetric detection and quantitation of total protein in a sample. This method uses bicinchoninic acid (BCA) as the detection reagent for copper, which is formed when the cupric ion is reduced by protein in an alkaline environment. A purple-colored reaction product is formed by the chelation of two molecules of BCA with one cuprous ion. This water-soluble complex exhibits a strong absorbance at 562nm that is linear with increasing protein concentrations.

In **CHAPTER 8**, the cumulative release of total protein was performed for emulsion electrospun anisotropic yarns and isotropic threads in both physiological and inflammatory settings to clearly understand the biological release of PL proteins. For the release, both anisotropic EE yarns and isotropic EE threads were collected and cut in pieces (20–30 mg) and shortly wetted in 50% ethanol and rinsed in MilliQ water. To replicate both physiological and inflammatory setups, a solution of PBS (solution adjusted to pH=7.4) and PBS with sodium bicarbonate (solution adjusted to pH=6.4) were prepared. Samples were left in contact with prepared solutions up to 31 days at 37°C, under 60 rpm constant agitation at established times, a total volume of 600 µl was collected. To quantitatively evaluate the cumulative release of total proteins, Pierce BCA protein assay (Micro BCATM Protein Assay Kit; Thermo Scientific™) was used according to the manufacturer protocol and measured in a microplate reader (Synergy HT, Bio-Tek Instruments). An equal volume of fresh solutions was added each time. Anisotropic HE yarns and isotropic HE threads were used as controls. Cumulative release was calculated in relation to the initial weight of samples for each tested condition.

Enzyme-linked immunosorbent assay (ELISA)

ELISA is an enzymatic immunoassay that allows the detection, in a solution, of a specific antigen. It consists in the immobilization of a specific antibody (capture antibody) in a solid surface, for instance 96-well plate polystyrene surface, to which the target molecule will specifically bind to. Afterwards a second antibody (detection antibody) will be bounded to the antigen. This detection antibody is usually linked to

an enzyme that will convert an adequate substrate into a measurable colorimetric signal, proportional to the amount of antigen in solution.

In CHAPTER 9, the cumulative release of platelet-derived growth factor BB (PDGF-BB), transforming growth factor beta (TGF-ß), insulin growth factor 1 (IGF-1), endothelial growth factor (EGF), vascular endothelia growth factor (VEGF), fibroblast growth factor ß (FGF-ß), RANTES and CXCL1 were performed using ELISA plate arrays (Signosis, INC.). Standard curves were performed for each protein ranging from 0 to 2 ng/mL. The concentration of released proteins was calculated in relation to the initial weight of samples for each tested condition and presented as ng/mL per mg of EE yarns/threads.

4.2.3. *IN VITRO* CELL CULTURE – BIOLOGICAL STUDIES

4.2.3.1. Cell sources

Human tendon derived cells (hTDCs)

Human tendon-derived cells (hTDCs) are a highly heterogeneous population composed not only of fully mature tenocytes, but also of tendon stem and progenitor cells (TDSCs) [80], as discussed in CHAPTER 2. Regarding tendon TE and regenerative medicine applications, transplantation of tendon cells, in particular TDSCs, has been reported to result in the formation of tendon-like tissue in vivo [81]. The isolation of hTDCs often requires invasive surgical procedures for harvesting tendon tissue biopsies. Nonetheless, tendon cells are considered a good cell source for replicating the cellular behavior of native tendon microenvironment. Having this into consideration, hTDCs were used in the studies developed in this thesis (**CHAPTERs 5, 6** and **9**). For this purpose, tendon tissue samples were collected during elective orthopedic surgeries and hTDCs were isolated by enzymatic digesting the tissue using collagenase type I. The obtained isolated cells were expanded and cultured in minimum essential medium (α-MEM, Invitrogen) supplemented with 10% (v/v) fetal bovine serum (FBS, Alfagene) and 1% (v/v) antibiotic/antimycotic (A/A). Cells were used at passages 2-3.

Adipose derived stem cells (hASCs)

Human adipose tissue-derived stem cells (hASCs) constitute a stem cell population of mesenchymal origin that are easily harvested using minimally invasive procedures, such as liposuction/lipoaspiration. As established by the International Society for Cellular Therapy, hASCs display features typical of mesenchymal stem cells (MSCs), including multilineage differentiation potential and expression of specific surface markers (CD105, CD73, CD90) [82]. These cells have been used as an alternative cell source for clinical applications, including tissue engineered strategies [83].

For the works performed under this thesis, hASCs were isolated from lipoaspirate samples by enzymatic digestion with collagenase type II and according to previously described protocols [84]. Isolated cells were expanded and cultured in α-MEM supplemented with 10% (v/v) FBS and 1% (v/v) A/A.

In **CHAPTERs 5, 6** and **8**, hASCs were differentiated towards the osteogenic lineage in the presence of α-MEM supplemented with 10 mmol/L β-glycerophosphate (G9422, Sigma-Aldrich), 10^{-8} mol/L dexamethasone (D2915, Sigma-Aldrich), and 50 μg/mL L-ascorbic acid 2-phosphate sesquimagnesium salt hydrate (013-12061, Wako) for 14 days in a humidified environment (37°C, 5% CO_2). Pre-differentiated cells were called pre-osteoblasts (pre-OBs). For all experiments, cells were used at passages 2-4.

4.2.3.2. Culture systems

Direct co-cultures

Most musculoskeletal tissue interfaces are composed of a variety of cells, therefore, over the years, a variety of cells sources and culture strategies have already been explored in interface tissue engineering as described in section I of this thesis. Generally, three different approaches can be distinguished: (1) co-culture of differentiated cells, (2) culture of one type of stem cell alone and (3) co-culture of differentiated cell with undifferentiated stem cell [85]. Co-culture systems can be either two-dimensional (2D) or three-dimensional (3D) – using scaffolds - and of direct or indirect contact (Figure 4.11). On direct contact cultures, cells are seeded together in 2D or 3D supports enabling the physical contact, while, on indirect contact cultures, cells are separated by a physical barrier (normally a porous membrane) and only interact through secreted soluble factors [86, 87] (Figure 4.11). Although these co-culture systems have demonstrated some feasibility, harvesting and seeding of different cell types into multiphasic scaffolds is still a challenge for clinical uses.

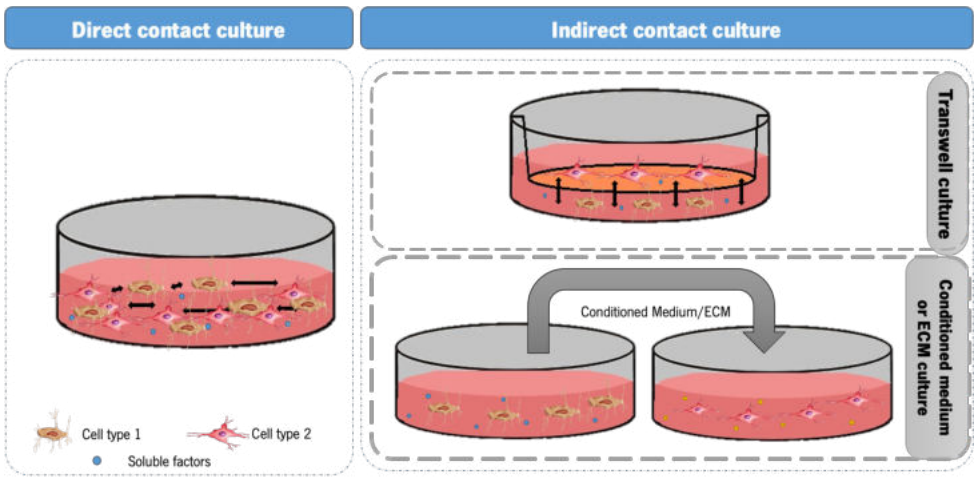

Figure 4.11 | Schematic representation of the direct and indirect contact co-culture systems used.

Direct co-culture systems were used in **CHAPTERs 5** and **6** to replicate as close as possible the cellular microenvironment found in the tendon-to-bone interface. To do so, hTDCs and pre-differentiated hASCs (pre-OBs) were seeded using a final density of 4×10^3 cells/well in a ratio of 1:1. Medium conditions were optimized allowing the maintenance of tenogenic and osteogenic phenotypes in singles cultures of hTDCs and pre-OBs, respectively, while enhancing the expression of interface-related markers in direct co-cultures (**CHAPTER 5**). After optimization, three conditions were used and direct-cocultures maintained under hypoxia (5% O_2) and normoxia (21% O_2) (**CHAPTER 6**).

4.2.3.3. Oxygen tension - Hypoxia vs Normoxia

The musculoskeletal system is a good example of tissues where hypoxia plays an important role during tissue development and homeostasis. Namely, in soft-to-hard tissue interfaces there is gradient in vascularity and, consequently, in oxygen concentrations. Given the physiology of the native tendon-to-bone interface, tendon cells are known to maintain their phenotype in vitro under hypoxic conditions, as the ones observed in the native hypo-vascular tendon niche (<5% oxygen tension) [61,62]. While, in bone, hypoxia has been shown to profoundly inhibit osteoclastogenesis in bone remodeling [63] given that bone physiological oxygen tension remains above 5% [64].

Mammalian cell culture represents a cornerstone of biomedical research. There is growing appreciation that the media conditions in which cells are cultured can remarkably influence the observed biological response and reproducibility.

In this thesis (**CHAPTER 6**), we considered a key variable, the oxygen tension. Therefore, we proposed the use of a direct co-culture system as an enthesis *in vitro* model to understand the influence of low oxygen tension (5% O_2, hypoxia) and osteogenic supplementation in the modulation of cellular phenotype *in vitro*. Briefly, as previously described, direct co-cultures were established, and single cultures were used as controls. Cells were left to adhere for a period of 24 h and then placed in a hypoxic vinyl chamber (Coy O_2 Control Glove Boxe; Coy/Esco) with a humidified environment at 37°C and lower oxygen tension (hypoxia, 5% O_2) for 14 days. Cells were also maintained under normal incubation conditions (normoxia, 21 % O_2).

4.2.3.4. Biological characterization

DNA quantification

Quant-iT™ PicoGreen® dsDNA reagent is an ultra-sensitive fluorescent nucleic acid stain for quantitating double-stranded DNA (dsDNA) in solution. Detecting and quantitating small amounts of DNA is extremely important in a wide variety of biological applications. In this thesis, Quant-iT™ PicoGreen® dsDNA kit (Molecular Probes, Invitrogen) was used to determine DNA content according to the manufacturer's protocol (**CHAPTERs 5, 6, 8** and **9**). For this purpose, cells were subjected to osmotic and thermal shocks using filtered ultra-pure Millipore water (pore size 0.22 µm) and storing at -80 °C. Cell lysates were used for dsDNA quantification, and fluorescence was measured in a microplate reader (Synergy HT, Bio-Tek Instruments) using an excitation wavelength of 485/20 nm and an emission wavelength of 538/20nm. A standard curve was prepared in a range of 0 to 1.5 µg/mL.

Metabolic activity quantification

AlamarBlue® is a colorimetric assay that gives information regarding cell viability. Resazurin is a non-toxic, cell-permeable blue dye that is weakly fluorescent and the active ingredient of AlamarBlue®. Living cells have the power to convert resazurin to a fluorescent molecule, resorufin, which is pink and highly fluorescent. Generally, the amount of measured fluorescence is proportional to the number of living cells; therefore, AlamarBlue® can be used to indirectly evaluate cell viability or cytotoxicity.

In the work performed throughout this thesis, AlamarBlue® was used to evaluate the impact of culturing cells in single microfibers (**CHAPTER 7**). Briefly, cell-seeded fibers were transferred to clean wells and washed twice with PBS. Then, 10% (v/v) Alamar blue (AbD SeroTec, Bio-Rad) in basal medium was added and cells were incubated overnight under standard culture conditions. The supernatant was collected, and the fluorescence measured using a microplate reader (Synergy HT, Bio-Tek Instruments) at an excitation wavelength of 530 nm and an emission wavelength of 590 nm.

Alkaline phosphatase activity quantification

As a representative mediator of biochemistry, alkaline phosphatase (ALP) participates in nearly every aspect of biological process. In the bone tissue, ALP is an ectoenzyme attached to the outer surface of the cell membrane of osteoblasts by glycosylphosphatidylinositol and it is partly released into the circulation [88]. Moreover, ALP is a major regulator of bone mineralization, as it hydrolyzes inorganic pyrophosphate which is a naturally occurring inhibitor of mineralization [88].

To date, several classical colorimetric methods has been developed for the ALP detection, based on the biological function of ALP [89]. One of these methods, uses as substrate, *p*-nitrophenyl phosphate (*p*NPP), that is dephosphorylated by ALP and its subsequent product (P-Nitrophenol) is coupled with obvious color-reactions, providing a metrological relation between colorimetric signals and ALP activity.
ALP activity was determined in **CHAPTER 5, 6** and **8** as a bone-related marker. Briefly, in all studies, samples were incubated with a substrate solution of 0.2% (w/v) *p*-nitrophenyl phosphate (pNPP) in 1 mmol diethanolamine (Sigma-Alrich). After 1-hour incubation at 37 °C, a stop solution of 2M NaOH/0.2 mM EDTA was added and the absorbance was measured (405 nm) using a microplate reader (Synergy HT, Bio-Tek Instruments). A standard curve was prepared using a *p*-nitrophenol (pNP) stock solution (Sigma-Alrich) with values ranging from 0 to 0.5 µmol/mL.

RT-PCR

Quantitative Real Time Reverse Transcriptase-Polymerase Chain Reaction (RT-PCR) was used to evaluate the expression of bone-, tendon and interface-associated markers at the gene level in **CHAPTERs 5**, **6** and **9**. This quantitative technique is divided into different steps: (1) mRNA extraction from cultured samples; (2) synthesis of single-stranded complementary DNA (cDNA) using first isolated mRNA; and (3) amplification and real-time quantification of target genes. In this thesis, after established time points, Total mRNA was extracted using RIBOZOLTM RNA extraction reagent (VWRCN580, VWR) and in **CHAPTER 9** RNA extraction was performed using RNeasy Mini Kit was according to the manufacturer's instructions. RNA quantity and purity were determined with a NanoDrop spectrophotometer (ND-1000, ThermoScientific, USA). The cDNA synthesis was performed with the qScript cDNA Synthesis kit and using the Mastercycler Realplex (Eppendorf, Germany). Transcripts quantification was carried out by quantitative polymerase chain reaction (qPCR) using the PerfeCTA SYBR Green FastMix kit following the manufacturer's protocol, in a Real-Time Mastercycler Realplex thermocycler (Eppendorf, Germany). Primer sequences (**Table 4.4**) were designed using Primer-BLAST tool and synthesized by Eurofins Genomics and IDT— Integrated DNA Technologies. The evaluation of the relative expression level was performed using the $2^{-\Delta\Delta ct}$ method. For this purpose, transcript expression of target genes was first normalized to the expression of the reference housekeeping and then to the respective calibrator sample, according to the experimental section in each chapter. Results are represented as fold change.

Table 4.4 | Primer sequences used for RT-PCR.

Chapter	Target gene	Sigla	Primer Sequence Forward Reverse	NCBI reference
5	*Glyceraldehyde 3-phosphate dehydrogenase*	*GAPDH*	AGCCTCAAGATCATCAGCAA GTCATGAGTCCTTCCAGGAT	NM_002046.5
9	*Tyrosine 3-Monooxygenase/Tryptophan 5-Monooxygenase Activation Protein Zeta*	*YWHAZ*		
	β-Actin	*ACTB*	CTGGAACGGTGAAGGTGACA AAGGGACTTCCTGTAACAA	AK223055
Tenogenic-related genes				
5, **6** and **9**	*Mohawk*	*MKX*	TGTTAAGGCCATAGCTGCGT TCGCACAGACACTCTGGAAAA	NM_173576.2
9	*Collagen I, α1*	*COL1A1*	CCTGACGCACGGCCAAGAGG GGCAGGGCTCGGGTTTCCAC	NM_000088.3
5 and **6**	*Collagen I, α1*	*COL1A1*	GTCACAGATCACGTCATCGC CGAAGACCCACCAATCAC	NM_000088.3
5 and **9**	*Collagen III, α1*	*COL3A1*	TTGGCATGGTTCTGGCTTCC GCTGGCTACTTCTCGTG	NM_000090.3
5 and **9**	*Decorin*	*DCN*	CAGCATTCCTCAAGGTCTTCC T GAGAGCCATTGTCAACAGCA	NM_001920.3
	Tenascin	*TNC*	ACTGCCAAGTTCACAACAGAC C CCCACAATGACTTCCTTGACT G	NM_002160.3

	Tenomodulin	*TNMD*	CCGCGTCTGTGAACCTTTAC CACCCACCAGTTACAAGGCA	NM_022144.2
9	*Scleraxis bHLH transcription factor*	*SCX*	AGAACACCCAGCCCAAACAGA T TCGCGGTCCTTGCTCAACTTT	NM_001080514. 2
5 and **6**	*Scleraxis bHLH transcription factor*	*SCX*	CGAGAACACCCAGCCCAAAC CTCCGAATCGCAGTCTTTCTG TC	NM_001717912
9	*Smooth muscle alpha actin*	*ACTA2*	AAAGCAAGTCCTCCAGCGTT TTAGTCCCGGGGATAGGCAA	NM_001141945. 1
Chondrogenic-related genes				
6 and **9**	*SRY-box 9*	*SOX9*	TTCATGAAGATGACCGACGC GTCCAGTCGTAGCCCTTGAG	NM_000346.3
5 and **6**	*Aggrecan*	*ACAN*	TGGTCTTGCAGCAGTTGATTC TAGAGTCCTCAAGCCTCCTGT	NM_013227.3
6	*Collagen type II, α1*	*COL2A1*	GAGCAGGAATTCGGTGTGGA GCCATTCAGTGCAGAGTCCT	NM_001844.5
6	*Collagen type X, α1*	*COL10A1*	CCCAGCACGCAGAATCCATC AGTGGGCCTTTTATGCCTGT	NM_000493.3
5 and **9**	*Cartilage oligomeric matrix protein*	*COMP*	AGGATGGAGACGGACATCAG TCTGCATCAAAGTCGTCCTG	NM_000095.2
Osteogenic-related genes				
9	*Runt related transcription factor 2*	*RUNX2*	TTCCAGACCAGCAGCACTC CAGCGTCAACACCATCATTC	NM_001024630
5 and **6**	*Runt related transcription factor 2*	*RUNX2*	TGTCTGTGCCTTCTGGGTTC CCGGCCTGCCTATGCTGTTA	NM_001024630. 3
5	*Alkaline Phosphatase*	*ALPL*	GAAGGAAAAGCCAAGCAGGC GGGGGCCAGACCAAAGATAG	NM_000478.5
	Secreted phosphoprotein 1 (Osteopontin)	*SPP1*	CAGACCTGACATCCAGTACCC GGTCATCCAGCTGACTCGTT	NM_001040058. 1

Metalloproteinases and inhibitors				
9	*Matrix metalloproteinase 1*	*MMP1*	ACCTGGAAAAATACTACAACCT GAA TTCAATCCTGTACAGATGTGTT	NM_002421.3
	Matrix metalloproteinase 3	*MMP3*	CACTCACAGACCTGACTCGG AGTCAGGGGGAGGTCCATAG	NM_002422.4
	Tissue inhibitor of metalloproteinases	*TIMP1*	CATCCGGTTCGTCTACACCC GGATAAACAGGGAAACACTGT GC	NM_003254.2
Hypoxia-related markers				
6	*Hypoxia-inducible factor 1-alpha*	*HIF1A*	AGAGGTTGAGGGACGGAGAT GACGTTCCAGAACTTATCCTA CCAT	NM_001243084.1
6	*Hypoxia-inducible factor 2-alpha*	*EPAS/HIF2A*	CAATGCAGTACCCAGACGGA TGGGGCTTAGCTGGAAGTCT	NM_001430.3
6	*Indian hedgehog*	*IHH*	CCGCGACCGCAATAAGTATG CGAGTGCTCGGACTTGACG	NM_002181.3
6	*Patched 1*	*PTCH1*	TGTCGCACAGAACTCCACTC GGCATAGGCGAGCATGAGTA	NM_001083605.2
6	*GLI family zinc finger 1*	*GLI1*	AAGCTAACCTCATGTCCGGC AAAAGAGTGGGCCCTCGGTG	NM_005269.3

Immunocytochemistry

Immunocytochemistry (ICC) is a common technique used to anatomically visualize the localization of a specific proteins or antigens in cells by the use of a specific primary antibody that binds to it. The primary antibody allows the visualization of the protein under a fluorescence microscope when it is bound to a secondary antibody that has a conjugated fluorophore.

Within this thesis, the expression of markers of interest was studied at the protein level, including ECM markers (**CHAPTERs 5**, **6**, **7**, **8** and **9**) and transcription factors.

For this purpose, after specific culture periods, samples were washed with PBS and fixed with 10 % (v/v) neutral buffered formalin for 20-30 min at room temperature. In Table 4.5 all the information regarding antibodies and dyes used is described. After samples treatment and incubation with primary and

secondary antibodies, actin filaments were stained with Phalloidin (Phalloidin-Tetramethylrhodamine B isothiocyanate from Amanita phalloides) solution at room temperature for 30 min and cell nuclei was counterstained with DAPI (4,6 – Diamidino-2-phenyindole dilactate) for 15 min at room temperature. Finally, immunostained samples were analyzed by confocal laser scanning microscopy (Leica TCS SP8, Microsystems, Wetzlar, Germany) or fluorescence (Axio Imager Z1m; Zeiss).

Table 4.5 | Summary of primary and secondary antibodies used for immunostaining and respective details.

	Chapt.	Antibody	Dilution	Treatment	Incubation	Company
Primary Antibodies	**5, 6**	*Mouse anti-human Tenascin-C*	TNC, 1:3000	0.25% Triton X-100/PBS solution for 5 min, non-specific binding blocked with 1% bovine serum albumin (w/v, BSA) for 30 minutes	Overnight, 4° C	Abcam/ Thermo Fisher
	5,6	*Mouse anti-human Collagen I*	COL1, 1:500			Abcam
	5 and **7**	*Rabbit anti-human Collagen III*	COL3, 1:100			Abcam
	6	*Rabbit anti-human Collagen type X*	COLX, 1:50			Millipore
	8	*Rabbit anti-human Scleraxis*	SCX, 1:100			Abcam
	8	*Mouse anti-human RUNX2*	RUNX2, 1:200			Merck
	8	*Mouse anti-human SOX9*	SOX9, 1:200			Millipore
	5	*Rabbit anti-human Osteopontin*	OPN, 1:100	0.025% Triton X-100/PBS solution for 30 min and nonspecific binding was blocked with 3% BSA.		Alfagene
	5	*Mouse anti-human Osteocalcin*	OCN, 1:50			Abcam
	5	*Mouse anti-human Decorin*	DCN, 1:100			Abcam
	5	*Mouse anti-human Aggrecan*	ACAN, 1:200			Abcam
	5	*Rabbit anti-human Collagen II*	COL2, 1:200			Abcam

	6	*Rabbit anti-human HIF1A*	HIF1A, 1:100			Abcam
	6	*Rabbit anti-human HIF2A*	HIF2A, 1:100			Thermo Fisher Scientific
	6	*Rabbit anti-human SOX9*	SOX9, 1:200			Abcam
	6	*Rabbit anti-human Collagen II*	COLII, 1:200			Abcam
	6	*Mouse anti-human Aggrecan*	ACAN, 1:200,			Abcam
	9	*Mouse anti-human Collagen I*	COL1, 1:500	0.1% Triton X-100/PBS solution for20 min, non-specific binding blocked with 1% bovine serum albumin (w/v, BSA) for 30 minutes. After incubation with primary antibody, 15 min with hydrogen peroxide 30%		Abcam
	9	*Rabbit anti-human Collagen III*	COL3, 1:100			Abcam
	9	*Mouse anti-human Decorin*	DCN, 1:100			Abcam
	9	*Mouse anti-human Tenomodulin*	TNMD, 1:200			Abcam
	9	*Rabbit anti-human Scleraxis*	SCX, 1:200			Abcam
	9	*Rabbit anti-human Elastin*	ELAS, 1:500			Abcam
Secondary	**5**, **6**, **7**, **8** and **9**	*Donkey anti-mouse alexafluor 488* *Mouse anti-rabbit alexafluor 488*		Dilution in 1% (w/v) BSA/PBS	1 h, RT	Thermo Fisher Scientific Thermo Fisher Scientific

	Rabbit anti-goat alexafluor 488	Thermo Fisher Scientific

Additionally, the signal emitted from the expression of the intended proteins was quantified using ImageJ software. Briefly, in **CHAPTER 9**, proteins expression was quantitatively analyzed by nuclei counting through DAPI staining and the protein of interest at 7 and 28 days of culture. Briefly, images from days 7 and 28 were split in 3 channels, being only the green analyzed and the fluorescence intensity measured. Results are expressed as normalized mean intensity. In **CHAPTER 8**, proteins expression was quantitively analyzed by dividing the green channel intensity by DAPI intensity in each image. Results were shown as DAPI/PROTEIN ratio intensity.

Reactive oxygen species (ROS) quantification

Oxygen radical absorbance capacity (ORAC) is a method used to measure the antioxidant capacity in biological samples *in vitro* [90]. The assay measures the oxidative degradation of a fluorescent molecule (either beta-phycoerythrin or fluorescein) after being mixed with free radical generators, such as azo-initiator compounds [90]. Azo initiators are considered to produce the peroxyl radical by heating, which damages the fluorescent molecule, resulting in the loss of fluorescence. Antioxidants are considered to protect the fluorescent molecule from the oxidative degeneration. The degree of protection is quantified using a fluorometer. Fluorescein is currently used most as a fluorescent probe [90].

In this thesis (**CHAPTER 6**) the production of ROS was measured using a modified method of oxygen radical absorbance capacity (ORAC). In brief, medium samples were thawed at room temperature in a closed vial and placed in a 96-well plate. A solution of fluorescein (Fluorescein sodium salt, Sigma), a fluorescent probe, in PBS was prepared and added to each well in a final concentration of $1.38x10^{-4}$ mol/L. Fluorescence intensity kinetics was measured every minute for 1 hour using a microplate fluorescence reader (excitation wavelength: 488 nm and emission wavelength: 528 nm). Different media freshly prepared were used as controls and PBS with fluorescein used as assay control. Results are presented as percentage of fluorescein intensity.

Enzyme-linked immunosorbent assay (ELISA)

ELISA was used for the quantification of hypoxia inducible factor 1 (HIF1A) in the extracellular medium of cells maintained under both normoxia (21% O_2) and hypoxia (5% O_2) (**CHAPTER 6**). To do so, at pre-

established time points, the different media were collected and placed at - 80°C until further analysis. Afterwards, a HIF1A ELISA Kit (AVIVA SYSTEMS BIOLOGY) was used for the quantification according to manufacturer protocol and the absorbance read at 405 nm in a microplate reader (Synergy HT; Bio-Tek Instruments). The percentage of extracellular HIF1A was calculated after normalization to condition 100 BM: 0 OM (basal condition) under normoxia.

4.2.3.5. Morphological characterization

F-actin alignment and nuclei aspect ratio

In **CHAPTERs 7**, **8** and **9**, actin filament alignment was determined through directionality analysis using the Fourier components method using the FIJI software (version 2.0.0). For this purpose, confocal images were converted to 32-bit images and cropped into three different images. The radial intensities were calculated, and the orientation map was also obtained. Nuclei aspect ratio was similarly performed. Elongation was determined measuring several nuclei in different labeled images of each sample, using ImageJ software (version 1.52d). The length was divided by the width to obtain the correspondent aspect ratio. If the ratio was higher than 1, more elongated nuclei were found, while the opposite demonstrated the presence of rounded-shaped nuclei.

4.2.3.6. Histochemical characterization

Alizarin Red Staining

Alizarin Red S is a water-soluble sodium salt of alizarin sulfonic acid with a chemical formula of $C_{14}H_7NaO_7S$ [91]. Alizarin Red is used in a biochemical assay to determine, quantitatively, the presence of calcific deposition by cells. Therefore, it can be used as an early-stage marker (days 10–16 of *in vitro* culture) of matrix mineralization. Alizarin's abilities to be used as a biological staining was first noted in 1567, when after fed to animals, it stained their teeth and bones red. The chemical is now commonly used in medical studies involving calcium. Free (ionic) calcium forms precipitates with alizarin, and tissue block containing calcium stain red immediately when immersed in alizarin solution. Thus, both pure calcium and calcium in bones and other tissues can be stained. These alizarin-stained elements can be better visualized under fluorescent lights, excited by 440–460 nm [92]. Moreover, acidic conditions (pH 4.1 to 4.3) are required for a high-quality staining of calcium deposits. This staining is particularly versatile as the dye can be extracted from the stained monolayer and quantified.

In **CHAPTERs 5**, **6**, **7** and **8**, calcium deposits were stained using alizarin red staining and afterwards quantified. Briefly, after established times, samples containing cells were fixed with 10% (v/v) neutral

buffered formalin for 20 min at room temperature. Afterwards, samples were washed with PBS and deionized water. Subsequently, a solution of 2% (w/v) AZ (Merck) was added for 10 min and the excess of dye removed with deionized water. Staining was visualized and images were acquired using the inverted microscope Vert A.1 Axio with Axiocam 503 color (Zeiss, Germany) and Zen 2.3 lite software (Zeiss, Germany). Quantitative data were obtained using the cetylpyridinium chloride (CPC) method. The dye was removed using a solution of 10% (w/v) CPC in 10×10^{-3} m sodium phosphate (Sigma-Aldrich) for 1 h, under gentle shaking, at RT and the absorbance measured at 562 nm in a microplate reader (Synergy HT, Bio-Tek Instruments).

Alcian blue staining

Alcian blue is commonly used to stain acidic polysaccharides such as glycosaminoglycans and some types of mucopolysaccharides [93]. Alcian Blue presents relatively high solubility in its salt form and stains slower than other dyes. The solid Alcian blue is obtained as greenish black crystals with metallic sheen. The aqueous solution is bright greenish blue. Though the compound alcian blue itself is unstable the staining it produces is stable and light fast. By changing pH or ambient salt concentrations characteristic staining patterns can be obtained. For instance, At pH 1.0, it stains only sulfated polysaccharides while at pH 2.5 also stains carboxyl group containing sugars, such as sialic acids and uronic acids [93].

In this thesis (**CHAPTER 6**), alcian blue staining was used to visualize the presence of glycosaminoglycans in single cultures of hTDCs and co-cultures of pre-OBs/hTDCs maintained under normoxia (21% O_2) and hypoxia (5% O_2). To do so, cells were washed with PBS and fixed with 10% (v/v) neutral buffered formalin for 20 min at room temperature. Afterward, the wells were washed twice with PBS, and alcian blue solution in 0.1M hydrochloric acid was added for 30min, at room temperature, under mild shaking. Stained samples were thoroughly washed with PBS and images acquired using a stereomicroscope (Discovery v8; Zeiss) coupled with a digital camera (EOS 1200D; Canon). Staining quantification was performed using a microplate reader (Synergy HT; Bio-Tek Instruments), and the absorbance measured at 620 nm.

Collagenous and non-collagenous ECM proteins

ECM deposition in the different scaffolds (**CHAPTERs 7** and **8**) was analyzed by quantification of collagen and other non-collagenous proteins using a semiquantitative colorimetric assay (Sirius Red/Fast Green Collagen Staining Kit, 9046, Chondrex), following the manufacturer's protocol. Briefly, gradient scaffolds

were washed with PBS and fixed with 10% (v/v) neutral buffered formalin for 20 min RT. Afterwards, samples were washed with PBS, and completely submersed in a dye solution for 1 h. The excess dye was rinsed off with distilled water and images acquired using a stereomicroscope (Discovery v8, Zeiss, Deutschland, Germany) with AxioCam ICC1 (Zeiss, Germany). A semiquantitative analyses was performed through dye extraction with a proper buffer and the OD reading taken at 540 and 605 nm using a microplate reader (Synergy HT, Bio-Tek Instruments). Collagenous and noncollagenous protein content were calculated from the formulae provided by the supplier.

4.2.4. STATISTICAL ANALYSIS

Throughout this thesis, data was obtained from at least 3 independent experiments with a minimum of 3 replicates for each condition. All data collected were presented as mean ± standard deviation (SD) or mean ± standard error of the mean (SEM), as indicated in the experimental of each chapter. Statistical analyses were performed using GaphPad Prism 8.0 software. Student's t-test was used for comparisons between two groups. One-way or two-way analysis of variance (ANOVA was used to compare between more than two groups and the test stated. A difference between experimental groups was considered significant with a confidence interval of 95%, whenever $p < 0.05$.

4.3. REFERENCES

[1] A.R. McLauchlin, N.L. Thomas, 13 - Biodegradable polymer nanocomposites, in: F. Gao (Ed.), Advances in Polymer Nanocomposites, Woodhead Publishing2012, pp. 398-430, 10.1533/9780857096241.2.398.

[2] K. Deshmukh, M. Basheer Ahamed, R.R. Deshmukh, S.K. Khadheer Pasha, P.R. Bhagat, K. Chidambaram, 3 - Biopolymer Composites With High Dielectric Performance: Interface Engineering, in: K.K. Sadasivuni, D. Ponnamma, J. Kim, J.J. Cabibihan, M.A. AlMaadeed (Eds.), Biopolymer Composites in Electronics, Elsevier2017, pp. 27-128, 10.1016/B978-0-12-809261-3.00003-6.

[3] D. Mondal, M. Griffith, S.S. Venkatraman, Polycaprolactone-based biomaterials for tissue engineering and drug delivery: Current scenario and challenges, International Journal of Polymeric Materials and Polymeric Biomaterials 65(5) (2016) 255-265, 10.1080/00914037.2015.1103241.

[4] C.X. Lam, D.W. Hutmacher, J.T. Schantz, M.A. Woodruff, S.H. Teoh, Evaluation of polycaprolactone scaffold degradation for 6 months in vitro and in vivo, J Biomed Mater Res A 90(3) (2009) 906-19, 10.1002/jbm.a.32052.

[5] H.-Y. Cheung, K.-T. Lau, T.-P. Lu, D. Hui, A critical review on polymer-based bio-engineered materials for scaffold development, Composites Part B: Engineering 38(3) (2007) 291-300, 10.1016/j.compositesb.2006.06.014.

[6] P. Gunatillake, R. Mayadunne, R. Adhikari, Recent developments in biodegradable synthetic polymers, in: M.R. El-Gewely (Ed.), Biotechnology Annual Review, Elsevier2006, pp. 301-347, 10.1016/S1387-2656(06)12009-8.

[7] M.J. Glimcher, Bone: Nature of the Calcium Phosphate Crystals and Cellular, Structural, and Physical Chemical Mechanisms in Their Formation, Reviews in Mineralogy and Geochemistry 64(1) (2006) 223-282, 10.2138/rmg.2006.64.8.

[8] R.A. Young, J.C. Elliott, Atomic-scale bases for several properties of apatites, Archives of Oral Biology 11(7) (1966) 699-707, 10.1016/0003-9969(66)90095-1.

[9] Y. Jiang, Z. Yuan, J. Huang, Substituted hydroxyapatite: a recent development, Materials Technology (2019) 1-12, 10.1080/10667857.2019.1664096.

[10] S. Adzila, I. Sopyan, M. Hamdi, Synthesis of hydroxyapatite through dry mechanochemical method and its conversion to dense bodies: preliminary result, 2011.

[11] B.O. Fowler, Infrared studies of apatites. II. Preparation of normal and isotopically substituted calcium, strontium, and barium hydroxyapatites and spectra-structure-composition correlations, Inorganic Chemistry 13(1) (1974) 207-214, 10.1021/ic50131a040.

[12] G. Ma, Three common preparation methods of hydroxyapatite, IOP Conference Series: Materials Science and Engineering 688 (2019) 033057, 10.1088/1757-899x/688/3/033057.

[13] Y. Wang, S. Zhang, K. Wei, N. Zhao, J. Chen, X. Wang, Hydrothermal synthesis of hydroxyapatite nanopowders using cationic surfactant as a template, Materials Letters 60(12) (2006) 1484-1487, 10.1016/j.matlet.2005.11.053.

[14] Y. Wang, J. Chen, K. Wei, S. Zhang, X. Wang, Surfactant-assisted synthesis of hydroxyapatite particles, Materials Letters 60(27) (2006) 3227-3231, 10.1016/j.matlet.2006.02.077.

[15] M. Canillas, R. Rivero, R. García-Carrodeguas, F. Barba, M.A. Rodríguez, Processing of hydroxyapatite obtained by combustion synthesis, Boletín de la Sociedad Española de Cerámica y Vidrio 56(5) (2017) 237-242, 10.1016/j.bsecv.2017.05.002.

[16] N.A.S. Mohd Pu'ad, P. Koshy, H.Z. Abdullah, M.I. Idris, T.C. Lee, Syntheses of hydroxyapatite from natural sources, Heliyon 5(5) (2019) e01588, 10.1016/j.heliyon.2019.e01588.

[17] J. Venkatesan, S.K. Kim, Effect of Temperature on Isolation and Characterization of Hydroxyapatite from Tuna (Thunnus obesus) Bone, Materials (Basel) 3(10) (2010) 4761-4772, 10.3390/ma3104761.

[18] D.S. Gomes, A.M.C. Santos, G.A. Neves, R.R. Menezes, A brief review on hydroxyapatite production and use in biomedicine, Cerâmica 65 (2019) 282-302.

[19] T.J. Webster, C. Ergun, R.H. Doremus, R.W. Siegel, R. Bizios, Enhanced functions of osteoblasts on nanophase ceramics, Biomaterials 21(17) (2000) 1803-10, 10.1016/s0142-9612(00)00075-2.

[20] V. Uskoković, Challenges for the Modern Science in its Descend Towards Nano Scale, Curr Nanosci 5(3) (2009) 372-389, 10.2174/157341309788921381.

[21] A. Olaechea, G. Mendoza-Azpur, F. O´Valle, M. Padial-Molina, N. Martin-Morales, P. Galindo-Moreno, Biphasic hydroxyapatite and ß-tricalcium phosphate biomaterial behavior in a case series of maxillary sinus augmentation in humans, Clinical Oral Implants Research 30(4) (2019) 336-343, 10.1111/clr.13419.

[22] V.S. Kattimani, S. Kondaka, K.P. Lingamaneni, Hydroxyapatite–-Past, Present, and Future in Bone Regeneration, Bone and Tissue Regeneration Insights 7 (2016) BTRI.S36138, 10.4137/btri.S36138.

[23] M.D. Pierschbacher, E. Ruoslahti, Cell attachment activity of fibronectin can be duplicated by small synthetic fragments of the molecule, Nature 309(5963) (1984) 30-3, 10.1038/309030a0.

[24] N. Davidenko, C.F. Schuster, D.V. Bax, R.W. Farndale, S. Hamaia, S.M. Best, R.E. Cameron, Evaluation of cell binding to collagen and gelatin: a study of the effect of 2D and 3D architecture and surface chemistry, J Mater Sci Mater Med 27(10) (2016) 148-148, 10.1007/s10856-016-5763-9.

[25] A. Page-McCaw, A.J. Ewald, Z. Werb, Matrix metalloproteinases and the regulation of tissue remodelling, Nature Reviews Molecular Cell Biology 8(3) (2007) 221-233, 10.1038/nrm2125.

[26] S. Galis Zorina, J. Khatri Jaikirshan, Matrix Metalloproteinases in Vascular Remodeling and Atherogenesis, Circulation Research 90(3) (2002) 251-262, 10.1161/res.90.3.251.

[27] G. Yang, Z. Xiao, H. Long, K. Ma, J. Zhang, X. Ren, J. Zhang, Assessment of the characteristics and biocompatibility of gelatin sponge scaffolds prepared by various crosslinking methods, Sci Rep 8(1) (2018) 1616, 10.1038/s41598-018-20006-y.

[28] T. Furuike, T. Chaochai, T. Okubo, T. Mori, H. Tamura, Fabrication of nonwoven fabrics consisting of gelatin nanofibers cross-linked by glutaraldehyde or N-acetyl-d-glucosamine by aqueous method, International Journal of Biological Macromolecules 93 (2016) 1530-1538, 10.1016/j.ijbiomac.2016.03.053.

[29] D. Achet, X.W. He, Determination of the renaturation level in gelatin films, Polymer 36(4) (1995) 787-791, 10.1016/0032-3861(95)93109-Y.

[30] R. Imani, M. Rafienia, S.H. Emami, Synthesis and characterization of glutaraldehyde-based crosslinked gelatin as a local hemostat sponge in surgery: an in vitro study, Biomed Mater Eng 23(3) (2013) 211-24, 10.3233/bme-130745.

[31] M. Liu, X. Zeng, C. Ma, H. Yi, Z. Ali, X. Mou, S. Li, Y. Deng, N. He, Injectable hydrogels for cartilage and bone tissue engineering, Bone Research 5(1) (2017) 17014, 10.1038/boneres.2017.14.

[32] A.B. Bello, D. Kim, D. Kim, H. Park, S.-H. Lee, Engineering and Functionalization of Gelatin Biomaterials: From Cell Culture to Medical Applications, Tissue Engineering Part B: Reviews 26(2) (2020) 164-180, 10.1089/ten.teb.2019.0256.

[33] G. Yang, H. Lin, B.B. Rothrauff, S. Yu, R.S. Tuan, Multilayered polycaprolactone/gelatin fiber-hydrogel composite for tendon tissue engineering, Acta Biomaterialia 35 (2016) 68-76, 10.1016/j.actbio.2016.03.004.

[34] B.B. Mendes, M. Gómez-Florit, P.S. Babo, R.M. Domingues, R.L. Reis, M.E. Gomes, Blood derivatives awaken in regenerative medicine strategies to modulate wound healing, Advanced Drug Delivery Reviews 129 (2018) 376-393, 10.1016/j.addr.2017.12.018.

[35] I. Martineau, E. Lacoste, G. Gagnon, Effects of calcium and thrombin on growth factor release from platelet concentrates: kinetics and regulation of endothelial cell proliferation, Biomaterials 25(18) (2004) 4489-502, 10.1016/j.biomaterials.2003.11.013.

[36] M. McLaughlin, P. Gagnet, E. Cunningham, R. Yeager, M. D'Amico, K. Guski, M. Scarpone, D. Kuebler, Allogeneic Platelet Releasate Preparations Derived via a Novel Rapid Thrombin Activation Process Promote Rapid Growth and Increased BMP-2 and BMP-4 Expression in Human Adipose-Derived Stem Cells, Stem Cells International 2016 (2016) 7183734, 10.1155/2016/7183734.

[37] G. Intini, S. Andreana, F.E. Intini, R.J. Buhite, L.A. Bobek, Calcium sulfate and platelet-rich plasma make a novel osteoinductive biomaterial for bone regeneration, J Transl Med 5 (2007) 13, 10.1186/1479-5876-5-13.

[38] M.R. Messora, M.J. Nagata, R.C. Mariano, R.C. Dornelles, S.R. Bomfim, S.E. Fucini, V.G. Garcia, A.F. Bosco, Bone healing in critical-size defects treated with platelet-rich plasma: a histologic and histometric study in rat calvaria, J Periodontal Res 43(2) (2008) 217-23, 10.1111/j.1600-0765.2007.01017.x.

[39] V.E. Santo, A.R. Duarte, E.G. Popa, M.E. Gomes, J.F. Mano, R.L. Reis, Enhancement of osteogenic differentiation of human adipose derived stem cells by the controlled release of platelet lysates from hybrid scaffolds produced by supercritical fluid foaming, J Control Release 162(1) (2012) 19-27, 10.1016/j.jconrel.2012.06.001.

[40] M.L. Chou, T. Burnouf, Current methods to manufacture human platelet lysates for cell therapy and tissue engineering: possible trends in product safety and standardization, ISBT Science Series 12(1) (2017) 168-175, 10.1111/voxs.12316.

[41] N. Fekete, M. Gadelorge, D. Fürst, C. Maurer, J. Dausend, S. Fleury-Cappellesso, V. Mailänder, R. Lotfi, A. Ignatius, L. Sensebé, P. Bourin, H. Schrezenmeier, M.T. Rojewski, Platelet lysate from whole blood-derived pooled platelet concentrates and apheresis-derived platelet concentrates for the isolation and expansion of human bone marrow mesenchymal stromal cells: production process, content and identification of active components, Cytotherapy 14(5) (2012) 540-54, 10.3109/14653249.2012.655420.

[42] D.M. Dohan Ehrenfest, L. Rasmusson, T. Albrektsson, Classification of platelet concentrates: from pure platelet-rich plasma (P-PRP) to leucocyte- and platelet-rich fibrin (L-PRF), Trends in Biotechnology 27(3) (2009) 158-167, 10.1016/j.tibtech.2008.11.009.

[43] N. Fekete, M. Gadelorge, D. Fürst, C. Maurer, J. Dausend, S. Fleury-Cappellesso, V. Mailänder, R. Lotfi, A. Ignatius, L. Sensebé, P. Bourin, H. Schrezenmeier, M.T. Rojewski, Platelet lysate from whole blood-derived pooled platelet concentrates and apheresis-derived platelet concentrates for the isolation and expansion of human bone marrow mesenchymal stromal cells: production process, content and identification of active components, Cytotherapy 14(5) (2012) 540-554, 10.3109/14653249.2012.655420.

[44] E. Anitua, M. Sánchez, A.T. Nurden, P. Nurden, G. Orive, I. Andía, New insights into and novel applications for platelet-rich fibrin therapies, Trends in Biotechnology 24(5) (2006) 227-234, 10.1016/j.tibtech.2006.02.010.

[45] E. Anitua, M. Sánchez, G. Orive, I. Andia, Delivering growth factors for therapeutics, Trends in Pharmacological Sciences 29(1) (2008) 37-41, 10.1016/j.tips.2007.10.010.

[46] D. Puppi, F. Chiellini, Wet-spinning of biomedical polymers: from single-fibre production to additive manufacturing of three-dimensional scaffolds, Polymer International 66(12) (2017) 1690-1696, 10.1002/pi.5332.

[47] A. Yaari, Y. Schilt, C. Tamburu, U. Raviv, O. Shoseyov, Wet Spinning and Drawing of Human Recombinant Collagen, ACS Biomaterials Science & Engineering 2(3) (2016) 349-360, 10.1021/acsbiomaterials.5b00461.

[48] O. Nechyporchuk, T. Yang Nilsson, H. Ulmefors, T. Köhnke, Wet Spinning of Chitosan Fibers: Effect of Sodium Dodecyl Sulfate Adsorption and Enhanced Dope Temperature, ACS Applied Polymer Materials 2(9) (2020) 3867-3875, 10.1021/acsapm.0c00562.

[49] P.F. Ng, K.I. Lee, S. Meng, J. Zhang, Y. Wang, B. Fei, Wet Spinning of Silk Fibroin-Based Core–Sheath Fibers, ACS Biomaterials Science & Engineering 5(6) (2019) 3119-3130, 10.1021/acsbiomaterials.9b00275.

[50] K.D. Nelson, A. Romero, P. Waggoner, B. Crow, A. Borneman, G.M. Smith, Technique paper for wet-spinning poly(L-lactic acid) and poly(DL-lactide-co-glycolide) monofilament fibers, Tissue Eng 9(6) (2003) 1323-30, 10.1089/10763270360728233.

[51] N. Abay Akar, G. Gürel Peközer, G. Torun Köse, Fibrous bone tissue engineering scaffolds prepared by wet spinning of PLGA, Turk J Biol 43(4) (2019) 235-245, 10.3906/biy-1904-63.

[52] N. Diban, S. Haimi, L. Bolhuis-Versteeg, S. Teixeira, S. Miettinen, A. Poot, D. Grijpma, D. Stamatialis, Development and characterization of poly(ε-caprolactone) hollow fiber membranes for vascular tissue engineering, Journal of Membrane Science 438 (2013) 29-37, 10.1016/j.memsci.2013.03.024.

[53] N. Diban, S. Haimi, L. Bolhuis-Versteeg, S. Teixeira, S. Miettinen, A. Poot, D. Grijpma, D. Stamatialis, Hollow fibers of poly(lactide-co-glycolide) and poly(ε-caprolactone) blends for vascular tissue engineering applications, Acta Biomater 9(5) (2013) 6450-8, 10.1016/j.actbio.2013.01.005.

[54] C.V. Boys, On the Production, Properties, and some suggested Uses of the Finest Threads, Proceedings of the Physical Society of London 9(1) (1887) 8-19, 10.1088/1478-7814/9/1/303.

[55] D. Li, Y. Xia, Electrospinning of Nanofibers: Reinventing the Wheel?, Advanced Materials 16(14) (2004) 1151-1170, 10.1002/adma.200400719.

[56] J. Xue, T. Wu, Y. Dai, Y. Xia, Electrospinning and Electrospun Nanofibers: Methods, Materials, and Applications, Chemical Reviews 119(8) (2019) 5298-5415, 10.1021/acs.chemrev.8b00593.

[57] J. Xue, J. Xie, W. Liu, Y. Xia, Electrospun Nanofibers: New Concepts, Materials, and Applications, Accounts of Chemical Research 50(8) (2017) 1976-1987, 10.1021/acs.accounts.7b00218.

[58] L. Persano, A. Camposeo, C. Tekmen, D. Pisignano, Industrial Upscaling of Electrospinning and Applications of Polymer Nanofibers: A Review, Macromolecular Materials and Engineering 298(5) (2013) 504-520, 10.1002/mame.201200290.

[59] J.A. Matthews, G.E. Wnek, D.G. Simpson, G.L. Bowlin, Electrospinning of Collagen Nanofibers, Biomacromolecules 3(2) (2002) 232-238, 10.1021/bm015533u.

[60] M. Laranjeira, R.M.A. Domingues, R. Costa-Almeida, R.L. Reis, M.E. Gomes, 3D Mimicry of Native-Tissue-Fiber Architecture Guides Tendon-Derived Cells and Adipose Stem Cells into Artificial Tendon Constructs, Small 13(31) (2017) 10.1002/smll.201700689.

[61] C. Wang, S.N. Tong, Y.H. Tse, M. Wang, Conventional Electrospinning vs. Emulsion Electrospinning: A Comparative Study on the Development of Nanofibrous Drug/Biomolecule Delivery Vehicles, Advanced Materials Research 410 (2012) 118-121, 10.4028/AMR.410.118.

[62] X. Xu, X. Zhuang, X. Chen, X. Wang, L. Yang, X. Jing, Preparation of Core-Sheath Composite Nanofibers by Emulsion Electrospinning, Macromolecular Rapid Communications 27(19) (2006) 1637-1642, 10.1002/marc.200600384.

[63] C. Zhang, Y. Li, P. Wang, H. Zhang, Electrospinning of nanofibers: Potentials and perspectives for active food packaging, Comprehensive Reviews in Food Science and Food Safety 19(2) (2020) 479-502, 10.1111/1541-4337.12536.

[64] Y. Yang, X. Li, W. Cui, S. Zhou, R. Tan, C. Wang, Structural stability and release profiles of proteins from core-shell poly (DL-lactide) ultrafine fibers prepared by emulsion electrospinning, J Biomed Mater Res A 86(2) (2008) 374-85, 10.1002/jbm.a.31595.

[65] X. Li, H. Zhang, H. Li, X. Yuan, Encapsulation of proteinase K in PELA ultrafine fibers by emulsion electrospinning: preparation and in vitro evaluation, Colloid and Polymer Science 288(10) (2010) 1113-1119, 10.1007/s00396-010-2235-5.

[66] P. McClellan, W.J. Landis, Recent Applications of Coaxial and Emulsion Electrospinning Methods in the Field of Tissue Engineering, Biores Open Access 5(1) (2016) 212-27, 10.1089/biores.2016.0022.

[67] L. Lu, S. Yuan, J. Wang, Y. Shen, S. Deng, L. Xie, Q. Yang, The Formation Mechanism of Hydrogels, Curr Stem Cell Res Ther 13(7) (2018) 490-496, 10.2174/1574888x12666170612102706.

[68] B.B. Mendes, M. Gómez-Florit, R.A. Pires, R.M.A. Domingues, R.L. Reis, M.E. Gomes, Human-based fibrillar nanocomposite hydrogels as bioinstructive matrices to tune stem cell behavior, Nanoscale 10(36) (2018) 17388-17401, 10.1039/C8NR04273J.

[69] P.S. Babo, R.L. Pires, L. Santos, A. Franco, F. Rodrigues, I. Leonor, R.L. Reis, M.E. Gomes, Platelet Lysate-Loaded Photocrosslinkable Hyaluronic Acid Hydrogels for Periodontal Endogenous Regenerative Technology, ACS Biomaterials Science & Engineering 3(7) (2017) 1359-1369, 10.1021/acsbiomaterials.6b00508.

[70] L.S. Neves, P.S. Babo, A.I. Gonçalves, R. Costa-Almeida, S.G. Caridade, J.F. Mano, R.M.A. Domingues, M.T. Rodrigues, R.L. Reis, M.E. Gomes, Injectable Hyaluronic Acid Hydrogels Enriched with Platelet Lysate as a Cryostable Off-the-Shelf System for Cell-Based Therapies, Regenerative Engineering and Translational Medicine 3(2) (2017) 53-69, 10.1007/s40883-017-0029-8.

[71] R. Costa-Almeida, I. Calejo, R. Altieri, R.M.A. Domingues, E. Giordano, R.L. Reis, M.E. Gomes, Exploring platelet lysate hydrogel-coated suture threads as biofunctional composite living fibers for cell delivery in tissue repair, Biomedical Materials 14(3) (2019) 034104, 10.1088/1748-605x/ab0de6.

[72] S.T. Robinson, A.M. Douglas, T. Chadid, K. Kuo, A. Rajabalan, H. Li, I.B. Copland, T.H. Barker, J. Galipeau, L.P. Brewster, A novel platelet lysate hydrogel for endothelial cell and mesenchymal stem cell-directed neovascularization, Acta Biomater 36 (2016) 86-98, 10.1016/j.actbio.2016.03.002.

[73] M. Akbari, A. Tamayol, S. Bagherifard, L. Serex, P. Mostafalu, N. Faramarzi, M.H. Mohammadi, A. Khademhosseini, Textile Technologies and Tissue Engineering: A Path Toward Organ Weaving, Adv Healthc Mater 5(7) (2016) 751-766, 10.1002/adhm.201500517.

[74] A. Fallahi, A. Khademhosseini, A. Tamayol, Textile Processes for Engineering Tissues with Biomimetic Architectures and Properties, Trends in Biotechnology 34(9) (2016) 683-685, 10.1016/j.tibtech.2016.07.001.

[75] D.J. Stokes, Principles of SEM, Principles and Practice of Variable Pressure/Environmental Scanning Electron Microscopy (VP-ESEM)2008, pp. 17-62, 10.1002/9780470758731.ch2.

[76] J.D. Boerckel, D.E. Mason, A.M. McDermott, E. Alsberg, Microcomputed tomography: approaches and applications in bioengineering, Stem Cell Res Ther 5(6) (2014) 144-144, 10.1186/scrt534.

[77] R. Song, M. Murphy, C. Li, K. Ting, C. Soo, Z. Zheng, Current development of biodegradable polymeric materials for biomedical applications, Drug Des Devel Ther 12 (2018) 3117-3145, 10.2147/DDDT.S165440.

[78] D. Ozdil, I. Wimpenny, H.M. Aydin, Y. Yang, 13 - Biocompatibility of biodegradable medical polymers, in: X. Zhang (Ed.), Science and Principles of Biodegradable and Bioresorbable Medical Polymers, Woodhead Publishing2017, pp. 379-414, 10.1016/B978-0-08-100372-5.00013-1.

[79] R.J. Markovich, C. Pidgeon, Introduction to Fourier Transform Infrared Spectroscopy and Applications in the Pharmaceutical Sciences, Pharmaceutical Research 8(6) (1991) 663-675, 10.1023/A:1015829412658.

[80] Y. Bi, D. Ehirchiou, T.M. Kilts, C.A. Inkson, M.C. Embree, W. Sonoyama, L. Li, A.I. Leet, B.M. Seo, L. Zhang, S. Shi, M.F. Young, Identification of tendon stem/progenitor cells and the role of the extracellular matrix in their niche, Nat Med 13(10) (2007) 1219-27, 10.1038/nm1630.

[81] P. Eliasson, T. Andersson, P. Aspenberg, Rat Achilles tendon healing: mechanical loading and gene expression, J Appl Physiol (1985) 107(2) (2009) 399-407, 10.1152/japplphysiol.91563.2008.

[82] M. Dominici, K. Le Blanc, I. Mueller, I. Slaper-Cortenbach, F. Marini, D. Krause, R. Deans, A. Keating, D. Prockop, E. Horwitz, Minimal criteria for defining multipotent mesenchymal stromal cells. The

International Society for Cellular Therapy position statement, Cytotherapy 8(4) (2006) 315-7, 10.1080/14653240600855905.

[83] R. Dai, Z. Wang, R. Samanipour, K.I. Koo, K. Kim, Adipose-Derived Stem Cells for Tissue Engineering and Regenerative Medicine Applications, Stem Cells Int 2016 (2016) 6737345, 10.1155/2016/6737345.

[84] A.I. Gonçalves, M.T. Rodrigues, S.-J. Lee, A. Atala, J.J. Yoo, R.L. Reis, M.E. Gomes, Understanding the Role of Growth Factors in Modulating Stem Cell Tenogenesis, PLOS ONE 8(12) (2014) e83734, 10.1371/journal.pone.0083734.

[85] S. Font Tellado, E.R. Balmayor, M. Van Griensven, Strategies to engineer tendon/ligament-to-bone interface: Biomaterials, cells and growth factors, Adv Drug Deliv Rev 94 (2015) 126-40, 10.1016/j.addr.2015.03.004.

[86] E. Cenni, F. Perut, N. Baldini, In vitro models for the evaluation of angiogenic potential in bone engineering, Acta Pharmacologica Sinica 32(1) (2011) 21-30, 10.1038/aps.2010.143.

[87] G.I. Im, Coculture in musculoskeletal tissue regeneration, Tissue Eng Part B Rev 20(5) (2014) 545-54, 10.1089/ten.TEB.2013.0731.

[88] P. Szulc, D.C. Bauer, Chapter 67 - Biochemical Markers of Bone Turnover in Osteoporosis, in: R. Marcus, D. Feldman, D.W. Dempster, M. Luckey, J.A. Cauley (Eds.), Osteoporosis (Fourth Edition), Academic Press, San Diego, 2013, pp. 1573-1610, 10.1016/B978-0-12-415853-5.00067-4.

[89] Z. Tang, H. Chen, H. He, C. Ma, Assays for alkaline phosphatase activity: Progress and prospects, TrAC Trends in Analytical Chemistry 113 (2019) 32-43,10.1016/j.trac.2019.01.019.

[90] B. Ou, M. Hampsch-Woodill, R.L. Prior, Development and Validation of an Improved Oxygen Radical Absorbance Capacity Assay Using Fluorescein as the Fluorescent Probe, Journal of Agricultural and Food Chemistry 49(10) (2001) 4619-4626, 10.1021/jf010586o.

[91] L. Legan, K. Retko, P. Ropret, Vibrational spectroscopic study on degradation of alizarin carmine, Microchemical Journal 127 (2016) 36-45, 10.1016/j.microc.2016.02.002.

[92] W.L. Smith, A.B. Chesney, S.O. Gregory, P.D. Matthew, P.M. Rene, Z.G. Sarah, G.G. Matthew, Improving Vertebrate Skeleton Images: Fluorescence and the Non-Permanent Mounting of Cleared-and-Stained Specimens, Copeia 106(3) (2018) 427-435, 10.1643/CG-18-047.

[93] M. Lai, B. Lü, 3.04 - Tissue Preparation for Microscopy and Histology, in: J. Pawliszyn (Ed.), Comprehensive Sampling and Sample Preparation, Academic Press, Oxford, 2012, pp. 53-93, 10.1016/B978-0-12-381373-2.00070-3.

SECTION III: Strategies for Tendon-to-Bone Interface Engineering

CHAPTER 5. "Bi-directional modulation of cellular interactions in an *in vitro* co-culture model of tendon-to-bone interface"

This chapter was adapted from the following publication:

I. Calejo, R. Costa-Almeida, A. I. Gonçalves, D. Berdecka, R. L. Reis, M. E. Gomes (2018) Bi-directional modulation of cellular interactions in an in vitro co-culture model of tendon-to-bone interface. *Cell Proliferation*, 51:e12493. DOI:10.1111/cpr.12493.

ABSTRACT

This work aimed at studying *in vitro* interactions between human tendon-derived cells (hTDCs) and pre-osteoblasts (pre-OBs) that may trigger a cascade of events involved in enthesis regeneration.

The effect of five osteogenic medium conditions over the modulation of hTDCs and pre-OBs toward the tenogenic and osteogenic phenotypes, respectively, was studied. Three different medium conditions were chosen for subsequently establishing a direct co-culture system in order to study the expression of bone, tendon and interface-related markers.

A higher matrix mineralization and ALP activity was observed in co-cultures in the presence of osteogenic medium. Higher transcription levels of bone- (*ALPL, RUNX2, SPP1*) and interface-related genes (*ACAN, COMP*) were found in co-cultures. The expression of aggrecan was influence by the presence of osteogenic medium and cell-cell interactions occurring in co-culture.

The present work assessed both the influence of osteogenic medium on cell phenotype modulation and the importance of co-culture models while promoting cell-cell interactions and the exchange of soluble factors in triggering an interface-like phenotype to potentially modulate enthesis regeneration.

Keywords: Cell crosstalk; Direct Co-culture; Single culture; Medium condition; Tendon-bone Interface

5.1. INTRODUCTION

The enthesis allows a smooth transition between tendon and bone. Typically, three continuous regions are distinguished: tendon, non-mineralized and mineralized fibrocartilage and bone, resulting in a gradient of composition, organization and, therefore, mechanical properties [1, 2]. This soft-hard tissue interface is vulnerable to acute or overuse sports injuries (e.g., golfer's elbow, jumper's knee and Achilles insertional tendinopathies) [3, 4]. Frequently, orthopedic surgeons face the challenge of partial or complete rupture of Achilles and rotator cuff tendons. Currently, grafts are most often applied but several problems are associated, including donor tissue availability and morbidity, host tissue reaction and time of biological incorporation [5-7], and high rupture recurrence rates due to neo-fibrovascular tissue formation that compromises stability and mechanical properties of repaired enthesis [6-8].

Thus, interface tissue engineering (ITE) aims at the recreating different tissues *in vitro* in order to repair or to regenerate diseased/damaged musculoskeletal interfaces.[9, 10] Several attempts have been made to improve enthesis repair and regeneration, considering a need to mimic the nano- and micro-structure of native tissue and replicate spatial distribution of cells and signaling factors [2, 3, 11]. Cell-based therapies provide new possibilities within tissue engineering to generate a functional enthesis, due to the central role of cell-cell interactions in developing a functional tissue. Particularly, the use of multiple cell types in co-culture systems is being increasingly explored aiming at mimicking the characteristic cellular environment found in the native tissue. Recent studies have shown that these strategies can affect cell fate and function [12-14]. Indeed, different strategies have been used to mimic the complex cellular composition of enthesis. Normally, *in vitro* co-culture approaches rely on the culture of differentiated cells (fibroblasts, osteoblasts, chondrocytes) and mesenchymal stem cells (MSCs) [12, 13, 15-17]. Here, compared to stem cells, the use of differentiated cells poses practical challenges for clinical applications given their lower regenerative power and longer *in vitro* expansion periods to obtain a sufficient cell number before transplantation. Therefore, MSCs, particularly bone marrow MSCs (BMSCs), have been explored in enthesis regeneration [17-19]. However, adipose derived stem cells (ASCs) offer some advantages: i) isolation from lipoaspirates provides an abundant autologous cell source, with relatively lower donor site morbidity and pain [20]; ii) ASCs exhibit higher *in vitro* proliferation capacity, lower senescence and ability to generate tendon [21-24], bone [25, 26] and cartilage-like [27-29] tissues.

Co-culture systems constitute interesting platforms to study cellular interactions occurring in enthesis, allowing a close replication of the native cellular environment [30, 31]. Several *in vitro* studies have reported the important role of cell-cell communication and paracrine factors on the expression of interface-

relevant markers, as well as the formation of fibrocartilage-like interface [12, 15, 17]. Nonetheless, the use of sources such as ASCs in co-culture is still unexplored, as option for ITE.

Herein, we propose optimizing a co-culture model to study cellular interactions between human ASCs (hASCs), pre-differentiated toward the osteogenic lineage (herein called pre-osteoblasts, pre-OBs) and human tendon-derived cells (hTDCs), used to replicate cellular environments found in bone and tendon, respectively. Firstly, the effect of different concentrations of osteogenic culture medium on tendon and bone niches maintenance was explored. Afterwards, a co-culture model was established to evaluate the effect of different medium conditions and the influence of direct cell contact on the expression of relevant tendon-, bone- and interface-related markers.

5.2. MATERIALS AND METHODS

5.2.1. Cell isolation and culture

Samples were obtained under protocols previously established with Hospital da Prelada (Porto, Portugal) and under informed consent of the patients, according to Helsinki's Declaration and as reviewed and approved by the Ethical Committee of Hospital da Prelada.

Human ASCs were isolated from subcutaneous fat tissue obtained from lipoaspirate samples of healthy female patients [32, 33] with ages in the range of 27- 42 years; hTDCs were isolated from tendon surplus samples of healthy male patients undergoing elective orthopedic surgeries [34, 35] with ages in the range of 25–30 years, as described in Supporting Information. Cells were cultured in basal medium composed of Minimum Essential Medium Eagle (α–MEM, Alfagene) supplemented with 10% (v/v) Fetal Bovine Serum (FBS, Alfagene) and 1% (v/v) antibiotic/antimitotic solution (A/A, Alfagene).

5.2.2. Osteogenic differentiation

Osteogenic pre-commitment was performed by culturing hASCs in osteogenic medium (OM) (basal medium with 10 mM β-glycerophosphate (βGP, G9422, Sigma-Aldrich), 10-8 M dexamethasone (DEX, D2915, Sigma-Aldrich), and 50 g/mL L-ascorbic acid 2-phosphate sesquimagnesium salt hydrate (AA, 013-12061, Wako). After selecting a 14-day pre-commitment period, hASCs were herein called pre-osteoblasts (pre-OBs) and used in both single and co-culture studies.

5.2.3. Culture Setup

Figure 5.1 depicts the experimental setup used for the experiments. In single cultures, pre-OBs and hTDCs were seeded separately at a density of 2×10^3 cells/cm2. Five medium conditions containing

different ratios of basal (BM) and osteogenic media (OM) were tested (**Table 5.1**). Three conditions were selected for establishing direct contact co-cultures by seeding pre-OBs and hTDCs together in a ratio of 1:1 using a final density of 2×103cells/cm2. Single cultures of pre-OBs and hTDCs were used as controls. Proliferation, alkaline phosphatase activity (ALP), alizarin red (AZ) staining, protein and gene expression were determined after 1, 7 and 14 days of culture.

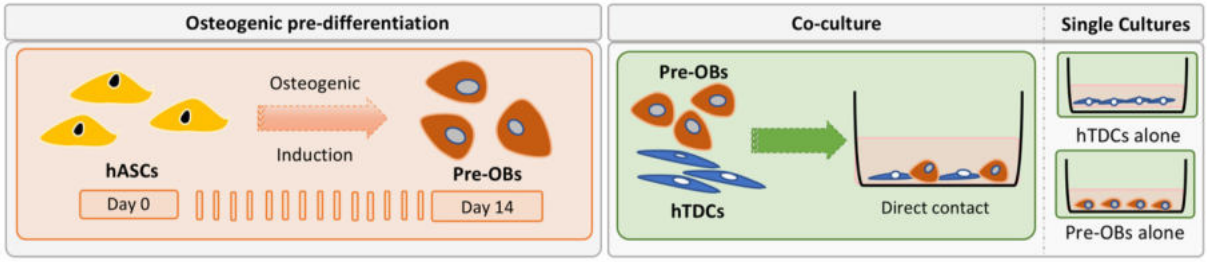

Figure 5.1 | Experimental setup illustrating the temporal approach used to induce the osteogenic differentiation of hASCs and consequent establishment of a direct co-culture model and correspondent single cultures. To assess the influence of different concentrations of osteogenic supplementation on culture medium, both pre-OBs and hTDCs were initially seeded separately in single culture systems. For this purpose, cellular responses were studied to simultaneously evaluate the effects on the osteogenic commitment of pre-OBs and the tenogenic phenotype of hTDCs. Subsequently, co-culture systems were established using pre-OBs and hTDCs under direct contact conditions to further investigate the crosstalk occurring between these two cell types under selected culture medium conditions. In this case, single culture systems were also performed in parallel as controls.

5.2.4. dsDNA quantification, Alizarin Red Staining and ALP activity

Cellular proliferation was evaluated using a fluorometric dsDNA quantification kit (PicoGreen, Molecular Probes, Invitrogen) to determine DNA content. Calcium deposition was assessed by AZ staining and quantitative analysis after 7 and 14 days of culture. ALP activity was determined using a colorimetric p-nitrophenol (pNp) assay. Details are provided in Supporting Information.

Table 5.1 | Composition of cell culture media used in single and co-cultures.

	Ratios (%)	
	Basal Medium (BM)	Osteogenic Medium (OM)
Condition 1 – 100 BM : 0 OM	100	0
Condition 2 – 75 BM : 25 OM	75	25
Condition 3 – 50 BM : 50 OM	50	50
Condition 4 – 25 BM : 75 OM	25	75
Condition 5 – 0 BM : 100 OM	0	100

Basal medium (BM): alpha-MEM supplemented with 10% FBS and 1% antibiotic/antimitotic solution; Osteogenic Medium (OM): basal medium supplemented with 10 mM βGP, 10^{-8} M DEX and 50 μg/mL AA;

5.2.5. Real-time Reverse Transcription Polymerase Chain Reaction (RT-PCR) analysis

Expression of tendon-, bone- and interface-related markers was analyzed. Total mRNA was extracted from single cultures (pre-OBs and hTDCs) and co-culture at days 0, 1, 7 and 14 days using RIBOZOL™ RNA extraction reagent (VWRCN580, VWR). Primer sequences (**Table 5.2**) were designed using Primer-BLAST tool and synthesized by Eurofins Genomics. The evaluation of the relative expression level was performed using the $2^{-\Delta\Delta Ct}$ method. Transcript levels of selected genes were analyzed and normalized to the expression of the selected housekeeping gene, glyceraldehyde-3-phosphate dehydrogenase (GAPDH). All values were firstly normalized against GAPDH housekeeping gene transcript values, and then to the basal condition (100BM:0OM, calibrator sample) of the respective collection day. Three samples were used for each condition. Results are represented as fold change.

5.2.6. Immunocytochemistry

Protein expression of tendon-, bone- and interface-related markers was evaluated using mouse anti-human Tenascin C (TNC, 1:3000, Abcam), mouse anti-human collagen I (COL1, 1:500, Abcam), rabbit anti-human collagen III (COL3, 1:100, Abcam), rabbit anti-human osteopontin (OPN, 1:100, Abcam), mouse anti-human osteocalcin (OCN,1:50, Abcam), mouse anti-human Decorin (DCN, 1:100, Abcam), mouse anti-human Aggrecan (ACAN,1:200, Alfagene) and rabbit anti-human Collagen II (COL2, 1:200, Abcam). Donkey anti-mouse AlexaFluor 488, mouse anti-rabbit AlexaFluor 488 or rabbit anti-goat

AlexaFluor 488 were used as secondary antibodies. Nuclei were counterstained with 4,6-diamidino-2-phenyindole dilactate (DAPI, Invitrogen). All samples were visualized, and images acquired by fluorescence microscopy (Axio Imager Z1m, Zeiss, Deutschland, Germany). Detailed protocol is provided in Supporting Information.

Table 5.2 | Primers used for quantitative RT-PCR analysis.

Target Gene	Gene Abbr.	Primer Sequence		NBCI Reference
		Forward	Reverse	
Glyceraldehyde 3-phosphate dehydrogenase	*GAPDH*	AGCCTCAAGATCATCAGCAA	GTCATGAGTCCTTCCAGGAT	NM_002046.5
Collagen, type I, α1	*COL1A1*	GTCACAGATCACGTCATCGC	CGAAGACCCACCAATCAC	NM_000088.3
Collagen, type III, α1	*COL3A1*	TTGGCATGGTTCTGGCTTCC	GCTGGCTACTTCTCGTG	NM_000090.3
Osteogenic related markers				
Secreted phosphoprotein 1 (Osteopontin)	*SPP1*	CAGACCTGACATCCAGTACCC	GGTCATCCAGCTGACTCGTT	NM_001040058.1
Run- related transcription factor 2	*RUNX2*	TGTCTGTGCCTTCTGGGTTC	CCGGCCTGCCTATGCTGTTA	NM_001024630.3
Alkaline Phosphatase	*ALPL*	GAAGGAAAAGCCAAGCAGGC	GGGGGCCAGACCAAAGATAG	NM_000478.5
Tenogenic related markers				
Scleraxis	*SCX*	CGAGAACACCCAGCCCAAAC	CTCCGAATCGCAGTCTTTCTGTC	NM_001717912
Mohawk	*MKX*	TGTTAAGGCCATAGCTGCGT	TCGCACAGACACCTGGAAAA	NM_173576.5
Decorin	*DCN*	CAGCATTCCTCAAGGTCTTCCT	GAGAGCCATTGTCAACAGCA	NM_001920.3
Tenascin-c	*TNC*	ACTGCCAAGTTCACAACAGACC	CCCACAATGACTTCCTTGACTG	NM_002160.3
Chondrogenic/Interface related markers				
Cartilage oligomeric matrix protein	*COMP*	AGGATGGAGACGGACATCAG	TCTGCATCAAAGTCGTCCTG	NM_000095.2
Aggrecan	*ACAN*	TGGTCTTGCAGCAGTTGATTC	TAGAGTCCTCAAGCCTCCTGT	NM_013227.3

5.2.7. Quantitative analysis of fluorescence images

All images were acquired by fluorescence microscope and the signal emitted from the expression of the intended proteins was, afterwards, quantified using ImageJ software. Briefly, proteins expression was quantitatively analyzed in stained captions of Phalloidin/DAPI and the protein of interest at 7 and 14 days of culture. The images were split in three channels, being only the green analyzed and the fluorescence intensity measured. A total of four images were analyzed and results are expressed as mean±SEM.

5.2.8. Statistical analysis

Results were obtained from three independent experiments with a minimum of three replicates for each condition. Results are presented as mean±SEM. Statistical analyses were performed using GaphPad Prism 7.0 software. Two-way analysis of variance (ANOVA) with Sidak and Tukey tests was performed. Differences between experimental groups were considered significant with a confidence interval of 95%, whenever $p<0.05$.

5.3. RESULTS

5.3.1. Pre-commitment of hASCs towards the osteogenic lineage

When comparing hASCs cultured in basal and osteogenic media, their pre-commitment toward the osteogenic lineage was evident as early as 14 days of culture (Supplementary Figure S5.1). Cells obtained at this stage (D14) were called pre-osteoblasts (pre-OBs) and used in subsequent studies.

The osteogenic differentiation of human adipose-derived stem cells (hASCs) was evaluated by alizarin red (AZ) staining to assess the degree of matrix mineralization and assessed by quantitative determination of the ALP activity levels. There was a clear increase of normalized ALP activity in cells cultured in the presence of osteogenic medium, with a 6-fold increase from day 7 to day 14 (σ, $p<0.0004$) (Supplementary Figure S5.1A). The presence of osteogenic medium induced a strong mineral deposition compared to the respective basal condition, as evidenced by the staining intensity as soon as after 14 days in culture (Supplementary Figure S5.1B).

5.3.2. Influence of increasing osteogenic medium concentrations at single culture level

5.3.2.1. *Influence of increasing osteogenic medium concentrations at single culture level*

The influence of different media on proliferation, ALP activity and mineralization of single cultures was studied (Figure 5.2). At 14 days, the presence of osteogenic medium (OM) in conditions 25BM:75OM and 0BM:100OM increased hTDCs proliferation, in comparison with the intermediate medium condition 50BM:50OM (0BM:100OM, $p<0.007$) and

lower concentrations in conditions 100BM:0OM (25BM:75OM, $p<0.05$; 0BM:100OM, $p<0.007$) and 75BM:25OM (0BM:100OM, $p<0.007$) (Figure 5.2A); whereas no significant differences were found for pre-OBs between medium conditions.

Regarding ALP activity (Figure 5.2B), at 14 days, pre-OBs exhibited the highest activity in conditions 25BM:75OM and 0BM:100OM ($p<0.0001$), followed by the intermediate condition 50BM:50OM ($p<0.02$). Although hTDCs exhibited a significant increased ALP activity with higher ratios of OM (25BM:75OM; 0BM:100OM) between days 7 and 14, no significant changes were observed between conditions.

Additionally, AZ staining confirmed that mineralized calcium depots increased with increasing OM ratios, which was more evident in pre-OBs, compared to hTDCs, as shown by staining intensity (Figure 5.2C-D).

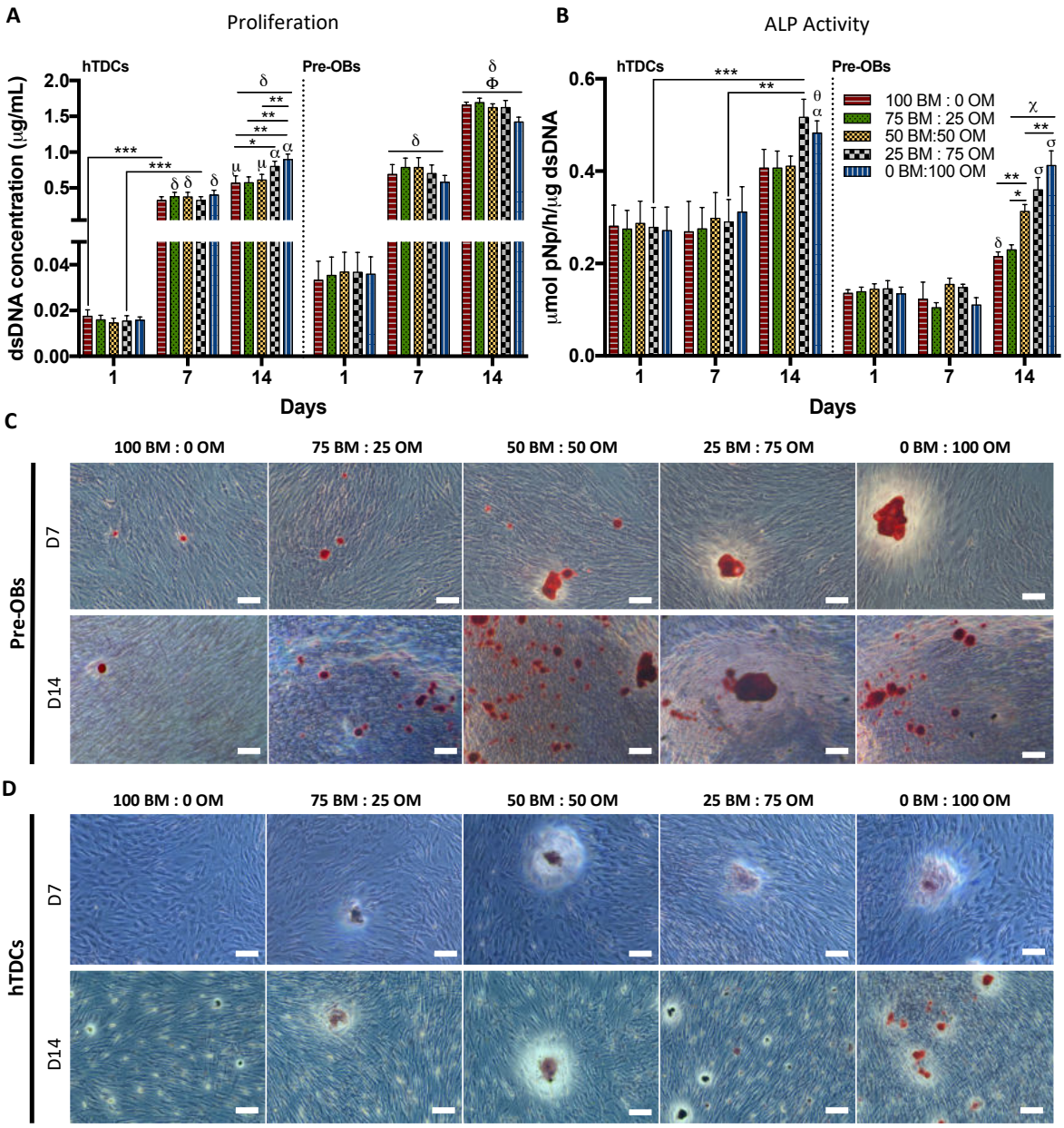

Figure 5.2 | Evaluation of cell proliferation, alkaline phosphatase activity and matrix mineralization in single cultures of pre-OBs and hTDCs in the presence of increasing concentrations of osteogenic medium. (A) Cell proliferation evaluated by dsDNA concentration. Results are presented as mean±SEM and statistically significant differences are *, $p<0.05$; **, $p<0.007$; ***, $p<0.0008$; µ, $p<0.02$ where µ is statistically significant in comparison with the same conditions at day 7α, $p<0.0001$, α is statistically significant in comparison with the same conditions at day 7; δ, $p<0.0001$, δ is statistically significant in comparison with the same conditions at day 1; Φ, $p<0.0001$, Φ is statistically significant in comparison with the same conditions at day 7. (B) Quantification of alkaline phosphatase (ALP) activity by the colorimetric *p*-nitrophenol (pNP) assay. Results were normalized against the amount of dsDNA of the correspondent sample and are presented as mean±SEM. Statistically

significant differences are shown as *, $p<0.02$; **, $p<0.003$; ***, $p<0.0009$; α, $p<0.02$, α is statistically significant in comparison with the same condition at day 7; δ, $p<0.004$, δ is statistically significant in comparison with the same conditions at day 1 and 7; θ, $p<0.003$, θ is statistically significant in comparison with the same condition at day 1; χ, $p<0.0001$, χ is statistically significant in comparison with the same conditions at days 1 and 7; σ, $p<0.0001$ σ is statistically significant in comparison with the conditions 100 BM: 0 OM and 75 BM: 25 OM. (C,D) Alizarin red staining, demonstrating matrix mineralization in both (C) pre-OBs and (D) hTDCs (scale bars, 100 μm). Legend: BM: basal medium; OM: osteogenic medium.

5.3.2.2. *Effect on osteogenic and tenogenic phenotype of pre-OBs and hTDCs: expression of bone and tendon-related markers*

Maintenance of pre-OBs phenotype was confirmed by analyzing the expression of *COL1A1, COL3A1* and bone-related genes (*SPP1, ALPL, RUNX2*) by RT-PCR (Figure 5.3A). No significant changes in the expression of the studied markers were detected after 7 days. Nonetheless, *SPP1* transcript levels (Figure 5.3A-i) increased significantly from 7 to 14 days ($p<0.0002$) in the highest concentration of OM and were significantly higher in cells cultured for 14 days in this condition (0BM:100OM), comparing to lower ratios of osteogenic supplementation (75BM:25OM, $p<0.004$; 50BM:50OM, $p<0.004$) and basal medium (100BM:0OM, $p<0.004$). Similarly, a significant increase of *ALPL* transcript levels (Figure 5.3A-ii) was observed from day 7 to 14 in 0BM:100OM, which were significantly higher in cells cultured for 14 days in this condition, compared to cells in basal medium (100BM:0OM, $p<0.004$) and in the intermediate condition (50BM:50OM, $p<0.04$). Also, *RUNX2* transcript levels (Figure 5.3A-iii) were significantly increased between 7 and 14 days in cells cultured with higher amounts of osteogenic supplementation (50BM:50OM, $p<0.004$; 25BM:75OM, $p<0.004$; 0BM:100OM, $p<0.0002$). Cells cultured for 14 days in 0BM:100OM showed an up-regulation of *RUNX2* in comparison with cells in BM (100BM:0OM, $p<0.004$) and with lower osteogenic supplementation (75BM:25OM, $p<0.004$; 50BM:50OM, $p<0.04$) (Figure 5.3A-iii). Concerning *COL1A1* expression, no significant changes were observed in the transcription levels between conditions (Figure 5.3A-iv). Similarly, to *SPP1, ALPL* and *RUNX2*, from day 7 to day 14, cells cultured in conditions with the highest concentration of osteogenic supplementation presented significantly higher *COL3A1* expression (75BM:25OM, $p<0.04$; 0BM:100OM, $p<0.004$, Figure 3A-v). After 14 days, *COL3A1* transcript levels in cells cultured in 0BM:100OM were significantly higher, compared to cells cultured in medium containing lower osteogenic supplementation (25BM:75OM, $p<0.04$; 50BM:50OM, $p<0.04$) and in BM (100BM:0OM, $p<0.004$) (Figure 5.3A-v).

Overall, higher concentrations of OM resulted in increased transcript levels of the studied bone-related markers, supporting osteogenic differentiation of pre-OBs. Furthermore, no significant differences were observed in OPN expression, an early osteogenic differentiation marker, in cells cultured in the presence of the different ratios of OM:BM at 7 and 14 days of culture (Figure 5.3B-C).

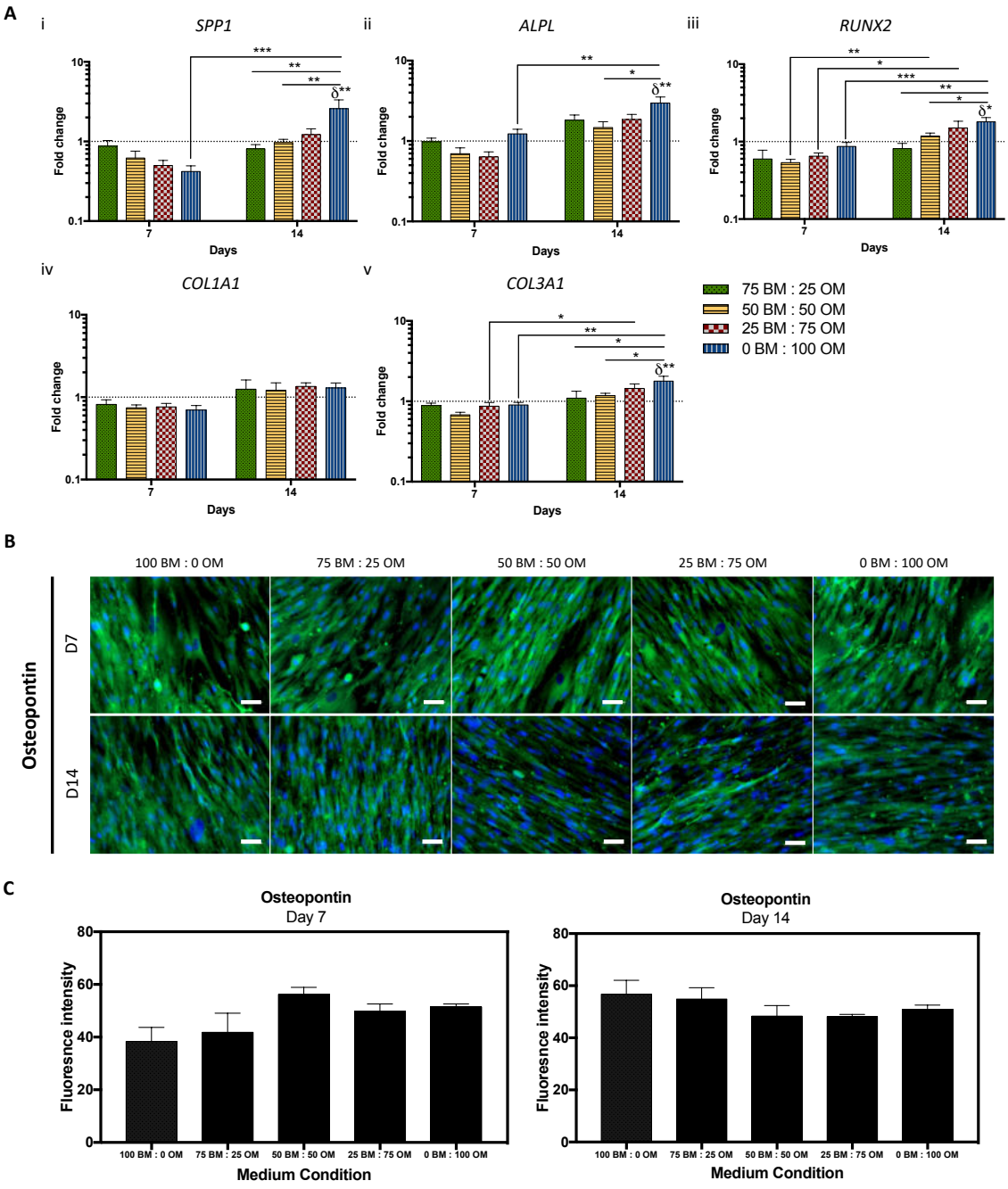

Figure 5.3 | Maintenance of osteogenic phenotype of pre-osteoblasts through culture time in the presence of different osteogenic medium conditions. (A) Gene expression of osteogenic-related markers, (i) bone sialoprotein 1/ osteopontin (*SPP1*), (ii) alkaline phosphatase (*ALPL*), (iii) runt-

related transcription factor 2 (*RUNX2*), (iv) collagen type I (*COL1A1*) and (v) collagen type III (*COL3A1*) evaluated by RT-PCR. Expression of target genes was normalized against *GAPDH* housekeeping gene and gene expression in all conditions was normalized to the basal condition (100BM:0OM) of the correspondent day. Results are presented as mean±SEM and statistically significant differences are shown as *, $p<0.04$; **, $p<0.004$; ***, $p<0.0002$; δ statistically significant differences in comparison to the basal condition of the correspondent day. (B) Fluorescence microscopy images of osteopontin (scale bars, 50 μm). (C) Fluorescence intensity quantification of osteopontin at days 7 and 14.

Maintenance of the tenogenic phenotype of hTDCs was also evaluated. The expression of tenogenic genes (*MKX*, *SCX*, *DCN*, *TNC*), as well as *COL1A1* and *COL3A1* and the bone-related marker *RUNX2* was assessed by RT-PCR (Figure 4). Strikingly, *MKX* was down-regulated in cells cultured with the highest concentration of OM after 7 days (0BM:100OM, $p<0.05$, compared to control) and at 14 days, conditions 25BM:75OM and 0BM:100OM resulted in a significant decrease of *MKX* transcript levels, compared to control ($p<0.01$; $p<0.05$, respectively, Figure 5.4A-i). The highest *MKX* expression was found for cells cultured with the lowest concentration of OM tested (75BM:25OM, $p<0.01$ comparing to 25BM:75OM; $p<0.05$ comparing to 0BM:100OM), with no differences compared to BM condition. Nonetheless, no differences were observed for *SCX* transcript levels between conditions (Figure 5.4A-ii). Cells cultured in the presence of only OM (0BM:100OM) presented significantly higher *DCN* and *TNC* transcript levels from days 7 to 14 (Figure 5.4Aiii-iv). At 14 days, *TNC* was up-regulated in cells cultured in 0BM:100OM, compared to basal condition ($p<0.01$) and *TNC* transcript levels in cells cultured in condition 0BM:100OM were significantly higher in comparison to those in lower ratios of osteogenic supplementation (75BM:25OM, $p<0.01$; 50BM:50OM, $p<0.01$; 25BM:75OM, $p<0.05$, Figure 5.4A-iv). Additionally, *COL1A1* was up-regulated in cells cultured in the highest concentration of osteogenic supplementation, as soon as 7 days of culture (0BM:100OM, $p<0.0005$, compared to basal condition) and in comparison, with cells cultured in the presence of lower OM ratios (50BM:50OM, $p<0.05$; 25BM:75OM, $p<0.01$, Figure 5.4A-v). *COL3A1* was up-regulated in cells cultured with 50BM:50OM ($p<0.05$) and 25BM:75OM ($p<0.0001$) in comparison with cells cultured in basal condition (100 BM:0OM, Figure 4A-vi). For both *COL1A1* and *COL3A1*, a significant decrease in the transcription levels of cells cultured in different conditions was noticed from day 7 to 14 (Figures 4Av-vi). *RUNX2* was up-
regulated in cells cultured in 50BM:50OM ($p<0.05$), 25BM:75OM ($p<0.05$) and 0BM:100OM ($p<0.01$) after 14 days, in comparison to basal condition (Figure 5.4A-vii).

Tendon-related ECM markers DCN, TNC, COL1 and COL3 were further studied at the protein level (Figure

5.4B-C). Interestingly, DCN was highly expressed at 14 days in cells cultured in the presence of lower OM concentrations, namely 100BM:0OM, 75BM:25OM and 50BM:50OM, in comparison with cells cultured for 7 days. TNC was detected at 7 days, but strongly expressed after 14 days by cells cultured in the presence of 100BM:0OM (p<0.0001), 75BM:25OM (p<0.0001) and 50BM:50OM (p<0.0005) (Figure 5.4B-C). Furthermore, at both 7 and 14 days of culture, cells expressed COL1 intracellularly and were able to synthesize and produce COL3, being only observed a significant increase in the expression of COL1 in cells cultured in the presence of 50BM:50OM (p<0.0001) for a period of 14 days. Overall, increasing concentrations of osteogenic supplementation affected the expression of tendon-related markers.

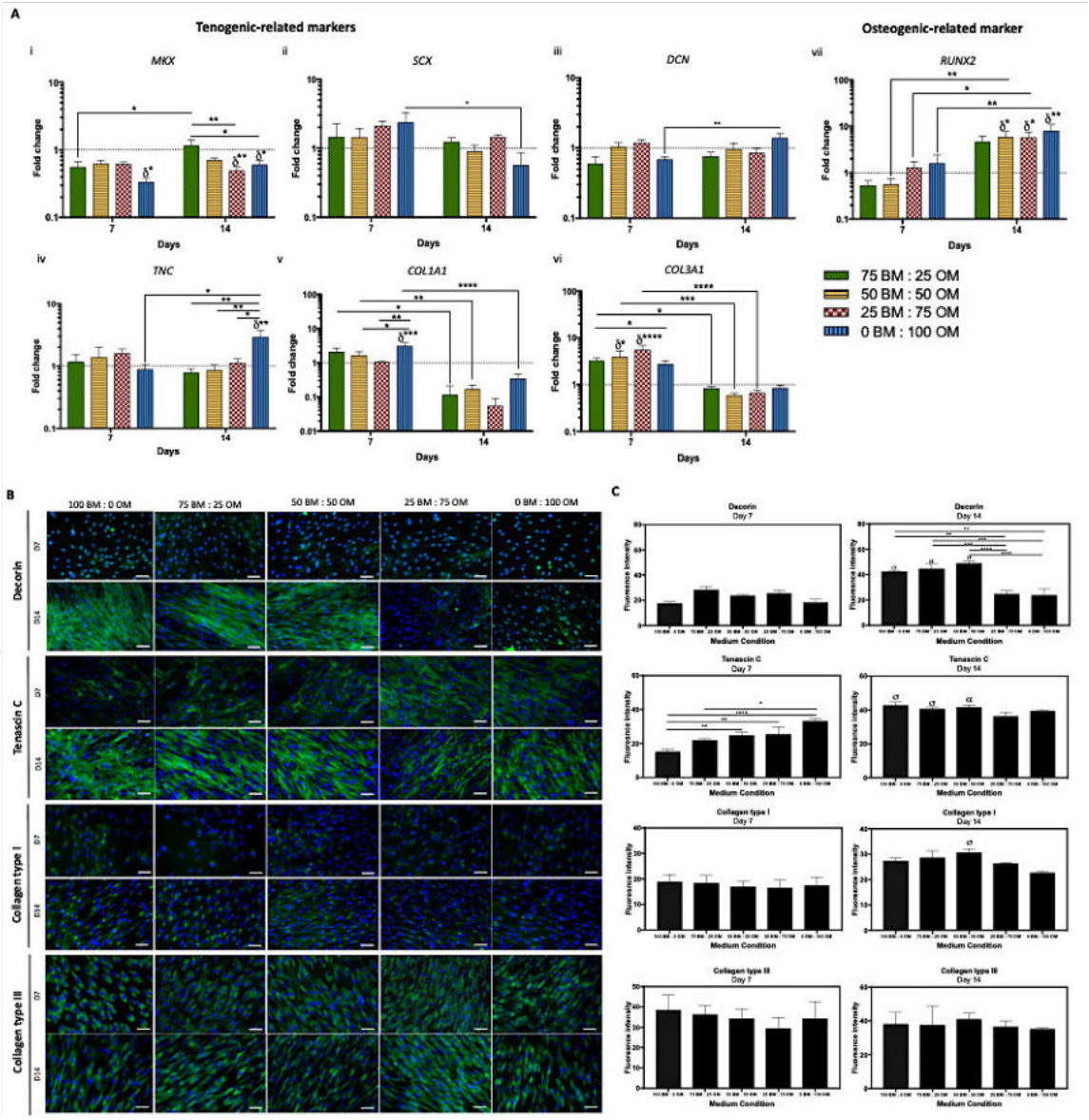

Figure 5.4 | Assessment of the expression of tenogenic and osteogenic markers by hTDCs through culture time in different osteogenic medium conditions after 7 and 14 days. (A)

Gene expression analysis of (i) mohawk (*MKX*), (ii) scleraxis (*SCX*), (iii) decorin (*DCN*), (iv) tenascin C (*TNC*), (v) collagen type I (*COL1A1*), (vi) collagen type III (*COL3A1*) and (vii) runt-related transcription factor 2 (*RUNX2*) by RT-PCR. Expression of target genes was normalized against *GAPDH* housekeeping gene and gene expression in all conditions was normalized to basal condition (100 BM: 0 OM) of the correspondent day. Results are presented as mean±SEM and statistically significant differences are shown as *, $p<0.05$; **, $p<0.01$; ***, $p<0.0005$; ****, $p<0.0001$; δ statistically significant differences in comparison to the basal condition of the correspondent day. (B) Fluorescence microscopy of tenogenic-related markers, decorin, tenascin-C, collagen type I and collagen type III (scale bars, 50 μm). Nuclei were counterstained with DAPI. (C) Fluorescence intensity quantification of decorin, tenascin-C, collagen type I and collagen type III at days 7 and 14. Results are presented as mean±SEM and statistically significant differences are shown as *, $p<0.04$; **, $p<0.006$; ***, $p<0.0006$; ****, $p<0.0001$; σ, $p<0.0001$, is statistically significant in correspondence to the same condition at day 7; α, $p<0.0005$, is statistically significant in correspondence to the same condition at day 7; μ, $p<0.009$, is statistically significant correspondence to the same condition at day 7.

5.3.3. Influence of direct pre-OBs–hTDCs crosstalk in co-culture systems

Based on obtained results, three medium conditions were chosen, maximizing cell growth and balancing tendon- and bone- related markers expression and matrix mineralization. Condition 50BM:50OM seemed to better maintain the osteogenic phenotype of pre-OBs without inducing rapid cell maturation and the tenogenic phenotype of hTDCs, without triggering phenotypic drift toward osteogenesis. Conditions 100BM:0OM and 0BM:100OM were used for comparison.

5.3.3.1. *Effects of direct contact co-culture: cell proliferation, ALP activity and matrix mineralization*

DNA content, ALP activity and mineralization were analyzed in co-cultures to evaluate the combined influence of direct contact and medium (Figure 5.5). Condition 50BM:50OM resulted in a significant increase in DNA content, in comparison with the basal condition ($p<0.03$) at 14 days, while no differences were observed for condition 0BM:100OM (Figure 5.5A). A significantly higher proliferation was observed in co-cultures compared to hTDCs in BM ($p<0.0002$) and condition 50BM:50OM ($p<0.0001$, Figure S5.2). At day 14, cells cultured with 0BM:100OM exhibited significantly higher ALP activity, compared to 50BM:50OM ($p<0.0001$) and 100BM:0OM ($p<0.0006$, Figure 5.5B). Strikingly, after 14 days, ALP activity was significantly higher in co-cultures, when compared to single cultures (pre-OBs and hTDCs) in

all conditions (Figure S5.3). Moreover, increasing OM ratios increased mineral deposition (Figures 5C, S5.4). After 7 days, higher concentrations were observed for pre-OBs and co-cultures in comparison with hTDCs in all conditions (Figure 5.5D-i). Interestingly, cells co-cultured for 14 days in the presence of 100% OM exhibited significantly increased mineralization, in comparison to pre-OBs and hTDCs alone (p<0.0001, Figure 5.5D-ii), suggesting a synergistic effect between osteogenic supplementation and direct cell-cell interactions.

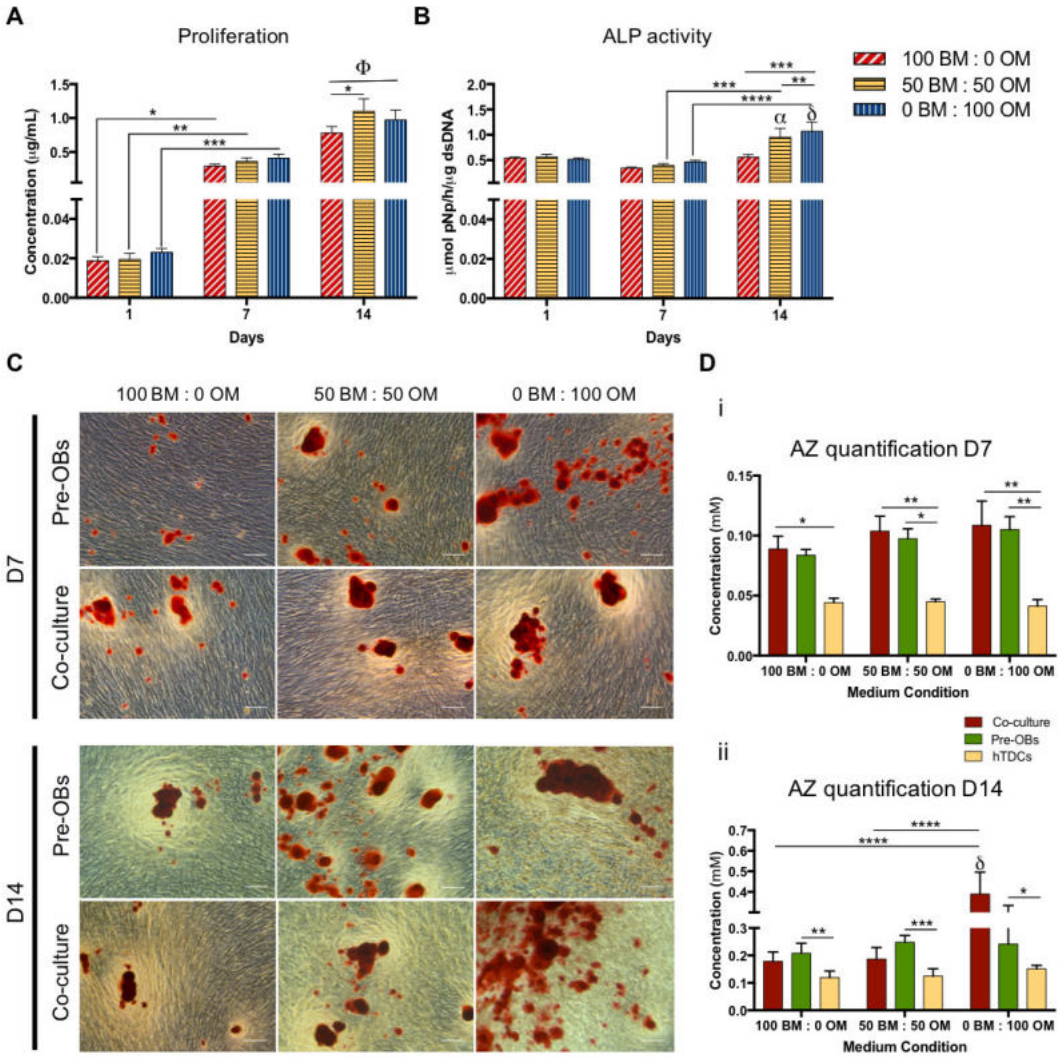

Figure 5.5 | Evaluation of cell proliferation, alkaline phosphatase activity and matrix mineralization in direct co-culture. (A) Cell proliferation was quantified by a fluorimetric dsDNA quantification kit. Results are presented as mean±SEM and statistically significant differences are shown as *, p<0.03; **, p<0.004; ***, p<0.0009; Φ, p<0.0001, Φ is statistically significant in correspondence to all the conditions at day 1 and 7. (B) Alkaline phosphatase (ALP) activity was quantified by the colorimetric p-nitrophenol (pNP). Results are presented as mean±SEM and statistically significant

differences are shown as **, $p<0.0001$; ***, $p<0.0006$; **** $p<0.0001$; α, $p<0.0002$, α is statistically significant in correspondence to the same condition at day 1; δ, $p<0.0001$, δ is statistically significant in correspondence to the same condition at day 1. (C) Alizarin red (AZ) staining was performed for both pre-OBs and direct co-cultures after 7 and 14 days of culture (scale bars, 100 μm). (D) Quantification of AZ staining was performed using cetylpyridinium chloride solution at 7 and 14 days of culture. Results are presented as mean±SEM and statistically significant differences are shown as *, $p<0.05$; **, $p<0.009$; ***, $p<0.0003$; ****, $p<0.0001$; δ, $p<0.0001$, δ is statistically significant in correspondence to pre-OBs and hTDCs in the same condition.

5.3.3.2. *Effects of direct contact co-culture: expression of bone-, tendon- and interface-related markers*

The expression of bone- (*ALPL*, *RUNX2* and *SPP1*), tendon- (SCX, *MKX* and *TNC*) and interface-related markers (*ACAN, COMP*), as well as *COL1A1* and *COL3A1* was analyzed by RT-PCR after 7 and 14 days of culture (Figure 6). Although no differences were found for *ALPL* transcript levels (Figure 5.6A), after 7 days, co-cultured cells in 50BM:50OM presented significantly higher *RUNX2* transcript levels ($p<0.0007$, versus pre-OBs; $p<0.009$ versus hTDCs, Figure 5.6B), but without differences comparing to basal condition. Interestingly, co-cultured cells expressed significantly higher *SPP1* transcript levels as soon as 7 days in 0BM:100OM comparing with pre-OBs in the same condition ($p<0.0007$, Figure 5.6C). From day 7 to 14, *SPP1* expression significantly decreased in co-cultures in condition 0BM:100OM ($p<0.0007$), but no differences were found comparing to basal condition.

Additionally, no significant differences were observed for *SCX* expression in co-cultures when comparing to pre-OBs and hTDCs single cultures, nor between medium conditions (Figure 5.6D). Strikingly, similarly to hTDCs alone, *MKX* transcript levels were significantly lower in co-cultures in 0BM:100OM after 14 days comparing to BM ($p<0.05$, Figure 5.6E). *TNC* was upregulated in co-cultures after 7 days in 50BM:50OM ($p<0.05$, versus BM), decreasing significantly from day 7 to 14 ($p<0.009$, Figure 5.6F). Interestingly, at day 14, the presence of only OM significantly decreased *TNC* transcript levels in co-cultures, comparing with hTDCs in the same medium condition ($p<0.0007$).

Furthermore, *ACAN* was up-regulated in co-cultures as soon as 7 days in 0BM:100OM ($p<0.05$, compared to pre-OBs and hTDCs, Figure 5.6G) and *COMP* was up-regulated in co-cultures in 0BM:100OM after 14 days ($p<0.05$, compared to 100BM:0OM Figure 6H). Strikingly, co-cultured cells expressed significantly higher *COMP* transcript levels after 14 days compared with pre-OBs and hTDCs cultured in the same conditions (50BM:50OM, $p<0.009$; 0BM:100OM, $p<0.0001$, Figure 5.6H). In pre-OBs, no

differences were observed for *ACAN* and *COMP* expression; whereas OM led to a significant decrease of *COMP* expression in conditions 50BM:50OM (p<0.05) and 0BM:100OM (p<0.009) in hTDCs from day 7 to 14.

Higher *COL1A1* (Figure 5.6I) and *COL3A1* (Figure 5.6J) transcript levels were noticed at 7 days in hTDCs in comparison with co-cultures in both medium conditions (*COL1A1*: 50BM:50OM, p<0.009; 0BM:100OM, p<0.0001; *COL3A1*: 50BM:50OM, p<0.0001; 0BM:100OM, p<0.0001). Nevertheless, after 14 days, co-cultured cells in 0BM:100OM expressed significantly higher *COL1A1* transcript levels (p<0.009, comparing to pre-OBs and hTDCs Figure 6I) and both medium conditions led to significantly higher *COL3A1* expression levels in co-cultures (p<0.05, comparing to pre-OBs and hTDCs Figure 5.6J). No differences were observed in comparison to basal condition.

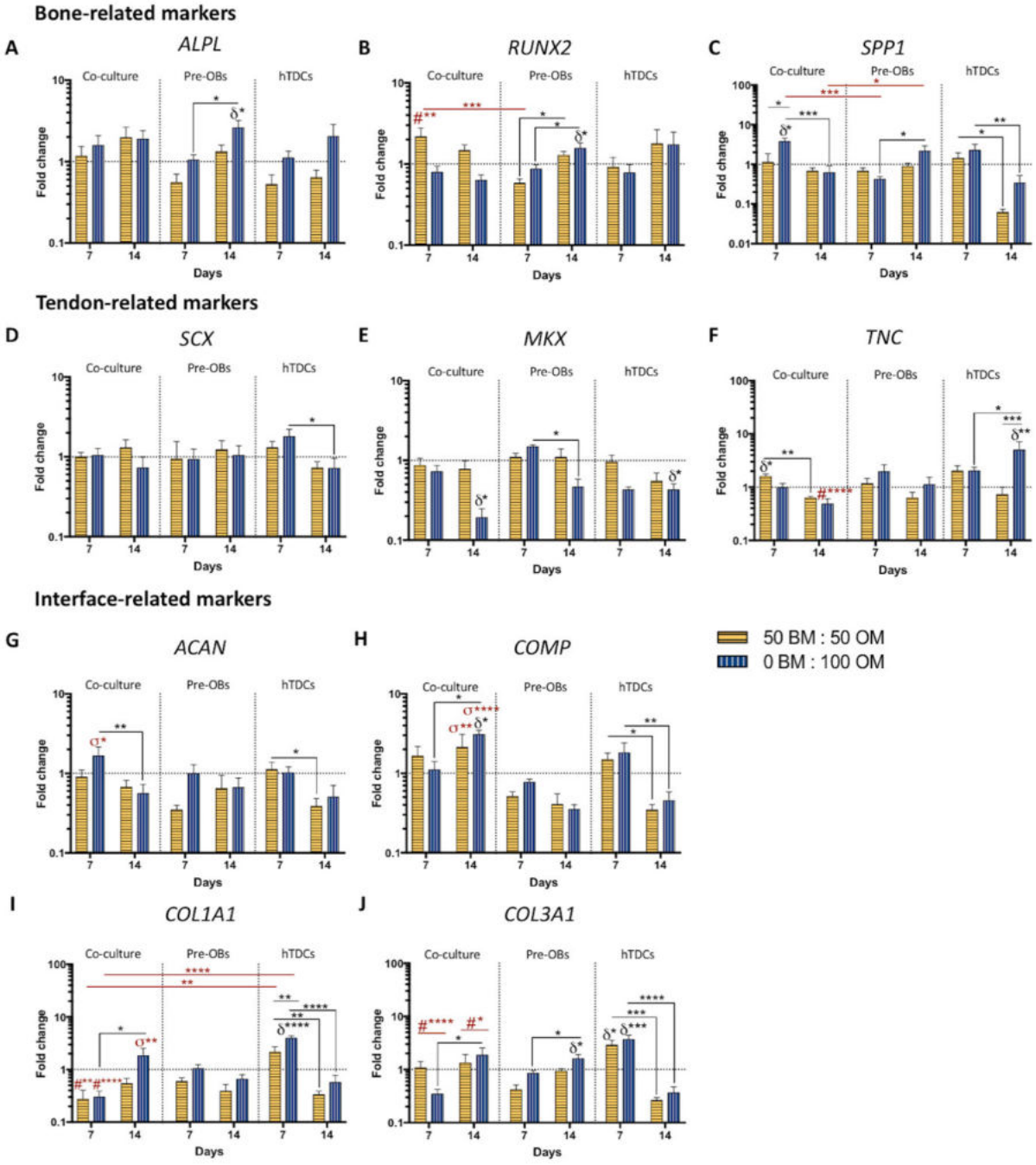

Figure 5.6 | Evaluation of the gene expression of bone-, tendon- and interface-related markers in single cultures and direct co-cultures up to 14 days in culture. Gene expression of (A) alkaline phosphatase (*ALPL*), (B) runt-related transcription factor 2 (*RUNX2*), (C) bone sialoprotein 1/ osteopontin (*SPP1*), (D) scleraxis (*SCX*), (E) homeobox mohawk (*MKX*), (F) tenascin C (*TNC*), (G) aggrecan (*ACAN*), (H) cartilage oligomeric matrix protein (*COMP*), (I) collagen type I (*COL1A1*) and (J) collagen type III (*COL3A1*) was analyzed by RT-PCR. Target genes were normalized against GAPDH housekeeping gene. The gene expression in all conditions was normalized to basal condition (100 BM: 0 OM) of the correspondent day. Results are presented as mean±SEM and statistically significant differences are

shown as *, $p<0.05$; **, $p<0.009$; ***, $p<0.0007$; ****, $p<0.0001$; δ statistically significant differences in comparison to the basal condition of the correspondent day; # statistically significant differences in comparison with hTDCs in the same condition; σ statistically significant differences in comparison pre-OBs and hTDCs in the same conditions.

Immunocytochemistry analysis was also performed against OCN, TNC, ACAN and COL2 (Figure 5.7). A higher OCN deposition was observed in co-cultures after both 7 and 14 days, whereas in pre-OBs, OCN was highly detected after 7 days in comparison with 14 days of culture (100BM:0OM, $p<0.006$; 50BM:50OM, $p<0.0001$; and 0BM:100OM, $p<0.006$) (Figure 5.7A). After 14 days, OM present in conditions 50BM:50OM and 0BM:100OM affected TNC expression, which was observed in hTDCs in all medium conditions, but only observed in basal condition (100BM:0OM) in co-cultures ($p<0.0001$) (Figure 5.7B). No ACAN expression was found in pre-OBs and hTDCs, while, in co-cultures, an abundant deposition was observed in conditions containing OM as soon as 7 days and maintained up to 14 days ($p<0.0001$) (Figure 5.7C). COL2 was deposited at a higher extent in co-cultures as soon as after 7 days in all conditions, whereas hTDCs expressed COL2 at 7 days mainly in the presence of OM and at 14 days in all medium conditions, being highly expressed in condition 50BM:50OM in comparison with conditions 100BM:0OM ($p<0.006$) and 0BM:100OM ($p<0.04$). COL2 expression was observed in pre-OBs at 14 days in condition 50BM:50OM and 0BM:100OM (Figure 5.7D), even though COL2 expression was significantly lower in comparison with co-cultures ($p<0.0001$). Altogether, these results support the influence of direct contact occurring between two types of cells in the modulation of cellular phenotype.

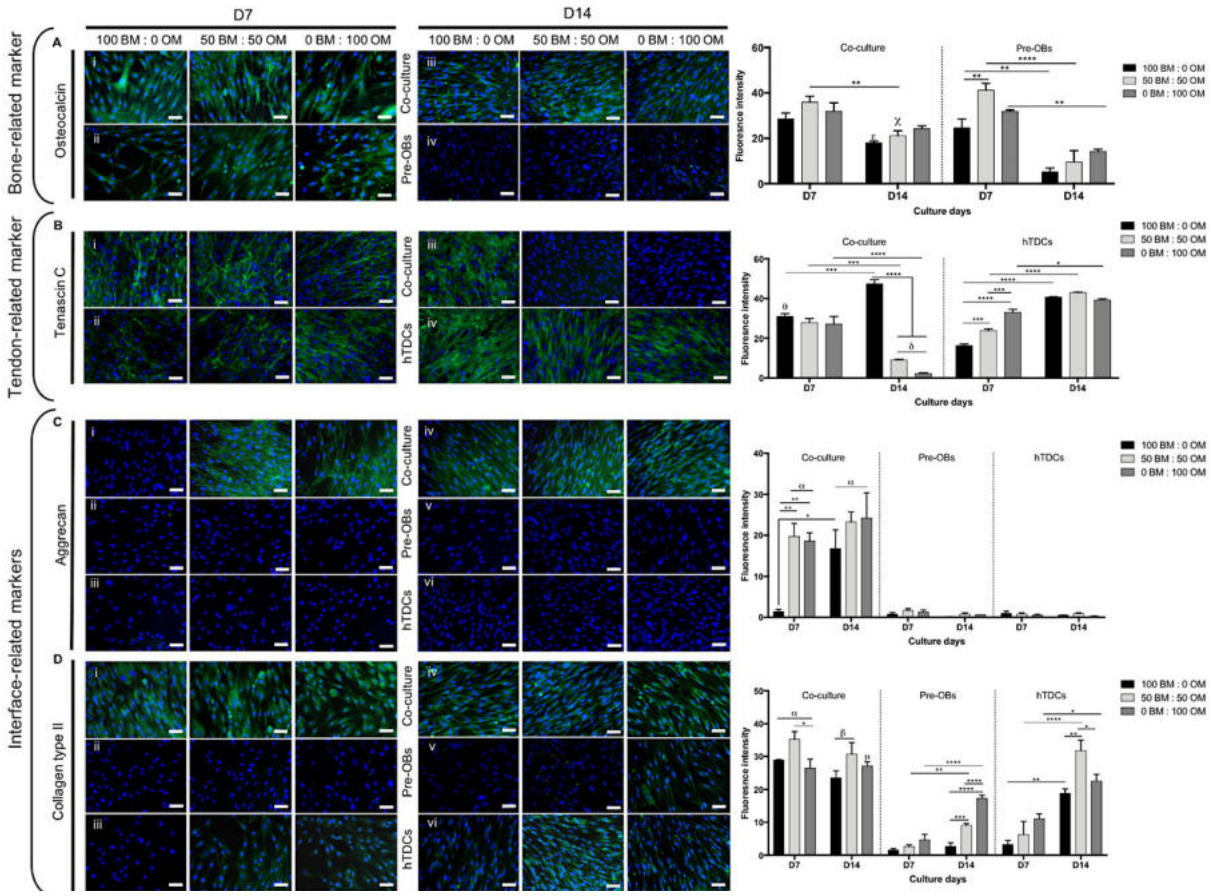

Figure 5.7 | Expression of bone, tendon- and interface-related proteins in single cultures of pre-OBs and hTDCs and in direct contact co-cultures. Fluorescence microscopy images of (A) osteocalcin, (B) tenascin C, (C) aggrecan and (D) collagen type II after 7 and 14 days of culture (scale bars, 50 μm). Nuclei were counterstained with DAPI (blue). Fluorescence intensity quantification was performed. Results are presented as mean ± SEM and statistically significant differences are shown as *, $p<0.05$; **, $p<0.006$; ***, $p<0.0007$; ****, $p<0.0001$; δ, $p<0.0001$, δ is statistically significant in comparison with hTDCs in the same day; α, $p<0.0001$, is statistically significant in comparison with pre-OBs and hTDCs in the same day; β, $p<0.0001$, is statistically significant in comparison with pre-OBs in the same day; σ, $p<0.0001$, is statistically significant in comparison with hTDCs in the same day; χ, $p<0.0003$, is statistically significant in comparison with pre-OBs in the same day; θ, $p<0.0006$, is statistically significant in comparison with hTDCs in the same day; μ, $p<0.04$, is statistically significant in comparison with pre-OBs in the same day; ε, $p<0.05$, is statistically significant in comparison with pre-OBs in the same day.

5.4. DISCUSSION

The success of ITE depends on optimal cell source selection and on the understanding of cellular interactions within native tissues. Strategies for enthesis tissue engineering and regeneration frequently disregard the existence of different cellular phenotypes and, thus, the need to establish adequate culture conditions to balance cellular behavior. Co-culture systems constitute platforms to study cellular communication through direct or indirect interactions between different cell types [30, 31, 36, 37]. Herein, we explored an *in vitro* strategy to modulate cellular phenotype for tissue engineering approaches, envisioning the combination of different cell types with medium supplementation. We first studied the effect of different osteogenic medium concentrations on the modulation of hASCs (pre-OBs) and hTDCs cellular responses and, afterwards, the influence of establishing a direct contact co-culture model on the expression of interface-relevant markers. Human ASCs constitute a promising cell source for tissue regeneration [38] and their osteogenic commitment has been well described [39]. Hence, this cell population was herein pre-committed toward the osteogenic lineage to obtain pre-OBs, aiming at mimicking, as close as possible, the cellular environment found in bone. Additionally, to mimic the cellular environment found in tendon counterpart of enthesis and given the lack of well-established protocols for tenogenic differentiation, hTDCs were used, which are composed by tenocytes/tenoblasts and stem/progenitor cells [40, 41] and hold potential for musculoskeletal tissue engineering [41, 42]. Both cell populations were chosen based on evidences that *in vitro* interactions between different cell types may modulate cellular trans-differentiation and lead to an eventual fibrocartilage formation [15], suggesting that heterotypic cellular interactions occurring between tendon and bone cells may initiate important events leading to interfacial regeneration.

Previous studies have addressed the formulation of optimal medium conditions in co-culture models, reporting that 1mM β-GP maximized cell growth and osteoblast mineralization, while minimizing ectopic fibroblast mineralization [15], whereas 3mM β-GP concentration promoted low fibroblast-osteoblast mineralization [16]. Therefore, co-culture medium should be tuned to each unique culture system toward improving tissue engineering strategies currently explored.

Our results clearly showed an osteogenic commitment of hASCs and the phenotype maintenance of pre-OBs during culture time, by an upregulation of *SPP1, RUNX2* and *ALPL.* During osteoblast-lineage differentiation and maturation, *RUNX2* expression is essential, as an important osteogenic master switch and regulator of ECM-related genes expression, like *SPP1*, and even *ALPL* [43, 44]. Increasing concentrations of OM promoted the expression of bone-related markers at the gene and protein level, simultaneously inducing matrix mineralization.

Additionally, maintenance of hTDCs tenogenic phenotype was also assessed. The intermediate condition (50BM:50OM) demonstrated a possible phenotypic modulation of hTDCs toward tenogenesis. Remarkably, increasing concentrations of osteogenic medium clearly downregulated *MKX* and *SCX*, transcription factors essential during tendon differentiation [45, 46], as well as *COL1A1* and *COL3A1*, while upregulating *DCN* and *TNC* expression after 14 days of culture. Collagen types I and III are the most abundant collagens found in tendon tissue; decorin and tenascin-C are known to be the major non-collagenous components of tendon ECM, and several authors reported their expression in bone cells [47-50]. At protein level, DCN and TNC were highly expressed in the presence of medium conditions containing lower ratios of osteogenic medium. Furthermore, *RUNX2* up-regulation in hTDCs may be strongly associated with the isolated mixed population of cells that could undergo osteogenic differentiation [41]. Thus, increasing concentrations of osteogenic medium may lead to a phenotypic drift of this population toward the osteogenic lineage. Nonetheless, condition 50BM:50OM seemed to modulate pre-OBs osteogenic commitment, while maintaining hTDCs tenogenic phenotype, without significant osteogenic drift. Thus, this intermediate medium condition was selected for further studies.

Subsequently, a direct co-culture system was established using three predetermined medium conditions. The co-culture system with different medium conditions offered a specific environment for the two cell types, not affecting cell proliferation, increasing matrix mineralization and ALP activity. The expression of bone-related markers was higher in co-cultures in the presence of osteogenic medium, as early as 7 days of culture. Particularly, the highest concentration of osteogenic medium (0BM:100OM) induced an up-regulation of *SPP1* at 7 days. Strikingly, the higher expression of *RUNX2* in condition 50BM:50OM may indicate the dynamic and evolving osteogenic process that is still occurring and explain higher ECM matrix mineralization observed in co-cultures after 14 days in the presence of osteogenic medium [51]. Higher *SPP1* and *RUNX2* transcript levels found in co-cultures after 7 days in comparison to pre-OBs alone suggest the existence of bi-directional cellular communication events orchestrating osteogenesis.

In turn, *SCX* and *MKX* expression in co-culture conditions exhibited no significant differences over time in the intermediate medium condition (50BM:50OM), when compared to BM, suggesting that a tenogenic phenotype may still be rescued in the presence of osteogenic medium, possibly as a result of heterotypic cellular interactions.

Interestingly, the presence of OM significantly increased the expression of interface-relevant markers, *ACAN* and *COMP*, in co-cultures, in comparison with pre-OBs and hTDCs single cultures. The production of extracellular molecules, such as tenascin and cartilage oligomeric matrix protein (COMP), activate intracellular signaling pathways of kinase and paxilin (focal adhesion enzymes) leading to the initiation of

a transition step from chondroprogenitor cells to fully committed chondrocytes [52]. Moreover, the presence of OM also influenced the deposition of ACAN and COL2. ACAN production was influenced by pre-OBs and hTDCs direct cell contact, given that it was only observed in co-culture conditions. Increasing ACAN expression in the matrix is normally observed in early differentiation periods where chondrocytes start to become hypertrophic [53]. Moreover, high levels of COL2 and ACAN are expressed by chondroprogenitor cells and chondrocytes in the extracellular matrix [53], being their deposition governed by the nuclear transcription factor Sox9 [54], being an important transcription factor to be considered in future studies. Interestingly, in co-cultures, *Runx2* is significantly increased as soon as 7 days of culture in comparison with hTDCs and Pre-OBs. Runx2 is expressed during the differentiation of chondrocytes to hypertrophic chondrocytes, being the BMP-induced Smad1 and Smad1 and Runx2/Cbfa1 interactions important for the hypertrophy [52, 55, 56]. Nevertheless, more studies at the molecular level will be useful to help clarifying the role of each cell type within the proposed system of heterotypic cell interactions. Altogether, these results suggest a possible targeting toward an osteochondral lineage, where the expression of both bone and chondrogenic-related markers is increased. Furthermore, since the expression of COL2 was observed in all medium conditions and the expression of ACAN was only observed after 14 days in basal condition, OM ratios and cell-cell interactions occurring in co-culture seem to play an important role in the maintenance of a chondrogenic-like ECM in longer culture periods [57].
Overall, our work suggests that a balanced process of osteogenic and tenogenic commitment of distinct cell populations may be achieved through the use of intermediate concentrations of osteogenic supplementation. Furthermore, interactions occurring in co-cultures play an important role in the expression of tendon-, bone- and interface-related markers. These findings serve as basis for understanding the effect of medium conditions on the modulation of cell phenotype along with the importance of cell-cell contact on the regulation of the biological environment with future application in studies involving more complex 3D systems in combination with dynamic platforms, such as bioreactors, to promote the formation of a new engineered enthesis-like tissue.

5.5. ACKNOWLEDGEMENTS

Authors thank Hospital da Prelada (Porto, Portugal) for providing tendon tissue (Orthopedics Department) and adipose tissue (Plastic Surgery Department) samples; the financial support from the European Union Framework Programme for Research and Innovation HORIZON2020, under the TEAMING Grant agreement No 739572 - The Discoveries CTR, FCT–Fundação para a Ciência e a Tecnologia for the PhD grant of IC (PD/BD/128088/2016); and the Project NORTE-01-0145-FEDER-000021:“Accelerating

tissue engineering and personalized medicine discoveries by the integration of key enabling nanotechnologies, marine-derived biomaterials and stem cells", supported by Norte Portugal Regional Operational Programme (NORTE 2020), under the PORTUGAL 2020 Partnership Agreement, through the European Regional Development Fund (ERDF).

5.6 REFERENCES

[1] L. Galatz, S. Rothermich, K. VanderPloeg, B. Petersen, L. Sandell, S. Thomopoulos, The development and morphogenesis of the tendon-to-bone insertion What development can teach us about healing, J Musculoskelet Neuronal Interact 10(1) (2010) 35-45.

[2] E. Zelzer, E. Blitz, M.L. Killian, S. Thomopoulos, Tendon-to-bone attachment: from development to maturity, Birth Defects Res C Embryo Today 102(1) (2014) 101-12, 10.1002/bdrc.21056.

[3] M. Benjamin, T. Kumai, S. Milz, B.M. Boszczyk, A.A. Boszczyk, J.R. Ralphs, The skeletal attachment of tendons—tendon 'entheses' Comp Biochem Physiol A Mol Integr Physiol 133(4) (2002) 931-945, 10.1016/S1095-6433(02)00138-1.

[4] M. Benjamin, H. Toumi, J.R. Ralphs, G. Bydder, T.M. Best, S. Milz, Where tendons and ligaments meet bone- attachment sites ('entheses') in relation to exercise and:or mechanical load, J Anat. 208(4) (2006) 471-490, 10.1111/j.1469-7580.2006.00540.x.

[5] A. Robertson, R.W. Nutton, J.F. Keating, Current trends in the use of tendon allografts in orthopaedic surgery, J Bone Joint Surg Br 88(8) (2006) 988-992, 10.1302/0301-620X.88B8.

[6] C.C. Kaeding, B. Aros, A. Pedroza, E. Pifel, A. Amendola, J.T. Andrish, W.R. Dunn, R.G. Marx, E.C. McCarty, R.D. Parker, R.W. Wright, K.P. Spindler, Allograft Versus Autograft Anterior Cruciate Ligament Reconstruction: Predictors of Failure From a MOON Prospective Longitudinal Cohort, Sports Health 3(1) (2011) 73-81, 10.1177/1941738110386185.

[7] S. Thomopoulos, Tendon to Bone Healing: Differences in Biomechanical, Structural, and Compositional Properties Due to a Range of Activity Levels, Journal of Biomechanical Engineering 125(1) (2003) 10.1115/1.1536660.

[8] P.P. Lui, P. Zhang, K. Chan, L. Qin, Biology and augmentation of tendon-bone insertion repair, Journal of Orthopaedic Surgery and Research 5(59) (2010) 10.1186/1749-799X-5-59.

[9] A. Seidi, M. Ramalingam, I. Elloumi-Hannachi, S. Ostrovidov, A. Khademhosseini, Gradient biomaterials for soft-to-hard interface tissue engineering, Acta Biomaterialia 7(4) (2011) 1441-1451, 10.1016/j.actbio.2011.01.011.

[10] J. Z. Paxton, Current Progress in Enthesis Repair: Strategies for Interfacial Tissue Engineering, Orthopedic & Muscular System 01(S1) (2013) 10.4172/2161-0533.s1-003.

[11] H.H. Lu, S. Thomopoulos, Functional attachment of soft tissues to bone: development, healing, and tissue engineering, Annual review of biomedical engineering 15 (2013) 201-26, 10.1146/annurev-bioeng-071910-124656.

[12] I.E. Wang, D.R. Bogdanowicz, S. Mitroo, J. Shan, S. Kala, H.H. Lu, Cellular interactions regulate stem cell differentiation in tri-culture, Connect Tissue Res 57(6) (2016) 476-487, 10.1080/03008207.2016.1230106.

[13] J. Jiang, S.B. Nicoll, H.H. Lu, Co-culture of osteoblasts and chondrocytes modulates cellular differentiation in vitro, Biochem Biophys Res Commun 338(2) (2005) 762-70, 10.1016/j.bbrc.2005.10.025.

[14] F. Veronesi, P. Torricelli, E. Della Bella, S. Pagani, M. Fini, In vitro mutual interaction between tenocytes and adipose-derived mesenchymal stromal cells, Cytotherapy 17(2) (2015) 215-23, 10.1016/j.jcyt.2014.10.006.

[15] I.E. Wang, J. Shan, R. Choi, S. Oh, C.K. Kepler, F.H. Chen, H.H. Lu, Role of osteoblast-fibroblast interactions in the formation of the ligament-to-bone interface, J Orthop Res 25(12) (2007) 1609-20, 10.1002/jor.20475.

[16] J.O. Cooper, J.D. Bumgardner, J.A. Cole, R.A. Smith, W.O. Haggard, Co-cultured tissue-specific scaffolds for tendon/bone interface engineering, J Tissue Eng 5 (2014) 2041731414542294, 10.1177/2041731414542294.

[17] P. He, K.S. Ng, S.L. Toh, J.C. Goh, In vitro ligament-bone interface regeneration using a trilineage coculture system on a hybrid silk scaffold, Biomacromolecules 13(9) (2012) 2692-703, 10.1021/bm300651q.

[18] B. Chen, B. Li, Y.J. Qi, Q.B. Ni, Z.Q. Pan, H. Wang, L.B. Chen, Enhancement of tendon-to-bone healing after anterior cruciate ligament reconstruction using bone marrow-derived mesenchymal stem cells genetically modified with bFGF/BMP2, Sci Rep 6 (2016) 25940, 10.1038/srep25940.

[19] L.V. Gulotta, D. Kovacevic, J.R. Ehteshami, E. Dagher, J.D. Packer, S.A. Rodeo, Application of bone marrow-derived mesenchymal stem cells in a rotator cuff repair model, The American journal of sports medicine 37(11) (2009) 2126-33, 10.1177/0363546509339582.

[20] K.L. Burrow, J.A. Hoyland, S.M. Richardson, Human Adipose-Derived Stem Cells Exhibit Enhanced Proliferative Capacity and Retain Multipotency Longer than Donor-Matched Bone Marrow Mesenchymal

Stem Cells during Expansion In Vitro, Stem Cells International 2017 (2017) 15, 10.1155/2017/2541275.

[21] X. Cheng, C. Tsao, V.L. Sylvia, D. Cornet, D.P. Nicolella, T.L. Bredbenner, R.J. Christy, Platelet-derived growth-factor-releasing aligned collagen–nanoparticle fibers promote the proliferation and tenogenic differentiation of adipose-derived stem cells, Acta Biomaterialia 10(3) (2014) 1360-1369, 10.1016/j.actbio.2013.11.017.

[22] D. Deng, W. Wang, B. Wang, P. Zhang, G. Zhou, W.J. Zhang, Y. Cao, W. Liu, Repair of Achilles tendon defect with autologous ASCs engineered tendon in a rabbit model, Biomaterials 35(31) (2014) 8801-8809, 10.1016/j.biomaterials.2014.06.058.

[23] C.A. Uysal, M. Tobita, H. Hyakusoku, H. Mizuno, Adipose-derived stem cells enhance primary tendon repair: Biomechanical and immunohistochemical evaluation, Journal of Plastic, Reconstructive & Aesthetic Surgery 65(12) (2012) 1712-1719, 10.1016/j.bjps.2012.06.011.

[24] G. Yang, B.B. Rothrauff, H. Lin, S. Yu, R.S. Tuan, Tendon-Derived Extracellular Matrix Enhances Transforming Growth Factor-beta3-Induced Tenogenic Differentiation of Human Adipose-Derived Stem Cells, Tissue engineering. Part A 23(3-4) (2017) 166-176, 10.1089/ten.TEA.2015.0498.

[25] S.M. Mihaila, A.M. Frias, R.P. Pirraco, T. Rada, R.L. Reis, M.E. Gomes, A.P. Marques, Human adipose tissue-derived SSEA-4 subpopulation multi-differentiation potential towards the endothelial and osteogenic lineages, Tissue engineering. Part A 19(1-2) (2013) 235-46, 10.1089/ten.TEA.2012.0092.

[26] C.M. Cowan, Y.Y. Shi, O.O. Aalami, Y.F. Chou, C. Mari, R. Thomas, N. Quarto, C.H. Contag, B. Wu, M.T. Longaker, Adipose-derived adult stromal cells heal critical-size mouse calvarial defects, Nature biotechnology 22(5) (2004) 560-7, 10.1038/nbt958.

[27] J. Lima, A.I. Gonçalves, M.T. Rodrigues, R.L. Reis, M.E. Gomes, The effect of magnetic stimulation on the osteogenic and chondrogenic differentiation of human stem cells derived from the adipose tissue (hASCs), Journal of Magnetism and Magnetic Materials 393 (2015) 526-536, 10.1016/j.jmmm.2015.05.087.

[28] L. Moradi, M. Vasei, M.M. Dehghan, M. Majidi, S. Farzad Mohajeri, S. Bonakdar, Regeneration of meniscus tissue using adipose mesenchymal stem cells-chondrocytes co-culture on a hybrid scaffold: In vivo study, Biomaterials 126 (2017) 18-30, 10.1016/j.biomaterials.2017.02.022.

[29] T. Rada, R.L. Reis, M.E. Gomes, Distinct stem cells subpopulations isolated from human adipose tissue exhibit different chondrogenic and osteogenic differentiation potential, Stem Cell Rev 7(1) (2011) 64-76, 10.1007/s12015-010-9147-0.

[30] S. Font Tellado, E.R. Balmayor, M. Van Griensven, Strategies to engineer tendon/ligament-to-bone interface: Biomaterials, cells and growth factors, Adv Drug Deliv Rev 94 (2015) 126-40, 10.1016/j.addr.2015.03.004.

[31] R. Costa-Almeida, R. Soares, P.L. Granja, Fibroblasts as maestros orchestrating tissue regeneration, J Tissue Eng Regen Med (2017) 10.1002/term.2405.

[32] P.P. Carvalho, X. Wu, G. Yu, I.R. Dias, M.E. Gomes, R.L. Reis, J.M. Gimble, The effect of storage time on adipose-derived stem cell recovery from human lipoaspirates, Cells Tissues Organs 194(6) (2011) 494-500, 10.1159/000324892.

[33] R. Costa-Almeida, I. Calejo, R.L. Reis, M.E. Gomes, Crosstalk between adipose stem cells and tendon cells reveals a temporal regulation of tenogenesis by matrix deposition and remodeling, Journal of Cellular Physiology n/a-n/a, 10.1002/jcp.26363.

[34] R. Costa-Almeida, L. Gasperini, J. Borges, P.S. Babo, M.T. Rodrigues, J.F. Mano, R.L. Reis, M.E. Gomes, Microengineered Multicomponent Hydrogel Fibers: Combining Polyelectrolyte Complexation and Microfluidics, ACS Biomaterials Science & Engineering 3(7) (2016) 1322-1331, 10.1021/acsbiomaterials.6b00331.

[35] T. Pesqueira, R. Costa-Almeida, S.M. Mithieux, P.S. Babo, A. Franco, B.B. Mendes, R.M.A. Domingues, P.P. Freitas, R.L. Reis, M.E. Gomes, A. Weiss, Engineering magnetically responsive tropoelastin spongy-like hydrogels for soft tissue regeneration, Journal of Materials Chemistry B (2018) 10.1039/C7TB02035J.

[36] R. Costa-Almeida, D. Berdecka, M.T. Rodrigues, R.L. Reis, M.E. Gomes, Tendon explant cultures to study the communication between adipose stem cells and native tendon niche, J Cell Biochem 119(4) (2018) 3653-3662, 10.1002/jcb.26573.

[37] R. Costa-Almeida, I. Calejo, R.L. Reis, M.E. Gomes, Crosstalk between adipose stem cells and tendon cells reveals a temporal regulation of tenogenesis by matrix deposition and remodeling, J Cell Physiol (2017) 10.1002/jcp.26363.

[38] C.Y. Li, X.Y. Wu, J.B. Tong, X.X. Yang, J.L. Zhao, Q.F. Zheng, G.B. Zhao, Z.J. Ma, Comparative analysis of human mesenchymal stem cells from bone marrow and adipose tissue under xeno-free conditions for cell therapy, Stem Cell Res Ther 6 (2015) 55, 10.1186/s13287-015-0066-5.

[39] B.E. Grottkau, Y. Lin, Osteogenesis of Adipose-Derived Stem Cells, Bone Res 1(2) (2013) 133-45, 10.4248/BR201302003.

[40] R. Costa-Almeida, A.I. Gonçalves, P. Gershovich, M.T. Rodrigues, R.L. Reis, M.E. Gomes, Tendon Stem Cell Niche, Tissue-Specific Stem Cell Niche2015, pp. 221-244, 10.1007/978-3-319-21705-5_10.

[41] Y. Bi, D. Ehirchiou, T.M. Kilts, C.A. Inkson, M.C. Embree, W. Sonoyama, L. Li, A.I. Leet, B.M. Seo, L. Zhang, S. Shi, M.F. Young, Identification of tendon stem/progenitor cells and the role of the extracellular matrix in their niche, Nat Med 13(10) (2007) 1219-27, 10.1038/nm1630.

[42] Q. Tan, P.P.Y. Lui, Y.F. Rui, Y.M. Wong, Comparison of Potentials of Stem Cells Isolated from Tendon and Bone Marrow for Musculoskeletal Tissue Engineering, Tissue engineering. Part A 18(7-8) (2012) 840-851, 10.1089/ten.tea.2011.0362.

[43] T. Komori, Regulation of Osteoblast Differentiation by Runx2, in: Y. Choi (Ed.), Osteoimmunology: Interactions of the Immune and skeletal systems II, Springer US, Boston, MA, 2010, pp. 43-49, 10.1007/978-1-4419-1050-9_5.

[44] G.S. Stein, J.B. Lian, A.J. van Wijnen, J.L. Stein, M. Montecino, A. Javed, S.K. Zaidi, D.W. Young, J.Y. Choi, S.M. Pockwinse, Runx2 control of organization, assembly and activity of the regulatory machinery for skeletal gene expression, Oncogene 23(24) (2004) 4315-29, 10.1038/sj.onc.1207676.

[45] K. Howell, C. Chien, R. Bell, D. Laudier, S.F. Tufa, D.R. Keene, N. Andarawis-Puri, A.H. Huang, Novel Model of Tendon Regeneration Reveals Distinct Cell Mechanisms Underlying Regenerative and Fibrotic Tendon Healing, Scientific Reports 7 (2017) 10.1038/srep45238.

[46] Y. Li, M. Ramcharan, Z. Zhou, D.J. Leong, T. Akinbiyi, R.J. Majeska, H.B. Sun, The Role of Scleraxis in Fate Determination of Mesenchymal Stem Cells for Tenocyte Differentiation, Sci Rep 5 (2015) 13149, 10.1038/srep13149.

[47] C.M. Webb, G. Zaman, J.R. Mosley, R.P. Tucker, L.E. Lanyon, E.J. Mackie, Expression of tenascin-C in bones responding to mechanical load, Journal of bone and mineral research : the official journal of the American Society for Bone and Mineral Research 12(1) (1997) 52-8, 10.1359/jbmr.1997.12.1.52.

[48] Y. Bi, C.H. Stuelten, T. Kilts, S. Wadhwa, R.V. Iozzo, P.G. Robey, X.D. Chen, M.F. Young, Extracellular matrix proteoglycans control the fate of bone marrow stromal cells, The Journal of biological chemistry 280(34) (2005) 30481-9, 10.1074/jbc.M500573200.

[49] E.J. Mackie, L.A. Abraham, S.L. Taylor, R.P. Tucker, L.I. Murphy, Regulation of Tenascin-C Expression in Bone Cells by Transforming Growth Factor-β, Bone 22(4) (1998) 301-307, https://doi.org/10.1016/S8756-3282(97)00297-4.

[50] E.D. Silva, P.S. Babo, R. Costa-Almeida, R.M.A. Domingues, B.B. Mendes, E. Paz, P. Freitas, M.T. Rodrigues, P.L. Granja, M.E. Gomes, Multifunctional magnetic-responsive hydrogels to engineer tendon-to-bone interface, Nanomedicine: Nanotechnology, Biology and Medicine (2017) https://doi.org/10.1016/j.nano.2017.06.002.

[51] B.A. Byers, A.J. Garcia, Exogenous Runx2 expression enhances in vitro osteoblastic differentiation and mineralization in primary bone marrow stromal cells, Tissue engineering 10(11-12) (2004) 1623-32, 10.1089/ten.2004.10.1623.

[52] A.M. DeLise, L. Fischer, R.S. Tuan, Cellular interactions and signaling in cartilage development, Osteoarthritis and Cartilage 8(5) (2000) 309-334, https://doi.org/10.1053/joca.1999.0306.

[53] R.S. Tuan, Biology of developmental and regenerative skeletogenesis, Clin Orthop Relat Res (427 Suppl) (2004) S105-17.

[54] M.B. Goldring, K. Tsuchimochi, K. Ijiri, The control of chondrogenesis, J Cell Biochem 97(1) (2006) 33-44, 10.1002/jcb.20652.

[55] P.S. Leboy, G. Grasso-Knight, M. D'Angelo, S.W. Volk, J.B. Lian, H. Drissi, G.S. Stein, S.L. Adams, Smad-Runx Interactions During Chondrocyte Maturation, JBJS 83(1_suppl_1) (2001).

[56] Q. Zheng, G. Zhou, R. Morello, Y. Chen, X. Garcia-Rojas, B. Lee, Type X collagen gene regulation by Runx2 contributes directly to its hypertrophic chondrocyte-specific expression in vivo, J Cell Biol 162(5) (2003) 833-842, 10.1083/jcb.200211089.

[57] M.T. Rodrigues, S.J. Lee, M.E. Gomes, R.L. Reis, A. Atala, J.J. Yoo, Bilayered constructs aimed at osteochondral strategies: the influence of medium supplements in the osteogenic and chondrogenic differentiation of amniotic fluid-derived stem cells, Acta Biomater 8(7) (2012) 2795-806, 10.1016/j.actbio.2012.04.013.

5.7. SUPPLEMENTARY INFORMATION

5.7.1. EXPERIMENTAL

5.7.1.1. Isolation of human adipose-derived stem cells

Fat tissue samples were immersed in a 0.05% (w/v) collagenase type II (Sigma/C6885) solution for 45 minutes at 37°C under mild agitation using an orbital shaker. The digested tissue was centrifuged at 304 g for 10 minutes at 4°C, after which the supernatant was eliminated. Lysis buffer (155 mM NH_4CL, 10 mM $KHCO_3$, 0.1 mM EDTA, pH=7.3) was used to separate the stromal vascular fraction followed by a centrifugation at 304 g for 5 minutes. Finally, isolated cells were expanded in basal medium composed of Minimum Essential Medium Eagle (α –MEM, Alfagene) supplemented with 10% (v/v) Fetal Bovine Serum (FBS, Alfagene) and 1% (v/v) antibiotic/antimitotic solution (A/A, Alfagene). Cells were seeded on culture flasks for expansion and incubated in a humidified environment at 37°C, 95% humidity with 5% CO_2. Medium was change every 3-4 days. Cells were used at passages 2-3.

5.7.1.2. Isolation of human tendon-derived cells

Surrounding non-tendon tissue was first carefully removed and then samples were minced and digested in the presence of 0.1% (w/v) collagenase type I solution (Sigma) for 1 hour at 37 °C, under mild orbital agitation. The obtained digested tissue was filtered and centrifuged at 1200 rpm for 5 minutes at 4°C. The supernatant was discarded and the cell pellet resuspended in basal medium composed of α-MEM supplemented with 10% (v/v) FBS (Invitrogen) and 1% (v/v) A/A. Cells were seeded on culture flasks for expansion and incubated in a humidified environment at 37°C, 95% humidity with 5% CO_2. Medium was change every 3-4 days. Cells were used at passages 2-4.

5.7.1.3. dsDNA quantification

Medium was removed and samples were washed with PBS. Then, filtered ultra-pure Millipore water (Pore size 0.22 μm) was added to subjecting cells to an osmotic shock. Lysed cell solution was collected and stored at -80°C, additionally promoting a thermal shock. Cell lysates were used for dsDNA quantification and fluorescence was measured in a microplate reader (Synergy HT, Bio-Tek Instruments) using an excitation wavelength of 485/20 nm and emission wavelength of 538/20nm. Standards were prepared in a range of concentrations between 0 and 1.5 μg/mL. Triplicates were used for each sample and condition. Results are presented as mean±standard error of the mean (SEM).

5.7.1.4. Alizarin Red Staining

Cells were fixed with a solution of 10% (v/v) neutral buffered formalin for 20 minutes at room temperature and washed with PBS. Prior to staining, cells were washed with deionized water. A solution of 2% (w/v) alizarin red (Merck) was added for 10 minutes and, subsequently, the cells were washed with deionized water until the excess of dye was removed. Staining was visualized and images were acquired using the inverted microscope Vert A.1 Axio with Axiocam 503 color (Zeiss, Germany) and Zen 2.3 lite software (Zeiss, Germany). To obtain the quantitative data, the staining was destained for 15-30 minutes, at room temperature, under smooth orbital agitation and the absorbance was measured at 562 nm in a microplate reader (Synergy HT, Bio-Tek Instruments). Standard curves were prepared and ranged from 0.007-0.46 mM. Triplicates were used for each sample and conditions. Results are presented as mean±SEM.

5.7.1.5. Alkaline phosphatase (ALP) activity

Briefly, cell lysates were incubated in a substrate solution of 0.2% (w/v) *p*-nitrophenyl phosphate (pNPP) in 1 M diethanolamine (Sigma-Alrich) and incubated for 1 hour at 37°C. Afterwards, a stop solution of

2M NAOH/0.2 mM EDTA was added and the absorbance was measured (405 nm) using a microplate reader (Synergy HT, Bio-Tek Instruments). Calibration curves were prepared using a *p*-nitrophenol (pNP) stock solution (Sigma-Alrich) with values ranging from 0 to 0.5 µmol/mL. Results were normalized against dsDNA and are presented as mean (µmol *p*NP/h/µg) ±SEM. Triplicates were used for each sample and per condition.

5.7.1.6. Immunocytochemistry

After 7 and 14 days, cells were washed twice with PBS and fixed with 10% (v/v) neutral buffered formalin for 20 minutes at room temperature. Fixed cells were washed with PBS, permeabilized with 0.25% Triton X-100/PBS solution for 5 minutes, non-specific binding was blocked with 1% bovine serum albumin (w/v, BSA) in PBS and samples were incubated overnight with mouse anti-human Tenascin C (TNC, 1:3000, Abcam), mouse anti-human collagen I (COLI, 1:500, Abcam) and rabbit anti-human collagen III (COLIII, 1:100, Abcam).

Samples incubated overnight with rabbit anti-human osteopontin (OPN, 1:100, Abcam), mouse anti-human osteocalcin (OCN,1:50, Abcam), rabbit anti-human Scleraxis (SCX, 1:200, Abcam), mouse anti-human Decorin (DCN, 1:100, Abcam), and in the case of co-cultures with mouse anti-human Aggrecan (ACAN,1:200, Alfagene) and rabbit anti-human Collagen II (COLII, 1:200, Abcam), were previously permeabilized with 0.025% Triton X-100/PBS solution for 30 minutes and non-specific binding was blocked with 3% BSA/PBS. Afterwards, cells were washed three times with PBS or rinsed twice with Triton X-100/PBS solution for 5 minutes in the case of primary antibody against OPN, OCN, ACAN and COL2. Cells were incubated with the secondary antibody for 1 hour at room temperature. All antibodies were diluted in 1% (w/v) BSA/PBS.

5.7.2. FIGURES

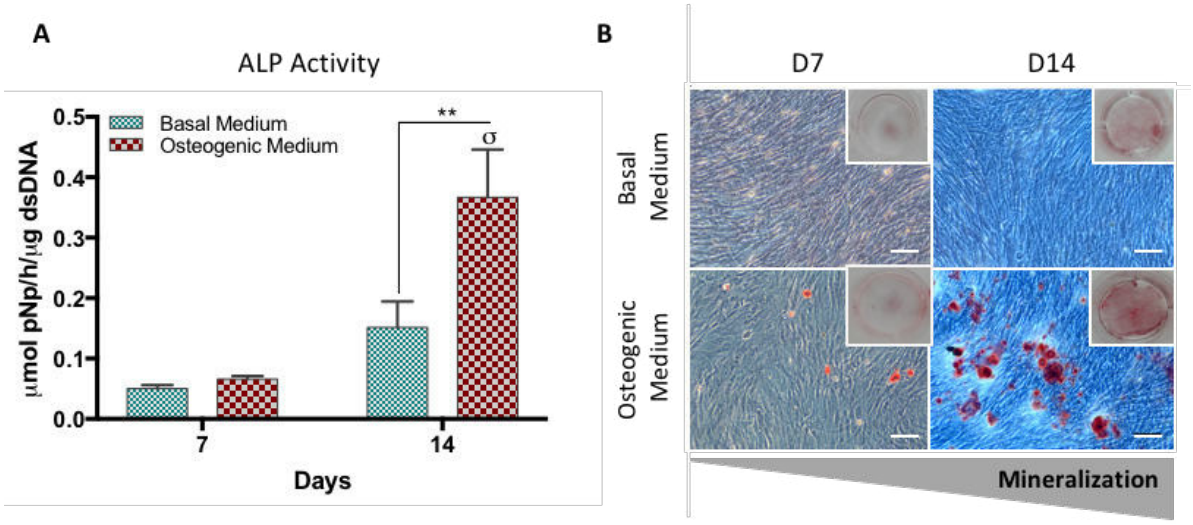

Supplementary Figure S5.1 | Osteogenic differentiation of hASCs. (A) Alkaline phosphatase (ALP) activity determined by the colorimetric p-nitrophenol (pNP) assay. Results are presented as mean±SEM and statistically significant differences are shown a *, $p<0.02$; ***, $p<0.0004$; σ, $p<0.0004$, σ is statistically significant differences in correspondence to day 7. (B) Alizarin red staining of hASCs cultured in basal medium (control group) and osteogenic medium after 7 and 14 days of culture (scale bars, 100 µm).

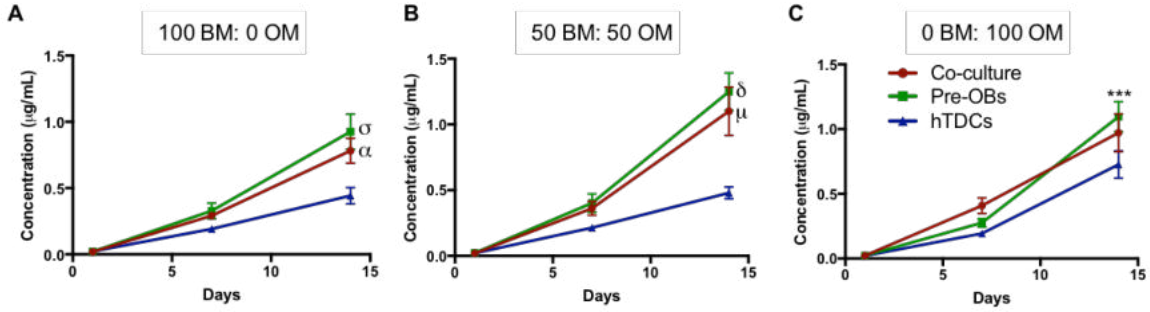

Supplementary Figure S5.2 | Comparative influence of media conditions on cell proliferation in single cultures and co-cultures. (A) Condition 100BM:0OM, statistically significant differences are shown as α, p<0.0002; σ, p<0.0001 where σ and α are statistically significant in correspondence to hTDCs in the correspondent day. (B) Condition 50BM:50OM, statistically significant differences are shown as δ, p<0.0001; µ, p<0.0001, where δ and µ are statistically significant in correspondence to hTDCs at the same day. (C) Condition 0BM:100OM, statistically significant differences are shown as ***, p=0.0003.

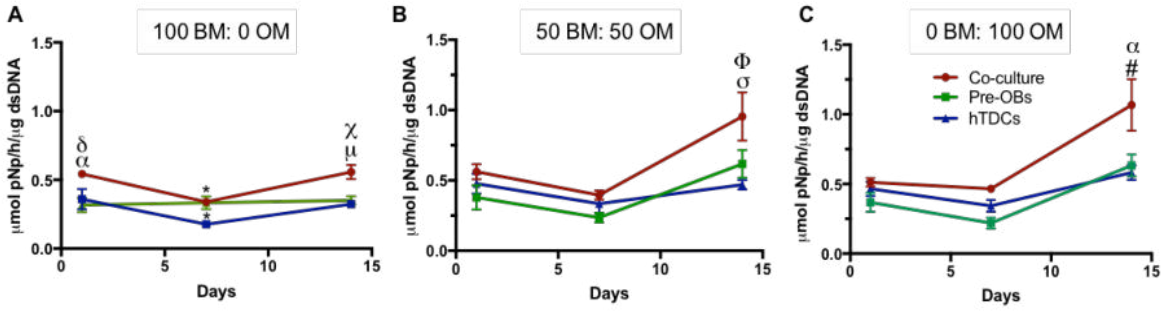

Supplementary Figure S5.3 | Comparative influence of media conditions on ALP activity in single cultures and co-cultures. (A) Condition 100BM:0OM, statistically significant differences are shown as *, $p<0.02$; α, $p<0.02$; δ, $p<0.003$; μ, $p<0.003$ and χ, $p<0.0006$, α, μ are statistically significant in correspondence to pre-OBs and δ, χ to hTDCs. (B) Condition 50BM:50OM, statistically significant differences are shown as σ, $p=0.01$; Φ, $p=0.0002$, σ is statistically significant in correspondence to pre-OBs and Φ to hTDCs. (C) 0BM:100OM, statistically significant differences are shown as #, $p=0.0003$; α, $p<0.0001$, # is statistically significant in correspondence to pre-OBs and α to hTDCs in the correspondent day

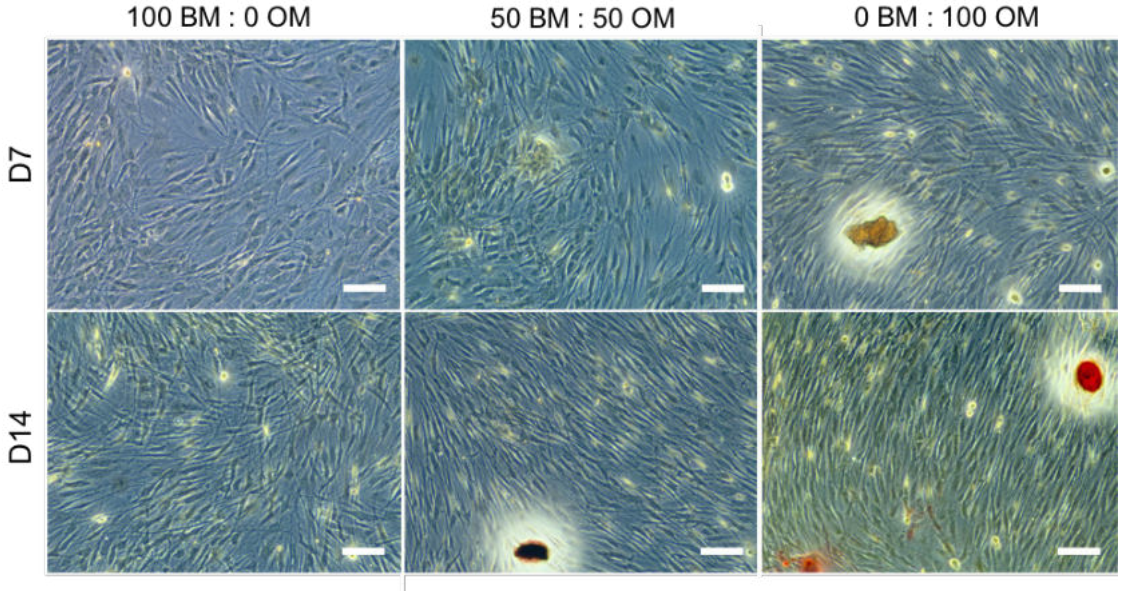

Supplementary Figure S5.4 | Matrix mineralization of single culture of hTDCs. Alizarin red staining in hTDCs after 7 and 14 days of culture (scale bars, 100 μm).

CHAPTER 6. "*In vitro* temporal HIF-mediated deposition of osteochondrogenic matrix governed by hypoxia and osteogenic factors synergy"

This chapter was adapted from the following publication:

I. Calejo, R. Costa-Almeida, R. L. Reis, M. E. Gomes (2020) *In vitro* temporal HIF-mediated deposition of osteochondrogenic matrix governed by hypoxia and osteogenic factors synergy. *Journal of Cellular Physiology*. DOI: 10.1002/jcp.30138

ABSTRACT

Musculoskeletal interfaces are naturally hypoxic. An understanding of key interactions occurring between different cell populations and its environment is critical for native tissue recapitulation. Here, an enthesis co-culture model (pre-osteoblasts and tendon-cells) was used to understand the influence of hypoxia (5% O_2) and osteogenic supplementation (OM) in cells' phenotype modulation. In single cultures, pre-osteoblasts were found to undergo osteogenic impairment while tendon-cells underwent a maturation process through ECM rescue. When in co-culture, hypoxia and osteoinduction promoted a temporal chondro/osteogenic pathway activation, as observed by an early deposition of cartilaginous ECM associated with HIF1A stabilization and *RUNX2* activation, and later hypertrophic differentiation resulting from HIF2A translocation and SOX9 activation. Moreover, the presence of OM under hypoxia was shown to influence the extracellular ROS/HIF1A interplay. Overall, this work revealed a link between biochemical factors and cell-cell crosstalk, providing a molecular framework for hypoxic control and modulation of cells' fate towards enthesis-like phenotypes.

Keywords: Cell modulation, Enthesis, Hedgehog signaling, Hypoxia-inducible factors, Osteogenic supplementation

6.1. INTRODUCTION

Mammalian physiology has shown to obtain beneficial effects from oxygen gradients, as demonstrated by the critical role of low oxygen tension (hypoxia) for proper embryogenesis or even wound healing [1]. Nevertheless, oxygen variations have also been correlated with tissue degeneration phenomena, including aging [2, 3] and tumor progression [4-6].

Hypoxia-inducible factors (HIF) are crucial mediators of hypoxic response [7] (reviewed in [8]). Amongst the three HIF α-subunits, HIF-1α and HIF-2α are the most studied. HIF-1α is mostly active during short periods of low oxygen tension hypoxia (or anoxia, when oxygen falls below 1%), whereas HIF-2α has been shown to undergo continuous activation under mild or physiological hypoxia. Strikingly, HIF-2α has been recognized to play an essential role in coordinating the hypoxic response during long time exposure, while HIF-1α is responsible for the preliminary response to hypoxia [9-11]. Under oxygen tensions between 10 – 21% (normoxia), HIF-1α is constitutively synthesized but simultaneously degraded, being this reflected in lower levels of HIF-1α protein expression [12].

Hypoxia-inducible factors have also been associated with the activation of numerous downstream pathways highlighted as important regulators of bone growth, coordinating chondrocyte proliferation, differentiation and hypertrophy, and osteoblast differentiation [13-16]. A good example of the critical role of these factors in tissue formation is their temporal involvement in organogenesis and osteogenesis coupling during endochondral ossification [17-19]. For example, in an *in vivo* mouse model, activation of the hypoxia pathway in osteoblasts resulted in elevated VEGF levels, promoting angiogenesis [20]. In contrast, mice lacking *Hif-1α* developed thinner and less vascularized long bones [20]. The spatio-temporal regulation of angiogenesis in the growth plate has also been addressed [21].

As mentioned above, considerable O_2 gradients can arise within a given organ. The musculoskeletal tendon-to-bone interface is a good example of this phenomenon, presenting very singular needs of oxygen tension and, therefore, supply, across the whole tissue. Tendon tissue saturation has been described as falling below skeletal muscle oxygen tension, which ranges from 3.6% to 4.0% [22], while, at the bony counterpart, where a higher vascularization has been reported, oxygen tension can go higher than 5.5% [23, 24]. Even though several cell- and culture-based strategies were developed to mimic, as close as possible, the interactions occurring in the native tissue [25], there is still a need for a deeper understanding of the physiological status of the junction when trying to explore new therapeutic approaches. In this regard, the oxygen tension must be recognized as a particular biochemical parameter critical when trying to address interface healing and proper regeneration.

Here, we propose the use of a direct co-culture system as enthesis *in vitro* model to understand the influence of low oxygen tension (5% O_2, hypoxia) and osteogenic supplementation in the modulation of cellular phenotype *in vitro*. In a first approach, single cultures of human adipose-derived stem cells (hASCs) pre-differentiated towards osteogenic lineage (herein called pre-osteoblasts, pre-OBs) and human tendon-derived cells (hTDCs) were used to determine the effect of hypoxia on tendon- and bone-like niches. Afterward, we established direct co-cultures to evaluate the influence of low oxygen tension on the cell-cell interaction and expression of interface-relevant markers in the presence of different ratios of osteogenic factors. Temporal expression of hypoxia-inducible factors, HIF1A and HIF2A, was assessed to understand the interaction of these factors on the transcriptional expression of interface markers and activation of Hedgehog signaling pathway. The potential role of nuclear accumulation of these hypoxia-inducible factors was similarly studied and associated with the activation of SOX9. This data was correlated with reactive oxygen species (ROS) production and secretion of HIF1A by co-cultured cells. Overall, this study allowed demonstrating the effects of low oxygen tension in an *in vitro* co-culture regime with possible translation to an *in vivo* setting to promote a proper *de novo* formation of the interface between tendon and bone that will closely resemble the native musculoskeletal tissue.

6.2. MATERIALS AND METHODS

6.2.1. Human samples and cell isolation

Adipose and tendon tissue samples were obtained under protocols previously established with Hospital da Prelada (Porto, Portugal). All samples were collected under the informed consent of the patients, according to the Declaration of Helsinki, and the content of the written informed consent and related procedures were reviewed and approved by the Ethical Committee of the Hospital.

Human adipose-derived stem cells (hASCs) were isolated from lipoaspirate samples of three healthy female patients (42-69 years old). Human tendon-derived cells (hTDCs), a heterogeneous tendon cell population, were obtained from tendon surplus tissue samples of three healthy male patients (25-30 years old) undergoing orthopedic surgeries. Cell isolation was performed as described in Calejo, et al [26]. Cells were expanded in basal medium (BM) composed of minimum essential medium (α-MEM; Alfagene, Carcavelos, Portugal) supplemented with 10% (v/v) fetal bovine serum (Alfagene) and 1% (v/v) antibiotic/antimitotic solution (A/A; Alfagene).

6.2.2. Experimental culture setups

The experimental setup used for the establishment of different oxygen concentrations is depicted in Supplementary Figure S6.1. Briefly, human adipose-derived stem cells (hASCs) were cultured in the presence of osteogenic medium (OM) consisting of BM supplemented with 10 mmol/L β-glycerophosphate (G9422, Sigma-Aldrich), 10^{-8} mol/L dexamethasone (D2915, Sigma-Aldrich), and 50 μg/mL L-ascorbic acid 2-phosphate sesquimagnesium salt hydrate (013-12061, Wako) for 14 days in a humidified environment (37 °C, 5% CO_2). Pre-differentiated cells were called pre-osteoblasts (pre-OBs). Human tendon derived cells (hTDCs) were simultaneously expanded in basal medium in a humidified environment at 37°C, 21% O_2 (normoxia). Direct contact co-culture systems were established afterward by seeding together pre-OBs and hTDCs using a final density of 4×10^3 cells/well in a ratio of 1:1 (Supplementary Figure S6.2), as previously described [26]. For visual evidence of the establishment of a direct contact co-culture, live staining was performed on pre-OBs (green, CellTrackerTM Green CMFDA Dye, C2925, Thermofisher) and hTDCs (red, CellTracker™ Red CMTPX Dye, C34552, Thermofisher) after 2 days of culture under both normoxia and hypoxia (Supplementary Figure S6.2). Single cultures of either pre-OBs or hTDCs seeded at a density of 4×10^3 cells/well were used as controls. Cells were left to adhere for a period of 24 hours and then, placed in a hypoxic vinyl chamber (Coy O2 Control Glove Boxe, Coy/ Esco) with a humidified environment at 37 °C and lower oxygen tension (hypoxia, 5% O_2) for 14 days. Three previously optimized medium conditions [26] with increasing ratios of osteogenic factors were used (100 BM: 0 OM, 50 BM: 50 OM, 0 BM: 100 OM; BM: basal medium, OM: osteogenic medium). Single cultures and co-cultures maintained under normoxia (21% O_2) were used for comparison. Samples were collected at specific timepoints as specified in Supplementary Figure S6.1.

6.2.3. Cell proliferation – dsDNA quantification

A fluorometric dsDNA quantification kit (PicoGreen, Molecular Probes, Invitrogen) was used to determine DNA content according to the manufacturer's protocol. For this purpose, cells were subjected to osmotic and thermal shocks using filtered ultra-pure Millipore water (Pore size 0.22 μm) and storing at -80 °C. Cell lysates were used for dsDNA quantification, and fluorescence was measured in a microplate reader (Synergy HT, Bio-Tek Instruments) using an excitation wavelength of 485/20 nm and an emission wavelength of 538/20nm. A standard curve was prepared in a range of 0 to 1.5 μg/mL.

6.2.4. Total protein concentration – Micro BCA assay

A specialized version of the Pierce BCA protein assay (Micro BCA™ Protein Assay Kit, Thermo Scientific™) was used according to the protocol, to determine the total protein content of collected samples. Briefly, 150 µL of standards and medium samples were added to 96 well-plates. A working reagent solution was prepared by mixing Reagent A, Reagent B, and Reagent C (25:24:1), added to each well, and plates incubated at 37 °C for 2 hours. After cooling at room temperature, absorbance was measured at 562 nm using a microplate reader (Synergy HT, Bio-Tek Instruments). A standard curve was prepared in a range of 0 to 200 µg/mL.

6.2.5. Alkaline Phosphatase (ALP)

A colorimetric *p*-nitrophenol (pNp) assay was used to quantify the activity of alkaline phosphatase in cell lysates. Briefly, samples were incubated with a substrate solution of 0.2% (w/v) *p*-nitrophenyl phosphate (pNPP) in 1 mmol diethanolamine (Sigma-Alrich). After 1-hour incubation at 37 °C, a stop solution of 2M NaOH/0.2 mM EDTA was added and the absorbance was measured (405 nm) using a microplate reader (Synergy HT, Bio-Tek Instruments). A standard curve was prepared using a *p*-nitrophenol (pNP) stock solution (Sigma-Alrich) with values ranging from 0 to 0.5 µmol/mL. Normalization against dsDNA was performed, and results presented as µmol *p*NP/h/µg.

6.2.6. Alizarin Red and Alcian Blue staining

Calcium deposition was assessed by alizarin red (AZ) staining. Cells were fixed with a solution of 10% (v/v) neutral buffered formalin for 20 minutes at room temperature, washed with PBS, and finally with deionized water to remove contaminating salts from PBS. A solution of 2% (w/v) alizarin red (Merck) was added for 10 minutes and, subsequently, cells were washed with deionized water until the excess of dye was removed. Images were acquired using an inverted microscope Vert A.1 Axio with Axiocam 503 color (Zeiss, Germany) and Zen 2.3 lite software (Zeiss, Germany). Quantitative data were obtained by removing the dye from the cell layer. In brief, a solution of 10% (w/v) cetylpyridinium chloride (CPC) in 10 mM sodium phosphate (Sigma-Alrich) was prepared and added to each well for 15-30 minutes, at room temperature, under smooth orbital agitation. The resulting destained solution was collected to a 96 well-plate, and the absorbance measured at 562 nm in a microplate reader (Synergy HT, Bio-Tek Instruments). Standard curves were prepared and ranged from 0.007 to 0.46 mmol/L.

Deposition of glycosaminoglycans was determined by alcian blue staining. Cells were washed with PBS and fixed with 10% (v/v) neutral buffered formalin for 20 minutes at room temperature. Afterward, wells

were washed twice with PBS, and alcian blue solution in 0.1 M hydrochloric acid was added for 30 minutes, at room temperature, under mild shaking. Stained samples were thoroughly washed with PBS and images acquired using a stereomicroscope (Discovery v8, Zeiss) coupled with a digital camera (EOS 1200D, Canon). Staining quantification was performed using a microplate reader (Synergy HT, Bio-Tek Instruments), and the absorbance measured at 620 nm.

6.2.7. Real-time Reverse Transcription Polymerase Chain Reaction (RT-PCR) analysis

Total mRNA was extracted using RIBOZOL™ RNA extraction reagent (VWRCN580, VWR), according to manufacturer's instructions, and mRNA was quantified using a NanoDrop® ND-1000 spectrophotometer (NanoDrop Technologies). Complementary DNA (cDNA) was synthesized from 100 ng of RNA of each sample using a qScript cDNA Synthesis Kit (Quanta Biosciences) in a final reaction volume of 20 µL. Quantification of transcripts was performed by RT-PCR using 50 ng of cDNA. PerfeCTA SYBR Green FastMix kit (Quanta Biosciences) was used as described in the manufacturer's protocol. Primer sequences (Supplementary Table S6.1) were designed using Primer-BLAST tool and synthesized by IDT – Integrated DNA Technologies. Having a amplification efficiency near 100% and equal amount of sample, cultures maintained in BM under normoxia were chosen as calibrators, and the relative expression level was determined using the $2^{-\Delta Ct}$ method [27-29]. Five samples were used for each condition and three independent experiments were performed (n=3). Results are represented as fold change and relative expression is normalized to the BM under normoxia.

6.2.8. Immunocytochemistry against osteogenic, tenogenic and interface-related markers

For immunocytochemistry, samples were fixed with 10% (v/v) neutral buffered formalin for 20 minutes at room temperature. Fixed cells were washed with PBS, permeabilized with 0.25% Triton X-100/PBS solution for 5 minutes; non-specific binding was blocked with 1% bovine serum albumin (w/v, BSA) in PBS and samples were incubated overnight with, mouse anti-human tenascin C (TNC, 1:3000, MA126779 Thermofisher), rabbit anti-human collagen I (COLI, 1:500, ab34710 Abcam) and rabbit anti-human collagen type X (COLX, 1:50, ab58632 Abcam). Samples incubated overnight with rabbit anti-human hypoxia-inducible factor 1-alpha (HIF1A, 1:100, ab82832 Abcam), rabbit anti-human hypoxia-inducible factor 2-alpha (HIF2A, 1:100, ab109616 Abcam) rabbit anti-SOX9 (SOX9, 1:200, AB5535 Millipore), mouse anti-human aggrecan (ACAN,1:200, MA316888 Thermofisher), rabbit anti-human

collagen II (COLII, 1:200, ab34712 Abcam), were previously permeabilized with 0.025% Triton X-100/PBS solution for 30 minutes and non-specific binding was blocked with 3% BSA.

Afterward, cells were washed three times with PBS or, in the case of the primary antibodies against ACAN, COLII, COLX, SOX9, HIF1A, and HIF2A, samples were rinsed with Triton X-100/PBS solution for 5 minutes. Cells were incubated with donkey anti-mouse AlexaFluor 488 (A21202, Thermofisher) or mouse anti-rabbit AlexaFluor 488 (A21206 Thermofisher), as secondary antibodies, for 1 hour at room temperature. All antibodies were diluted in 1% (w/v) BSA/PBS. Cell nuclei were counterstained with 4,6-diamidino-2-phenyindole dilactate (DAPI, Invitrogen). Images were acquired by fluorescence microscopy (Axio Imager Z1m, Zeiss, Deutschland, Germany).

6.2.9. Measurement of ROS production

The production of ROS was measured using a modified method of oxygen radical absorbance capacity (ORAC) [30, 31]. In brief, medium samples were thawed at room temperature in a closed vial and placed in a 96-well plate. A solution of fluorescein (Fluorescein sodium salt, Sigma), a fluorescent probe, in PBS was prepared and added to each well in a final concentration of 1.38×10^{-4} mol/L. Fluorescence intensity kinetics was measured every minute for 1 hour using a microplate fluorescence reader (excitation wavelength: 488 nm and emission wavelength: 528 nm). Different media freshly prepared were used as controls and PBS with fluorescein used as assay control. Triplicates were used. Results are presented as percentage of fluorescein intensity.

6.2.10. Quantification of extracellular HIF1A

The concentration of extracellular HIF1A was performed using an HIF1A ELISA Kit (OKEH02771, AVIVO SYSTEM BIOLOGY). Briefly, collected medium samples were left to thaw at room temperature, added to wells and incubated. Afterwards, wells were washed 3x and Avidin-Peroxidase Conjugate added. After incubation, wells were washed and TMB substrate added, generating a blue color. After addition of the stop solution, a yellow color was visible and therefore absorbance read at 450 nm in a microplate reader (Synergy HT, Bio-Tek Instruments). Data was normalized to the basal condition under normoxia and presented as percentage (%) of extracellular HIF1A.

6.2.11. Statistical Analysis

Results were obtained from three independent experiments with a minimum of three replicates for each condition. Statistical analyses were performed using GraphPad Prism 8.0 software

(https://www.graphpad.com/scientific-software/prism/). Two-way analysis of variance (ANOVA) with Sidak and Tukey tests were performed. For ROS production analysis, t-test (nonparametric, Mann-Whitney test) was used. Data are represented as means ± standard deviation (SD). Differences between experimental groups were considered significant, with a confidence interval of 95%, whenever $p < 0.05$.

6.3. RESULTS

6.3.1. Hypoxia effects on the osteogenic response cascade of pre-OBs is independent of osteogenic supplementation

The influence of a restricted oxygen environment on pre-osteoblasts (pre-OBs) phenotype was first investigated in the presence of basal medium (100 BM: 0 OM), a combination of basal and osteogenic media (50 BM: 50 OM) and complete osteogenic medium (0 BM: 100 OM) while exposed to normal and restricted oxygen environments (21% and 5% O_2) for 14 days (Supplementary Figure S6.1). Proliferation, alkaline phosphatase activity, gene expression of bone-related markers, and deposition of the bone-like matrix were studied.

Although pre-OBs proliferated over time in all conditions, the restricted oxygen environment (5% O_2) impacted pre-OBs proliferation when compared to equal cultures maintained under normoxia (21% O_2) (Figure 6.1A). After 14 days of culture, a synergistic effect on the reduction of cell proliferation by hypoxia and osteogenic supplementation was observed. At this time, a significant reduction on DNA content was registered for both osteogenic medium (OM) conditions (50 BM:50BM, $p < 0.05$; 0 BM:100BM, $p < 0.001$) under hypoxia in comparison to cells under normoxia.

Alkaline phosphatase (ALP) activity was determined as a biochemical indicator of osteogenesis (Figure 6.1B), and a similar behavior was observed when comparing both oxygen tensions, as 5% O_2 reduced the activity of this enzyme. Yet, the presence of OM, under hypoxia, enhanced the expression of this biomarker after 14 days compared with cells in basal medium (BM) (0 BM: 100 OM: $p < 0.009$).

We next evaluated the transcription of osteogenic markers runt-related transcription factor 2 (*RUNX2*) and collagen type I alpha 1 chain (*COL1A1*) (Figure 6.1C). Transcription levels of *RUNX2* were found to be only influenced by a mild osteogenic supplementation at early times, independently of 21% or 5% O_2 tension. This was observed under hypoxia, by the significantly higher levels observed for day 7 compared to day 14 (Figure 6.1C, i; day 7, 50BM:50OM, $p < 0.05$). On the other hand, the same was not observed *COL1A1* transcription levels, where 5% O_2 clearly induced an upregulation, when compared to the levels observed for cultures in BM under normoxia, being this expression independent of the presence of pro-osteogenic factors in the medium, both at 7 and 14 days of culture (Figure 6.1C, ii). To further assess

the impact of oxygen tension and osteogenic supplementation on osteogenesis, the deposition of collagen type I (COLI) was studied at the protein level by immunocytochemistry (Figure 6.1D). Culturing pre-OBs at 5% O_2 revealed a nonfibrillar and presumably intracellular collagen localization (Figure 6.1D, ii). Moreover, during culture time, significantly higher COLI synthesis was observed in pre-OBs cultured at 5% O_2 compared with cells under normoxia, independently of osteogenic medium supplementation (Figure 6.1D, iii). These data can be correlated with gene expression and result from *COL1A1* transcription to protein level.

Concerning matrix mineralization, alizarin red staining confirmed a significantly lower deposition of mineralized calcium in the matrix of pre-OBs cultured in restricted oxygen tension compared with normoxia, independently of the presence of osteogenic medium (Figure 6.1E, iii, $p < 0.0001$).

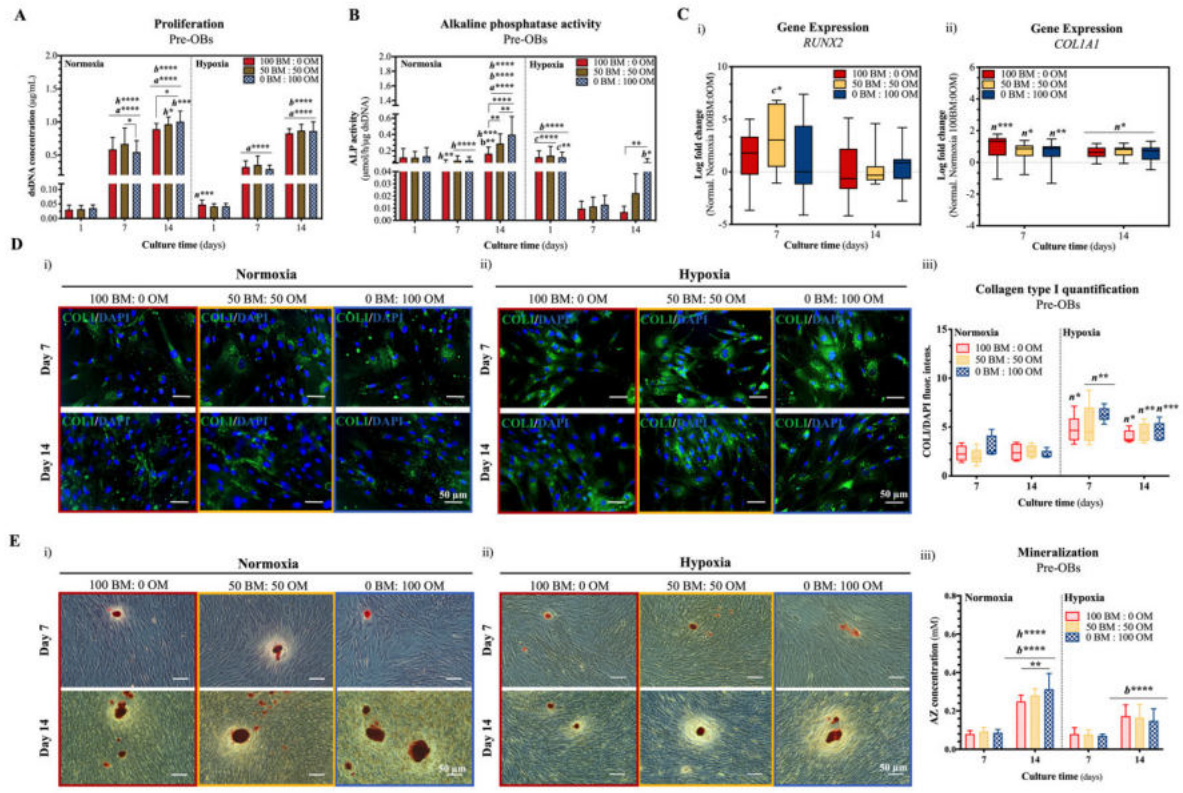

Figure 6.1 | Expression of osteogenic markers by pre-OBs cultured under normoxia and hypoxia in the presence of increasing ratios of osteogenic medium. (**A**) Cell proliferation evaluated by dsDNA quantification of pre-OBs cultured under normoxia and hypoxia for 14 days. Data are represented as means ± SD (n=3). (B) Activity of alkaline phosphatase in pre-OBs under normoxia and hypoxia. Results were normalized against the amount of dsDNA of the correspondent sample. Data are represented as means ± SD (n=3). (C) Gene expression of osteogenic-related markers, runt-related transcription factor 2 (*RUNX2*) (i), and collagen type I alpha 1 chain (*COL1A1*) (ii) were analyzed under

normoxia and hypoxia. Expression of target genes was normalized to the basal condition (100 BM: 0 OM) of the correspondent day under normoxia and the log fold change calculated (n=3, five replicates). (D) Fluorescence microscopy of collagen type I (COLI) of pre-OBs under (i) normoxia and (ii) hypoxia. Scale bars, 50 μm. (iii) Fluorescence intensity ratio quantification. (E) Matrix mineralization by alizarin red (AZ) staining of pre-OBs cultured under (i) normoxia and (ii) hypoxia, and correspondent (iii) quantification by CPC methods. Data are represented as means ± SD (n=3). Scale bars, 50 μm. For A-E, statistically significant differences are shown as *, $p < 0.05$; **, $p < 0.01$; ***, $p < 0.001$; ****, $p < 0.0001$; a, b and c are statistically significant in comparison with the same condition at days 1, 7 and 14, respectively; h is statistically significant in relation to the same condition at hypoxia; n is statistically significant in relation to the same condition at normoxia. Legend: BM: basal medium; OM: osteogenic medium.

6.3.2. Osteogenic supplementation under hypoxia rescues ECM tenogenic protein deposition but not total glycosaminoglycans

The combined influence of 5% O_2 and increasing ratios of pro-osteogenic factors on a tendon-like niche was investigated using single cultures of hTDCs. Cell proliferation, gene expression, and deposition of the characteristic tenogenic-like matrix were assessed up to 14 days of culture under both normoxia and hypoxia.

An increase of DNA content was registered for cultures maintained under hypoxia up to 14 days (Figure 6.2A). A co-effect between low oxygen tension and increasing ratios of OM was observed at 14 days of culture, when hTDCs proliferation was significantly reduced in comparison with normoxia (50 BM: 50 OM, 0 BM: 100 OM, $p < 0.0001$).

We also evaluated the impact of oxygen tension and osteogenic supplementation at the transcript level by analyzing the expression of tenogenic-related transcription factors, scleraxis (*SCX*), and mohawk (*MKX*) by RT-PCR (Figure 6.2B, i-ii). An absence (100BM:0 OM) and mild presence (50 BM: 50 OM) of osteogenic factors under 5% O_2, as soon as 7 days, induced a significant increase of *SCX* transcription levels compared to the same conditions at 14 days of culture, where this expression was reduced (Figure 6.2B, i; 7 days, 100 BM: 0 OM, $p < 0.001$; 50 BM: 50 OM, $p < 0.05$). At this timepoint, an absence of osteogenic factors under hypoxia clearly induced a downregulation of this gene when compared to the *SCX* levels in basal conditions under normoxia (Figure 6.2B, i; $p < 0.05$). Opposingly, transcriptions levels of *MKX* were upregulated in cells maintained in basal medium under hypoxia when compared with the cells maintained at the same conditions under normoxia at both 7 and 14 days of culture (Figure **6.2B**, ii; 100BM: 0 OM: 7 days, $p < 0.01$, 14 days, $p < 0.05$). Given the critical role of *MKX* in tendon maturation

through the regulation of type I collagen production by tendon cells [32], we further assessed the expression of collagen type I at the protein level (Supplementary Figure S6.3). Following the pattern observed at the gene level, hypoxia-induced a higher deposition of this fibrillar collagen, the main component of the tendon extracellular matrix (ECM). On the contrary, tenascin C deposition by hTDCs in hypoxia was significantly decreased during culture time in comparison with cells under normoxia (Figure 6.2C, i-iii). However, the presence of high ratios of osteogenic supplementation (0 BM: 100 OM) rescued the deposition of this protein at both 7 and 14 days compared to hTDCs cultured in BM (day 7: $p < 0.04$, day 14: $p < 0.0001$) and intermediate OM condition (day 7: $p < 0.001$; day 14: $p < 0.0001$).

Since ECM is critical in coordinating tenogenesis, as well as both physiological and pathological events within the tendon niche, the deposition of glycosaminoglycans (GAGs) was evaluated by alcian blue staining of hTDCs cultured for 14 days under normoxia and hypoxia (Figure 6.2D, i-ii). GAGs deposition was significantly reduced under 5% O_2, particularly at 7 and 14 days in BM and high OM conditions when compared with hTDCs maintained under the same conditions in 21% O_2 (Figure 6.2D, iii, 7 days: 100BM: 0 OM, $p < 0.0001$; 14 days: 100BM:0 OM and 0 BM:100 OM, $p < 0.001$).

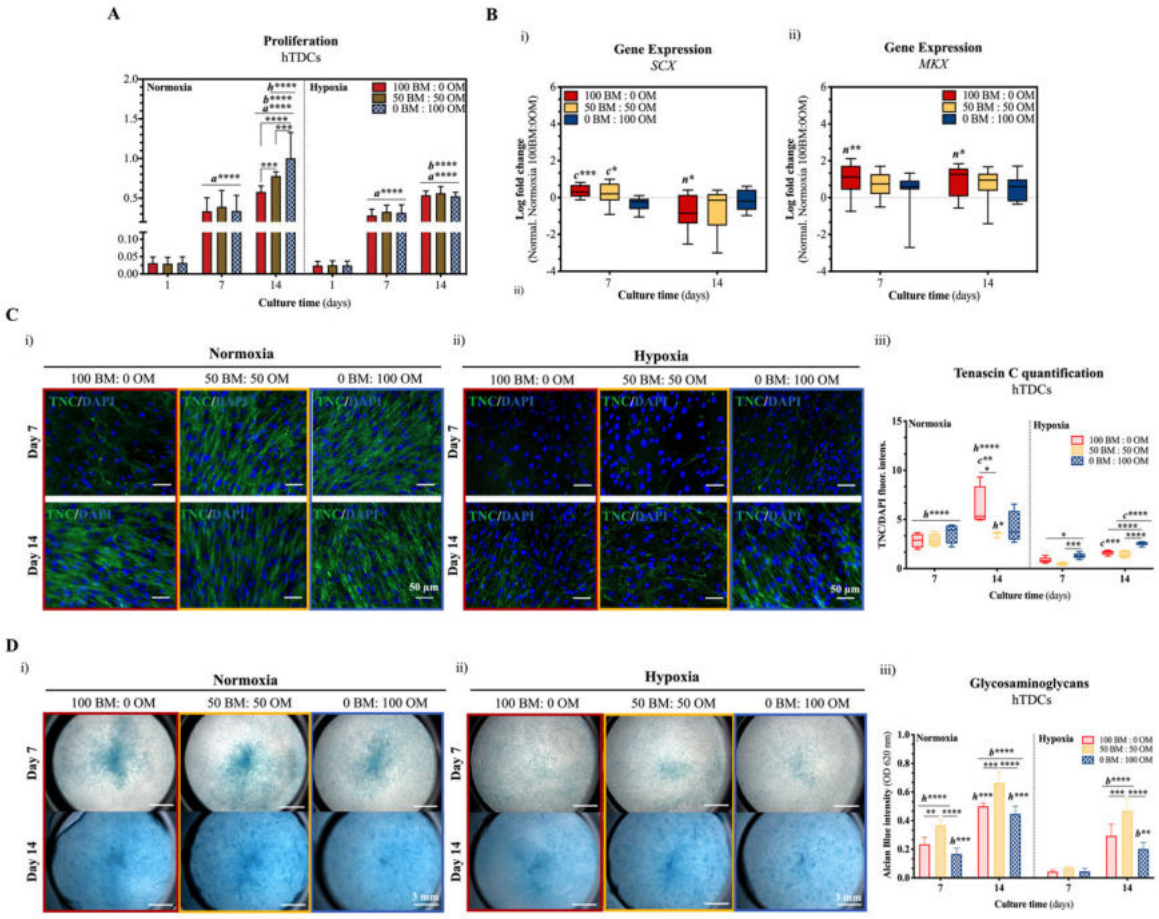

Figure 6.2 | Effect of hypoxia on the expression of tenogenic markers by hTDCs in the presence of increasing osteogenic supplementation during culture time. (A) Cell proliferation of hTDCs up to 14 days of culture under both normoxia and hypoxia and increasing OM ratio. Data are represented as means ± SD (n=3). (B) Gene expression of tenogenic-related markers (i) scleraxis (SCX) and (ii) mohawk (MKX) at 7 and 14 days of culture evaluated by RT-PCR. Expression of target genes was normalized to the basal condition (100 BM: 0 OM) of the correspondent day under normoxia and the log fold change calculated (n=3, five replicates). (C) Immunofluorescence of tenascin C under (i) normoxia and (ii) hypoxia at days 7 and 14, and correspondent (iii) fluorescence intensity ratio quantification. Scale bars, 50 μm. (D) Glycosaminoglycans deposited by hTDCs maintained under (i) normoxia and (ii) hypoxia in the presence of increasing ratios of OM. Data are represented as means ± SD (n=3). Scale bars, 3 mm. (iii) Glycosaminoglycan quantification at 7 and 14 days of culture. For A-D, statistically significant differences are shown as *, $p < 0.05$; **, $p < 0.01$; ***, $p < 0.001$; ****, $p < 0.0001$; a, b and c are statistically significant in comparison with the same condition at days 1, 7 and 14, respectively; h is statistically significant in relation to the same condition at hypoxia; n is statistically significant in relation to the same condition at normoxia. Legend: BM: basal medium; OM: osteogenic medium.

6.3.3. Crosstalk between pre-OBs and hTDCs under hypoxia regulates the expression of osteogenic-markers regardless of OM supplementation in contrast with the expression of tenogenic-markers

We first determined how the combination of 5% O_2, increasing ratios of osteogenic supplementation, and crosstalk between pre-OBs and hTDCs (direct contact co-culture system) would influence the expression of bone- and tendon-related markers.

Similarly, to single cultures, exposure to low oxygen tension resulted in a significant decrease in DNA content compared to normoxia (Supplementary Figure S6.4A). We further assessed the effect of low oxygen tension on the expression of bone-related markers in direct contact co-cultures biochemically, and gene and protein levels. The activity of ALP was found to be significantly reduced under hypoxia compared to normoxia. Still, compared to single cultures of pre-OBs cultured under the same conditions, the crosstalk occurring at direct co-cultures induced a higher activity of this enzyme, independently of OM supplementation (Supplementary Figure S6.4B, day 7: d^{**}, $p < 0.01$; d^{****}, $p < 0.0001$; day 14: d^{***}, $p < 0.001$; d^{****}, $p < 0.0001$). The synergy between hypoxia and increasing osteogenic supplementation induced a significantly lower deposition of mineralized matrix compared to the basal medium condition, at 14 days of culture, and also co-cultures under normoxia (Supplementary Figure S6.4C). Surprisingly,

when compared to pre-OBs, an absence of OM enabled a higher matrix mineralization in co-cultured cells in comparison with pre-OBs (Supplementary Figure S6.4C, iii, $p< 0.05$), suggesting a role for cell-to-cell communication. At the transcript level, the expression of osteogenic markers (*RUNX2* and *COL1A1*) was analyzed (Figure 6.3A). Expression of studied osteogenic-related markers was found to be influenced by the restricted oxygen environment and crosstalk occurring in co-cultures, independently of OM supplementation (Figure 6.3A, i-ii). This effect was reflected, as soon as 7 days of culture, by the significant upregulation of the transcript levels of *RUNX2* and *COL1A1* under hypoxia compared to normoxia. Transcription levels of *COL1A1* were increased from day 7 to day 14 under 5% O_2 (Figure 6.3A, ii, $p< 0.05$). Additionally, significantly higher levels of *RUNX2* and *COL1A1* were observed in co-cultures under hypoxia compared to transcript levels evaluated in single cultures of pre-OBs under the same culture conditions (Figure 6.3A, 7/14 days, $p < 0.05$; $p < 0.01$; $p < 0.001$; $p < 0.0001$), being this expression independent of osteogenic medium supplementation. Yet, the same was not observed at the protein level. Even though co-culturing cells at 5% O_2 induced intracellular accumulation of COLI, this was significantly lower compared with single cultures of pre-OBs both at 7 and 14 days of culture (Figure 6.3D, i-iii; Pre-OBs, f; $p < 0.01$; $p < 0.0001$). Nevertheless, in co-cultures, the effect of hypoxia was observed at 7 days of culture by a higher synthesis of COLI compared with normoxia, regardless of OM supplementation (Figure 6.3D, iii: 100BM 0 OM, $p < 0.05$; 50 BM: 50 OM, $p < 0.01$).

Next, we evaluated the expression of tenogenic-related markers up to 14 days in co-cultures under normoxia and hypoxia by assessing GAGs deposition, gene expression of *SCX* and *MKX* and protein expression of tenascin C. First, exposure to hypoxia resulted in a reduction of GAGs deposition during culture time compared to normoxia (Supplementary Figure S6.4D). However, at 14 days of culture, the interaction between low oxygen and high OM supplementation induced a lower deposition of GAGs (Figure 6.3D, iii, 14 days: 0 BM: 14 OM, $p < 0.001$). At gene level, co-cultures maintained under low oxygen tension exhibited significantly higher transcript levels of *MKX* independently of OM supplementation, in comparison with cells under normoxia (Figure 6.3B, ii, 7 days: 100 BM: 0 OM, $p < 0.001$; 50 MB: 50 OM, $p < 0.05$; 0 BM: 100 OM, $p < 0.01$; 14 days: 100 BM: 0 OM, $p < 0.0001$; 50 MB: 50 OM, $p < 0.0014$; 0 BM: 100 OM, $p < 0.0001$) But the same was not observed for *SCX* transcript levels, which were only significantly higher in the presence of 100 BM: 0 OM and 0 BM: 100 OM compared with cells cultured in BM under normoxia (Figure 6.3B, i, $p < 0.01$). Nevertheless, cells co-cultured under 5% O_2 in high osteogenic supplementation presented significantly higher transcription levels of *MKX*, at both 7 and 14 days, in comparison with transcription levels for hTDCs maintained under the same conditions (Figure 6.3B, ii, 7 days: $p < 0.01$; 14 days: $p < 0.0001$). Yet, at 14 days of culture under hypoxia, transcription

levels of both *SCX* and *MKX* were simultaneously increased in BM condition in comparison with transcription levels of single cultures of hTDCs maintained under the same culture conditions (Figure 6.3B; $p < 0.0001$). Concerning the deposition of tenascin c, even though significantly lower at 7 days compared to normoxia (Figure 6.3E, i-iii, $p < 0.0001$), the synergy between 5% O_2 and OM supplementation recovered the deposition of TNC at 14 days of culture, although only significantly in 0 BM: 100 OM (Figure 6.3E, iii, $p < 0.001$).

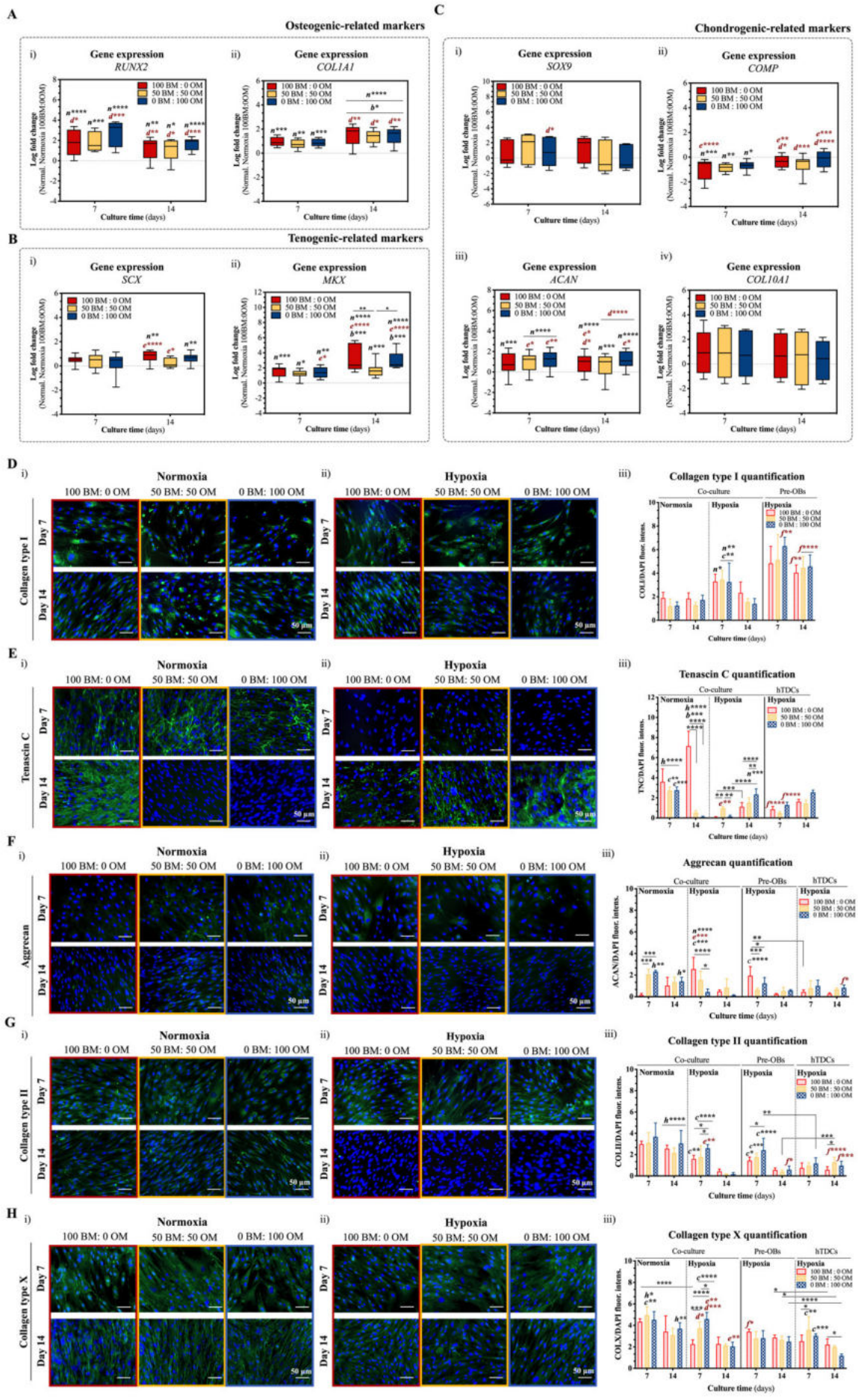
A
Osteogenic-related markers
i) Gene expression RUNX2
ii) Gene expression COL1A1
B
Tenogenic-related markers
i) Gene expression SCX
ii) Gene expression MKX
C
Chondrogenic-related markers
i) Gene expression SOX9
ii) Gene expression COMP
iii) Gene expression ACAN
iv) Gene expression COL10A1
100 BM : 0 OM
50 BM : 50 OM
0 BM : 100 OM
Log fold change (Normal. Normoxia 100BM:0OM)
Culture time (days)
D
Collagen type I
E
Tenascin C
F
Aggrecan
G
Collagen type II
H
Collagen type X
i) Normoxia
ii) Hypoxia
iii) Collagen type I quantification
Tenascin C quantification
Aggrecan quantification
Collagen type II quantification
Collagen type X quantification
Co-culture
Pre-OBs
hTDCs
Day 7
Day 14
50 µm

Figure 6.3 | Temporal expression of osteogenic-, tenogenic- and chondrogenic-related markers in direct co-cultures maintained in different ratios of osteogenic supplementation in hypoxic and normoxic setups. Gene expression of (A) osteogenic-related markers, (i) runt-related transcription factor 2 (*RUNX2*) and (ii) collagen type I alpha 1 chain (*COL1A1*); (B) Tenogenic-related markers (i) scleraxis (*SCX*) and (ii) mohawk (*MKX*); and (C) chondrogenic-related markers, sex-determining region Y-box 9 (*SOX9*) (i), cartilage oligomeric matrix protein (*COMP*) (ii), aggrecan (*ACAN*) (iii) and collagen type X alpha 1 chain (*COL10A1*) was determined by RT-PCR. Expression of target genes was normalized to the basal condition (100 BM: 0 OM) of the correspondent day under normoxia and the log fold change calculated (n=3, five replicates). Immunofluorescence of (D) collagen type I (COLI), (E) tenascin C, (F) aggrecan (ACAN), (G) collagen type II (COLII) and (H) collagen type X (COLX) in co-culture and single cultures at (i) normoxia and (ii) hypoxia for 14 days in the presence of increasing ratios of OM. Scale bars, 50 μm. Fluorescence intensity ratio quantification (iii) of proteins deposition. Data are represented as means ± SD. For A-H, statistically significant differences are shown as *, $p < 0.05$; **, $p < 0.01$; ***, $p < 0.001$; ****, $p < 0.0001$; b and c are statistically significant in comparison with the same condition at 7 and 14 days, respectively; d is statistically significant in correspondence with the same condition and culture time in pre-OBs; e is statistically significant in correspondence with the same condition and culture time in hTDCs; f is statistically significant in correspondence with the same condition in co-cultures maintained under hypoxia; h is statistically significant in correspondence with the same condition maintained under hypoxia at the correspondent culture time; n is statistically significant in correspondence with the same condition maintained under normoxia at the correspondent culture time; Legend: BM: basal medium; OM: osteogenic medium.

6.3.4. Deposition of hypertrophic matrix in direct contact co-cultures associated with chronic hypoxia exposure in the presence of osteogenic supplementation

We evaluated the expression of sex-determining region Y-box 9 (*SOX9*), cartilage oligomeric matrix protein (*COMP*), aggrecan (*ACAN*), and collagen type X alpha 1 chain (*COL10A1*) (Figure 6.3C). Transcription levels of *ACAN* were found to be upregulated during the culture period in hypoxia regardless of the presence of osteogenic factors compared with transcription levels in cells co-cultured in BM under normoxia (Figure 6.3C, iii, $p < 0.001$; $p < 0.0001$). However, the same was not observed for single cultures of pre-OBs and hTDCs (Supplementary Figure S6.5A, iii). On the contrary, *COMP* transcript levels were downregulated throughout culture time, even though only significantly at 7 days of culture (Figure

6.3C, ii, 100 BM: 0 OM: $p < 0.001$; 50 BM: 50 OM: $p < 0.01$; 0 BM: 100 OM: $p < 0.05$). Similarly, a down-regulation was observed for *COMP* transcription levels of hTDCs during culture time compared to the levels observed in hTDCs in BM under normoxia (Figure 6.3C, ii; Supplementary Figure S6.5A, ii). Still, these levels were significantly lower in comparison with direct co-cultures in the presence of BM at both 7 and 14 days (Figure 6.3C, ii, 7 days: $p < 0.0001$; 14 days: $p < 0.01$) and OM at only 14 days ($p < 0.001$) of culture. Pre-OBs expressed significantly higher *COMP* transcript levels at 7 days compared with direct co-culture levels (Supplementary Figure S6.5A, ii, $p < 0.0001$), although at 14 days of culture the opposite was observed (Figure 6.3C, ii, 100 BM: 0 OM: $p < 0.05$; 50 BM: 50 OM: $p < 0.001$; 0 BM: 100 OM: $p < 0.0001$). No significant differences were observed for *SOX9* (Figure 6.3C, i) and *COL10A1* (Figure 6.3C, iv) transcript levels.

We further assessed the deposition of chondrogenic ECM at the protein level by immunocytochemistry (Figure 6.3F-H). Matrix protein deposition in co-cultures was significantly affected by both low oxygen tension and the presence of high concentration of pro-osteogenic factors. Concerning ACAN deposition, an opposite effect was observed as soon as 7 days (Figure 6.3F). At this time, under hypoxia, the presence of OM resulted in a reduced deposition of ACAN compared with normoxia and even compared to cells maintained under BM conditions ($p < 0.0001$). On the contrary, besides the sustained deposition of collagenous matrix observed under hypoxia, the presence of OM in culture significantly induced the deposition of both COLII (Figure 6.3G, 0 BM: 100 OM, COLII: $p < 0.05$) and COLX (Figure 6.3H, COLX: $p < 0.05$, $p < 0.0001$) in comparison with basal medium and intermediate OM conditions. Compared with single cultures, the direct contact occurring at co-cultures induced higher deposition of COLII in comparison with hTDCs (Figure 6.3G, $p < 0.01$) and COLX in comparison with both hTDCs and pre-OBs (Figure 6.3H, hTDCs: $p < 0.01$; pre-OBs: $p < 0.0001$) maintained under the same culture conditions. Nevertheless, the hypoxic environment clearly induced an early expression of ACAN and COLII in single cultures of pre-OBs, while the opposing effect was observed for hTDCs where the highest deposition was found to occur at 14 days of culture, compared with cells maintained under normoxia (Supplementary Figure S6.5B-G). Co-cultures maintained in a hypoxic environment for long periods (14 days), exhibited a lower deposition of both COLII, ACAN and COLX, although this last one was much more sustained independently of medium supplementation (Figure 6.3F-G). Strikingly, when analyzing COLX/COLII ratio, a particularly higher deposition of hypertrophic matrix was observed co-cultures maintained under 5% O_2 in comparison with 21% (Table 6.1, Supplementary Table S7.2). A similar ratio of COLX/COLII was observed for pre-OBs under normoxia at 7 days, although only significantly for BM and intermediate OM

condition (Supplementary Table S6.2, pre-OBs, $p<0.01$). No significant differences were observed for single cultures of hTDCs.

Table 6.1 | Summary table of the ratio between COLX/COLII ratio in cells exposed to 5% O_2 for 7 and 14 days.

		Ratio COLX/COLII		
	Time	7 days	14 days	
Medium condition	100 BM: 0 OM	1.49±0.41	8.01±2.52 $^{b**, n****}$	Co-culture
	50 BM: 50 OM	2.31±1.71 ^{x*}	13.25±2.48 $^{b****, e****, n****}$	
	0 BM: 100 OM	1.78±0.22	11.15±5.23 $^{b****, d*, e****, n****}$	
	100 BM: 0 OM	3.46±2.07	6.02±1.91	Pre-OBs
	50 BM: 50 OM	1.59±0.45	8.40±4.63 ^{b**}	
	0 BM: 100 OM	2.54±2.31	5.88±3.94	
	100 BM: 0 OM	3.01±1.33	4.63±2.39 $^{x*, y*}$	hTDCs
	50 BM: 50 OM	4.10±2.23	1.74±0.68	
	0 BM: 100 OM	2.19±0.38	1.55±1.08	

Statistically significant differences are shown as *, $p<0.05$; **, $p<0.01$; ****, $p<0.0001$; x and y are statistically significant in comparison with cells in 100 BM: 0 OM and 50 BM: 50 OM, respectively; b is statistically significant in comparison with the same condition at 7 days; d and e are statistically significant in comparison with the same condition in pre-OBs and hTDCs, respectively; n is statistically significant to normoxia.

6.3.5. Gene activation of hypoxia-inducible factors, interface-related markers and hedgehog pathway cascade activation are governed by osteogenic supplementation in direct co-cultures under acute exposure to hypoxia

Both HIF1A and HIF2A participate in the regulation of hypoxia-dependent genes through complex and, sometimes, antagonistic interactions binding to the same hypoxia response elements (reviewed in [33]). In some cell types (namely from cancer), the highest activity of HIF1A is rapidly observed, while HIF2A activity is continuous even after long periods [9].

Therefore, we started by determining the temporal expression of both hypoxia-inducible factors at the gene level, and its influence on the expression of relevant interface markers by cells co-cultured at 21% O_2 and 5% O_2 in the presence of increasing concentrations of osteogenic medium (Figure 6.4). An early increase of *HIF1A* transcription levels was observed for co-cultured cells in the presence of OM as soon

as 10 minutes in comparison with cells maintained in BM under normoxia, although not significantly (Figure 6.4B-C). While, in the absence of osteogenic factors, *HIF1A* transcript levels were only increased, compared to normoxia, after 3 hours (Figure 6.4A). The combined influence of 5% O_2 and OM supplementation was found to coordinate the transcriptional levels of *HIF2A*, as observed by a significant upregulation after 3 hours of culture compared with *HIF2A* transcript levels of cells co-cultured in BM (Figure 6.4A-C, 50 BM: 50 OM, $p < 0.05$; 0 BM: 100 OM, $p < 0.05$). Transcription levels of *RUNX2* were found to suffer a temporal activation governed by the presence of OM when under hypoxia. After 45 minutes, an increase in *RUNX2* transcription levels was registered for OM conditions when compared with cells in BM under normoxia. However, at 24 hours of culture, this effect was not observed as a significant upregulation was visualized in all tested medium conditions (Figure 6.4A-C, ii, 100 BM: 0 OM, $p < 0.01$; 50 BM: 50 OM; 0 BM: 100 OM, $p < 0.0001$). Transcriptional levels of *SOX9* were only found to be significantly upregulate, compared with BM in normoxia, after 48 hours of culture in BM conditions (Figure 6.4A, ii, 100 BM: 0 OM, $p <0.0001$). Regarding the expression of collagenous matrix genes, transcriptional levels of *COL2A1* and *COL10A1* were found to follow the expression of both *HIF1A* and *HIF2A* when cells were maintained in the presence of OM supplementation (Figure 6.4A, C). This was observed by the significantly higher transcription levels of *COL10A1* (50 BM: 50 OM: $p <0.05$; 0 BM: 100 OM, $p <0.001$) and *COL2A1* (50 BM: 50 OM; 0 BM: 100 OM, $p <0.0001$) at 3 hours of exposure of direct co-cultures to hypoxia compared with BM under normoxia.

We also explored the activation of the hedgehog (Hh) signaling cascade (Figure 6.4D). Strikingly, a direct correlation between hypoxic conditions coupled with the presence of osteogenic factors was found to temporally influence the transcription levels of Indian Hedgehog (*IHH*), responsible for the activation of the Hh pathway in the fibrocartilaginous insertion site. This was observed by high levels of *IHH* transcript at condition 50 BM: 50 OM, coordinated with the high transcription's levels of *HIF1A* and *HIF2A* at 3 hours of exposure, resulting in membrane-bound receptor Patched1 (*PTCH1*) and zinc finger protein (*GLI*1) transcription factor downstream activation at 24 h (Figure 6.4B-D, i-ii). High content of osteogenic factors under hypoxia was found to induce a faster or repress the activation of *IHH* pathway cascade (Figure 6.4D, iii). Nonetheless, under basal conditions (100BM:0OM), even though *IHH* was found to be upregulated at 48 h in coordination with *HIF2A* and *SOX9* upregulation, transcription levels of *PTCH1* and *GLI*1 were downregulated (Figure 6.4D, i).

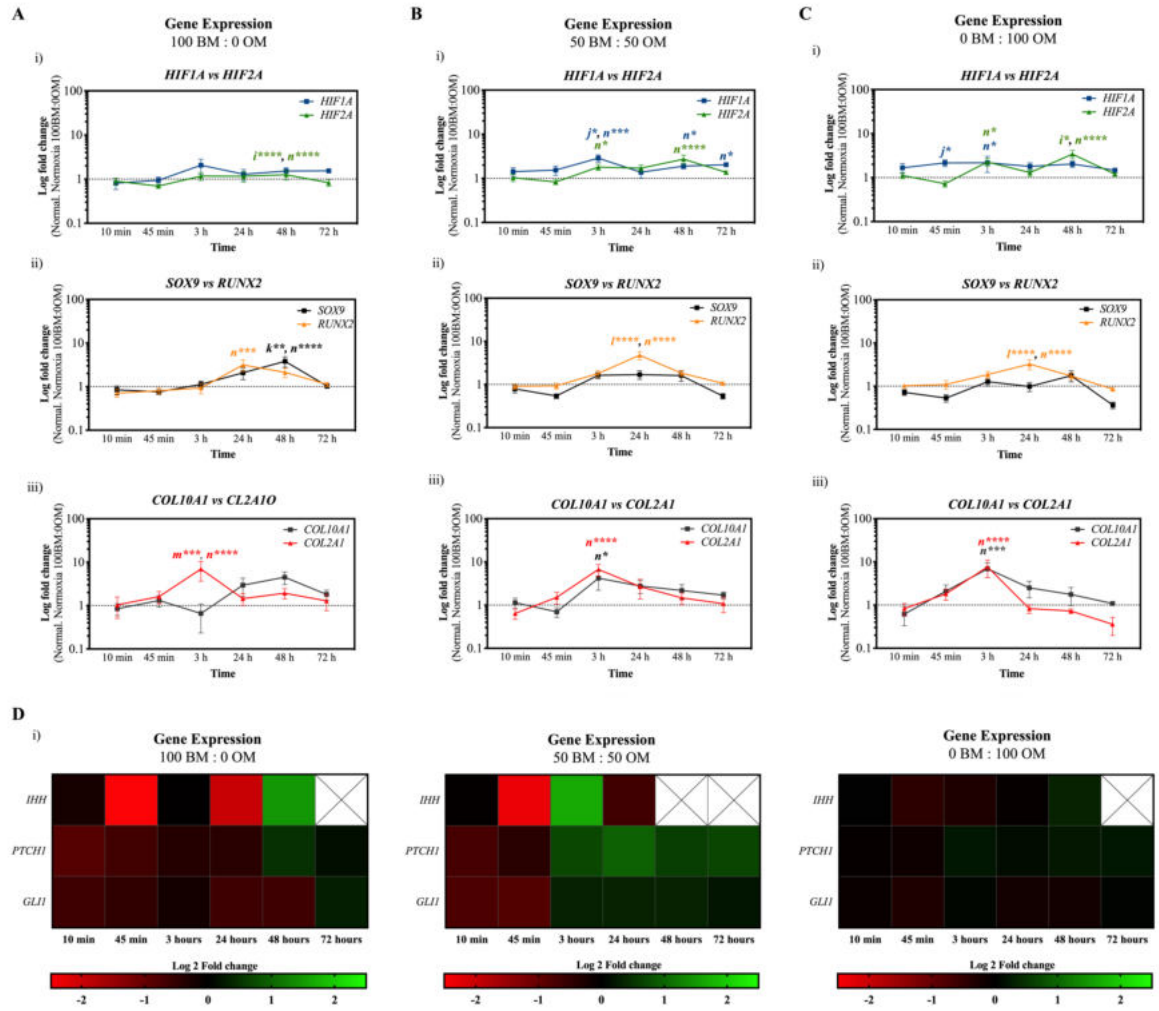

Figure 6.4 | Early gene expression of hypoxia-inducible factors, transcription factors and chondrogenic-related matrix genes in direct co-cultures at low oxygen tension in increasing ratios of osteogenic supplementation. (A-C) Temporal transcriptional expression of (i) hypoxia inducible factor 1 alpha (*HIF1A*) and hypoxia inducible factor 2 alpha (*HIF2A*), (ii) sex-determining region Y-box 9 (*SOX9*) and runt-related transcription factor 2 (*RUNX2*), and (iii) collagen type X alpha 1 chain (*COL10A1*) and collagen type II alpha 1 chain (*COL2A1*) was determined after 10 minutes and up to 3 hours in co-cultures in the presence of (A) 100BM:0 OM, (B) 50 BM: 50 OM and (C) 0 BM: 100 OM by RT-PCR. Expression of target genes was normalized to the basal condition (100 BM: 0 OM) of the correspondent day under normoxia and the log fold change calculated (n=3, five replicates). (D) Heatmap mapped to the transcriptional expression of Indian hedgehog (*IHH*), patched 1 (*PTCH1*) and zinc finger protein GLI1 (*GLI1*) in cells co-cultured in the presence of only basal medium (i), basal and osteogenic medium (ii) and only osteogenic medium (iii). Expression of target genes was normalized to the basal condition (100 BM: 0 OM) of the correspondent day under normoxia and the log 2 fold change calculated (n=3, five replicates).The cluster separates the differently expressed genes by color with positive or

negative row-scaled scores represented in green and red, respectively. For A-C, statistically significant differences are shown as *, $p < 0.05$; **, $p < 0.01$; ***, $p < 0.001$; ****, $p < 0.0001$; i, j, k, l, m and o are statistically significant in correspondence with the transcription levels of *HIF1A, HIF2A, RUNX2, SOX9, COL10A1* and *COL2A1* at the respective time in normoxia; n is statistically significant in correspondence with the same condition maintained under normoxia at the correspondent culture time. Color is in correspondence with the analyzed gene. Legend: BM: basal medium; OM: osteogenic medium.

6.3.6. Co-effect between cellular crosstalk and osteogenic factors is an important regulator of HIF1A stabilization, and HIF2A and SOX9 translocation under prolonged exposure to hypoxia

We further studied the localization and stabilization of both HIF1A and HIF2A in co-culture systems, under 5% O_2, and in the presence of increasing ratios of OM, at protein level. First, the concentration of HIF1A in the extracellular environment was detected in the different medium conditions by ELISA (Figure 6.5). In comparison with co-cultured cells maintained in BM under normoxia, the presence of OM in hypoxia clearly reduced the concentration of extracellular HIF1A (Figure 6.5A). Simultaneously, when assessing the levels of reactive oxygen species (ROS) in the extracellular environment, once again the same tendency was observed for cells co-cultured in the presence of OM, as extracellular ROS was significantly reduced when compared to cells in BM (Figure 6.5B; 10-45 minutes: $p < 0.0001$; 3 hours: 50 BM: 50 OM, $p < 0.01$, 0 BM: 100 OM, $p < 0.0001$; 24 hours: 50 BM: 50 OM, $p < 0.001$, 0 BM: 100 OM, $p < 0.01$; 48 hours: 50 BM: 50 OM, $p < 0.001$, 0 BM: 100 OM, $p < 0.0001$; 72 hours: 50 BM: 50 OM, $p < 0.05$, 0 BM: 100 OM, $p < 0.01$) and in comparison with co-cultures maintained under BM in normoxia for the same time periods (Figure 6.5B, $p < 0.0001$). Interestingly, at 3 hours of culture under hypoxia, HIF1A was also found to be accumulated around the cell nuclei near the mitochondria (Figure 6.5C, i-iii). Whereas cells under normoxia, presented a highly dispersed HIF1A distributed across the cell cytoplasm.

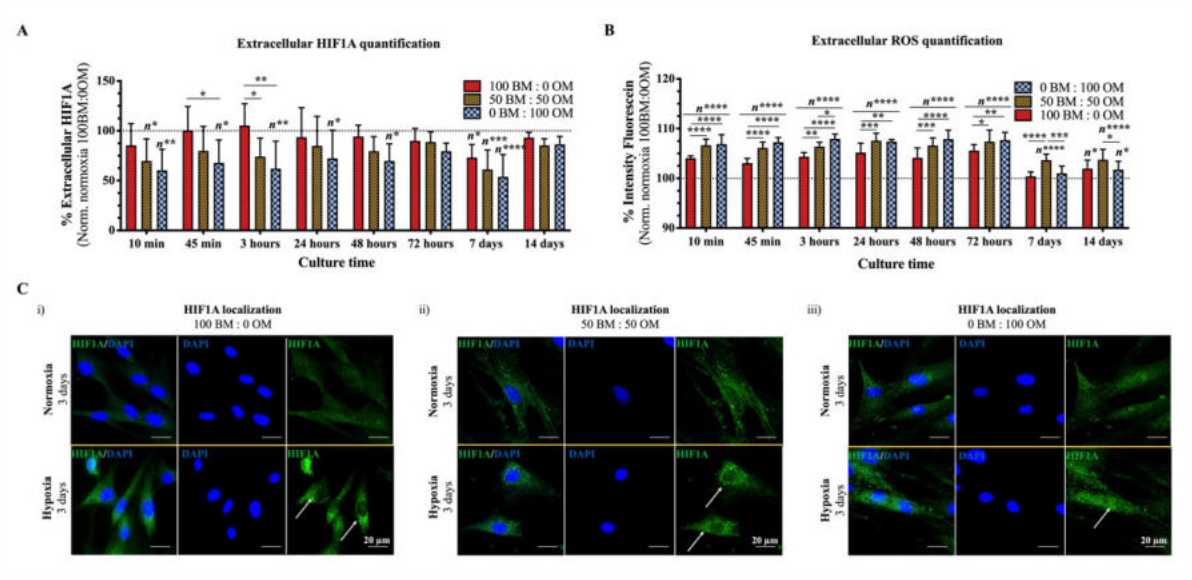

Figure 6.5 | Temporal extracellular HIF1A and ROS quantification in direct co-cultures. (A) Protein levels of extracellular HIF1A. Results were normalized to the basal condition of normoxia at the correspondent timepoint and represented as % extracellular HIF1A ± SD. (B) Temporal production of ROS under hypoxia in the presence of different ratios of OM. Results were normalized to the basal condition of normoxia at the correspondent timepoint and data are represented as % intensity of fluorescence ± SD. Statistically significant differences are shown as *, $p < 0.05$; **, $p < 0.01$; ***, $p < 0.001$; ****, $p < 0.0001$. (C) Immunolabelling of HIF1A (green) under normoxia and hypoxia at day 3. Arrows point the localization closer to the mitochondria. Scale bar, 20 µm. For B-C, n is statistically significant in correspondence with the same condition maintained under normoxia at the correspondent culture time. Legend: BM: basal medium; OM: osteogenic medium.

Assessing nuclei co-localization of HIF1A under hypoxia, a significant reduction from day 3 to day 7 was noticed only in cells maintained in BM conditions (Figure 6.6B, ii, 50 BM: 50 OM, 0 BM: 100 OM, $p < 0.0001$), suggesting stabilization of HIF1A inside the cells in the presence of OM. The same tendency was observed compared with single cultures of pre-OBs and hTDCs maintained under the same conditions (Figure 6.6B, ii, pre-OBs, hTDCs, $p < 0.0001$). In single cultures, the effect of hypoxia on HIF1A nuclei co-localization was only noticeable on pre-OBs after 7 days of exposure, given by the increase observed independently of medium supplementation compared to normoxia (Supplementary Figure S6.6A-B). In the case of HIF2A, a clear and significant influence of hypoxia and OM was observed at 7 days of culture under hypoxia (Figure 6.6C). By this time, the direct contact occurring in the presence of osteogenic medium, induced a robust nuclear co-localization of HIF2A compared to normoxia (Figure 6.6D, $p < 0.0001$) and with single cultures of pre-OBs (50 BM: 50 OM, $p < 0.001$; 0 BM: 100 OM, $p <$

0.01) and hTDCs (50 BM: 50 OM, $p < 0.001$; 0 BM: 100 OM, $p < 0.05$). Up to 14 days of culture, even though still localized in the nucleus, HIF2A was found to suffer a translocation outside. Interestingly, the opposite was observed for singles cultures. Under hypoxia, HIF2A co-localization in pre-OBs was found to be influenced by the presence of OM at 14 days (Supplementary Figure S6.7A-B, ii) whilst the highest co-localization in hTDCs was found to occur under normoxia independently of medium supplementation (Supplementary Figure S6.7C-D).

As previously demonstrated, HIF2A has an important role in SOX9 activation [34]. We wanted to understand how the crosstalk occurring in direct co-cultures alongside the presence of different concentrations of pro-osteogenic factors would influence the activation of this transcription factor. Even though SOX9 nuclei translocation was observed in direct co-cultures at 7 days of culture due to HIF2A activation (Figure 6.6C, v; 6.6D, iii), the bi-directional crosstalk coupled with the presence of osteogenic factors clearly resulted in a significantly higher co-localization of SOX9 in the nuclei compared with basal condition (Figure 6.6F, $p < 0.05$; $p < 0.01$). After 14 days, the highest co-localization of SOX9 was found to occur in direct co-cultures under hypoxia, even when compared with single cultures, and independently of HIF2A nuclei localization (Figure 6.6F, ii). Nevertheless, the effect of HIF2A and presence of osteogenic medium was also observed in single cultures of pre-OBs (Supplementary Figure S6.8A-B), but SOX9 nuclei translocation in hTDCs was found to occur independently of HIF2A translocation under hypoxia and osteogenic supplementation (Supplementary Figure S6.8C-D).

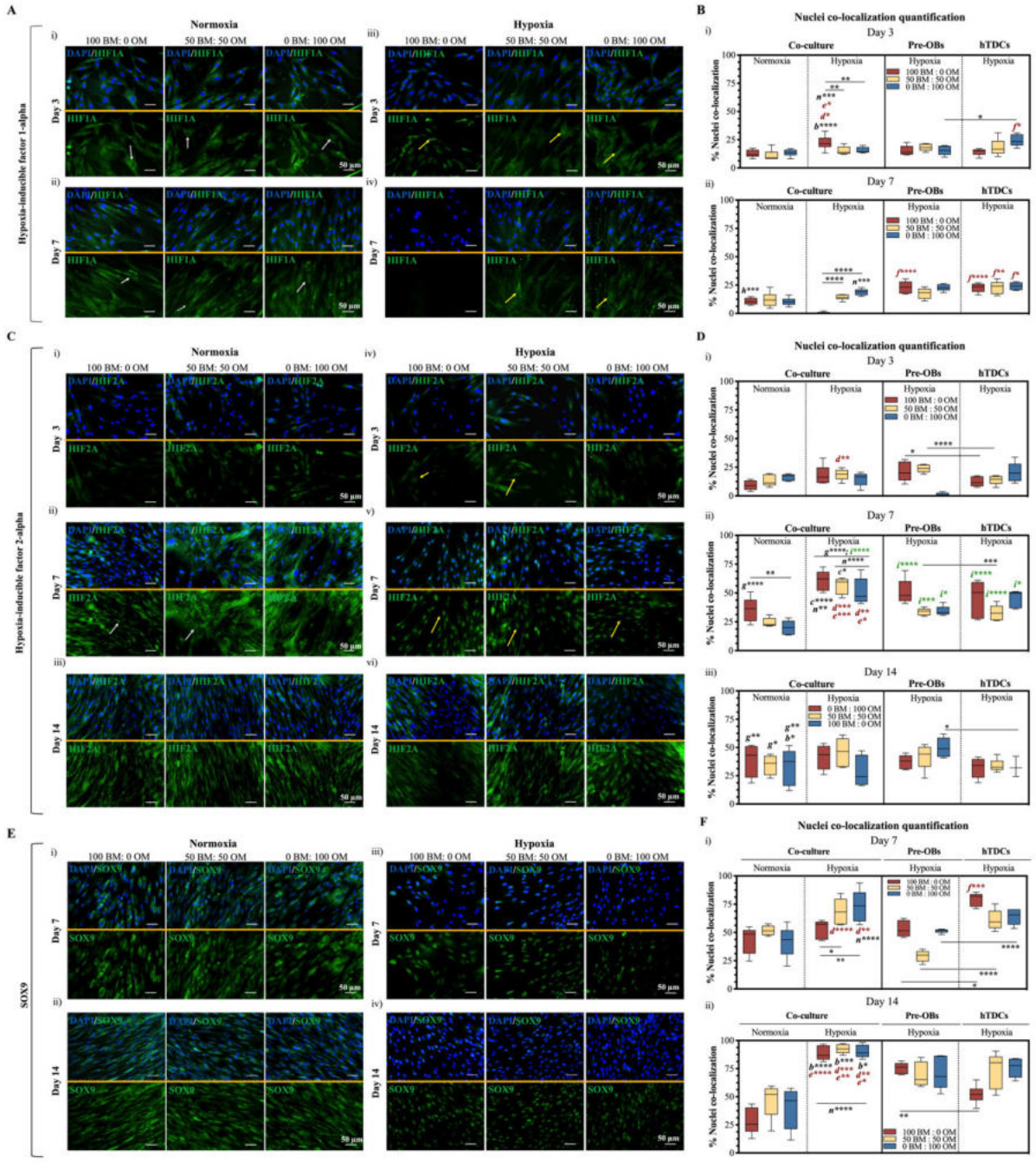

Figure 6.6 | Hypoxia increases HIF2A nuclear accumulation and SOX9 activation in direct co-cultured cells under hypoxia. Nuclear protein localization was assessed by immunofluorescence of (A) hypoxia inducible factor 1 alpha (HIF1A), (C) hypoxia inducible factor 2 alpha (HIF2A) and (E) sex-determining region Y-box 9 (*SOX9*), and nuclei staining with DAPI for co-cultures maintained under both 21% O_2 and 5% O_2 in the presence of increasing ratios of OM. (B, D, F) Percentage of nuclei co-localization. Scale bars, 50 µm. Arrows point the nuclei localization. Data are represented as % co-localization ± SD. Statistically significant differences are shown as *, $p < 0.05$; **, $p < 0.01$; ***, $p < 0.001$; ****, $p < 0.0001$; g, b and c are statistically significant in comparison with the same condition at 3, 7 and 14

days, respectively; d is statistically significant in correspondence with the same condition and culture time in pre-OBs; e is statistically significant in correspondence with the same condition and culture time in hTDCs; f is statistically significant in correspondence with the same condition in co-cultures maintained under hypoxia; h is statistically significant in correspondence with the same condition maintained under hypoxia at the correspondent culture time; n is statistically significant in correspondence with the same condition maintained under normoxia at the correspondent culture time; i is statistically significant in correspondence with HIF1A quantification for the respective condition and day under hypoxia. Legend: BM: basal medium; OM: osteogenic medium.

6.4. DISCUSSION

Oxygen tensions are reported to widely vary across human tissues. Organs such as large intestine, uterus, and skeletal muscle are in the lower spectrum of oxygen tension, presenting variations between 0 – 6.5% O_2 tension [35]. On the opposite side of the spectrum, tissues associated with the respiratory and circulatory systems can reach tensions up to 15% O_2 [35]. Notably, O_2 tensions can suffer sequential fluctuations after exposure to a demanding metabolic activity, as already described for the skeletal muscle, which, after incremental exercise, has presented lower levels of oxygenation [36]. In musculoskeletal interfaces, such as the one found in tendon-to-bone, different oxygen levels are required for the maintenance and determination of cells fate in their natural environment. When trying to understand important cell interactions *in vitro* as models of the native tissue, there is a huge need to perform more robust and relevant cell cultures. Having this into consideration, in this study, the effect of two very important biochemical factors, oxygen supply, and media composition, were assessed in an optimized *in vitro* model of tendon-to-bone interface [26].

As a first step to understand the modulatory effect of different oxygen tensions (21% O_2 and 5% O_2), we investigated the expression of bone- and tendon-related markers on single culture systems of pre-OBs and hTDCs maintained in the presence of previously optimized medium condition up to 14 days of culture. Concerning single cultures of pre-OBs, we observed an independent effect of hypoxia on the osteogenic cascade. Long culture exposure to low oxygen tension resulted in a down-regulation of *RUNX2*, alkaline phosphatase activity, and matrix mineralization, demonstrating an impairment in osteoblast differentiation as a response to stress [37]. A similar effect was observed in human pre-osteoblastic cell lines and human mesenchymal stem cells, where the exposure to low oxygen tensions before a proper osteoblast differentiation, clearly affected matrix mineralization and expression of osteogenic markers [37-39]. Moreover, this impairment could also be related to simultaneous activation of HIF2A activation, known to

negatively regulate osteoblastogenesis [34]. Interestingly, the synthesis of collagen type I was found to be uncompromised, leading to intracellular accumulation.

Focusing on the tendon-like niche, represented by single cultures of hTDCs, the synergistic effect of hypoxia and osteogenic supplementation was clearly found to rescue the deposition of tenascin c, a tenogenic ECM protein. Additionally, the hypoxic environment resulted in an early cell differentiation and maturation, as suggested by the initial *SCX* transcription simultaneous to the high transcription levels of *MKX*, playing a critical role in the deposition of COLI [32]. Nevertheless, when exposed to 21% O_2 hTDCs deposited increased amounts of glycosaminoglycans, as demonstrated by alcian blue staining. This high deposition is associated with human tendon degeneration, commonly resulting from the formation of scar tissue [40] and aberrant cartilaginous-like matrix [41], validating the beneficial effect of hypoxia (5% O_2) in *in vitro* single cultures of hTDCs.

Subsequently, a direct co-culture system was established to understand the influence of direct crosstalk under low oxygen tension on the modulation and expression of interface-related markers. Additionally, the expression of hypoxia-inducible factors was explored and correlated with the expression of different markers. At the gene level, we were able to see that, under hypoxia, the presence of OM in early time points induced an early transcriptional activation of *HIF1A*, that significantly increase the transcription of *RUNX2*, indicating an early induction of hypertrophic differentiation governed by *HIF1A*, as also observed by Lee et al both *in vitro* and *in vivo* [42]. This was confirmed at the protein level by studying the deposition of characteristic ECM found in the tendon-to-bone interface using the established co-cultures. After chronic exposure to hypoxia in the presence of osteogenic factors, while deposition of aggrecan and type I and type II collagens started to diminish, a high deposition of a hypertrophic matrix was determined by the high ratio of COLX compared with COLII in direct co-cultures. The stated phenotypic changes were also found in the growth plate during endochondral bone formation, in which chondrocytes undergo a chronological phenotypic change, first associated with a hypoxic environment, towards the formation of bone tissue always under the influence of oxygen [43]. Nevertheless, chronic exposure (7 days) has also induced HIF2A translocation and nuclear accumulation, followed by SOX9 translocation and activation. Concurring with Dy et al [44], we also observed that SOX9 is required for final hypertrophy, alongside the expression and deposition of collagen type X in direct co-cultures under hypoxia. Additionally, the coordination between hypoxia and the presence and absence of osteogenic factors was found to induce different responses in the Hh pathway cascade. In the development of the musculoskeletal system namely during endochondral bone ossification, indian hedgehog (Ihh) is known to be expressed by pre-hypertrophic chondrocytes while it stimulates the expression of parathyroid hormone-related peptide

(PTHrP) [45]. Acting together, Ihh and PTHrP form a negative feedback loop that regulates chondrogenic differentiation, from pre-hypertrophic to hypertrophic chondrocytes [46]. Moreover, Hh signaling cell-signaling cascade results in the final activation of Gli expression, in particular Gli1, serving as a marker of active Hh signaling [47, 48]. Interestingly, in our study, the downstream activation of Hh that resulted in the final upregulation of *GLI1* was found to be correlated with the activation of both hypoxia inducible factors (*HIF1A* and *HIF2A*) when under the presence of mild osteogenic supplementation resulting in a hypertrophy of chondrocytes in later time points. Strikingly, the expression of Gli1 in the insertion site has suggested that Hh signaling pathway is involved in the differentiation of the fibrocartilaginous insertion site [49]. In contrast, even though, *IHH* was upregulated under hypoxia in basal culture conditions, the downstream activation of *GLI1* was not observed not either the deposition of hypertrophic matrix. Nonetheless, high osteogenic factors were found to inhibit the expression of *GLI1* at later stages of culture, maybe due to an inhibition of osteogenesis under hypoxia.

Several studies have also demonstrated the beneficial effect of HIF1A in reducing ROS cellular production by switching energy production to glycolysis via numerous pathways [50-53] and the important role of ROS in HIF1A stabilization. Alongside, HIF1A has been reported as an essential regulator of the response to oxidative stress and ROS production by targeting the mitochondria [52, 54]. However, some controversy still arises concerning ROS origin and hypoxia, as some works have reported that ROS production requires O2, being assumed that ROS generation is attenuated when cells are maintained under hypoxic conditions [55] while others suggested a direct link between high mitochondrial ROS production and HIF-1α stabilization [56]. In our work, lower ROS levels were observed in the extracellular environment of cells maintained under 5% O2 compared with 21% O2. Moreover, while assessing the expression of HIF1A at the protein level, low quantities of extracellular HIF1A were found in hypoxic environment compared to the levels in normoxia, which could be associated with the low levels of ROS quantified in the extracellular medium [53], meaning that extracellular ROS could have a triggering effect on the secretion of HIF1A-containing exosomes or vesicles. Strikingly, the higher concentration of extracellular HIF1A in co-cultures under normoxia could be associated with a mediation signaling occurring in between cells as a response to oxidative stress, constituting a mechanism to make the recipient cell more tolerant to oxidative processes, reducing cell death [57]. Additionally, we found that HIF1A accumulate within the cell, mainly near the mitochondria, sustaining a probable stabilization of HIF1A [52]. However, the mechanism behind ROS/HIF-1 stabilization should be addressed in future studies and correlated with the expression of important tendon-to-bone interface-markers, as recent works

have also demonstrated the important role of ROS and HIF-1 interplay in cells osteochondrogenic differentiation, namely in vascular smooth muscle [58, 59]

In summary, we have demonstrated that exposure of pre-OBs and hTDCs to lower oxygen tension induces phenotypic changes by impairing osteogenesis and inducing cell maturation, respectively. Moreover, low oxygen tension and cell-cell interactions occurring in direct co-cultures, in the presence of osteogenic factors, clearly modulates the downstream activation of chondrogenic and osteoblastic pathways towards the expression of an osteochondrogenic phenotype. The effect of hypoxia in promoting this progression requires an initial transcriptional activation *HIF1A* and stabilization near the nucleus, and a later activation *HIF2A* governing the final hypertrophic differentiation regulated by SOX9. These results highlight the importance of biochemical factors on the establishment of *in vitro* models that aim to mimic as close as possible the physiological conditions found in complex tissues as the tendon-to-bone interface.

6.5. ACKNOWLEDGEMENTS

The authors thank to Hospital da Prelada (Porto, Portugal) for providing lipoaspirate tissue (Plastic Surgery Department) and tendon tissue (Orthopedic Department) samples. The authors acknowledge the financial support from the European Union Framework Programme for Research and Innovation HORIZON2020, under the TEAMING Grant agreement No 739572 - The Discoveries CTR, the ERC Grant CoG MagTendon nr 772817, FCT– Fundação para a Ciência e a Tecnologia for the PhD grant of IC (PD/BD/128088/2016).

6.6. REFERENCES

[1] M.C. Simon, B. Keith, The role of oxygen availability in embryonic development and stem cell function, Nat Rev Mol Cell Biol 9(4) (2008) 285-296, 10.1038/nrm2354.

[2] E.-J. Yeo, Hypoxia and aging, Experimental & Molecular Medicine 51(6) (2019) 67, 10.1038/s12276-019-0233-3.

[3] Y. Yuan, V.F. Cruzat, P. Newsholme, J. Cheng, Y. Chen, Y. Lu, Regulation of SIRT1 in aging: Roles in mitochondrial function and biogenesis, Mech Ageing Dev 155 (2016) 10-21, 10.1016/j.mad.2016.02.003.

[4] H.E. Ryan, J. Lo, R.S. Johnson, HIF-1 alpha is required for solid tumor formation and embryonic vascularization, EMBO J 17(11) (1998) 3005-3015, 10.1093/emboj/17.11.3005.

[5] P. Carmeliet, Y. Dor, J.-M. Herbert, D. Fukumura, K. Brusselmans, M. Dewerchin, M. Neeman, F. Bono, R. Abramovitch, P. Maxwell, C.J. Koch, P. Ratcliffe, L. Moons, R.K. Jain, D. Collen, E. Keshet, Role

of HIF-1α in hypoxia-mediated apoptosis, cell proliferation and tumour angiogenesis, Nature 394(6692) (1998) 485-490, 10.1038/28867.

[6] M. Reiterer, R. Colaco, P. Emrouznejad, A. Jensen, H. Rundqvist, R.S. Johnson, C. Branco, Acute and chronic hypoxia differentially predispose lungs for metastases, Sci Rep 9(1) (2019) 10246, 10.1038/s41598-019-46763-y.

[7] G.L. Semenza, G.L. Wang, A Nuclear Factor Induced by Hypoxia via De Novo Protein Synthesis Binds to the Human Erythropoietin Gene Enhancer at a Site Required for Transcriptional Activation, Mol Cell Biol. 12(12) (1992) 5447-5454, 10.1128/mcb.12.12.5447.

[8] M.Y. Koh, G. Powis, Passing the baton: the HIF switch, Trends Biochem Sci 37(9) (2012) 364-72, 10.1016/j.tibs.2012.06.004.

[9] L. Holmquist-Mengelbier, E. Fredlund, T. Lofstedt, R. Noguera, S. Navarro, H. Nilsson, A. Pietras, J. Vallon-Christersson, A. Borg, K. Gradin, L. Poellinger, S. Pahlman, Recruitment of HIF-1alpha and HIF-2alpha to common target genes is differentially regulated in neuroblastoma: HIF-2alpha promotes an aggressive phenotype, Cancer Cell 10(5) (2006) 413-23, 10.1016/j.ccr.2006.08.026.

[10] M.Y. Koh, R. Lemos, Jr., X. Liu, G. Powis, The hypoxia-associated factor switches cells from HIF-1alpha- to HIF-2alpha-dependent signaling promoting stem cell characteristics, aggressive tumor growth and invasion, Cancer Res 71(11) (2011) 4015-27, 10.1158/0008-5472.CAN-10-4142.

[11] R. Noguera, E. Fredlund, M. Piqueras, A. Pietras, S. Beckman, S. Navarro, S. Pahlman, HIF-1alpha and HIF-2alpha are differentially regulated in vivo in neuroblastoma: high HIF-1alpha correlates negatively to advanced clinical stage and tumor vascularization, Clin Cancer Res 15(23) (2009) 7130-6, 10.1158/1078-0432.CCR-09-0223.

[12] J.-W. Lee, S.-H. Bae, J.-W. Jeong, S.-H. Kim, K.-W. Kim, Hypoxia-inducible factor (HIF-1)α: its protein stability and biological functions, Experimental & Molecular Medicine 36(1) (2004) 1-12, 10.1038/emm.2004.1.

[13] S.J. Karp, E. Schipani, B. St-Jacques, J. Hunzelman, H. Kronenberg, A.P. McMahon, Indian Hedgehog coordinates endochondral bone growth and morphogenesis via Parathyroid Hormone related-Protein-dependent and -independent pathways, Sci Rep 5 (2015) 10.1038/srep10290.

[14] B. Lanske, A.C. Karaplis, K. Lee, A. Luz, A. Vortkamp, A. Pirro, M. Karperien, L.H.K. Defize, C. Ho, R.C. Mulligan, A.-B. Abou-Samra, H. Jüppner, G.V. Segre, H.M. Kronenberg, PTH/PTHrP Receptor in Early Development and Indian Hedgehog–Regulated Bone Growth, Science 273(5275) (1996) 663, 10.1126/science.273.5275.663.

[15] F. Long, X.M. Zhang, S. Karp, Y. Yang, A.P. McMahon, Genetic manipulation of hedgehog signaling in the endochondral skeleton reveals a direct role in the regulation of chondrocyte proliferation, Development 128(24) (2001) 5099-5108.

[16] B. St-Jacques, M. Hammerschmidt, A.P. McMahon, Indian hedgehog signaling regulates proliferation and differentiation of chondrocytes and is essential for bone formation, Genes Dev. 13(16) (1999) 2072-2086, 10.1101/gad.13.16.2072.

[17] E.B. Rankin, A.J. Giaccia, E. Schipani, A central role for hypoxic signaling in cartilage, bone, and hematopoiesis, Curr Osteoporos Rep 9(2) (2011) 46-52, 10.1007/s11914-011-0047-2.

[18] P.C. W., P.J. Ratcliffe, Regulation of angiogenesis by hypoxia: role of the HIF system, Nat Med. 9(6) (2003) 677-684, 10.1038/nm0603-677.

[19] E. Zelzer, R. Mamluk, N. Ferrara, R.S. Johnson, E. Schipani, B.R. Olsen, VEGFA is necessary for chondrocyte survival during bone development, Development 131(9) (2004) 2161, 10.1242/dev.01053.

[20] Y. Wang, C. Wan, L. Deng, X. Liu, X. Cao, S.R. Gilbert, M.L. Bouxsein, M.C. Faugere, R.E. Guldberg, L.C. Gerstenfeld, V.H. Haase, R.S. Johnson, E. Schipani, T.L. Clemens, The hypoxia-inducible factor alpha pathway couples angiogenesis to osteogenesis during skeletal development, J Clin Invest 117(6) (2007) 1616-26, 10.1172/JCI31581.

[21] A.P. Kusumbe, S.K. Ramasamy, R.H. Adams, Coupling of angiogenesis and osteogenesis by a specific vessel subtype in bone, Nature 507(7492) (2014) 323-328, 10.1038/nature13145.

[22] R.S. Richardson, S. Duteil, C. Wary, D.W. Wray, J. Hoff, P.G. Carlier, Human skeletal muscle intracellular oxygenation: the impact of ambient oxygen availability, J Physiol 571(Pt 2) (2006) 415-24, 10.1113/jphysiol.2005.102327.

[23] P.M. Gross, D.D. Heistad, M.L. Marcus, Neurohumoral regulation of blood flow to bones and marrow, American Journal of Physiology-Heart and Circulatory Physiology 237(4) (1979) H440-H448, 10.1152/ajpheart.1979.237.4.H440.

[24] J.A. Spencer, F. Ferraro, E. Roussakis, A. Klein, J. Wu, J.M. Runnels, W. Zaher, L.J. Mortensen, C. Alt, R. Turcotte, R. Yusuf, D. Cote, S.A. Vinogradov, D.T. Scadden, C.P. Lin, Direct measurement of local oxygen concentration in the bone marrow of live animals, Nature 508(7495) (2014) 269-73, 10.1038/nature13034.

[25] I. Calejo, R. Costa-Almeida, R.L. Reis, M.E. Gomes, Enthesis Tissue Engineering: Biological Requirements Meet at the Interface, Tissue Eng Part B Rev 25(4) (2019) 330-356, 10.1089/ten.TEB.2018.0383.

[26] I. Calejo, R. Costa-Almeida, A.I. Goncalves, D. Berdecka, R.L. Reis, M.E. Gomes, Bi-directional modulation of cellular interactions in an in vitro co-culture model of tendon-to-bone interface, Cell Prolif 51(6) (2018) e12493, 10.1111/cpr.12493.

[27] T.D. Schmittgen, K.J. Licak, Analyzing real-time PCR data by the comparative CT method, Nat Protocols 3 (2008) 1101–1108, 10.1038/nprot.2008.73.

[28] K.J. Livak, T.D. Schmittgen, Analysis of relative gene expression data using real-time quantitative PCR and the 2(-Delta Delta C(T)) Method, Methods 25(4) (2001) 402-8, 10.1006/meth.2001.1262.

[29] M.W. Pfaffl, A new mathematical model for relative quantification in real-time RT-PCR, Nucleic Acids Res 29(9) (2001) e45-e45, 10.1093/nar/29.9.e45.

[30] M. Lúcio, C. Nunes, D. Gaspar, H. Ferreira, J.L.F.C. Lima, S. Reis, Antioxidant Activity of Vitamin E and Trolox: Understanding of the Factors that Govern Lipid Peroxidation Studies In Vitro, Food Biophysics 4(4) (2009) 312-320, 10.1007/s11483-009-9129-4.

[31] D. Huang, B. Ou, M. Hampsch-Woodill, J.A. Flanagan, R.L. Prior, High-Throughput Assay of Oxygen Radical Absorbance Capacity (ORAC) Using a Multichannel Liquid Handling System Coupled with a Microplate Fluorescence Reader in 96-Well Format, Journal of Agricultural and Food Chemistry 50(16) (2002) 4437-4444, 10.1021/jf0201529.

[32] Y. Ito, N. Toriuchi, T. Yoshitaka, H. Ueno-Kudoh, T. Sato, S. Yokoyama, K. Nishida, T. Akimoto, M. Takahashi, S. Miyaki, H. Asahara, The Mohawk homeobox gene is a critical regulator of tendon differentiation, Proc Natl Acad Sci U S A 107(23) (2010) 10538-10542, 10.1073/pnas.1000525107.

[33] R.H. Wenger, D.P. Stiehl, G. Camenisch, Integration of Oxygen Signaling at the Consensus HRE, Science Signaling 2005(306) (2005) re12, 10.1126/stke.3062005re12.

[34] C. Merceron, K. Ranganathan, E. Wang, Z. Tata, S. Makkapati, M.P. Khan, L. Mangiavini, A.Q. Yao, L. Castellini, B. Levi, A.J. Giaccia, E. Schipani, Hypoxia-inducible factor 2alpha is a negative regulator of osteoblastogenesis and bone mass accrual, Bone Res 7 (2019) 7, 10.1038/s41413-019-0045-z.

[35] T. Ast, V.K. Mootha, Oxygen and mammalian cell culture: are we repeating the experiment of Dr. Ox?, Nature Metabolism 1(9) (2019) 858-860, 10.1038/s42255-019-0105-0.

[36] K.-i. Shibuya, J. Tanaka, Skeletal Muscle Oxygenation During Incremental Exercise, Archives of Physiology and Biochemistry 111(5) (2003) 475-478, 10.3109/13813450312331342355.

[37] A. Salim, R.P. Nacamuli, E.F. Morgan, A.J. Giaccia, M.T. Longaker, Transient changes in oxygen tension inhibit osteogenic differentiation and Runx2 expression in osteoblasts, J Biol Chem 279(38) (2004) 40007-16, 10.1074/jbc.M403715200.

[38] C. Nicolaije, M. Koedam, J.P.T.M. van Leeuwen, Decreased oxygen tension lowers reactive oxygen species and apoptosis and inhibits osteoblast matrix mineralization through changes in early osteoblast differentiation, Journal of Cellular Physiology 227(4) (2012) 1309-1318, 10.1002/jcp.22841.

[39] G. D'Ippolito, S. Diabira, G.A. Howard, B.A. Roos, P.C. Schiller, Low oxygen tension inhibits osteogenic differentiation and enhances stemness of human MIAMI cells, Bone 39(3) (2006) 513-522, 10.1016/j.bone.2006.02.061.

[40] N. Gagliano, A. Menon, C. Martinelli, L. Pettinari, A. Panou, A. Milzani, I. Dalle-Donne, N.M. Portinaro, Tendon structure and extracellular matrix components are affected by spasticity in cerebral palsy patients, Muscles Ligaments Tendons J 3(1) (2013) 42-50, 10.11138/mltj/2013.3.1.042.

[41] K. Howell, C. Chien, R. Bell, D. Laudier, S.F. Tufa, D.R. Keene, N. Andarawis-Puri, A.H. Huang, Novel Model of Tendon Regeneration Reveals Distinct Cell Mechanisms Underlying Regenerative and Fibrotic Tendon Healing, Scientific Reports 7(1) (2017) 45238, 10.1038/srep45238.

[42] S.-H. Lee, X. Che, J.-H. Jeong, J.-Y. Choi, Y.-J. Lee, Y.-H. Lee, S.-C. Bae, Y.-M. Lee, Runx2 protein stabilizes hypoxia-inducible factor-1α through competition with von Hippel-Lindau protein (pVHL) and stimulates angiogenesis in growth plate hypertrophic chondrocytes, The Journal of biological chemistry 287(18) (2012) 14760-14771, 10.1074/jbc.M112.340232.

[43] P. Aghajanian, S. Mohan, The art of building bone: emerging role of chondrocyte-to-osteoblast transdifferentiation in endochondral ossification, Bone Research 6(1) (2018) 19, 10.1038/s41413-018-0021-z.

[44] P. Dy, W. Wang, P. Bhattaram, Q. Wang, L. Wang, R.T. Ballock, V. Lefebvre, Sox9 Directs Hypertrophic Maturation and Blocks Osteoblast Differentiation of Growth Plate Chondrocytes, Developmental Cell 22(3) (2012) 597-609, 10.1016/j.devcel.2011.12.024.

[45] A.M. DeLise, L. Fischer, R.S. Tuan, Cellular interactions and signaling in cartilage development, Osteoarthritis and Cartilage 8(5) (2000) 309-334, 10.1053/joca.1999.0306.

[46] B. St-Jacques, M. Hammerschmidt, A.P. McMahon, Indian hedgehog signaling regulates proliferation and differentiation of chondrocytes and is essential for bone formation, Genes Dev 13(16) (1999) 2072-2086, 10.1101/gad.13.16.2072.

[47] S. Ahn, A.L. Joyner, Dynamic Changes in the Response of Cells to Positive Hedgehog Signaling during Mouse Limb Patterning, Cell 118(4) (2004) 505-516, 10.1016/j.cell.2004.07.023.

[48] C.B. Bai, W. Auerbach, J.S. Lee, D. Stephen, A.L. Joyner, Gli2, but not Gli1, is required for initial Shh signaling and ectopic activation of the Shh pathway, Development 129(20) (2002) 4753.

[49] C.-F. Liu, A. Breidenbach, L. Aschbacher-Smith, D. Butler, C. Wylie, A Role for Hedgehog Signaling in the Differentiation of the Insertion Site of the Patellar Tendon in the Mouse, PLOS ONE 8(6) (2013) e65411, 10.1371/journal.pone.0065411.

[50] I. Papandreou, R.A. Cairns, L. Fontana, A.L. Lim, N.C. Denko, HIF-1 mediates adaptation to hypoxia by actively downregulating mitochondrial oxygen consumption, Cell Metab 3(3) (2006) 187-97, 10.1016/j.cmet.2006.01.012.

[51] G.L. Semenza, Hypoxia-inducible factor 1: regulator of mitochondrial metabolism and mediator of ischemic preconditioning, Biochim Biophys Acta 1813(7) (2011) 1263-8, 10.1016/j.bbamcr.2010.08.006.

[52] H.S. Li, Y.N. Zhou, L. Li, S.F. Li, D. Long, X.L. Chen, J.B. Zhang, L. Feng, Y.P. Li, HIF-1alpha protects against oxidative stress by directly targeting mitochondria, Redox Biol 25 (2019) 101109, 10.1016/j.redox.2019.101109.

[53] F. Chen, J. Chen, L. Yang, J. Liu, X. Zhang, Y. Zhang, Q. Tu, D. Yin, D. Lin, P.P. Wong, D. Huang, Y. Xing, J. Zhao, M. Li, Q. Liu, F. Su, S. Su, E. Song, Extracellular vesicle-packaged HIF-1alpha-stabilizing lncRNA from tumour-associated macrophages regulates aerobic glycolysis of breast cancer cells, Nat Cell Biol 21(4) (2019) 498-510, 10.1038/s41556-019-0299-0.

[54] H. Zhang, M. Bosch-Marce, L.A. Shimoda, Y.S. Tan, J.H. Baek, J.B. Wesley, F.J. Gonzalez, G.L. Semenza, Mitochondrial autophagy is an HIF-1-dependent adaptive metabolic response to hypoxia, J Biol Chem 283(16) (2008) 10892-903, 10.1074/jbc.M800102200.

[55] T.P. Cash, Y. Pan, M.C. Simon, Reactive oxygen species and cellular oxygen sensing, Free Radic Biol Med 43(9) (2007) 1219-1225, 10.1016/j.freeradbiomed.2007.07.001.

[56] A. Hielscher, S. Gerecht, Hypoxia and free radicals: role in tumor progression and the use of engineering-based platforms to address these relationships, Free Radic Biol Med 79 (2015) 281-291, 10.1016/j.freeradbiomed.2014.09.015.

[57] M. Eldh, K. Ekström, H. Valadi, M. Sjöstrand, B. Olsson, M. Jernås, J. Lötvall, Exosomes Communicate Protective Messages during Oxidative Stress; Possible Role of Exosomal Shuttle RNA, PLOS ONE 5(12) (2010) e15353, 10.1371/journal.pone.0015353.

[58] E. Balogh, A. Tóth, G. Méhes, G. Trencsényi, G. Paragh, V. Jeney, Hypoxia Triggers Osteochondrogenic Differentiation of Vascular Smooth Muscle Cells in an HIF-1 (Hypoxia-Inducible Factor 1)–Dependent and Reactive Oxygen Species–Dependent Manner, Arteriosclerosis, Thrombosis, and Vascular Biology 39(6) (2019) 1088-1099, 10.1161/ATVBAHA.119.312509.

[59] S. Mokas, R. Larivière, L. Lamalice, S. Gobeil, D.N. Cornfield, M. Agharazii, D.E. Richard, Hypoxia-inducible factor-1 plays a role in phosphate-induced vascular smooth muscle cell calcification, Kidney International 90(3) (2016) 598-609, 10.1016/j.kint.2016.05.020

6.7. SUPPLEMENTARY INFORMATION

6.7.1. FIGURES

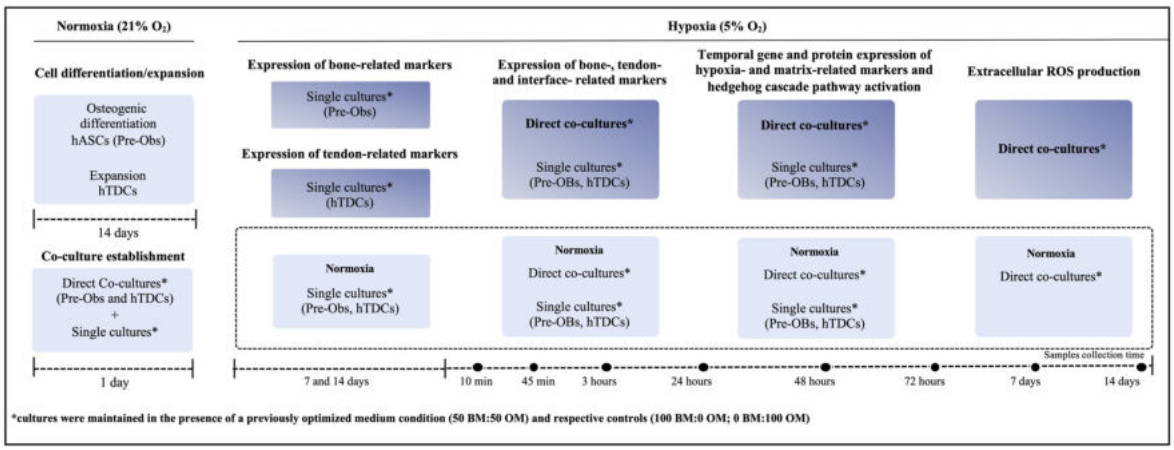

Supplementary Figure S6.1 | Illustration of experimental setup. Before the establishment of an oxygen restricted environment, the osteogenic differentiation of hASCs (pre-OBs) and expansion of hTDCs occurred in a humidified environment (37°C, 5% CO_2) under normal atmospheric oxygen tension (21% O_2). After 14 days, cells were seeded together in a direct-co-culture and, simultaneously pre-OBs and hTDCs were seeded separately – single cultures – and used as controls. In both cases, a previously optimized medium condition composed of a 1:1 ratio of basal and osteogenic media was used alongside the respective controls composed of only basal medium (BM) and only osteogenic medium. Cells were left to adhere for 24 hours at 21% O_2. Afterwards, both single and direct co-cultures were exposed to 5% O_2 tension, in a humidified environment (37 °C). Simultaneously, similar cultures were maintained under the same conditions in normoxia (21% O_2) and used as controls. The influence of restricted oxygen supply and different medium conditions on the expression of bone- and tendon- markers was assessed after 7 and 14 days in bone- and tendon-like niches, respectively. The expression of bone-, tendon- and interface markers was similarly assessed in direct co-culture systems and single cultures. Afterwards, the expression of hypoxia inducible factors was explored at gene level and correlated with the expression of interfacial matrix markers and hedgehog signaling pathway. Additionally, protein localization of HIF1A and HIF2A was assessed and correlated with the transcriptional activation of SOX9. Nevertheless, extracellular ROS was quantified.

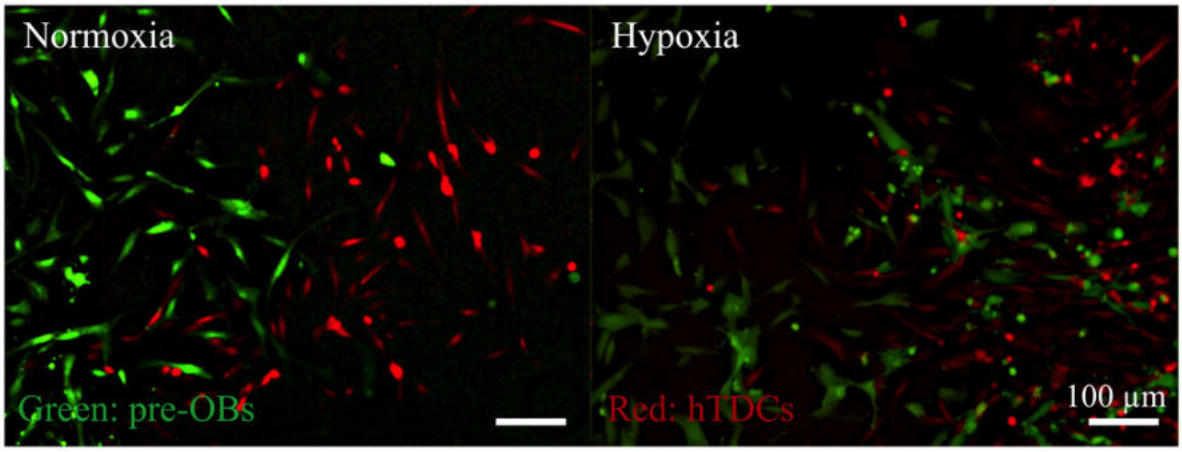

Supplementary Figure S6.2 | Direct o-culture setup of pre-OBs (green) and hTDCs (red) under normoxia and hypoxia. Fluorescence images were acquired after 2 days of culture under basal media condition (100 BM: 0OM). Scale bar, 100 µm.

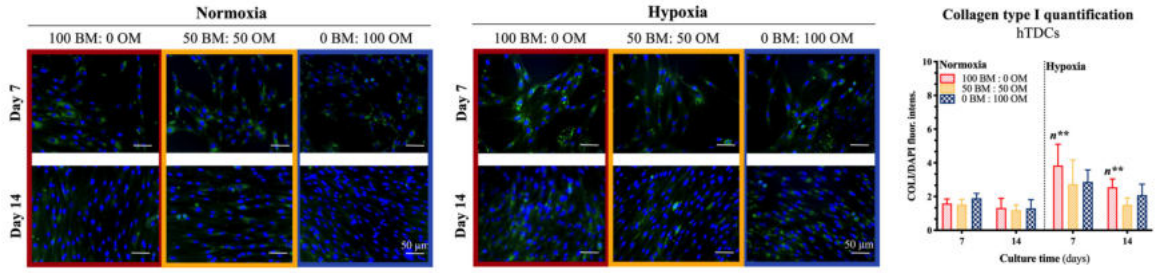

Supplementary Figure S6.3 | Expression of collagen type I by hTDCs. Immunofluorescence staining for collagen type I (COLI) deposited by hTDCs up to 14 days of culture under hypoxia and normoxia. Scale bars, 50 µm. Representative images were displayed. Nuclei were counterstained with DAPI. Fluorescence intensity ratio was quantified for the studied culture conditions at established culture times. Data are represented as means ± SD. Statistically significant differences are shown as **, $p < 0.01$; n is statistically significant in correspondence with the same condition maintained under normoxia at the correspondent culture time.

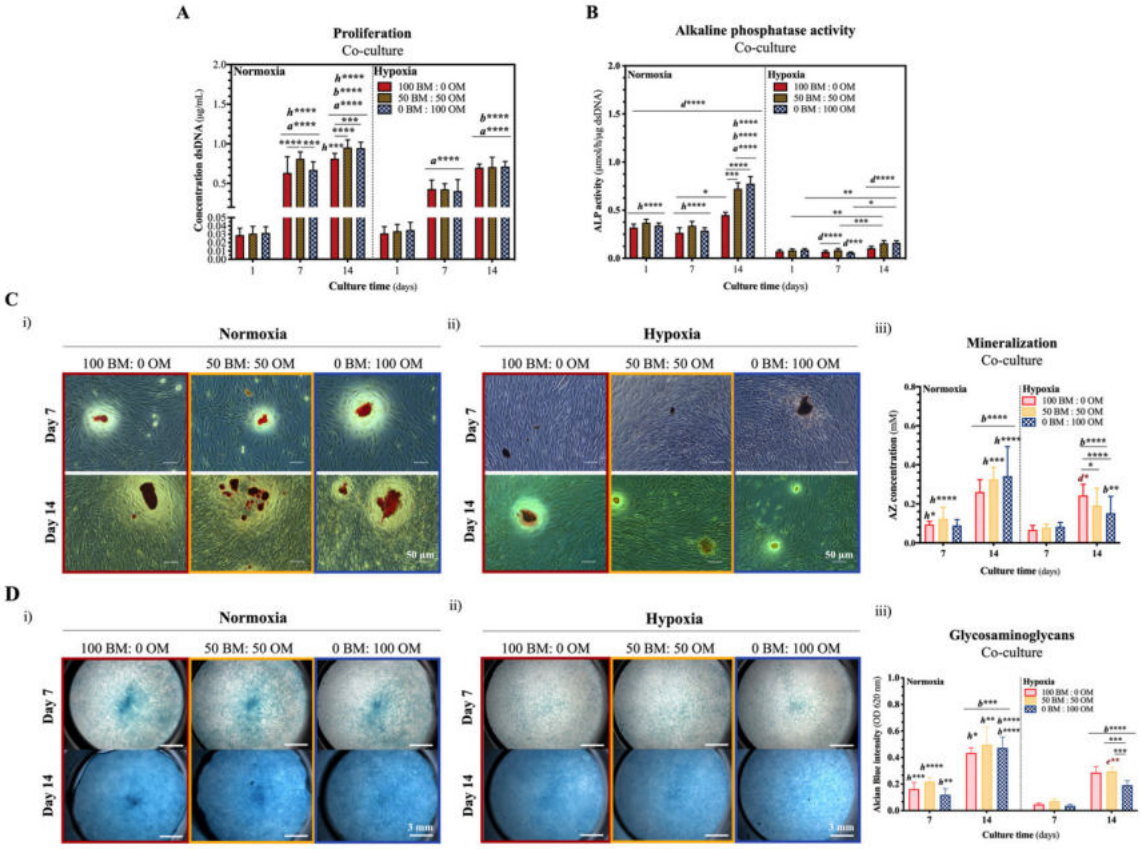

Supplementary Figure S6.4 | Proliferation, ALP activity and gene expression of osteogenic- and tenogenic-related markers in direct co-cultures under hypoxia and normoxia and ratios of pro-osteogenic factors. (A) Proliferation of co-cultured cells up to 14 days under normoxia and hypoxia in the presence of increasing ratios of OM. Data are represented as means ± SD (n=3). (B) Alkaline phosphatase activity quantified in co-cultured cells at both 7 and 14 days under both oxygen tensions. Data are represented as means ± SEM (n=3). (C) Matrix mineralization was assessed in co-cultures maintained under (i) normoxia and (ii) hypoxia. Scale bars, 50 µm. (iii) Quantification of alizarin red staining for 7 and 14 days of culture. Data are represented as means ± SD (n=3). (D) Alcian blue staining was used to study the deposition of glycosaminoglycans in cultures maintained under (i) normoxia and (ii) hypoxia. Scale bars, 3 mm. (iii) Quantification of alcian blue staining was performed for all tested conditions. Data are represented as means ± SD (n=3). For A-D, statistically significant differences are shown as *, $p < 0.05$; **, $p < 0.01$; ***, $p < 0.001$;****, $p < 0.0001$; b and c are statistically significant in comparison with the same condition at 7 and 14 hours, respectively; d is statistically significant in correspondence with the same condition and culture time in pre-OBs; e is statistically significant in correspondence with the same condition and culture time in hTDCs; h is statistically significant in correspondence with the same condition maintained under hypoxia at the correspondent culture time; n

is statistically significant in correspondence with the same condition maintained under normoxia at the correspondent culture time; Legend: BM: basal medium; OM: osteogenic medium.

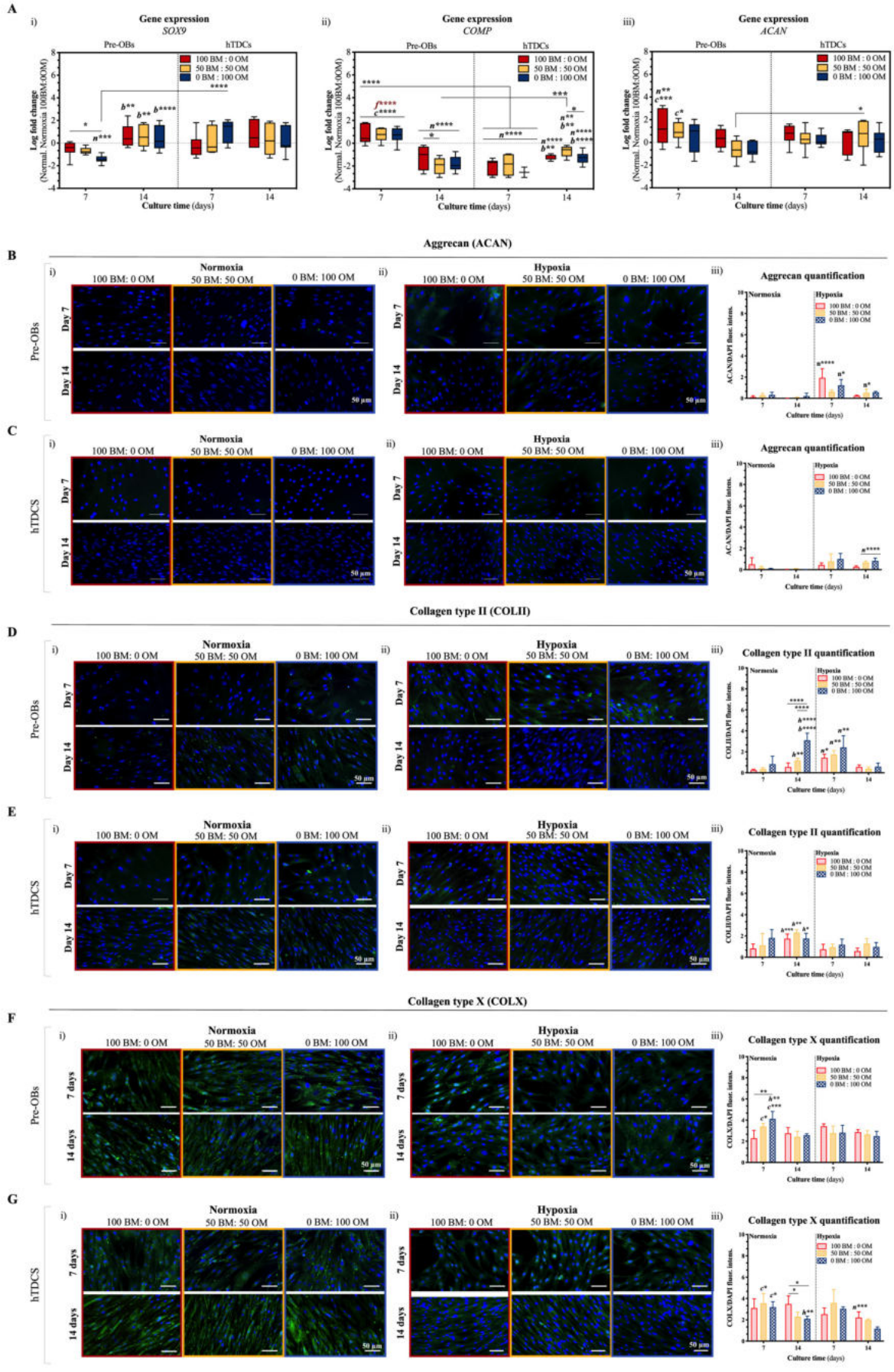
A
i)
Gene expression
SOX9
ii)
Gene expression
COMP
iii)
Gene expression
ACAN
Pre-OBs
hTDCs
100 BM : 0 OM
50 BM : 50 OM
0 BM : 100 OM
Log fold change (Normal. Normoxia 100BM:0OM)
Culture time (days)
B
Aggrecan (ACAN)
C
Collagen type II (COLII)
D
E
Collagen type X (COLX)
F
G
Normoxia
Hypoxia
Aggrecan quantification
Collagen type II quantification
Collagen type X quantification
Pre-OBs
hTDCS
Day 7
Day 14
7 days
14 days
50 µm

Supplementary Figure S6.5 | Gene and protein expression of chondrogenic-related markers in both single cultures of hTDCs and pre-OBs under hypoxia and normoxia and osteogenic supplementation ratios. (A) Gene expression of (i) sex-determining region Y-box 9 (*SOX9*), (ii) cartilage oligomeric matrix protein (*COMP*) and (iii) aggrecan (*ACAN*). Expression of target genes was normalized to the basal condition (100 BM:0 OM) of normoxia at the correspondent day. Expression of target genes was normalized to the basal condition (100 BM: 0 OM) of the correspondent day under normoxia and the log fold change calculated (n=3, five replicates). Immunofluorescence analysis of (B-C) aggrecan (AGG), (D-E) collagen type II (COLII) and (F-G) collagen type X (COLX) deposition by pre-OBs and hTDCs cultured under normoxia (i) and hypoxia (ii) for 7 and 14 days in the presence of increasing ratios of OM. Scale bars, 50 μm. (iii) Fluorescence intensity ratio quantification of matrix protein. Data are represented as means ± SD. For A-G, statistically significant differences are shown as *, $p < 0.05$; **, $p < 0.01$; ***, $p < 0.001$; ****, $p < 0.0001$; b and c are statistically significant in comparison with the same condition at 7 and 14 days, respectively; h is statistically significant in correspondence with the same condition maintained under hypoxia at the correspondent culture time; n is statistically significant in correspondence with the same condition maintained under normoxia at the correspondent culture time. Legend: BM: basal medium; OM: osteogenic medium.

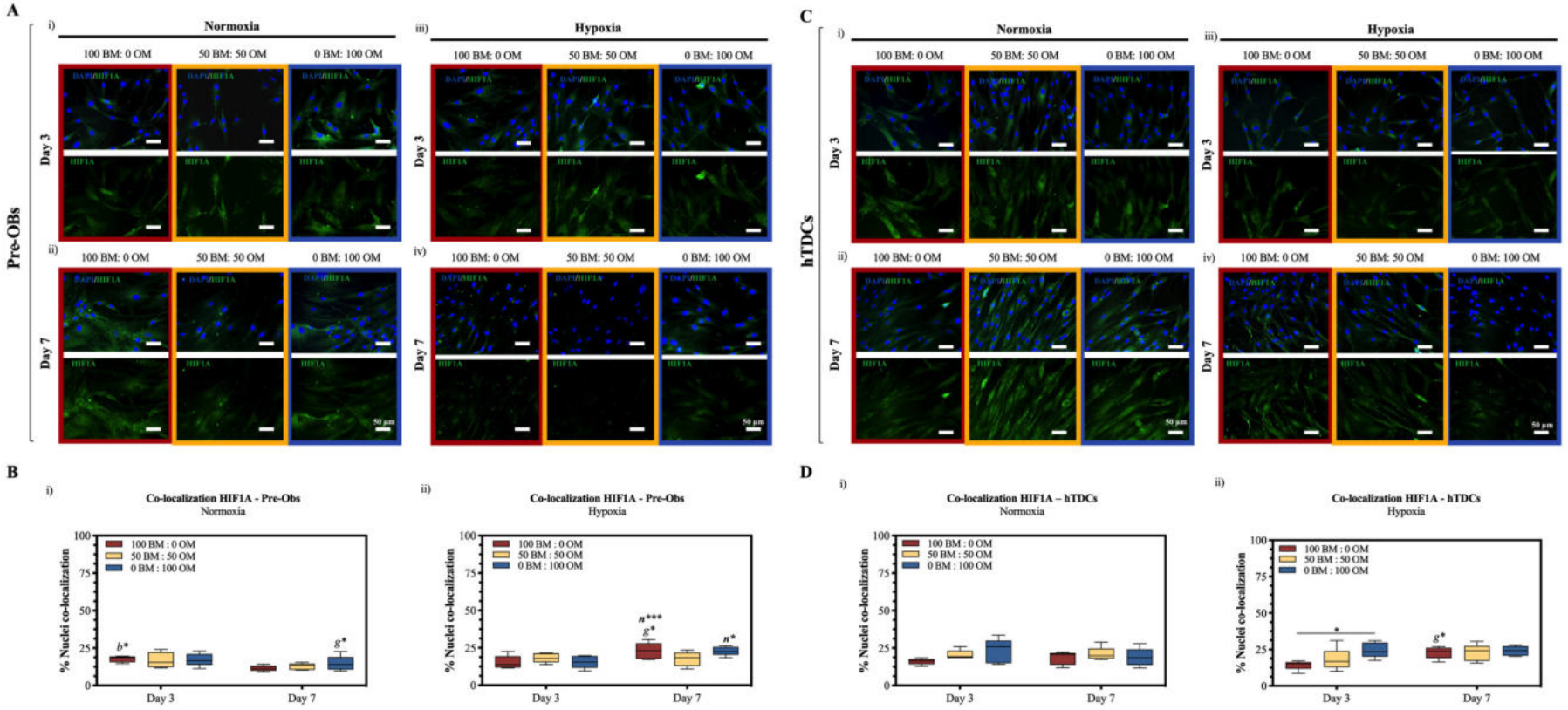

Supplementary Figure S6.6 | Nuclei co-localization of HIF1A in single cultures of pre-OBs and hTDCs under normoxia and hypoxia. (A, C) Immunofluorescence of hypoxia inducible factor 1 alpha (HIF1A) in single cultures of (A) pre-OBs and (C) hTDCs at both 3 and 7 days of culture. (B-D) The percentage of nuclei co-localization was calculated from obtained immunofluorescence. Scale bars, 50 µm. For B and D, statistically significant differences are shown as *, $p < 0.05$; **, $p < 0.01$; ***, $p < 0.001$; g and b are statistically significant in comparison with the same condition at 3 and 7 days, respectively; h is statistically significant in correspondence with the same condition maintained under hypoxia at the correspondent culture time; n is statistically significant in correspondence with the same condition maintained under normoxia at the correspondent culture time. Legend: BM: basal medium; OM: osteogenic medium.

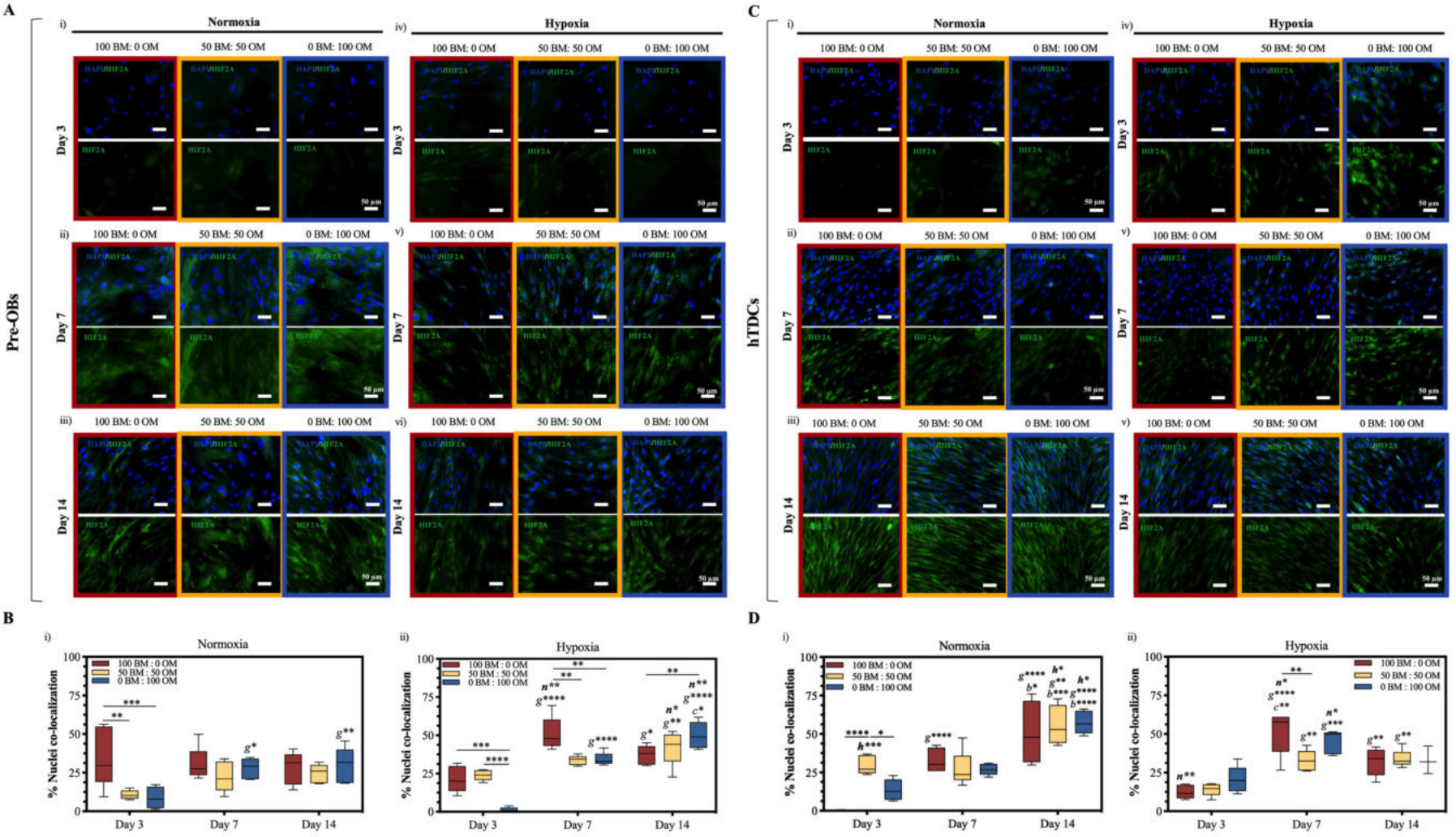

Supplementary Figure S6.7 | Nuclei co-localization of HIF2A in single cultures of pre-OBs and hTDCs under different oxygen tensions. (A-C) Immunofluorescence of hypoxia inducible factor 2 alpha (HIF2A) in single cultures of (A) pre-OBs and (C) hTDCs maintained under hypoxia and normoxia up to

14 days in the presence of increasing ratios of OM. (B-D) The percentage of nuclei co-localization was calculated from obtained immunofluorescence images acquired after 3, 7 and 14 days of culture. Scale bars, 50 μm. For B and D, statistically significant differences are shown as *, $p < 0.05$; **, $p < 0.01$; ***, $p < 0.001$;****, $p < 0.0001$; g, b and c are statistically significant in comparison with the same condition at 3, 7 and 14 days, respectively; h is statistically significant in correspondence with the same condition maintained under hypoxia at the correspondent culture time; n is statistically significant in correspondence with the same condition maintained under normoxia at the correspondent culture time. Legend: BM: basal medium; OM: osteogenic medium.

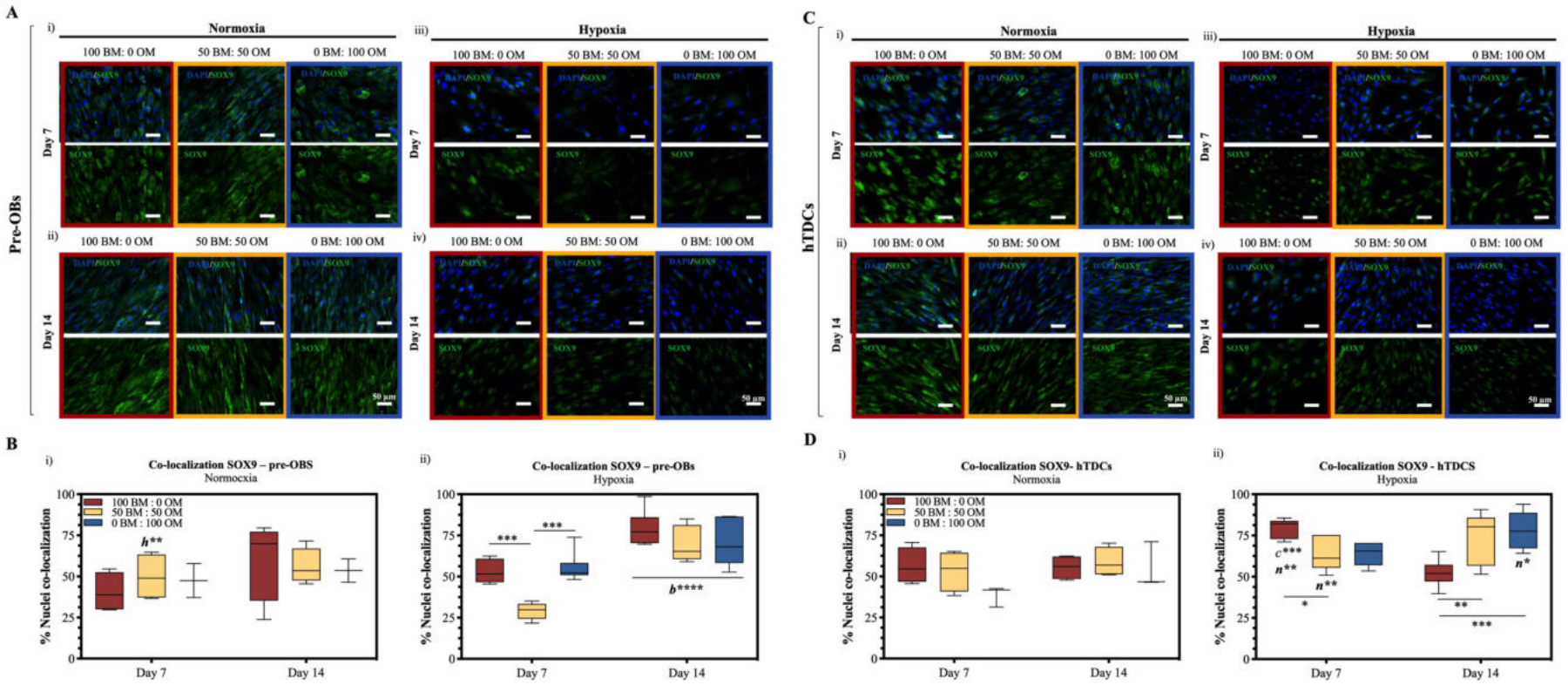

Supplementary Figure S6.8 | Nuclei co-localization of SOX9 in single cultures of pre-OBs and hTDCs maintained under normoxia and hypoxia.

(A-C) Immunofluorescence of sex-determining region Y-box 9 (SOX9) in single cultures of (A) pre-OBs and (C) hTDCs maintained under hypoxia and normoxia up to 14 days in the presence of increasing ratios of OM. (B-D) The percentage of nuclei co-localization was calculated from obtained immunofluorescence images acquired after 7 and 14 days of culture. Scale bars, 50 µm. For B and D, statistically significant differences are shown as *, $p < 0.05$; **, $p < 0.01$; ***, $p < 0.001$;****, $p < 0.0001$; b and c are statistically significant in comparison with the same condition at 7 and 14 days, respectively; h is statistically significant in

correspondence with the same condition maintained under hypoxia at the correspondent culture time; n is statistically significant in correspondence with the same condition maintained under normoxia at the correspondent culture time. Legend: BM: basal medium; OM: osteogenic medium.

6.7.2. TABLES

Supplementary Table S6.1 | Primers used for quantitative RT-PCR analysis.

Target Gene	Gene Abbreviation	Primer Sequence		NBCI Reference
		Forward	Reverse	
Collagen type I, α1	*COL1A1*	GTCACAGATCACGTCATCGC	CGAAGACCCACCAATCAC	NM_000088.3
Tenogenic-related markers				
Scleraxis	*SCX*	CGAGAACACCCAGCCCAAAC	CTCCGAATCGCAGTCTTTCTGTC	NM_001717912
Mohawk	*MKX*	TGTTAAGGCCATAGCTGCGT	TCGCACAGACACCTGGAAAA	NM_173576.5
Interface-related markers				
Cartilage oligomeric matrix protein	*COMP*	AGGATGGAGACGGACATCAG	TCTGCATCAAAGTCGTCCTG	NM_000095.2
Aggrecan	*ACAN*	TGGTCTTGCAGCAGTTGATTC	TAGAGTCCTCAAGCCTCCTGT	NM_013227.3
SRY-box 9	*SOX9*	TTCATGAAGATGACCGACGC	GTCCAGTCGTAGCCCTTGAG	NM_000346.4
Collagen type II, α1	*COL2A1*	GAGCAGGAATTCGGTGTGGA	GCCATTCAGTGCAGAGTCCT	NM_001844.5
Collagen type X, α1	*COL10A1*	CCCAGCACGCAGAATCCATC	AGTGGGCCTTTTATGCCTGT	NM_000493.3
Osteogenic-related markers				
Run-related transcription factor 2	*RUNX2*	TGTCTGTGCCTTCTGGGTTC	CCGGCCTGCCTATGCTGTTA	NM_001024630.3
Oxygen-related markers				
Hypoxia-inducible factor 1-alpha	*HIF1A*	AGAGGTTGAGGGACGGAGAT	GACGTTCCAGAACTTATCCTACCAT	NM_001243084.1
Hypoxia-inducible factor 2-alpha	*EPAS/HIF2A*	CAATGCAGTACCCAGACGGA	TGGGGCTTAGCTGGAAGTCT	NM_001430.3
Indian Hedgehog pathway markers				
Indian hedgehog	*IHH*	CCGCGACCGCAATAAGTATG	CGAGTGCTCGGACTTGACG	NM_002181.3
Patched 1	*PTCH1*	TGTCGCACAGAACTCCACTC	GGCATAGGCGAGCATGAGTA	NM_001083605.2
GLI family zinc finger 1	*GLI1*	AAGCTAACCTCATGTCCGGC	AAAAGAGTGGGCCCTCGGTG	NM_005269.3

Supplementary Table S6.2 | Summary table of the COLX/COLII ratio in cells exposed to 21% O_2 for 7 and 14 days of culture.

Ratio COLX/COLII

	Time (hours)	168	336	
Medium condition	100 BM: 0 OM	1.45±0.09	1.33±0.57	Co-culture system
	50 BM: 50 OM	1.85±0.60 ^{z*}	1.43±0.29	
	0 BM: 100 OM	1.23±0.21	1.21±0.19	
	100 BM: 0 OM	13.69±5.40 $^{f****, y*, z**, h**}$	6.89±1.4.58 $^{b*, y*, z*}$	Pre-Obs
	50 BM: 50 OM	7.74±0.80 $^{f*, z*, h**}$	1.95±0.41$^{b*, f****}$	
	0 BM: 100 OM	4.86±0.84	0.83±0.05 ^{f****}	
	100 BM: 0 OM	5.18±2.91 ^{z*}	2.04±0.32 $^{c**, f*}$	hTDCs
	50 BM: 50 OM	3.81±1.53	0.99±0.18$^{c*, f****}$	
	0 BM: 100 OM	1.76±0.28	1.19±0.14 ^{f****}	

Statistically significant differences are shown as: *, p<0.05; **, p<0.01; ****, p<0.0001; y and z are statistically significant in comparison with cells in 50BM:50OM and 0BM:100OM, respectively; b and c are statistically significant in comparison with the same condition at 7 and 14 days, respectively; f is statistically significant in comparison with the same condition in direct co-cultures; h is statistically significant in relation to hypoxia.

CHAPTER 7. "A textile platform using continuous aligned and textured composite microfibers to engineer tendon-to-bone interface gradient scaffold"

This chapter was adapted from the following publication:

I. Calejo, R. Costa-Almeida, R. L. Reis, M. E. Gomes (2019) A Textile Platform Using Continuous Aligned and Textured Composite Microfibers to Engineer Tendon-to-Bone Interface Gradient Scaffolds. *Advanced Healthcare Materials*, 8(15) 1900200. DOI: 10.1002/adhm.201900200.

ABSTRACT

Tendon-to-bone interfaces exhibit a hierarchical multi-tissue transition. To replicate the progression from mineralized to non-mineralized tissue, a novel 3D fibrous scaffold was fabricated with spatial control over mineral distribution and cellular alignment. For this purpose, wet-spun continuous microfibers were produced using polycaprolactone (PCL)/ Gelatin and PCL/Gelatin/hydroxyapatite nano-to-microparticles (HAp). Higher extrusion rates resulted in aligned PCL/Gelatin microfibers while, in the case of PCL/Gelatin/HAp, the presence of minerals led to a less organized structure. Biological performance using human adipose-derived stem cells (hASCs) demonstrated that topography of PCL/Gelatin microfibers could induce cytoskeleton elongation, resembling native tenogenic organization. Matrix mineralization on PCL/Gelatin/HAp wet-spun composite microfibers suggested the production of an osteogenic-like matrix, without external addition of osteogenic medium supplementation. As proof of concept, a 3D gradient structure was produced by assembling PCL/Gelatin and PCL/Gelatin/HAp microfibers, resulting in a fibrous scaffold with a continuous topographical and compositional gradient. Overall, it was demonstrated the feasibility of wet-spinning for the generation of continuously aligned and textured microfibers, which can be further assembled into more complex 3D gradient structures to mimic characteristic features of tendon-to-bone interface.

Keywords: Biotextiles; Cell-Laden Microfibers; Gradient Biomaterials; Tendon-To-Bone Interface; Wet-Spinning.

7.1. INTRODUCTION

Tendon-to-bone failure due to trauma or severe illness is an increasing healthcare problem. Conservative treatments are often not effective or inadequate and surgical application of grafts is the gold standard approach to clinical management of such injuries. Despite recent advances in surgical techniques, interface repair still fails up to 95% of the time due to the formation of fibrotic tissue [1]. The major problem associated with tendon-to-bone junction regeneration is the fact that, after failure, there is a disordered matrix deposition rather than the formation of organized collagen fibers, affecting tendon tissue integration and leading to a disorganized graded interface [2, 3]. Moreover, the gradual loss of mineral content is also believed to contribute to the observed mechanically inferior interface, resulting in tissue rupture [4]. Therefore, tissue engineered approaches combining biological and engineering sciences are essential to regenerate these complex interfaces. In this regard, interfacial tissue engineering is a fascinating research field with substantial focus on the development of strategies to emulate complex and multiphasic tissue interfaces, such as the one interconnecting tendon to bone. Particularly, providing the necessary biological cues in one single unit, while recreating the mechanical requirements of the native tissue would be of great importance.

Several approaches are available for the fabrication of naturally derived or synthetic fibers for tissue engineering applications, including electrospinning, meltspinning, interfacial complexation or microfluidic spinning [5]. However, these techniques present some limitations as the use of highly toxic organic solvents, voltages and temperatures known to partially denature the structure of natural polymers [6, 7], lack of control of scaffold porosity involving the use of other techniques to obtain larger pores to enable cell infiltration [8] and the impossibility to scale-up the fiber production limiting the application to large lab-scale systems [5]. Strikingly, among available fiber processing techniques, wet-spinning appears as a powerful tool to convert biomolecules into fibers without the need of high voltages or temperatures and likely less denaturation [9, 10]. This manufacturing process has been present in textile industry for many years and is based on a non-solvent-induced phase inversion which involves the extrusion of a polymeric solution directly into a coagulation bath [10]. This bath is normally composed of a poor solvent (non-solvent) or a nonsolvent/solvent mixture having in mind the processed polymer to form a coagulating filament, that will solidify as a continuous polymeric fiber [11, 12]. Compared to other available techniques, wet-spinning presents several advantages such as low cost, high yield, adjustable fibers diameter and, ultimately scaffolds porosity, and mild production conditions [6, 7, 12]. Furthermore, fibers are very easy to handle and assemble by textile techniques [11, 12]. Therefore, wet-spun fibers have

been used to produce different tissue analogs such as cartilage [13], bone [14] and even neural tissue [15].

Herein, we aimed at developing a gradient scaffold by assembling microfibers with distinct topographical and compositional features tailored to guide cell alignment and simultaneously match the mechanical properties of the native tissue. Wet-spinning was used to produce two types of microfibers toward mimicking the soft (tendon) and hard (bone) tissues constituting the tendon-to-bone interface. For this purpose, synthetic/natural origin blend formulations of polycaprolactone and gelatin (PCL/Gelatin) and PCL/Gelatin incorporating nano-to-micro sized hydroxyapatite (HAp) particles were used. Different flow rates were tested to assess their effect on wet-spun fibers diameter and mechanical properties. The biological performance of the developed microfibers was assessed by culturing human adipose-derived stem cells (hASCs) onto the fibers for a period of 14 days. As proof of concept, knitting (crochet) was used to create a 3D fibrous scaffold using the produced fibers to generate a mineral gradient within the developed structure. Also, the formation of specific regions was assessed by studying the deposition of characteristic collagen matrices by hASCs cultured onto scaffolds.

7.2. MATERIALS AND METHODS

7.2.1. Materials

Poly-ε-caprolactone (PCL, average Mn = 80 000), gelatin (type A, from porcine skin), phosphate buffered saline (PBS), 4,6-diamidino-2-phenyindole dilactate (DAPI, 5 μg μL^{-1}), bovine serum albumin (BSA) and CellcrownTM 24-well plate inserts were purchased from Sigma-Aldrich (Germany). Formic acid 98% was purchased from Laborspirit (Spain). Glacial acetic acid and 25% (v/v) glutaraldehyde were obtained from VWR (Belgium). Antibiotic/antimycotic solution (A/A), fetal bovine serum (FBS) and minimum essential medium alpha (α-MEM) were purchased from Alfagene (United Kingdom). Phalloidin-iFluorTM Conjugate was purchased from ATT Bioquest (USA). Basal medium was prepared using α-MEM supplemented with 10% (v/v) FBS and 1% (v/v) A/A.

7.2.2. Hydroxyapatite Nano-to-microparticles Synthesis (HAp)

A precipitation reaction of calcium hydroxide (Riedel-de Haën, Germany) and orthophosphoric acid 85% (Panreac, Spain) solutions was performed in an aqueous system at room temperature in order to obtain HAp. The mixing was performed in a basic environment (pH=11), adjusted with concentrated ammonium hydroxide (1 M, Riedel-de Haën, Germany) at a continuous flow rate ranging from 8 to 15 mL min^{-1}. The formed ceramic powder was sieved to obtain particles smaller than 63 μm X-ray.

7.2.3. Fabrication of continuous PCL/Gelatin and PCL/Gelatin/HAp fibers by wet spinning

A PCL solution (22% w/v, initial concentration) was prepared by dissolving PCL in formic acid/acetic acid (3:1 v/v) and stirring at 150 rpm for 4 hours. Gelatin (9% w/v, initial concentration) was dissolved in a solution of 80% acetic acid/water (v/v) and stirred at 150 rpm for 4 hours. The final solution of PCL/Gelatin was prepared by mixing PCL and gelatin solutions at a ratio of 70:30, respectively. In the case of PCL/Gelatin/HAp blend, HAp nano-to-microparticles were first completely dispersed in PCL solution and, afterwards, gelatin (9% w/v) solution was added to the mixture. HAp content represents 7.7% w/v of the final solution. Both solutions were prepared at room temperature and used within the day of preparation. Fibers were fabricated using the wet spinning method. A customized device was used to produce textured wet-spun microfibers. A coagulation bath containing 1.25% (v/v) glutaraldehyde/water solution was used as crosslinker. The prepared solutions were injected using a 10 mL syringe with a 21G needle and extruded to the coagulation bath at a constant flow rate. Three different flow rates were tested: 1 mL/h, 0.5 mL/h and 0.25 mL/h. The vertical distance from the needle to the surface of the coagulation bath (**Figure 7.1A**) was set at 6 cm. A collector was set after the coagulation bath at a horizontal distance of 8 cm from the needle and the fibers were collected at a constant speed (2 rotations per minute) (**Figure 7.1A**). All fibers were left inside the hood overnight to eliminate possible solvent and/or glutaraldehyde residues from the production process.

7.2.4. Morphological Characterization

Fibers obtained from different formulations and flow rates were observed and photographed under an optical microscope. Fiber diameter was determined by measuring three different regions in the images. Images were obtained from six independent samples per condition. The morphology of the different fibers was analyzed by scanning electron microscopy (SEM, MP1000001280128, JSM-6010 LV, JEOL). All samples were previously coated with 2 nm of platinum (Cressigton). The degree of surface alignment was determined through directionality analysis applying the Fourier components method using the FIJI® software (version 2.0.0). For this purpose, scanning electron images were converted to 32-bit images and cropped into three different images. The radial intensities were calculated, and the orientation map was also obtained.

In order to evaluate its microstructure, single microfibers of PCL/Gelatin/HAp were analyzed by X-rays micro-computed tomography (micro-CT) using a high-resolution X-ray microtomography system was used:

Skyscan 1 scanner (Skyscan 1272; Bruker, Billerica, MA, USA). The acquisition of X-ray images was performed with a pixel size of 10 µm, a rotation step of 0.4° over 360°, and a smoothing averaging of every 3 images. The X-ray source was fixed at 50 keV and 200 µA, of voltage and current, respectively. Following the acquisition, grey-scale images were reconstructed using the NRecon software (version 1.7.1.0, Bruker, Billerica, MA, USA). Then, the samples were vertically aligned for the longitudinal analysis of the fibers using the DataViewer software (version 1.5.3.6, Bruker, Billerica, MA, USA). Qualitative visualization of the 3D morphology and the different phases of the polymer and hydroxyapatite was performed using CT-Vox software (version 3.3.0, Bruker, Billerica, MA, USA). Finally, the quantitative analysis was performed after converting the regions of interest into binary images, by a dynamic threshold (30–255 – polymeric phase; 80-255 ceramic phase). So, the binary images were used for morphometric examination (CT Analyzer v1.12.0.0, SkyScan, Kontich, Belgium) of porosity amount, pore volume and interconnectivity.

7.2.5. Chemical Characterization

Fourier-transform infrared spectroscopy (FTIR, IRPrestige 21, Shimadzu) was used for chemical analysis of the developed fibers. Briefly, all samples were mixed with potassium bromide (KBr) and pressed into transparent pellets prior to FTIR analysis. Infrared spectra of PCL, gelatin, HAp and PCL/Gelatin and PCL/Gelatin/HAp fibers were recorded by averaging 32 individual scans, at a resolution of 4 cm^{-1}, over a wavenumber range between 4000 - 400 cm^{-1} at room temperature.

7.2.6. Mechanical Characterization

Mechanical properties of produced wet spun fibers were assessed using the universal mechanical testing machine (5543K2942, 5543, Instron) equipped with a 1 kN load cell. Images from optical microscope (DM750, Leica, Schweiz, Germany) were acquired and used for cross-sectional area calculations. Each specimen was measured along the length at three different locations using the ImageJ software (version 1.52d). Samples were cut into testing specimens with 1.5 cm and fixed in paper frames with a window of 1.2×1.2 cm. After mounting the frames onto the tester grips, the lateral sides were cut and the crosshead speed set at a constant rate of 1 mm min^{-1}. At least six samples per condition were tested. The elastic modulus was calculated from the tangent slope of the linear section of the stress-strain curve.

7.2.7. Biological assays and characterization

7.2.7.1. *Cell seeding*

Human-adipose derived cells (hASCs) were isolated by enzymatic digestion of lipoaspirate samples obtained under previously established protocols with Hospital da Prelada (Porto, Portugal), as described elsewhere [16]. Human lipoaspirate samples were collected under informed consent following protocols approved by the ethical committee of the hospital and according to the Declaration of Helsinki. Human lipoaspirate samples (n=3) of healthy female patients with ages in the range of 60-70 were used. Isolated cells were cultured and expanded in basal medium.

Prior to seeding, both wet-spun fibers and fibrous scaffolds were immersed in 70% ethanol for 15 minutes, followed by a washing step with PBS for 15 minutes to remove the remaining ethanol residues.

Single fibers were then fixed inside 24-well plate inserts and left overnight in basal medium. Afterwards, after removing the medium, hASCs were seeded on the fibers at a density of $2x10^4$ cells using 400 µl per well in basal medium. After 1 hour of incubation in a humidified environment (37 °C, 5% CO2), culture medium was added up to 1 mL.

Scaffolds were fixed with 6 well-plate inserts and left overnight with basal medium. Cells were seeded on the scaffolds at a density of $1x10^5$ cells using 1 mL per well in basal medium. After 1h of incubation (37 °C, 5% CO2), basal culture medium was added up to 4 mL. Cells were used at passage 2-3 and culture medium was changed twice a week over 14 days of culture.

7.2.7.2. *Determination of metabolic activity by Alamar Blue Assay*

After 1, 7 and 14 days in culture, the metabolic activity of hASCs was evaluated by Alamar blue assay, according to manufacturer's instructions (AbD SeroTec, Bio-Rad). Briefly, cell-seeded fibers were transferred to clean wells and washed twice with PBS. Then, 10% (v/v) Alamar blue in basal medium was added and cells were incubated overnight under standard culture conditions. The supernatant was collected, and the fluorescence measured using a microplate reader (Synergy HT, Bio-Tek Instruments) at an excitation wavelength of 530 nm and an emission wavelength of 590 nm. Quadruplicates were used for each fiber.

7.2.7.3. *Alizarin Red (AZ) staining and quantification*

Matrix mineralization was analyzed by alizarin red staining after 7 and 14 days of culture. Briefly, fibers were fixed with 10% (v/v) neutral buffered formalin for 20 minutes at room temperature (RT). Afterwards, samples were washed with PBS and deionized water. Subsequently, a solution of 2% (w/v) AZ (Merck)

was added for 10 minutes and the excess of dye removed with deionized water. Staining was visualized and images were acquired using the inverted microscope Vert A.1 Axio with Axiocam 503 color (Zeiss, Germany) and Zen 2.3 lite software (Zeiss, Germany). Quantitative data was obtained using the cetylpyridinium chloride (CPC) method. The dye was removed using a solution of 10% (w/v) CPC in 10 mM sodium phosphate (Sigma-Alrich) for 1 hour, under gentle shaking, at RT and the absorbance measured at 562 nm in a microplate reader (Synergy HT, Bio-Tek Instruments). Fibers without cells were used as controls and the dye quantification used as background control for fibers with cells. Triplicates were used for each sample and conditions.

7.2.7.4. *Morphological evaluation of seeded hASCs by SEM*

The organization and morphology of hASCs cultured on developed microfibers was analyzed by SEM. Briefly, after 7 and 14 days, cell-seeded fibers were washed three times with PBS, fixed with 2.5% (v/v) glutaraldehyde in PBS solution and stored at 4°C until preparation. After this, all samples were dehydrated in a series of increasing concentrations of ethanol in water (10% to 100%, 30 minutes of incubation in each solution). After dehydration, all samples were left to air-dry and mounted on aluminum stubs. Prior to SEM analysis, a coating with platinum was performed and the samples were observed at an accelerating voltage of 5kV.

7.2.7.5. *Immunofluorescence and F-actin staining*

After 7 and 14 days of culture, fibers seeded with hASCs were washed with PBS and fixed with 10% (v/v) neutral buffered formalin for 20 minutes at RT. To assess the deposition of collagen type III, fibers were first washed with PBS and permeabilized with 0.25% Triton X-100/PBS solution for 5 minutes. To block non-specific binding, a solution of 1% bovine serum albumin (w/v, BSA) in PBS was added and left for 30 minutes at RT. Samples were afterwards incubated overnight with rabbit anti-human collagen type III (COLIII, 1:100, Abcam, ab7778). After incubation with the primary antibody, mouse anti-rabbit AlexaFluor 488 was used as secondary antibody. All antibodies were diluted in 1% (w/v) BSA. Cell nuclei were counterstained with 4,6-diamidino-2-phenyindole dilactate (DAPI, Invitrogen) in a dilution of 1:1000. All samples were visualized, and images acquired using Z-stack method by fluorescence microscopy (Axio Imager Z1m, Zeiss, Deutschland, Germany).

Actin filaments of cell cytoskeleton were stained with phalloidin. Briefly, samples were washed three times with PBS after formalin fixation and incubated with phalloidin solution for 90 minutes at room

temperature. Then, samples were washed with PBS and analyzed by confocal laser scanning microscopy (Leica TCS SP8, Microsystems, Wetzlar, Germany).

7.2.7.6. *Organization of actin filaments and nuclei elongation*

The degree of actin filament alignment was determined through directionality analysis using the Fourier components method using the FIJI® software (version 2.0.0). For this purpose, confocal images were converted to 32-bit images and cropped into three different images. The radial intensities were calculated, and the orientation map was also obtained. Nuclei aspect ratio was determined measuring at least 40 nuclei in different labeled images of each fiber, using ImageJ software (version 1.52d). The length was divided by the width to obtain the correspondent aspect ratio.

7.2.8. Assembly of a 3D gradient scaffold using textile techniques

To fabricate a scaffold with a gradient of HAp content, knitting (crochet) was used as the main textile technique. Briefly, fibers from each formulation produced at 1 mL/h were used. First, four PCL/Gelatin fibers were knot together and, with a hook needle, over hook and draw through to form a new loop without tightening the previous one, forming a chain stitch. In the middle region of the 3D scaffold, two PCL/Gelatin fibers were removed, and two fibers of PCL/Gelatin/HAp were interlocked with the remaining ones to produce the interface. Finally, PCL/Gelatin fibers were completely removed to obtain a third part of the scaffold comprising only PCL/Gelatin/HAp fibers. The mineral content along the gradient scaffold was determined.

7.2.8.1. *Immunohistochemical staining of gradient scaffolds*

After 14 days of culture scaffolds seeded with hASCs were washed with PBS and fixed with 10% (v/v) neutral buffered formalin for 20 minutes at RT. For the detection of collagen type II and X protein, scaffolds were washed with PBS and quenched of peroxidase activity with 3% oxygen peroxide (H_2O_2) solution in water. Afterwards, samples were blocked with 2.5% normal horse serum for 30 min at RT (VECTASTAIN® Elite® ABC HRP Kit, Vector Lab, UK) and incubated either with mouse anti-collagen type II (COLIII, 1:200, Merck, MAB1330) or rabbit anti-collagen type X (COLX, 1:50, Abcam, ab58632) for 2h at RT. The secondary antibody was then applied for 30 min. Samples color was developed using the Vectastain ABC reagent for 30 min, followed by an exposure to 3,3-diaminobenzidine substrate (DAB) for 3 min (DAB Peroxidase (HRP) Substrate Kit (with Nickel), Vector Lab, UK). Stained samples were visualized, and images acquired under a stereomicroscope (Stemi 2000-C, Zeiss, Deutschland, Germany) with AxioCam

ICC1 (Zeiss, Germany). Quantitative data was obtained using the IHC profiler plugin of ImageJ software (version 1.52d). Scaffolds made of only PCL/Gelatin and PCL/Gelatin/HAp were used as controls. Duplicates were used and data acquired from three different parts of each image/section.

7.2.8.2. *Semi-quantitative analysis of collagen and non-collagenous proteins*

To detect collagen and non-collagenous proteins across the scaffolds, Sirius red/fast green staining kit (Chondrex, Inc., Washington, USA) was used in fixed samples according manufacturer's instructions. Briefly, after 14 days of culture, scaffolds fixed with 10% (v/v) neutral buffered formalin for 20 minutes at room temperature (RT) and washed with PBS, were completely submersed in a dye solution for 1h at RT. Afterwards, the excess dye was rinsed off with distilled water and images acquired using a stereomicroscope (Stemi 2000-C, Zeiss, Deutschland, Germany) with AxioCam ICC1 (Zeiss, Germany). Semi-quantification was performed trough the dye extraction with a buffer and the OD reading taken at 540 nm and 605 nm using a microplate reader (Synergy HT, Bio-Tek Instruments). Collagen and non-collagen proteins content was calculated from the formulae provided by the supplier. Triplicates were used for each section. PCL/Gelatin and PCL/Gelatin/HAp scaffolds were used as controls.

7.2.8.3. *Morphological characterization of the scaffold*

Developed 3D fibrous scaffolds were analyzed by micro-computed X-ray tomography (μ-CT). Several images from different parts of the fibrous scaffold were acquired by X-ray diffraction, and then used for analysis and 3D reconstruction. The HAp profile was traced and quantified. 3D projections of the specimens were performed. The 3D gradient structures were acquired with a SkyScan 1272 scanner (v1.1.3, Bruker, Boston, USA), with a pixel size of 11 μm. Approximately 1300 to 1700 projections were acquired over a rotation angle of 360°, with a rotation step of 0.20°. Data sets were reconstructed using a standardized cone-beam reconstructed software (NRecon v1.7.1.0, Bruker). Bitmap images were obtained as final output. Representative data set of the slices was segmented into binary images with a dynamic threshold of approximately 100 to 255 for the analysis of the ceramic phase, and from 16 to 255 for soft polymeric phase (grey scale values – optimized per sample and analysis). Then, the binary images were used for morphometric analysis (CT Analyser, v1.17.0.0, Bruker) and to build the 3-D models (CTvox, v 3.3.0, Bruker). When needed, samples were oriented in DataViewer (v1.5.3.6, Bruker) before proceeding to CT Analyser and CTvox.

7.2.9. Statistical Analysis

Results were obtained from three independent experiments with a minimum of three replicates for each condition. Results are presented as mean ± standard deviation (SD). Statistical analyses were performed using GaphPad Prism 7.0 software. Two-way analysis of variance (ANOVA) with Sidak and Tukey tests and multiple comparisons with Tukey tests were performed. Differences between experimental groups were considered significant with a confidence interval of 95%, whenever $p<0.05$.

7.3. RESULTS

7.3.1. Fabrication and morphological characterization of wet-spun composite microfibers

Wet-spun fiber production set-up is shown in Figure 7.1A. Two different polymeric solutions were injected into a supporting coagulation bath. While the solutions were injected, fibers were instantaneously being formed while a roller was collecting them at a constant speed. This fabrication set-up allowed obtaining a continuous thread that could be easily manipulated and stored (Figure 7.1A). The initial polymeric solutions were designed to mimic the collagenous composition of tendon (gelatin) and the mineral composition of bone (HAp), along with the topography of both tissues. In order to evaluate the effect of collection speed on the wet-spun fibers diameter, as well as, alignment, three different flow rates (1 mL/h, 0.5 mL/h and 0.25 mL/h) were tested (Figure 7.1B). By varying the flow rates, wet-spun fibers could be obtained with diameters in the range of 110-400 μm. The highest extraction rate (1 mL/h) resulted in significantly thicker fibers (368.25 ± 29.47 μm for PCL/Gelatin and 332.99 ± 41.85 μm for PCL/Gelatin/HAp) compared with lower flow rates of 0.5 and 0.25 mL/h ($p<0.0001$, Figure 7.1C i-ii). The lowest flow rate resulted in significantly thinner fibers ($p<0.0001$, 126.32 ± 7.87 μm for PCL/Gelatin and 182.50 ± 22.22 μm for PCL/Gelatin/HAp). Interestingly, the conjugation of HAp in the polymeric solution and lower extrusion rates led to the production of fibers with higher diameters (Supplementary Table S7.1). Furthermore, HAp incorporation also led to different topographical orientation (Figure 7.1D). In the directionality graphs, an absence of a peak means a random orientation of fibers, as observed in the case of PCL/Gelatin/HAp fibers, while the presence of a sharp peak in the orientation angle frequency represents a tendency to align in a specific orientation. Strikingly, a flow rate of 1 mL/h, seemed to induce a higher anisotropic alignment in PCL/Gelatin fibers, while in contrast fiber alignment was less evident in the case of PCL/Gelatin/HAp fibers.

Additionally, as observed in figure 7.1, PCL/Gelatin/HAp fibers were characterized by the presence of pores due to the incorporation of differently sized HAp particles. Interestingly, a flow rate of 1 mL/h, lead

to the accumulation of larger particles in fibers (0.5 mL/h, p<0.008; 0.25 mL/h, p<0,0009; Supplementary Figure S7.1A, i), while no significant differences were found between particles size on fibers produced at lower flow rates. Therefore, a significantly higher pore volume was found in the highest flow rate in comparison with the lowest (0.25 mL/h, p<0,02, Supplementary Figure S7.1A, ii). Similarly, lowering the flow rate, resulted in a decrease of porosity amount. When addressing the interconnectivity of these fibers, it was observed a significantly higher interconnection of pores in flow rates of 0.5 mL/h and 0.25 mL/h in comparing with 1 mL/h (p<0.008, Supplementary Figure S7.1A, iv).

7.3.2. Chemical and mechanical characterization

The characterization of the functional groups of PCL, gelatin, hydroxyapatite, PCL/Gelatin and PCL/Gelatin/HAp was performed by FTIR. Infrared spectra of raw materials and developed fibers are shown in Figure 7.2A, i-ii. In both PCL/Gelatin and PCL/Gelatin/HAp several PCL characteristic bands are observed in 2931 (asymmetric stretching-CH_2), 2858 (symmetric stretching-CH_2), 1292 (C-O and C-C stretching) and 1239 (C-O-C, asymmetric stretching). The characteristic bands for gelatin were also found in 3433 (N-H stretching, amide bond), 1653 (C=O stretching, amide I) and 1543 cm^{-1} (N-H bending, amide II), being also observed in both fibers. Additionally, HAp particles presented one critical infrared band located in 1041 cm^{-1} corresponding to the group of υ3 PO4 which appeared for PCL/Gelatin/HAp fibers (Figure 7.2A, ii).

Concerning the mechanical performance of composite fibers, tensile properties of PCL/Gelatin and PCL/Gelatin/HAp are summarized in Figure 7.2B and Table 7.1. The mechanical properties were examined in terms of young's modulus, yield strength, yield strain and strain to failure. Different blend formulations and tested flow rates resulted in a significant impact on the Young's modulus of produced wet-spun fibers. Regarding PCL/Gelatin fibers, the highest extrusion flow rate (1 mL/h) resulted in fibers with significantly lower Young's modulus (115.30 ± 16.33 MPa, p<0.0001) in comparison with fibers produced at lower flow rates (0.5 mL/h, 251.80 ± 25.51 MPa; 0.25 mL/h, 241.10 ± 41.92 MPa, Figure 7.2B, iii). An opposite tendency was observed for PCL/Gelatin/HAp fibers where Young's modulus ranged from 35.39±6.19 to 59.13±7.87 MPa (Figure 7.2B, iii), without significant differences between Young's moduli of fibers obtained from different flow rates. Additionally, results indicated that the addition of HAp particles caused a decrease in the tensile properties of composite fibers, in comparison to

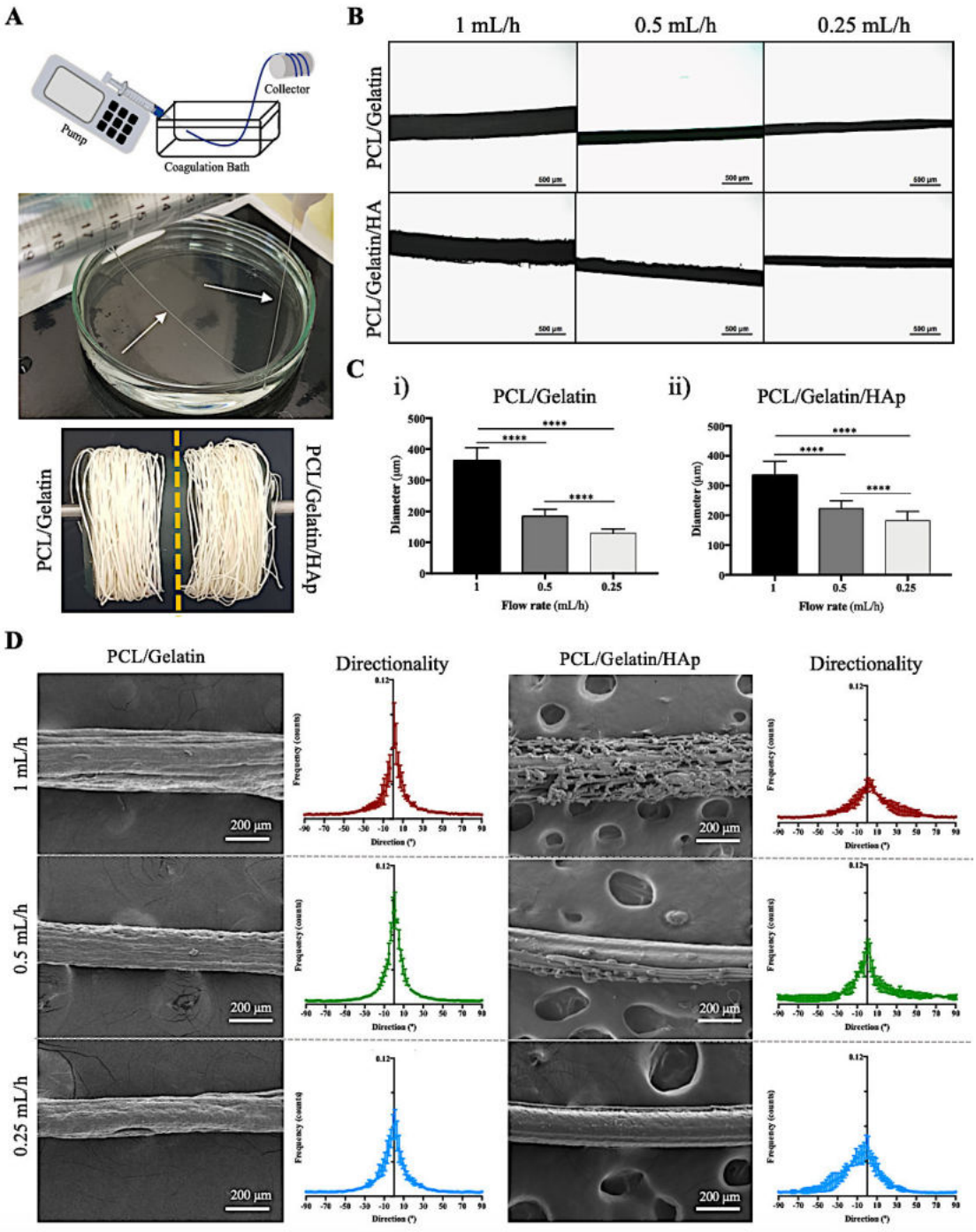

Figure 7.1 | Schematic representation of wet-spinning setup and morphology of PCL/Gelatin and PCL/Gelatin/HAp wet-spun fibers. (A) Continuous wet-spinning system. Arrows point fibers formation. Wet-spun fibers can be easily manipulated and collected in rollers for further use. (B) Optical microscopy images of produced wet-spun fibers according to the different formulations and flow rates. Scale bars, 500 µm. (C) Average diameter of the produced (i) PCL/Gelatin (n=6) and (ii) PCL/Gelatin/HAp fibers (n=6) (****, $p<0.0001$). (D) Scanning electron microscopy images were obtained for the different fibers and the topographical directionality was assessed, as observed by the frequency counts represented in the graphs in the left.

PCL/Gelatin fibers, as observed by the lower young's modulus (Figure 7.2B, ii-iii; Table 7.1). Interestingly, fibers produced at lower extrusion flow rates present higher plasticity, having higher strain-to-failure. In contrast, fibers produced at 1mL/h are more elastic, exhibiting higher yield strain and strain to failure (Table 7.1).

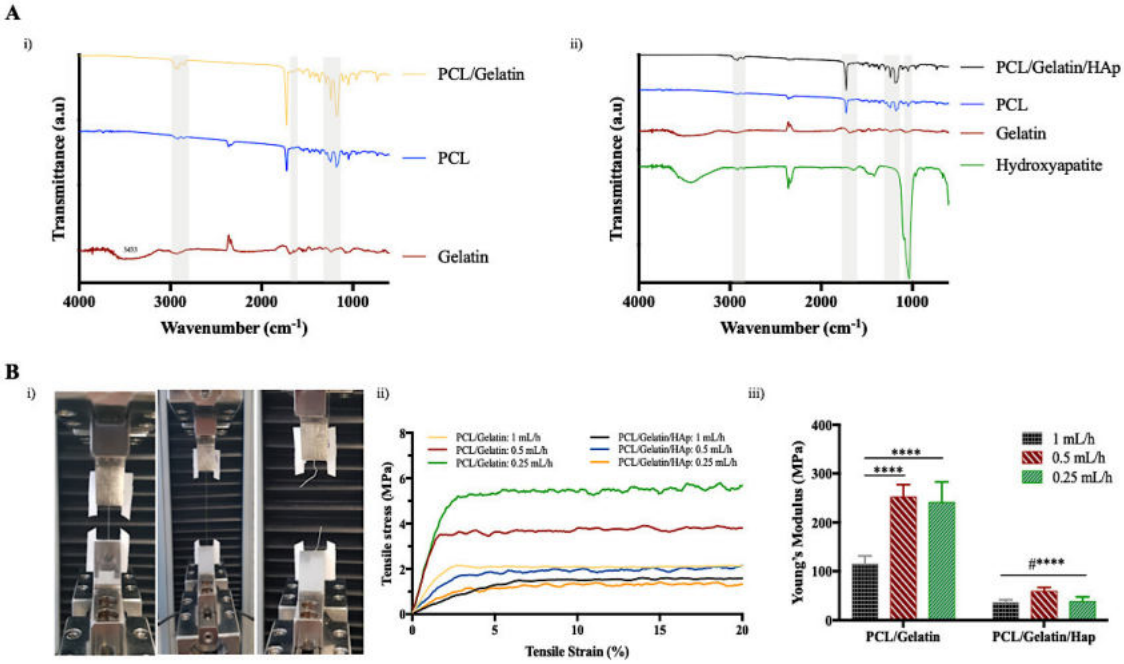

Figure 7.2 | Chemical analysis and mechanical properties of PCL/Gelatin and PCL/Gelatin/HAp wet-spun fibers. (A) FTIR spectra of neat PCL, gelatin and hydroxyapatite, as well as (i) PCL/Gelatin and (ii) PCL/Gelatin/HAp wet-spun fibers with bands of interest identified. (B) Mechanical testing of specimens. (i) The samples were placed between the tester grips and the tensile tests were performed until break point. (ii) Characteristic tensile stress-tensile strain curves of the distinct formulations and respective flow rates were obtained and (iii) the young's modulus calculated. Statistically significant differences between tested flow rates in PCL/Gelatin fibers production in comparison with the same tested conditions in PCL/Gelatin/HAp fibers are shown as #****; ****, $p<0.0001$; n=6.

7.3.3. Biological performance of wet-spun composite microfibers

Human adipose-derived stem cells were used to study the ability of PCL/Gelatin and PCL/gelatin/HAp wet-spun fibers to provide the appropriate microstructural and topographical cues to support a tenogenic-like cellular organization or osteogenic-like matrix compositional features, respectively. For this reason, fibers produced at a flow rate of 1 mL/h were chosen for biological studies with seeded cells for a culture

Table 7.1 | Mechanical properties of wet-spun fibers produced at different flow rates.

Specimen		Yield Strength [MPa]	Yield Strain [%]	Strain to Failure [%]
PCL/Gelatin	1 mL/h	2.12 ± 0.38	2.02 ± 0.28	164.45 ± 60.41
	0.5 mL/h	4.67 ± 1.29	1.93 ± 0.42	295.08 ± 95.04
	0.25 mL/h	3.69 ± 0.70	1.63 ± 0.21	476.15 ± 224.00
PCL/Gelatin/HAp	1 mL/h	0.61 ± 0.12	2.10 ± 0.32	360.77 ± 69.13
	0.5 mL/h	1.05 ± 0.21	1.81 ±0.24	442.59 ± 143.12
	0.25 mL/h	0.72 ± 0.17	2.33 ± 1.46	492.31 ± 264.48

period of 14 days in basal medium. The rationale for selecting this fabrication condition relies on the aforementioned topographical and structural features of obtained microfibers. On one hand, the anisotropic alignment of PCL/Gelatin wet-spun composite microfibers extruded at a rate of 1 mL/h was hypothesized to support cell alignment, replicating tendon cell organization. On the other hand, the compositional and isotropic features of PCL/Gelatin/HAp were envisioned to trigger an osteogenic behavior on seeded hASCs.

7.3.3.1. Cell viability and morphology of hASCs-seeded microfibers

After seeding of hASCs, microfibers were visually inspected daily under an optical microscope to monitor cell distribution and organization along the fibers. A well-distributed layer of cells and new matrix enveloping the microfibers could be observed after 7 days of culture (Figure 7.3A, I; 7.3B). This initial observation suggests that the developed PCL/Gelatin and PCL/Gelatin/HAp wet-spun microfibers were able to support the adhesion, proliferation and possible new matrix synthesis by seeded cells. Hence, cell viability was further assessed by alamar blue assay using 1 cm long hASCs-seeded microfibers (Figure 7.3A, ii). A significant increase on hASCs metabolic activity was registered from day 1 to days 7 and 14 in both PCL/Gelatin (Day7, $p<0.03$, Day 14, $p<0.001$) and PCL/Gelatin/HAp microfibers (Day7, $p<0.001$, Day 14, $p<0.0001$). No differences were observed at the correspondent days between both fiber formulations.

7.3.3.2. F-actin alignment and nuclei elongation

Given the importance of replicating the topography of two different tissues composing tendon-to-bone junction, it was also investigated whether produced fibers would modulate hASCs alignment and nuclei elongation. For that, confocal images were acquired after 7 and 14 days of culture and both cytoskeletal

alignment and nuclei aspect ratio were evaluated. In figure 7.3B, i, acquired images of actin filaments of hASCs cultured for 14 days on PCL/Gelatin show that cell cytoskeleton followed the topography of microfibers, as seen by the resulting layer of highly aligned and elongated cells and organization of actin filaments. In contrast, even though some alignment is observed in cells cytoskeleton in contact with PCL/Gelatin/HAp microfibers, a layer of randomly organized/ non-aligned cells was also observed (Figure 7.3B, ii). This behavior was confirmed by the directionality analysis of confocal images. The layer of highly aligned hASCs observed in PCL/Gelatin microfibers led to the presence of a sharper peak in a specific orientation angle frequency, representing an alignment tendency to one specific orientation (Figure 7.3B, iii), resembling tendon anisotropic cellular alignment; while, in contrast, a smoother peak was noticed in the case of PCL/Gelatin/HAp microfibers, suggesting a more random cytoskeleton orientation (Figure 7.3B, iv). Additionally, the average aspect nuclei ratio of hASCs in contact with PCL/Gelatin microfibers after 7 and 14 days of culture was found to range between 2.07±0.67 and 2.56±0.75, respectively, which is considerably high. Moreover, hASCs tended to elongate overtime in culture (Figure 7.3C, i, iii, p<0.0001). In contrast, hASCs cultured on PCL/Gelatin/HAp microfibers presented statistically significant lower nuclei aspect ratio (between 1.51±0.41 at day 7 and 1.44±0.23 at day 14; p<0.0001), which was confirmed by the presence of more round-shaped nuclei (Figure 7.3C, ii)

7.3.3.3. Extracellular matrix production and organization

The extracellular cellular matrix is a dynamic structure which interacts with cells regulating important processes such as proliferation, migration and differentiation. Therefore, to better understand the effect of both wet-spun fibers on hASCs ECM deposition and organization, SEM images of both hASCs-seeded microfibers were acquired. In accordance to optical microscopy findings, it was clear the existence of a layer of cells and matrix covering the surface of PCL/Gelatin fibers, as well as PCL/Gelatin/HAp fibers (Figure 7.3D) after 7 and 14 days of culture. Remarkably, the presence of HAp on the surface of PCL/Gelatin/HAp fibers, which led to an increased surface roughness, enabled cells to stretch (Figure 7.3D, ii, arrows). Additionally, due to increased evidence of the key role of ECM components, mainly the deposition of collagen type III (COLIII) known to be involved in the development and healing process of bone [17] and tendon/ligament [18], the expression of COLIII was evaluated in hASCs-seeded microfibers after 7 and 14 days of culture by immunostaining. Acquired fluorescence images demonstrated that collagen type III was synthesized over time by hASCs in both PCL/Gelatin and PCL/Gelatin/HAp fibers (Figure 7.3E). Furthermore, the widespread immunolabeling observed over the surface of PCL/Gelatin and PCL/Gelatin/HAp fibers was indicative of a cell migration over culture time while demonstrating the

ability of produced fibers to support the growth of cells within the 14 days of culture in basal conditions (Figure 7.3E).

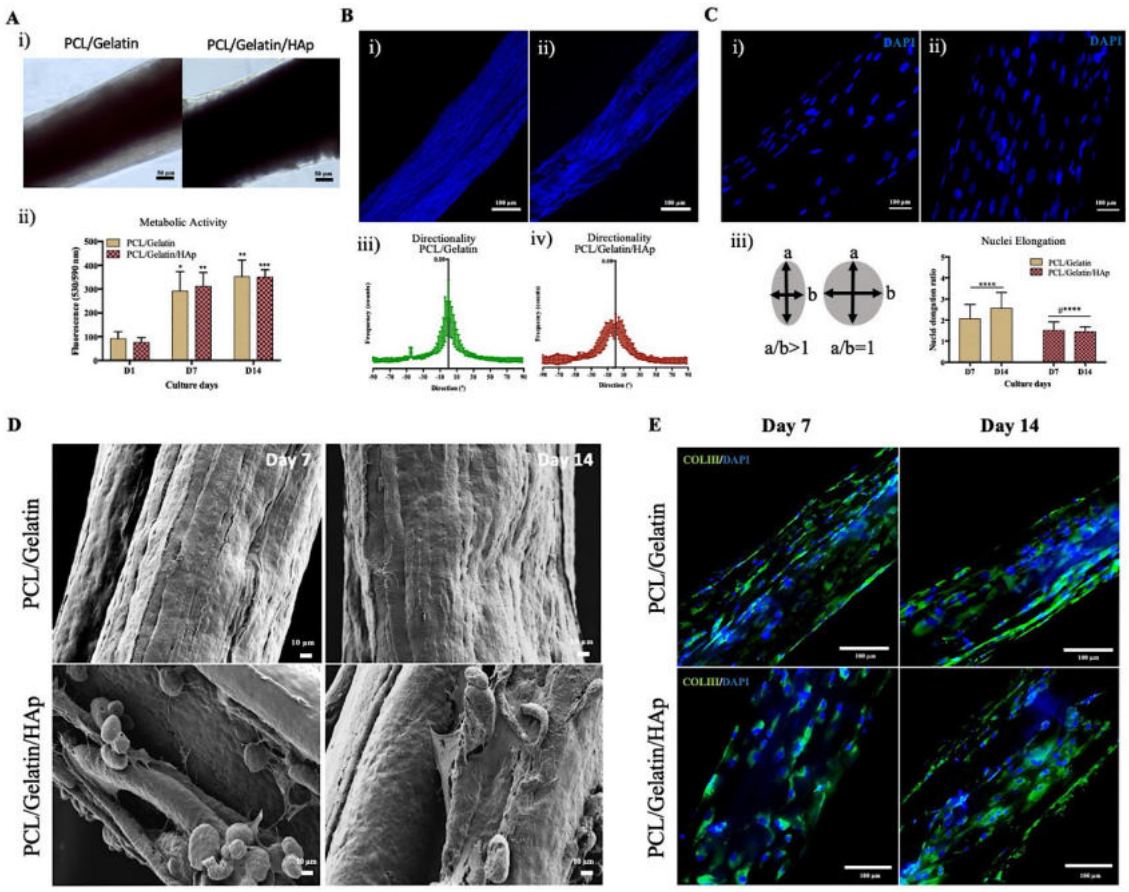

Figure 7.3 | Cell activity, morphometric analysis of hASCs and ECM organization in PCL/Gelatin and PCL/Gelatin/HAp wet-spun composite microfibers produced at 1 mL/h. (A) (i) Optical microscopy images of hASCs-seeded microfibers after 7 days of culture in basal medium condition. Scale bars, 50 μm. (ii) Metabolic activity of seeded hASCs during 14 days of culture, determined by Alamar blue assay. Statistically significant differences are shown as *, $p<0.03$, **, $p<0.001$, ***, $p<0.0003$; n=4. (B) Confocal images of actin filaments of hASCs (phalloidin, blue) and directionality of actin filaments orientation angle in (i, iii) PCL/Gelatin (n=3) and (ii, iv) PCL/Gelatin/HAp (n=3) after 14 days of culture. Scale bars, 100 μm. (C) Fluorescence microscopy images of cell nuclei (DAPI, blue) on (i) PCL/Gelatin and (ii) PCL/Gelatin/HAp wet-spun composite microfibers after 14 days of culture. Scale bars, 100 μm. (iii) Nuclei aspect ratio of hASCs cultured on both types of microfibers. Statistically significant differences between nuclei elongation in PCL/Gelatin microfibers in comparison with PCL/Gelatin/HAp microfibers are shown as #****; ****, $p<0.0001$; n=3. (D) Scanning electron microscope images of hASCs-seeded PCL/Gelatin and PCL/Gelatin/HAp fibers both at 7 and 14 days.

Scale bars, 10 µm. (E) Expression of matrix proteins observed by immunolabeling against collagen type III after 7 and 14 days of culture in both microfiber formulations. Scale bars, 100 µm.

7.3.3.4. Matrix mineralization

The mineralization of ECM is regarded as an important event during osteoblast differentiation [19]. Therefore, the ability of wet-spun composite microfibers to support bone-like extracellular matrix deposition was evaluated by AZ staining of both fibers after culturing with hASCs for 7 and 14 days in basal medium (Figure 7.4A). Optical images of stained fibers confirmed an absence of mineralization in PCL/Gelatin microfibers, while an extensive mineral deposition was observed in PCL/Gelatin/HAp microfibers, as soon as 7 days of culture in basal medium conditions. Moreover, fibers without cells were used as controls, demonstrating the presence of HAp particles in PCL/Gelatin/HAp microfibers (Figure 7.4B). Matrix mineralization in fibers was further confirmed by AZ quantification (Figure 7.4C). Statistically significant differences were observed between hASCs cultured in PCL/Gelatin and PCL/Gelatin/HAp fibers at 7 (p<0.04) and 14 days of culture (p<0.0001). This effect was more pronounced with time in culture in PCL/Gelatin/HAp microfibers. Indeed, a significant increase was observed in AZ quantification from day 7 to day 14 (p<0.0001), demonstrating intensification of mineral deposition. These results are attributed to the presence of HAp, which led to increased matrix mineralization, indicating a possible differentiation of hASCs toward the osteogenic lineage, without any osteogenic-inductive medium supplementation.

7.3.4 Textile assembling of a 3D gradient fibrous scaffold

Taking advantage of the main characteristic of textile techniques which relies on the possibility to assemble fibers into bigger and adjustable constructs while preserving the characteristics of the single units [5], produced fibers were incrementally assembled by knitting (crochet) aiming at the generation of a 3D fibrous structure with a compositional and topographical gradient to mimic the tendon-to-bone junction.

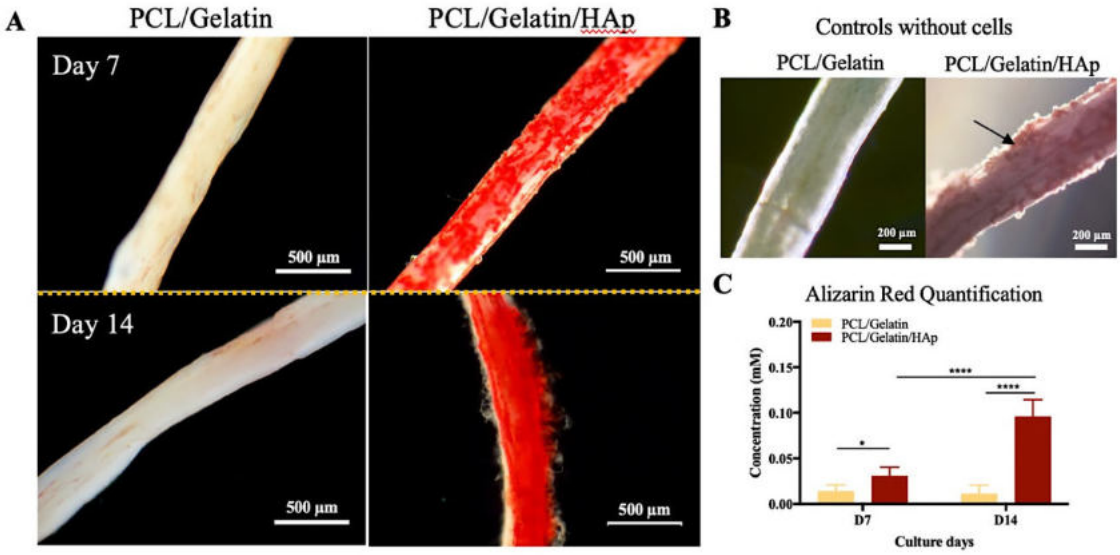

Figure 7.4 | Alizarin Red staining of PCL/Gelatin and PCL/Gelatin/HAp wet-spun composite microfibers. (A) Matrix mineralization observed by optical microscopy after 7 and 14 days of culture of hASCs in PCL/Gelatin and PCL/Gelatin/HAp fibers. Scale bars, 500 µm. (B) Fibers without cells were used as controls. The presence of HAp particles is observed in the case of PCL/Gelatin/HAp fibers. Scale bars, 200 µm. (iii) Alizarin red dye quantification performed after 7 and 14 days of culture, using the cetylpyridinium method. Statistically significant differences are shown as *, p<0.04, ****, p<0.0001, n=3.

Macroscopic images show a fibrous scaffold where PCL/Gelatin and PCL/Gelatin/HAp microfibers were knitted together by crochet (Figure 7.5A, top), creating a uniform structure with diameters of 423.20 ± 99.94 µm for tendon (PCL/Gelatin microfibers only), 410.45 ± 56.06 µm for the interface (PCL/Gelatin plus PCL/Gelatin/HAp microfibers) and 381.60 ± 45.47 µm for bone (PCL/Gelatin/Hap microfibers only). Staining with AZ clearly showed a gradient of HAp (Figure 7.5A, bottom), being these observations confirmed by dye quantification of the different parts of the scaffold (Figure 7.5B). A significant increase was demonstrated by AZ quantification when comparing the different parts, from tendon to bone (tendon *versus* interface, $p<0.002$; interface *versus* bone, $p<0.00001$; and tendon *versus* bone, $p<0.00001$). Additionally, micro-CT scanning was used to confirm the HAp content along the length of the fibrous scaffold (Figure 7.5C). Scan images allowed a clear visualization of a continuous and a gradual increase in HAp as observed in Figure 7.5C, i-ii. This increasing gradient was additionally confirmed by quantification of HAp content by micro-CT image analysis, which demonstrated a steady increase of mineral content along the scaffold, as observed in Figure 7.5D.

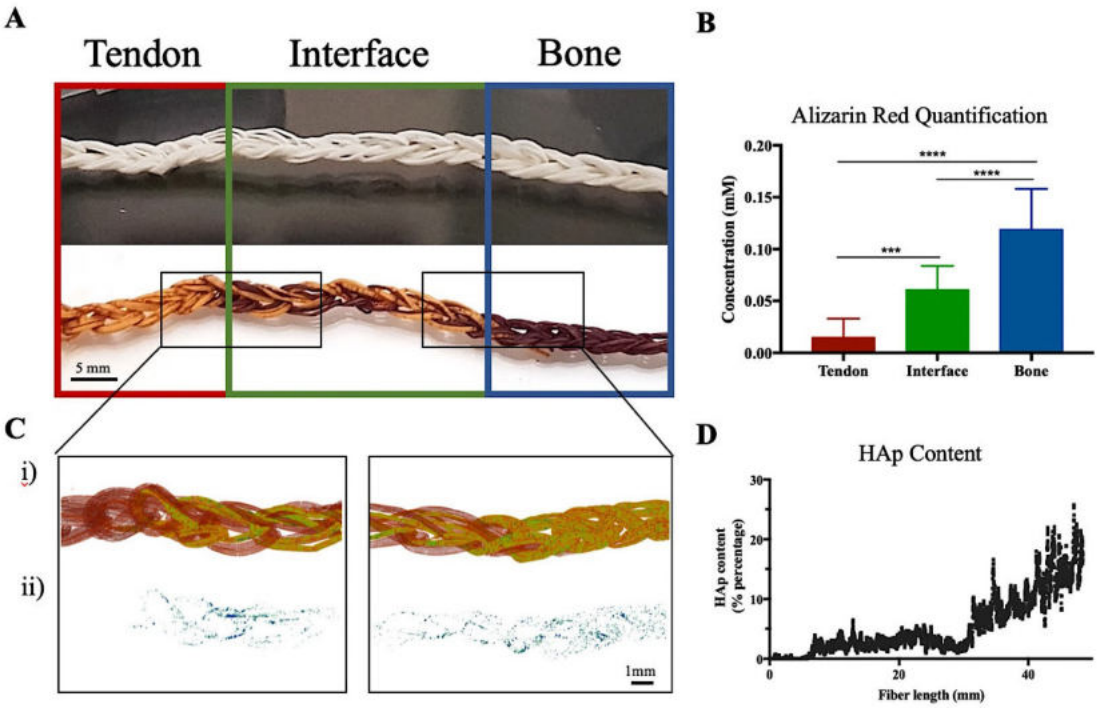

Figure 7.5 | Morphology and composition of produced scaffolds with HAp gradient. (A) 3D scaffolds were produced by crochet using PCL/Gelatin and PCL/Gelatin/HAp microfibers to mimic tendon, interface and bone. Scale bar, 5 mm. (B) Alizarin red staining was used to dye the scaffold showing a gradient in HAp content. (ii) Alizarin red quantification was performed using different sections of the scaffold through the cetylpyridinium method. Statistically significant differences are shown as ***, $p<0.002$, ****, $p<0.00001$, $n=3$. (C) Micro-CT scans of (i) different sections of the scaffold and (ii) HAp particles content. Scale bar, 1 mm. (D) Graphical demonstration of HAp content increase along the scaffold.

7.3.4.1. Collagenous matrix production and deposition

Given the importance of collagen matrix deposition in tendon-to-bone interface, the production of collagen and non-collagenous proteins was assessed in gradient scaffolds. The collagen was examined across different sections of the scaffold (Figure 7.6A-B, i-ii) and semi-quantification was performed for different sections the fibrous scaffolds, the tendon (PCL/Gelatin fibers only), interface (PCL/Gelatin and PCL/Gelatin/HAp fibers) and bony parts (PCL/Gelatin/HAp only). Interestingly, quantitative data demonstrated higher collagen accumulation in the bony-part of the scaffold (****, $p<0.0001$, Figure 7.6C), even though the tendon extremity (only PCL/Gelatin fibers) presented significantly higher collagen deposition in comparison with the interface (*, $p<0.014$). Remarkably, when assessing non-collagenous

proteins, the opposite was observed, where the highest accumulation occurred in the tendinous sections of the scaffolds (****, p<0.0001, Figure 7.6C).

Additionally, the presence of collagens types II and X was also studied (Figure 7.6B, i-ii) due to their contribution to the non-mineralized and mineralized fibrocartilage regions of tendon-to-bone interface. Strikingly, it was observed a positive scoring of collagen type II in both tendon and interface sections of the scaffolds, while a low positive was obtained for the bony-part (Figure 7.6D). In contrast, highly positive staining score of collagen type X was found in the interface, while tendon and bone scored low positive and positive, respectively (Figure 7.6D).

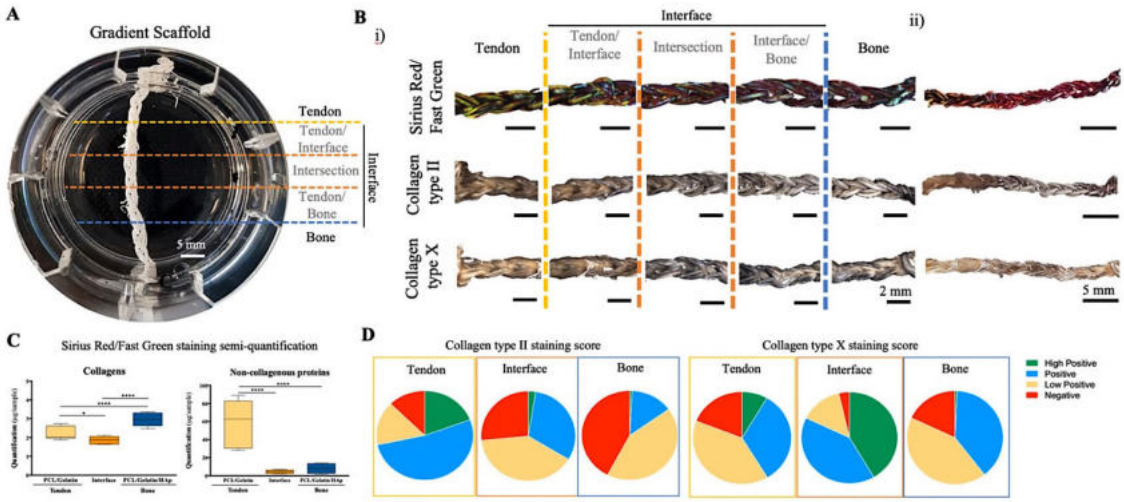

Figure 7.6 | Histochemical staining of 3D gradient scaffolds. (A) Gradient scaffolds were produced and seeded with hASCs for 14 days of culture in basal conditions. Scale bar, 5 mm. (B) Sirius red/ Fast Green and immunostaining with DAB exposure (i-ii) were used to detect a gradient in collagens and non-collagenous proteins deposition and collagen types II and X along the fibrous scaffolds, respectively. Scale bar, 2 mm (i) and 5 mm (ii). (C) Quantification of collagen (left) and non-collagenous proteins (right) was performed using different sections of the scaffold through the extraction of Sirius red and fast green stain. Statistically significant differences are shown as *, p<0.014, ****, p<0.00001; n=3. (D) DAB staining for collagen types II (n=3) and X (n=3) was scored in several parts of scaffolds.

7.4. DISCUSSION

Macro- and microstructural features of developed biomaterials are known to affect cell survival and growth, as well as to play a key role in modulating cell phenotype and function [20, 21]. In this regard, new biomaterials for tendon-to-bone interface should mimic structural and compositional properties of this soft-hard tissue transition, comprising both non-mineralized and mineralized ECM components. In

this work, two different polymeric solutions were used to mimic tendon (PCL/Gelatin) and bone tissues (PCL/Gelatin /HAp). Biodegradable synthetic polymers such as poly(lactic-co-glycolic acid) (PLGA) [22], poly-ε-caprolactone (PCL) [12], poly(lactic acid) (PLLA) [23], have demonstrated suitability to wet-spinning processing. Among these, PCL has been widely used due to its compatibility, mechanical strength, low cost and solubility in most solvents. However, its weak hydrophilicity affects cell adhesion and proliferation. Wet-spinning technique has been also widely used for processing natural origin polymers. The combination of PCL with natural polymers derived from ECM proteins, such as gelatin, has increased the biocompatibility of the fabricated fibers [24]. Gelatin, which is derived from the controlled hydrolysis of collagen, is widely used in tissue engineering due to adequate low thermal stability [12], better solubility and reduced antigenicity, in comparison to native collagen, as well as the presence of cell-binding motifs, like arginine-glycine-aspartic acid (RGD) sequences [25] and MMP-sensitive degradation sites [26]. Moreover, the addition of gelatin has been shown to result in more homogeneous fibers by electrospinning in comparison with pure PCL scaffolds [27]. The formulations proposed herein have been previously used in the fabrication of electrospun scaffolds [27] but these combinations have been relatively unexplored using wet-spinning as the fiber production method. Since natural polymers usually dissolve in aqueous environments, being gradually released, a coagulation bath with a crosslinking agent was included in the wet-spinning set-up to assure gelatin was incorporated into the collected fiber. Glutaraldehyde is the most commonly used cross-linking agent which has the ability to cross-link the primary amine groups of collagenous tissues [28]. Even though percentages above 8% of glutaraldehyde have been reported to be cytotoxic [29], lowering the concentration has been reported to be biocompatible, as already described for anionic collagenous membranes [30]. In this work, a solution of 1.25% (v/v) glutaraldehyde/water was used to produce the polymeric wet-spun microfibers. After injecting the polymeric solutions into the coagulation bath, composite microfibers could be collected in a continuous and large-scale manner. In addition, cell viability up to 14 days of culture suggests that the proposed system was harmless to seeded hASCs.

Mechanically, tendons and ligaments are demanding tissues exhibiting different mechanical properties depending on body location [31]. At the interface, semitendinosus and Achilles tendons have higher young's modulus in the ranges of 540-1081 and 819±208 MPa [32], respectively. Typically, electrospun based scaffolds proposed for tendon or ligament tissue engineering fail in meeting the native tissue's mechanical requirements, presenting tensile properties in lower ranges, normally with Young's modulus up to 30 MPa [33, 34]. In this regard, produced wet-spun PCL/Gelatin microfibers extruded at 1 mL/h

have demonstrated to have an adequate mechanical performance, meeting the tendon mechanical requirements in a biomimetic manner.

Furthermore, to mimic as close as possible the composition of bone, micro-to-nanosized hydroxyapatite particles were incorporated in the polymeric solution. Hydroxyapatite is a well-established material for bone regeneration due to its biocompatibility, chemical resemblance with the inorganic part of bone and osteoconductive properties. Several studies have demonstrated that mesenchymal stem cells of both rat and human origins were sensitive to HAp concentrations as low as 1% w/w of solid scaffold weight and, increasing this concentration would result in different cells responses [35-37]. Therefore, in this study, hydroxyapatite was used at percentages that trigger, in a controllable manner, an osteogenic-like cellular behavior without the need for osteogenic medium supplementation.

Additionally, topography has been shown to strongly affect cells response resulting in cells commitment to different lineages, which can be induced directly by the surface topography or from an altered ECM layer deposition on the surface of the biomaterial [33, 38-40]. In wet-spinning, fiber topography, as well as diameter can be tuned by changing the flow rate during injection. Therefore, three different extrusion flow rates were tested to study the topography of produced fibers. Interestingly, 1 mL/h extrusion flow rate seemed to induce a better alignment on PCL/Gelatin microfibers, which is an important characteristic for the tendon counterpart of the junction, as already described in the literature [33, 38]. Several studies have shown that individual fiber anisotropy guides cell alignment potentially leading to a better control over pro-regenerative events, while 3D fibrous scaffolds can match the mechanical properties required at the tissue-level [38, 41-43]. Herein, the aligned arrangement of the PCL/Gelatin wet-spun composite microfibers induced a high cytoskeleton alignment and nuclei elongation, resembling native tendon anisotropic organization. This was observed after seeding hASCs, which were able to align following the direction of the surface topography of PCL/Gelatin microfibers through contact guidance mechanisms, even after prolonged times in culture.

In contrast, PCL/Gelatin/HAp microfibers produced at the same extrusion rate presented HAp particles distributed along the surface of the fiber, sticking out and creating lumps and beads. This morphology resulted from the presence of larger sized particles as observed by the micro-CT analysis. Moreover, changing the flow rate also affected the porosity of PCL/Gelatin/HAp fibers. Extrusion of fibers at 1mL/h, resulted in higher pore volumes and pore amount. This may be correlated with the amount of polymeric solution extruded, meaning that a high flow rate leads to higher amounts of polymeric solution to be extruded to the crosslinking bath which resulted in the accumulation of HAp particles in the surface of larger fibers. The same was not observed for lower extrusion rates, where the amount and time of

polymeric solution in contact with the bath is decreased, leading to thinner fibers incorporating small sized particles.

Fibers topography and flow rate can potentially be correlated to the "Kelvin-Helmholtz instability" (**EQUATION 7.1**), as demonstrated elsewhere [44]:

Equation 7.1: $$(U1 - U2)\text{^}2 > 2\sqrt{g\sigma(\rho 1 - \rho 2(\rho 1 + \rho 2)\left(\frac{1}{\rho 1 \rho 2}\right)}$$

Where, ρ1, ρ2, U1, and U2 are the densities and velocities of liquids 1 and 2, g is the acceleration due to gravity, and σ is the interfacial tension between the two fluids. In the present study conditions, U2 tends to 0 as it corresponds to the coagulation bath.

Likewise, fibers diameter can also be correlated with the flow rate as described by Han et al [45], who demonstrated that the volumetric flow rate is directly proportional to the filament cross-sectional area (**EQUATION 7.2**):

Equation 7.2: $$A(x) = \frac{Q}{V(x)},$$

where A(x) is the filament cross-sectional area, V(x) is the axial velocity and Q is the volumetric flow rate. Similarly, this is also observed in electrospinning technique, where the flow rate influences both the diameter and morphology of fibers, meaning that high flow rate results in longer drying time due to greater volume of polymeric solution drawn from the needle [46].

Incorporation of HAp decreased the Young's modulus of PCL/Gelatin/HAp microfibers in comparison with PCL/Gelatin wet spun fibers, according to what has been previously reported [47]. Moreover, the presence of HAp led to a higher matrix mineralization as soon as 7 days, suggesting an induction of osteogenic differentiation of hASCs. Results from the literature show that the micro-pattern of hydroxyapatite in materials seem to induce a higher promotion in early cells adhesions and subsequent osteogenic differentiation [48].

The fabrication of a suitable interface engineered approach is based on the design of stratified or multi-graded biomimetic scaffolds able to replicate the complex and hierarchical organization, structure and mechanical properties present in tendon-to-bone junction [49]. Great attention has been given to the potential use of textile technologies for the biofabrication of tissue engineered constructs. Different textile techniques, among knitting, weaving, braiding, can be used to create fibrous structures with the

demanded properties of different tissues, using a rational assembly of fibers into bigger textile constructs while conserving the main features of the single unit [50, 51]. In tendon-to-bone interface, changes in structure, composition and mineralization are gradual and continuous and aid an efficient transfer of load between the two dissimilar tissues [52]. Thus, taking advantage of textile techniques, the produced polymeric fibers (PCL/Gelatin and PCL/Gelatin/HAp, 1 mL/h) were knitted together by crochet to create a gradient in composition along the scaffold. This technique differs from knitting because the stitches are built on top of each other and the active loop is the only place from which the scaffold is prone to unraveling, making the construct more stable. To mimic the tendon structure, PCL/Gelatin fibers were crochet together and afterwards, to create the interface, PCL/Gelatin/HAp microfibers were gradually incorporated until only this material was left. Alizarin red staining and HAp profile from micro-CT allowed to confirm the presence of a mineral gradient in HAp content. Overall, these results show that engineered microfibers could be handled manually and were able to withstand the textile assembling to produce 3D gradient scaffolds.

Tendon-to-bone interface is also characterized by the presence of four different zones (tendon, non-mineralized and mineralized fibrocartilage and bone), with collagen as major component [53]. These transitions were also observed in produced fibrous scaffolds. Strikingly, it was possible to distinguish four different zones: tendon (first sections), interface which was composed by the tendon/intersection and intersection/bone, and bone (last section). Taking advantage of the topological and compositional differences across the gradient scaffolds, it was possible to induce the deposition of different collagens in the distinctive parts of the construct. Even though collagens were quantified in all parts, non-collagenous proteins were highly present in the tendon section. In tendon, collagen fibers are interspersed by a variety of non-collagenous matrix components, namely proteoglycans, glycoproteins and glycoconjugates, playing an important role within the tissue [54]. The presence of collagen type II and collagen type X was observed in the interfaced section, as demonstrated by the score obtained along the scaffolds. This is also observed in the native tissue, where non-mineralized fibrocartilage is characterized by a collagenous matrix composed of collagen types II and III, with small amounts of types I, IX, and X collagen [55]. The mineralized fibrocartilage also contains collagen type II, with significant higher amounts of type X collagen [55].

A similar work was developed by Sun et al [56] in which co-electrospun dual scaffolds, poly(lactic-co-glycolic acid)/collagen I-polycaprolactone/nanohydroxyapatite (PLGA/Col-PCL/nHA), were used to bridge massive rotator cuff tears in rabbit models [56]. However, the authors did not truly generate a gradient of mineral and collagen composition, which is addressed by the gradient developed in the present study.

On the other hand, Li et al [57] developed gradients of mineral content in PCL and PLGA nanofibers using concentrated simulated body fluid. However, only randomly aligned non-woven mats coated with calcium phosphate were used to mimic the tendon-to-bone insertion site, not truly mimicking the topological features of the native multi-tissue transition. Moreover, gradient scaffolds were not able to uniformly support pre-osteoblast cells adhesion [57]. Comparably, Nowlin et al [58] produced random-to-aligned nanofiber scaffolds to mimic the micro-topology of tendon-to-bone interface. Even though a transitional region was obtained, authors seeded terminally cells (fibroblasts and osteosarcoma cells) on the different regions and did not demonstrate de ability of cells to differentiate towards specific lineages due to the influence of fibers topology and composition.

Overall, produced scaffolds demonstrated the potential use in tendon-to-bone tissue regeneration by replicating the transition between tissues and collagen matrix deposition observed in the native interface. In summary, through the addition of HAp into the initial polymeric solutions, structural and compositional properties could be tuned. The developed microfibers can potentially guide a single cell source toward different behaviors. Cellular morphometric characteristics demonstrated that the topography of PCL/Gelatin wet-spun composite microfibers could induce a preferential alignment of seeded hASCs, resembling the anisotropic cellular organization found in native tendon niches. Matrix mineralization on PCL/Gelatin/HAp wet-spun composite microfibers suggested that seeded hASCs were able to produce an osteogenic-like ECM, without the external addition of any osteoinductive factors. Altogether, these results demonstrate the feasibility of using wet-spinning method to generate continuous aligned and textured composite microfibers, which can be further assembled into more complex 3D gradient structures through the application of textile techniques to closely resemble tendon-to-bone microstructure.

7.5. CONCLUSIONS

Tendon-to-bone interface is a complex hierarchical tissue, exhibiting unique structural and compositional characteristics. The development of advanced tissue engineered approaches should focus the use of straightforward techniques toward mimicking the native features of the different tissues forming the junction. In this study, a wet-spinning technique was used to produce two different wet spun microfibers with compositional and structural differences in order to mimic tendon anisotropic organization and mineral composition of bone. Biological studies revealed that the fibers were not only able to support cell proliferation but also to favor cellular anisotropic alignment or to induce an osteogenic-like phenotype on human adipose derived stem cells in the presence of HAp. In fact, the continuous wet-spinning technique in combination with textile technologies enabled the generation of a fibrous scaffold with a gradient in

polymer composition, resulting in a mineral gradient of HAp content. Altogether, results clearly demonstrated the feasibility of using simple fiber processing techniques, such as wet-spinning, to tailor cells response while having a precise control over fibers topography and composition. Moreover, the combination with advanced textile techniques allowed the development of 3D fibrous scaffolds envisioning tendon-to-bone regeneration.

7.6. ACKNOWLEDGEMENTS

The authors thank to Hospital da Prelada (Porto, Portugal) for providing lipoaspirate tissue (Plastic Surgery Department) samples; Dr. Rui Domingues and Dr. Pedro Babo for the technical help with confocal microscopy and micro-CT analysis. The authors acknowledge the financial support from the European Union Framework Programme for Research and Innovation HORIZON2020, under the TEAMING Grant agreement No 739572 - The Discoveries CTR, the ERC Grant CoG MagTendon nr 772817, FCT– Fundação para a Ciência e a Tecnologia for the PhD grant of IC (PD/BD/128088/2016); and the Project NORTE-01-0145-FEDER-000021: "Accelerating tissue engineering and personalized medicine discoveries by the integration of key enabling nanotechnologies, marine-derived biomaterials and stem cells", supported by Norte Portugal Regional Operational Programme (NORTE 2020), under the PORTUGAL 2020 Partnership Agreement, through the European Regional Development Fund (ERDF).

7.7. REFERENCES

[1] K.A. Derwin, A.R. Baker, J.P. Iannotti, J.A. McCarron, Preclinical Models for Translating Regenerative Medicine Therapies for Rotator Cuff Repair, Tissue Engineering Part B 16(1) (2010) 10.1089=ten.teb.2009.0209.

[2] S. Thomopoulos, G.R. Williams, L.J. Soslowsky, Tendon to Bone Healing: Differences in Biomechanical, Structural, and Compositional Properties Due to a Range of Activity Levels, Journal of Biomechanical Engineering 125(1) (2003) 10.1115/1.1536660.

[3] S. Thomopoulos, G. Hattersley, V. Rosen, M. Mertens, L. Galats, G.R. Williams, L.J. Soslowsky, The localized expression of extracellular matrix components in healing tendon insertion sites: an in situ hybridization study, Journal of Orthopaedic Research 20 (2002) 454-463.

[4] R.K. Roeder, A.G. Schwartz, J.D. Pasteris, G.M. Genin, T.L. Daulton, S. Thomopoulos, Mineral Distributions at the Developing Tendon Enthesis, PLoS ONE 7(11) (2012) 10.1371/journal.pone.0048630.

[5] A. Tamayol, M. Akbari, N. Annabi, A. Paul, A. Khademhosseini, D. Juncker, Fiber-based tissue engineering: Progress, challenges, and opportunities, Biotechnol Adv 31(5) (2013) 669-87, 10.1016/j.biotechadv.2012.11.007.

[6] J. Burck, S. Heissler, U. Geckle, M.F. Ardakani, R. Schneider, A.S. Ulrich, M. Kazanci, Resemblance of electrospun collagen nanofibers to their native structure, Langmuir 29(5) (2013) 1562-72, 10.1021/la3033258.

[7] L. Yang, C.F. Fitie, K.O. van der Werf, M.L. Bennink, P.J. Dijkstra, J. Feijen, Mechanical properties of single electrospun collagen type I fibers, Biomaterials 29(8) (2008) 955-62, 10.1016/j.biomaterials.2007.10.058.

[8] D.R. Nisbet, J.S. Forsythe, W. Shen, D.I. Finkelstein, M.K. Horne, Review paper: a review of the cellular response on electrospun nanofibers for tissue engineering, J Biomater Appl 24(1) (2009) 7-29, 10.1177/0885328208099086.

[9] E. Mathiowitz, M.D. Lavin, R. Hopkins, Wet spun microfibers - potential in the design of controlled-release scaffolds?, Therapeutic Delivery 4(9) (2013) 1075–1077.

[10] J.M. Caves, V.A. Kumar, J. Wen, W. Cui, A. Martinez, R. Apkarian, J.E. Coats, K. Berland, E.L. Chaikof, Fibrillogenesis in continuously spun synthetic collagen fiber, J Biomed Mater Res B Appl Biomater 93(1) (2010) 24-38, 10.1002/jbm.b.31555.

[11] D. Puppi, A.M. Piras, F. Chiellini, E. Chiellini, A. Martins, I.B. Leonor, N. Neves, R. Reis, Optimized electro- and wet-spinning techniques for the production of polymeric fibrous scaffolds loaded with bisphosphonate and hydroxyapatite, Journal of Tissue Engineering and Regenerative Medicine 5(4) (2011) 253-263, 10.1002/term.310.

[12] D. Puppi, F. Chiellini, Wet-spinning of biomedical polymers: from single-fibre production to additive manufacturing of three-dimensional scaffolds, Polymer International 66(12) (2017) 1690-1696, 10.1002/pi.5332.

[13] S.C. Neves, L.S. Moreira Teixeira, L. Moroni, R.L. Reis, C.A. Van Blitterswijk, N.M. Alves, M. Karperien, J.F. Mano, Chitosan/poly(epsilon-caprolactone) blend scaffolds for cartilage repair, Biomaterials 32(4) (2011) 1068-79, 10.1016/j.biomaterials.2010.09.073.

[14] D. Puppi, C. Mota, M. Gazzarri, D. Dinucci, A. Gloria, M. Myrzabekova, L. Ambrosio, F. Chiellini, Additive manufacturing of wet-spun polymeric scaffolds for bone tissue engineering, Biomed Microdevices 14(6) (2012) 1115-27, 10.1007/s10544-012-9677-0.

[15] Y. Yang, J. Sun, X. Liu, Z. Guo, Y. He, D. Wei, M. Zhong, L. Guo, H. Fan, X. Zhang, Wet-spinning fabrication of shear-patterned alginate hydrogel microfibers and the guidance of cell alignment, Regen Biomater 4(5) (2017) 299-307, 10.1093/rb/rbx017.

[16] I. Calejo, R. Costa-Almeida, A.I. Goncalves, D. Berdecka, R.L. Reis, M.E. Gomes, Bi-directional modulation of cellular interactions in an in vitro co-culture model of tendon-to-bone interface, Cell Prolif 51(6) (2018) e12493, 10.1111/cpr.12493.

[17] S.W. Volk, S.R. Shah, A.J. Cohen, Y. Wang, B.K. Brisson, L.K. Vogel, K.D. Hankenson, S.L. Adams, Type III collagen regulates osteoblastogenesis and the quantity of trabecular bone, Calcif Tissue Int 94(6) (2014) 621-31, 10.1007/s00223-014-9843-x.

[18] C.S. Chamberlain, E.M. Crowley, H. Kobayashi, K.W. Eliceiri, R. Vanderby, Quantification of collagen organization and extracellular matrix factors within the healing ligament, Microsc Microanal 17(5) (2011) 779-87, 10.1017/S1431927611011925.

[19] H.C. Blair, Q.C. Larrouture, Y. Li, H. Lin, D. Beer-Stoltz, L. Liu, R.S. Tuan, L.J. Robinson, P.H. Schlesinger, D.J. Nelson, Osteoblast Differentiation and Bone Matrix Formation In Vivo and In Vitro, Tissue Eng Part B Rev 23(3) (2017) 268-280, 10.1089/ten.TEB.2016.0454.

[20] J. Leijten, J. Rouwkema, Y.S. Zhang, A. Nasajpour, M.R. Dokmeci, A. Khademhosseini, Advancing Tissue Engineering: A Tale of Nano-, Micro-, and Macroscale Integration, Small 12(16) (2016) 2130-2145, 10.1002/smll.201501798.

[21] W. Liu, J. Lipner, J. Xie, C.N. Manning, S. Thomopoulos, Y. Xia, Nanofiber scaffolds with gradients in mineral content for spatial control of osteogenesis, ACS Appl Mater Interfaces 6(4) (2014) 2842-9, 10.1021/am405418g.

[22] K. Wanawananon, S.E. Moulton, G.G. Wallace, S. Liawruangrath, Fabrication of novel core-shell PLGA and alginate fiber for dual-drug delivery system, Polymers for Advanced Technologies 27(8) (2016) 1014-1019, 10.1002/pat.3763.

[23] J.S. Fernandes, R.L. Reis, R.A. Pires, Wetspun poly-L-(lactic acid)-borosilicate bioactive glass scaffolds for guided bone regeneration, Mater Sci Eng C Mater Biol Appl 71 (2017) 252-259, 10.1016/j.msec.2016.10.007.

[24] J. Lee, G. Tae, Y.H. Kim, I.S. Park, S.-H. Kim, S.H. Kim, The effect of gelatin incorporation into electrospun poly(l-lactide-co-ε-caprolactone) fibers on mechanical properties and cytocompatibility, Biomaterials 29(12) (2008) 1872-1879, 10.1016/j.biomaterials.2007.12.029.

[25] Y. Liu, M.B. Chan-Park, A biomimetic hydrogel based on methacrylated dextran-graft-lysine and gelatin for 3D smooth muscle cell culture, Biomaterials 31 (2010) 1158–1170, 10.1016/j.biomaterials.20.

[26] J. Vandooren, P.E. Van den Steen, G. Opdenakker, Biochemistry and molecular biology of gelatinase B or matrix metalloproteinase-9 (MMP-9): the next decade, Crit Rev Biochem Mol Biol 48(3) (2013) 222-72, 10.3109/10409238.2013.770819.

[27] M. Sattary, M.T. Khorasani, M. Rafienia, H.S. Rozve, Incorporation of nanohydroxyapatite and vitamin D3 into electrospun PCL/Gelatin scaffolds: The influence on the physical and chemical properties and cell behavior for bone tissue engineering, Polymers for Advanced Technologies 29(1) (2018) 451-462, 10.1002/pat.4134.

[28] L.H.H.O. Damink, P.J. Dijkstra, M.J.A. Van Luyn, P.B. Van Wachem, P. Nieuwenhuis, J. Feijen, Glutaraldehyde as a crosslinking agent for collagen-based biomaterials, Journal of Materials Science 6 (1995) 450-472.

[29] P.R. Umashankar, P.V. Mohanan, T.V. Kumari, Glutaraldehyde treatment elicits toxic response compared to decellularization in bovine pericardium, Toxicol Int 19(1) (2012) 51-8, 10.4103/0971-6580.94513.

[30] G. Goisis, E.M. Junior, A.C. Marcantonio, R.C.C. Lia, D.C.J. Cancian, W.M. Carvalho, Biocompatibility studies of anionic collagen membranes with different degree of glutaraldehyde cross-linking, Biomaterials 20 (1999) 27-34, 0142-9612/98/$.

[31] J.G. Barber, A.M. Handorf, T.J. Allee, W.J. Li, Braided nanofibrous scaffold for tendon and ligament tissue engineering, Tissue Eng Part A 19(11-12) (2013) 1265-74, 10.1089/ten.tea.2010.0538.

[32] H.-J. Jung, M.B. Fisher, S.L.Y. Woo, Role of biomechanics in the understanding of normal, injured, and healing ligaments and tendons, BMC Sports Science, Medicine and Rehabilitation 1(1) (2009) 10.1186/1758-2555-1-9.

[33] Z. Yin, X. Chen, J.L. Chen, W.L. Shen, T.M. Hieu Nguyen, L. Gao, H.W. Ouyang, The regulation of tendon stem cell differentiation by the alignment of nanofibers, Biomaterials 31(8) (2010) 2163-2175, 10.1016/j.biomaterials.2009.11.083.

[34] S.B. Orr, A. Chainani, K.J. Hippensteel, A. Kishan, C. Gilchrist, N.W. Garrigues, D.S. Ruch, F. Guilak, D. Little, Aligned multilayered electrospun scaffolds for rotator cuff tendon tissue engineering, Acta Biomater 24 (2015) 117-26, 10.1016/j.actbio.2015.06.010.

[35] N. Barbani, G.D. Guerra, C. Cristallini, P. Urciuoli, R. Avvisati, A. Sala, E. Rosellini, Hydroxyapatite/gelatin/gellan sponges as nanocomposite scaffolds for bone reconstruction, J Mater Sci Mater Med 23(1) (2012) 51-61, 10.1007/s10856-011-4505-2.

[36] J.H. Lee, N.G. Rim, H.S. Jung, H. Shin, Control of osteogenic differentiation and mineralization of human mesenchymal stem cells on composite nanofibers containing poly[lactic-co-(glycolic acid)] and hydroxyapatite, Macromol Biosci 10(2) (2010) 173-82, 10.1002/mabi.200900169.

[37] T.T. Ruckh, D.A. Carroll, J.R. Weaver, K.C. Popat, Mineralization content alters osteogenic responses of bone marrow stromal cells on hydroxyapatite/polycaprolactone composite nanofiber scaffolds, J Funct Biomater 3(4) (2012) 776-98, 10.3390/jfb3040776.

[38] M. Laranjeira, R.M.A. Domingues, R. Costa-Almeida, R.L. Reis, M.E. Gomes, 3D Mimicry of Native-Tissue-Fiber Architecture Guides Tendon-Derived Cells and Adipose Stem Cells into Artificial Tendon Constructs, Small 13(31) (2017) 1700689, 10.1002/smll.201700689.

[39] G. Abagnale, M. Steger, V.H. Nguyen, N. Hersch, A. Sechi, S. Joussen, B. Denecke, R. Merkel, B. Hoffmann, A. Dreser, U. Schnakenberg, A. Gillner, W. Wagner, Surface topography enhances differentiation of mesenchymal stem cells towards osteogenic and adipogenic lineages, Biomaterials 61 (2015) 316-26, 10.1016/j.biomaterials.2015.05.030.

[40] F. Luthen, R. Lange, P. Becker, J. Rychly, U. Beck, J.G. Nebe, The influence of surface roughness of titanium on beta1- and beta3-integrin adhesion and the organization of fibronectin in human osteoblastic cells, Biomaterials 26(15) (2005) 2423-40, 10.1016/j.biomaterials.2004.07.054.

[41] S.K. Madhurakkat Perikamana, J. Lee, T. Ahmad, Y. Jeong, D.-G. Kim, K. Kim, H. Shin, Effects of Immobilized BMP-2 and Nanofiber Morphology on In Vitro Osteogenic Differentiation of hMSCs and In Vivo Collagen Assembly of Regenerated Bone, ACS Applied Materials & Interfaces 7(16) (2015) 8798-8808, 10.1021/acsami.5b01340.

[42] Z. Zheng, J. Ran, W. Chen, Y. Hu, T. Zhu, X. Chen, Z. Yin, B.C. Heng, G. Feng, H. Le, C. Tang, J. Huang, Y. Chen, Y. Zhou, P. Dominique, W. Shen, H.W. Ouyang, Alignment of collagen fiber in knitted silk scaffold for functional massive rotator cuff repair, Acta Biomater 51 (2017) 317-329, 10.1016/j.actbio.2017.01.041.

[43] R. Costa-Almeida, R.M.A. Domingues, A. Fallahi, H. Avci, I.K. Yazdi, M. Akbari, R.L. Reis, A. Tamayol, M.E. Gomes, A. Khademhosseini, Cell-laden composite suture threads for repairing damaged tendons, Journal of Tissue Engineering and Regenerative Medicine 12(4) (2018) 1039-1048, 10.1002/term.2605.

[44] S.-K. Chae, E. Kang, A. Khademhosseini, S.-H. Lee, Micro/Nanometer-Scale Fiber with Highly Ordered Structures by Mimicking the Spinning Process of Silkworm, Advanced Materials 25(22) (2013) 3071-3078, 10.1002/adma.201300837.

[45] C.D. Han, L. Segal, A study of fiber extrusion in wet spinning. II. Effects of spinning conditions on fiber formation, Journal of Applied Polymer Science 14(12) (1970) 2999-3019, 10.1002/app.1970.070141206.

[46] G.C. Rutledge, S.V. Fridrikh, Formation of fibers by electrospinning, Adv Drug Deliv Rev 59(14) (2007) 1384-91, 10.1016/j.addr.2007.04.020.

[47] G. Tetteh, A.S. Khan, R.M. Delaine-Smith, G.C. Reilly, I.U. Rehman, Electrospun polyurethane-hydroxyapatite bioactive Scaffolds for bone tissue engineering- The role of solvent and hydroxyapatite particles, journal of the mechanical behavior of biomedical materials 39 (2014) 95-110, 10.1016/j.jmbbm.2014.06.019.

[48] C. Zhao, X. Wang, L. Gao, L. Jing, Q. Zhou, J. Chang, The role of the micro-pattern and nano-topography of hydroxyapatite bioceramics on stimulating osteogenic differentiation of mesenchymal stem cells, Acta Biomater 73 (2018) 509-521, 10.1016/j.actbio.2018.04.030.

[49] H.H. Lu, J. Jiang, Interface Tissue Engineeringand the Formulation of Multiple-Tissue Systems, Tissue Engineering I2006, pp. 91-111, 10.1007/b138509.

[50] M. Akbari, A. Tamayol, S. Bagherifard, L. Serex, P. Mostafalu, N. Faramarzi, M.H. Mohammadi, A. Khademhosseini, Textile Technologies and Tissue Engineering: A Path Toward Organ Weaving, Adv Healthc Mater 5(7) (2016) 751-66, 10.1002/adhm.201500517.

[51] A. Maziz, A. Concas, A. Khaldi, J. Stalhand, N. Persson, E.W.H. Jager, Knitting and weaving artificial muscles, Science Advances (3) (2017) 1-11.

[52] S. Thomopoulos, G.M. Genin, L.M. Galatz, The development and morphogenesis of the tendon-to-bone insertion What development can teach us about healing, J Musculoskelet Neuronal Interact 10(1) (2010) 35-45.

[53] M. Benjamin, H. Toumi, J.R. Ralphs, G. Bydder, T.M. Best, S. Milz, Where tendons and ligaments meet bone: attachment sites ('entheses') in relation to exercise and/or mechanical load, Journal of Anatomy 208 (2006) 471–490.

[54] C.T. Thorpe, H.L. Birch, P.D. Clegg, H.R.C. Screen, The role of the non-collagenous matrix in tendon function, International Journal of Experimental Pathology 94(4) (2013) 248-259, 10.1111/iep.12027.

[55] S. Thomopoulos, J.P. Marquez, B. Weinberger, V. Birman, G.M. Genin, Collagen fiber orientation at the tendon to bone insertion and its influence on stress concentrations, Journal of Biomechanics 39(10) (2006) 1842-1851, 10.1016/j.jbiomech.2005.05.021.

[56] Y. Sun, F. Han, P. Zhang, Y. Zhi, J. Yang, X. Yao, H. Wang, C. Lin, X. Wen, J. Chen, P. Zhao, A synthetic bridging patch of modified co-electrospun dual nano-scaffolds for massive rotator cuff tear, Journal of Materials Chemistry B 4(45) (2016) 7259-7269, 10.1039/c6tb01674j.

[57] X. Li, J. Xie, J. Lipner, X. Yuan, S. Thomopoulos, Y. Xia, Nanofiber Scaffolds with Gradations in Mineral Content for Mimicking the Tendon-to-Bone Insertion Site, Nano Letters 9(7) (2009) 2763-2768, 10.1021/nl901582f.

[58] J. Nowlin, M.A. Bismi, B. Delpech, P. Dumas, Y. Zhou, G.Z. Tan, Engineering the hard–soft tissue interface with random-to-aligned nanofiber scaffolds, Nanobiomedicine 5 (2018) 1849543518803538, 10.1177/1849543518803538.

7.8. SUPPLEMENTARY INFORMATION

7.8.1. FIGURES

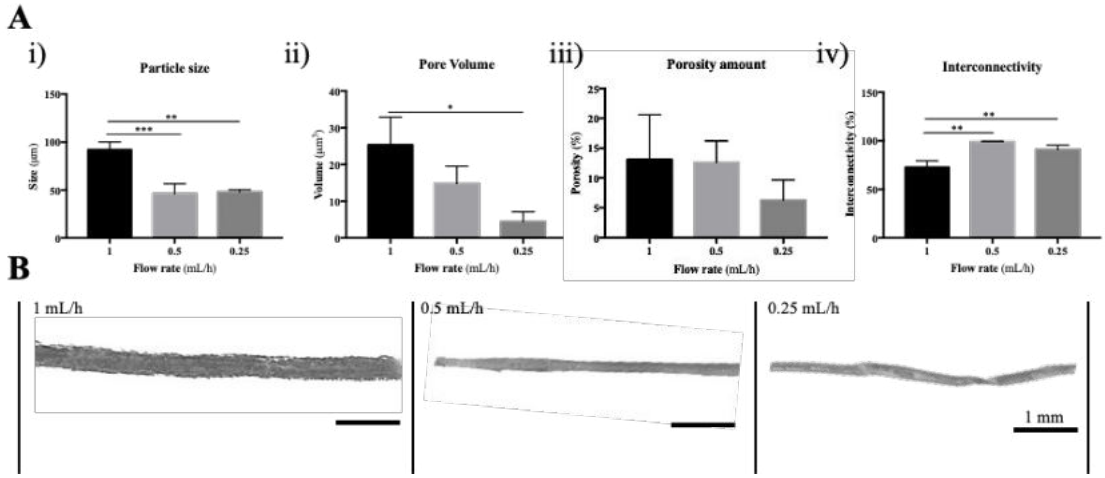

Supplementary Figure S7.1 | Microtomography (micro-CT) analysis of PCL/Gelatin/HAp fibers. (A) Morphometric analysis of (i) particle size, (ii) pore volume, (iii) porosity amount and (iv) interconnectivity of fibers produced at different flow rates. Statistically significant differences are shown as *, p<0,02 **, p<0.008, ***, p<0,0009; n=3. (B) Micro-CT 3D reconstruction of PCL/Gelatin/HAp microfibers. Scale bar, 1 mm.

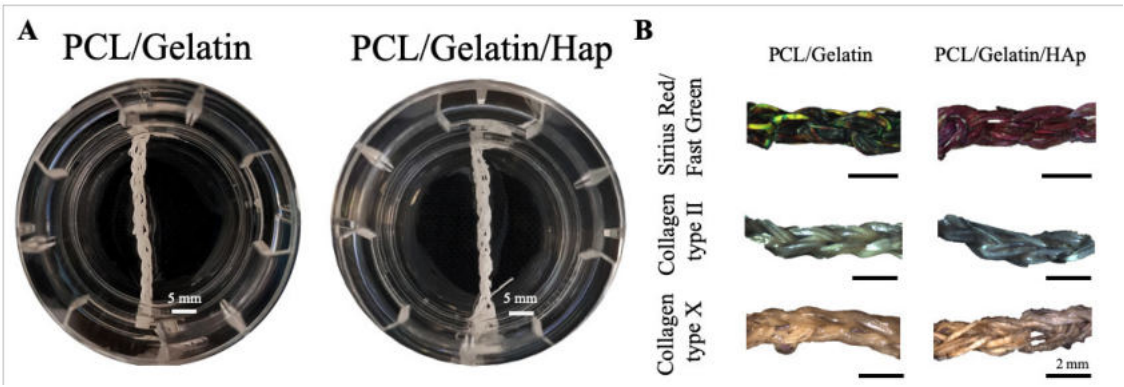

Supplementary Figure S7.2 | Histochemical staining of fibrous scaffolds after 14 days of culture. (A) Scaffolds of only PCL/Gelatin and PCL/Gelatin/HAp were used as controls. Scale bar, 2 mm. (B) Sirius red/ Fast Green and DAB staining for collagen and non-collagen proteins and collagens type II and X, respectively. Scale bar, 2 mm.

7.8.2. TABLES

Supplementary Table S7.1 | Wet-spun fibers diameters extruded at different flow rates.

Flow rate [mL/h]	Fibers Diameter [µm]		Significance (*p*)
	PCL/Gelatin	PCL/Gelatin/HAp	
1	368.25 ± 29.47	332.99 ± 41.85	**
0.5	181.15 ± 15.32	223.00 ± 12,09	****
0.25	126.32 ± 7.87	182.50 ±2 2.22	****

Statistically significant differences shown as: **, $p<0.002$; ****, $p<0.0001$

CHAPTER 8. "Functionally graded fibrous scaffolds as tendon-to-bone tissue interface replicates"

This chapter was adapted from the following publication:

I. Calejo, R.M.A Domingues, R. L. Reis, M. E. Gomes (2021) Functionally graded fibrous scaffolds as tendon-to-bone tissue interface replicates (submitted)

ABSTRACT

The heterogeneity of the tendon-to-bone interface requires complex engineered constructs as suitable tissue replacements. Herein, we propose the fabrication of functionally graded 3D scaffolds through the integration of biological, biochemical and tissue engineered cues. For this purpose, polycaprolactone anisotropic yarns (A-Yarns) and isotropic threads (I-Threads) were produced and incorporated with platelet lysate (PL) using emulsion electrospinning, enabling the production of tendon- and bone-mimetic structures, respectively. Besides recreating the architecture of the target tissues, threads were incorporated with nanohydroxyapatite (I-Threads/PL@nHAp) to replicate the bone organic mineral content. The incorporation of PL into fiber's core enabled a sustained delivery of growth factors, cytokines and chemokines under both physiological (pH=7.4) and inflammatory (pH=6.4) settings. Biological performance assessed using human adipose-derived stem cells (hASCs) demonstrated that A-Yarns/PL induced a high expression of scleraxis, a tenogenic-marker, comparably to plain controls. Also, high alkaline phosphatase activity and matrix mineralization in I-Threads/PL@nHAp suggested an osteogenic commitment without the need for external biochemical supplementation. As proof of concept, functional 3D gradient scaffolds were fabricated using weaving technique, resulting in high-throughput and reproducible hierarchical constructs with gradients in composition and topography. Additionally, the precise delivery of bioactive cues together with in situ biophysical features tailored the commitment of hASCs into a phenotypic gradient exhibiting tenogenic, osteochondrogenic and osteogenic profiles in specific sections of scaffolds. Overall, we demonstrate a promising solution for the regeneration of tendon-to-bone tissue interface through the fabrication of bio-functional 3D gradient constructs.

Keywords: Emulsion Electrospinning; Functionally graded scaffolds; Platelet lysates; Tendon-to-bone interface

8.1. INTRODUCTION

The tendon-to-bone interface is a musculoskeletal tissue divided into four continuous zones – tendon, mineralized-, non-mineralized fibrocartilage, and bone - composed of various cell types and extracellular matrix (ECM) composition, resulting in a structural and compositional gradient, reflected in its capacity of load-bearing [1, 2]. Tendon-bone interface injuries are highly prevalent, and currently used tissue-grafts face several significant shortcomings, such as adverse host tissue reaction, donor site morbidity, and formation of neofibrovascular tissue, compromising graft integrity [1, 3] and resulting in high re-tear rates [4, 5]. Therefore, in light of tendon-to-bone interface complexity, there is a need to develop improved systems that meet the biophysical, biochemical, and mechanical requirements of this highly heterotypic tissue, generating suitable tissue replacements.

In this regard, functionally graded materials constructs (FGMs) have been presented as promising biomaterials in the field of tissue engineering, designed to mimic native gradients in composition, structure, mechanical properties, and signaling cues found in the native tissue [6]. With the increased use of FGMs in tissue engineering, fiber-based systems have been used as building blocks of biotextiles, playing an essential role in controlling a myriad of properties of resulting 3D gradient constructs. Thus, several technologies have been developed for the fabrication of synthetic and natural fibrous biomaterials, namely microfluidics [7, 8], melt spinning [9, 10], wet-spinning [11, 12] and electrospinning [13, 14]. Electrospinning is one of the most widely used techniques, mainly due to its relative simplicity, efficient control over processing parameters, scaling up possibility, and practicability to fabricate micro/nanosized fibers with as ECM-like structure [15]. As an example, our group recently reported the fabrication of continuous electrospun anisotropic nanofibers threads that were then hierarchically assembled by textile into 3D scaffolds recreating the fibrillar hierarchical organization and topography of tendon tissues [16, 17]. Similarly, Moffat et al. demonstrated the capability of isotropic nanofiber poly(lactic-co-glycolic acid) (PLGA) scaffolds to induce human rotator cuff fibroblasts attachment and deposition of collagenous matrix according to substrate orientation [18]. Yet, reported nanofiber units still fail to incorporate and/or release important biological factors for cell signaling in a controlled spatiotemporal manner. Thus, different materials engineering approaches for the incorporation of drugs and bioactive molecules within fibers have been investigated over the years, particularly exploring fabrication methods such as coaxial electrospinning [19]. This technique relies on the production of core-shell structures, in which two solutions can be coaxially and simultaneously electrospun by different capillary channels, enabling the incorporation of bioactive molecules within fibers [20]. However, besides the inherent complexity associated with its setup, several parameters, including apparatus design, flow rate of the inner and outer

solutions, as well as their viscoelasticity and interfacial tension, need to be considered since they can affect the entrainment and production of required core-shell fiber morphology [21, 22]. Alternatively, emulsion electrospinning has gained attention as a suitable substitute to overcome these problems, especially using water-in-oil emulsions. Under electric force, the emulsion containing the polymeric solution and the water phase made of sub- to micron-spheres is elongated and converted into core-shell structure fibers [23], enabling an easy and continuous incorporation of biomolecules into electrospun fibers core. Thus, raising the potential application of this fabrication technique for the development of functionally graded materials for tendon-to-bone interface, through the integration of both biological, biochemical and tissue engineered cues, shall enable the regeneration of injured tissue interfaces by the local and controlled release of biochemical factors and consequent deposition of architecturally oriented ECM.

Biological factors can play a significant role in tissue healing, as cellular activities are regulated by a panoply of growth factors (GFs), cytokines, and chemokines. Therefore, over the years, several material and drug delivery engineering have relied on the encapsulation of biomolecules into fibrous constructs and theirs subsequent controlled release to achieve specific therapeutic effects in the targeted microenvironments [24]. However, despite several biomolecules have been encapsulated in core-shell fibers through co-electrospinning [25-27], the proposed strategies frequently rely on single GF encapsulation, while tissue healing is a finely orchestrated process involving multiple signaling biomolecules [28], thus limiting the therapeutic potential of these biomaterials. Moreover, the high costs of recombinant GFs and the difficulty of adequately controlling its programmed release kinetics to match the healing time are other major limitations hindering the implementation of such strategies [29]. The use of platelet lysates (PLs) as an alternative to recombinant GFs, might contribute to overcome some of these issues. This biomolecule cocktail can be obtained through cost-effective and straightforward protocols [30, 31], has numerous bioactive components, including GFs with known important roles in several biological processes (e.g., cell adhesion, proliferation, and differentiation) [32] and proved efficiency on promoting tissue healing and regeneration [31-33]. As an example, PDGF, FGF, VEGF and TGF-ß have been shown, by different effects, to accelerate interfacial healing and enhance the insertional strength of tendon grafts both in vitro and in vivo models [34-38]. Further, chemokines such as RANTES and CXCL1 have been described to have a potential role in fracture repair and tendon healing mainly associated with inflammatory response and macrophages recruitment [39, 40]. Currently, particular emphasis is given to strategies that enable to control their spatiotemporal delivery and improve the selectivity of presentation profiles of growth factors derived from platelet lysates. So, the development of

advanced functional and controllable systems, through the coupling of biological factors release with advanced tissue engineered strategies, might enable the development of functional systems for the in-situ delivery of well characterized populations of biomolecules improving the therapeutic efficiency during healing phases.

Building on the concept of functional graded materials, we hypothesized that by coupling the incorporation of PL with hierarchical assembly biofunctionalized fibers, we would be able to recapitulate the native tendon-to-bone tissue interface, while enabling the precise and controlled release of biological molecules important for interface tissue regeneration. So, electrospinning was first used for the production of biodegradable polycaprolactone (PCL) nanofiber threads with two different topographies, anisotropic and isotropic. Then, the concept of emulsion electrospinning was applied and optimized for the incorporation of biological factors (PLs) in these fibrous units under mild processing conditions. As tendon-to-bone is composed of structurally dissimilar tissues, the tendon's architecture was replicated by hierarchically assembling anisotropic nanofiber threads with PL into yarns (A-Yarn/PL), while isotropic threads with PL (I-Thread/PL) were produced to replicate the random organization of bone ECM. In addition, nHAp was incorporated within isotropic threads (I-Thread/PL@nHAp) to mimic bone's organic phase [42] while enhancing its osteogenic potential, namely by inducting matrix mineralization without the need for external medium supplementation. Beyond recreating the architecture of different tissue, the release profile of encapsulated PL bioactive components was assessed, mainly focusing on the delivery kinetics of GFs, cytokines and chemokines in a healthy (physiological) and injured (inflammatory) settings. Human adipose-derived stem cells (hASCs) were selected to study the tenogenic and osteogenic potential of produced A-Yarn/PL and I-Thread/PL, respectively, to clearly understand the temporal combinatory effect of topography and biomolecules release over stem cell phenotype commitment. Finally, as a proof-of-concept, textile techniques were applied for the fabrication 3D functionally graded constructs with spatially distributed gradients of architecture, topography, biological and biochemical composition that characterize the tendon-to-bone interface, to create microenvironments capable of inducing a spatial-specific stem cell commitment according to the native tissue. Overall, the developed approach holds great promise for the fabrication of 3D functional gradient scaffolds through easy and scalable techniques for tendon-to-bone tissue integration and proper regeneration.

8.2. MATERIALS AND METHODS

8.2.1. Fabrication of electrospun and emulsion nanofiber yarns/threads

8.2.1.1. Preparation of human platelet lysates

Platelet concentrates (PC) from healthy human blood donors were used to obtain platelet lysates (PLs). The PC samples were provided by Hospital de São João (Serviço de Imunohemoterapia do Centro Hospitalar São João, Porto, Portugal) under a previously established protocol. PL was obtained according to optimized protocols [43]. Briefly, PC with a platelet count of 1 million platelets/µL were used. PC were pooled using ten donors and then, to promote platelet lysis and protein release, the pools were subjected to three different freeze/thaw cycles using liquid nitrogen and a water bath, respectively. Platelet debris was removed after centrifugation at 1400g for 10 minutes at 4 °C and supernatants were stored at -80 °C. Prior to use, platelet lysates (PLs) samples were allowed to thaw at room temperature (RT), filtered using a pore size of 0.22 µm and kept on ice until solution preparation.

8.2.1.2. Optimization of water-in-oil emulsions

A pure polymeric solution (oil phase) of 17% (w/v) polycaprolactone (PCL, average Mn = 80 000, Merck, Germany) was prepared by dissolving the polymer in a mixture of chloroform /DMF (7:3, v/v; Merck, Germany) overnight at RT. Afterward, water-in-oil (W/O) emulsions were prepared by the addition of a mixture of blue food coloring and MilliQ water to PLs (1:1, v/v). The obtained solution was sonicated using an ultra-sonicator probe (Sonics&Materials, INC., VCX-130PB-220, EUA) for 2 min at 20, 30, 40 and 50% amplitude and 3 min at 20 and 30% amplitude. For an initial characterization prior to electrospinning, few drops w/o emulsions were mounted on a glass slide and observed under a reflected light microscope (Microscope Leica DM750, Germany). Images of emulsion droplets were acquired and analyzed for average diameter and dispersion. To study emulsions stability and phase separation, all solutions were left 24h inside the containers (Supplementary information, Figure S1).

For the analysis of PL distribution after electrospinning, w/o emulsions were prepared containing FITC-BSA (Thermofisher, EUA; 5 mg/mL in MilliQ water) and PLs (1:1 ratio, v/v) in the aqueous phase. Afterward, using a previously optimized electrospinning setup, emulsions were electrospun and a thin layer of fibers collected on a glass slide allowed to dry overnight at RT, and observed under confocal laser scanning microscopy (Leica TCS SP8, Microsystems, Wetzlar, Germany) to visualize the presence and distribution of molecules within the electrospun fibers. To do so, Z-stack images were acquired for each tested solution.

8.2.1.3. Production of plain and emulsion fiber threads with anisotropic and isotropic topographies

Water-in-oil (W/O) emulsions with PLs were prepared on the same day of electrospinning. Briefly, for the aqueous phase preparation, filtered PLs and MilliQ were mixed together in a ratio of 1:1 (v/v), and a final volume of 200 μL dropped-wise to the polymeric solution (oil phase, 17% PCL solution) under constant agitation. Afterward, using previously optimized conditions, the obtained solution was ultrasonicated on ice for 2 minutes at 50% amplitude. Within a period of 1 – 2 h, the acquired emulsion solutions were used for electrospinning. Continuous electrospun fiber threads with and without PLs were produced using a previously optimized electrospinning system developed by our group [17] with some modifications. Briefly, pure polymeric or emulsion solutions contained in a syringe with a 21G needle were electrospun at a constant flow rate of 1.00 mL/h and a voltage of 8-12 KV to a grounded liquid support bath of water/ethanol (8:2, v/v), and continuously pulled by a winding collector placed at defined distances. For the production of anisotropic fiber threads, the vertical distance (dBath, Figure 1A) from the needle to the support liquid bath was set at 16 cm, and the horizontal distance (dCollector) to the collector was set at 20 cm. For the production of isotropic fiber threads, the vertical and horizontal distances were set at 13 and 13 cm, respectively. Electrospun fiber threads were collected at RT (23±2 °C) and humidity ranging from 45% to 50%. Several collection speeds were tested (v1, 0.14 cm s-1; v2, 0.34 cm s-1; v3, 0.54 cm s-1; v4, 0.68 cm s-1; v5, 0.82 cm s-1and v6, 1.09 cm s-1). Optimal collection speed conditions were set at 0.14 (v1) and 1.09 cm/s (v6) to produce anisotropic and isotropic threads, respectively. All fibers were left inside a desiccator switched on with a vacuum pump overnight to eliminate possible solvent from the production process. Produced anisotropic and isotropic fiber threads without PLs were thereafter called as A-Threads and I-Threads, respectively, while anisotropic and isotropic emulsion electrospun fiber threads containing PLs were denominated as A-Threads/PL and I-Threads/PL respectively. Concerning the fabrication of yarns, 12 anisotropically aligned fiber threads were grouped together and twisted at 4 turns cm−1 and produced yarns without and with PLs were thereafter denominated as A-Yarns and A-Yarns/PL, respectively.

8.2.1.4. Incorporation of nHAp in isotropic threads

To replicate the organic phase composition of bone tissue as accurately as possible, I-Threads and I-Threads/PL were incorporated with nano-hydroxyapatite (nHAP, nanopowder, <200 nm particle size (BET), ≥97%, synthetic, Merck, Germany) particles. Briefly, nHAp was added to a PCL solution (17% w/v), representing 1% w/w of PCL. The obtained mixture was stirred at 150 rpm for 1-3 hours, at room

temperature, and sonicated for 2 minutes until all the nHAP powder was blended. For emulsion preparation, the aqueous phase (PL/MilliQ, 1:1, v/v) was added to the obtained blended solution and the preparation ultrasonicated for 2 minutes at 50% amplitude. Right afterward, the obtained solutions were contained in a syringe fitted with a 21G needle and electrospun at a constant flow rate of 1.00 mL h−1 and a voltage of 8-9 kV was applied during the process. Vertical and horizontal distance to the bath of 12 and 13 cm, respectively, and produced electrospun threads were collected at RT (25 ± 2°C) and humidity ranging from 45% to 50%. Incorporated isotropic fiber threads without and with PLs were thereafter called as I-Threads@nHAp and I-Threads/PL@nHAp, respectively.

8.2.2. Textile assembling of 3D gradient scaffolds for tendon-to-bone hierarchical replication

To fabricate a 3D construct, weaving textile technique was applied to assemble the fibrous structures following a previously reported process [17] with some adaptations. A handmade platform was produced, where 8 cotton threads were placed side by side with a distance of 0.5 cm. Anisotropic yarns and isotropic threads were sequentially used as warp/weft threads. This sequence was adjusted during the fabrication of scaffolds. In the middle, threads were interlocked, creating a continuous gradient of threads topography and composition. As a final step, respective threads were passed in between warp/weft threads and in the middle, as a way to maintain the structural integrity of the scaffold. Three constructs were produced: 1) Yarns-Threads (plain control); 2) Yarns-Threads@nHAp; 3) Yarns-Threads/PL@nHAp were produced with dimensions ranging from 10,69 ± 0.78 to 11,39 ± 2.13 mm.

8.2.3. Morphological, mechanical and chemical characterization of yarns, threads and 3D scaffolds

8.2.3.1. *Scanning electron microscopy (SEM) analysis and directionality analysis*

The morphology of produced yarns and threads were analyzed by scanning electron microscope (SEM, MP1000001280128, JSM-6010 LV, JEOL). Samples were coated with 2 nm of platinum (Cressigton) before analysis. For I-Threads/PL@nHAp, samples were coated with 2 nm of gold (Cressigton) and analyzed by High-Resolution Field Emission Scanning Electron Microscope with Focused Ion Beam (FIB – SEM).

Concerning the degree of topographical alignment, this parameter was determined through directionality analysis applying the Fourier components method using the FIJI software (version 2.0.0-rc-69/1.52p).

For this purpose, scanning electron images were converted to 8-bit images and cropped into three different images. The radial intensities were calculated, and the orientation map was also obtained.

8.2.3.2. *Micro-CT analysis*

Plain and PL-incorporated yarns and threads microstructure was evaluated by X-rays micro-computed tomography (micro-CT) using a high-resolution system Skyscan scanner (Skyscan 1272; Bruker, Billerica, MA, USA). The acquisition of X-ray images was performed with a pixel size of 4.25 μm, a rotation step of 0.2° over 360°, and a smoothing averaging of every two images, using the SkyScan acquisition software version 1.1.3. The X-ray source was fixed at 35 kV and 181 μA of voltage and current, respectively. Following the acquisition, gray-scale images were reconstructed using the NRecon software (version 1.7.1.0). Then, when needed, the samples were vertically aligned for the cross-sectional analysis of the fibers using the DataViewer software (version 1.5.3.6). Qualitative visualization of the 3D morphology was performed using CT-Vox software (version 3.3.0). Quantitative analysis was performed after converting the regions of interest into binary images by a dynamic threshold of 35-255 (CT Analyzer v1.17.0.0). The binary images were used for morphometric examination of inner-porosity, pore size, and interconnectivity. The microstructure and nHAp composition in the fabricated scaffolds were also evaluated by micro-CT. In this case, acquisition of X-ray images was performed with a pixel size ranging from 8 to 14 μm, a rotation step of 0.6° over 360°, and a smoothing averaging of every two images, using the SkyScan acquisition software version 1.1.3. The X-ray source was fixed at 35 kV and 181 μA, of voltage and current, respectively. Following the acquisition, gray-scale images were reconstructed and, when necessary, aligned using NRecon software (version 1.7.1.0) DataViewer software (version 1.5.3.6) as previously described, respectively. Qualitative visualization of the cross-sectional morphology and the 3D polymer (black) and nano-hydroxyapatite (red) phases were obtained using CT-Vox software (version 3.3.0). Finally, two dynamic thresholds of 20-255 for the whole structure and 90-255 for the ceramic phase were applied (CT Analyzer v1.17.0.0) and used for the quantification of nHAp percentage over the polymeric composition.

8.2.3.3. *Alizarin red staining of nHAp particles in 3D scaffolds*

Nano-HAp content across produced scaffolds with Yarns-Threads@nHAp and Yarns-Threads/PL@nHAp was analyzed by alizarin red staining. Briefly, samples were washed with deionized water, followed by incubation with a solution of 2% (w/v) AZ (Merck) for 20 minutes under gentle shaking. Afterward, samples

were thoughtfully washed with deionized water and visualized under fluorescence microscopy (Axio Imager Z1m; Zeiss).

8.2.3.4. *Chemical characterization*

Fourier-transform infrared spectroscopy (FTIR, A21004200704, IRPrestige 21, Shimadzu) was used for chemical analysis of the produced nanofiber threads. Briefly, prior to FTIR analysis by attenuated total reflectance (ATR), all samples without PL were dissolved with a small amount of chloroform and allowed to dry at RT to form a small pellet. In the case of samples incorporating PLs, several replicates were combined and smashed to form a small pellet. Infrared spectra of only PCL, PL-incorporated yarns/threads and PLs only were recorded by averaging 32 individual scans, at a resolution of 4 cm, over a wavenumber range between 4000 and 1000 cm−1 at RT.

8.2.3.5. *Mechanical characterization*

The mechanical properties of both a A-Yarns and -PL, I-Threads and -PL and I-Threads@nHAp and -PL@nHAp were assessed using a universal mechanical testing machine (5543K2942, 5543, INSTRON) equipped with a 50N load cell. Images from optical microscope (DM750, Leica, Schweiz, Germany) were acquired and used for cross-sectional area calculations. Each specimen was measured along the length at six different locations using the ImageJ software (version 1.52d). Samples were cut into testing specimens with 2 cm and fixed in paper frames with a window of 1 × 1 cm. After mounting the frames onto the tester grips, the lateral sides were cut, and the crosshead speed was set at a constant rate of 10 mm/min. At least six samples per condition were tested. The young modulus was calculated from the tangent slope of the linear section of the stress-strain curve, and the ultimate tensile strength and load were determined by calculating the maximum of the stress-strain curve.

8.2.3.6. *Water-uptake and release kinetics*

Both A-Yarns and -/PL, and I-Threads and -/PL were cut into pieces (20–30 mg). To replicate both physiological and inflammatory setups, a solution of PBS (solution adjusted to pH=7.4) and PBS with sodium bicarbonate (solution adjusted to pH=6.4) were used. At the end of each time point, samples of each formulation were collected and rinsed with distilled water (dH2O), and the weight of the samples measured. The percentage of weight loss kinetics was calculated according to the following equation:

Equation 8.1: Weight loss=(mi-mf)× 100%.

Where mi is the initial weight and mf the final weight.

8.2.3.7. *Cumulative release of total proteins and PLs growth factors, cytokines and chemokines*

A-Yarns/PL and I-Threads/PL were collected and cut in pieces (20–30 mg) and shortly rinsed in MilliQ water. Samples were left in contact with physiological (PBS solution adjusted to pH=7.4, total volume = 1 mL) and inflammatory environments (sodium bicarbonate solution adjusted to pH=6.4, total volume =1 mL) up to 31 days at 37°C, under 60 rpm constant agitation. At 0, 0.125, 1, 3 5 and 14 days, a total volume of 600 µl was collected. To quantitatively evaluate the cumulative release of total proteins, Pierce BCA protein assay (Micro BCATM Protein Assay Kit; Thermo ScientificTM) was used according to the manufacturer protocol and measured in a microplate reader (Synergy HT, Bio-Tek Instruments). An equal volume of fresh solutions was added each time. A-Yarn and I-Thread were used as controls. Cumulative release was calculated in relation to the initial weight of samples for each tested condition.

For the cumulative release of PLs factors, after electrospinning, produced A-Yarn/PL and I-Thread/PL were maintained at 37°C in both physiological and inflammatory environments under 60 rpm constant agitation. At 0, 0.125, 1, 3 5 and 14 days, 600 µl of solution was collected and stored at -80°C until further analysis. An equal volume of fresh solutions was added each time. Platelet lysates GFs, cytokines and chemokines were quantitatively studied using an ELISA plate array assay. Customized ELISA plates for platelet-derived growth factor-BB (PDGF-BB), transforming growth factor beta (TGF-ß), insulin growth factor 1 (IGF-1), endothelial growth factor (EGF), vascular endothelia growth factor (VEGF), fibroblast growth factor ß (FGF-ß), RANTES and CXCL1 (Signosis, INC.) were used. Standard curves were performed for each protein ranging from 0 to 2 ng/mL. The concentration of released proteins was calculated in relation to the initial weight of samples for each tested condition and presented as ng/mL per mg of A-Yarns/PLs or I-Threads/PL.

8.2.4. Biological characterization

8.2.4.1. *Isolation, seeding and culture of human adipose-derived stem cells*

Human stem cells from adipose source were isolated by enzymatic digestion of surplus lipoaspirate samples [44] obtained under previously established protocols with Hospital da Prelada (Porto, Portugal). All human samples were obtained under informed consent following protocols approved by the ethical committee of the hospital and according to the Declaration of Helsinki. Afterward, cells were expanded in basal medium (Alpha-MEM medium (Alfagene, Lisboa) supplemented with 10% FBS (Thermofisher, EUA)

and 1% A/A (Thermofisher,EUA)). Prior to seeding, A-Yarn, I-Thread (with and without nHAp), A-Yarn/PL and I-Thread/PL (with and without nHAp), and 3D scaffolds were placed inside the 24-well plate and 12-well plate inserts (Merck, Germany), respectively, and immersed in 70% ethanol for 45 min for sterilization, followed by several washing steps with PBS for 15 min to remove the remaining ethanol residues. As a final step, samples were incubated overnight with basal medium to improve cells attachment. The following day, hASCs were seeded at a density of 3x104 cells onto each sampled yarn/thread, and at a density of 30x104 cells/per scaffold. Samples were afterward incubated overnight to allow cells adhesion. Fresh basal medium was added up to 0.6 mL in yarns/threads and 2 mL in 3D scaffolds, and cell were cultured for 15 days and 21 days, respectively. Culture medium was changed twice a week. Cells were used at passages 2-3.

8.2.4.2. *Evaluation of cell proliferation*

On days 5, 10 and 15, cellular proliferation was evaluated using a fluorometric dsDNA quantification kit (PicoGreen; Molecular Probes, Invitrogen, Carlsbad, CA, USA) to determine DNA content. After the established culture times, hASCs-seeded fiber threads and yarns were washed twice with PBS. Then, filtered ultra-pure Millipore water (Pore size 0.22 μm) was added to subject cells to an osmotic shock. The collected cell solution was stored at -80°C to promote an additional thermal shock. After defrosting, cell lysates were used for dsDNA quantification and fluorescence was measured in a microplate reader (Synergy HT, Bio-Tek Instruments) using an excitation wavelength of 485/20 nm and an emission wavelength of 538/20 nm. Standards were prepared in a range of concentrations between 0 and 1.5 μg/mL. The fold increase was calculated using A-Yarns or I-Threads as normalizer group.

8.2.4.3. *Alkaline phosphatase activity quantification*

At pre-determined days, intracellular alkaline phosphatase was determined using the colorimetric n-nitrophenol (pNp) assay. Cell lysates were incubated with a substrate solution composed of 0.2% (w/v) p-nitrophenyl phosphate (pNPP) in 1 mmol diethanolamine (Sigma-Aldrich). After incubation (1h, 37°C), a stock solution of 2 M NaOH/0.2 mM ethylenediaminetetraacetic acid was added. Absorbance was measured (405 nm) using a microplate reader (Synergy HT; Bio-Tek Instruments). A standard curve was prepared using a pNP stock solution (Sigma-Aldrich) with values ranging from 0 to 0.5 μmol/ml. The fold increase was calculated using A-Yarns and I-Threads as normalizer group.

8.2.4.4. *Matrix mineralization*

Matrix mineralization was analyzed by alizarin red staining in hASCs-seeded threads (with and without nHAp) after 5 and 15 days, and in scaffolds after 14 days of culture. Briefly, samples were washed with deionized water, followed by incubation with a solution of 2% (w/v) AZ (Merck) for 20 minutes under gentle shaking. Afterward, samples were thoughtfully washed with deionized water and images acquired using a stereomicroscope (Discovery v8, Zeiss, Deutschland, Germany) with AxioCam ICC1 (Zeiss, Germany).

8.2.4.5. *Immunofluorescence of tendon-, bone- and interface-related markers*

Seeded yarns/threads (with and without PL) and gradient scaffolds were fixed with 10% (v/v) neutral buffered formalin for 20 minutes at RT. Briefly, to assess the expression of tenogenic and extracellular matrix (ECM) related markers in Yarns-Empty/PLs and Iso-Empty/PLs, and the expression of tenogenic-, osteogenic-and interface-related markers in 3D scaffolds, samples were first washed with PBS and permeabilized with 0.25% Triton X-100/PBS solution for 30 minutes. To block non-specific binding, a solution of 1% bovine serum albumin (w/v, BSA, Thermofisher, EUA) in PBS was added and left for 30 minutes at RT. Afterward, A-Yarn, A-Yarn/PL, I-Thread and I-Thread/PL were incubated with anti-Scleraxis antibody (rabbit anti-human SCX 1:100; Abcam) and anti-collagen type III (rabbit anti-human COLIII, 1:500, Abcam) overnight at 4 °C with gentle shaking. In the case of 3D scaffolds, sampled were incubated with anti-Scleraxis antibody (rabbit anti-human SCX, 1:100; Abcam), anti-runt related transcription factor 2 (mouse anti-human RUNX2, 1:100, Merck), anti-SRY-Box Transcription Factor 9 (mouse anti-human SOX9, 1:200, Millipore) and anti-collagen II (rabbit anti-human COLII, 1:100, Abcam) overnight at 4 °C with gentle shaking. After incubation with the primary antibody, mouse anti-rabbit AlexaFluor 488, goat anti-rabbit AlexaFluor 594 and donkey anti-mouse AlexaFluor 488 were used secondary antibody. All antibodies were diluted in 1% (w/v) BSA. Cell nuclei and cytoskeleton were counterstained with 4,6-diamidino-2-phenyindole dilactate (DAPI, 1:1000, Thermofisher, EUA) and phalloidin solution (PHA, 1:200, Merck, Germany), respectively.

In the case of yarns/threads, samples were visualized and acquired using a fluorescence microscopy (Axio Imager Z1m; Zeiss). While 3D scaffolds were visualized and acquired by confocal laser scanning microscopy (Leica TCS SP8, Microsystems, Wetzlar, Germany).

8.2.5. Statistical analysis

Results are presented as mean ± standard deviation (SD) if not stated otherwise. Statistical analyses were performed using GraphPad Prism 8.4.0 software. Two-way analysis of variance (ANOVA) with Sidak and Tukey tests was used. Nonparametric t-test (Mann-Whitney test) and unpaired t-test were performed for mechanical tensile testing. Differences between experimental groups were considered significant, with a confidence interval of 95%, whenever $p<0.05$.

8.3. RESULTS and DISCUSSION

8.3.1. Fabrication of electrospun fiber threads with different surface topographies

Within every tissue, the properties of cell's supporting environment are sensed at multiple length scales. Interestingly, the conjugation of tissue-generated forces at the macroscale with cellular forces at the microscale, are paramount for guiding multi-cell differentiation during development, particularly on musculoskeletal tissues [45]. For instance, stem cell lineage specification can be governed by the physical contact with specific architectures of the surrounding microenvironment [46, 47]. As previously reported, the topography of electrospun fibers plays an important role in maintaining and inducing a specific phenotype in stem cells [13, 48, 49]. In this work, textured electrospun fiber threads were produced with anisotropic and isotropic topographies (Figure 8.1B, i-ii). Specifically, during electrospinning, the highest anisotropic degree was observed in A-Threads collected at higher speeds (v6, 1.09 cm s^{-1}) presenting diameters of 104.3 ± 3.1 μm, and fiber widths of 1.3 ± 0.4 μm (Figure 8.1C-D, i). Remarkably, obtained fibers closely resembled the dimensions of the elementary unit of tendon tissue - primary collagen fibers [50, 51]. Nonetheless, to replicate the fiber bundles macro-architecture of tendon fascicles, A-Threads/PL were twisted into yarns consisting of 12 threads covering the full-length scale units of tendon tissue [51]. Isotropic fiber threads were also fabricated to replicate the randomly organized ECM of cancellous bone, specifically the fibrillar collagen network [42]. In figure 8.1C, ii, a peak absence in the orientation angle frequency of I-Threads confirmed the production of isotropic topography induced by the lowest collection speed (v1, 0.17 cm s^{-1}). Threads were produced with dimensions of 379.7 ± 70.3 μm and formed by fibers ranging within 1.2 ± 0.3 μm (Figure 8.1D, ii), measurements falling within the dimensions of targeted trabecular network and mineralized collagen bundles [52, 53].

Based on these results, the speed of 1.06 cm s^{-1} was selected for production of A-Threads whereas 0.17 cm s^{-1} was selected for production of I-Threads aiming at tendon and bone ECM structural replication, respectively.

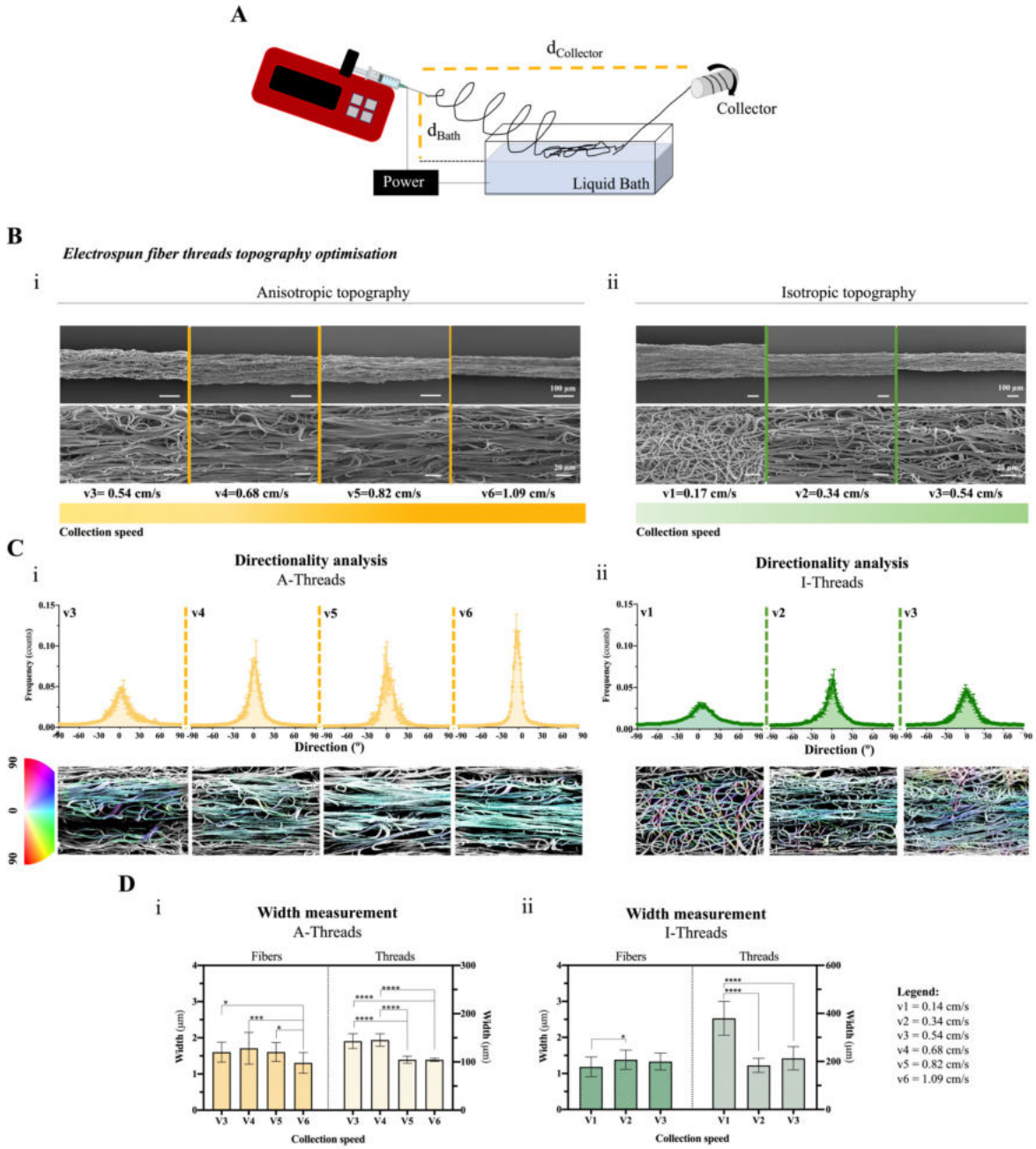

Figure 8.1 | Optimization of electrospun fiber threads topographies for tendon and bone structure replication. (A) Schematics representation of electrospinning setup used for fiber threads fabrication. (B) SEM images of (i) anisotropic (A-Threads) and (ii) isotropic electrospun fiber threads (I-Threads) fabricated with increasing collection speeds (v1, 0.17 cm s^{-1}; to v6, 1.09 cm^{-1}). Scale bars, 100 µm and 20 µm. (C) Directionality analysis (top) and orientation maps (bottom) of collected A-Threads (i) and I-Threads (ii). (D) Average width of single fibers (left) and threads (right) produced with anisotropic (i, *, p = 0.011; ***, p = 0.0003; ****, p = 0.0001) and isotropic topographies (ii, *, p = 0.026; ****, p = 0.0001). Error bars represent standard error deviation (SD) (Fibers, n=24; Threads, n=12).

8.3.2. Optimization and characterization of emulsion solutions and PLs incorporation in fiber threads

In an emulsion electrospinning process, emulsion droplets move perpendicularly from the surface to the center suffering an enrichment in the axial region, where droplets are stretched into an elliptical shape in the direction of the fiber trajectory, becoming entrapped inside electrospun fibers [23]. Thus, in this work, emulsion electrospinning was used as fabrication strategy to incorporate bioactive molecules present in PL within fiber cores (Figure 8.2A, i). Therefore, before electrospinning, droplets' diameter and dispersion of aqueous phase were two critical W/O emulsion parameters optimized for achieving a continuous spinning and efficient incorporation of PL within fibers [54, 55]. Light microscope images revealed that homogenous emulsions could be acquired through the application of increasing ultrasonication amplitude percentages (Figure 8.2B, i). Specifically, among tested conditions, an amplitude of 50% for 2 minutes induced the formation of droplets with the smallest diameter (Figure 8.2B, i; 6.34 ± 3.39 μm) with lower polydispersion (Figure 8.2B, ii). As defined by Pal et al. emulsions with droplet size of 4–12 μm as fine and 25–30 μm as coarse [54]. Thus, the obtained emulsion can be classified as fine without big phase separations, suggesting that an amplitude of 50% for 2 minutes is well suited for the PL emulsions preparation.

Recently, emulsion centrifugal spinning has been recently applied for the incorporation platelet lyophilizes within microfibrous scaffolds [56]. Yet, the need for high amounts of surfactants to produce the spinning emulsions and its colloidal low stability are among the identified limitations of this strategy of fiber scaffolds production [56]. In the present work, PLs were incorporated in the aqueous phase of the W/O emulsions without requiring additional surfactants. This was observed in tests of emulsions stability, where no separation between the polymeric solution and aqueous phase was observed after leaving emulsion solutions to rest for 1 day (Supplementary Figure S8.1). This could be explained following the thermodynamic laws that all systems should be at their global minimum energy state, W/O dispersions rapidly separate into 2 phases to minimize the interfacial contact area and the free energy [57]. Separation or de-emulsification rate can be controlled by reducing the interfacial tension between the continuous phase and the dispersed droplets by adding an amphiphilic molecule, such as albumin, that acts as surfactant by adsorbing to and orienting itself at the interface in such a way that its nonpolar (hydrophobic) segment is partitioned into the polymeric phase of the solution and its hydrophilic part exposed to the aqueous phase, protecting more protein of interest [57-60]. So, the stability observed in prepared solutions might be explained by the high concentrations of albumin present in PL [31].

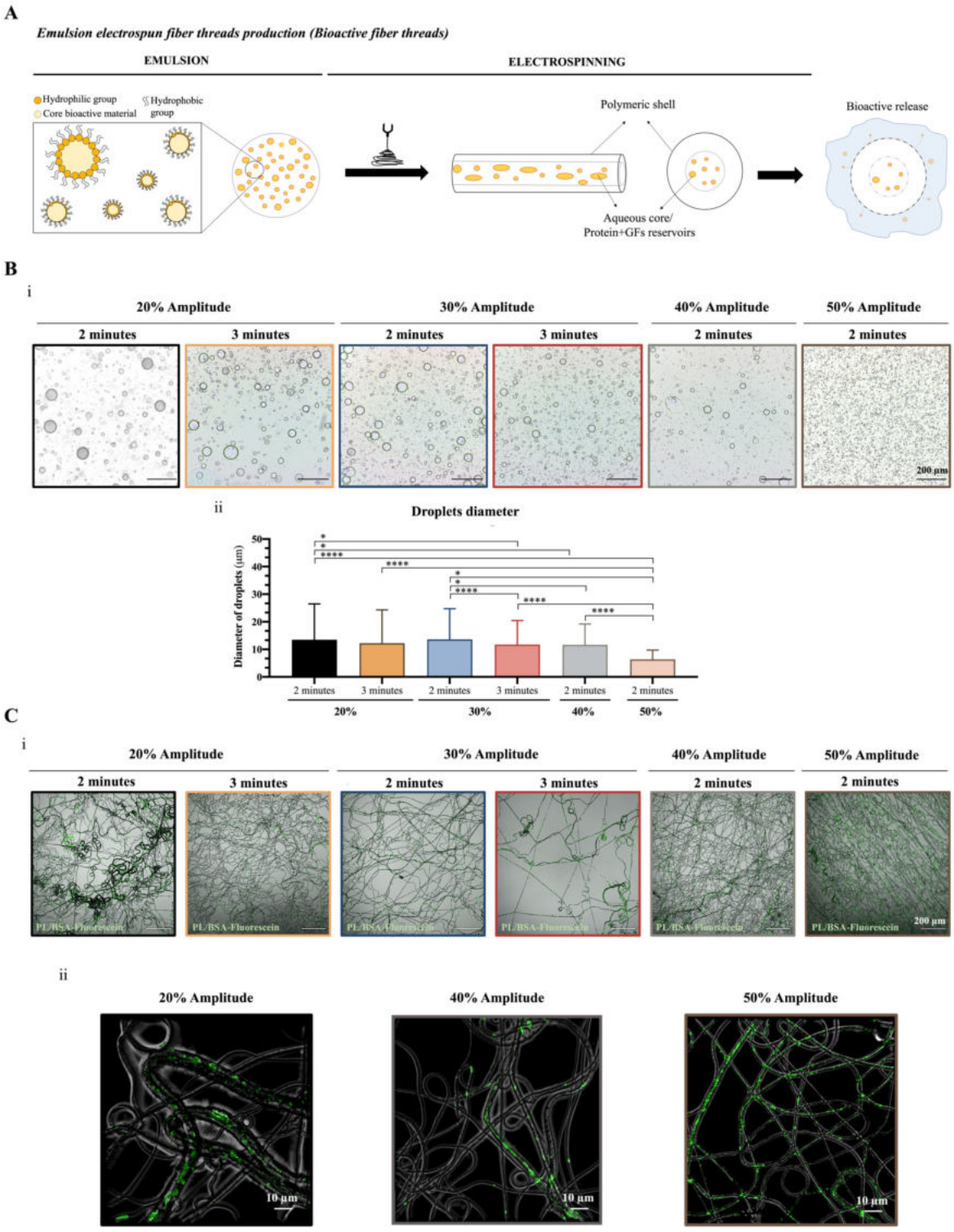

Figure 8.2 | Emulsion solution parameters optimization and fibers production. (A) Schematics of emulsion electrospinning demonstrating the incorporation of bioactive molecules within electrospun fibers for a controlled local release. (B) Light reflect images of (i) emulsion droplets containing PLs and color dye after the application of increasing ultrasonication amplitudes: 20% and 30% for 2-3 minutes, and 40% and 50% for 2 minutes. Scale bars, 200 µm. Droplets average diameter (ii, *, p =

0.028; ****, $p < 0.0001$) evaluated for the different tested ultrasonication amplitudes. Error bars represent SD. (C) Confocal fluorescence microscopy images of emulsion electrospun fibers incorporating PL/BSA-fluorescein after (i) 20% and 30% for 2-3 minutes, and 40% and 50% for 2 minutes. (ii) Higher magnifications obtained of fibers obtained after emulsions preparation using 20%, 40% and 50% ultrasonication amplitudes for 2 minutes. Scale bars: 200 μm (i) and 10 μm (ii).

The impact of emulsion quality on the entrapment of aqueous phase molecules on electrospun fibers was also assessed adding small amounts of fluorescent BSA-fluorescein to PL for visualization (Figure 8.2C). As shown by confocal imaging, fluorescent BSA-fluorescein were poorly dispersed within fibers when using emulsion solutions prepared using lower ultrasonication amplitudes (Figure 8.2C, i-ii; 20% - 30%). On the other hand, as observed in Figure 8.2C, ii, well-dispersed incorporation was observed for the sonication at highest amplitude (50%, 2 minutes), resulting in bead-free and highly homogeneous nanofibers with PL cores. This results from the W/O emulsification process, where shell formation is associated with the evaporation of solvents in the hydrophobic polymeric solution (oil phase) [61] followed by a solidification process as result of surface precipitation in the non-solvent bath [62]. Biomolecules present in the water phase are elongated and migrate to the center of the jet due to the viscosity gradient, instead of escaping onto fibers surface [61], enabling the formation of continuous core-shell fibers.

8.3.3. Comparative analysis of PL-incorporated yarns and threads: chemical, morphological and mechanical assessment

After the acquisition of fiber threads with anisotropic and isotropic topographies, the chemical composition of PCL and PLs in A-Yarns/PL and I-Threads/PL was assessed (Figure 8.3A, i-ii). FTIR-spectra exhibited several PCL characteristic bands at 1239 (C-O-C, asymmetric stretching), 1292 (C-O and C-C stretching), 1653 (C=O stretching, amide I), 2931 (asymmetric stretching -CH2) and 2858 cm^{-1} (symmetric stretching -CH2) [12]. The characteristic bands of PL around 3286 cm^{-1}, commonly amide A, attributed to the -NH group from PL proteins, and by a band around 1600-1690 cm^{-1} (amides I, C=O stretching) [63, 64] confirmed its presence in A-Yarns/PL and I-Threads/PL (Figure 8.3A, ii).

Further, the morphology of produced A-Yarns/PL and I-Threads/PL was evaluated using SEM and micro-CT analysis. As depicted in Figure 8.3B, the topographical orientation of fiber threads in A-Yarns/PL was not affected by manufacturing process, as also confirmed by the directionality frequency graphs, where the presence of a sharp peak in the orientation angle frequency demonstrated a tendency of fiber threads alignment in a single direction (Supplementary Figure S8.2A, i). In contrast, a peak absence in I-

Threads/PL demonstrated no preferential orientation as result of its random organization (Supplementary Figure S8.2A, ii). Also, Figure 8.3B, i, c shows the influence of PL incorporation in fibers and yarns/threads diameters. It was observed an overall decrease in fibers diameters in the range of 0.75 ± 0.19 μm and 0.91 ± 0.26 μm for A-Yarns/PL and I-Threads/PL, respectively, comparably to A-Yarns and I-Threads (1.31 ± 0.29 μm; 1.18 ± 0.27 μm, respectively, Figure 8.1C, i-ii). This effect could derive from changes in the w/o emulsion solution properties (namely lower viscosity, surface tension and high conductivity) resulting from the addition of an aqueous phase [65, 66]. Additionally, the porosity of manufactured A-Yarns/PL and I-Threads/PL was evaluated as this is one key parameter that favors cell infiltration, nutrient and oxygen diffusion and colonization [67]. A-Yarns/PL presented a full-length porosity of 20.56 ± 3.45% while in I-Threads/PL it fell around 19.51 ± 1.14% (Figure 8.3B, iii-iv). Furthermore, while higher inner porosity and pore size were obtained for A-Yarns/PL comparably to A-Yarns, similar values were found in between I-Threads/PL and I-Threads (Supplementary Figure S8.2A, iii-iv, b), not being observed an influence of PL incorporation on threads inner porosity and pore size.

The impact of PL incorporation in the tensile mechanical properties of yarns and threads was also evaluated (Figure 8.3C and Figure S2B, i-ii). No significant differences were observed between Young's modulus and ultimate tensile strength of A-Yarn/PL (23.78 ± 2.5 MPa; i, UTS: 4.7 ± 0.6 MPa) and A-Yarn (24.1 ± 3.9 MPa; UTS: 3.6 ± 0.9 MPa; Figure 8.3C, i, b; Supplementary Figure S8.2B, i, respectively). The Young's modulus and ultimate tensile strength of A-Yarns/PL are within the lower range of native tendons tensile properties (20-1200 MPa and 5-100 MPa, respectively) [68]. I-Threads/PL (4.2 ± 1.4 MPa; UTS: 1.0 ± 0.2 MPa) and I-Threads (6.1 ± 1.5 MPa; UTS: 0.9 ± 0.2 MPa) also revealed similar mechanical performance when compared in between them (Figure 8.3C, ii, b; Supplementary Figure S8.2B, ii). Overall, incorporation of PLs was found to not affect the morphology and mechanical properties of A-Yarns/PL and I-Threads/PL compared with empty controls, which might be explained by the good dispersion of aqueous solution inside the fibers (Supplementary Figure S8.3), that could have filled possible structural defects that could affect the mechanical performance of tested specimens.

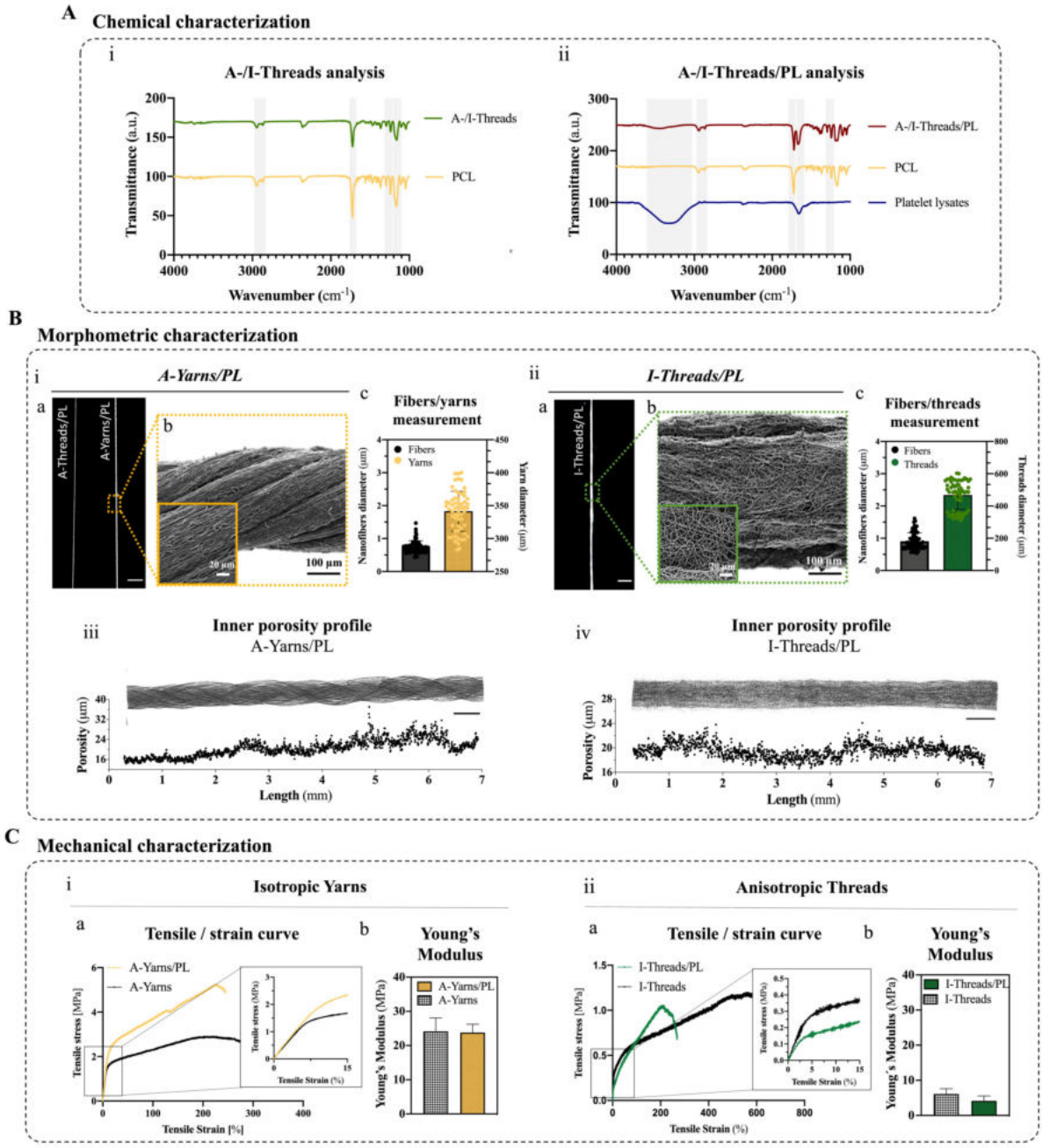

Figure 8.3 | Chemical, morphometric and mechanical characterization of A-Yarns/PL and I-Threads/PL. (A) FTIR spectra of neat PCL, PLs, and (i) A-/I-Threads and (ii) A-/I-Threads/PL with respective bands of interest identified. (B) Morphometric analysis of assembled (i) A-Yarns/PL and produced (ii) I-Threads/PL with (a) macro-scale images, (b) scanning-electron microscopy images, and (c) fiber and yarns/threads diameter measurements. Scale bars, 500 µm, 20 µm and 100 µm. Error bars represent SD (Fibers, n=60; Yarns/Threads, n=60). Microtomography (Micro-CT) 3D reconstruction and respective longitudinal porosity analysis of (i) A-Yarns/PL and (ii) I-Threads/PL. Scale bars, 500 µm. Error bars represent SD. (C) Mechanical tensile testing of specimens with (a) representative tensile/strain

curves and (b) calculated young's modulus for (i) A-Yarns vs A-Yarns/PL and (ii) I-Threads vs I-Threads/PL.

8.3.4. Characterization of nano-hydroxyapatite incorporated isotropic threads

As a heterotypic tissue, the tendon-to-bone interface is constituted by distinctive ECMs [47]. To closely replicate these matrices, at first, bioactive fiber threads were hierarchically assembled to mimic tendon's full-length architecture. Besides tendon-counterpart representation, bone tissue ECM organization mimicry was achieved through the production of bioactive fiber threads with isotropic topography. Yet, this factor was not enough to induce the commitment of stem cells and resulting deposition of a mineralized matrix required for a proper bone ECM-likeliness. So, to enhance the potential of I-Threads/PL to induce osteogenic-like ECM deposition and mineralization, threads were modified with incorporation of nano-hydroxyapatite (nHAp) and thus closely resembling bone's nanocomposite nature, specifically the interconnected intrafibrillar and extrafibrillar minerals on the nanometer scale [69]. As reported in the literature, concentrations as low as 1% w/w of solid scaffold weight were shown to increase ALP activity and matrix mineralization in pre-osteoblast-like cells [70] and induce mesenchymal stem cells osteogenic commitment [71]. So, to boost the osteogenic potential of isotropic fiber threads without the need of pro-osteogenic factors and also a smooth fabrication of continuous I-Threads/PL incorporating these nanoparticles (I-Threads/PL@nHAp), a solid weight of 1% (w/w) was used during polymeric solution preparation. As observed in figure 8.4A-i, after alizarin red staining, I-Threads/PL@nHAp presented a good dispersion and incorporation of nHAp. Additionally, SEM imaging confirmed the absence of particles on the surface of the fibers, but an increased roughness was found when compared with I-Threads (Figure 8.4A-ii). Interestingly, fiber roughness has been shown to have an effect on human mesenchymal stem cells compared with smoother electrospun materials, namely higher surface roughness were shown to support the expression of osteogenic genes such as osteopontin (OPN), bone morphogenetic protein 2 (BMP2), and runt-related transcription factor 2 (RUNX2) [72]. So, the presence of fiber roughness in I-Threads/PL@nHAp may act as an additional physical cue for stem cells differentiation. Concerning the tensile mechanical performance of I-Threads/PL@nHAp, the incorporation of nHAp resulted in significantly lower Young's modulus (2.49 ± 1.50 MPa, Figure 8.4B, ii) and UTS (0.60 ± 0.17 MPa, Figure 8.4B, iii) compared to I-Threads@nHAp (5.72 ± 1.34 MPa and 1.51 ± 0.75 MPa). This could be explained by the conjugation of PL and higher agglomeration of nHAp within fibers, resulting in less resistant and brittle fibers. Overall, nHAp was successfully incorporated within I-Threads/PL@nHAp resulting in a

topological alteration on fibers surface, by increasing its roughness, important as an osteo-inductive cue for stem cells differentiation without the need of pro-osteogenic supplementation of medium.

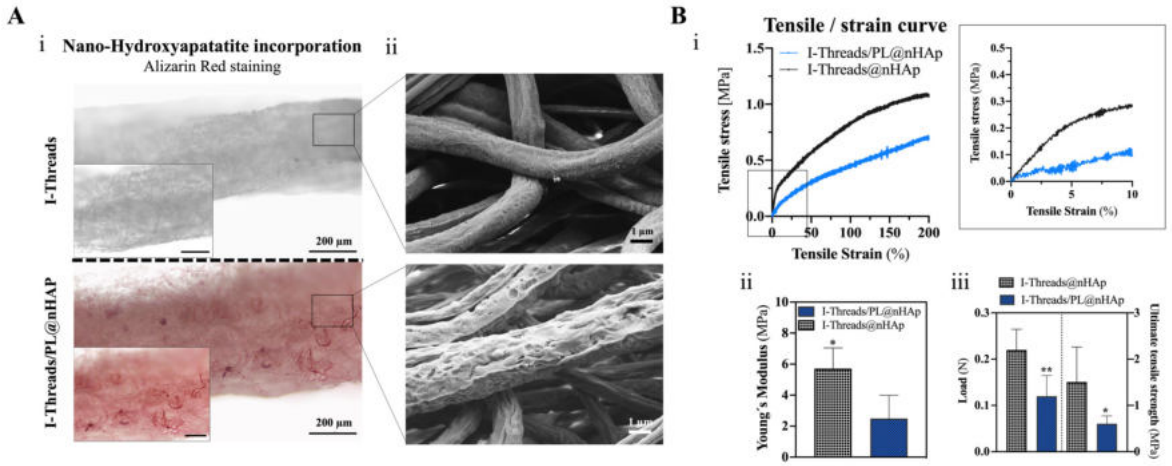

Figure 8.4 | Morphometric and mechanical characterization of I-Threads and I-Threads/PL incorporated with nHAp. (A) Optical microscope images of (i) alizarin red staining of I-Threads (Top) and I-Threads/PL@nHAp (bottom). Scale bars, 200 µm. (ii) SEM images of fibers in both I-Threads (Top) and I-Threads/PL@nHAp (bottom). Scale bars, 1 µm. (B) Mechanical tensile testing of I-Threads @nHAp and I-Threads/PL@nHAp with (i) representative tensile/strain curves, (ii) calculated young's modulus and (iii) analysis of (*, $p = 0.016$) and tensile load and ultimate tensile (*, $p = 0.031$; **, $p = 0.0077$). Error bars represent SD (n=5).

8.3.5. A-Yarns/PL and I-Threads/PL as biological delivery systems

Tissue's pH is tightly regulated in the living organism, ranging from 7.35 to 7.45 [73]. After injury, pH-associated deviations occur under conditions in which oxygen cannot be properly transported, resulting in tissues damage [74]. Further, in wound healing, the tissues microenvironment pH value is suggested as a parameter for diagnostic purposes [75], and more recently, advances in the field of stimuli-responsive drug delivery used the pH as an endogenous trigger for programmed in situ drug release [76]. So, defining and controlling the environmental tissues niche alterations is the key for a successful tissue regeneration. In this study, two different pH conditions (7.4 and 6.4) were used to replicate the physiological (healthy) and injured (inflammatory) states of tendon-to-bone tissue interface aiming at understanding the release kinetics of incorporated molecules in A-Yarns/PL and I-Threads/PL (Figure 8.5).

First, the cumulative release of total proteins was evaluated up to 31 days. Since proteins were in the core of fibers, in figure 8.5A, a sustained and slow released is observed for both A-Yarns/PL and I-

Threads/PL under physiological and inflammatory conditions. Interestingly, higher amounts of proteins were released under inflammatory pH comparably to physiological pH, which might be associated with the polymer degradation, namely accelerated hydrolysis under acidic conditions, and solubilization of easily accessible proteins [77]. Additionally, higher release was observed for I-Threads/PL comparably with A-Yarns/PL (Figure 8.5B, i-ii), which could be related with threads microstructural differences, namely threads dimensions, fibers number, and porosity. This behavior could be observed in terms of water uptake/weight loss kinetics (Supplementary Figure S8.4), where the highest uptake was observed in threads independently of the incorporation of PL. Nevertheless, it should be noted that these mechanism can differ in an *in vivo* setting, where the presence of macrophages or even metalloproteinases at a wound site can contribute to an accelerated polymer degradation [83].

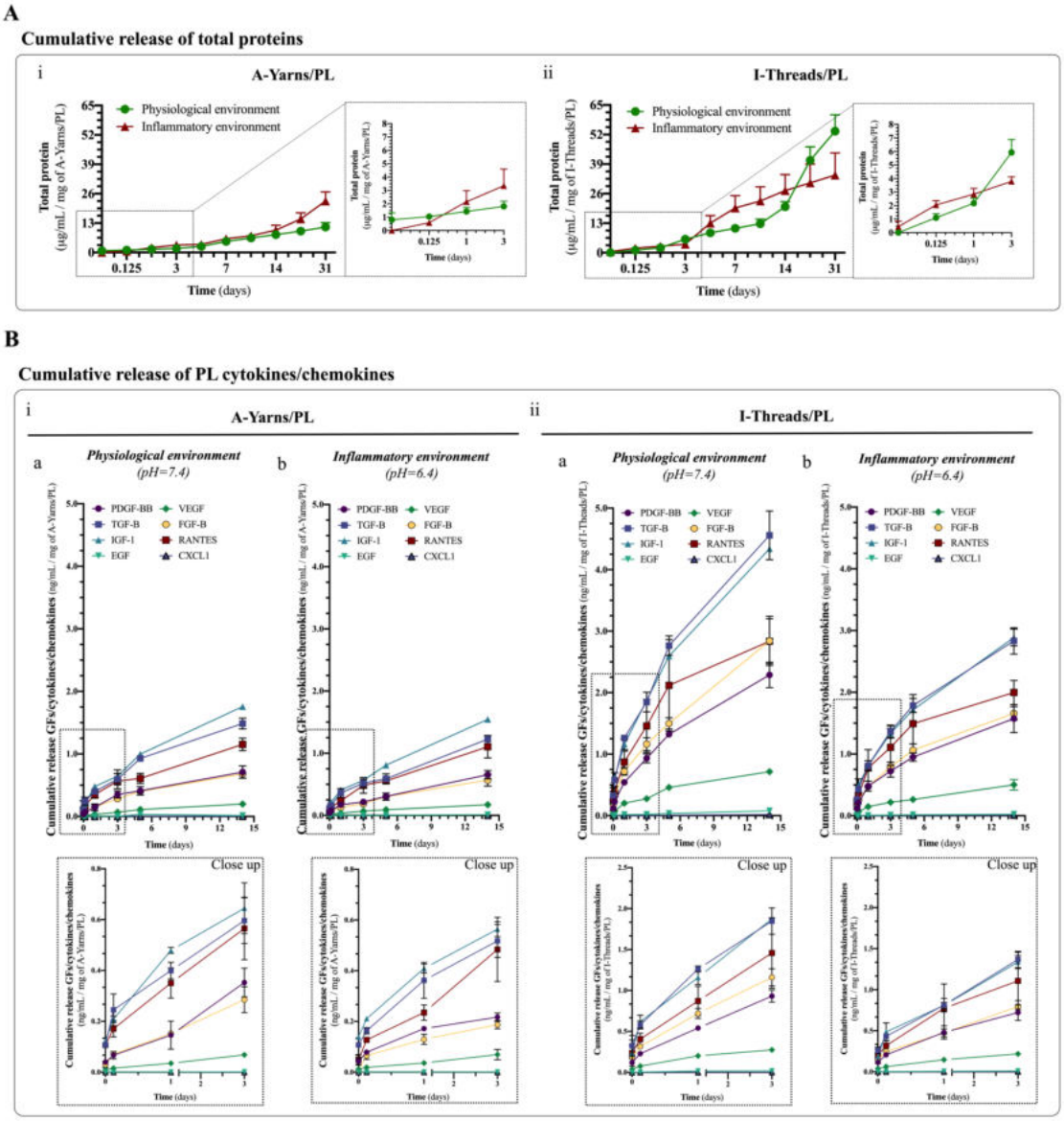

Figure 8.5 | Profile release of total proteins and PL growth factors, chemokines and cytokines in physiological and inflammatory environments. (A) Cumulative total protein release from (i) A-Yarns/PL and (ii) I-Threads/PL after contact with physiological and inflammatory environments for 31 days. Error bars represent standard error mean (SEM) (n=5). (C) Cumulative release of PL growth factors (GFs), cytokines and chemokines, namely PDGF-ß, TGF- ß, IGF-1, EGF, VEGF, FGF, ß, RANTES and CXCL1, quantified by ELISA in both (i) A-Yarns/PL and (ii) I-Threads/PL in both (a) physiological and (b) inflammatory settings for 14 days. Error bars represent SD (n=3).

The release of the PL components with known relevant roles on tendon-to-bone healing [78] namely, platelet-derived growth factor-BB subunit (PDGF-BB), transforming growth factor-ß (TGF-ß), insulin growth factor-1 (IGF-1), epidermal growth factor (EGF), vascular endothelia growth factor (VEGF), fibroblast growth factor-ß (FGF-ß), RANTES and CXCL1 were similarly evaluated up to 14 days. As depicted in Figure 8.5B and Table 8.1, I-Threads/PL presented higher concentrations of GFs, cytokines and chemokines when compared with A-Yarns/PL at both testing settings. This expected difference might have resulted from the higher diameter of threads comparably with yarns, and thus increased presence of PL-incorporated fibers. When assessing the release profile of both tested yarns and threads after 14 days, higher amounts of PDGF, IGF-1, TGF-ß, FGF- ß and RANTES, important factors for mesenchymal stem cells osteogenic induction [79] were observed for I-Threads/PL, whilst TGF-ß, IGF-1 and RANTES, described together as inducers of tenogenic matrix synthesis and/or cell proliferation [80], showed higher release in A-Yarns/PL, at both physiological and inflammatory settings (Figure 8.5B, Table 8.1). Nevertheless, when evaluating the cumulative concentration of PDGF-BB in the collected solution in contact with yarns and threads after 14 days, this GF was found to be released within a range (~0.2 to 10.0 ng/mL; Table 8.1) described to induce *in vitro* cells proliferation and differentiation [81, 82]. However, even though the release of biomolecules is within the pretended concentrations, it is widely dependent of the volume of external solution/medium used during release test. Yet, when seeded with cells, the presentation of PL biomolecules in close proximity to the cell receptor at the surface of the fibers is a much more biomimetic way of presenting PL biomolecules that adding it to culture media, as commonly performed in the daily basis, potentiating their effects and prevent a fast proteolytic degradation [28].

Table 8.1 | Average cumulative release of GFs, cytokines and chemokines of A-Yarns/PL and I-Threads/PL after 14 days under physiological and inflammatory settings.

Average cumulative release (ng/ml/mg sample)		***Growth Factors/cytokines/chemokines***							
		PDGF-BB	**TGF-B**	**IGF-1**	**EGF**	**VEGF**	**FGF-B**	**RANTES**	**CCLX1**
A-Yarns/PL	Physiolog	0.71± 0.10	1.49± 0.09	1.76± 0.05	0.016± 0.0002	0.20± 0.03	0.68± 0.05	1.15± 0.10	0.004± 0.0001
	Inflamm.	0.66± 0.07	1.23± 0.01	1.55± 0.01	0.012± 0.001	0.17± 0.02	0.57± 0.09	1.11± 0.18	0.001± 0.0001
I-Threads/PL	Physiolog	2.29± 0.21	4.56± 0.40	4.34± 0.01	0.08±0. 02	0.71± 0.03	2.84± 0.40	2.84±0. 37	0.02± 0.003
	Inflamm.	1.57± 0.23	2.83± 0.21	2.89± 0.14	0.024± 0.004	0.50± 0.09	1.66± 0.11	1.99±0. 20	0.010± 0.0001

8.3.6. Biological performance of biofunctional yarns and threads

To evaluate the effects stemming from the synergy between the biological activity of PLs components and topographical cues of anisotropic yarns and isotropic threads, A-Yarns/PL and I-Threads/PL and compared with the empty controls were seeded with hASCs, an easily available stem-cell source for tendon- and bone-tissue engineering [84, 85]. Figure 6A reveals a significant increase in hASCs proliferation after 10 and 15 days of culture in contact with A-Yarns/PL and I-Threads/PL comparably to A-Yarns and I-Threads, respectively, indicating a biological activity of incorporated PLs that results in the observed increase in cellular proliferation. Interestingly, the intracellular alkaline phosphatase (ALP) activity, an important indicator of osteogenic commitment [86], of hASCs seeded in I-Threads/PL was 5.1-, 1.7- and 1.4-fold increased at days 5, 10, and 15 in comparison with the values found in I-Threads (Figure 8.6B), demonstrating the potential of bioactive threads to induce an osteogenic response in stem cells. In the case of hASCs seeded A-Yarns/PL, ALP activity is reduced during culture time.

The expression of scleraxis (SCX), an important transcription factor in tendon tissue formation and expressed during tendon development [87], was assessed in both hASCs-seeded A-Yarns/PL, I-Threads/PL and respective plain controls (Figure 8.6C, i-ii). A-Yarns/PL showed a significantly higher expression of SCX at 5 and 10 days comparably to A-Yarns. Remarkably, SCX expression was accompanied by a translocation into cells' nuclei (Figure 8.6C, i, c-d), demonstrating an activation of this transcription factor, and resultant commitment of stem cells towards the tenogenic lineage [88]. Nevertheless, even though a temporal increase in SCX expression was observed in I-Threads/PL, nuclei

translocation did not occur (Figure 8.6C, ii, c-d). Therefore, the conjugation of biological factors release and anisotropic orientation of produced A-Yarns/PL was found to induce a tenogenic response in hASCs. In Figure 8.6D, expression of collagen type III (COL3) was evaluated in hASCs seeded onto A-Yarns/PL, I-Threads/PL and respective plain controls, due to reported evidence of this protein key role in bone ECM during tissues development and healing [89] and associated role in tendon degeneration and pathophysiology [90]. During culture time, no differences were observed in the expression of COL3 between A-Yarns/PL and A-Yarns (Figure 8.6D, i, a-b). In contrast, at both 5 and 10 days of culture, I-Threads/PL induced a significant higher deposition of COL3 compared with I-Threads (Figure 8.6D, i, a-b), demonstrating the potential use of these fibers to sustain the deposition of an osteogenic-like ECM. Nevertheless, the pro-osteogenic potential of fiber threads incorporated with nHAp was similarly assessed, envisioning its use as reliable biomaterials for osteo-commitment of stem cells. So, the biological performance of hASCs in terms of cell proliferation and ALP activity was also assessed in I-Threads/PL@nHAp over a culture period of 15 days in basal medium conditions and compared with respective controls (I-Threads@nHAp) (Figure 8.6E). As expected, I-Threads/PL@nHAp induced a significantly higher proliferation with a fold increase of 1.2- and 3.1- at days 5 and 10, respectively, and enhanced ALP activity compared to I-Threads@nHAp. Additionally, and given the importance of ECM mineralization on the determination of cells commitment towards the osteogenic lineage [91], alizarin red was performed at both 5 and 15 days of culture in several groups, namely I-Threads, I-Threads@nHAp, I-Threads/PL and I-Threads/PL@nHAp (Figure 8.6F, i-ii). Optical images of stained threads confirmed an absence of matrix mineralization in I-Threads in both 5 and 15 days. Even though, some mineralization was found in I-Threads@nHAp and I-Threads/PL, an extensive staining was observed in I-Threads/PL@nHAp (Figure 8.6F, i). This visual information was afterward confirmed by alizarin red quantification (Figure 8.6F, ii), where significantly higher AZ dye concentration was obtained for I-Threads/PL@nHAp, at both 5 and 10 days of culture under basal conditions, comparably with other tested threads formulations. Overall, the synergistic effect between the mineral component, fibers topography and PLs biological factors enabled to induce the commitment of hASCs towards osteogenic lineage without the need of an external biochemical supplementation.

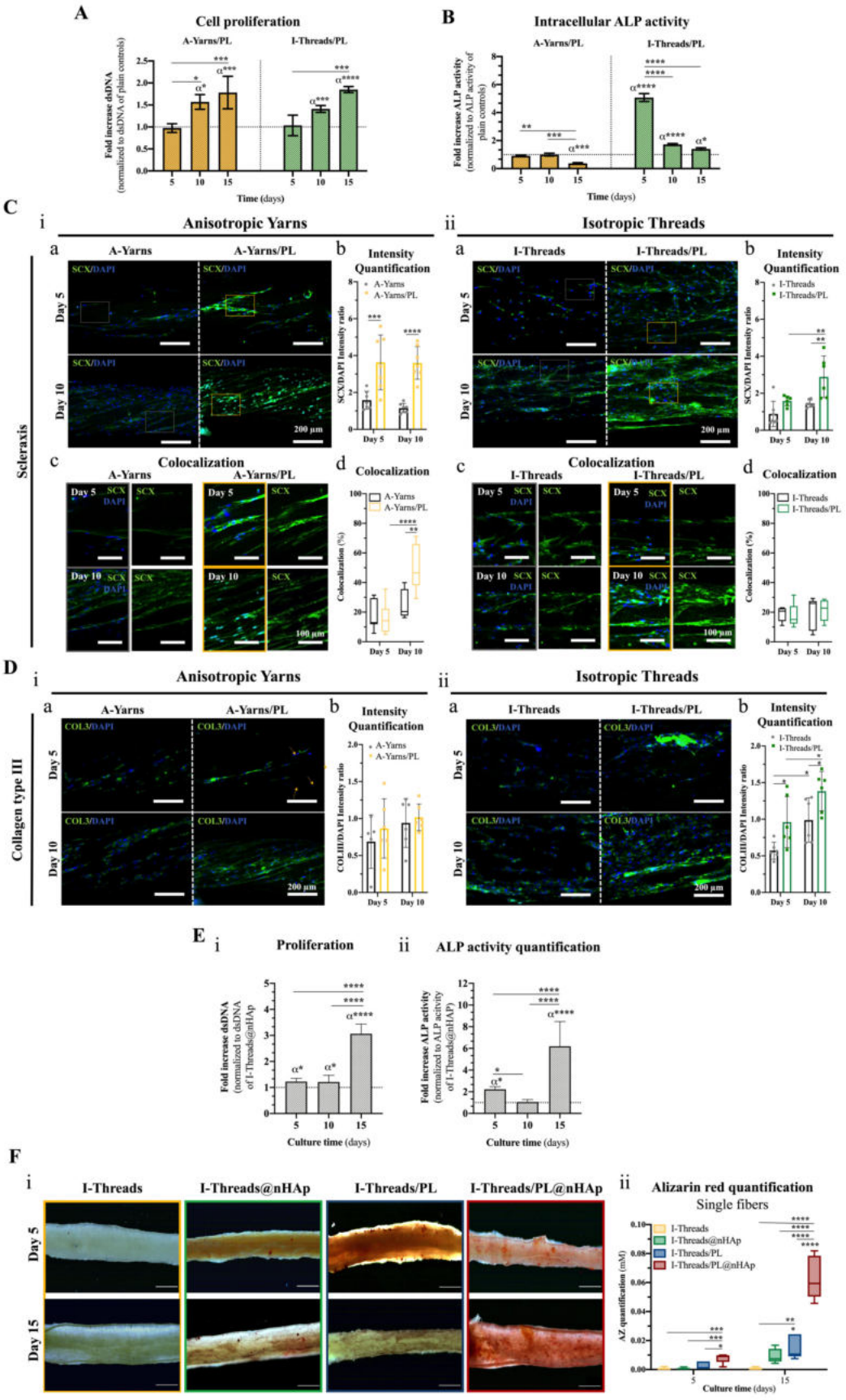

Figure 8.6 | Cell proliferation, ALP activity, protein expression and matrix mineralization of hASCs seeded A-Yarns/PL, I-Threads/PL and I-Threads/PL@nHAp. (A) Fold increase in

hASCs proliferation in A-Yarns/PL (*, p = 0.020; ***, p = 0.0004) and I-Threads/PL (***, p = 0.0005; ****, p < 0.0001) compared with A-Yarns and I-Threads, respectively, at 5, 10 and 15 days of culture. Error bars represent SEM (n=9) (B) Fold increase in intracellular ALP activity in A-Yarns/PL (**, p = 0.0019; ***, p = 0.0003) and I-Threads/PL (*, p = 0.028; ****, p < 0.0001) compared with A-Yarns and I-Threads at 5, 10 and 15 days of culture. Error bars represent SEM (n=9). (C) Immunofluorescence imaging of (a) scleraxis (SCX) and respective (b) intensity ratio in A-Yarns vs A-Yarns/PL (***, p = 0.0006; ****, p < 0.0001) and I-Threads vs I-Threads/PL (**, p = 0.0053). (c) Nuclei colocalization after 5 and 10 days of culture in both (i) A-Yarns vs A-Yarns/PL and (ii) I-Threads vs I-Threads/PL and respective (d) colocalization percentage (**, p = 0.0016; ****, p < 0.0001) at 5 and 10 days of culture. Scale bars, 200 μm and 100 μm. Error bars represent SD (n=7). (D) Immunolabeling of matrix protein, (a) collagen type III (COL3) after 5 and 10 days of culture in (i) A-Yarns vs A-Yarns/PL and (ii) I-Threads vs I-Threads/PL and respective (b) intensity ratio (*, p = 0.045). Scale bars, 200 μm. Error bars represent SD (n=5). (E) Cell's proliferation (i, *, p = 0.039; ****, p < 0.0001) and intracellular ALP activity (ii, *, p = 0.031; ****, p < 0.0001) of seeded hASCs up 15 days of culture in I-Threads/PL@nHAp. Fold increase obtained through normalization against the values obtained for I-Threads@nHAp. Bars represent SD (n=9). Statistical differences between I-Threads/PL@nHAp and I-Threads@nHAp are shown as α. (G) Optical microscopy images of (i) alizarin red staining after 5 and 15 days of culture of hASCs seeded I-Threads, I-Threads@nHAp, I-Threads/PL and I-Threads/PL@nHAp. Scale bars, 500 μm. (ii) Alizarin red quantification performed at 5 and 15 days of culture for the previously stained isotropic threads (*, p = 0.015; **, p = 0.0046; ***, p = 0.0004; ****, p < 0.0001). Bars represent the maximum and minimum values (n=5).

8.3.7. Fabrication of 3D functionally graded scaffolds: textile assembling technique

Over the past year, various-biomaterials have focused on the replication of the hierarchical organization of soft-to-hard tissue interfaces. Much attention has been given, in particular to textile technologies for the fabrication of mechanically and biologically competent 3D scaffolds. Knitting, weaving and braiding have been used to create constructs closely reaching the properties of different soft-to-hard tissues, while conserving key features of their single units in an assembled hierarchical construct [92]. Still, developed technologies fail in providing crucial bioactive signals in a precise and controllable manner, not reaching the required biological response. As observed in Figure 8.7A, by simply interlocking anisotropic yarns and isotropic threads, we developed continuous, easily handled and highly reproducible (Supplementary Table S8.1) gradient scaffolds with three distinct zones: a tendon insertion, an interface resultant of the

conjugation of yarns and threads, and a bony part (Figure 8.7A, iv), within the micro-scale range of tendon-to-bone tissue interface [93]. Micro-CT analysis allowed the confirmation of both the change in topographical cues in Yarns-Threads, Yarns-Threads/PL@nHAp (Figure 8.7B, i-ii) and Yarns-Threads@nHAp scaffolds (Supplementary Figure S8.5), and the presence of a mineral gradient of nHAp (Figure 8.7C and Supplementary Figure S8.5, ii, a). Further, the presence of nHAp within threads was confirmed by immunofluorescence microscopy after alizarin red staining (Figure 8.7D, i-ii).

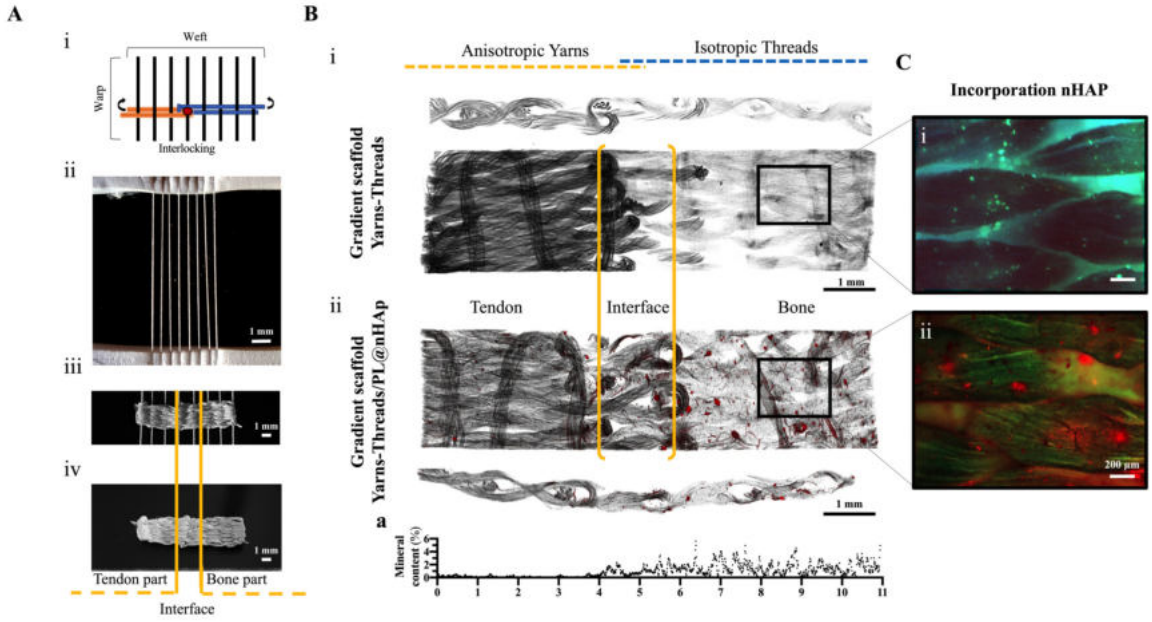

Figure 8.7 | Production and morphometric analysis of developed 3D gradient scaffolds. (A) Schematics of textile assembling taking advantage of (i) weaving technique and (ii) used platform for the continuous weft of anisotropic yarns and isotropic threads, resulting in the fabrication of continuous gradient scaffold (iii-iv). Scale bars, 1 mm. (B) Micro-CT scans of full-length and transversal cuts of (i) gradient scaffolds produced using A-Yarns and I-Threads (Scaffold Yarns-Threads) and (ii) A-Yarns/PL and I-Threads/PL@nHAp (Scaffold Yarns-Threads/PL@nHAp) . Hydroxyapatite particles are represented in red. Scale bar, 1 mm. (a) Graphical demonstration of the mineral content of across produced Yarns-Threads/PL@nHAp scaffold. (C) Immunofluorescence imaging of alizarin red-stained (i) Yarns-Threads and (ii) Yarns-Threads/PL@nHAp scaffolds. Particles are identified in red. Scale bar, 200 µm.

8.3.8. Biological performance of 3D gradient scaffolds: expression of tendon, interface and bone-related markers

Focus centered on assessment of the biological performance of biofunctional gradient scaffolds since, and considering their microstructural and compositional properties, we foresee a higher potential of this

biotextile as suitable scaffolds for tendon-to-bone tissue engineering. So, hASCs were used to evaluate if the microstructural, topographical and compositional cues provided by the fabricated biofunctional gradient constructs would induce the localized expression of specific tissue-related markers and thus recapitulate cells behavior on native niches, without any additional biochemical supplementation. The expression of tendon-(SCX), bone- (runt-related transcription factor 2, RUNX2) and interface-related markers (type II collagen, COLII, and SRY-box transcription factor 9, SOX9) was assessed on the different zones constituting Yarns-Threads (plain control), Yarns-Threads@nHAp and Yarns/Threads/PL@nHAp scaffolds at 14 and 21 days of culture (Figure 8.8A-B). Results indicate a high expression of RUNX2 at the tendon-, interface and bone-sections of seeded Yarns-Threads/PL@nHAp scaffolds (Figure 8.8A, iii, green and red, respectively), whilst RUNX2 expression was mainly localized in the interface-, bone-parts of Yarns-Threads@nHAp scaffolds. Nonetheless, the random orientation of threads in Yarns-Threads scaffolds seemed to induce a high expression of RUNX2 in the bone-section (Figure 8.8A, iii, green). The requirement of RUNX2 for commitment to the osteogenic lineage and support final progression to the mature osteocyte and expression of important molecules for mineralization of the bone extracellular matrix has been described [94]. Therefore, alizarin red staining was performed for produced scaffolds (Supplementary Figure S8.6, ii) to assessed matrix mineralization in the several sections. Interestingly, matrix mineralization was concentrated in the interface-bone sections of Yarns-Threads/PL@nHAp and Yarns-Threads@nHAp scaffolds (Supplementary Figure S8.6, ii), demonstrating a possible commitment of hASCs into the osteogenic lineage in that region associated with the presence of nHAp. As an important tenogenic markers associated with tendon development and differentiation [88] the expression of SCX was similarly explored. An increase expression was observed when going from the tendon part to the bony part of Yarns-Threads/PL@nHAp (Figure 8.8A, i, red). In contrast, no changes were observed for the expression of SCX in Yarns-Threads (plain control) and Yarns-Threads@nHAp. To investigate the capacity of produced functionally graded scaffolds to induce the expression of interface-related markers, while inducing the deposition of characteristic collagenous matrix commonly found in the interface [1], the expression of both SOX9 and COL2 were studied in fabricated scaffolds after 21 days of culture under basal conditions (Figure 8.8B). Remarkably, higher COL2 deposition was observed in both tendon- and interface parts of the Yarns-Threads/PL@nHAp (Figure 8.8B, iii, red), whilst SOX9 expression was mainly localized in the interface- and bony-sections (Figure 8.8B, iii, green). In contrast, Yarns-Threads@nHAp and Yarns-Threads a dispersed expression of both proteins was observed through scaffolds full-length (Figure 8.8B, i-ii).

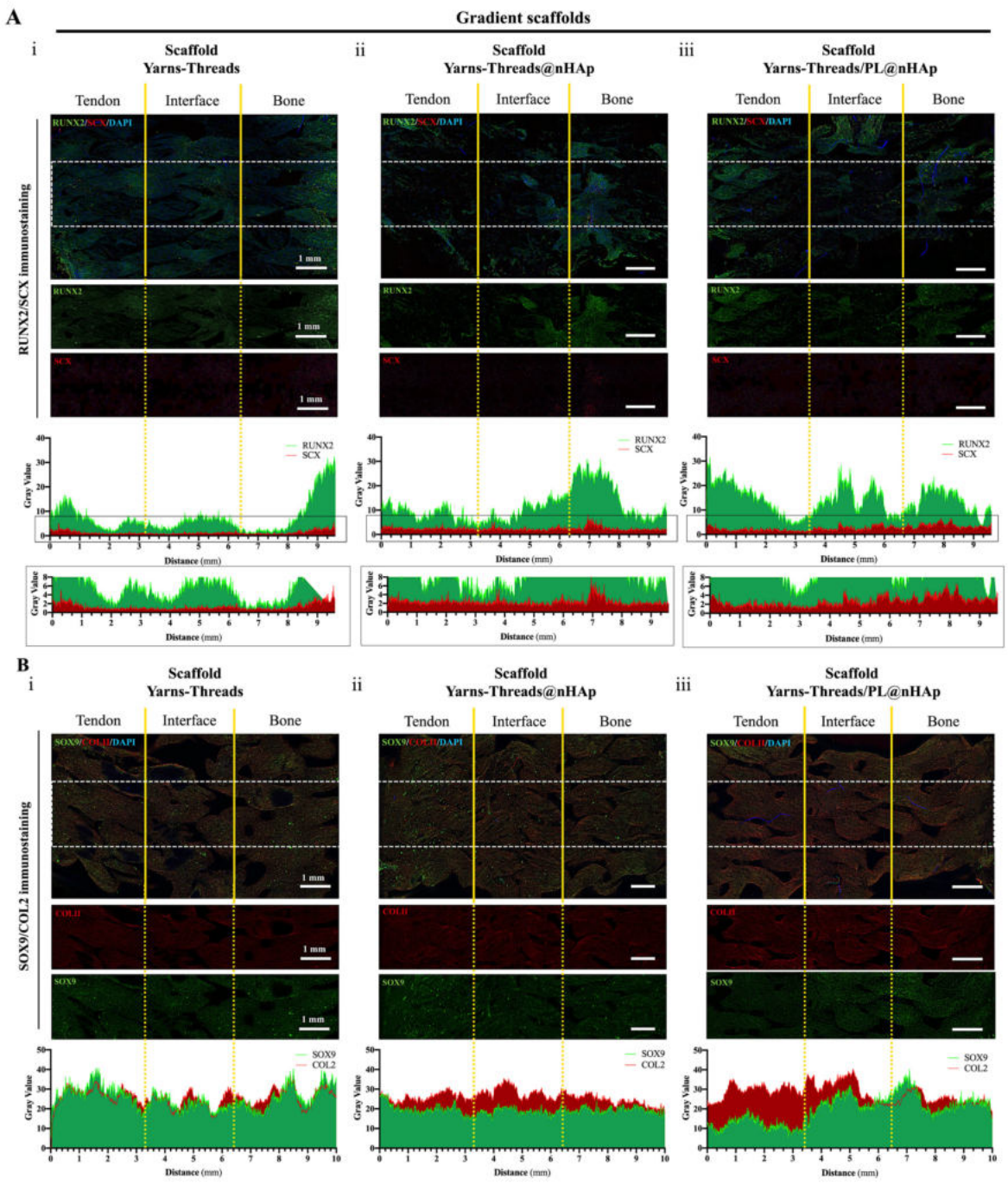

Figure 8.8 | Expression of tenogenic, osteogenic and interface-relevant markers in hASCs-seeded 3D graded scaffolds. Immunostaining of (E) tendon- (scleraxis, SCX) and bone-related markers (runt-related transcription factor 2, RUNX2) and (F) interface-related markers (collagen type II, COLII; SRY-Box transcription factor SOX9, SOX9) after 14 and 21 days of culture, respectively, in Yarns-Threads, Yarns-Threads@nHAp and Yarn-Threads/PL@nHAp scaffolds seeded with hASCs. Scale bar, 500 μm. The respective gray value of immunolabeling for each marker was determined across scaffolds length and divided according to the different parts (dotted lines).

Overall, these results demonstrate that the 3D hierarchical architecture, topography and composition of the proposed functionally graded scaffolds can synergistically boost the deposition of tenogenic-like matrix in the tendon counterpart, the osteochondrogenic commitment of stem cells at the interface, while inducing matrix mineralization at bony-part, promoting that way the deposition of ECM that resembles that of native tendon-to-bone interface. It should be noted that these constructs can be used as complete replacements of injured tendon-to-bone interface tissues, namely tendon detachment or rupture, as these are able to mimic heterogenic structure and biological gradients present in this interface. Nevertheless, *in vivo* studies using clinically relevant models of tendon injury will need to be conducted to quantitatively evaluate their regenerative performance.

8.4. CONCLUSIONS

In this work, we developed functionally graded 3D scaffolds containing bioactive factors for tendon to bone interface tissue replacement. This was achieved using emulsion electrospinning for the incorporation of PL within tendon- and bone-tissue mimetic structures, namely anisotropic yarns and isotropic threads, respectively. Additionally, nHAp was incorporated in threads to closely replicate the bone mineral content. PL-incorporated yarns and threads demonstrated to support a sustained release of biological factors when maintained in physiological (neutral pH) and inflammatory (acidic pH) settings without losing their bioactivity. In fact, this was confirmed in biological studies with hASCs, where seeded A-Yarns/PL and I-Threads/PL@nHAp revealed not only to be able to support cell proliferation but also to favor the expression of tenogenic-markers or to induce an osteogenic-like phenotype, respectively, without the need of external biochemical supplementation. Nevertheless, the combination of emulsion electrospinning and weaving technique, enabled the generation of 3D functional scaffolds with gradients in composition and topography, important to tailor hASCs commitment into tenogenic, osteochondrogenic and osteogenic lineages in the different sections of the constructs. Altogether, our results represent a promising strategy for the fabrication of easy reproducible and high-throughput 3D functionally graded scaffolds for tendon-to-bone tissue regeneration.

8.5. ACKNOWLEDGEMENTS

The authors would like to thank to Hospital da Prelada (Porto, Portugal) for the lipoaspirate tissue samples (Plastic Surgery Department). The authors acknowledge the financial support from the European Union Framework Programme for Research and Innovation HORIZON2020, Achilles (grant nr 810850) and

MagTendon (nr 772817), and Fundação para a Ciência e a Tecnologia for MagTT (nr 029930) and SmarTendon (PTDC/NAN-MAT/30595/2017) projects and the PhD grant of IC (PD/BD/128088/2016).

8.6. REFERENCES

[1] I. Calejo, R. Costa-Almeida, R.L. Reis, M.E. Gomes, Enthesis Tissue Engineering: Biological Requirements Meet at the Interface, Tissue Eng Part B Rev 25(4) (2019) 330-356, 10.1089/ten.teb.2018.0383.

[2] S. Thomopoulos, G.R. Williams, J.A. Gimbel, M. Favata, L.J. Soslowsky, Variation of biomechanical, structural, and compositional properties along the tendon to bone insertion site, Journal of Orthopaedic Research 21(3) (2003) 413-419, 10.1016/S0736-0266(03)00057-3.

[3] C.C. Kaeding, B. Aros, A. Pedroza, E. Pifel, A. Amendola, J.T. Andrish, W.R. Dunn, R.G. Marx, E.C. McCarty, R.D. Parker, R.W. Wright, K.P. Spindler, Allograft Versus Autograft Anterior Cruciate Ligament Reconstruction: Predictors of Failure From a MOON Prospective Longitudinal Cohort, Sports Health 3(1) (2011) 73-81, 10.1177/1941738110386185.

[4] G. Gasbarro, J. Ye, H. Newsome, K. Jiang, V. Wright, D. Vyas, J.J. Irrgang, V. Musahl, Morphologic Risk Factors in Predicting Symptomatic Structural Failure of Arthroscopic Rotator Cuff Repairs: Tear Size, Location, and Atrophy Matter, Arthroscopy 32(10) (2016) 1947-1952, 10.1016/j.arthro.2016.01.067.

[5] N.N. Verma, W. Dunn, R.S. Adler, F.A. Cordasco, A. Allen, J. MacGillivray, E. Craig, R.F. Warren, D.W. Altchek, All-arthroscopic versus mini-open rotator cuff repair: a retrospective review with minimum 2-year follow-up, Arthroscopy 22(6) (2006) 587-94, 10.1016/j.arthro.2006.01.019.

[6] J.M. Lowen, J.K. Leach, Functionally Graded Biomaterials for Use as Model Systems and Replacement Tissues, Advanced Functional Materials 30(44) (2020) 1909089, 10.1002/adfm.201909089.

[7] Y. Jun, E. Kang, S. Chae, S.-H. Lee, Microfluidic spinning of micro- and nano-scale fibers for tissue engineering, Lab on a Chip 14(13) (2014) 2145-2160, 10.1039/C3LC51414E.

[8] X.-Y. Du, Q. Li, G. Wu, S. Chen, Multifunctional Micro/Nanoscale Fibers Based on Microfluidic Spinning Technology, Advanced Materials 31(52) (2019) 1903733, 10.1002/adma.201903733.

[9] M.E. Gomes, H.S. Azevedo, A.R. Moreira, V. Ellä, M. Kellomäki, R.L. Reis, Starch–poly(ε-caprolactone) and starch–poly(lactic acid) fibre-mesh scaffolds for bone tissue engineering applications: structure, mechanical properties and degradation behaviour, Journal of Tissue Engineering and Regenerative Medicine 2(5) (2008) 243-252, 10.1002/term.89.

[10] M.L. Muerza-Cascante, D. Haylock, D.W. Hutmacher, P.D. Dalton, Melt Electrospinning and Its Technologization in Tissue Engineering, Tissue Engineering Part B: Reviews 21(2) (2014) 187-202, 10.1089/ten.teb.2014.0347.

[11] D. Puppi, F. Chiellini, Wet-spinning of biomedical polymers: from single-fibre production to additive manufacturing of three-dimensional scaffolds, Polymer International 66(12) (2017) 1690-1696, 10.1002/pi.5332.

[12] I. Calejo, R. Costa-Almeida, R.L. Reis, M.E. Gomes, A Textile Platform Using Continuous Aligned and Textured Composite Microfibers to Engineer Tendon-to-Bone Interface Gradient Scaffolds, Advanced Healthcare Materials 8(15) (2019) 1900200, 10.1002/adhm.201900200.

[13] R.F. Canadas, J.M. Cavalheiro, J.D. Guerreiro, M.C. de Almeida, E. Pollet, C.L. da Silva, M.M. da Fonseca, F.C. Ferreira, Polyhydroxyalkanoates: waste glycerol upgrade into electrospun fibrous scaffolds for stem cells culture, Int J Biol Macromol 71 (2014) 131-40, 10.1016/j.ijbiomac.2014.05.008.

[14] N. Nagiah, C.J. Murdock, M. Bhattacharjee, L. Nair, C.T. Laurencin, Development of Tripolymeric Triaxial Electrospun Fibrous Matrices for Dual Drug Delivery Applications, Scientific Reports 10(1) (2020) 609, 10.1038/s41598-020-57412-0.

[15] X. Wang, B. Ding, B. Li, Biomimetic electrospun nanofibrous structures for tissue engineering, Mater Today (Kidlington) 16(6) (2013) 229-241, 10.1016/j.mattod.2013.06.005.

[16] A.R. Tomás, A.I. Gonçalves, E. Paz, P. Freitas, R.M.A. Domingues, M.E. Gomes, Magneto-mechanical actuation of magnetic responsive fibrous scaffolds boosts tenogenesis of human adipose stem cells, Nanoscale 11(39) (2019) 18255-18271, 10.1039/C9NR04355A.

[17] M. Laranjeira, R.M.A. Domingues, R. Costa-Almeida, R.L. Reis, M.E. Gomes, 3D Mimicry of Native-Tissue-Fiber Architecture Guides Tendon-Derived Cells and Adipose Stem Cells into Artificial Tendon Constructs, Small 13(31) (2017) 1700689, 10.1002/smll.201700689.

[18] K.L. Moffat, A.S. Kwei, J.P. Spalazzi, S.B. Doty, W.N. Levine, H.H. Lu, Novel nanofiber-based scaffold for rotator cuff repair and augmentation, Tissue Eng Part A 15(1) (2009) 115-26, 10.1089/ten.tea.2008.0014.

[19] M. Buzgo, A. Mickova, M. Rampichova, M. Doupnik, 11 - Blend electrospinning, coaxial electrospinning, and emulsion electrospinning techniques, in: M.L. Focarete, A. Tampieri (Eds.), Core-Shell Nanostructures for Drug Delivery and Theranostics, Woodhead Publishing2018, pp. 325-347, 10.1016/B978-0-08-102198-9.00011-9.

[20] D. Han, A.J. Steckl, Coaxial Electrospinning Formation of Complex Polymer Fibers and their Applications, ChemPlusChem 84(10) (2019) 1453-1497, 10.1002/cplu.201900281.

[21] M. Li, Y. Zheng, B. Xin, Y. Xu, Coaxial Electrospinning: Jet Motion, Core–Shell Fiber Morphology, and Structure as a Function of Material Parameters, Industrial & Engineering Chemistry Research 59(13) (2020) 6301-6308, 10.1021/acs.iecr.9b05866.

[22] H. Jiang, Y. Hu, P. Zhao, Y. Li, K. Zhu, Modulation of protein release from biodegradable core–shell structured fibers prepared by coaxial electrospinning, Journal of Biomedical Materials Research Part B: Applied Biomaterials 79B(1) (2006) 50-57, 10.1002/jbm.b.30510.

[23] N. Nikmaram, S. Roohinejad, S. Hashemi, M. Koubaa, F.J. Barba, A. Abbaspourrad, R. Greiner, Emulsion-based systems for fabrication of electrospun nanofibers: food, pharmaceutical and biomedical applications, RSC Advances 7(46) (2017) 28951-28964, 10.1039/C7RA00179G.

[24] A.C. Mitchell, P.S. Briquez, J.A. Hubbell, J.R. Cochran, Engineering growth factors for regenerative medicine applications, Acta biomaterialia 30 (2016) 1-12, 10.1016/j.actbio.2015.11.007.

[25] H. Zhang, K. Wang, T. Gao, R. Zhang, Z. Cai, J. Liu, H. Ma, W. Zhang, Controlled release of bFGF loaded into electrospun core–shell fibrous membranes for use in guided tissue regeneration, Biomedical Materials 15(3) (2020) 035021, 10.1088/1748-605x/ab7979.

[26] J. Hu, Y. Song, C. Zhang, W. Huang, A. Chen, H. He, S. Zhang, Y. Chen, C. Tu, J. Liu, X. Xuan, Y. Chang, J. Zheng, J. Wu, Highly Aligned Electrospun Collagen/Polycaprolactone Surgical Sutures with Sustained Release of Growth Factors for Wound Regeneration, ACS Applied Bio Materials 3(2) (2020) 965-976, 10.1021/acsabm.9b01000.

[27] O. Evrova, G.M. Burgisser, C. Ebnother, A. Adathala, M. Calcagni, E. Bachmann, J.G. Snedeker, C. Scalera, P. Giovanoli, V. Vogel, J. Buschmann, Elastic and surgeon friendly electrospun tubes delivering PDGF-BB positively impact tendon rupture healing in a rabbit Achilles tendon model, Biomaterials 232 (2020) 119722, 10.1016/j.biomaterials.2019.119722.

[28] S.P.B. Teixeira, R.M.A. Domingues, M. Shevchuk, M.E. Gomes, N.A. Peppas, R.L. Reis, Biomaterials for Sequestration of Growth Factors and Modulation of Cell Behavior, Advanced Functional Materials 30(44) (2020) 1909011, 10.1002/adfm.201909011.

[29] E. Anitua, M. Sánchez, G. Orive, Potential of endogenous regenerative technology for in situ regenerative medicine, Advanced Drug Delivery Reviews 62(7) (2010) 741-752, 10.1016/j.addr.2010.01.001.

[30] E. Anitua, M. Sánchez, A.T. Nurden, P. Nurden, G. Orive, I. Andía, New insights into and novel applications for platelet-rich fibrin therapies, Trends in Biotechnology 24(5) (2006) 227-234, 10.1016/j.tibtech.2006.02.010.

[31] N. Fekete, M. Gadelorge, D. Fürst, C. Maurer, J. Dausend, S. Fleury-Cappellesso, V. Mailänder, R. Lotfi, A. Ignatius, L. Sensebé, P. Bourin, H. Schrezenmeier, M.T. Rojewski, Platelet lysate from whole blood-derived pooled platelet concentrates and apheresis-derived platelet concentrates for the isolation and expansion of human bone marrow mesenchymal stromal cells: production process, content and identification of active components, Cytotherapy 14(5) (2012) 540-554, 10.3109/14653249.2012.655420.

[32] B.B. Mendes, M. Gómez-Florit, P.S. Babo, R.M. Domingues, R.L. Reis, M.E. Gomes, Blood derivatives awaken in regenerative medicine strategies to modulate wound healing, Advanced Drug Delivery Reviews 129 (2018) 376-393,1 0.1016/j.addr.2017.12.018.

[33] S.C.N.d.S. Santos, Ó.E. Sigurjonsson, C.d.A. Custódio, J.F.C.d.L. Mano, Blood Plasma Derivatives for Tissue Engineering and Regenerative Medicine Therapies, Tissue Eng Part B Rev 24(6) (2018) 454-462, 10.1089/ten.TEB.2018.0008.

[34] R. Yonemitsu, T. Tokunaga, C. Shukunami, K. Ideo, H. Arimura, T. Karasugi, E. Nakamura, J. Ide, Y. Hiraki, H. Mizuta, Fibroblast Growth Factor 2 Enhances Tendon-to-Bone Healing in a Rat Rotator Cuff Repair of Chronic Tears, The American Journal of Sports Medicine 47(7) (2019) 1701-1712, 10.1177/0363546519836959.

[35] C.C. Würgler-Hauri, L.M. Dourte, T.C. Baradet, G.R. Williams, L.J. Soslowsky, Temporal expression of 8 growth factors in tendon-to-bone healing in a rat supraspinatus model, J Shoulder Elbow Surg 16(5 Suppl) (2007) S198-S203, 10.1016/j.jse.2007.04.003.

[36] Y. Huang, M. Pan, H. Shu, B. He, F. Zhang, L. Sun, Vascular endothelial growth factor enhances tendon-bone healing by activating Yes-associated protein for angiogenesis induction and rotator cuff reconstruction in rats, Journal of Cellular Biochemistry 121(3) (2020) 2343-2353, 10.1002/jcb.29457.

[37] S. Yamazaki, K. Yasuda, F. Tomita, H. Tohyama, A. Minami, The effect of transforming growth factor-beta1 on intraosseous healing of flexor tendon autograft replacement of anterior cruciate ligament in dogs, Arthroscopy 21(9) (2005) 1034-41, 10.1016/j.arthro.2005.05.011.

[38] A. Weiler, C. Förster, P. Hunt, R. Falk, T. Jung, F.N. Unterhauser, V. Bergmann, G. Schmidmaier, N.P. Haas, The influence of locally applied platelet-derived growth factor-BB on free tendon graft remodeling after anterior cruciate ligament reconstruction, Am J Sports Med 32(4) (2004) 881-91, 10.1177/0363546503261711.

[39] B. Edderkaoui, Potential Role of Chemokines in Fracture Repair, Front Endocrinol (Lausanne) 8 (2017) 39-39, 10.3389/fendo.2017.00039.

[40] A. Stålman, D. Bring, P.W. Ackermann, Chemokine expression of CCL2, CCL3, CCL5 and CXCL10 during early inflammatory tendon healing precedes nerve regeneration: an immunohistochemical study in the rat, Knee Surg Sports Traumatol Arthrosc 23(9) (2015) 2682-9, 10.1007/s00167-014-3010-9.

[41] S. Von Euw, Y. Wang, G. Laurent, C. Drouet, F. Babonneau, N. Nassif, T. Azaïs, Bone mineral: new insights into its chemical composition, Scientific Reports 9(1) (2019) 8456, 10.1038/s41598-019-44620-6.

[42] V.E. Santo, M.E. Gomes, J.F. Mano, R.L. Reis, Chitosan–chondroitin sulphate nanoparticles for controlled delivery of platelet lysates in bone regenerative medicine, Journal of Tissue Engineering and Regenerative Medicine 6(S3) (2012) s47-s59, 10.1002/term.1519.

[43] P.P. Carvalho, X. Wu, G. Yu, I.R. Dias, M.E. Gomes, R.L. Reis, J.M. Gimble, The effect of storage time on adipose-derived stem cell recovery from human lipoaspirates, Cells Tissues Organs 194(6) (2011) 494-500, 10.1159/000324892.

[44] N. Felsenthal, E. Zelzer, Mechanical regulation of musculoskeletal system development, Development 144(23) (2017) 4271, 10.1242/dev.151266.

[45] J. Lee, A.A. Abdeen, K.A. Kilian, Rewiring mesenchymal stem cell lineage specification by switching the biophysical microenvironment, Scientific Reports 4(1) (2014) 5188, 10.1038/srep05188.

[46] I. Calejo, R. Costa-Almeida, R.L. Reis, M.E. Gomes, A Physiology-Inspired Multifactorial Toolbox in Soft-to-Hard Musculoskeletal Interface Tissue Engineering, Trends in Biotechnology 38(1) (2020) 83-98, 10.1016/j.tibtech.2019.06.003.

[47] L. Krishna, K. Dhamodaran, C. Jayadev, K. Chatterjee, R. Shetty, S.S. Khora, D. Das, Nanostructured scaffold as a determinant of stem cell fate, Stem Cell Research & Therapy 7(1) (2016) 188, 10.1186/s13287-016-0440-y.

[48] R. Ravichandran, S. Liao, C.C. Ng, C.K. Chan, M. Raghunath, S. Ramakrishna, Effects of nanotopography on stem cell phenotypes, World J Stem Cells 1(1) (2009) 55-66, 10.4252/wjsc.v1.i1.55.

[49] S.P. Magnusson, K. Qvortrup, J.O. Larsen, S. Rosager, P. Hanson, P. Aagaard, M. Krogsgaard, M. Kjaer, Collagen fibril size and crimp morphology in ruptured and intact Achilles tendons, Matrix Biol 21(4) (2002) 369-77, 10.1016/s0945-053x(02)00011-2.

[50] P. Kannus, Structure of the tendon connective tissue, Scand J Med Sci Sports 10(6) (2000) 312-20, 10.1034/j.1600-0838.2000.010006312.x.

[51] E.A. McNally, H.P. Schwarcz, G.A. Botton, A.L. Arsenault, A Model for the Ultrastructure of Bone Based on Electron Microscopy of Ion-Milled Sections, PLOS ONE 7(1) (2012) e29258, 10.1371/journal.pone.0029258.

[52] A. Boyde, Scanning Electron Microscopy of Bone, Methods Mol Biol 1914 (2019) 571-616, 10.1007/978-1-4939-8997-3_31.

[53] R. Pal, Effect of droplet size on the rheology of emulsions, AIChE Journal 42(11) (1996) 3181-3190, 10.1002/aic.690421119.

[54] F.L. Román, M. Schmidt, H. Löwen, Colloidal particles in emulsions, Physical Review E 61(5) (2000) 5445-5451, 10.1103/PhysRevE.61.5445.

[55] M. Buzgo, M. Rampichova, K. Vocetkova, V. Sovkova, V. Lukasova, M. Doupnik, A. Mickova, F. Rustichelli, E. Amler, Emulsion centrifugal spinning for production of 3D drug releasing nanofibres with core/shell structure, RSC Advances 7(3) (2017) 1215-1228, 10.1039/C6RA26606A.

[56] S. Damodaran, Protein Stabilization of Emulsions and Foams, Journal of Food Science 70(3) (2005) R54-R66, 10.1111/j.1365-2621.2005.tb07150.x.

[57] E. Bouyer, G. Mekhloufi, V. Rosilio, J.-L. Grossiord, F. Agnely, Proteins, polysaccharides, and their complexes used as stabilizers for emulsions: Alternatives to synthetic surfactants in the pharmaceutical field?, International Journal of Pharmaceutics 436(1) (2012) 359-378, 10.1016/j.ijpharm.2012.06.052.

[58] D.J. McClements, Food Emulsions: Principles, Practices, and Techniques, CRC Press2004, 10.1201/9781420039436.

[59] D.J. Burgess, O.N. Sahin, Influence of protein emulsifier interfacial properties on oil-in-water emulsion stability, Pharm Dev Technol 3(1) (1998) 21-9, 10.3109/10837459809028476.

[60] X. Xu, X. Zhuang, X. Chen, X. Wang, L. Yang, X. Jing, Preparation of Core-Sheath Composite Nanofibers by Emulsion Electrospinning, Macromolecular Rapid Communications 27(19) (2006) 1637-1642, 10.1002/marc.200600384.

[61] P. Lu, Y. Xia, Maneuvering the Internal Porosity and Surface Morphology of Electrospun Polystyrene Yarns by Controlling the Solvent and Relative Humidity, Langmuir 29(23) (2013) 7070-7078, 10.1021/la400747y.

[62] Ş. Şeker, A.E. Elçin, Y.M. Elçin, Autologous protein-based scaffold composed of platelet lysate and aminated hyaluronic acid, Journal of Materials Science: Materials in Medicine 30(12) (2019) 127, 10.1007/s10856-019-6334-7.

[63] S.A. Bernal-Chávez, S. Alcalá-Alcalá, D. Cerecedo, A. Ganem-Rondero, Platelet lysate-loaded PLGA nanoparticles in a thermo-responsive hydrogel intended for the treatment of wounds, European Journal of Pharmaceutical Sciences 146 (2020) 105231, 10.1016/j.ejps.2020.105231.

[64] A. Camerlo, A.M. Bühlmann-Popa, C. Vebert-Nardin, R.M. Rossi, G. Fortunato, Environmentally controlled emulsion electrospinning for the encapsulation of temperature-sensitive compounds, Journal of Materials Science 49(23) (2014) 8154-8162, 10.1007/s10853-014-8524-5.

[65] F. Cengiz Çallıoğlu, H. Kesici Güler, E. Sesli Çetin, Emulsion electrospinning of bicomponent poly (vinyl pyrrolidone)/gelatin nanofibers with thyme essential oil, Materials Research Express 6(12) (2019) 125013, 10.1088/2053-1591/ab5387.

[66] J. Wu, Y. Hong, Enhancing cell infiltration of electrospun fibrous scaffolds in tissue regeneration, Bioactive Materials 1(1) (2016) 56-64, 10.1016/j.bioactmat.2016.07.001.

[67] A.S. LaCroix, S.E. Duenwald-Kuehl, R.S. Lakes, R. Vanderby, Jr., Relationship between tendon stiffness and failure: a metaanalysis, J Appl Physiol (1985) 115(1) (2013) 43-51, 10.1152/japplphysiol.01449.2012.

[68] A.S. Deshpande, P.-A. Fang, X. Zhang, T. Jayaraman, C. Sfeir, E. Beniash, Primary structure and phosphorylation of dentin matrix protein 1 (DMP1) and dentin phosphophoryn (DPP) uniquely determine their role in biomineralization, Biomacromolecules 12(8) (2011) 2933-2945, 10.1021/bm2005214.

[69] M. Carles-Carner, L.S. Saleh, S.J. Bryant, The effects of hydroxyapatite nanoparticles embedded in a MMP-sensitive photoclickable PEG hydrogel on encapsulated MC3T3-E1 pre-osteoblasts, Biomed Mater 13(4) (2018) 045009-045009, 10.1088/1748-605X/aabb31.

[70] R. Kang, Y. Luo, L. Zou, L. Xie, H. Lysdahl, X. Jiang, C. Chen, L. Bolund, M. Chen, F. Besenbacher, C. Bünger, Osteogenesis of human induced pluripotent stem cells derived mesenchymal stem cells on hydroxyapatite contained nanofibers, RSC Advances 4(11) (2014) 5734-5739, 10.1039/C3RA44181D.

[71] H. Chen, X. Huang, M. Zhang, F. Damanik, M.B. Baker, A. Leferink, H. Yuan, R. Truckenmüller, C. van Blitterswijk, L. Moroni, Tailoring surface nanoroughness of electrospun scaffolds for skeletal tissue engineering, Acta Biomaterialia 59 (2017) 82-93, 10.1016/j.actbio.2017.07.003.

[72] J.C. Berkmann, A.X. Herrera Martin, A. Ellinghaus, C. Schlundt, H. Schell, E. Lippens, G.N. Duda, S. Tsitsilonis, K. Schmidt-Bleek, Early pH Changes in Musculoskeletal Tissues upon Injury—Aerobic Catabolic Pathway Activity Linked to Inter-Individual Differences in Local pH, Int J Mol Sci 21(7) (2020) 10.3390/ijms21072513.

[73] B.S. Sørensen, M. Busk, J. Overgaard, M.R. Horsman, J. Alsner, Simultaneous Hypoxia and Low Extracellular pH Suppress Overall Metabolic Rate and Protein Synthesis In Vitro, PLOS ONE 10(8) (2015) e0134955, 10.1371/journal.pone.0134955.

[74] M. Chen, C. Chen, Z. Shen, X. Zhang, Y. Chen, F. Lin, X. Ma, C. Zhuang, Y. Mao, H. Gan, P. Chen, X. Zong, R. Wu, Extracellular pH is a biomarker enabling detection of breast cancer and liver cancer using CEST MRI, Oncotarget 8(28) (2017) 45759-45767, 10.18632/oncotarget.17404.

[75] A. Raza, T. Rasheed, F. Nabeel, U. Hayat, M. Bilal, H.M.N. Iqbal, Endogenous and Exogenous Stimuli-Responsive Drug Delivery Systems for Programmed Site-Specific Release, Molecules 24(6) (2019) 1117, 10.3390/molecules24061117.

[76] L. Macdougall, H. Culver, C.-C. Lin, C. Bowman, K. Anseth, 1.3.2F - Degradable and Resorbable Polymers, in: W.R. Wagner, S.E. Sakiyama-Elbert, G. Zhang, M.J. Yaszemski (Eds.), Biomaterials Science (Fourth Edition), Academic Press2020, pp. 167-190, 10.1016/B978-0-12-816137-1.00015-5.

[77] J.M. Anderson, A. Rodriguez, D.T. Chang, Foreign body reaction to biomaterials, Seminars in Immunology 20(2) (2008) 86-100, 10.1016/j.smim.2007.11.004.

[78] S. Font Tellado, E.R. Balmayor, M. Van Griensven, Strategies to engineer tendon/ligament-to-bone interface: Biomaterials, cells and growth factors, Advanced Drug Delivery Reviews 94 (2015) 126-140, 10.1016/j.addr.2015.03.004.

[79] F. Ng, S. Boucher, S. Koh, K.S.R. Sastry, L. Chase, U. Lakshmipathy, C. Choong, Z. Yang, M.C. Vemuri, M.S. Rao, V. Tanavde, PDGF, TGF-β, and FGF signaling is important for differentiation and growth of mesenchymal stem cells (MSCs): transcriptional profiling can identify markers and signaling pathways important in differentiation of MSCs into adipogenic, chondrogenic, and osteogenic lineages, Blood 112(2) (2008) 295-307, 10.1182/blood-2007-07-103697.

[80] T. Molloy, Y. Wang, G. Murrell, The roles of growth factors in tendon and ligament healing, Sports Med 33(5) (2003) 381-94, 10.2165/00007256-200333050-00004.

[81] Z. Mihaylova, R. Tsikandelova, P. Sanimirov, N. Gateva, V. Mitev, N. Ishkitiev, Role of PDGF-BB in proliferation, differentiation and maintaining stem cell properties of PDL cells in vitro, Archives of Oral Biology 85 (2018) 1-9, 10.1016/j.archoralbio.2017.09.019.

[82] A. Colciago, F. Celotti, L. Casati, R. Giancola, S.M. Castano, G. Antonini, M.C. Sacchi, P. Negri-Cesi, In Vitro Effects of PDGF Isoforms (AA, BB, AB and CC) on Migration and Proliferation of SaOS-2 Osteoblasts and on Migration of Human Osteoblasts, Int J Biomed Sci 5(4) (2009) 380-389.

[83] A.I. Gonçalves, M.T. Rodrigues, S.J. Lee, A. Atala, J.J. Yoo, R.L. Reis, M.E. Gomes, Understanding the role of growth factors in modulating stem cell tenogenesis, PLoS One 8(12) (2013) e83734, 10.1371/journal.pone.0083734.

[84] S.M. Mihaila, A.K. Gaharwar, R.L. Reis, A. Khademhosseini, A.P. Marques, M.E. Gomes, The osteogenic differentiation of SSEA-4 sub-population of human adipose derived stem cells using silicate nanoplatelets, Biomaterials 35(33) (2014) 9087-99, 10.1016/j.biomaterials.2014.07.052.

[85] J.R. Farley, D.J. Baylink, Skeletal alkaline phosphatase activity as a bone formation index in vitro, Metabolism - Clinical and Experimental 35(6) (1986) 563-571, 10.1016/0026-0495(86)90016-8.

[86] Y. Yoshimoto, A. Takimoto, H. Watanabe, Y. Hiraki, G. Kondoh, C. Shukunami, Scleraxis is required for maturation of tissue domains for proper integration of the musculoskeletal system, Scientific Reports 7(1) (2017) 45010, 10.1038/srep45010.

[87] N.D. Murchison, B.A. Price, D.A. Conner, D.R. Keene, E.N. Olson, C.J. Tabin, R. Schweitzer, Regulation of tendon differentiation by scleraxis distinguishes force-transmitting tendons from muscle-anchoring tendons, Development 134(14) (2007) 2697, 10.1242/dev.001933.

[88] S.W. Volk, S.R. Shah, A.J. Cohen, Y. Wang, B.K. Brisson, L.K. Vogel, K.D. Hankenson, S.L. Adams, Type III collagen regulates osteoblastogenesis and the quantity of trabecular bone, Calcif Tissue Int 94(6) (2014) 621-631, 10.1007/s00223-014-9843-x.

[89] H.A. Eriksen, A. Pajala, J. Leppilahti, J. Risteli, Increased content of type III collagen at the rupture site of human Achilles tendon, Journal of Orthopaedic Research 20(6) (2002) 1352-1357, 10.1016/S0736-0266(02)00064-5.

[90] Y. Mikuni-Takagaki, Y. Kakai, M. Satoyoshi, E. Kawano, Y. Suzuki, T. Kawase, S. Saito, Matrix mineralization and the differentiation of osteocyte-like cells in culture, J Bone Miner Res 10(2) (1995) 231-42, 10.1002/jbmr.5650100209.

[91] S. Wu, Y. Wang, P.N. Streubel, B. Duan, Living nanofiber yarn-based woven biotextiles for tendon tissue engineering using cell tri-culture and mechanical stimulation, Acta Biomater 62 (2017) 102-115, 10.1016/j.actbio.2017.08.043.

[92] L. Rossetti, L.A. Kuntz, E. Kunold, J. Schock, K.W. Müller, H. Grabmayr, J. Stolberg-Stolberg, F. Pfeiffer, S.A. Sieber, R. Burgkart, A.R. Bausch, The microstructure and micromechanics of the tendon–bone insertion, Nature Materials 16(6) (2017) 664-670, 10.1038/nmat4863.

[93] G.S. Stein, J.B. Lian, A.J.v. Wijnen, J.L. Stein, M. Montecino, A. Javed, S.K. Zaidi, D.W. Young, J.-Y. Choi, S.M. Pockwinse, Runx2 control of organization, assembly and activity of the regulatory machinery for skeletal gene expression, Oncogene 23(24) (2004) 4315-4329, 10.1038/sj.onc.1207676.

8.7. SUPPLEMENTARY INFORMATION

8.7.1. FIGURES

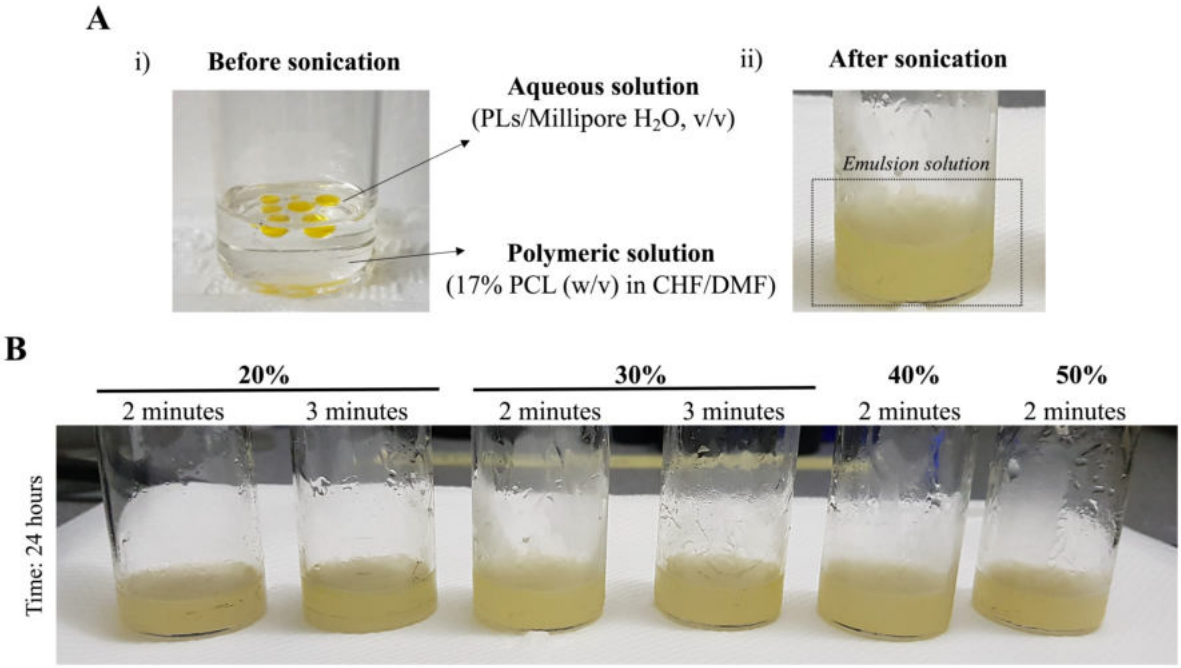

Supplementary Figure S8.1 | Stability of emulsion solutions after the application of increasing ultrasonication amplitudes. (A) W/O emulsion composed of (i) polymeric solution of 17% PCL (w/v) in chloroform/dimethylformamide (CHF/DMF) and an aqueous phase composed of PL/MilliQ water with food coloring (1:1, v/v) before sonification. (ii) Emulsion solution obtained right after ultrasonication for 2 minutes under 20% amplitude (ii). (B) Images acquired after 24 hours following emulsion preparation using increasing ultrasonication amplitudes.

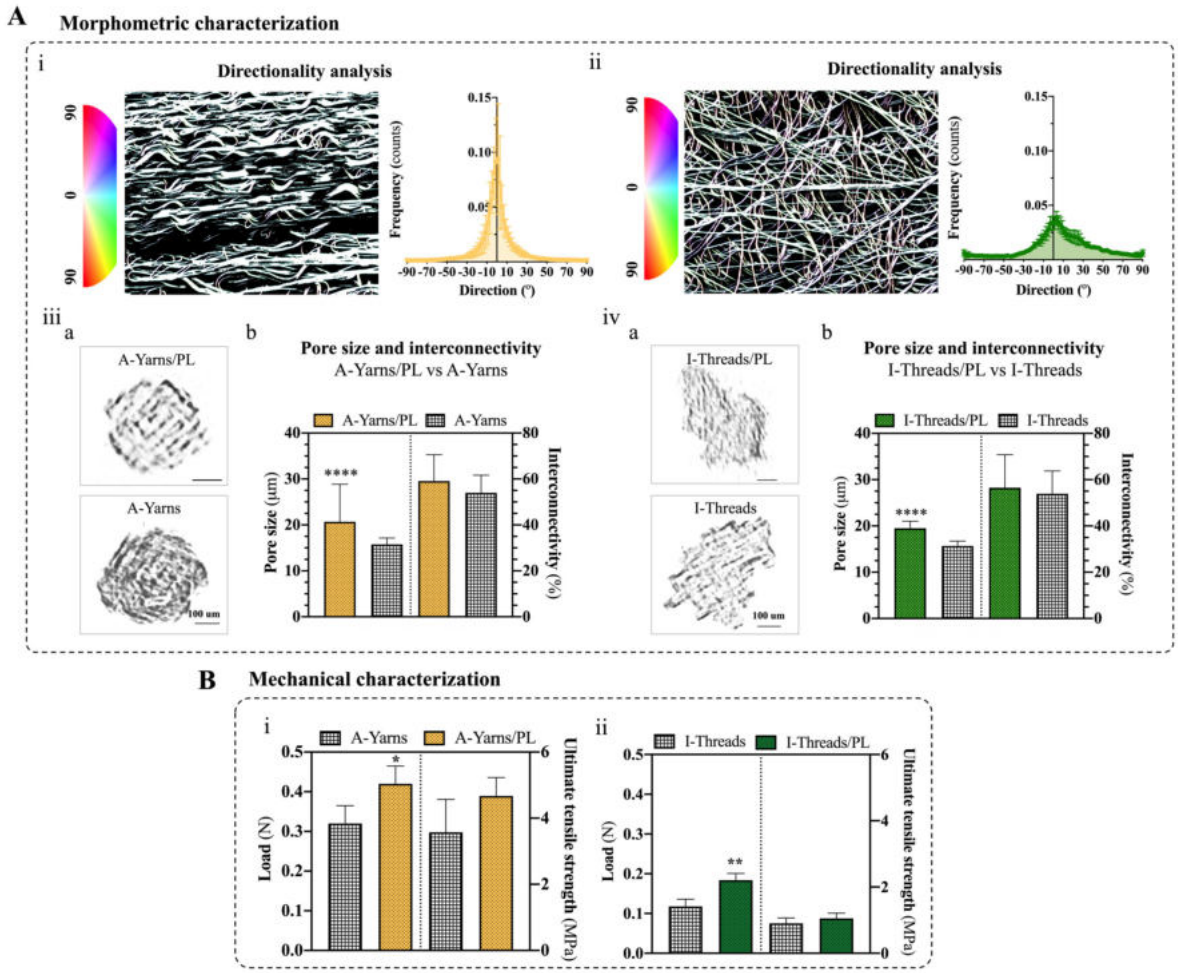

Supplementary Figure S8.2 | Comparative morphometric and mechanical characterization of A-Yarns/PL and I-Threads/PL with empty controls. (A) Morphometric analysis of (i-iii) A-Yarns vs A-Yarns/PL and (ii - iv) I-Threads vs I-Threads/PL through (i) fibers directionality analysis and (ii) transversal porosity profiling by (b) pore size (left) and interconnectivity (right) evaluation. Scale bar, 100 μm. Error bars represent SD (n=4). (B) Mechanical characterization with analysis of tensile load and ultimate tensile for A-Yarns vs A-Yarns/PL (*, p = 0.0397) and I-Threads vs I-Threads/PL (**, p = 0.0079). Error bars represent SD (n=5).

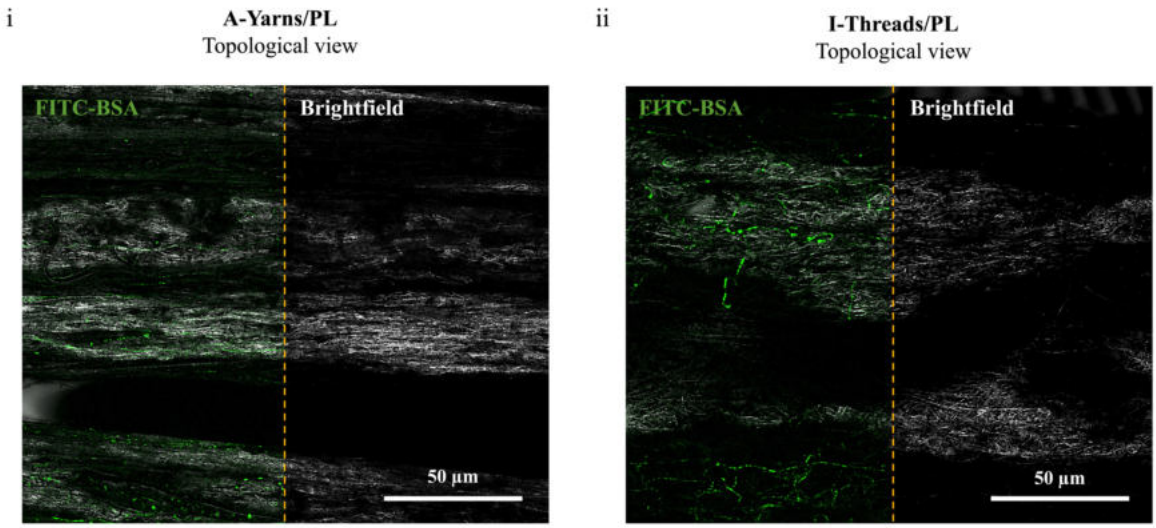

Supplementary Figure S8.3 | Distribution of PL/FITC-BSA within fibers. Confocal images of the topological view of (i) A-Yarns/PL and (ii) I-Threads/PL with incorporated PL/FITC-BSA (green) in the aqueous fraction of the polymeric solution.

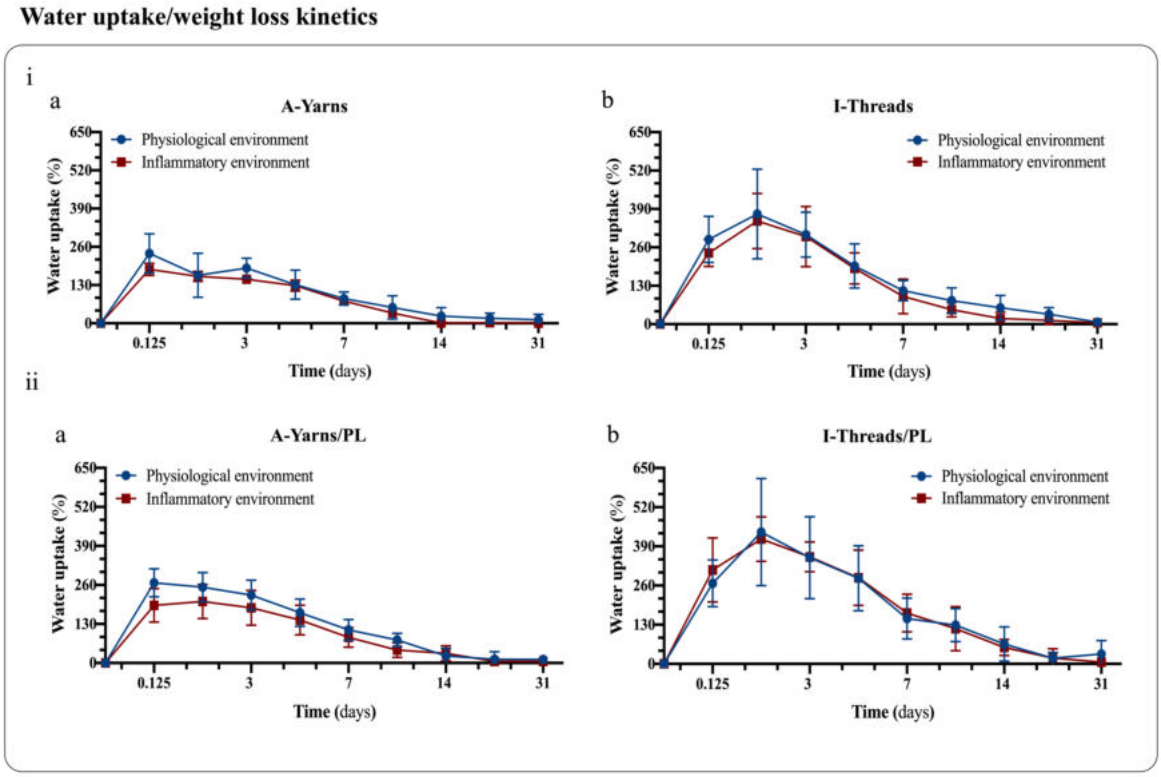

Supplementary Figure S8.4 | Water uptake under physiological and inflammatory environments. Water uptake/ weight loss kinetics profile of both (i) A-Yarns (a) and I-Threads (b) and (ii) A-Yarns/PL (a) and I-Threads/PL (b) in physiological (pH=7.4) and inflammatory (pH=6.4) environments up to 31 days. Error bars represent SD (n=5).

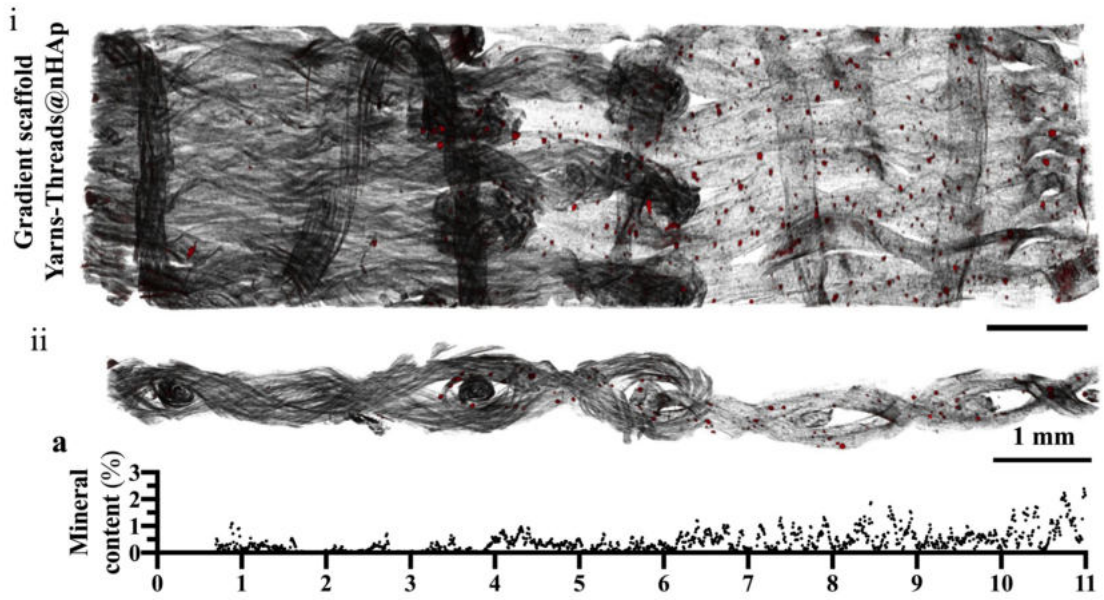

Supplementary Figure S8.5 | Morphological analysis of Yarns-Threads@nHAp scaffold. Micro-CT scans of (i) full length and (ii) transversal cut of gradient scaffolds produced using anisotropic A-Yarns I-Threads@nHAp. Scale bar, 1 mm. (a) Graphical demonstration of the mineral content of across produced gradient scaffold. Scale bar, 1 mm.

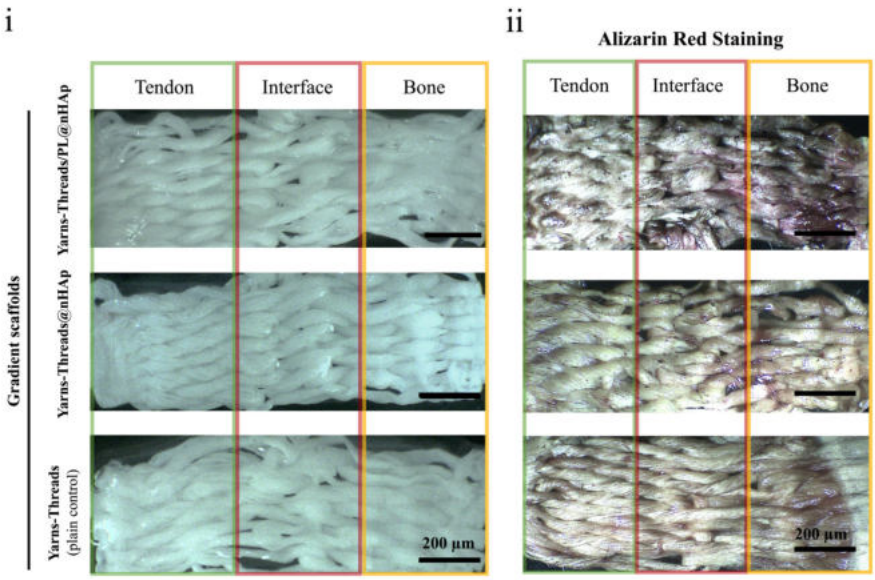

Supplementary Figure S8.6| Matrix mineralization in fabricated 3D gradient scaffolds. (i) Optical images of hASCs-seeded scaffolds after 14 days of culture under basal medium conditions. Scale bar, 200 µm. (ii) Alizarin red staining of 3D gradient scaffolds. Scale bar, 200 µm.

8.7.2. TABLES

Supplementary Table S8.1 | Length measurement of produced scaffolds.

Scaffold	**Yarns-Threads**	**Yarns-Threads@nHAp**	**Yarns-Threads/PL@nHAp**
Length (mm)	11.39 ± 2.13	10.69 ± 0.78	10.72 ± 0.39

CHAPTER 9. "Microengineered composite living fibers as 3D in vitro models of tendon physiology and pathology"

This chapter was adapted from the following publication:

I. Calejo, C. J. Labrador-Rached, M. Gomez-Florit, D. Docheva, R. L. Reis, R.M.A Domingues, M. E. Gomes (2021) 3D multiplex bioengineered model for tendon tissue microenvironment replication. (submitted)

ABSTRACT

Clinically relevant models of tendon health and disease are urgently needed for a better understanding of associated cellular mechanisms and functions that can foster the development and testing of novel therapeutic approaches. In this work, multiplex 3D bioengineered tendon units were produced for the replication of both physio- and pathophysiological tendon microenvironments. For this purpose, composite living fibers (CLFs) were produced with polycaprolactone yarns (anisotropic) and threads (isotropic) core coated with a bioactive platelet lysate (PL) hydrogel layer encapsulating human tendon-derived cells (hTDCs) to mimic both healthy and diseased 3D tissue architectures, respectively. In CLF-healthy, hTDCs presented high cytoskeleton alignment while expressing tendon-related genes, scleraxis, tenomodulin, and mohawk, and depositing a tenogenic rich extracellular matrix (ECM). Contrarily, cell crowding without marked preferential orientation and high ECM deposition were observed in CLF-diseased. Moreover, deposition of collagen type III was favored over collagen type I, in association with a phenotypic drift characterized by early gene expression of osteogenic and chondrogenic markers and later expression of smooth alpha muscle actin, a myofibroblastic marker, were observed. Furthermore, an imbalance between matrix remodeling and degradation was demonstrated by the enzymatic activity of matrix metalloproteinase-1, -3, -9, and tissue metallopeptidase inhibitor 1. In summary, we report the fabrication of health and disease bioengineered 3D *in vitro* tendon models taking advantage of biophysical and biological cues for the induction of regenerative and pro-fibrotic phenotypes in human tendon-derived cells. These innovative alternatives to currently available models offer several advantages and thus envisions promising applications for drug screening and for supporting the research and development of new therapies.

Keywords: Composite living fibers; Fiber-based techniques; Tendon tissue engineering; Tendon units; 3D multiplex model

9.1. INTRODUCTION

Tendons are well-organized and dense connective tissues that can respond and adapt to the transmission of contraction forces by muscles to the skeleton, allowing motion and maintenance of posture. Healthy tendon encompasses highly aligned and hierarchical type I collagen fibrous structures with few tendon cells located in between [1]. Nowadays, as the human lifespan expands and sedentary lifestyle increases, tendon-associated injuries and pathologies are extremely prevalent leading to patients' disabilities and pain [2]. Frequently, loss of tendon functionality, as observed in tendinopathies, is caused by the poor rearrangement of collagen fibrils, deposited fibrocartilaginous ECM, and type III collagen [3, 4], a typical characteristic of scarring (fibrotic) tissue formation, neovascularization, and inflammation [3, 5]. Furthermore, the hypovascular and hypocellular nature of the tendon limits its healing capacity resulting in injury recurrence [6]. Notwithstanding, tendon healing is a complex process influenced by several factors described in distinctive stages, namely inflammation, proliferation, and remodeling [7]. Thus, it is particularly important to understand the intricate interactions between tendon tissue 3D architecture, organization, and cell composition to recapitulate both healthy and disease physiology in a model, for the development of effective new therapies. Clearly, despite presenting lower complexity and high practicability, currently used 2D *in vitro* static culture models cannot accurately recreate the level of complexity found at the native tendon tissue [8]. Therefore, to unravel intricate mechanisms involved in tendon homeostasis and disease, a wide range of animal models (e.g. mouse, rat, rabbit, murine have been used to evaluate the cascade of processes that occur throughout both tendon pathology and repair, as these are cheaper, easier to handle and allow to study the disease in the naturally occurring environment [9]. However, due to species-specific differences, several therapeutics fail when translating animal models to human clinics, given often unclear results compared to the human homolog [10]. So, *ex vivo* explants models (e.g. digital flexor tendons [11], Achilles tendon [12]) have been used as alternatives for the above-mentioned models as they allow a deep study of the biological responses with minimal stress to animals, such as mouse, rabbit, and horses, and using molecular tools developed for standard cell culture [8]. Yet, due to limited knowledge about *ex vivo* tissue homeostasis, culture conditions still need to be optimized to have a homeostatic baseline in which tendon cells remain quiescent, thus introducing a time-related constraint [8, 13]. Overall, a major obstacle to the scientific and clinical advancement of tendon therapies is still the lack of reliable and valid models of tendon physiology and pathology. Innovative *in vitro* bioengineered 3D models might be developed using advanced fabrication strategies and following tissue engineering principles, enabling the mimicry of the native tissue's structure and function through the precise deposition and assembly of materials and cells.

Among the biochemical and biomechanical factors in the extracellular niche that regulate tendon cells behavior, the extracellular matrix (ECM) structure, particularly fiber alignment, has been highlighted as an important biophysical cue governing tendon cells behavior. Recent works have demonstrated the importance of topography on cell commitment towards a tenogenic phenotype [14, 15]. For example, our group has produced anisotropic electrospun fibrous scaffolds able to replicate the 3D nano-to-macro hierarchical architecture of native tendon ECM [14]. The physical cues stemming from this tendon inspired 3D architecture favored the tenogenic commitment of human adipose-derived stem cells and prevented the phenotype drift of tendon cells [14]. Similarly, Schoenenberger *et al.* [16] studied the influence of either aligned or misaligned 2D PCL mats on tendon fibroblasts' behavior. Cells morphology, phenotype, and matrix turnover were markedly influenced by substrate orientation, being favoring a downregulation of the matrix proteins and ECM-remodeling enzymes by cells in contact with random nanofiber scaffolds, in contrast to cells in aligned substrates [16]. Moreover, in an inflammatory setting characterized by macrophage-tendon fibroblast crosstalk, macrophages seeded in randomly orientated displayed a unique pro-inflammatory signature providing new insights into how biological response can be modulated by biomaterial designs that address the biomechanical niche of cells [17]. Thus, when aiming at replicate the tendon microenvironment, one should consider that 3D architecture and topography of engineered systems, deliver biophysical cues that induce powerful modulatory effects over tendon cells' behavior. Aside from the hierarchical structure of tendon, tendon cells are embedded in a peri-cellular ECM niche composed of fibrillar collagens type III, V, and XI, and non-fibrillar collagens type VI, XII, and XIV, important in fibrillogenesis and tendon development [18, 19], and by non-collagenous components, such as proteoglycans (e.g. decorin), elastin and other glycoproteins (e.g. fibronectin, tenascin-c) which provide resistance to compression, support collagen matrix assembly and regulate cellular processes during tendon development and healing [20-22]. Currently, the engineering of a rich extracellular matrix tenocyte-assembled tendon equivalent requires the use of prolonged *in vitro* cultures, normally associated with phenotypic drift, besides its associated high costs and time consumption for modeling. Molecular crowding has been proposed to mitigate this problem as means to increase ECM deposition in cell culture systems by accelerating the enzymatic conversion of soluble procollagen in insoluble collagen [23, 24]. However, the inherent complexity associated with this technique makes it difficult to implement in a miniaturized 3D tissue equivalent as additional cues from ECM signaling are necessary to maintain tissue homeostasis or guide matrix remodeling.

Blood derivatives such as platelet lysate (PL), have attracted great attention in regenerative medicine as an inexpensive milieu of bioactive molecules (e.g., growth factors, cytokines, adhesion, and structural

proteins). Interestingly, growth factors encountered in PL have been suggested to be involved in several tendon homeostasis. For example, platelet-derived growth factor (PDGF) has been suggested to be involved in the regulation of tendon cells fate [25]. One study specifically showed that PDGF immobilized on aligned substrates promoted the tenogenic differentiation of adipose-derived stem cells [26]. Similarly, transforming growth factor-beta (TGF-β) has been established to play central roles in early events of tendon development, tendon neonatal cells recruitment [27] and tendon cells maintenance [28]. Additionally, several growth factors present in platelet derivatives, including PDGF and TGF-β, but also vascular endothelial growth factor (VEGF), endothelial growth factor (EGF), insulin-like growth factor (IGF-I), fibroblast growth factor (FGF), and hepatocyte growth factor (HGF), have been shown to significantly enhance the healing process in tendinopathies [29-31]. On the other hand, PL is also rich in several structural proteins (e.g. fibrin(ogen) or fibronectin) that are essential as temporary scaffolds for the first phases of the wound healing process [32]. We have recently shown that their composition and intrinsic bioactivity can be leveraged to develop fast cellularized tissue-engineered constructs [33, 34]. Interestingly, fibrin-based hydrogels have been used as *in vitro* model systems to explore cellular roles in embryonic tendon formation [35]. These fibrillary gels could mimic the soft matrix and high cell density representative of embryonic tissues [35], although not replicating the structural complexity of the native hierarchical tissue and 3D matrix of tendon. Moreover, supplementation of fibrin gels with a combination of recombinant BMP-14, TGF-β3, and VEGF enhanced the tenogenic commitment of encapsulated bone marrow stem cells, supporting the notion that multiple biological signaling pathways are involved in the regulation of this mechanism [36, 37]. Together, these studies suggest that, if combined with fabrication strategies enabling control over tenoinductive physical cues, PL might be an interesting bioactive biomaterial for the development of advanced in vitro 3D tendon models.

We have recently used PL as hydrogel coatings on sutures cores to produce composite living fibers (CLFs) for potential surgical tissue repair and showed that it induces fast deposition of collagen types I and III by encapsulated human adipose-derived stem cells (hASCs) [38]. Building on this CLFs concept, we hypothesized that by combining PL hydrogel coatings with tendon inspired nanofiber assemblies with defined 3D architecture, we would be able to recapitulate the biophysical and biological cues of both healthy and diseased tendon microenvironments, at the required throughput and in a time and cost-effective manner for *in vitro* modeling. Thus, in the present study, electrospinning was used for the production of continuous anisotropic fibers that were afterward twisted into more complex yarns to recreate the hierarchical 3D structure of healthy tendon fascicles and used as core elements for the production of CLFs. Beyond recreating the anisotropic fiber alignment existing in heathy tendon

microenvironments, fibrous cores with isotropic topographies were also fabricated to recreate diseased-like ECM organization and induce the production of degenerative-related markers, as commonly observed in tendinopathies [3, 4]. Human tendon-derived cells (hTDCs) were selected as the heterogeneous population of stem/progenitor cells and tenocytes found in the native tissue that are widely used in *in vitro* tendon modeling studies [39]. To fabricate the CLFs, they hTDCs were then encapsulated within PL hydrogel coatings shells, which replicated the interstitial ECM and constituted a source of growth factors, proteins, and other signaling biomolecules that promote fast construct cellularization, effective matrix deposition, while directing hTDCs phenotype depending on the core's topography. Combined with 3D printing technologies, the proposed concept allows the rapid generation of large numbers of highly reproducible sample replicates fitting multi-well plate formats. Overall, the developed approach holds great promise for the fabrication of high-throughput 3D *in vitro* models to study tendon physiology and pathology, offering a reliable alternative to existing options as tools for drug screening in the search for new tendon therapies.

9.2. MATERIALS AND METHODS

9.2.1. Materials

Poly-ε-caprolactone (PCL, average MW 80,000), thrombin from bovine plasma lyophilized powder (40-300 NIH units/mg protein), gelatin from porcine skin (type A, gel strength ~300 bloom), phosphate-buffered saline (PBS), bovine serum albumin (BSA) and phalloidin-tetramethylrhodamine B isothiocyanate were purchased from Sigma-Aldrich, USA. Chloroform was purchased from Honeywell, Switzerland while N, N'-dimethylformamide (DMF) was purchased from Carlo Erba Reagents, France. Calcium chloride ($CaCl_2$) was purchased from Merk KGaA, Germany. Polylactic acid (PLA) filaments were purchased from Beeverycreative, Portugal. ACTIVA WM transglutaminase was purchased from Ajinomoto, Germany. Ethanol 70% (v/v) was purchased from AGA, Portugal. Formalin 10% solution neutral buffered was purchased from Bio-Optica Milano, Italy. Minimum essential medium alpha (α-MEM), Dulbecco's phosphate-buffered saline (DPBS), trypsin-EDTA solution, fetal bovine serum (FBS), antibiotic/antimycotic solution (A/A) were purchased from Life Technologies, USA. Triton X-100 was purchased from ThermoFisher Scientific. 4,6-Diamidino-2-phenyindole dilactate (DAPI) was purchased from VWR, USA. PerfeCTa SYBR Green FastMix and qScript cDNA Synthesis Kit were purchased from Quanta Biosciences, USA. RNeasy Mini Kit (RNA extraction) was purchased from Quiagen, Germany. Hydrogen peroxide 30% w/v was purchased from Panreac Applichem, Barcelona.

9.2.2. Production of poly-ε-caprolactone (PCL) anisotropic and isotropic fiber yarns and threads

An electrospinning solution was prepared with 17% w/v of PCL dissolved in a chloroform/DMF (v/v, 7:3) solution, and stirred overnight at room temperature (RT). Both anisotropic and isotropic PCL fiber threads were produced using a customized electrospinning setup [15]. Briefly, a syringe with a 21G needle was filled with the PCL solution and jetted, under a constant flow rate of 1.0 mL/h and voltage of 8.0-9.0 kV, into a 20% (v/v) ethanol/water bath. Continuous anisotropic fiber threads were collected with the jetting needle at 16 cm from the surface of the bath by a roller located 20 cm away from the needle at a constant winding speed of 1.09 cm/s. For isotropic fiber threads, the needle was placed 13 cm above the surface of the bath, the roller was located 13 cm away from the needle, and threads were collected at a constant winding speed of 0.14 cm/s. Throughout the process, the temperature was maintained at 21-23°C with a relative humidity of 43-45%. Threads with anisotropic fibers were further assembled into yarns by twisting twelve threads together (4 turns/cm) to mimic the collagen architecture in the tendon fascicles in terms of alignment and anisotropy [22]. Threads with isotropic fibers were no further treated since they matched well the targeted tendon fascicle dimensions and mimicked the more randomly oriented fiber organization seen in fibrosis [5, 16].

9.2.2.1. *Characterization by scanning electron microscopy (SEM) and directionality analysis*

Threads topography was observed using a high-resolution field scanning electron microscope (JSM-6010 LV, JEOL, Japan). Briefly, samples were prepared by placing random pieces of around 1 cm on adhesive carbon films and coated with gold under vacuum for one minute (Cressington, UK) before visualization. Images were collected at an acceleration voltage of 10 kV. ImageJ software was used to measure threads and fiber diameters (n=50). The degree of surface alignment was determined by using directionality analysis applying the Fourier components method within ImageJ software (version 2.1.0/1.43c). For this purpose, scanning electron images were converted to 32-bit images and cropped into three different images. The radial intensities were calculated, and the orientation map was also obtained.

9.2.3. Fabrication of CLFs support platform fitting multi-well plate format

Customizable three-dimensional (3D) polylactic acid (PLA) holders were designed using AutoCAD (version 2019, student license) to hold up to four yarns/threads simultaneously with an approximate length of 2.5 cm. The top and bottom parts were designed with an outer diameter of 3.4 cm and an inner diameter of

3.0 cm to fit into 6-well plates. A pillar-to-hole mechanism was designed to trap yarns/threads between the bottom and top pieces. Moreover, an adjustable bottom piece was designed to separate four CLFs yarns/threads into different channels, presenting a height of 0.5 cm, a diameter of 0.2 cm, and a depth of 0.4 cm. The different parts were 3D printed using B2X300 printer (Beeverycreative, Portugal).

9.2.4. Platelet lysates (PL) and gelatin (GEL) coatings for production of CLFs

9.2.4.1. *Platelet lysate preparation*

Platelet lysate (PL) was prepared from platelet concentrates (PC) obtained from healthy human blood donors under a cooperation protocol previously established with the Hospital de São João, Portugal (Serviço de Imunohemoterapia) and approved by the Ethical Committee [38, 40]. Briefly, PC with a platelet count of one million platelets/µL were pooled from 80 donors and subjected to three freeze/thaw cycles with liquid nitrogen at -196°C and a 37°C water bath, respectively. These cycles allowed for platelet lysis and protein content release. PL aliquots were then stored at -80°C. Before use, PL was thawed, and platelet debris was removed by centrifugation at 3000 g for 10 min at RT.

9.2.4.2. *Optimization of PL hydrogel coating*

Yarns/threads were coated with a hydrogel layer composed of PL. For this purpose, samples were fixed inside the 3D-printed holder and immersed into thrombin solution prepared in 5 mM $CaCl_2$ at a final concentration of 5 and 10 U/mL for 15, 30, 45, and 90 minutes at RT. Then, a clean multichannel part was placed and filled with equal amounts of fresh PL. Yarns/threads were incubated in PL at 37° C for 2 hours under humidified conditions to allow PL gelation. The morphology of PL hydrogel coated yarns/threads were analyzed by optical microscopy (DM750, Leica, Schweiz), to observe hydrogel layer formation around yarns/threads core. Herein, four images per sample were acquired immediately after the coating (day 0) and after 24 hours (day 1), where PL hydrogel layer thickness was assessed using ImageJ software (version 2.1.0/1.43c). Upon hydrogel optimization, the 45 minutes incubation time in thrombin solution at a final concentration of 10 U/mL was selected for subsequent assays.

9.2.4.3. *Preparation of gelatin (GEL) coatings*

Enzymatically crosslinked gelatin prepared according to our previously established protocol [41] was used as control hydrogel coatings for the PL-coated structures. Briefly, 5% gelatin from porcine skin (w/v in PBS) was dissolved at 60°C for 2h under constant stirring and allowed to cool down to 37°C. A previously prepared stock solution (20% w/v in PBS) of transglutaminase (100 U/g) was then thoroughly mixed with

the gelatin solution to obtain a 10 U/g gelatin enzymatic activity. Then, yarns were incubated in gelatin at the same density under humidified conditions for 2h at 37°C.

9.2.5. Isolation of human tendon derived-stem cells

Tendon tissue was collected from patients undergoing elective orthopedic surgeries at the Hospital da Prelada (Porto, Portugal) under informed consent and according to protocols approved by the Ethical Committee of Hospital da Prelada. Herein, human tendon-derived cells (hTDCs) were isolated as previously described [42] using three healthy tendon autografts were collected from male patients with ages in the range of 25–30 years. Briefly, tissue samples were rinsed in PBS solution containing 10% (v/v) of A/A. Samples were minced and then digested in 0.1% (w/v) type I collagenase solution at 37 °C for at least 1h in an orbital shaker at 200 rpm. Following filtration (100 μm filter) and double centrifugation at 4 °C for 5 min each cycle at 1250 rpm, the supernatant was discarded, and the cell pellet was resuspended in α-MEM. Cells were incubated in standard humidified conditions of 5% CO_2 at 37 °C until confluency, where media was removed, and cells were washed with PBS and trypsinized before adding fresh media for cell counting. A portion of counted cell suspension was transferred to a new treated culture flask with fresh media and returned to the incubator. Culture medium was changed every two to three days while splitting protocol was repeated at confluency for cell maintenance. Cells were used at passages 3-4.

9.2.6. Production and culture of cell-laden CLFs

9.2.6.1. *Encapsulation in platelet lysates (PL) and gelatin (GEL) hydrogels*

Previously produced yarns (PCL-anisotropic/healthy) and threads (PCL-isotropic/diseased) were placed in the 3D-printed holders. Holders with four sample replicate each were placed in 6-well plates and sterilized by immersion in 70% (v/v) ethanol for 30 min followed by two washes with sterile DPBS for 30 min. Afterward, yarns/threads were pre-incubated in a solution of thrombin (10 U/mL) in calcium chloride (5 mM) for an optimized time of 45 min at RT. Following pre-incubation, yarns/threads were incubated with a solution of hTDCs in PL at a density of $2.5x10^5$ cells/mL (200 μL per sample) under humidified conditions for 2h at 37°C. In the case of cells seeded in enzymatically crosslinked gelatin, the prepared solution of transglutaminase and gelatin was added to a pellet of $2.5x10^5$ cells/mL, immediately distributed to yarns, and incubated under humidified conditions for 2h at 37°C. After incubation, templating molds for CLF coatings were removed and fresh α-MEM was added. CLFs were transferred to

a new 6-well plate 24h upon seeding and maintained in culture for up to 28 days, depending on the assay, changing the media every two to three days. Non-seeded yarns were used as blanks.

Encapsulated hTDCs in PL-coated and GEL-coated yarns were thereafter called as CLF-healthy and CLF-control, respectively, while encapsulated cells in PL-coated threads were denominated as CLF-diseased.

9.2.6.2. *Cell morphology, cytoskeleton organization and proliferation analysis*

Actin filaments of cell cytoskeleton were stained with phalloidin at 7 and 28 days of culture. Briefly, samples were washed three times with PBS after formalin fixation and incubated with phalloidin solution for 1h at RT. Then, samples were washed with PBS and analyzed by confocal laser scanning microscopy (Leica TCS SP8, Microsystems, Wetzlar, Germany). The degree of actin filament alignment was determined through directionality analysis using the Fourier components method using ImageJ software (version 2.1.0/1.43c), as previously described.

For nuclei counterstaining, samples were incubated with 4′,6-diamidino-2-phenylindole (DAPI, 1:1000) for 15 min at room temperature. Nuclei aspect ratio was determined by measuring at least 100 nuclei in different labeled images of each sample, using ImageJ software (version 2.1.0/1.43c). The length was divided by the width to obtain the correspondent aspect ratio.

For proliferation, the number of nuclei per area of CLFs was calculated. Briefly, blue channel images corresponding to DAPI staining were thresholded, and then the particle analyzer plugin of ImageJ used to count nuclei numbers. The area of CLFs was measured using ImageJ. Afterward, the number of nuclei divided by the area and the proliferation obtained.

9.2.6.3. *Immunocytochemistry of coated CLF-healthy/diseased*

Samples (n=4) were rinsed with PBS and fixed with 10% formalin at days 7 and 28 after hTDCs encapsulation. After thorough washing with PBS, cellular membranes were permeabilized with 0.1% Triton X-100 in PBS for 20 min at RT. Following washing steps, samples were blocked with 1% BSA in PBS for 30 min. Then, cells were incubated overnight with primary antibodies against anti-collagen type I (COL1, ab90395, 1:500), anti-collagen type III (COL3, ab175404, 1:100), anti-decorin (DCN, ab7778, 1:100), anti-scleraxis (SCX, ab58655, 1:200) and anti-elastin (ELAS, E4013, 1:500) diluted in 0.1% BSA in PBS at 4°C. The rabbit polyclonal anti-C-terminal tenomodulin (TNMD, 1:200) antibody against a synthetic polypeptide compliant to amino acids 245–252 of mouse and human was kindly produced and provided by Prof. Denitsa Docheva. Samples were afterward rinsed in PBS and incubated for 15 min with 30%

hydrogen peroxide. After PBS rinsing, samples were incubated for 1h at RT with the respective Alexa Fluor 488 secondary antibodies. Finally, nuclei were counterstained with DAPI for 30 min at RT. Immunolabeled samples were analyzed through confocal laser scanning microscopy.

9.2.6.4. *Quantitative analysis of immunofluorescence images*

All images were acquired by confocal fluorescence microscope and the signal emitted from the expression of the intended proteins was quantified using ImageJ software. Expression of proteins of interest was quantitatively analyzed and normalized by cell nuclei number at 7 and 28 days of culture. Briefly, images from days 7 and 28 were first split into 3 channels, blue, green, and red. The fluorescence intensity of the green channel corresponding to the protein of interest was measured in several images (n>6) acquired from the different sample replicates. Image's thresholding was performed to separate the signal from the background. Blue channel images corresponding to DAPI staining were thresholded and then the particle analyzer plugin of ImageJ was used to count nuclei numbers. Afterward, the mean fluorescence intensity of each protein marker was normalized by the corresponding number of nuclei, and results expressed as normalized mean intensity.

9.2.6.5. *CLFs hydrogel thickness*

Confocal 3D transversal fluorescence images were acquired for both CLF-healthy and CLF-control. For hydrogel thickness measurement, the fluorescence intensity of blue (DAPI) and red (Phalloidin) channels were split into two separate channels. Afterward, the thickness of hydrogels was measured using the red channel by evaluating the distance between the surface of the core fiber and the end of the hydrogel using ImageJ. Several images (n>3) from different sample replicates were measured.

9.2.6.6. *mRNA extraction and real-time PCR analysis (RT-PCR)*

Total mRNA was extracted from PL-yarns/threads (healthy/diseased) at days 0, 4, and 10 using RNeasy Mini Kit, according to the manufacturer's instructions. RNA quantity and purity were determined with a NanoDrop spectrophotometer (ND-1000, ThermoScientific, USA). The cDNA synthesis was performed with the qScript cDNA Synthesis kit and using the Mastercycler Realplex (Eppendorf, Germany). Transcript's quantification was carried out by quantitative polymerase chain reaction (qPCR) using the PerfeCTA SYBR Green FastMix kit following the manufacturer's protocol, in a Real-Time Mastercycler Realplex thermocycler (Eppendorf, Germany). Primer sequences (Table 9.1) were designed using the Primer-BLAST tool and synthesized by Eurofins Genomics. The evaluation of the relative expression level

was performed using the 2−ΔΔCt method. Transcript levels of selected genes were analyzed and normalized to the expression of the selected reference genes, ß-actin (*ACTB*) and Tyrosine 3-Monooxygenase/Tryptophan 5-Monooxygenase Activation Protein Zeta (*YWHAZ*), due to stability of their expression across the sample sets. All values were firstly normalized against the average value of reference genes transcript values, and then to the transcript values of hTDCs at day 0. Samples were collected and analyzed in quadruplets.

Table 9.1 | Primers used for quantitative RT-PCR analysis.

Gene	Nomenc.		Sequence	Reference
Housekeeping genes				
Tyrosine 3-Monooxygenase/Tryptophan 5-Monooxygenase Activation Protein Zeta	*YWHAZ*	F'	ACTTTTGGTACATTGtGGCTTCAA	NM_001135701.2
		R'	CCGCCAGGACAAACCAGTAT	
β-Actin	*ACTB*	F'	CTGGAACGGTGAAGGTGACA	AK223055
		R'	AAGGGACTTCCTGTAACAA	
Tenogenic-related				
Mohawk	*MKX*	F'	TCGCACAGACACTCTGGAAAA	NM_173576.2
		R'	TGTTAAGGCCATAGCTGCGT	
Collagen I, α1	*COL1A1*	F'	CCTGACGCACGGCCAAGAGG	NM_000088.3
		R'	GGCAGGGCTCGGGTTTCCAC	
Collagen III, α1	*COL3A1*	F'	TTGGCATGGTTCTGGCTTCC	NM_000090.3
		R'	GCTGGCTACTTCTCGTG	
Decorin	*DCN*	F'	CAGCATTCCTCAAGGTCTTCCT	NM_001920.3
		R'	GAGAGCCATTGTCAACAGCA	
Tenascin	*TNC*	F'	ACTGCCAAGTTCACAACAGACC	NM_002160.3
		R'	CCCACAATGACTTCCTTGACTG	
Tenomodulin	*TNMD*	F'	CCGCGTCTGTGAACCTTTAC	NM_022144.2
		R'	CACCCACCAGTTACAAGGCA	
Scleraxis bHLH transcription factor	*SCX*	F'	AGAACACCCAGCCCAAACAGAT	NM_001080514.2
		R'	TCGCGGTCCTTGCTCAACTTT	
	ACTA2	F'	AAAGCAAGTCCTCCAGCGTT	NM_001141945.1

Smooth muscle alpha actin		R'	TTAGTCCCGGGGATAGGCAA	
Chondrogenic-related				
SRY-box 9	*SOX9*	F'	TTCATGAAGATGACCGACGC	NM_000346.3
		R'	GTCCAGTCGTAGCCCTTGAG	
Osteogenic-related				
Runt related transcription factor 2 (RUNX2)	*RUNX2*	F'	TTCCAGACCAGCAGCACTC	NM_001024630
		R'	CAGCGTCAACACCATCATTC	
Metalloproteinases				
Matrix metalloproteinase 1	*MMP1*	F'	ACCTGGAAAAATACTACAACCTGAA	NM_002421.3
		R'	TTCAATCCTGTACAGATGTGTT	
Matrix metalloproteinase 3	*MMP3*	F'	CACTCACAGACCTGACTCGG	NM_002422.4
		R'	AGTCAGGGGGAGGTCCATAG	
Tissue inhibitor of metalloproteinases	*TIMP1*	F'	CATCCGGTTCGTCTACACCC	NM_003254.2
		R'	GGATAAACAGGGAAACACTGTGC	

9.2.6.7. *Multiplex immunoassay*

Multianalyte profiling in the supernatant of healthy and diseased CLF was performed using the Luminex MagPix system (Luminex, Austin, TX, USA). Concentrations of matrix metalloproteinase (MMP)-1, 2, 3, 8, 9, and 13, as well as tissue inhibitor of metalloproteinases (TIMP)-1 were measured using a custom ProcartaPlex human magnetic assay (ThermoFisher Scientific, Austria). The assay was performed as instructed by the manufacturer. The concentration of each analyte was calculated using the Luminex xPONENT 4.2 software. Data is plotted as mean ± standard deviation where n=4 for each timepoint.

9.2.7. Statistical Analysis

Statistical analysis of data was performed using GraphPad PRISM version 8.4.0. Results were presented as mean ± standard error of the mean (SD) when not stated otherwise. One-way and two-way analysis of variance (ANOVA) were performed in normally distributed populations followed by Tukey post hoc test for multiple comparisons, whereas the Kruskal-Wallis non-parametric test was performed, unless specified

otherwise. Non-parametric tests were performed using Mann-Whitney test. Differences between experimental groups were considered significant with a confidence interval of 95%, whenever $p < 0.05$.

9.3. RESULTS and DISCUSSION

9.3.1. Fabrication of a multiplex *in vitro* platform of micro-engineered tendon units

Understanding of the mechanisms governing tendon physiology and pathophysiology has been hampered by the lack of valid *in vitro* and *in vivo* models of tendon health and disease states. The search for physiologically (health and diseased) relevant *in vitro* models enabling high throughput testing are needed not only to study molecular mechanisms and predict preclinical drug efficacy of new therapies in humans but also for enabling the development of improved tissue-engineered constructs for tendon regeneration. To allow an effective mimicry of tendon microenvironment at the required experimental replication for *in vitro* modeling, we fabricated a multiplexed system supporting multiple micro-engineered 3D tendon units fitting in standard multi-well plates (Figure 9.1A). The proposed system not only assists in the fabrication and maturation steps, enables assay parallelization and provides a physical support device, allowing easy sample handling for biological testing during and after in vitro cell culture. The micro-engineered 3D units were developed to emulate both physiological and pathological tendon microenvironments taking advantage of: 1) the bioinspired topography and architecture of continuous electrospun PCL fiber threads (Figure 9.1C, i-iv) to control cell cytoskeleton tension and orientation; and 2) PL coating (Figure 9.1D) to provide the biological signaling for supporting hTDCs proliferation and promote fast ECM deposition. The synergy between these biophysical and biological cues are expected to direct hTDCs toward different healthy or diseased (fibrotic) phenotypes. First, and using a previously customized electrospinning setup [15], the spinning conditions were optimized (Supplementary Figure S9.1) to produce continuous PCL fiber threads with anisotropic and isotropic topographies, aiming the mimicry of healthy and diseased tendon ECM organization, respectively. Morphometric SEM analysis demonstrated that obtained fiber diameters remained at the primary collagen fiber range for both PCL-anisotropic/healthy (Figure 1B, iii, a; 2.30 ± 0.38 μm) and PCL-isotropic/diseased threads (Figure 9.1B, iv, a; 2.35 ± 0.33 μm), resembling the microscale dimensions of mature human collagen fibrils bundles (fibers) (~1 to 300 μm) [43, 44]. For recreation of the tendon's multilevel fibrous architecture, PCL-anisotropic/healthy threads were then hierarchically assembled into yarns (328.6 ± 15.98 μm) with diameters within the range of tendon fascicles (150 to 1000 μm) [22]. This step was not applied for PCL-isotropic/diseased threads (Figure 9.1B, iv, a, 444.3 ± 108.7 μm) as their dimensions already fall within the targeted fascicle's range, but also because this lower level of hierarchical fiber organization will contribute to confer it a more

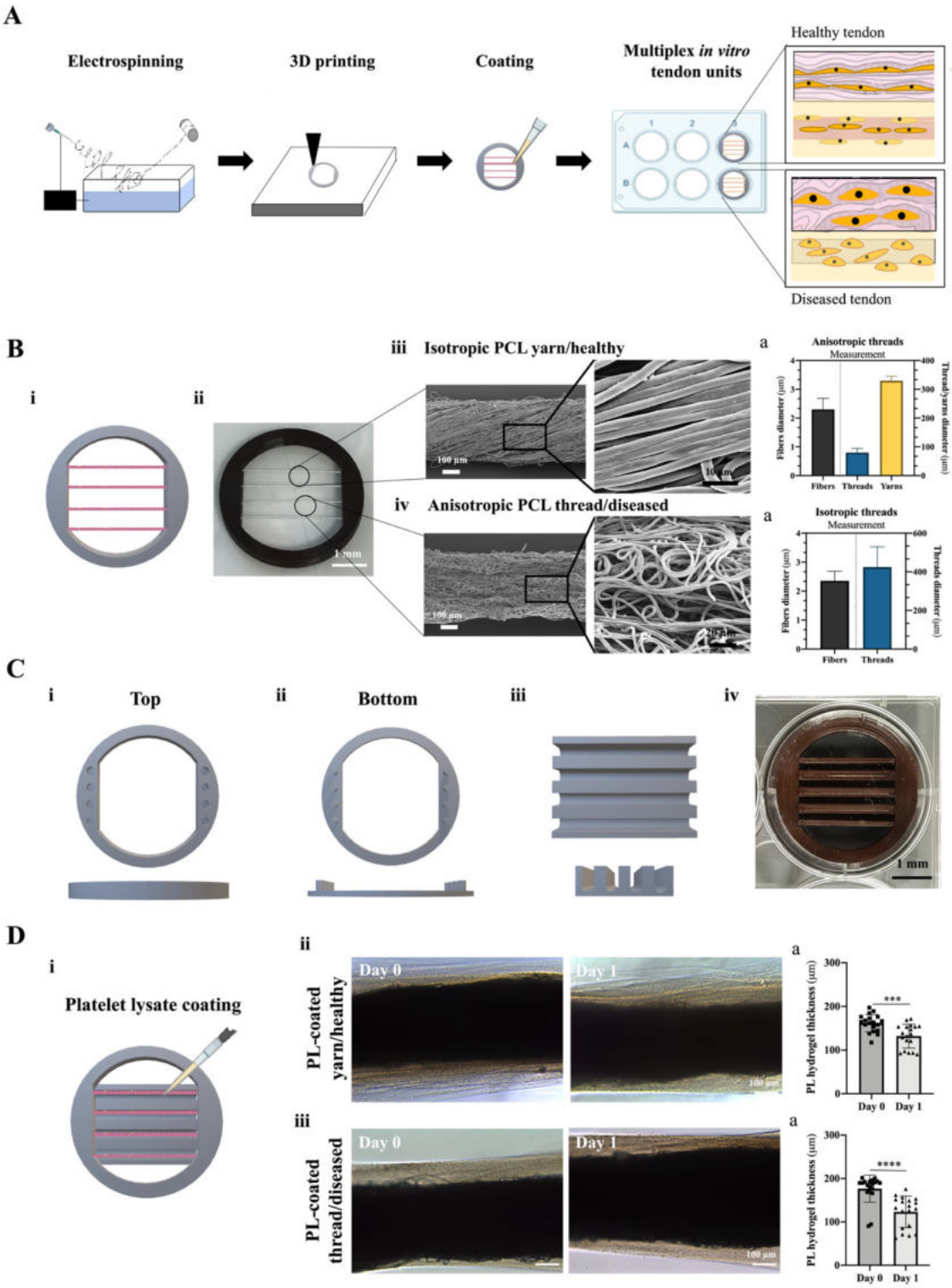

Figure 9.1 | Design of multiplex micro-engineered 3D *in vitro* tendon units. (A) Schematic illustration of the experimental procedure for the fabrication of 3D health and disease tendon models *in vitro*. Electrospinning was used for the production of anisotropic and isotropic threads, while the multiplexing platform was printed using a 3D-printer. Samples were placed in printed holders and coated with a bioactive hydrogel. (B) Mounted 3D tendon units (i-ii) with electrospun (iii) anisotropic yarns (PCL-

healthy) and (iv) isotropic threads (PCL-diseased) for physiological and pathophysiological tendon tissue replication. (a) Measurement of electrospun fibers, threads and yarns diameter for both anisotropic yarns and isotropic threads. Data are presented as mean ± standard deviation (SD). (C) Three-dimensionally printed holders depicting (i) top, (ii) bottom, and (iii) channels pieces, and (iv) complete structure in 6 well-plate. (D) Schematics of (i) platelet lysate (PL) coating and optimized PL-coated (ii) anisotropic yarns and (iii) isotropic threads at days 0 and 1. Scale bars, 100 μm. (a) Hydrogel thickness evaluation in PL-healthy (***, $p = 0.0008$) and PL-diseased (****, $p < 0.00001$). Data are presented as mean ± SD (n=19).

diseased-like character. The electrospun fiber cores were then assembled on the 3D printed support holders (Figure 9.1B, i and Figure 9.1C, i-ii). The customized design of this system consisted of a top part with pillars able to fix the fiber samples when attached to a bottom twin part (Figure 9.1C, i-ii), and a removal multi-basin part designed as molds for the building of the hydrogel shells using lower amounts of reagents and biological samples (Figure 9.1C, iii). Here, we designed it to fit standard 6 well-plates and support up to 4 different sample replicates per well (Figure 9.1C, iv), but this technology can be easily adapted to the specific needs of the user.

The tendon ECM houses tendon cells within a complex niche that can be roughly defined as load-bearing fibrous collagen bundles embedded within a mostly non-collagen matrix [45]. To closely replicate this matrix and cellular organization, we next built hydrogel shells on the PCL fibers cores. Besides providing a hydrated and soft biodegradable matrix for cell encapsulation recreating the organization of native tendon fascicles, PL is also a xenofree source of bioactive biomolecules with known roles in tendon healing and regeneration processes that we aim to explore for the maturation of micro-engineered CLFs. To achieve PL gelation and consequent hydrogel formation starting from PLC fiber core, the thrombin concentration required to induce fibrinogen self-assembly [38] and create a homogenous hydrogel layer, was optimized (Supplementary Figure S9.2). Optical microscopy images show that uniform and homogenous PL hydrogel layers are formed in samples incubated with 10 U/mL of thrombin for 45 minutes (Figure 9.1D, ii-iii). Additionally, PL-CLFs stability was tested by leaving samples in PBS solution for 1 day (Supplementary Figure S9.2). Although the PL hydrogel shell suffered an expected retraction of approximately 15% in thickness typically seen in this type of soft matrix [34], it remained stable and well attached to the fiber core. This retraction of PL matrix that, as discussed further ahead will be even more evident when encapsulating cells, is an important feature of the proposed concept because it will rapidly bring cell in contact with threads surface thus allowing it to exert cell contact guidance, governing cells orientation [46].

9.3.2. Healthy tendon microenvironment replicated through tenogenic phenotype maintenance and ECM synthesis

9.3.2.1. CLFs-healthy induce high f-actin alignment and nuclei aspect ratio in encapsulated hTDCs

Within their 3D microenvironment, tendon resident cells play critical roles in regulating tissue physiological functions and hemostasis, namely on the formation and remodeling of ECM [47, 48]. Moreover, tenocytes show spindle-shaped morphology, aligned following the anisotropic orientation of the dense network of collagen fibers [49]. Having as target the recreation of these native cell niche characteristics and function, the performance of the developed model was first evaluated regarding the capacity of CLFs to induce cell contact guidance, a mechanism that will depend on hydrogel shell thickness and how fast cells will be brought in contact with the core fibers surface. F-actin alignment and nuclei aspect ratio of hTDCs over culture time within CLF-healthy were used to measure the extent of these effects. CLFs based on gelatin (hydrolyzed collagen) (CLF-control) coatings, a biomaterial widely used to replicate the collagenous component of ECM [50], were used as non-bioactive reference controls for PL CLFs.

As expected, the soft nature of PL gels and their susceptibility to cell contractility [34, 38] promoted the fast reaction of the hydrogel shell. The cellularized PL hydrogel layers show a significant gradual contraction mostly occurring over the initial culture period (Figure 9.2A, i-ii). As shown in Figure 9.2A, i, this effect brings cells in contact with the topography of the fiber's surface. In contrast, CLF-control (Figure 9.2A, i-ii) shows a thick hydrogel layer with a dispersed distribution of cells that is maintained up to day 28, resulting in low cell contact with fibers surface. To evaluate the impact of these effects on cell morphology and organization, both cytoskeletal alignment and nuclei aspect ratio of encapsulated cells were investigated. As hypothesized, images and directionality analysis of hTDCs actin filaments in CLF-healthy up to 28 days show that cell cytoskeleton organization followed the topography of yarns (Figure 9.3A), resulting in uniaxially aligned and elongated cells, as characteristic of tenocytes embedded within tendon fascicles [49]. In contrast, hTDCs encapsulated within CLF-control were found to be more randomly organized and mainly at the surface of the hydrogel (Figure 9.3A, ii). Similar results have been previously described for cells encapsulated within unpatterned methacrylated gelatin hydrogels [51].

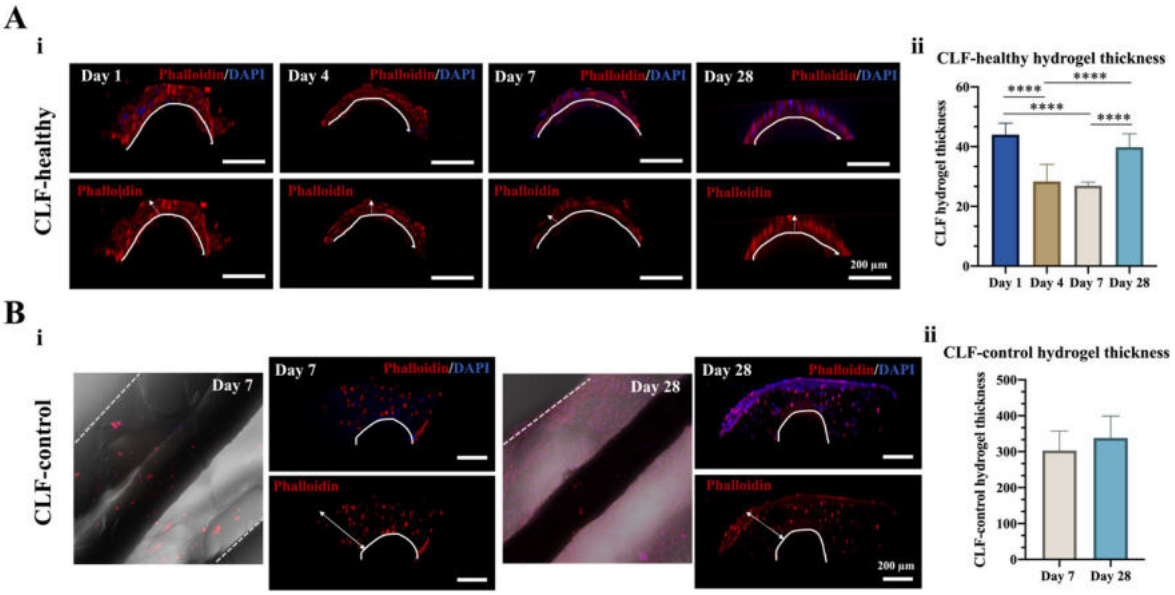

Figure 9.2 | Assessment of CLFs-healthy and -control hydrogel thickness. (A) Confocal three-dimensional imaging of PL hydrogel coating with encapsulated hTDCs in (i) CLFs-healthy at 1, 4, 7 and 28 days of culture. White lines represent the interface between the coating and the PCL-yarn core of CLFs. Scale bars, 200 µm. (ii) CLFs-healthy hydrogel thickness measurement (****, $p<0.0001$). Data are presented as mean ±SD (n=10). (B) Confocal imaging of gelatin hydrogel coating with encapsulated hTDCs in (i) CLFs-control at days 7 and 28 days. White lines represent the interface between the coating and the PCL-yarn core of CLFs. Scale bars, 200 µm. (ii) CLFs-control hydrogel thickness measurement. Data are presented as mean ±SD (n=10).

Additionally, the nuclei aspect ratio of cells in CLF-healthy after 7 and 28 days was considerably high (Figure 9.3A, i, a; 2.56 ± 0.71 µm and 3.28 ± 0.90 µm, respectively), an effect that is typically correlated with the effective cytoskeletal tension stemming from its pronounced elongation in a preferential axis direction [52]. In contrast, cells in CLF-control presented a significant lower nuclei aspect ratio (between 1.07 ± 0.23 µm - day 7, and 1.53 ± 0.28 µm - day 28; Figure 9.3B, ii, a), confirming their less elongated morphology and respective lower cytoskeletal tension. These results demonstrate the suitability of the hierarchically assembled PL-CLF to guide cell orientation through contact guidance mechanisms while simultaneously recreating the organization of native tendon ECM fibrillar structure with tendon cells embedded in a peri-cellular gel-like matrix. The ability to recreate these tendon mimetic features in CLFs is critical for the proposed concept because cells can adapt their differentiation decisions or phenotype profiles through mechanotransduction mechanisms mediated by cytoskeleton organization in response to biophysical inputs associated with 3D ECM architecture [53], feedback that we have previously shown

for both tendon and stem cells under the context of tendon tissue engineering [14, 15], as well as to its surrounding stromal composition.

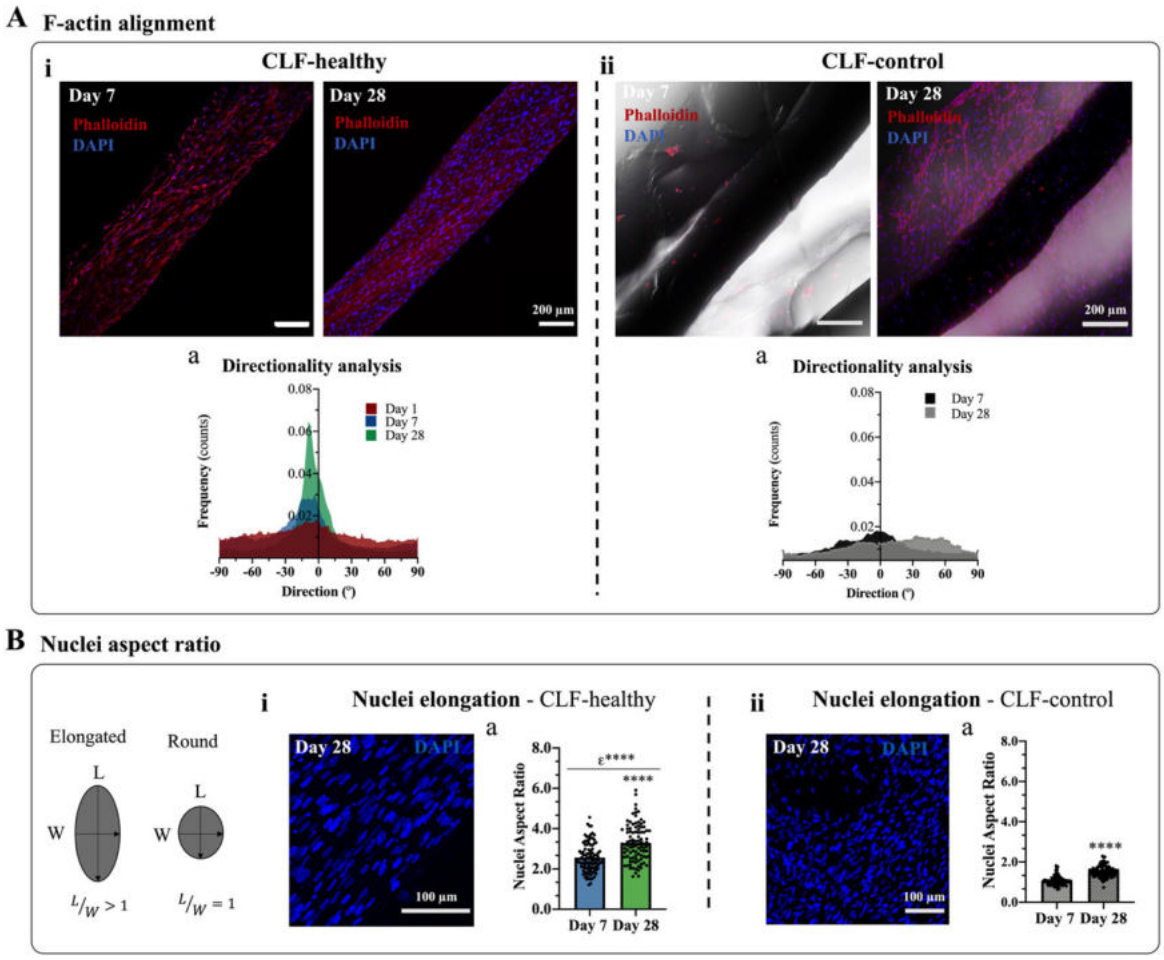

Figure 9.3 | Morphometric analysis of hTDCs encapsulated in CLF-healthy and -control. (A) Confocal images of gelatin F-actin filaments of hTDCs (phalloidin, red; DAPI, blue) and (a) directionality analysis of F-actin filaments orientation angle in hTDCs in (i) CLF-healthy and (ii) CLF-control at days 1, 7 and 28. Scale bars, 200 µm. (B) Confocal microscopy images of cell nuclei (DAPI, blue) on (i) CLF-healthy and (ii) CLF-control after 28 days of culture. Scale bars, 100 µm. (a) Nuclei aspect ratio of hTDCs encapsulated on both types of coatings. Scale bars, 100 µm. Statistically significant differences between nuclei elongation in CLF-healthy in comparison with CLF-control are shown as ε****; ****, $p < 0.0001$. Data are presented as mean ±SD (n=4).

9.3.2.2. CLFs-healthy sustain the expression of tenogenic-related markers and synthesis of tenogenic-rich ECM

To evaluate the potential of CLFs to sustain the tenogenic commitment of encapsulated hTDCs, most widely recognized tendon-related markers, tenomodulin (TNMD), scleraxis (SCX), and mohawk (MKX) were assessed through gene and protein expression. TNMD is a type II transmembrane glycoprotein highly expressed by tenocytes as a regulator of matrix remodeling [54] and widely accepted as a marker of mature tendon/ligament lineage [55]. SCX is a transcription factor expressed during tendon development and differentiation [56], also known to be a positive regulator of tendon differentiation and downstream promoter type I collagen expression [57], while MKX is a transcription factor described as an important regulator of tendon differentiation [58]. Results showed that transcript levels of *SCX*, *TNMD,* and *MKX* experienced a gradual upregulation from day 0 to day 10 (Figure 9.4A, i). At the protein level, TNMD was significantly deposited from day 7 to day 28, while SCX was constitutively expressed during culture time (Figure 9.4A, ii a-d), indicating the maintenance of cells tenogenic phenotype [59] and maturation [60] when encapsulated in CLF-healthy. Also, the expression of TNMD was shown to be positively regulated by the transcription factor SCX [61]. The opposite was observed in CLF-control, where no differences were found in the deposition of TNMD, while SCX expression was significantly decreased over culture time (Supplementary Figure S9.3, iii), suggesting a possible temporal inhibition of tenogenic phenotype or hTDCs transdifferentiation.

To evaluate the quality of the *de novo* synthesized matrix by hTDCs by encapsulated within CLF-healthy, we then assessed the expression of several tendon-related ECM components, namely the gene expression of collagen type I (*COL1A1*) and III (*COL3A1*), decorin (*DCN*), and tenascin C (*TNC*). Collagen type I is the main collagen type found in tendon tissues ECM (~60-85% dry weight), followed by collagen type III (~3-5% of total collagen) and noncollagenous matrix components, namely proteoglycans (including decorin) and collagen oligomeric matrix proteins, such as lubricin and tenascin C [4, 62]. Although collagen type I and III and tenascin are not considered specific markers for tendon as they are ubiquitous components present in different tissues, they are often included in selected panels of tendon markers [63], while DCN is a proteoglycan highly expressed during tendon development by fibrillogenesis regulation [64]. Transcription levels of *COL3A1* and *DCN* were found to be upregulated at day 10 (Figure 9.4B, i), while *COL1A1* and *TNC* were continuously expressed during culture time (Figure 9.4B, i). Results were complemented with immunocytochemistry of collagen type I (COL1) and III (COL3), elastin (ELAS), and decorin (DCN).

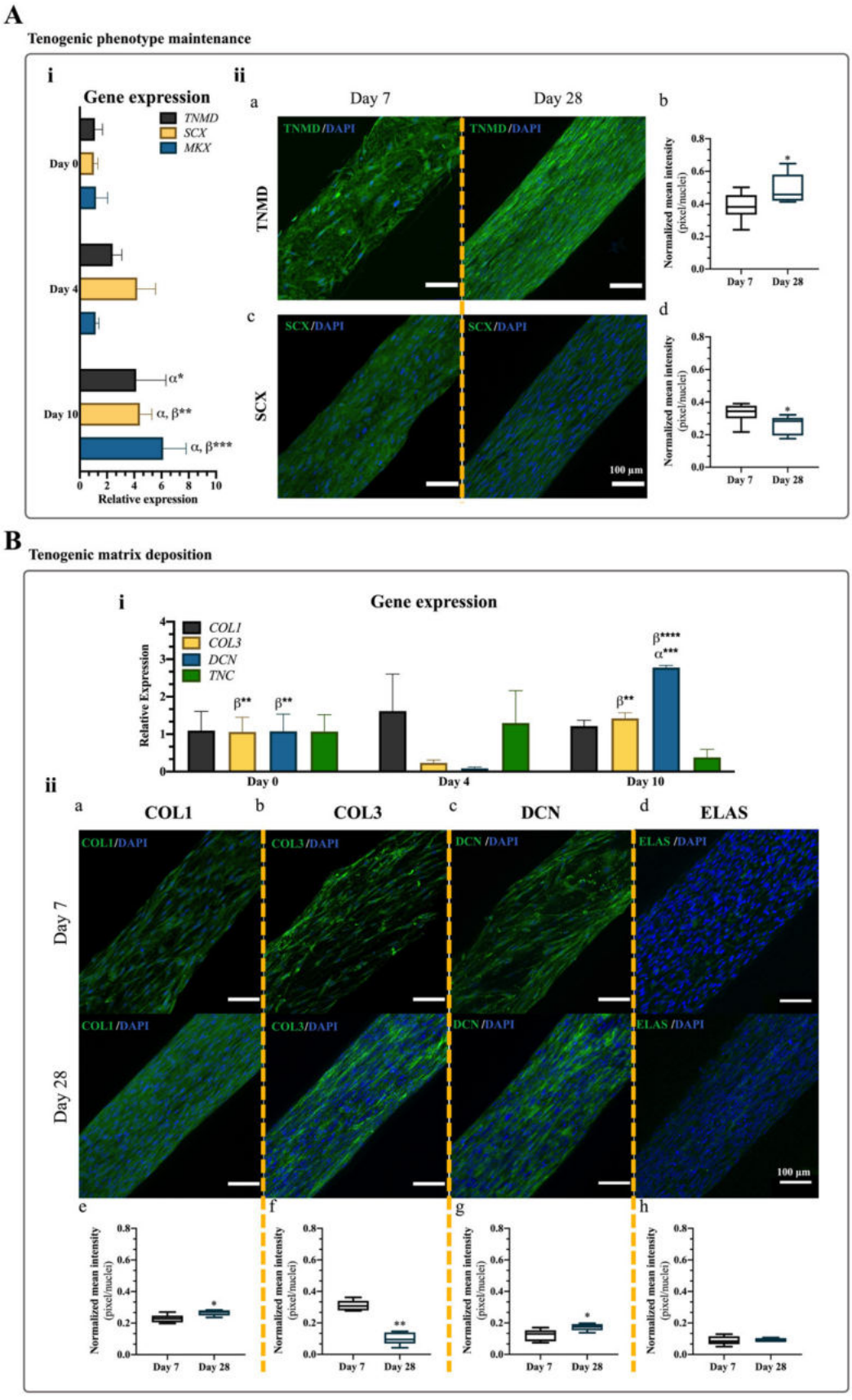

Figure 9.4 | Gene and protein expression of tenogenic markers by hTDCs encapsulated in CLF-healthy. (A) Phenotype maintenance evaluated by gene expression of (a) tenomodulin (*TNMD;* *, *p*

= 0.028), (b) scleraxis (*SCX*; **, p = 0.0026) and (c) mohawk (*MKX*; ***, p = 0.0003) at 0, 4 and 10 days of culture. Data are presented as mean ± SD (n=4). α and ß are statistically significant in comparison with day 0 and day 4, respectively. Expression of target genes was normalized against the average of *ß-actin/ YWHAZ* reference genes and gene expression in all conditions was normalized to day 0. (ii) Fluorescence microscopy of tenogenic markers (a) tenomodulin (TNMD) and (c) transcription factor scleraxis (SCX) at 7 and 28 days. Nuclei were counterstained with DAPI. Scale bars, 100 μm. Fluorescence intensity quantification of (b) TNMD (*, p = 0.038, n=6) and (d) SCX (*, p = 0.026, n=6) evaluated at 7 and 28 days of culture. (B) Matrix deposition assessed by (i) gene expression of (a) collagen type I, alpha chain 1 (*COL1A1*), (b) collagen type III, alpha chain 1 (*COL3A1*; **, p = 0.0029; ***, p = 0.0002), (c) decorin (*DCN*; **, p = 0.0029; ***, p = 0.0001; ****, p < 0.0001), (d) tenascin (*TNC*), by RT-PCR at 0, 4 and 10 days of culture. Data are presented as mean ± SD (n=4). α and ß are statistically significant in comparison with day 0 and day 4, respectively. Expression of target genes was normalized against the average of *ß-actin/ YWHAZ* reference genes and gene expression in all conditions was normalized to day 0. (ii) Fluorescence microscopy of ECM-related tenogenic markers, (a) type I collagen (COL1), (b) type I collagen (COL1), (c) decorin (DCN) and (d) elastin (ELAS) at 7 and 28 days. Nuclei were counterstained with DAPI. Scale bars, 100 μm. Fluorescence intensity quantification (bottom) of (e) COLI (*, p = 0.026, n=6), (f) COLIII (b, **, p = 0.0022, n=6), (g) DCN (*, p = 0.022, n=6) and (h) ELAS (n=6) evaluated at 7 and 28 days of culture.

The expression of tendon ECM-related markers was evident as early as 7 days of culture. Interestingly, after 28 days of culture, CLF-healthy presented a high ECM density (Supplementary Figure S9.4) comparably to previously described works taking advantage of similar 3D hierarchical structures as cell's support [14, 15]. Further, this ECM was found to be composed of higher amounts of COL1 and DCN (Figure 9.4B, ii, a-c), while COL3 synthesis suffered a decrease when compared to day 7 (Figure 9.4B, ii, b). At the same time, elastin, an ECM component known for its role in facilitating fascicle sliding and recoil [65, 66], was deposited in CLF-healthy (Figure 9.4B, ii, d). The composition of this *de novo* deposited matrix in the fabricated CLFs match well with the reported in *in vivo* and explants-based studies that described COL1, DCN, and ELAS as important functional ECM components for a proper tendon function [65, 67, 68]. It should be noted that the synergy between the engineered tendon 3D architecture mimicry and biological factors directed the natural healing character, inherent to the biological signaling triggered by the PL hydrogel components, toward a regenerative response resulting in micro-engineered CLFs showing a healthy organotypic profile. Notwithstanding, the obtained results supported the proposed

hypothesis, actually demonstrating that biofabricated multiplex tendon units can be advantageously explored for *in vitro* modeling as suitable alternatives for currently used explants and/or animal models.

9.3.3. Fibrotic matrix deposition associated with cells morphological phenotypic changes and unbalanced matrix turnover

9.3.3.1. Encapsulated hTDCs in CLF-diseased present a higher proliferation and cytoskeleton misalignment

The fabricated diseased tendon units were first evaluated in terms of hTDCs proliferation and organization. Over time of culture, a significant increase in proliferation was observed from day 7 to day 28 (Figure 9.5A, i). This behavior was accompanied by a lower degree of cytoskeleton alignment in cells within CLF-diseased (Figure 9.5A) compared to the CLF-healthy. Indeed, staining of the cytoskeletal actin filaments at day 7 shows that encapsulated cells were able to migrate without showing a marked preferential orientation (Figure 9.5A, ii), as sustained by the results of f-actin directionality analysis (Figure 9.5A, ii, a). After 28 days, a small peak is observed in the orientation map, probably associated with cell crowding and high ECM deposition occurring over time, normally associated with a high proliferative phase occurring tendon remodeling phase [72], resulting in cell polarization and leading to some degree of alignment along the fibers.

9.3.3.2. CLF-diseased induced a tenogenic drift over culture time

The effect of CLF-diseased surface on encapsulated hTDCs phenotype and ECM deposition was then evaluated at both gene and protein levels. First, the potential phenotypic drift/degeneration was studied by RT-PCR, through the expression of tendon markers (TNMD, SCX, and MKX). While cells in CLF-diseased showed significantly increased TNMD transcript levels at day 10, SCX and MKX transcript levels were found to be decreased with culture time (Figure 9.5B, i, a-c). Additionally, complementary immunocytochemistry imaging quantification revealed an almost absent protein expression of SCX, with lower levels compared to the CLF-healthy (Figure 9.5B, ii, f), TNMD was still significantly deposited at 28 days of culture, even though at significantly lower levels compared to the ones found in CLF-healthy (Figure 9.5B, ii, a-c). The absence of these markers has been correlated with a loss or depletion of TSPC's capacity to differentiate into tenocytes and deposit a characteristic teno-rich ECM [57, 73], contributing to pathogenesis, namely tendinopathies [74]. Further, the expression profiles of osteoblastic and chondrogenic genes associated with common tenogenic drift/degeneration pathways [75] were found to be favored over tenogenic ones. Levels of the osteogenic-related markers runt-related transcription factor

2 (RUNX2) were significantly increased at day 4, suffering a temporal decrease after 10 days, while levels of the chondrogenic marker SRY-Box transcription factor 9 (SOX9) [76] were significantly increased at day 10 compared with both 0 and 4 days of culture (Figure 9.5B, i). The expression trend of these two transcription factors is consistent with tendon degeneration associated with detrimental effects over tissue mechanical loading capacity [77]. Furthermore, the levels of smooth alpha muscle actin (ACTA2), a marker associated with "myofibroblast" phenotype acquisition associated with tendinopathy and tissue fibrogenesis [78], were significantly increased at 4 days of culture compared with both 0 and 4 days of culture and also with the levels observed for CLF-healthy (Figure 9.5B, iii), indicating a myofibroblast differentiation/activation and suggesting the commitment of hTDCs toward a fibrotic phenotype.

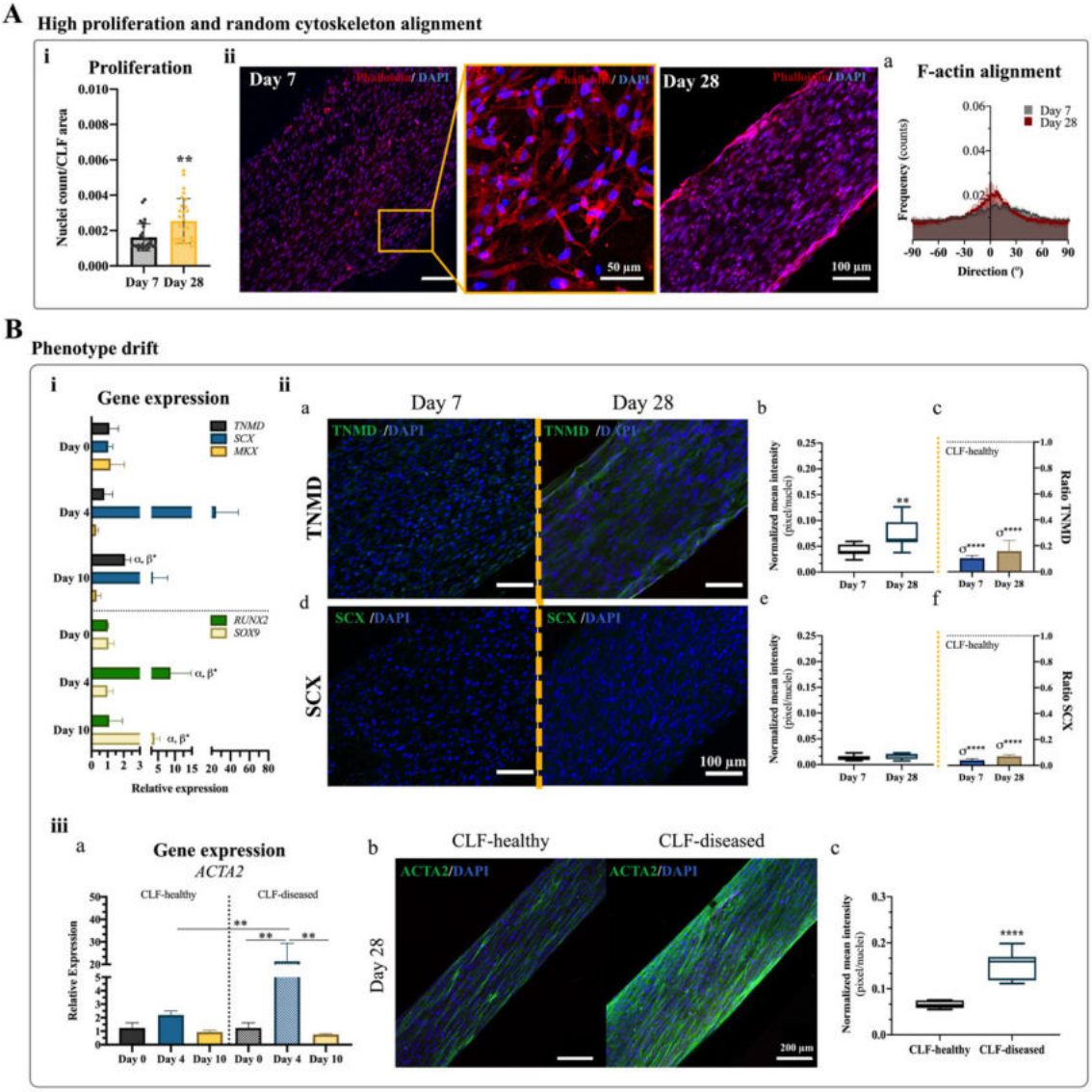

Figure 9.5 | Analysis of proliferation, F-actin alignment and phenotype drift in hTDCs encapsulated in CLF-diseased. (A) Cell's proliferation (i) evaluated at 7 and 14 days of culture. (ii)

Confocal imaging of nuclei (DAPI, blue) and actin filaments (F-actin, phalloidin, red) staining of encapsulated hTDCs in (i) CLF-diseased after 7 and 28 days of culture, and respective image magnification. Scale bars, 100 and 25 μm. (a) Directionality analysis of actin filaments orientation for CLF-diseased at 7 and 28 days. (B) Phenotype drift evaluation through (i) gene expression of (a) TNMD (*, p = 0.05), (b) SCX, (c) MKX, (d) RUNX2 (*, p = 0.05), and (e) SOX9 (*, p = 0.01) by RT-PCR analysis at 0, 4 and 10 days of culture. Data are presented as mean ± SD (n=4). α and ß are statistically significant in comparison with day 0 and day 4, respectively. Expression of target genes was normalized against the average of ß-actin/YWHAZ reference genes and gene expression in all conditions was normalized to day 0. (ii) Fluorescence microscopy of (a) TNMD and (c) SCX at 7 and 28 days. (b-d) Fluorescence intensity quantification of respective proteins evaluated at 7 and 28 days of culture (n=6) and (c-f) ratio of proteins of interest between CLF-healthy and CLF-diseased at both culture times. σ is statistically significant in comparison with the correspondent day in CLF-healthy. Nuclei were counterstained with DAPI. Scale bars, 100 μm. (iii) Fibrotic myofibroblastic marker evaluation. (a) Gene expression of smooth alpha muscle actin (ACTA2) at days 0, 4 and 10 in both CLF-healthy and -diseased (**, p = 0.009). Data are presented as mean ± SD (n=4). Expression of target genes was normalized against the average of ß-actin/YWHAZ reference genes and gene expression in all conditions was normalized to day 0. (b) Confocal images acquired for the expression of smooth alpha muscle actin (ACTA2) at 28 days of culture in CLF-healthy and CLF-diseased. Nuclei were counterstained with DAPI. Scale bars, 200 μm. (c) Mean intensity quantification (****, p < 0.0001) performed for the respective samples (n=6).

9.3.3.3. CLF-diseased induce a temporal unbalanced matrix turnover favoring the deposition of fibrotic ECM

The pathologic hallmark of tendon fibrosis is underlined by changes in the composition of interstitial ECM [79]. This involves altered gene expression of the structural ECM proteins including *COL1*, *COL3, DCN,* and certain metalloproteinases that regulate the biological tissue homeostasis [80]. Accordingly, *COL1A1*, *COL3A1*, *DCN*, and *TNC* gene levels were evaluated (Figure 9.6A, i). Increased *COL1A1* and *TNC* transcription levels were found in CLF-diseased at early time points (4 days) yet suffering a significant downregulation at later culture times. *COL3A1* levels were decreased after 4 and 10 days of culture whilst a significant increase was observed for *DCN* levels after 10 days compared to day 0 (Figure 9.6A, i).

At the protein level, while not very significant differences were observed on the deposition of the proteoglycan DCN (Figure 9.6A, ii, b) compared to CLF-healthy, interesting finds were seen on the effects of core fiber architecture over COLI and COL3 ratios (Figure 9.6A, iii). Indeed, as soon as 7 days, CLF-

diseased exhibited the highest COL1/COL3 ratio (Figure 9.6A, iii, a). Yet, after 28 days, COL3 deposition was favored against COL1 synthesis, while the opposite was verified in CLF-healthy. In these systems, COL1/COL3 ratio was significantly higher at 28 days, demonstrating a preference for the deposition of COL1 over COL3 (Figure 9.6A, iii, b). So, in CLF-diseased an impairment in cells repair mechanism was associated with an increased accumulation of COL3 [81] and the formation of a fibrotic-like tissue [82]. Similar observations occur in pathologic tendons, which show microscopic irregular fibrillar collagen alignment and molecular changes in collagen composition involving an increased ratio of type III and type I collagen [81, 83, 84]. Nonetheless, after 28 days of culture, cells in CLF-diseased were found to express significantly higher amounts of ACTA2 compared to hTDCs in CLF-healthy (Figure 9.5B, iii, b-c), suggesting the deposition of a fibrotic-like matrix. Interestingly, altered collagen microstructure is a known promoter of stromal/stem cells myofibroblast differentiation [85], a process that is further induced by TGF-β1 [86, 87], a main component of PL.

Considering that ECM remodeling is a process dependent on the balanced expression and activity of matrix metalloproteinases (MMPs) and their inhibitors (tissue inhibitors of metalloproteinases, TIMPs), the *MMP1*, *MMP3,* and *TIMP1* gene expression and enzymes secretome was studied in both CLF-healthy and CLF-diseased (Figure 9.6B). MMPs are actively involved in ECM remodeling, a critical and continuous process that maintains the healthy state of tendon tissues but also contributes to tendon healing [88, 89]. A temporal increase trend was observed for *MMP1* transcript levels in both CLF-healthy and CLF-diseased up to 10 days (Figure 9.6B, i, a). Yet, when assessing the secretome in both systems, after 10 days significantly higher concentrations of MMP-1 were observed in CLF-diseased comparably to CLF-healthy (Figure 9.6B, ii), reflecting an early cleavage of fibrillar collagens [89]. On day 4, only MMP-2 was found to be overexpressed in the extracellular medium of CLF-diseased in comparison with CLF-healthy, suffering a decrease over time of culture (Figure 9.6B, ii). A decreased activity of the MMP-2 associated with a higher activity of the collagenase MMP-1 is described to lead to an enhanced collagen turnover followed by a deterioration in the quality of the collagen network commonly associated with tendinopathies [90], concomitantly reflected in the favored COL3 over COL1 deposition in CLF-diseased. Levels of *MMP3* were upregulated in CLF-healthy within 4 days of culture and significantly increased compared to the levels in CLF-diseased (Figure 9.6B, i, b).

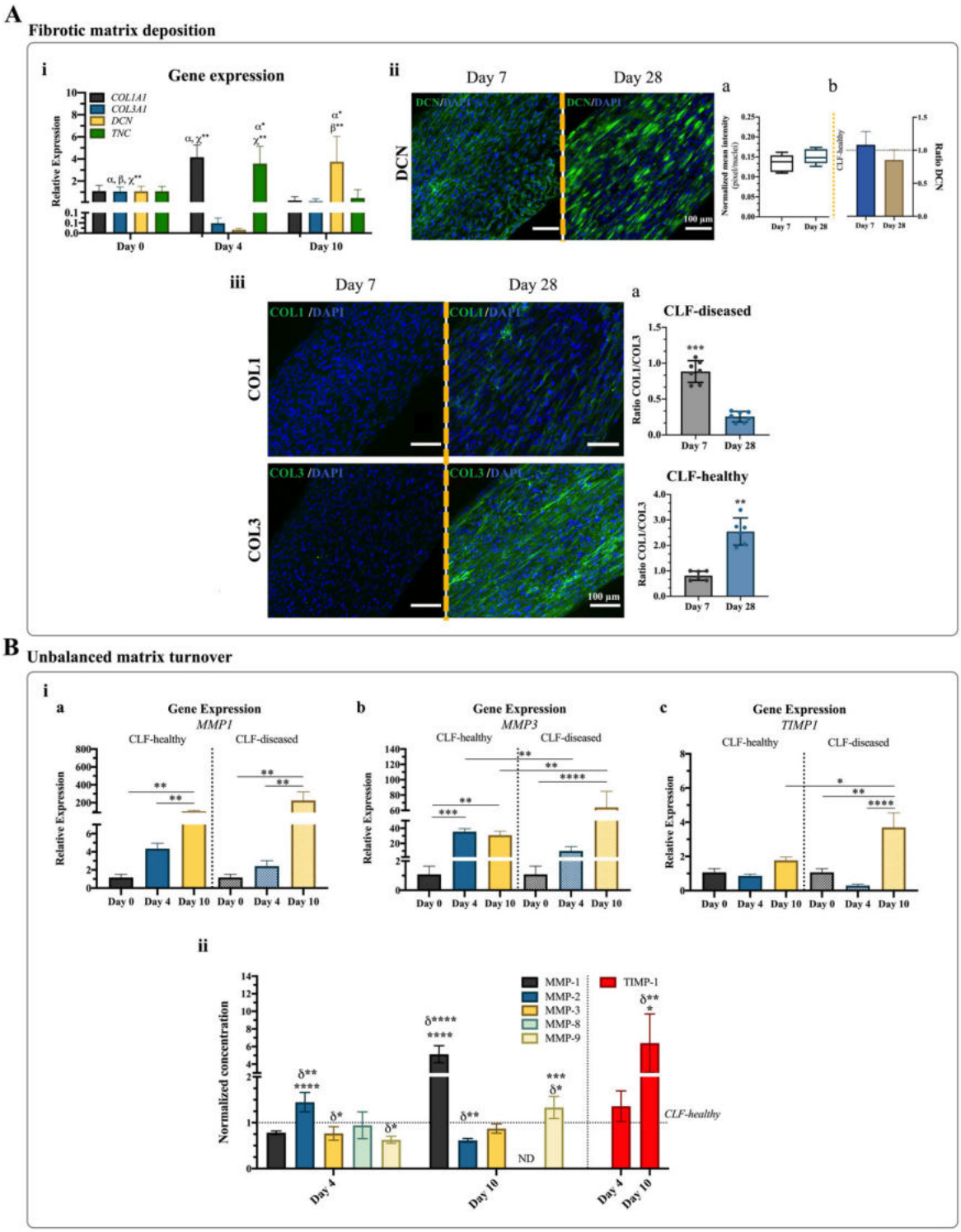

Figure 9.6 | Evaluation of fibrotic matrix deposition and unbalanced matrix turnover in hTDCs encapsulated in CLF-diseased. (A) Matrix deposition assessed by (i) gene expression of (a) COL1A1 (***, p = 0.0008), (b) COL3A1 (**, p = 0.003), (c) DCN (*, p = 0.05; **, p = 0.009) and (d) TNC (*, p = 0.02; **, p = 0.006) by RT-PCR analysis at 0, 4 and 10 days of culture. Data are presented as mean ± SD (n=4). α, ß and χ are statistically significant in comparison with day 0, day 4 and day 10,

respectively. Expression of target genes was normalized against the average of ß-actin/YWHAZ reference genes and gene expression in all conditions was normalized to day 0. (ii) Fluorescence microscopy of tenogenic-ECM related marker, DCN, (a) respective fluorescence intensity quantification and (b) ratio between CLF-healthy and CLF-diseased at 7 and 28 days of culture (n=6). (iii) Confocal imaging of (i) COL1 and (ii) collagen type III (COL3) deposition after 7 and 28 days. Scale bars, 100 μm. Measurement of (a) COL1/COL3 ratio (***, p = 0.0006) in CLF-diseased and (b)) COL1/COL3 ratio (**, p = 0.002) in CLF-healthy at 7 and 28 days of culture. Data are presented as mean ± SD (CLF-diseased, n=7; CLF-healthy, n=6). (B) Unbalanced matrix turnover evaluated through (i) Gene expression of (a) matrix metalloproteinase 1 (MMP1; **, p = 0.002), (b) matrix metalloproteinase 3 (MMP3; **, p = 0.004; ***, p = 0.0003; ****, p < 0.0001) and (c) tissue inhibitor of metalloproteinase 1 (TIMP1; *, p = 0.02; **, p = 0.001; ****, p < 0.0001). Data are presented as mean ± SD (n=4). Expression of target genes was normalized against the average of ß-actin/YWHAZ reference genes and gene expression in all conditions was normalized to day 0. (ii) Expression of matrix metalloproteinases-1 (MMP-1; ****, p<0.0001), -2 (MMP-2; **, p=0.005, ****, p<0.0001), -3 (MMP-3; *, p=0.03), -8 (MMP-8) and -9 (MMP-9; *, p=0.03, ***, p=0.0002) and tissue inhibitor of metalloproteinase 1 (TIMP-1; *, p=0.012; **, p=0.0080) detected in the extracellular medium of CLF-diseased. Data was normalized to CLF-healthy. δ are statistically significant in comparison with CLF-healthy at the correspondent day. Data are presented as mean ± SD (n=4).

Notably, after 10 days, even though a significant increase was observed for both systems, CLF-diseased presented higher levels compared to CLF-healthy, probably associated with a high degradation activity of matrix proteins typical of pathological tendons [91, 92]. Extracellular MMP-9 was significantly higher in CLF-diseased comparably to CLF-healthy (Figure 6B, ii). In parallel, TIMP1 levels were significantly upregulated in CLF-diseased and comparatively higher than CLF-healthy at day 10 (Figure 6B, i, c). The same was stated for the secreted levels of TIMP1 (Figure 6B, ii,c) which were significantly higher in CLF-diseased compared to CLF-healthy after 10 days. Together with MMP-1 and MMP-9 high activity, the role of these enzymes has been associated with tendon retraction after rotator cuff tear [93] and possibly related with the lower collagen remodeling, high degradation and fibrotic-like ECM formation also reflected by its low COL1/COL3 ratio [94, 95].

It should be noted that the 3D isotropic architecture coupled with a source of biological factors, found in the PL, induced a phenotypic drift, and unbalanced matrix turnover, reinforced by the deposition of a fibrotic like-ECM, towards the in vitro formation of a pathophysiological scenario commonly observed in

pathological tendon tissue. Moreover, 3D bioengineered diseased tendon units were fabricated to be used as suitable models for drug screening and new therapies development.

9.4. CONCLUSIONS

In this work, through the coupling of the well-defined 3D architecture of electrospun PCL yarns/threads with a source of biological factors derived from platelet lysates, bioengineered 3D models of physiological and pathological tendon tissue were developed. Combined with 3D printing, composite living fibers were fabricated allowing the fast generation of several numbers of highly reproducible sample replicates fitting 6-well plate formats. Cellularized PL-CLFs presented higher efficacy in promoting cell contact with the topography of fiber's surface compared with Gel-CLFs, reflected by hTDCs uniaxially alignment and elongation in CLF-healthy comparably with the dispersed and random organization of cells in CLF-control. Furthermore, CLF-healthy sustained the expression of tenogenic-related markers while allowing the deposition of a teno-rich ECM, characteristic of a regenerative response resulting in micro-engineered CLFs showing a healthy organotypic profile. In contrast, CLF-diseased, characterized by an isotropic PCL core with PL coating, drove hTDCs response toward a fibrotic profile. This was reflected in a phenotypic drift through an early expression of osteo and chondrogenic markers. Moreover, a favored collagen type III deposition over collagen type I coupled with a later expression of myofibroblastic protein demonstrated a clear commitment of hTDCs toward a pro-fibrotic profile. Nevertheless, a pathogenic matrix turnover was also observed in CLF-diseased through an unbalanced expression of metalloproteinases and tissue inhibitors of metalloproteinases.

Altogether, our results represent a promising strategy for the fabrication of innovative and high-throughput 3D *in vitro* models of tendon health and disease biology, offering a suitable and reliable alternative to existing tendon models with possible application for the discovery of new molecular mechanisms, drug screening, and development of advanced tendon therapies.

9.5. ACKNOWLEDGEMENTS

Work developed under the framework of the Cooperation Agreement established with the Serviço de Imuno-Hemoterapia do Centro Hospitalar de S. João, EPE. The authors would like to thank the Plastic Surgery Department of Hospital da Prelada (Porto, Portugal) for providing tendon tissue samples. Authors acknowledge the financial support from the ERC Grant CoG MagTendon nr 772817; FCT–Fundação para a Ciência e a Tecnologia for the PhD grant of IC (PD/BD/128088/2016) and CLR

(PD/BD/150515/2019); for the contract to MGF (CEECIND/01375/2017); and for project SmarTendon (PTDC/NAN-MAT/30595/2017).

9.6. REFERENCES

[1] B.K. Connizzo, S.M. Yannascoli, L.J. Soslowsky, Structure-function relationships of postnatal tendon development: a parallel to healing, Matrix biology: journal of the International Society for Matrix Biology 32(2) (2013) 106-116, 10.1016/j.matbio.2013.01.007.

[2] S. Steinmann, C.G. Pfeifer, C. Brochhausen, D. Docheva, Spectrum of Tendon Pathologies: Triggers, Trails and End-State, Int J Mol Sci 21(3) (2020) 844, 10.3390/ijms21030844.

[3] N.L. Millar, G.A. Murrell, I.B. McInnes, Inflammatory mechanisms in tendinopathy - towards translation, Nat Rev Rheumatol 13(2) (2017) 110-122, 10.1038/nrrheum.2016.213.

[4] N.L. Millar, K.G. Silbernagel, K. Thorborg, P.D. Kirwan, L.M. Galatz, G.D. Abrams, G.A.C. Murrell, I.B. McInnes, S.A. Rodeo, Tendinopathy, Nature Reviews Disease Primers 7(1) (2021) 1, 10.1038/s41572-020-00234-1.

[5] S.S. Nikolaeva, Y.A. Khoroshkov, V.A. Dubinskaya, Structure and properties of tendon collagen complex during disorganization of the ground substance of connective tissue, Bulletin of Experimental Biology and Medicine 92(2) (1981) 1115-1118, 10.1007/BF00829805.

[6] C.F. Liu, L. Aschbacher-Smith, N.J. Barthelery, N. Dyment, D. Butler, C. Wylie, What we should know before using tissue engineering techniques to repair injured tendons: a developmental biology perspective, Tissue Eng Part B Rev 17(3) (2011) 165-76, 10.1089/ten.TEB.2010.0662.

[7] P. Sharma, N. Maffulli, Tendon Injury and Tendinopathy: Healing and Repair, JBJS 87(1) (2005).

[8] S.L. Wunderli, U. Blache, J.G. Snedeker, Tendon explant models for physiologically relevant in vitro study of tissue biology – a perspective, Connective Tissue Research 61(3-4) (2020) 262-277, 10.1080/03008207.2019.1700962.

[9] M.W. Hast, A. Zuskov, L.J. Soslowsky, The role of animal models in tendon research, Bone Joint Res 3(6) (2014) 193-202, 10.1302/2046-3758.36.2000281.

[10] M.A. Brehm, L.D. Shultz, J. Luban, D.L. Greiner, Overcoming current limitations in humanized mouse research, J Infect Dis 208 Suppl 2(Suppl 2) (2013) S125-30, 10.1093/infdis/jit319.

[11] G. Fessel, J. Cadby, S. Wunderli, R. van Weeren, J.G. Snedeker, Dose- and time-dependent effects of genipin crosslinking on cell viability and tissue mechanics – Toward clinical application for tendon repair, Acta Biomaterialia 10(5) (2014) 1897-1906, https://doi.org/10.1016/j.actbio.2013.12.048.

[12] Y.-T. Wu, Y.-T. Wu, T.-C. Huang, F.-C. Su, I.M. Jou, C.-C. Wu, Sequential inflammation model for Achilles tendinopathy by elastin degradation with treadmill exercise, Journal of Orthopaedic Translation 23 (2020) 113-121, https://doi.org/10.1016/j.jot.2020.03.004.

[13] T. Stauber, U. Blache, J.G. Snedeker, Tendon tissue microdamage and the limits of intrinsic repair, Matrix Biology 85-86 (2020) 68-79, https://doi.org/10.1016/j.matbio.2019.07.008.

[14] A.R. Tomás, A.I. Gonçalves, E. Paz, P. Freitas, R.M.A. Domingues, M.E. Gomes, Magneto-mechanical actuation of magnetic responsive fibrous scaffolds boosts tenogenesis of human adipose stem cells, Nanoscale 11(39) (2019) 18255-18271, 10.1039/C9NR04355A.

[15] M. Laranjeira, R.M.A. Domingues, R. Costa-Almeida, R.L. Reis, M.E. Gomes, 3D Mimicry of Native-Tissue-Fiber Architecture Guides Tendon-Derived Cells and Adipose Stem Cells into Artificial Tendon Constructs, Small 13(31) (2017) 10.1002/smll.201700689.

[16] A.D. Schoenenberger, J. Foolen, P. Moor, U. Silvan, J.G. Snedeker, Substrate fiber alignment mediates tendon cell response to inflammatory signaling, Acta Biomaterialia 71 (2018) 306-317, https://doi.org/10.1016/j.actbio.2018.03.004.

[17] A.D. Schoenenberger, H. Tempfer, C. Lehner, J. Egloff, M. Mauracher, A. Bird, J. Widmer, K. Maniura-Weber, S.F. Fucentese, A. Traweger, U. Silvan, J.G. Snedeker, Macromechanics and polycaprolactone fiber organization drive macrophage polarization and regulate inflammatory activation of tendon in vitro and in vivo, Biomaterials 249 (2020) 120034, https://doi.org/10.1016/j.biomaterials.2020.120034.

[18] D.E. Birk, J.M. Fitch, J.P. Babiarz, K.J. Doane, T.F. Linsenmayer, Collagen fibrillogenesis in vitro: interaction of types I and V collagen regulates fibril diameter, J Cell Sci 95 (Pt 4) (1990) 649-57.

[19] C.C. Banos, A.H. Thomas, C.K. Kuo, Collagen fibrillogenesis in tendon development: current models and regulation of fibril assembly, Birth Defects Res C Embryo Today 84(3) (2008) 228-44, 10.1002/bdrc.20130.

[20] J.A. Martin, D. Mehr, P.D. Pardubsky, J.A. Buckwalter, The role of tenascin-C in adaptation of tendons to compressive loading, Biorheology 40(1-3) (2003) 321-9.

[21] L. Jozsa, M. Lehto, P. Kannus, M. Kvist, A. Reffy, T. Vieno, M. Järvinen, S. Demel, E. Elek, Fibronectin and laminin in Achilles tendon, Acta Orthop Scand 60(4) (1989) 469-71, 10.3109/17453678909149322.

[22] P. Kannus, Structure of the tendon connective tissue, Scandinavian Journal of Medicine & Science in Sports 10(6) (2000) 312-320, https://doi.org/10.1034/j.1600-0838.2000.010006312.x.

[23] P. Kumar, A. Satyam, X. Fan, E. Collin, Y. Rochev, B.J. Rodriguez, A. Gorelov, S. Dillon, L. Joshi, M. Raghunath, A. Pandit, D.I. Zeugolis, Macromolecularly crowded in vitro microenvironments accelerate the production of extracellular matrix-rich supramolecular assemblies, Scientific Reports 5(1) (2015) 8729, 10.1038/srep08729.

[24] D. Tsiapalis, A. De Pieri, K. Spanoudes, I. Sallent, S. Kearns, J.L. Kelly, M. Raghunath, D.I. Zeugolis, The synergistic effect of low oxygen tension and macromolecular crowding in the development of extracellular matrix-rich tendon equivalents, Biofabrication 12(2) (2020) 025018, 10.1088/1758-5090/ab6412.

[25] A.L. Titan, M.T. Longaker, A fine balance in tendon healing, Nature Cell Biology 21(12) (2019) 1466-1467, 10.1038/s41556-019-0432-0.

[26] S.K. Madhurakkat Perikamana, J. Lee, T. Ahmad, E.M. Kim, H. Byun, S. Lee, H. Shin, Harnessing biochemical and structural cues for tenogenic differentiation of adipose derived stem cells (ADSCs) and development of an in vitro tissue interface mimicking tendon-bone insertion graft, Biomaterials 165 (2018) 79-93, 10.1016/j.biomaterials.2018.02.046.

[27] D.A. Kaji, K.L. Howell, Z. Balic, D. Hubmacher, A.H. Huang, Tgfβ signaling is required for tenocyte recruitment and functional neonatal tendon regeneration, eLife 9 (2020) e51779, 10.7554/eLife.51779.

[28] G.-K. Tan, B.A. Pryce, A. Stabio, J.V. Brigande, C. Wang, Z. Xia, S.F. Tufa, D.R. Keene, R. Schweitzer, Tgfβ signaling is critical for maintenance of the tendon cell fate, eLife 9 (2020) e52695, 10.7554/eLife.52695.

[29] L. Chen, S.W. Dong, X. Tao, J.P. Liu, K.L. Tang, J.Z. Xu, Autologous Platelet-Rich Clot Releasate Stimulates Proliferation and Inhibits Differentiation of Adult Rat Tendon Stem Cells towards Nontenocyte Lineages, Journal of International Medical Research 40(4) (2012) 1399-1409, 10.1177/147323001204000418.

[30] Y. Zhou, J.H.C. Wang, PRP Treatment Efficacy for Tendinopathy: A Review of Basic Science Studies, BioMed Research International 2016 (2016) 9103792, 10.1155/2016/9103792.

[31] X.-x. Tan, H.-y. Ju, W. Yan, H.-j. Jiang, J.-p. Su, H.-j. Dong, L.-s. Wang, D.-b. Zou, Autologous platelet lysate local injections for the treatment of refractory lateral epicondylitis, J Orthop Surg Res 11 (2016) 17-17, 10.1186/s13018-016-0349-2.

[32] B.B. Mendes, M. Gómez-Florit, P.S. Babo, R.M. Domingues, R.L. Reis, M.E. Gomes, Blood derivatives awaken in regenerative medicine strategies to modulate wound healing, Advanced Drug Delivery Reviews 129 (2018) 376-393, https://doi.org/10.1016/j.addr.2017.12.018.

[33] B.B. Mendes, M. Gómez-Florit, A.G. Hamilton, M.S. Detamore, R.M.A. Domingues, R.L. Reis, M.E. Gomes, Human platelet lysate-based nanocomposite bioink for bioprinting hierarchical fibrillar structures, Biofabrication 12(1) (2019) 015012, 10.1088/1758-5090/ab33e8.

[34] B.B. Mendes, M. Gómez-Florit, R.A. Pires, R.M.A. Domingues, R.L. Reis, M.E. Gomes, Human-based fibrillar nanocomposite hydrogels as bioinstructive matrices to tune stem cell behavior, Nanoscale 10(36) (2018) 17388-17401, 10.1039/C8NR04273J.

[35] N.S. Kalson, D.F. Holmes, Z. Kapacee, I. Otermin, Y. Lu, R.A. Ennos, E.G. Canty-Laird, K.E. Kadler, An experimental model for studying the biomechanics of embryonic tendon: Evidence that the development of mechanical properties depends on the actinomyosin machinery, Matrix Biology 29(8) (2010) 678-689, https://doi.org/10.1016/j.matbio.2010.08.009.

[36] M. Bottagisio, S. Lopa, V. Granata, G. Talò, C. Bazzocchi, M. Moretti, A. Barbara Lovati, Different combinations of growth factors for the tenogenic differentiation of bone marrow mesenchymal stem cells in monolayer culture and in fibrin-based three-dimensional constructs, Differentiation 95 (2017) 44-53, https://doi.org/10.1016/j.diff.2017.03.001.

[37] I. Rajpar, J.G. Barrett, Optimizing growth factor induction of tenogenesis in three-dimensional culture of mesenchymal stem cells, Journal of Tissue Engineering 10 (2019) 2041731419848776, 10.1177/2041731419848776.

[38] R. Costa-Almeida, I. Calejo, R. Altieri, R.M.A. Domingues, E. Giordano, R.L. Reis, M.E. Gomes, Exploring platelet lysate hydrogel-coated suture threads as biofunctional composite living fibers for cell delivery in tissue repair, Biomed Mater 14(3) (2019) 034104, 10.1088/1748-605X/ab0de6.

[39] C. Lehner, G. Spitzer, R. Gehwolf, A. Wagner, N. Weissenbacher, C. Deininger, K. Emmanuel, F. Wichlas, H. Tempfer, A. Traweger, Tenophages: a novel macrophage-like tendon cell population expressing CX3CL1 and CX3CR1, Disease Models & Mechanisms 12(12) (2019) dmm041384, 10.1242/dmm.041384.

[40] P. Babo, V. Santo, iacute, E. tor, A.R.C. Duarte, C. Correia, aacute, udia, M.H.G. Costa, J. Mano, atilde, F. o, R.L. Reis, M.E. Gomes, Platelet lysate membranes as new autologous templates for tissue engineering applications, Inflammation and Regeneration 34(1) (2014) 033-044, 10.2492/inflammregen.34.033.

[41] M.C. Echave, R.M.A. Domingues, M. Gómez-Florit, J.L. Pedraz, R.L. Reis, G. Orive, M.E. Gomes, Biphasic Hydrogels Integrating Mineralized and Anisotropic Features for Interfacial Tissue Engineering, ACS Applied Materials & Interfaces 11(51) (2019) 47771-47784, 10.1021/acsami.9b17826.

[42] R.M.A. Domingues, S. Chiera, P. Gershovich, A. Motta, R.L. Reis, M.E. Gomes, Enhancing the Biomechanical Performance of Anisotropic Nanofibrous Scaffolds in Tendon Tissue Engineering: Reinforcement with Cellulose Nanocrystals, Advanced Healthcare Materials 5(11) (2016) 1364-1375, https://doi.org/10.1002/adhm.201501048.

[43] F.H. Silver, Y.P. Kato, M. Ohno, A.J. Wasserman, Analysis of mammalian connective tissue: relationship between hierarchical structures and mechanical properties, J Long Term Eff Med Implants 2(2-3) (1992) 165-98.

[44] F.H. Silver, J.W. Freeman, G.P. Seehra, Collagen self-assembly and the development of tendon mechanical properties, J Biomech 36(10) (2003) 1529-53, 10.1016/s0021-9290(03)00135-0.

[45] C.T. Thorpe, H.L. Birch, P.D. Clegg, H.R.C. Screen, Chapter 1 - Tendon Physiology and Mechanical Behavior: Structure–Function Relationships, in: M.E. Gomes, R.L. Reis, M.T. Rodrigues (Eds.), Tendon Regeneration, Academic Press, Boston, 2015, pp. 3-39, https://doi.org/10.1016/B978-0-12-801590-2.00001-6.

[46] R.G. Flemming, C.J. Murphy, G.A. Abrams, S.L. Goodman, P.F. Nealey, Effects of synthetic micro- and nano-structured surfaces on cell behavior, Biomaterials 20(6) (1999) 573-88, 10.1016/s0142-9612(98)00209-9.

[47] M. Benjamin, E. Kaiser, S. Milz, Structure-function relationships in tendons: a review, J Anat 212(3) (2008) 211-28, 10.1111/j.1469-7580.2008.00864.x.

[48] M. O'Brien, Structure and metabolism of tendons, Scandinavian Journal of Medicine & Science in Sports 7(2) (1997) 55-61, https://doi.org/10.1111/j.1600-0838.1997.tb00119.x.

[49] C.M. McNeilly, A.J. Banes, M. Benjamin, J.R. Ralphs, Tendon cells in vivo form a three dimensional network of cell processes linked by gap junctions, J Anat 189 (Pt 3)(Pt 3) (1996) 593-600.

[50] A.B. Bello, D. Kim, D. Kim, H. Park, S.-H. Lee, Engineering and Functionalization of Gelatin Biomaterials: From Cell Culture to Medical Applications, Tissue Engineering Part B: Reviews 26(2) (2020) 164-180, 10.1089/ten.teb.2019.0256.

[51] H. Aubin, J.W. Nichol, C.B. Hutson, H. Bae, A.L. Sieminski, D.M. Cropek, P. Akhyari, A. Khademhosseini, Directed 3D cell alignment and elongation in microengineered hydrogels, Biomaterials 31(27) (2010) 6941-6951, https://doi.org/10.1016/j.biomaterials.2010.05.056.

[52] D. Wang, W. Zheng, Y. Xie, P. Gong, F. Zhao, B. Yuan, W. Ma, Y. Cui, W. Liu, Y. Sun, M. Piel, W. Zhang, X. Jiang, Tissue-specific mechanical and geometrical control of cell viability and actin cytoskeleton alignment, Scientific Reports 4(1) (2014) 6160, 10.1038/srep06160.

[53] A. Totaro, T. Panciera, S. Piccolo, YAP/TAZ upstream signals and downstream responses, Nature Cell Biology 20(8) (2018) 888-899, 10.1038/s41556-018-0142-z.

[54] H. Yin, M.D. Caceres, Z. Yan, M. Schieker, M. Nerlich, D. Docheva, Tenomodulin regulates matrix remodeling of mouse tendon stem/progenitor cells in an ex vivo collagen I gel model, Biochemical and Biophysical Research Communications 512(4) (2019) 691-697, https://doi.org/10.1016/j.bbrc.2019.03.063.

[55] S. Dex, D. Lin, C. Shukunami, D. Docheva, Tenogenic modulating insider factor: Systematic assessment on the functions of tenomodulin gene, Gene 587(1) (2016) 1-17, 10.1016/j.gene.2016.04.051.

[56] D. Ramos, M.S. Peach, A.D. Mazzocca, X. Yu, S.G. Kumbar, 8 - Tendon tissue engineering, in: S.P. Nukavarapu, J.W. Freeman, C.T. Laurencin (Eds.), Regenerative Engineering of Musculoskeletal Tissues and Interfaces, Woodhead Publishing2015, pp. 195-217, https://doi.org/10.1016/B978-1-78242-301-0.00008-2.

[57] N.D. Murchison, B.A. Price, D.A. Conner, D.R. Keene, E.N. Olson, C.J. Tabin, R. Schweitzer, Regulation of tendon differentiation by scleraxis distinguishes force-transmitting tendons from muscle-anchoring tendons, Development 134(14) (2007) 2697, 10.1242/dev.001933.

[58] Y. Ito, N. Toriuchi, T. Yoshitaka, H. Ueno-Kudoh, T. Sato, S. Yokoyama, K. Nishida, T. Akimoto, M. Takahashi, S. Miyaki, H. Asahara, The Mohawk homeobox gene is a critical regulator of tendon differentiation, Proceedings of the National Academy of Sciences 107(23) (2010) 10538, 10.1073/pnas.1000525107.

[59] R. Schweitzer, J.H. Chyung, L.C. Murtaugh, A.E. Brent, V. Rosen, E.N. Olson, A. Lassar, C.J. Tabin, Analysis of the tendon cell fate using Scleraxis, a specific marker for tendons and ligaments, Development 128(19) (2001) 3855.

[60] D. Docheva, E.B. Hunziker, R. Fässler, O. Brandau, Tenomodulin Is Necessary for Tenocyte Proliferation and Tendon Maturation, Molecular and Cellular Biology 25(2) (2005) 699, 10.1128/MCB.25.2.699-705.2005.

[61] C. Shukunami, A. Takimoto, M. Oro, Y. Hiraki, Scleraxis positively regulates the expression of tenomodulin, a differentiation marker of tenocytes, Developmental Biology 298(1) (2006) 234-247, https://doi.org/10.1016/j.ydbio.2006.06.036.

[62] H.R.C. Screen, D.E. Berk, K.E. Kadler, F. Ramirez, M.F. Young, Tendon functional extracellular matrix, Journal of orthopaedic research : official publication of the Orthopaedic Research Society 33(6) (2015) 793-799, 10.1002/jor.22818.

[63] Y. Bi, D. Ehirchiou, T.M. Kilts, C.A. Inkson, M.C. Embree, W. Sonoyama, L. Li, A.I. Leet, B.M. Seo, L. Zhang, S. Shi, M.F. Young, Identification of tendon stem/progenitor cells and the role of the extracellular matrix in their niche, Nat Med 13(10) (2007) 1219-27, 10.1038/nm1630.

[64] G. Zhang, Y. Ezura, I. Chervoneva, P.S. Robinson, D.P. Beason, E.T. Carine, L.J. Soslowsky, R.V. Iozzo, D.E. Birk, Decorin regulates assembly of collagen fibrils and acquisition of biomechanical properties during tendon development, Journal of Cellular Biochemistry 98(6) (2006) 1436-1449, https://doi.org/10.1002/jcb.20776.

[65] C.T. Thorpe, H.L. Birch, P.D. Clegg, H.R.C. Screen, The role of the non-collagenous matrix in tendon function, Int J Exp Pathol 94(4) (2013) 248-259, 10.1111/iep.12027.

[66] R.T. Kohrs, C. Zhao, Y.L. Sun, G.D. Jay, L. Zhang, M.L. Warman, K.N. An, P.C. Amadio, Tendon fascicle gliding in wild type, heterozygous, and lubricin knockout mice, J Orthop Res 29(3) (2011) 384-9, 10.1002/jor.21247.

[67] Z. Yin, X. Chen, H.X. Song, J.J. Hu, Q.M. Tang, T. Zhu, W.L. Shen, J.L. Chen, H. Liu, B.C. Heng, H.W. Ouyang, Electrospun scaffolds for multiple tissues regeneration in vivo through topography dependent induction of lineage specific differentiation, Biomaterials 44 (2015) 173-85, 10.1016/j.biomaterials.2014.12.027.

[68] J. Foolen, S.L. Wunderli, S. Loerakker, J.G. Snedeker, Tissue alignment enhances remodeling potential of tendon-derived cells - Lessons from a novel microtissue model of tendon scarring, Matrix Biology 65 (2018) 14-29, https://doi.org/10.1016/j.matbio.2017.06.002.

[69] D.L. Matera, W.Y. Wang, B.M. Baker, New directions and dimensions for bioengineered models of fibrosis, Nature Reviews Materials (2021) 10.1038/s41578-021-00288-x.

[70] M. Järvinen, L. Józsa, P. Kannus, T.L.N. Järvinen, M. Kvist, W. Leadbetter, Histopathological findings in chronic tendon disorders, Scandinavian Journal of Medicine & Science in Sports 7(2) (1997) 86-95, https://doi.org/10.1111/j.1600-0838.1997.tb00124.x.

[71] N.M. Lee, C. Erisken, T. Iskratsch, M. Sheetz, W.N. Levine, H.H. Lu, Polymer fiber-based models of connective tissue repair and healing, Biomaterials 112 (2017) 303-312, https://doi.org/10.1016/j.biomaterials.2016.10.013.

[72] D. Docheva, S.A. Müller, M. Majewski, C.H. Evans, Biologics for tendon repair, Advanced Drug Delivery Reviews 84 (2015) 222-239, https://doi.org/10.1016/j.addr.2014.11.015.

[73] Y. Ito, N. Toriuchi, T. Yoshitaka, H. Ueno-Kudoh, T. Sato, S. Yokoyama, K. Nishida, T. Akimoto, M. Takahashi, S. Miyaki, H. Asahara, The Mohawk homeobox gene is a critical

regulator of tendon differentiation, Proceedings of the National Academy of Sciences 107(23) (2010) 10538, 10.1073/pnas.1000525107.

[74] Y.F. Rui, P.P.Y. Lui, Y.M. Wong, Q. Tan, K.M. Chan, Altered fate of tendon-derived stem cells isolated from a failed tendon-healing animal model of tendinopathy, Stem Cells Dev 22(7) (2013) 1076-1085, 10.1089/scd.2012.0555.

[75] C. Zhang, J. Zhu, Y. Zhou, B.P. Thampatty, J.H.C. Wang, Tendon Stem/Progenitor Cells and Their Interactions with Extracellular Matrix and Mechanical Loading, Stem Cells International 2019 (2019) 3674647, 10.1155/2019/3674647.

[76] W. Bi, J.M. Deng, Z. Zhang, R.R. Behringer, B. de Crombrugghe, Sox9 is required for cartilage formation, Nature Genetics 22(1) (1999) 85-89, 10.1038/8792.

[77] J. Zhang, J.H.C. Wang, Mechanobiological response of tendon stem cells: Implications of tendon homeostasis and pathogenesis of tendinopathy, Journal of Orthopaedic Research 28(5) (2010) 639-643, https://doi.org/10.1002/jor.21046.

[78] W. Zhao, X. Wang, K.-H. Sun, L. Zhou, α-smooth muscle actin is not a marker of fibrogenic cell activity in skeletal muscle fibrosis, PLOS ONE 13(1) (2018) e0191031, 10.1371/journal.pone.0191031.

[79] L.M. Galatz, L. Gerstenfeld, E. Heber-Katz, S.A. Rodeo, Tendon regeneration and scar formation: The concept of scarless healing, J Orthop Res 33(6) (2015) 823-31, 10.1002/jor.22853.

[80] M. de Mos, B. van El, J. DeGroot, H. Jahr, H.T. van Schie, E.R. van Arkel, H. Tol, R. Heijboer, G.J. van Osch, J.A. Verhaar, Achilles tendinosis: changes in biochemical composition and collagen turnover rate, Am J Sports Med 35(9) (2007) 1549-56, 10.1177/0363546507301885.

[81] N. Maffulli, S.W.B. Ewen, S.W. Waterston, J. Reaper, V. Barrass, Tenocytes from Ruptured and Tendinopathic Achilles Tendons Produce Greater Quantities of Type III Collagen than Tenocytes from Normal Achilles Tendons: An in Vitro Model of Human Tendon Healing, The American Journal of Sports Medicine 28(4) (2000) 499-505, 10.1177/03635465000280040901.

[82] H.A. Eriksen, A. Pajala, J. Leppilahti, J. Risteli, Increased content of type III collagen at the rupture site of human Achilles tendon, J Orthop Res 20(6) (2002) 1352-7, 10.1016/s0736-0266(02)00064-5.

[83] S. Tom, J. Parkinson, M.Z. Ilic, J. Cook, J.A. Feller, C.J. Handley, Changes in the composition of the extracellular matrix in patellar tendinopathy, Matrix Biology 28(4) (2009) 230-236, https://doi.org/10.1016/j.matbio.2009.04.001.

[84] G.P. Riley, M.J. Goddard, B.L. Hazleman, Histopathological assessment and pathological significance of matrix degeneration in supraspinatus tendons, Rheumatology (Oxford) 40(2) (2001) 229-30, 10.1093/rheumatology/40.2.229.

[85] B.R. Seo, X. Chen, L. Ling, Y.H. Song, A.A. Shimpi, S. Choi, J. Gonzalez, J. Sapudom, K. Wang, R.C. Andresen Eguiluz, D. Gourdon, V.B. Shenoy, C. Fischbach, Collagen microarchitecture mechanically controls myofibroblast differentiation, Proceedings of the National Academy of Sciences 117(21) (2020) 11387, 10.1073/pnas.1919394117.

[86] V.J. Thannickal, D.Y. Lee, E.S. White, Z. Cui, J.M. Larios, R. Chacon, J.C. Horowitz, R.M. Day, P.E. Thomas, Myofibroblast Differentiation by Transforming Growth Factor-β1 Is Dependent on Cell Adhesion and Integrin Signaling via Focal Adhesion Kinase*, Journal of Biological Chemistry 278(14) (2003) 12384-12389, https://doi.org/10.1074/jbc.M208544200.

[87] V.F. Achterberg, L. Buscemi, H. Diekmann, J. Smith-Clerc, H. Schwengler, J.J. Meister, H. Wenck, S. Gallinat, B. Hinz, The nano-scale mechanical properties of the extracellular matrix regulate dermal fibroblast function, J Invest Dermatol 134(7) (2014) 1862-1872, 10.1038/jid.2014.90.

[88] M. Kjaer, Role of extracellular matrix in adaptation of tendon and skeletal muscle to mechanical loading, Physiol Rev 84(2) (2004) 649-98, 10.1152/physrev.00031.2003.

[89] G.P. Riley, V. Curry, J. DeGroot, B. van El, N. Verzijl, B.L. Hazleman, R.A. Bank, Matrix metalloproteinase activities and their relationship with collagen remodelling in tendon pathology, Matrix Biology 21(2) (2002) 185-195, https://doi.org/10.1016/S0945-053X(01)00196-2.

[90] M. Tsuzaki, D. Bynum, L. Almekinders, X. Yang, J. Faber, A.J. Banes, ATP modulates load-inducible IL-1beta, COX 2, and MMP-3 gene expression in human tendon cells, J Cell Biochem 89(3) (2003) 556-62, 10.1002/jcb.10534.

[91] C.T. Thorpe, S. Chaudhry, I.I. Lei, A. Varone, G.P. Riley, H.L. Birch, P.D. Clegg, H.R.C. Screen, Tendon overload results in alterations in cell shape and increased markers of inflammation and matrix degradation, Scandinavian Journal of Medicine & Science in Sports 25(4) (2015) e381-e391, https://doi.org/10.1111/sms.12333.

[92] A. Castagna, E. Cesari, A. Gigante, M. Conti, R. Garofalo, Metalloproteases and their inhibitors are altered in both torn and intact rotator cuff tendons, Musculoskelet Surg 97 Suppl 1 (2013) 39-47, 10.1007/s12306-013-0264-1.

[93] S. Lakemeier, S.A. Schwuchow, C.D. Peterlein, C. Foelsch, S. Fuchs-Winkelmann, E. Archontidou-Aprin, J.R.J. Paletta, M.D. Schofer, Expression of matrix metalloproteinases 1, 3, and 9 in degenerated long head biceps tendon in the presence of rotator cuff tears: an immunohistological study, BMC Musculoskeletal Disorders 11(1) (2010) 271, 10.1186/1471-2474-11-271.

[94] A. Del Buono, F. Oliva, L. Osti, N. Maffulli, Metalloproteases and tendinopathy, Muscles Ligaments Tendons J 3(1) (2013) 51-57, 10.11138/mltj/2013.3.1.051.

[95] G. Riley, Tendinopathy–from basic science to treatment, Nat Clin Pract Rheumatol 4(2) (2008) 82-9, 10.1038/ncprheum0700.

9.7. SUPPLEMENTARY INFORMATION

9.7.1. FIGURES

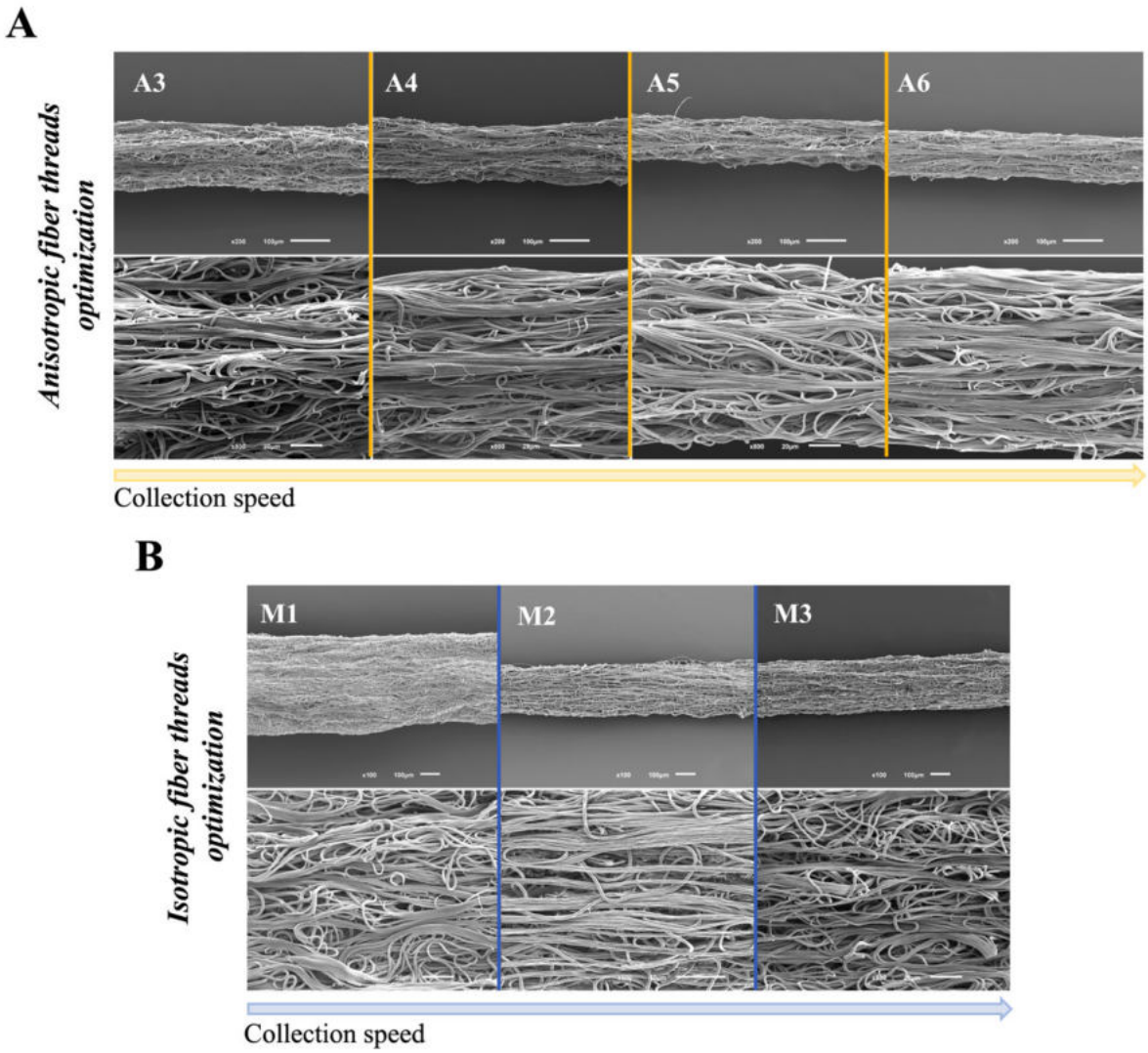

Supplementary Figure S9.1 | Optimization of anisotropic and isotropic fiber threads production. Representative scanning electron microscopy images of (A) anisotropic and (B) isotropic fiber threads acquired at increasing collection speeds.

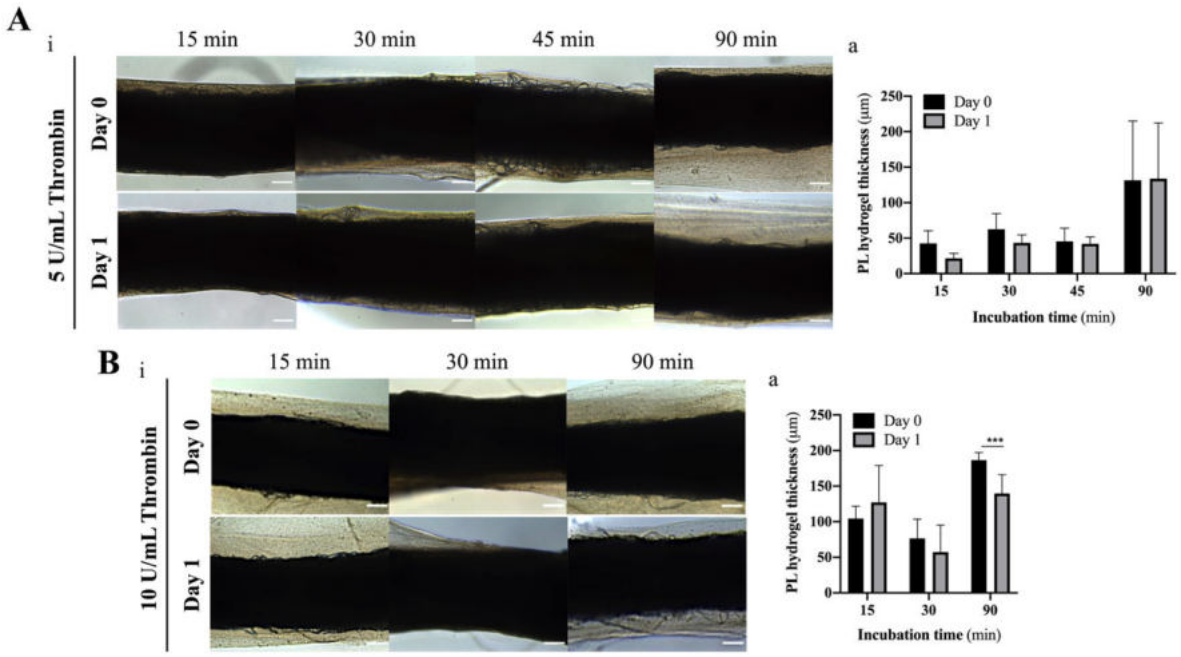

Supplementary Figure S9.2 | Morphology of functional PL-yarns/healthy and hydrogel thickness. Representative optical microscopy images of PCL yarns incubated with a thrombin/$CaCl_2$ (5mM) solution with a final concentration of thrombin of (A) 5 U/mL and (B) 10 U/mL for 15, 30, 45 and 90 minutes. Scale bars, 100 µm. (a) Changes of hydrogel thickness as a function of thrombin/$CaCl_2$ incubation time. Statistically significant differences are shown as ***, p<0.0003. Data are presented as mean ± SD (n=19).

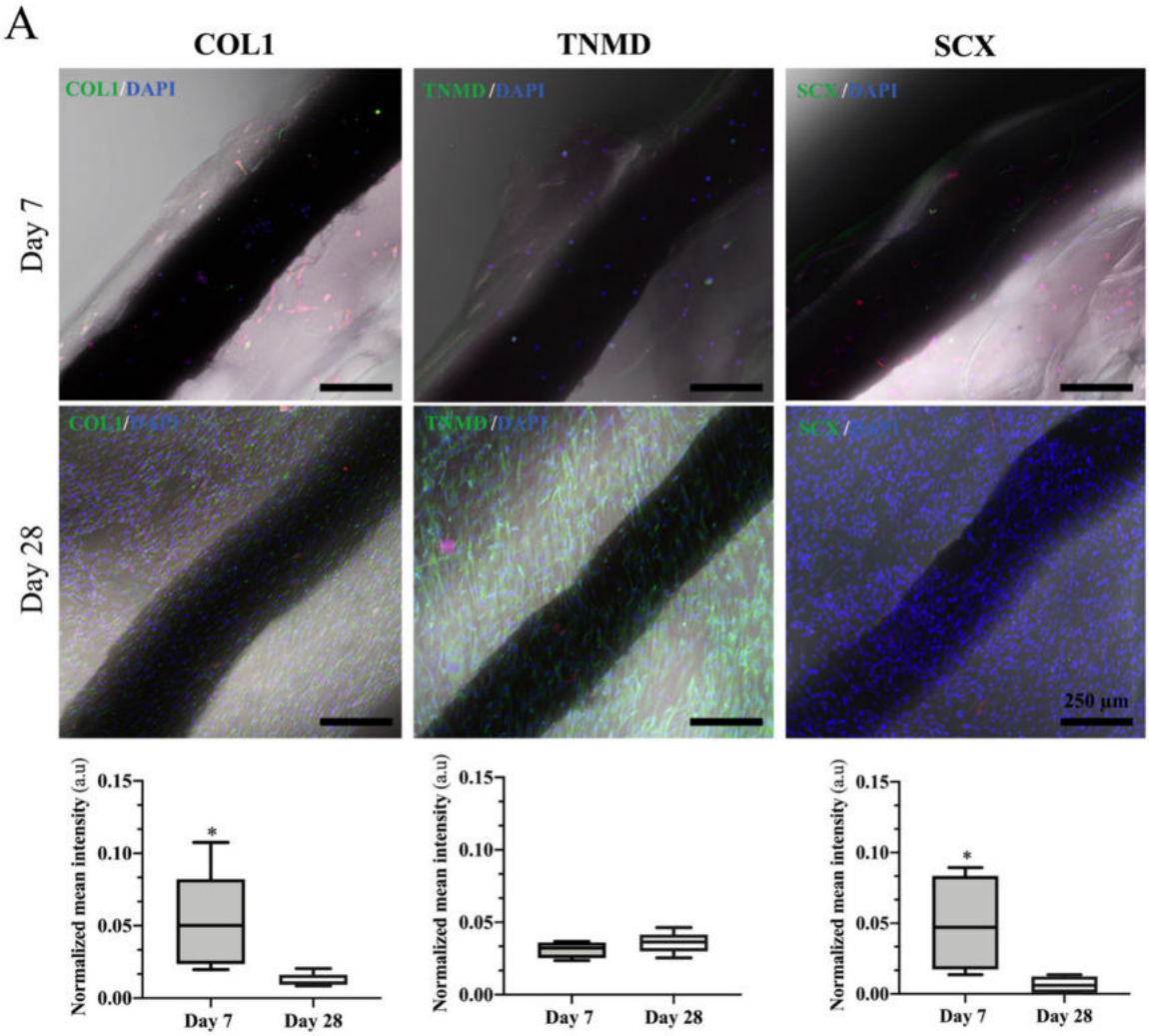

Supplementary Figure S9.3 | Protein expression of tenogenic markers by hTDCs encapsulated in CLF-control. (A) Confocal imaging of (i) COL1 (*, $p = 0.016$, n=6), (ii) TNMD (n=6) and (iii) SCX (*, $p = 0.029$, n=6) in CLF-control and respective mean intensity quantification (bottom). Scale bars, 250 µm.

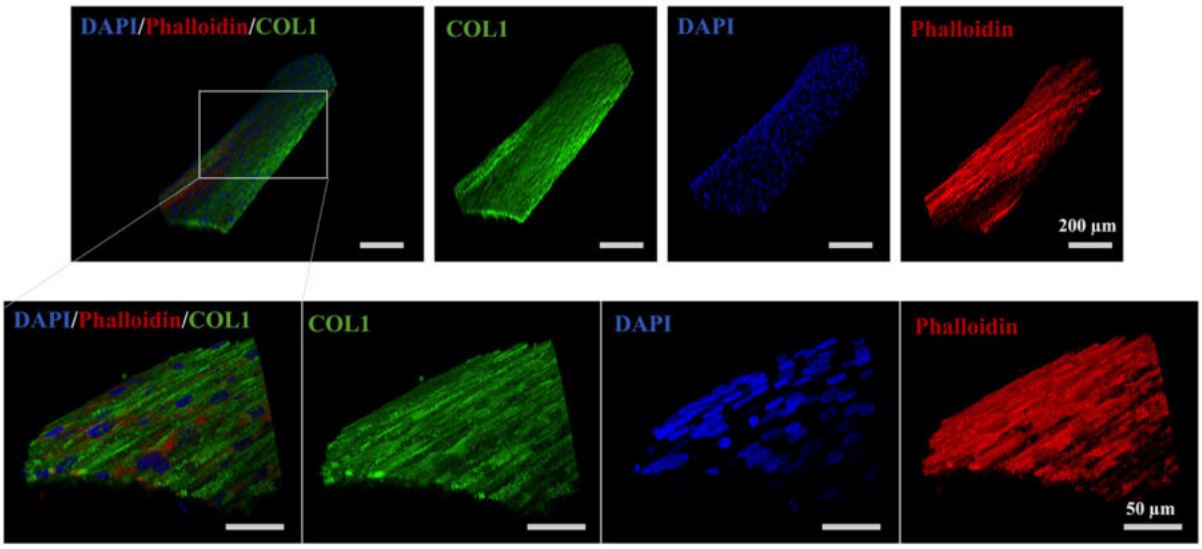

Supplementary Figure S9.4 | ECM deposition in CLF-healthy after 28 days of culture. Three-dimensional confocal imaging of COL1 (green channel), nuclei (blue channel) and cytoskeleton (red channel) density in CLF-healthy.

SECTION IV: Final remarks

CHAPTER 10. Conclusions and future perspectives

10.1. CONCLUSIONS

Over the past decade, efforts have been made in the field of Interfacial Tissue Engineering to address the need for advanced strategies to improve tendon-to-bone interface repair and ultimately achieve a proper interface integration and regeneration. Yet, the inexistence of satisfactory clinical outcomes is a commonplace in the treatment of injuries, often resulting in problems such as detachment of the tendon from the bony insertion or even rupture of the interface. Besides, tendon-to-bone interfaces are present in different anatomic locations and are exposed to severe mechanical loadings, which result in injuries with very dissimilar characteristics. To overcome these problems, several interfacial tissue engineering strategies targeting soft-to-hard interfaces have been proposed, encompassing the combination of biochemical and biophysical tools to recreate the native morphological and regional features of soft-to-hard tissue interfaces, while carefully controlling stem cells fate to mimic the naturally present cellular microenvironments. These strategies focus on a broad spectrum of approaches, including those based on the development of fibrous biomaterials, cell-based therapies, growth factor delivery, gene therapy, among others. However, even though several advances have been made in the field, to date, there is no successful therapy for tendon-to-bone interface regeneration and major challenges remain to be overcome, namely: (i) the mimicry of tissue complex architecture and hierarchical organization; (ii) the replication of the tissue´s adequate biomechanical properties; (iii) the search for an ideal cell source, given the lack of complete knowledge of the cellular microenvironment present in tendon-to-bone interface and (iv) the lack of well-established biochemical/biophysical cues to trigger the orchestration of regenerative processes in situ upon injury. Overall, the ideal strategy for tendon-to-bone interface tissue regeneration would lay on the recreation of the interfacial physiological complexity, assuring the mechanical performance of the tissue during the reparative process, and delivery of essential therapeutic elements to promote tissue regeneration and modulate the inflammatory milieu. Besides this, healing must occur within an optimal temporal window toward limiting scar tissue formation.

Over the years, several studies addressed the role of biological actors, including competent regenerative cells and inflammatory cells, as well as biochemical factors, namely cytokines and growth factors. Alternatively, recent progresses on biomaterial-guided cell behaviors have been providing novel tools to direct cell fate. Additionally, and taking advantage of fiber-based technologies and textile techniques, different strategies have been explored towards the development of an optimal scaffold that can temporarily substitute the injured tissue while triggering its regeneration. Nonetheless, current TE strategies frequently lack the ability of merging biomechanical support and a cellular instructive

microenvironment into a single construct or do not address the need of fulfilling different requirements according to the type of injury.

With this in mind, the major objective of this thesis was to tackle these concerns by exploring different routes towards advancing *in vitro* strategies envisioning innovative set-ups, as well as for clinically relevant and translatable biomaterials. Through these studies, some important/major outcomes could be achieved, as discussed in detail below.

(1) Co-culture systems as platforms to optimize culture conditions and study bidirectional interactions between native tendon cells and pre-osteoblasts towards the establishment of novel *in vitro* models and cellular based therapies for the tendon-to-bone interface (Chapter 5)

Co-culture systems constitute a tool for the study of complex interactions occurring at the cellular level, enabling the recreation of heterotypic cell interactions and production of soluble factors. In interfacial tissue engineering, cell-based therapies face the great challenge of finding an ideal cell source and to orchestrate the co-existence of several cell populations, as mixed populations are commonly found at the tendon-to-bone interface and are known to contribute at distinct levels to coordinate tissue's healing and regeneration Nature provides tissues with top-notch engineers, yet how these cellular populations perform their job, is still to be completely uncover.

In this thesis (Chapter 5), we proposed the optimization of a co-culture model to study cellular interactions between human ASCs (hASCs), pre-differentiated toward the osteogenic lineage (pre-osteoblasts, pre-OBs) and human tendon-derived cells (hTDCs), used to replicate cellular environments found in bone and tendon, respectively. The main purpose was to clearly understand and modulate the cellular interactions occurring at the tendon-to-bone interface microenvironment through the optimization of extracellular medium content, one of the major lacks observed in the literature, as no described medium was found for the maintenance of the tenogenic phenotype of tendon cells and/or for the maintenance of both tenogenic and osteogenic phenotypes simultaneously. In this regard, intermediate concentrations of both basal medium and osteogenic medium (50 BM: 50 OM) were found to enable the maintenance of both phenotypes *in vitro*, through the deposition of characteristic ECMs and gene expression of specific markers. After the establishment a co-culture using the optimized medium condition, the influence of direct cell contact on the expression of relevant tendon-, bone- and interface-related markers was also evaluated. Strikingly, cellular crosstalk's occurring in co-cultures were found to play an important role in the expression of interface-related markers, namely by deposition of an osteochondrogenic ECM. These

findings served as basis for understanding the effect of medium conditions on the modulation of cell phenotype along with the importance of cell-cell contact on the regulation of the biological environment with future application in studies involving more complex tissue engineered systems to promote the formation of a new engineered tendon-to-bone like tissues.

(2) Tuning of oxygen tension as a key feature for the modulation of cells behavior towards the expression of interface-related markers (Chapters 6)

Oxygen tension is an important signal for the development and maintenance of several tissues. Tendon-to-bone interface presents a "critical zone" near the tendon-bone attachment, poorly vascularized, where the oxygen supply is very low. Similarly, tendon tissue is also poorly vascularized with oxygen saturation falling below 3.6-4.0% while, opposingly, bone is highly vascularized, presenting oxygen concentrations ranging from 5.5% to 15%. Hence, oxygen variations in the culture environment seem to play an important role cell's fate. Additionally, when trying to engineer the tendon-to-bone interface, it is of major importance to have in mind the gradual heterotypic cellular environment. Yet, no data was found in the literature reporting an ideal oxygen tension for tendon-to-bone microenvironment replication *in vitro*. Therefore, the aim of this work was to, first, recreate the oxygen environment found in the tendon and bone tissues, for the simultaneous maintenance of tenogenic and osteogenic phenotypes. Additionally, based on the previously optimized culturing conditions, in this chapter we aimed to mimicry the proper interface microenvironment through a balanced oxygen concentration to unravel important events that pave the way to the expression of important interface-related markers. Having this key aspect in mind, in Chapter 6, we proposed the use of a direct co-culture system as tendon-to-bone *in vitro* model to clearly understand the influence of low oxygen tension (5% O_2, hypoxia) and osteogenic supplementation in the modulation of cellular phenotype. To do so, single cultures of hASCs pre-differentiated towards osteogenic lineage (pre-osteoblasts) and hTDCs were used to determine the effect of hypoxia on tendon- and bone-like niches. Afterward, direct co-cultures were established to evaluate the influence of low oxygen tension on the cell-cell interaction and expression of interface-relevant markers in the presence of different ratios of osteogenic factors. Temporal expression of HIF1A and HIF2A was assessed, as well as activation of Hedgehog signaling pathway and reactive oxygen species (ROS) production and secretion of HIF1A by co-cultured cells. In summary, we demonstrated that exposure of pre-OBs and hTDCs to lower oxygen tension induces phenotypic changes by impairing osteogenesis and inducing cell maturation, respectively. Moreover, low oxygen tension and cell-cell interactions occurring in direct co-cultures, in the presence of osteogenic factors, clearly tunes the downstream activation of chondro- and osteoblastic pathways

towards the expression of an osteochondrogenic phenotype. The effect of hypoxia in promoting this progression requires an initial transcriptional activation *HIF1A* and stabilization near the nucleus, and a later activation *HIF2A* governing the final hypertrophic differentiation regulated by SOX9. Overall, the development of this *in vitro* system allowed the demonstration of the importance of the low oxygen tension in a co-culture regime with possible translation to an *in vivo* setting to promote a proper *de novo* formation of the interface between tendon and bone that will closely resemble the native musculoskeletal tissue.

(3) Combination of simple fabrication techniques and textile assembling towards the development of 3D functionally graded constructs with tunable properties that closely replicate the tendon-to-bone complex structure (Chapters 7 and 8)

Tendon-to-bone interfaces exhibit a characteristic hierarchical multi-tissue transition, specifically when going from the tendon part to the bony insertion. Currently described tissue engineered strategies rely on the use multiphasic and gradient scaffolds for tendon-to-bone tissue regeneration. Yet, developed approaches were reported no to comply with the required biomechanical and biochemical - relying on the use of single molecules - features necessary for a proper tissue replication. Moreover, in the case of multiphasic scaffolds, mostly failed in the mimicry of the smooth transition observed in between tissues composing the tendon-to-bone interface. So, in this thesis (Chapter 7), a novel 3D fibrous scaffold was fabricated with distinct topographical and compositional features tailored to guide cell alignment and simultaneously approximate the mechanical properties of the native tissue, to replicate the smooth progression from mineralized to non-mineralized tissue. To do so, wet-spinning was taken advantage, as this is a simple method for the continuous fabrication of fibers. Two types of microfibers were produced using PCL/ Gelatin and PCL/Gelatin/hydroxyapatite nano-to-microparticles to replicate both the soft (tendon) and hard (bone) tissues constituting the tendon-to-bone interface. Higher extrusion rates resulted in aligned PCL/Gelatin microfibers while, in the case of PCL/Gelatin/HAp, the presence of minerals led to a less organized structure. Biological studies with hASCs revealed that the fibers were not only able to support cell proliferation but also to favor cellular anisotropic alignment or to induce an osteogenic-like phenotype on human adipose derived stem cells in the presence of HAp. In fact, the continuous wet-spinning technique in combination with textile technologies enabled the generation of a more complex fibrous scaffold with a gradient in polymer composition, resulting in a mineral gradient of HAp content. Altogether the obtained results clearly demonstrated the feasibility of using simple fiber processing techniques, such as wet-spinning, to tailor cells response while having a precise control over fibers

topography and composition. Moreover, the combination with advanced textile techniques allowed the development of 3D fibrous scaffolds envisioning tendon-to-bone regeneration.

Lately, and taking advantage of both emulsion electrospinning and textile assembling (Chapter 8), 3D functionally graded scaffolds were similarly fabricated by continuously assembling anisotropic and isotropic emulsion electrospun yarns/threads, resulting in a multi-scale hierarchical construct that precisely deliver *in situ* multiple bioactive factors from platelet lysates in conjugation with biophysical and biochemical cues. Biological studies using hASCs clearly demonstrated the ability of produced constructs to tailor the commitment of hASCs into a phenotypic gradient exhibiting tenogenic, osteochondrogenic and osteogenic profiles in specific sections of scaffolds.

Altogether, it was demonstrated the feasibility of wet-spinning and electrospinning for the generation of textured and biofunctionalized micro- to nanofibers, which can be further assembled into more complex 3D gradient structures to mimic distinguishing features of tendon-to-bone interface.

(4) Platelet lysates as a source of depots of human-derived therapeutic factors with promising bioinstructive and pro-regenerative features (Chapter 8 and 9)

Platelet derivatives have been widely explored as they present a gigantic potential for endogenous regenerative medicine. Recently, blood derivatives such as platelet lysates (PLs) have been receiving increased attention as cost-effective sources of human therapeutic factors that can be used in both autologous and allogeneic applications in regenerative medicine. Indeed, PL is recognized as a stable alternative to several blood derivatives as it shows a comparatively lower batch-to-batch variability in batches prepared from platelet concentrates of different donors, potentially resulting in more predictable clinical outcomes. Several reports have been demonstrating the special interest for treating tendon injuries, as these cocktails of biomolecules are applied aiming at modulating the inflammatory response in difficult-to-heal tendinopathies that are not resolved by the substitution of the tissue due to the altered properties of the surrounding microenvironment. Yet, no studies were reported with the application of a source of multiple growth factors, such as PL, for tendon-to-bone interface repair.

In Chapter 8, we explored the use of platelet lysates as bioactive factors used in the biofunctionalization of fiber threads to sustain stem cells fate. We proposed the development of anisotropic and isotropic electrospun nanofiber threads incorporating platelet lysates and and/or nanohydroxyapatite (@nHAp), and their subsequent hierarchical assembling to produce tendon-similar structures – yarns (A-Yarn/PL) or bone collagen/mineral replicates – threads (I-Threads/PL@nHAp). Biological studies were performed using hASCs and demonstrated that A-Yarn/PL induce the expression of tenogenic markers, while matrix

mineralization on I-Threads/PL@nHA fostering the deposition of an osteogenic-ECM, without the need of pro-osteogenic supplementation. 3D functionally graded scaffolds were fabricated by continuously assembling A-Yarn/PL and I-Threads/PL@nHAp, resulting in hierarchically assembled bioactive scaffold which enabled the tailoring of hASCs differentiation into three different lineages, tenogenic, osteochondrogenic and osteogenic.

Afterwards, in Chapter 9, PL-hydrogel coated yarns and threads were used for the recreation *in vitro* of healthy and diseased tendon tissue. Nevertheless, coatings of platelet lysates were used as PL was intended to provide a vast source of biomolecules vital for regeneration. Additionally, PL coating have demonstrated to be a suitable tool for hTDCs encapsulation, as it allowed contact guidance with the core fiber due to its shrinking, which was not observed when compared to gelatin coating.

Overall, in this thesis we reported a reproducible and feasible method which enabled, for the first time, the incorporation of platelet lysates within nanofiber threads without denaturation and the use of an easy source of multiple growth factors for tendon and tendon-to-bone tissue regeneration.

(5) Physiological and pathological multiplex bioengineered tendon *in vitro* models as platforms to study key molecular pathways and drug screening (Chapter 9)

Clinically appropriate models of tendon tissue healthy and diseased microenvironments are a current need in cell biology and tissue engineering, as currently used *in vivo, ex vivo* and *in vitro* models still fail to capture reach the indispensable human transability. Moreover, optimal conditions for tendon explants that enable tissue homeostasis are yet to be described, being observed a huge gap for a proper tendon tissue model. So, when trying to engineer tissue substitutes it is required a multi-component and scalable approach that combines together physical, chemical and biological cues in single units. Therefore, in Chapter 9, we engineered a 3D multifunctional *in vitro* model for the mimicry of both physiological and pathological tendon microenvironments. First, and taking advantage of 3D printing, a simple holder was designed, allowing the user to prepare four different samples in each well of a 6-well plate. Afterward, composite living fibers (CLFs) were produced with polycaprolactone yarns (anisotropic) and threads (isotropic) core coated with a bioactive platelet lysate (PL) hydrogel layer encapsulating human tendon-derived cells (hTDCs) to mimic both healthy and diseased 3D tissue architectures, respectively. Human TDCs in CLF-healthy (anisotropic yarns) were found to be highly aligned, express tendon-related genes while synthetizing and depositing a teno-rich ECM. On the other hand, cell crowding without marked preferential orientation and high ECM deposition were observed in CLF-diseased accompanied by a phenotypic drift characterized by early gene expression of osteogenic and chondrogenic markers and later

expression of smooth alpha muscle actin. Moreover, CLF-diseased presented an imbalance between matrix remodeling and degradation, as normally observed in fibrotic tissue. In summary, in this thesis, a promising strategy was explored with the development of a 3D microengineered *in vitro* model for the replication of the physiological and pathophysiological microenvironments found in the native healthy and diseased tendon tissues, as possible alternatives for existing *in vivo* models of tendon development, rupture and repair, and suitable models for drug screening.

10.1. FUTURE PERSPECTIVES

The integration of both structural, biophysical, biochemical and cellular cues in a single system has been pursued over the last century in Tissue Engineering. Particularly for tendon-to-bone interface, the poor clinical outcomes of currently used therapeutic approaches are driving the current research toward the discovery of an optimal substitute that can ideally restore the proper tissue functionality at an unprecedented level. Nonetheless, it is extremely clear that some basic steps are still missing in this path. The present thesis recognizes the relevance of addressing the problem from different viewpoints, namely starting at the biological level and growing up to the gold standard approach of tissue engineering, i.e. development of novel biomaterials and scaffolds that can reflect the need for a proper tissue healing and regeneration. Yet, advanced integration of produced fibrous scaffolds (Chapter 7) and 3D fibrous gradient constructs (Chapter 8) can be further exploited for *in vivo* performance in a tendon-to-bone interface defect animal model. Moreover, when trying to clearly understand cellular mechanisms and interactions occurring at the native tissue, optimized co-culture systems should also be used in conjugation with bioinstructive 3D gradient scaffolds (Chapter 7 and 8), as these replicate the tendon-to-bone structure. Besides supportive biomaterials and biochemical cues, mechanical loading also plays an active role in tendon-to-bone interface formation. Therefore, the developed work would significantly improve with the use of a bioreactor system to mechanically simulate the body movements while using the developed 3D structures and assessing cellular responses occurring at each part the scaffold.

Generally, the work developed throughout this thesis proved to have potential utility in a broader range of areas, however some applications still need more exploration.